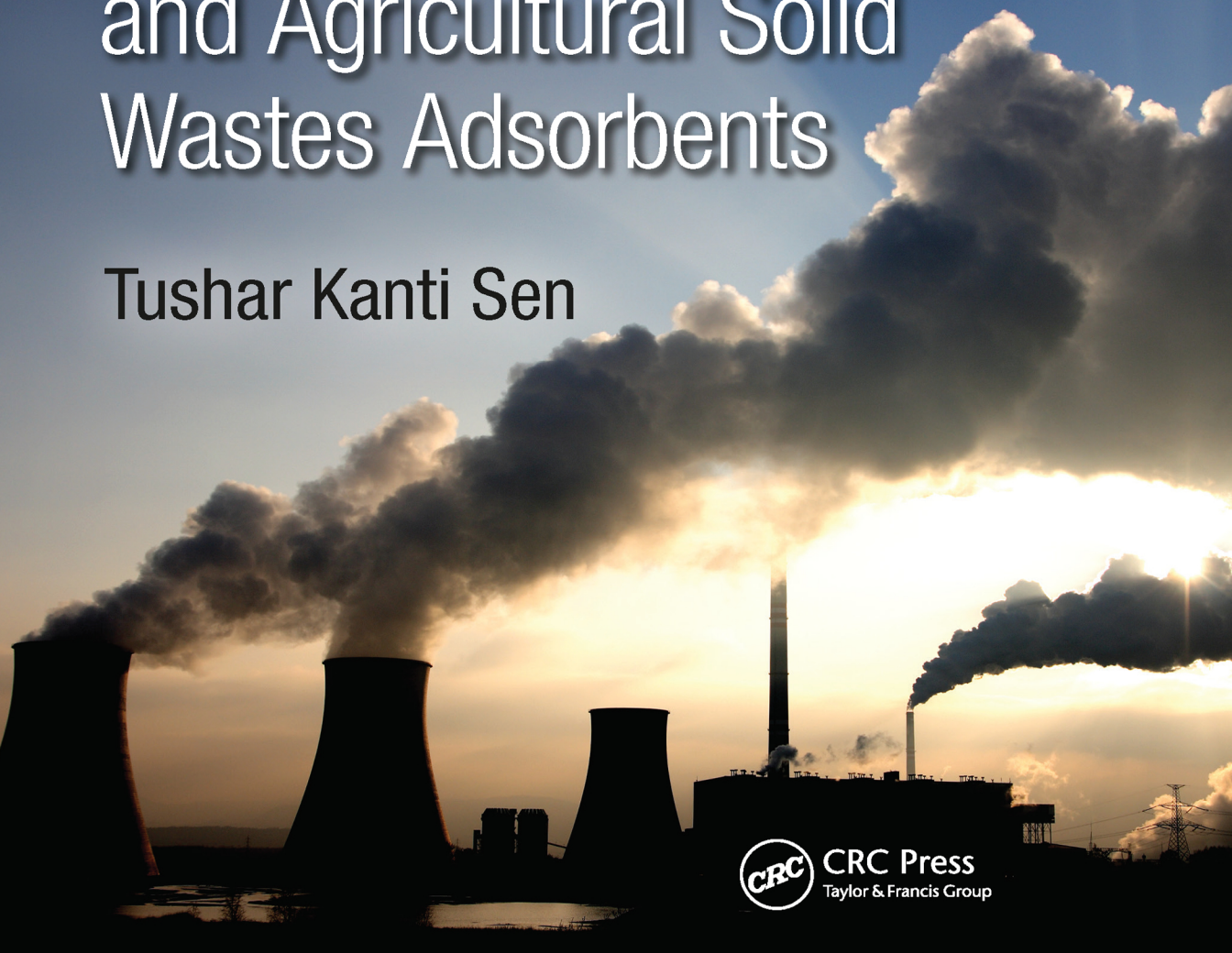


Air, Gas, and Water Pollution Control Using Industrial and Agricultural Solid Wastes Adsorbents

Tushar Kanti Sen



Air, Gas, and Water Pollution Control Using Industrial and Agricultural Solid Wastes Adsorbents



Taylor & Francis

Taylor & Francis Group

<http://taylorandfrancis.com>

Air, Gas, and Water Pollution Control Using Industrial and Agricultural Solid Wastes Adsorbents

Edited by
Tushar Kanti Sen



CRC Press

Taylor & Francis Group
Boca Raton London New York

CRC Press is an imprint of the
Taylor & Francis Group, an **informa** business

CRC Press
Taylor & Francis Group
6000 Broken Sound Parkway NW, Suite 300
Boca Raton, FL 33487-2742

© 2018 by Taylor & Francis Group, LLC
CRC Press is an imprint of Taylor & Francis Group, an Informa business

No claim to original U.S. Government works

Printed on acid-free paper

International Standard Book Number-13: 978-1-138-19673-5 (Hardback)

This book contains information obtained from authentic and highly regarded sources. Reasonable efforts have been made to publish reliable data and information, but the author and publisher cannot assume responsibility for the validity of all materials or the consequences of their use. The authors and publishers have attempted to trace the copyright holders of all material reproduced in this publication and apologize to copyright holders if permission to publish in this form has not been obtained. If any copyright material has not been acknowledged please write and let us know so we may rectify in any future reprint.

Except as permitted under U.S. Copyright Law, no part of this book may be reprinted, reproduced, transmitted, or utilized in any form by any electronic, mechanical, or other means, now known or hereafter invented, including photocopying, micro-filming, and recording, or in any information storage or retrieval system, without written permission from the publishers.

For permission to photocopy or use material electronically from this work, please access www.copyright.com (<http://www.copyright.com/>) or contact the Copyright Clearance Center, Inc. (CCC), 222 Rosewood Drive, Danvers, MA 01923, 978-750-8400. CCC is a not-for-profit organization that provides licenses and registration for a variety of users. For organizations that have been granted a photocopy license by the CCC, a separate system of payment has been arranged.

Trademark Notice: Product or corporate names may be trademarks or registered trademarks, and are used only for identification and explanation without intent to infringe.

Visit the Taylor & Francis Web site at
<http://www.taylorandfrancis.com>

and the CRC Press Web site at
<http://www.crcpress.com>

To my parents, the late Jahar lal Sen and Smt. Mira Sen, and to my family, Kabita and Anindya.



Taylor & Francis

Taylor & Francis Group

<http://taylorandfrancis.com>

Contents

Preface.....	ix
Acknowledgments	xiii
Editor.....	xv
Contributors.....	xvii

Section I Industrial and Agricultural Solid Wastes-Based Adsorbents in Gas/Air Purification

1. Gaseous Pollutant Removal Using Solid Wastes Adsorbents.....	3
<i>Sumathi Sethupathi, Lau Lee Chung, Muhammad Younas, Abdul Rahman Mohamed, and Mohammed J. K. Bashir</i>	
2. Solid Waste Adsorbents for Volatile Organic Compounds Removal by Biofiltration	21
<i>Hussein Znad, Benjamin Alliss, and Hari Vuthaluru</i>	
3. Carbon Dioxide (CO₂) Capture from Industrial Flue Gas: A Review	35
<i>Dipa Das and B. C. Meikap</i>	
4. Carbon Dioxide (CO₂) Capture by Calcium-Based Industrial Solid Wastes in Calcium Looping Process.....	57
<i>Yingjie Li, Xiaotong Ma, Lunbo Duan, and Chunmei Lu</i>	

Section II Industrial and Agricultural Solid Wastes-Based Adsorbents in Water Purification

5. Current Progress on the Removal of Hazardous Pollutants from Water Using Agricultural Wastes.....	79
<i>Suryadi Ismadji, Felycia Edi Soetaredjo, and Yi Hsu Ju</i>	
6. Biosorption of Divalent Heavy Metal Ions by Rice Husk: A Review	109
<i>Anteneh Mesfin Yeneneh, Tushar Kanti Sen, Murugesan Thanabalan, and Eugene Hong</i>	
7. Utilization of Red Mud for Environmental Applications.....	135
<i>Manoj Kumar Sahu and Raj Kishore Patel</i>	
8. Dolochar as a Low-Cost Adsorbent for the Removal of Pb(II) from Aqueous Solutions.....	163
<i>Gayatree Patra and B. C. Meikap</i>	

9. A Review on Potential Reusability of Industrial Solid Wastes as Adsorbents.....	179
<i>Gopinath Halder and Soumya Banerjee</i>	
10. A Review of Agricultural Solid Waste Materials as Potential Adsorbents for Copper Ions from Water and Wastewater	197
<i>Mohd Rafatullah, Syed Zaghun Abbas, Akil Ahmad, and David Lokhat</i>	
 Section III Solid Wastes-Based Emerging Adsorbents in Gaseous/Water Purification	
11. Mesoporous Adsorbents from Biomass: Opportunities and Challenges in Hydrothermal Treatment	225
<i>Akshay Jain, Kubilay Tekin, and Madapusi P. Srinivasan</i>	
12. Sustainable Biochar Derived from Agricultural Wastes for Removal of Methylene Green 5 from Aqueous Solution: Adsorption Kinetics, Isotherms, Thermodynamics, and Mechanism Analysis	255
<i>Hai Nguyen Tran, Sheng-Jie You, Huan-Ping Chao, and Ya-Fen Wang</i>	
13. Impact of Surface Modification of Activated Carbon on BTEX Removal from Aqueous Solutions: A Review	293
<i>Hirra Anjum, Fareeda Chemat, Nirmala Gnanasundaram, Appusami Arunagiri, and Murugesan Thanabalan</i>	
Index.....	313

Preface

Air and water pollution occur when toxic pollutants of varying kinds (organic, inorganic, radioactive, and so on) are directly or indirectly discharged into the environment without adequate treatment to remove these potential pollutants. The main sources of these toxic pollutants are industrialization, human activities such as agriculture and deforestation, and other environmental and global changes. As an example, the process of drilling oil and natural gas can create toxic by-products such as hydrogen sulfide, methane, benzene, toluene and xylenes, nitrogen oxides, toxic metals, and sulfur dioxide. These chemicals and waste products can contaminate air, soil, and water. Today, carbon dioxide, a greenhouse gas, is the main pollutant that is warming Earth. The main sources of carbon dioxide are power plants and other human activities that involve the burning of fossil fuels such as gasoline and natural gas and coal combustion. When our water and air are polluted, it is not only devastating to the environment but also to human health. Therefore, sustainable cost-effective development of removal techniques to alleviate such environmental pollution has been a challenging and demanding task for engineers, scientists, and researchers. Further there are various federal and state government and environmental protection agencies that strictly enforce regulations on minimizing pollutants from gaseous and liquid discharge effluent streams. Hence, it is important to take appropriate measures to make sure that all effluents streams are being treated properly before being discharged into the environment or recycled.

Air pollutants are mostly gaseous pollutants and odors. Some of the gaseous pollutants produced during industrial and human activities are sulfur dioxide (SO_2); sulfur trioxide (SO_3); oxides of nitrogen (NO_x); carbon monoxide (CO); hydrocarbons; hydrogen sulfide (H_2S); halogen; and greenhouse gases mainly composed of carbon dioxide (CO_2), methane, chlorinated hydrocarbon, and nitrogen dioxide (NO_2). Also, the quality of water resources is deteriorating day by day due to the continuous addition of undesirable chemicals/contaminants into them. These chemicals include both inorganic and organic pollutants, which contaminate water resources. Among inorganic water pollutants, heavy metal ions such as mercury (Hg^{2+}), lead (Pb^{2+}), copper (Cu^{2+}), cadmium (Cd^{2+}), zinc (Zn^{2+}), chromium (Cr^6), and nickel (Ni^{2+}) are the most hazardous pollutants found in industrial effluents. Various types of organic pollutants, including pesticides, fertilizers, hydrocarbons, phenols, detergents, oils, grease, dyes, and pharmaceuticals, have also been found in different water bodies.

A number of treatment technologies, such as reverse osmosis, filtration, adsorption, chemical precipitation, coagulation, foam flotation, solvent extraction, electroplating, oxidation/reduction, ion exchange, activated sludge, aerobic and anaerobic treatment, and membrane filtration have been used to remove those potential pollutants/contaminants from gaseous and liquid effluents. Among these separation techniques, adsorption is considered to be a superior technique because of its simple design, universal nature, and ease of operation, regeneration, and inexpensiveness. *Adsorption* may be defined as selective concentration or retention of one or more components of a mixture on a solid surface or at the solid–fluid interface. The solid that adsorbs a component/pollutant is called the *adsorbent*, and the pollutant component adsorbed/accumulated on the solid surface is called the *adsorbate*.

Numerous works have been reported within the last 2 to 3 decades with the primary goal being the investigation of removal of different pollutants (either in gas or liquid medium) using *solid adsorbents*. Commercially, activated carbons (ACs) are widely used and they are highly effective adsorbents for the removal of organic/inorganic pollutants from both gaseous and liquid effluents. However, activated carbons are expensive and the regeneration operation is not easy. Therefore, current research is focused on finding cost-effective alternatives. In this research direction, advancement has been made on the utilization of various nonconventional, alternative, cost-effective adsorbents derived from natural materials, industrial solid wastes, agricultural solid wastes, and biosorbents that not only remove pollutants from effluents but also provide a solution for waste disposal problems.

In view of the importance of air and water quality and the environmental aspect, it is considered worthwhile to address the state of the art of adsorption for the removal of gaseous and water pollutants using various sustainable cost-effective alternative adsorbents. The nature and types of adsorbents are the main controlling parameters for effectiveness of the adsorption process. With these objectives, this book was written in order to provide various research results and compilation, and up-to-date development on the current state of knowledge on various industrial and agricultural solid waste based adsorbents and their applications in the broad field of separation and purification of air, gaseous, and water pollutants. The synthesis, characteristics of adsorbents based on industrial and agricultural solid, and their adsorptive effectiveness under various physicochemical process parameters will be discussed. Basically, this book will give a comprehensive understanding and advancement and application of various nonconventional alternative solid waste-based adsorbents in the reduction of potential pollutants (inorganics/organics) from gaseous and liquid effluents.

There are a total of three sections containing 13 chapters written by a significant number of expert authors from around the world. Chapter 1 reviews the occurrences and utilization of various industrial, agricultural, construction, and municipal solid wastes as adsorbents in the removal of gaseous and air pollutants. Greenhouse gas and flue gas separation technologies by the sorbents made from solid wastes are highlighted here. Chapter 2 discusses the impact of solid-waste adsorbents as a cost-effective biofilter media on the performance and the removal efficiency of volatile organic compounds (VOCs) for different biofilter designs. Chapter 3 presents the CO₂ capture technology and role of adsorption in the removal of CO₂ from industrial flue gas. Chapter 4 notes that calcium-based industrial solid wastes have been used to capture CO₂ in the calcium looping process. This chapter reviews the latest progress of research on industrial solid wastes as potential candidates for CO₂ capture in the calcium looping process. Chapter 5 deals with the current progress of various agricultural solid waste-based adsorbents in water and wastewater treatment. Biosorption of heavy metals by agricultural lignocellulosic waste has proven to be an efficient, low cost, and environmentally viable separation method. Therefore, Chapter 6 reviews the biosorption of heavy metals by natural or chemically and thermally modified rice husk under different physicochemical process conditions. Red mud is a heterogeneous mineral that emerges as a by-product after the caustic leaching of bauxite to produce alumina via the Bayer process. In recent years, a lot of research has been done to utilize red mud for environmentally benign applications such as gas cleaning and wastewater treatment. Therefore, Chapter 7 reviews varying innovative applications of red mud as an adsorbent for wastewater and gas treatment. Chapter 8 presents the experimental results on the adsorptive removal of lead (Pb²⁺) from its aqueous solution by cost-effective industrial solid wastes (dolomite). A detailed comparative critical discussion on application of various industrial solid wastes such as blast furnace slag, sludge, flue dust, alumina

industry waste, paper industry waste, fertilizer industry waste, and other solid wastes in the removal of aqueous phase heavy metal ions and air pollutants is presented in Chapter 9. Chapter 10 reviews various agricultural-based solid wastes in aqueous phase copper (Cu^{2+}) metal ion removal. Chapter 11 presents the synthesis methods and characterization of emerging mesoporous adsorbents and their various challenges and opportunities. Chapter 12 presents the synthesis and characterization of various biochars derived from golden shower pod (GSB), coconut shell (CCB), and orange peel (OPB) and finally testing their effectiveness in the removal of methylene green (MG5) dye by adsorption. Chapter 13 discusses activated carbon and various agricultural solid wastes-based activated carbon in the removal of BTEX (benzene, toluene, ethylbenzene, and xylene) from aqueous solutions under various process conditions.

This book is useful for practicing engineers, scientists, researchers, academics, and undergraduate and postgraduate students interested in this specific area.



Taylor & Francis

Taylor & Francis Group

<http://taylorandfrancis.com>

Acknowledgments

I would like to take this opportunity to express my sincere gratitude to all the contributing authors for their great endeavors and their help in peer-reviewing all the chapters. I also wish to thank all reviewers, namely, Professor Sumathi Sethupathi of Universiti Tunku Abdul Rahman, Malaysia; Professor Amalesh Sirkar of Haldia Institute of Technology, India; Professor B. C. Meikap of Indian Institute of Technology, Kharagpur, India; Professor Yingjie Li of Shandong University, China; Professor Suryadi Ismadji of Widya Mandala Surabaya Catholic University, Indonesia; Dr. Anteneh Mesfin Yeneneh of Curtin University, Australia; Professor Faisal Anwar of Curtin University, Australia, Professor Raj Kishore Patel of National Institute of Technology, Rourkela, India; Professor Gopinath Halder of National Institute of Technology, Durgapur, India; Professor Mohd Raftullah of Universiti Sains Malaysia; Professor Shariff Che Ibrahim of Universiti Teknologi MARA, Malaysia; and Dr. Hai Nguyen Tran of Chung Yuan Christian University, Taiwan.

My special thanks to Professor Ha Ming Ang of the Chemical Engineering Department of Curtin University, Australia, for his continuous support in completion of this book.

I wish to acknowledge Dr. Gagandeep Singh of CRC Press/Taylor & Francis Group for his initial book write-up invitation and prompt responses to all my queries. I also thank all other staff of CRC Press, particularly Mouli Sharma, for their help in all other editorial work during final manuscript submission. Finally, I would like to thank my wife, Kabita, and son, Anindya, for their patience and support in completing the book.

Tushar Kanti Sen



Taylor & Francis

Taylor & Francis Group

<http://taylorandfrancis.com>

Editor



Dr. Tushar Kanti Sen is a full-time associate professor in the Department of Chemical Engineering at Curtin University, Perth, Australia. Prior to joining Curtin, he worked at Universiti Teknologi PETRONAS (UTP), Malaysia, and also with National Institute of Technology, Rourkela, India. Sen obtained his B.Sc. (Hons.) B.Tech in chemical engineering from the University of Calcutta, India, and master's of chemical engineering from Jadavpur University, Kolkata, India. He obtained his Ph.D. in chemical engineering from the Indian Institute of Technology

(IIT), Bombay, and Mumbai, India. He has more than 25 years of teaching and research experience in chemical engineering. Sen is continuously engaged in undergraduate and postgraduate teaching and learning, supervision, and research activities. Sen has an excellent track record in the broad field of water research, wastewater treatment, adsorption at solid-liquid interface, anaerobic digestion and dewatering of wastewater sludge, rheology of colloidal slurry/sludge, colloids in groundwater contamination, and separation processes. He has made significant contributions in the field of adsorption in water treatment, anaerobic digestion processes, and colloid and interface area. He has edited two research books: one on physical, chemical, and biological treatment processes for water and wastewater, and another on clay minerals. Sen is an associate editor of the journal *Adsorption Science & Technology*. He has developed many novel cost-effective agricultural solid wastes-based adsorbents and biomass-based activated carbons, magnetic nanocomposites, and their effective utilization in industrial wastewater treatment. Further, Sen and his research group have also developed a novel sludge pretreatment method that is a combination of microwave and ultrasonication. Compared to all other pretreatment methods studied (ultrasonication, microwave), this novel method has given the most promising results in terms of methane production, solids reduction, and improved dewaterability. Currently, Sen and his research group are working on the rheological behaviors of wastewater treatment plant sludge and its implication on wastewater treatment process parameters optimization including conditioning polymer dose optimization.

Sen has published more than 145 research papers including books and book chapters. Sen has guided eight Ph.Ds., one M.Phil., and many master's candidates. Currently, five Ph.D. students and many postgraduate/undergraduate students are working under him. He is a recipient of the HORN Scholarship (2012, 2014) Japan; the Ganga Ram Memorial Prize (Gold Medal) (2009, 2011), instituted by the Institution of Engineers (India), the Certificate of Merit in 2008 by the Institution of Engineers (India), the Shah-Schulman award, instituted by Indian Institute of Chemical Engineers (IICChE), India; and an Australian Academy of Science scientific visit Award (2011) for his outstanding contribution in research. He is also the recipient of the University Gold Medal from Jadavpur University, Kolkata, India; a Visiting Fellowship at the Australian National University, Australia; a Visiting Professorship at the University of Hyogo, Himeji, Japan; a Senior Research Fellowship from the Ministry of Human Resource Development (MHRD), New Delhi, India; and a Travel award from the All India Council for Technical Education (AICTE), New Delhi. He is also associated with many professional activities such as a regular reviewer of many international journals, journal editorial board members, and session chair of international conferences. Sen also

has life memberships in many professional bodies including the Institution of Chemical Engineers (IChemE; United Kingdom), Adsorption Society, Australian Association of Engineering Education, Indian Institute of Chemical Engineers, Institution of Engineers (India), Indian Institute of Public Health Engineers, Computer Society of India, and Indian Institute of Metals. Sen has given many invited talks on adsorption, water, and wastewater treatment processes at many universities and international conferences.

Contributors

Syed Zaghum Abbas

School of Industrial Technology
Universiti Sains Malaysia
Penang, Malaysia

Akil Ahmad

Department of Chemical Engineering
University of KwaZulu-Natal
Durban, South Africa

Benjamin Alliss

Department of Chemical Engineering
Curtin University
Perth, Australia

Hirra Anjum

Chemical Engineering Department
Universiti Teknologi PETRONAS
Perak, Malaysia

Appusami Arunagiri

Department of Chemical Engineering
National Institute of Technology
Tiruchirappalli, India

Soumya Banerjee

Department of Chemical Engineering
National Institute of Technology, Durgapur
Durgapur, India

Mohammed J. K. Bashir

Faculty of Engineering and Green
Technology
Universiti Tunku Abdul Rahman
Perak, Malaysia

Huan-Ping Chao

Department of Environmental Engineering
Chung Yuan Christian University
Taoyuan City, Taiwan

Fareeda Chemat

Chemical Engineering Department
Universiti Teknologi PETRONAS
Perak, Malaysia

Lau Lee Chung

Faculty of Engineering and Green
Technology
Universiti Tunku Abdul Rahman
Perak, Malaysia

Dipa Das

Department of Chemical Engineering
Indian Institute of Technology Kharagpur
Kharagpur, India

and

Department of Chemical Engineering
Indira Gandhi Institute of Technology
Sarang, India

Lunbo Duan

School of Energy and Environment
Southeast University
Nanjing, China

Nirmala Gnanasundaram

Department of Chemical Engineering
Vellore Institute of Technology University
Vellore, India

Gopinath Halder

Department of Chemical Engineering
National Institute of Technology, Durgapur
Durgapur, India

Eugene Hong

Department of Chemical Engineering
Curtin University
Perth, Australia

Suryadi Ismadji

Department of Chemical Engineering
Widya Mandala Surabaya Catholic
University
Surabaya, Indonesia

Akshay Jain

Centre of Innovation (Environment
and Water Technology)
Ngee Ann Polytechnic
Clementi, Singapore

Yi Hsu Ju

Department of Chemical Engineering
National Taiwan University of Science
and Technology
Taipei, Taiwan

Yingjie Li

School of Energy and Power Engineering
Shandong University
Jinan, China

David Lokhat

Department of Chemical Engineering
University of KwaZulu-Natal
Durban, South Africa

Chunmei Lu

School of Energy and Power Engineering
Shandong University
Jinan, China

Xiaotong Ma

School of Energy and Power Engineering
Shandong University
Jinan, China

B. C. Meikap

Department of Chemical Engineering
Indian Institute of Technology Kharagpur
Kharagpur, India

and

Department of Chemical Engineering
School of Engineering
University of Kwazulu-Natal
Durban, South Africa

Abdul Rahman Mohamed

School of Chemical Engineering
Universiti Sains Malaysia
Pulau Pinang, Malaysia

Raj Kishore Patel

Department of Chemistry
National Institute of Technology, Rourkela
Rourkela, India

Gayatree Patra

Department of Chemical Engineering
Indian Institute of Technology Kharagpur
Kharagpur, India

Mohd Rafatullah

School of Industrial Technology
Universiti Sains Malaysia
Penang, Malaysia

Manoj Kumar Sahu

Department of Chemistry
National Institute of Technology, Rourkela
Rourkela, India

Tushar Kanti Sen

Department of Chemical Engineering
Curtin University
Perth, Australia

Sumathi Sethupathi

Faculty of Engineering and Green
Technology
Universiti Tunku Abdul Rahman
Perak, Malaysia

Felycia Edi Soetaredjo

Department of Chemical Engineering
Widya Mandala Surabaya Catholic
University
Surabaya, Indonesia

Madapusi P. Srinivasan

School of Engineering
RMIT University
Melbourne, Australia

Kubilay Tekin

Occupational Health and Safety
Karabuk University
Karabuk, Turkey

Murugesan Thanabalan

Chemical Engineering Department
Universiti Teknologi PETRONAS
Perak, Malaysia

Hai Nguyen Tran

Department of Environmental Engineering
and
Department of Civil Engineering
Chung Yuan Christian University
Taoyuan City, Taiwan

Hari Vuthaluru

Department of Chemical Engineering
Curtin University
Perth, Australia

Ya-Fen Wang

Department of Environmental Engineering
Chung Yuan Christian University
Taoyuan City, Taiwan

Anteneh Mesfin Yeneneh

Department of Chemical Engineering
Curtin University
Perth, Australia

Sheng-Jie You

Department of Environmental Engineering
Chung Yuan Christian University
Taoyuan City, Taiwan

Muhammad Younas

Faculty of Engineering and Green
Technology
Universiti Tunku Abdul Rahman
Perak, Malaysia

Hussein Znad

Department of Chemical Engineering
Curtin University
Perth, Australia



Taylor & Francis

Taylor & Francis Group

<http://taylorandfrancis.com>

Section I

Industrial and Agricultural Solid Wastes-Based Adsorbents in Gas/Air Purification



Taylor & Francis

Taylor & Francis Group

<http://taylorandfrancis.com>

1

Gaseous Pollutant Removal Using Solid Wastes Adsorbents

Sumathi Sethupathi, Lau Lee Chung, Muhammad Younas,
Abdul Rahman Mohamed, and Mohammed J. K. Bashir

CONTENTS

1.1	Introduction	3
1.2	Industrial Waste	4
1.2.1	Types of Industrial Waste	5
1.2.2	Synthesis of Industrial Waste Adsorbents	6
1.2.3	Utilization of Industrial Waste.....	7
1.3	Agricultural Waste	8
1.3.1	Synthesis of Agricultural Waste Adsorbents.....	8
1.3.2	Utilization of Agricultural Waste	10
1.4	Other Types of Waste	11
1.4.1	Utilization of Other Waste Adsorbents for Gas Adsorption	13
1.5	Pros and Cons of Separation Technologies and Future Developments.....	14
	References.....	15

1.1 Introduction

Gaseous pollutants are created from natural and anthropogenic activities. Natural activities are, for example, volcanic eruptions, forest fires, plant and animal decomposition, and ocean spray, whereas anthropogenic activities are mainly from human-induced activities such as power generation, commercial use, industrial combustion, and transportation. The pollutants can be divided into two major categories: primary and secondary. Primary air pollutants are the ones directly emitted into the atmosphere from the sources (such as coal-burning plants). Secondary air pollutants are formed as a result of reactions between primary pollutants and other elements in the atmosphere, such as ozone. One of the most important characteristics of gaseous pollutants is their transboundary nature whereby they can effortlessly transport and affect areas far away from their points of origin.

The major gaseous pollutants include carbon monoxide (CO), carbon dioxide (CO₂), nitrogen oxides (NO_x), sulfur dioxide (SO₂), ammonia (NH₃), unburned hydrocarbon (UHC), and volatile organic compounds (VOCs), as well as ozone (O₃). CO₂ is produced as a waste product of human and animal respiration. However, when it is generated in large quantity it becomes a pollutant that reduces the oxygen concentration in the air. The combustion of carbon-based fuels also produces CO₂ and incomplete combustion leads to the production of CO. CO is a colorless, poisonous, odorless, and tasteless gas. Generally, it occurs when a fuel is burned under a limited supply of oxygen. SO₂ is a colorless and corrosive gas with

a pungent, suffocating odor. Fossil fuel combustion accounts for almost all anthropogenic sulfur emissions. Ammonia is a colorless, pungent, hazardous caustic gas composed of nitrogen and hydrogen. Agriculture waste from vegetation, life stock farming, and animal waste account for the biggest percentage of total ammonia emissions. VOCs are defined as organic compounds that easily evaporate and enter the atmosphere. VOCs may include a wide range of organic air pollutants, from pure hydrocarbons to partially oxidized hydrocarbons to organic compounds containing chlorine, sulfur, or nitrogen (Jeremy, 2002).

These gaseous pollutants affect the earth, buildings, water, and air. Moreover, secondary pollutants consequently result in acid rain, fog, smog, and global warming, which deteriorate vegetation, forests, and even human health. Human beings may be affected in the form of asthma, cancer, and heart and lung diseases. It was reported that thousands of people in the world die each year due to air pollution. Even animals are affected vulnerable. Moreover, it was also reported that these gases also cause damage to plant tissue, and some compounds from photochemical reactions produce a burn on the leaves of many vegetables (Foster and Kumar, 2011; Najjar, 2011; Pope et al., 2002).

Therefore, in order to reduce the harmful effects of these gaseous pollutants, much research work has been done using various technologies, namely, combined cycles, fuel cells, fluidized bed combustion, renewable energy, adsorption, nuclear power, energy conservation, energy storage, oxy-fuel combustion, and chemical looping combustion (Najjar, 2011).

The World Bank has estimated that cities currently generate about 1.3 billion tonnes of solid waste per year as of 2013, and with the current urbanization trends the figure is expected to grow further to about 2.2 billion tonnes per year by 2025, which is an increase of 70% (Daniel and Perinaz, 2012). Thus, managing waste will become more expensive. The best way to solve the problem is either change the way we use or reuse the waste. Recently, many initiatives have been made to reutilize solid waste. One such initiative is converting the solid waste into value-added product. Sorbent is a type of product made from solid waste and the successful usage of these sorbents for gas separation processes has been reported. Moreover, the development of inexpensive and high capacity sorbents has been getting extensive interest from various researchers for the removal of toxic substances from gases such as sulfur oxides (SO_2), nitrogen oxides (NO_x , NO , and NO_2), carbon dioxide (CO_2), and hydrogen sulfide (H_2S). The effectiveness of adsorbents in removing pollutants has been recognized by many other applications because of their high adsorption capacity, ease of operation, and simplicity of design (Hayashi et al., 2005). Furthermore, there is a need to produce adsorbents from alternative materials that are renewable, cheap, and readily available as commercial coal-based adsorbents, which are relatively expensive (Attia et al., 2008). For this reason, research interest in the production of adsorbents from cheaper and renewable precursors is intensive.

In this chapter, detailed and efficacious work on the utilization of industrial, agricultural, construction, and municipal solid wastes as sorbents for gas separation processes is discussed. Greenhouse gas and flue gas separation technologies by the sorbents made from solid wastes are highlighted. The pros and cons of the separation technologies of solid wastes in gas separation are reviewed.

1.2 Industrial Waste

Rapid population growth requires the support of the supply chain of goods for daily activities. In order to meet this demand, large-scale production of these goods are necessary.

Therefore, various industries have been well developed to fulfill the needs of society. Unfortunately, industrial activities to extract and process raw materials into useful final products produce millions of tons of industrial solid wastes daily. These wastes pose a great threat to the environment and must be disposed of properly so that environmental deterioration will not occur. Luckily, research studies showed these solid wastes can be converted into something useful for environmental protection, especially in gas separation. Industrial wastes that are suitable to be converted into adsorbents generally come from agriculture, power plants, and mining. Due to their carbonaceous nature, almost every type of agriculture waste can be converted in adsorbents. Therefore, they are categorized into another section for detailed discussion. In this section, three major industrial solid wastes used for gas cleaning processes—fly ash from coal-fired power plants, slag from iron and steel mills, and red mud from aluminum industries—are discussed (Kaithwas et al., 2012).

1.2.1 Types of Industrial Waste

A coal-fired power plant generates a large amount of solid waste in the power generation process. In a combustion chamber, most carbon from coal is burned, but inorganic and noncombustible material is released as coal fly ash. Fly ash is fine particles captured from flue gas using an electrostatic precipitator before the flue gas is emitted into the atmosphere through a chimney. The diameters of the particles range between 1 and 150 μm (Kaithwas et al., 2012). The composition of fly ash is highly dependent on the source of the coal. The main components are silicon dioxide (SiO_2) and calcium oxide (CaO) (Kaithwas et al., 2012). They possess dielectric and pozzolanic properties, and therefore can be used for various applications in soil amelioration, construction, the ceramic industry, and environmental protection (Yao et al., 2015). The amount of fly ash produced is about 500 million tons per year and it is projected to increase further. Therefore, proper handling or disposal of this solid waste has become an important issue (Hui and Chao, 2006).

In the manufacturing process in a steel mill, slags are produced. In 2009, 12.2 billion tons of steel was produced globally. An estimated 0.2 tons of steel slag is produced from every ton of steel; the steel slag production was about 2.44 billion tons (Yu and Wang, 2011). The primary composition of steel slag is calcium and magnesium silicates, but it will vary depending on source and particle size (Das et al., 2007). In general, smaller particle size slag contains more CaO and SiO_2 and less Fe_2O_3 (Pan et al., 2013; Zhang et al., 2011). In addition, slag also contains several types of heavy metals such as As, Cd, and Hg that will cause severe environmental pollution if they are not handled or disposed properly (Das et al., 2007). Currently, slags are utilized in road building, cement and concrete production, phosphate fertilizer production, and iron recycling (Yi et al., 2012; Yu and Wang, 2011). The utilization of steel slags will slow the exploitation of unmined resources and enhance environmental protection.

Additionally, in aluminum industries, alumina must be first extracted from bauxite, a common aluminum ore using the Bayer process, before it can be refined into aluminum metal. During the process, an alkaline bauxite residue or red mud is produced, as sodium hydroxide is used to dissolve the ore. Typically, about 1.5 tons of red mud is produced to obtain 1 ton of alumina. Due to the huge demand on aluminum, more than 66 million tons of red mud was produced annually (Agrawal et al., 2004; Yang and Xiao, 2008). Therefore, environmental deterioration will occur if the large amount of high alkalinity waste red mud is not handled appropriately. The main components of red mud are Fe_2O_3 , Al_2O_3 , and SiO_2 . The actual composition will vary depending on the type and bauxite quality used in the Bayer process (Sushil and Batra, 2008). Fortunately, red mud's high Fe_2O_3 content enables it to be a cheap and efficient adsorbent for the removal of heavy metals such as

lead, chromium, and arsenic from wastewaters (Altundogan et al., 2002). Apart from that, red mud can be used in several applications such as acid amender, building materials, ceramics, and tiles (Yadav et al., 2010).

1.2.2 Synthesis of Industrial Waste Adsorbents

Fly ash can be used to synthesize adsorbent. Nevertheless, fly ash is treated as a support rather than catalyst itself. Fly ash can be a good catalyst support because it has a high surface area, attributed to the unburned carbon content remained in the particles. Therefore, it can be further activated by increasing its surface area. For instance, activation of fly ash can be done using steam at 900°C and then acid nitric treatment at 70°C for 1 hour (Lu and Do, 1991). Steam activation was found to develop a porous structure for fly ash, which increases the surface area up to 900 m²/g. A high surface area is the key property for a high adsorption capacity of an adsorbent (Izquierdo and Rubio, 2008). After that, fly ash can be impregnated with various types of metals such as Cu, Fe, and Ni by using metal nitrates. Subsequent calcination at about 300°C is necessary to decompose the nitrate added (Xuan et al., 2003). Apart from that, impregnating fly ash with amine is a common method to synthesize adsorbent for CO₂ adsorption. Amine solutions such as monoethanolamine, diethanolamine, and methyldiethanolamine can be used to perform surface modification to enhance fly ash's affinity and selectivity toward CO₂ (Gray et al., 2004). The preparation step was just a simple soaking of fly ash in amine solution for one hour in ambient temperature and subsequently dried in an oven.

A simple approach to utilize red mud was reported by Yadav et al. (2010). Dried red mud was grinded and sieved into three fractions with different densities (1.5, 1.8, and 2.2 g cm⁻³). Without any modification, the red mud was used to remove CO₂. In addition, in the work of Sahu et al. (2011), no modification of red mud was necessary for the removal of hydrogen sulfide. In general, red mud in the form of dried clay can be modified using various types of chemicals that are suitable for pollutant gas removal. Chemical impregnation was typically performed by soaking or stirring the adsorbent in the chemical precursors. Subsequently, calcination was used to enhance chemical distribution of the adsorbent surface. For instance, acid-treated (Sushil and Batra, 2012) and CuO (Hu et al., 2016) impregnated red mud were reported to remove CO effectively. Acid-treated red mud was prepared by digesting red mud with 37% hydrochloric acid at 80°C. After washing and drying, the samples were calcined in static air at 500°C for 2 hours (Sushil and Batra, 2012). On the other hand, acid treatment was also demonstrated for CuO-impregnated red mud adsorbent. After acid treatment, red mud was added and stirred in a copper nitrate solution. After stirring for 1 hour, the washed and dried adsorbent was calcined at 200°C for 2 hours (Hu et al., 2016).

Slag's chemical properties are fit for usage as an adsorbent. However, useful chemicals can be leached from slag and then used for CO₂ sequestration. The leaching process was reported using chemicals such as HNO₃ (Doucet, 2010), acetic acid (Eloneva et al., 2008), and NH₄Cl (Sun et al., 2011). Doucet (2010) reported slag leaching process using 0.5 M HNO₃ at 22°C for an hour. The liquid-to-solid ratio was 10 kg/kg. The main extracted metal was calcium hydroxide, which can be further utilized for CO₂ adsorption. Apart from that, acetic acid was also used to dissolve slag (Eloneva et al., 2008) in an aqueous solution of 20% acetic acid at 70°C. Continuous bubbling of N₂ at 1 L/min was employed for 2 hours. The solution was then filtered to obtain calcium acetate salt that can be used for carbonation. On the other hand, NH₄Cl can also be used in the slag leaching process (Sun et al., 2011). The leaching conditions were optimum at the solid-to-liquid ratio of 10, 2M NH₄Cl, 60°C, and 120 min duration. NH₄Cl was found to react with lime in the slag to form NH₄OH that can also be used for carbonation.

1.2.3 Utilization of Industrial Waste

Fly ash, slag, and red mud have been widely used as adsorbents for pollutant gas cleaning. Recently, research on the use of fly ash as an adsorbent for pollutant gas cleaning for SO_2 (Izquierdo and Rubio, 2008), NO_x (Lu and Do, 1991; Xuan et al., 2003), and CO_2 (Arenillas et al., 2005; Gray et al., 2004; Mercedes et al., 2008; Sarmah et al., 2013) removal has gained increasing attention. An SO_2 adsorption test using a fly ash-based adsorbent indicated an adsorption capacity of over 60 mg SO_2 /g adsorbent. The adsorption capacity was enhanced by the presence of calcium and iron oxide (Izquierdo and Rubio, 2008). Fly ash catalyst was also employed in selective catalytic reduction (SCR) of NO_x . In fact, both SO_2 and NO_x were pollutant gases emitted during coal combustion in a power plant. Therefore, it is reasonable to utilize fly ash from the same industry to remove SO_2 and NO_x from the flue gas. In SCR of NO_x , an oxidizing agent such as O_2 or NH_3 must be supplied in order to convert NO_x into a harmless compound such as N_2 . NO conversion above 90% was achieved (Xuan et al., 2003). CO_2 is a pollutant more stable than SO_2 and NO_x . Therefore, it is more difficult to remove CO_2 comparatively. Despite that, using fly ash to remove CO_2 was achieved by several researchers (Arenillas et al., 2005; Gray et al., 2004; Mercedes et al., 2008). Study showed that amine-based fly ash adsorbent was cheap and efficient for CO_2 adsorption compared to other materials (Sarmah et al., 2013).

Steel slags also have been used in carbon capture and sequestration technology. Slag has been used in carbonation without any chemical modification (Yu and Wang, 2011). The carbonation reaction chemistry was reported by Bonenfant et al. (2009). CO_2 adsorption on slag surface was mainly on three types of metal oxides: basic, amphoteric, and acid oxides. Basic oxides (CaO , MgO), amphoteric (Al_2O_3 , Fe_2O_3), and acidic (SiO_2) oxides can adsorb CO_2 up to 0.25 kg CO_2 /kg of slag to form stable carbonate compounds. The affinity toward CO_2 was reported in the order basic oxides > amphoteric oxides > acidic oxides. On top of that, several studies also showed that similar CO_2 adsorption capacity between 0.21 and 0.23 kg CO_2 /kg of slag was obtained for chemical-treated slag-based adsorbent (Eloneva et al., 2008; Sun et al., 2011).

Likewise, alkaline red mud, which contains various metal oxides, is also suitable for pollutant gas removal. Research studies showed that red mud was successfully applied in removal of CO_2 (Yadav et al., 2010), CO (Hu et al., 2016; Sushil and Batra, 2012) and H_2S (Sahu et al., 2011). Aluminum industries itself is energy intensive and produces more than 590 million tons of carbon dioxide annually (Tsai et al., 2013). The increasing emission of CO_2 worsens the impact from global warming. Therefore, there is an urgent need to reduce CO_2 emission from aluminum industries. Coincidentally, the waste red mud can be used to capture CO_2 easily. The metal oxides and alkaline nature of red mud are important characteristics for CO_2 adsorbent. By keeping this red mud under carbon dioxide atmosphere, a high carbonation capacity of 5.3 g CO_2 /100 g red mud was reported for red mud fraction with 1.8 g cm^{-3} . The red mud fraction contains a higher mineral phase amount of chautalite and cancrinite that was responsible for high carbonization capacity (Yadav et al., 2010). CO as a toxic component of exhaust gas can be removed using catalytic oxidation. Research studies showed that metal oxides were a good catalytic to serve this purpose, even though they are less reactive than precious metals such as Au, Pt, and Pd. Red mud, with a large iron oxide content, is able to be chemically modified to enhance its catalytic oxidation activity. For instance, 90% CO conversion was successfully achieved using acid-treated red mud (Sushil and Batra, 2012). On top of that, acid-treated red mud improved by CuO impregnation achieved complete removal of CO for more than 12 hours (Hu et al., 2016). On the other hand, direct utilization of red mud to remove hydrogen sulfide at

ambient condition was demonstrated by Sahu et al. (2011). Suspension of red mud in aqueous solution was found to successfully adsorb the hydrogen sulfide bubbled through the solution. This was attributed to the high iron oxide content of red mud. The reaction products were found to be FeS_2 , FeS , S , and sulfide minerals (Sahu et al., 2011).

1.3 Agricultural Waste

Agricultural waste is defined as the residues from growing and processing of raw agricultural products such as vegetables, fruits, meat, dairy products, poultry, and crops. Agricultural wastes can be in the form of a solid, liquid, or slurry, depending on the nature of agricultural activities in a farm or agricultural field, and can be both natural (organic) and nonnatural wastes. Agricultural residues, refuse, and wastes constitute a significant proportion of worldwide agricultural productivity, and these wastes can account for over 30% of worldwide agricultural productivity (Ajith, 2009). According to the U.S. Department of Energy, under baseline assumptions, there are currently about 200 million dry tons of primary crop residues generated in the United States alone. Moreover, it is estimated that by 2030, the total primary residue will be about 320 million dry tons, with 85% of this quantity composed of corn stover (U.S. Department of Energy, 2011). Therefore, there is a huge necessity in reutilizing this solid waste. It is known that abundant agricultural wastes pose serious issues to both the environment and society. The huge volume of agricultural waste generated is increasingly enormous due to the high demand of fresh and processed agricultural products. Some of them have little or no economic value. There are two common practices of agricultural waste disposal—dumping in the landfill and open burning—that will lead to the air pollution problems. Hence, conversion of agricultural waste into adsorbent will lead to a double purpose: (1) unwanted agricultural waste is converted to value-added adsorbents and (2) decreasing the agricultural waste disposal. The availability of agricultural wastes at a low price became a major advantage of using raw material for the gas separation processes.

There are many types of agricultural wastes. Some examples are palm shell (Sumathi et al., 2010), rice husk (Lau et al., 2010), coconut shell (Guo et al., 2015), palm stones (Lua and Guo, 2000), hay (Kazmierczak-Razna et al., 2016), olive stones (Ghouma et al., 2015), wood (Bashkova and Bandosz, 2009), corn cobs (Kazmierczak et al., 2013), and date pits (Belhachemi et al., 2014), all of which can be used as adsorbents for gas pollutants.

1.3.1 Synthesis of Agricultural Waste Adsorbents

There are two main steps in the preparation and manufacturing of adsorbents: first, the carbonization of the raw material in the absence of oxygen to break down the cross-linkage between carbon atoms, and then activation of the carbonized product, for further pore development (Ioannidou and Zabaniotou, 2007). The term *carbonization* means to convert the carbonaceous material into elemental carbon at a high temperature (400°C–850°C) in an inert atmosphere. This process enriches carbon content and develops initial porosity in the char produced.

The second step is the activation process to increase the char porosity and discharge the tar clogging pores (Turmuzi et al., 2004). There are two main activation processes, which are physical activation and chemical activation. Physical activation involves activation of the resulting char at elevated temperature in the presence of suitable oxidizing gases such as CO_2 , steam, air, or their mixtures. The reaction between the carbon atom and oxidizing

gas gives rise to the pore creation and enlarge the existing pores. Aworn et al. (2008) found that the optimum condition for activated carbon production from agricultural wastes depended on the raw material itself, the activation temperature, the activating agent, and the amount of volatile matter in the materials.

The chemical activation process involves the impregnation of char with chemical agents as dehydrating agents and oxidants, such as potassium hydroxide (KOH), potassium carbonate (K_2CO_3), sodium hydroxide (NaOH), sodium carbonate (Na_2CO_3), zinc chloride ($ZnCl_2$), phosphoric acid (H_3PO_4), and sulfuric acid (H_2SO_4) (Rajgopal et al., 2006). Furthermore, the activated carbon's yield from chemical activation tends to be greater than physical activation since burn-off char is not required, as the pores are developed by dehydration and oxidation reactions of the chemicals (Acharya et al., 2009). Table 1.1 lists the preparation methods of several types of agricultural waste with their application for gas separation processes.

TABLE 1.1

Preparation Methods of Several Types of Agricultural Waste

Types of Agro Waste	Preparation Method	Source	Application	References
Palm kernel shell	Single step CO_2 activation	Local palm oil mill	–	Rashidi et al., 2012
	Physical activation using CO_2 gas	Local palm oil mill	SO_2 and NO_x removal	Sumathi et al., 2010
Rice husk	Single-step CO_2 activation	Local rice mill	–	Rashidi et al., 2012
	Impregnation with copper nitrate	Kilang Beras and Minyak Sin Guan Hup Sdn Bhd, Nibong Tebal, Malaysia	SO_2 and NO removal	Lau et al., 2010
Coconut shell	Physical activation process	Jibei activated carbon plant in Hebei province	SO_2 and NO removal	Guo et al., 2015
	One-step CO_2 activation	–	CO_2 removal	Ello et al., 2013
Palm stones	One-step CO_2 activation	Local palm oil mill	NO_2 removal	Lua and Guo, 2000
Hay	Physical activation ($T = 500^\circ C$, CO_2 flow rate of 0.250 L/min, for 15 min)	–	NO_2 and H_2S removal	Kazmierczak-Razna et al., 2016
Corn cobs	Physical activation ($T = 800^\circ C$, CO_2 flow rate of 0.250 L/min, for 30 min)	–	NO_2 removal	Kazmierczak et al., 2013
Cherry stones	Physical and chemical activation with CO_2 and KOH	–	NO_2 and H_2S removal	Nowicki et al., 2015
Coffee waste	Physical activation	Coffee industry	H_2S removal	Nowicki et al., 2014
Sargassum	Physical and chemical activation	–	NO removal	Li et al., 2015
Olive stones	Physical activation using water vapor at $750^\circ C$	Olive oil factories	NO_2 removal	Ghouma et al., 2015
Pine sawdust	CO_2 activation at $800^\circ C$ for 90 min	–	NO_2 removal	Nowicki and Pietrzak, 2010
Wood	Urea impregnation and heat treatment at $950^\circ C$	–	NO_2 removal	Bashkova and Bandosz, 2009
Date pits	Physical and chemical activation using CO_2 (CCO_2) and $ZnCl_2$ (CZn)	–	NO_2 removal	Belhachemi et al., 2014

1.3.2 Utilization of Agricultural Waste

Over the last few decades, utilization of activated carbon as an adsorbent has become increasingly more widespread, especially in environmental protection for removing SO_2 and NO_x gases. This is because activated carbon poses suitable surface characteristics like a large number of micropores, high surface area, and suitable pore size distribution. They are prepared from a different variety of carbonaceous precursors such as lignite, coal, peat, wood, coconut, palm shell, and industrial by-product (Davini, 1999; Guo and Lua, 1999, 2000; Li et al., 2001; Liu et al., 2003).

Activated carbon prepared from palm oil mill waste has been extensively studied (Guo and Chong, 2003; Guo and Lua, 1999, 2000, 2002). Oil palm shell (also known as endocarp) has been used as a precursor for the impregnation of activated carbon, since this material has high density, relatively high carbon content and low ash content. Various methods were applied during the preparation of such activated carbon, which include physical or thermal activation and with or without impregnation. The effect of activation temperature and holding time were investigated during the physical activation process. The activation temperature and holding time were found to have important influences on the BET (Brunauer–Emmett–Teller) surface areas of the activated carbon. The optimum conditions for CO_2 activation to obtain the maximum BET surface area were found to be at an activation temperature of 900°C and a holding time of 30 min. Under these conditions, the largest BET surface area for oil palm shell-activated carbon was about $1366 \text{ m}^2/\text{g}$. From the sorption test, the sorption capacity of oil palm shell-activated carbon was slightly higher than that of the commercial product (Microcarb). The sorption capacity was found to be linearly proportional to its BET surface area or textural characteristics. This was due to the neutral (or slightly acidic) surface organic functional groups of the oil palm shell activated carbons as detected by the Fourier transform infrared spectroscopy (Lua and Guo, 2001).

In a series of research work carried out by Davini (Davini, 1999, 2001, 2002, 2003a, 2003b), the sorption of SO_2 was studied using activated carbon prepared from low ash petroleum pitches, oil-fired fly ash particulates, polyacrylonitrile textile by-products, and chars. His work focused on the sorption capacity of SO_2 using different types and amounts of support materials with various gas composition mixtures during the sorption processes. For activated carbon prepared from polyacrylonitrile textile by-product, it was shown that the amount of sorbed SO_2 was enhanced by the presence of nitrogen-based surface groups for the temperature range between 100°C and 160°C . The low ash petroleum pitches and chars, on the other hand, produced activated carbon with high surface area, high oxygen content, and surface sites with prevalent basic characteristics. The activated carbon produced from oil-fired fly ash particulates gave a surface area of about $1000 \text{ m}^2/\text{g}$. It also has basic surface characteristics that promote the sorption of SO_2 gas.

Activated carbon fiber has also been tested as a sorbent, since it has a uniform micropore structure and lower pressure drop in comparison to granular activated carbons. Li et al. (2001) studied the SO_2 sorption capacity of ammonia-activated carbon fibers. Nitrogen-containing functional groups were introduced onto the surface of activated carbon fibers by activating an ethylene tar pitch-based carbon fiber with ammonia solution. The activity of the activated carbon fibers for the conversion of SO_2 to H_2SO_4 in the presence of water vapor and O_2 was found to be significantly higher than that of other commercially activated carbon fibers studied. This was due to the presence of nitrogen-containing functional groups since they were able to enhance the sorption capacity of SO_2 and H_2O and the catalytic activity for oxidation of SO_2 to SO_3 .

1.4 Other Types of Waste

As the world moves toward urbanization, it has been reported that the amount of municipal solid waste (MSW) is growing even faster than the rate of urbanization. It was estimated that 3 billion residents of the world are generating about 1.2 kg per person per day (1.3 billion tonnes per year) of MSW. Additionally, by 2025 the numbers are projected to increase to about 1.42 kg/capita/day of MSW, amounting to about 2.2 billion tonnes per year (Daniel and Perinaz, 2012). The ideal solid waste management solution is to minimize the volume of waste at both the generation and disposal stages followed by preventive environmental management actions. Recycling of waste materials is another major productive area that can be employed for producing new products. MSW includes wastes generated from residential, commercial, industrial, institutional, construction, demolition, process, and municipal services. Nevertheless, this definition varies significantly among waste studies, and some sources are usually excluded, such as industrial, construction and demolition, and municipal services. General MSW is a collection of waste. Table 1.2 highlights eight major classifications of MSW generators.

TABLE 1.2

Source and Types of Solid Waste

Source	Typical Waste Generators	Types of Solid Wastes
Residential	Single and multifamily dwellings	Food wastes, paper, cardboard, plastics, textiles, leather, yard wastes, wood, glass, metals, ashes, special wastes (e.g., bulky items, consumer electronics, white goods, batteries, oil, tires), and household hazardous wastes
Industrial	Light and heavy manufacturing, fabrication, construction sites, power and chemical plants	Housekeeping wastes, packaging, food wastes, construction and demolition materials, hazardous wastes, ashes, special wastes
Commercial	Stores, hotels, restaurants, markets, office buildings	Paper, cardboard, plastics, wood, food wastes, glass, metals, special wastes, hazardous wastes
Institutional	Schools, hospitals, prisons, government centers	Same as commercial
Construction and demolition	New construction sites, road repair, renovation sites, demolition of buildings	Wood, steel, concrete, dirt
Municipal services	Street cleaning, landscaping, parks, beaches, other recreational areas, water and wastewater treatment plants	Street sweepings; landscape and tree trimmings; general wastes from parks, beaches, and other recreational areas; sludge
Process (manufacturing, etc.)	Heavy and light manufacturing, refineries, chemical plants, power plants, mineral extraction and processing	Industrial process wastes, scrap materials, off-specification products, slay, tailings
All of the above should be included as municipal solid waste		
Agriculture	Crops, orchards, vineyards, dairies, feedlots, farms	Spoiled food wastes, agricultural wastes, hazardous wastes (e.g., pesticides)

Source: Daniel, H., Laura, T., Keshav, V., 1999, *What a Waste: Solid Waste Management in Asia*, Urban Development Sector Unit East Asia and Pacific Region, The International Bank for Reconstruction and Development/The World Bank, Washington, D.C.

One MSW classification that was not covered earlier in this chapter is construction waste. Masonry materials and construction wastes such as brick, concrete, and tile constitute a significant part of construction and demolition debris. These bulky materials, if not reused or recycled, are mostly landfilled for disposal. Globally, it is estimated that around 10% to 30% of waste in landfills originate from the construction industry and demolition activities. The Malaysian construction industry is rapidly growing, benefiting the country's economy and providing essential infrastructure. However, this flourishing industry is responsible for one of the single largest waste streams in the country causing environmental pollution and degradation (Papargyropoulou et al., 2011). Only around 5% of total waste is recycled in Malaysia and the remaining 95% is disposed at the country's 112 landfills. According to the Ministry of Housing and Local Government (MHLG) Malaysia, the most landfills are at full capacity and operate to old standards with limited leachate and landfill gas control (Vasudevan, 2015). As a result, the construction industry ought to promote sustainable waste management practices guided by the 3Rs of reducing, reusing, and recycling. This will lead to economic benefits including cost reduction in material purchasing, saving transportation costs to landfills, saving in disposal costs at landfills, and revenue from selling waste-derived materials such as adsorbents (Bakshan et al., 2017). Recently, an increasing trend has been noticed in utilizing construction waste as adsorbent precursors. However, very little has been done in developing potential adsorbents for the separation of gases.

There are several types of construction wastes, which can be mainly classified into organic and inorganic materials. Construction waste materials include woody and plant materials, carpet, cardboard, concrete gravel, aggregate, asphaltic roofing, gypsum board, clay minerals, and asbestos. Most of these materials are benign, but some of the materials such as asbestos and asphalt roofing cause risks to human health and the environment. Turning these waste materials to valuable adsorbents for gas separation will have both environmental and economic benefits (Arabyarmohammadi et al., 2014; Kousaiti et al., 2011; Ottaviani and Venturi, 1996). To date, various kinds of construction waste materials have been reused. The prominent ones are Portland cement mixture, clay minerals, asbestos, and other organic materials (Ottaviani and Venturi, 1996; Ramakrishnan and Orlov, 2014). Most of these construction wastes are used for the adsorption of impurities in the liquid phase. Kousaiti et al. (2011) treated used waste asbestos under hydrothermal conditions applying different acids in various temperatures in order to produce an adsorbent material that is used to remove petroleum pollutants. Ottaviani and Venturi (1996) used asbestos fibers for the adsorption of organic molecules from solutions onto asbestos fibers. Arabyarmohammadi et al. (2014) investigated the removal of zinc (II) using clay-based demolition wastes as adsorbents for the treatment of aqueous solutions. These studies revealed that the adsorbent preparation techniques from construction waste helped in morphological degradation, which leads to and increase in the BET surface area and tuning porosity. Thus, it is believed that the morphology of these materials may be tuned for the separation of gases.

Moreover, an adsorbent preparation procedure commonly aims to improve functional groups, surface area, and porosity. Thus, preparation methods will strongly depend on the kind of materials being used. For noncarbonaceous materials such as ceramics, clay-based bricks, marble, fluorspar, lime, and hot metal steel slags, and mining wastes were basically washed with distilled water to remove surface impurities, dried, crushed, and sieved to the desired particle sizes. Some studies used chemicals to modify adsorbent characteristics. Cheng (2016) modified adsorbent from clay-based masonry materials using 10% NaCl. Zeolite is a very common adsorbent from MSW incinerator ash. MSW fly ash has

a significant content of SiO_2 and Al_2O_3 (15%–30%). Different types of zeolites have been synthesized by utilizing MSW fly ash by fusion or the hydrothermal process (Lam et al., 2010). Fan et al. (2008) even demonstrated that the properties of zeolite products made from MSW fly ash mainly depend on NaOH concentration, reaction temperature, and crystallization time. The development of zeolite is favorable under a lower NaOH-to-ash ratio and operating temperature. In another study carried out by Penilla et al. (2003), zeolite was also successfully synthesized by alkaline hydrothermal treatment of MSW bottom ash. Nevertheless, the use of bottom ash from MSW for zeolite synthesis is less common than using fly ash.

1.4.1 Utilization of Other Waste Adsorbents for Gas Adsorption

Only a few studies have been carried out to convert construction waste and other types of waste into gas adsorbents. Construction materials such as CaO or calcined rocks are mainly used as adsorbents for CO_2 capture in gasification processes. However, these materials suffer from various problems during long operation hours, predominately deactivation and particle attrition due to the weak mechanical strength. Most of these problems can be avoided largely using construction and demolition waste, which possess good activity and does not suffer from attrition problems associated with low mechanical strength. Moghtaderi et al. (2012) employed construction and demolition waste (CDW), calcined limestone (CL), silica sand, and hydrated Portland cement (HPC) for CO_2 adsorption in chemical looping gasification of biomass. The results confirmed CO_2 capture efficiencies as high as 56.4% and ranked the adsorbents as silica sand < CDW < HPC < CL. The durability, high mechanical strength, and abundant availability makes the CDW an attractive sorbent for CO_2 in chemical looping gasification of biomass. The age of the waste concrete materials is the important parameter to be considered in the gas adsorption, particularly in CO_2 adsorption. The surface chemistry and acidity of concrete material depends on the environmental conditions and the age of the concrete. Fresh concrete material possesses a considerable concentration of surface $\text{Ca}(\text{OH})_2$ that comes in contact with CO_2 during the adsorption process and converts to CaCO_3 . The surface of an aged concrete sample was neutralized over time due to the exposure of surfaces to the environment, which resulted in a significant decrease in the CO_2 uptake (Heng and Murata, 2004; Ramakrishnan and Orlov, 2014). Similarly, Ramakrishnan and Orlov (2014) used waste concrete as adsorbent for the mitigation of NOx. The results revealed that the decrease in surface basicity of waste concrete due to carbonation is the main reason for the decrease in NO_2 uptake as a function of concrete age. The experiments demonstrated that NO_2 uptake for relatively fresh concrete samples exhibited almost 100% NO_2 removal and a 12-year-old sample showed about 60% NO_2 removal.

Wu et al. (2008) used waste cement particles for the dry desulfurization with a laboratory-scale thermogravimetric analyzer based on the weight change of the sample exposed to a SO_2 -containing gas stream. In waste cement, calcium was the main component, making an equivalent of about 38 wt% of calcium oxide (CaO). These calcium contents in the waste cement react with SO_2 and form solid products of CaSO_3 and CaSO_4 . According to the stoichiometry, 1 metric ton of waste cement particles could almost capture 0.44 ton of SO_2 . The surface chemistry as well as the morphology and porosity of the construction-waste derived adsorbents are very important. The required characteristics of the potential gas adsorbents can be achieved by carefully treating construction waste. Therefore, it is confirmed that construction waste could be applicable as a precursor in developing inexpensive adsorbents for gas separation. Moreover, construction industries

have also undertaken initiatives to reduce CO₂ emission by the CO₂ sink effect of concrete carbonation. The CO₂ reacts with the alkaline components of concrete, primarily portlandite, and with the hydrated phases, resulting in the formation of CaCO₃ (Galan et al., 2010).

Zhuang et al. (2016) studied the feasibility of utilizing plastic solid waste as a membrane material for gas separation. In their study, polystyrene (PS) waste was directly reused for gas-separation membranes by a solution-casting technique. The waste materials comprise three types: (1) oriented polystyrene, (2) expandable polystyrene, and (3) high-impact polystyrene. The waste materials have the same composite and specification as the raw materials except for waste expandable polystyrene, which contains a partially broken molecular chain. In addition to the waste expandable polystyrene, the waste PS-derived membranes were homogenous and symmetrical. The gas permeation results of the membranes were tested by using the time-lag method at different working pressures. It was observed that the results of the waste PS- and raw PS-derived membranes are similar. In the meantime, a high-impact polystyrene membrane comprising of butadiene rubber displayed high CO₂ plasticization resistance at high pressure with a CO₂ permeability of 67 Barrer and CO₂/N₂ selectivity of 10–11 at a working pressure of 5 atm. As a conclusion, the novel reuse process of PS waste is feasible as an environmentally friendly and economically method for disposing plastic solid waste.

Nylo de Aguiar et al. (2012) investigated the hot metal desulfurization by residual marble waste and fluorspar. This study involved the use of marble waste, fluorspar, lime, and hot metal. Four mixtures were made and added to a liquid hot metal at a temperature of 1450°C. The results indicated that marble waste can be used effectively for gas desulfurization. This was due to the fact that marble waste when mixed with CaF₂ gathers interesting characteristics from both the thermodynamic as well as kinetic aspect to its use in the process of hot metal desulfurization. As a deduction, it can be concluded that waste can be reutilized for gas phase adsorption.

1.5 Pros and Cons of Separation Technologies and Future Developments

It is evident that waste material from industry, agricultural activities, municipal solid waste, and other wastes can be modified into value-added product and reutilized for gas phase pollutants. Furthermore, the control of pollutant gas emissions has become an issue of great importance to governmental regulatory agencies and the general public due to their negative effects toward the environment and human health. This has led to forcing countries around the world to impose a more stringent regulation on the release of these air pollutants into the atmosphere. Adsorption through flue gas cleanup is the most promising alternative among other currently used technologies, both environmentally and economically. The status research of this approach has been compiled and analyzed here with a focus on adsorbent materials that indirectly enhance the use of waste material as potential adsorbent material.

These waste-derived adsorbents have been modified in terms of physical, chemical, and structural properties that lead to better cleanup performance compared with the current state-of-the-art materials. Moreover, the main advantage of adsorbents derived from waste material is its low cost. For instance, steel slag utilization enables low-cost CO₂ sequestration using on-site waste slag. Carbonized slag was not disposed as waste. It possesses enhanced properties for construction and reduced heavy metal leaching. Apart from that,

a study showed that CO₂ sequestration performed in a packed back reactor can remove 32 ktons of CO₂ by using 140 ktons of steel slag. The cost of CO₂ sequestration was merely \$8/ton of CO₂. Hence, the implementation of this technology is feasible in terms of economical consideration (Bonenfant et al., 2009). On the other hand, by using zero economic value red mud, removal of hydrogen sulfide from coal gasification can be achieved without additional cost. In addition, carbonation using red mud is inexpensive and relatively safe. In fact, formation of stable carbonate products in this carbonation technology is a great advantage compare to other technologies (Cengeloglu et al., 2006).

However, realizing the advantages of adsorption-based gas cleanup technology using these materials requires overcoming several barriers to allow for practical utility. One of the greatest barriers to the application of agricultural-based adsorbents for flue gas cleanup are their high costs of synthesis, narrow range of useful operation conditions, lack of long-term stability, and the ability to remove multiple impurity gases simultaneously. Besides, operation at relatively high temperatures, especially to capture NO_x gases, still remains one of the major issues. Hence, much work needs to be done in developing various types of adsorbents that can interact with SO₂ and NO_x gases at low temperatures (Rezaei et al., 2015).

Despite many recent advances, much of the potential remains untapped and need to be explored. Novel materials such as metal-organic frameworks (MOFs) appear to have many of the hallmarks of high-performance adsorbents. Nevertheless, more fundamental and applied research is required for these advanced materials to find widespread use of adsorption-based gases clean-up processes (Rezaei et al., 2015). Besides that, some waste material such as MSW has side effects as well. For example, one of the major concerns for using incinerator ash is the leachability of heavy metals. The use of MSW fly ash as the adsorbent is less common than bottom ash. This is due to the existence of toxic heavy metals in the fly ash. Moreover, the new application of construction wastes, including ceramic, marble, concrete, and clay bricks, are still not mature, and are mostly in the stage of laboratory research without relevant industrial application experiments. This is due to the fact that construction waste materials have less adsorption capacity compared to activated carbons.

Therefore, before these technologies can be fully utilized at the industrial scale, further improvement in adsorption capacity of adsorbents must be researched. This would reduce the operating cost for the separation process. In addition, even though the adsorbent cost is low or practically none, the adsorption process still requires high capital investment and operating cost, especially when the industry does not regard environmental protection as profitable action. Therefore, with no stringent policy regarding waste gas emission, the industry is reluctant to invest in the new technology and process. Thus, it is recommended that in order to realize industrialization, future work should concentrate on scaling up equipment design and buildup, recycling materials, and residue treatment.

References

- Acharya, J., Sahu, J. N., Sahoo, B. K., Mohanty, C. R., Meikap, B. C. 2009. Removal of chromium(VI) from wastewater by activated carbon developed from Tamarind wood activated with zinc chloride. *Chemical Engineering Journal* 150: 25–39.
- Agrawal, A., Sahu, K. K., Pandey, B. D. 2004. Solid waste management in non-ferrous industries in India. *Resources, Conservation and Recycling* 42: 99–120.

- Ajith, K. S., Geoffrey, S. A., Pablo, A. 2009. *Agricultural Wastes*. Nova Science Publishers, New York.
- Altundogan, H. S., Altundogan, S., Tumen, F., Bildik, M. 2002. Arsenic adsorption from aqueous solutions by activated red mud. *Waste Management* 22: 357–363.
- Arabyarmohammadi, H., Salarirad, M. M., Behnamfard, A. 2014. Characterization and utilization of clay-based construction and demolition wastes as adsorbents for zinc (II) removal from aqueous solutions: An equilibrium and kinetic study. *Environmental Progress & Sustainable Energy* 33: 777–789.
- Arenillas, A., Smith, K. M., Drage, T. C., Snape, C. E. 2005. CO₂ capture using some fly ash derived carbon materials. *Fuel* 84: 2204–2210.
- Attia, A. A., Girgis, B. S., Fathy, N. A. 2008. Removal of methylene blue by carbons derived from peach stones by H₃PO₄ activation: Batch and column studies. *Dyes and Pigments* 76: 282–289.
- Aworn, A., Thiravetyan, P., Nakbanpote, W. 2008. Preparation and characteristics of agricultural waste activated carbon by physical activation having micro- and mesopores. *Journal of Analytical and Applied Pyrolysis* 82: 279–285.
- Bakshan, A., Srouf, I., Chehab, G., El-Fadel, M., Karaziwan, J. 2017. Behavioral determinants towards enhancing construction waste management: A Bayesian network analysis. *Resources, Conservation and Recycling* 117: 274–284.
- Bashkova, S., Badosz, T. J. 2009. The effects of urea modification and heat treatment on the process of NO₂ removal by wood-based activated carbon. *Journal of Colloid and Interface Science* 333: 97–103.
- Belhachemi, M., Jeguirim, M., Limousy, L., Addoun, F. 2014. Comparison of NO₂ removal using date pits activated carbon and modified commercialized activated carbon via different preparation methods: Effect of porosity and surface chemistry. *Chemical Engineering Journal* 253: 121–129.
- Bonenfant, D., Kharoune, L., Sauve, S., Hausler, R., Niquette, P., Mimeault, M., Kharoune, M. 2009. Molecular analysis of carbon dioxide adsorption processes on steel slag oxides. *International Journal of Greenhouse Gas Control* 3: 20–28.
- Cengeloglu, Y., Tor, A., Ersoz, M., Arslan, G. 2006. Removal of nitrate from aqueous solution by using red mud. *Separation and Purification Technology* 51: 374–378.
- Cheng, H. 2016. Reuse research progress on waste clay brick. *Procedia Environmental Sciences* 31: 218–226.
- Daniel, H., Laura, T., Keshav, V. 1999. *What a Waste: Solid Waste Management in Asia*. Urban Development Sector Unit East Asia and Pacific Region, The International Bank for Reconstruction and Development/The World Bank, Washington, D.C.
- Daniel, H., Perinaz, B. T. 2012. *What a Waste: A Global Review of Solid Waste Management*, No. 15, Urban Development Series, Urban Development & Local Government Unit, The World Bank, 8–12.
- Das, B., Prakash, S., Reddy, P. S. R., Misra, V. N. 2007. An overview of utilization of slag and sludge from steel industries. *Resources, Conservation and Recycling* 50: 40–57.
- Davini, P. 1999. Desulphurization properties of active carbons obtained from petroleum pitch pyrolysis. *Carbon* 37: 1363–1371.
- Davini, P. 2001. The effect of certain metallic derivatives on the adsorption of sulphur dioxide on active carbon. *Carbon* 39: 419–424.
- Davini, P. 2002. Flue gas treatment by activated carbon obtained from oil-fired fly ash. *Carbon* 40: 1973–1979.
- Davini, P. 2003a. Behaviour of activated carbons obtained from mixtures of oil-fired fly ash and oil refining pitch. *Carbon* 41: 1559–1565.
- Davini, P. 2003b. Flue gas desulphurization by activated carbon fibers obtained from polyacrylonitrile by-product. *Carbon* 41: 277–284.
- Doucet, F. J. 2010. Effective CO₂-specific sequestration capacity of steel slags and variability in their leaching behaviour in view of industrial mineral carbonation. *Mineral Engineering* 23: 262–269.
- Ello, A. S., de Souza, L. K. C., Trokourey, A., Jaroniec, A. M. 2013. Coconut shell-based microporous carbons for CO₂ capture. *Microporous and Mesoporous* 180: 280–283.
- Eloneva, S., Teir, S., Salminen, J., Fogelholm, C. J., Zevenhoven, R. 2008. Fixation of CO₂ by carbonating calcium derived from blast furnace slag. *Energy* 33: 1461–1467.

- Fan, Y., Zhang, F. S., Zhu, J., Liu, Z. 2008. Effective utilization of waste ash from MSW and coal co-combustion power plant-zeolite synthesis. *Journal Hazardous Materials* 153: 382–388.
- Foster, A., Kumar, N. 2011. Health effects of air quality regulations in Delhi, India. *Atmospheric Environment* 45: 1675–1683.
- Galan, I., Andrade, C., Mora, P., Sanjuan, M. 2010. Sequestration of CO₂ by concrete carbonation. *Environmental Science and Technology* 44: 3181–3186.
- Ghouma, I., Jeguirim, M., Dorge, S., Limousy, L., Ghimbeu, C. M., Ouederni, A. 2015. Activated carbon prepared by physical activation of olive stones for the removal of NO₂ at ambient temperature. *Comptes Rendus Chimie* 18: 63–74.
- Gray, M. L., Soong, Y., Champagne, K. J., Baltrus, J., Stevens, R. W., Toochinda Jr., P., Chuang, S. S. C. 2004. CO₂ capture by amine-enriched fly ash carbon sorbents. *Separation and Purification Technology* 35: 31–36.
- Guo, J., Chong, A. 2003. Adsorption of sulphur dioxide onto activated carbon prepared from oil-palm shells with and without pre-impregnation. *Separation and Purification Technology* 30: 265–273.
- Guo, J., Lua, A. C. 1999. Textural and chemical characterisations of activated carbon prepared from oil-palm stone with H₂SO₄ and KOH impregnation. *Microporous and Mesoporous Materials* 32: 111–117.
- Guo, J., Lua, A. C. 2000. Effect of surface chemistry on gas-phase adsorption by activated carbon prepared from oil-palm stone with pre-impregnation. *Separation and Purification Technology* 18: 47–55.
- Guo, J., Lua, A. C. 2002. Microporous activated carbons prepared from palm shell by thermal activation and their application to sulfur dioxide adsorption. *Journal of Colloid and Interface Science* 251: 242–247.
- Guo, Y., Li, Y., Zhu, T., Ye, M. 2015. Investigation of SO₂ and NO adsorption species on activated carbon and the mechanism of NO promotion effect on SO₂. *Fuel* 143: 536–542.
- Hayashi, J., Yamamoto, N., Horikawa, T., Muroyama, K., Gomes, V. G. 2005. Preparation and characterization of high-specific-surface-area activated carbons from K₂CO₃-treated waste polyurethane. *Journal of Colloid and Interface Science* 281: 437–443.
- Heng, M., Murata, K. 2004. Aging of concrete buildings and determining the pH value on the surface of concrete by using a handy semi-conductive pH meter. *Analytical Sciences* 20: 1087–1090.
- Hu, Z. P., Zhu, Y. P., Gao, Z. M., Wang, G., Liu, Y., Liu, X., Yan, Z. Y. 2016. CuO catalysts supported on activated red mud for efficient catalytic carbon monoxide oxidation. *Chemical Engineering Journal* 302: 23–32.
- Hui, K. S., Chao, C. Y. H. 2006. Effects of step-change of synthesis temperature on synthesis of zeolite 4A from coal fly ash. *Microporous and Mesoporous Materials* 88: 145–151.
- Ioannidou, O., Zabaniotou, A. 2007. Agricultural residues as precursors for activated carbon production—A review. *Renewable and Sustainable Energy Reviews* 11: 1966–2005.
- Izquierdo, M. T., Rubio, B. 2008. Carbon-enriched coal fly ash as a precursor of activated carbons for SO₂ removal. *Journal of Hazardous Materials* 155: 199–205.
- Jeremy, C. 2002. *Air Pollution*, 2nd ed. Spon Press, London.
- Kaithwas, A., Prasad, M., Kulshreshtha, A., Verma, S. 2012. Industrial wastes derived solid adsorbents for CO₂ capture: A mini review. *Chemical Engineering Research and Design* 90: 1632–1641.
- Kazmierczak, J., Nowicki, P., Pietrzak, R. 2013. Sorption properties of activated carbons obtained from corn cobs by chemical and physical activation. *Adsorption* 19: 273–281.
- Kazmierczak-Razna, J., Nowicki, P., Pietrzak, R. 2016. Toxic gases removal onto activated carbons obtained from hay with the use of microwave radiation. *Chemical Engineering Research and Design* 109: 346–353.
- Kousaiti, A., Anastasiadou, K., Aivalioti, M., Gidarakos, E. 2011. Use of treated asbestos waste in the adsorption of BTEX, MTBE and TAME. Proceedings of the 3rd International CEMEPE & SECOTOX Conference, Skiathos, June 19–24.
- Lam, C. H. K., Ip, A. W. M., Barford, J. P., McKay, G. 2010. Use of incineration MSW ash: A review. *Sustainability* 2: 1943–1968.

- Lau, L. C., Lee, K. T., Mohamed, A. R. 2010. Rice husk ash sorbent doped with copper for simultaneous removal of SO₂ and NO: Optimization study. *Journal of Hazardous Materials* 183: 738–745.
- Li, K., Ling, L., Lu, C., Qiao, W., Liu, Z., Liu, L., Mochida, I. 2001. Catalytic removal of SO₂ over ammonia-activated carbon fibers. *Carbon* 39: 1803–1808.
- Li, W., Tan, S., Shi, Y., Li, S. 2015. Utilization of sargassum based activated carbon as a potential waste derived catalyst for low temperature selective catalytic reduction of nitric oxides. *Fuel* 160: 35–42.
- Liu, Q., Guan, J. S., Li, J., Li, C. 2003. SO₂ removal from flue gas by activated semi-cokes 2: Effects of physical structures and chemical properties on SO₂ removal activity. *Carbon* 41: 2225–2230.
- Lu, G. Q., Do, D. D. 1991. Adsorption properties of fly ash particles for NO_x removal from flue gases. *Fuel Processing Technology* 27: 95–107.
- Lua, A. C., Guo, J. 2000. Activated carbon prepared from oil palm stone by one-step CO₂ activation for gaseous pollutant removal. *Carbon* 38: 1089–1097.
- Lua, A. C., Guo, J. 2001. Microporous oil-palm-shell activated carbon prepared by physical activation for gas-phase adsorption. *Langmuir* 17: 7112–7117.
- Mercedes, M. V. M., Zhe, L., Zhang, T. 2008. Sorbents for CO₂ capture from high carbon fly ashes. *Waste Management* 28: 2320–2328.
- Moghtaderi, B., Zanganeh, J., Shah, K., Wu, H. 2012. Application of concrete and demolition waste as CO₂ sorbent in chemical looping gasification of biomass. *Energy & Fuels* 26: 2046–2057.
- Najjar, Y. S. H. 2011. Gaseous pollutants formation and their harmful effects on health and environment. *Innovative Energy Policies* 1: 1–8.
- Nowicki, P., Kazmierczak, J., Pietrzak, R. 2015. Comparison of physicochemical and sorption properties of activated carbons prepared by physical and chemical activation of cherry stones. *Powder Technology* 269: 312–319.
- Nowicki, P., Pietrzak, R. 2010. Carbonaceous adsorbents prepared by physical activation of pine sawdust and their application for removal of NO₂ in dry and wet conditions. *Bioresource Technology* 101: 5802–5807.
- Nowicki, P., Skibiszewska, P., Pietrzak, R. 2014. Hydrogen sulphide removal on carbonaceous adsorbents prepared from coffee industry waste materials. *Chemical Engineering Journal* 248: 208–215.
- Nylo de Aguiar, F., Fardin Grillo, F., Soares Tenório, J. K., Roberto de Oliveira, J. 2012. Hot metal desulfurization by marble waste and fluorspar. *Rem: Revista Escola de Minas* 65: 233–239.
- Ottaviani, M. F., Venturi, F. 1996. Physicochemical study on the adsorption properties of asbestos. 1. EPR study on the adsorption of organic radicals. *Journal of Physical Chemistry* 100: 265–273.
- Pan, S. Y., Chiang, P. C., Chen, Y. H., Chen, C. D., Lin, H. Y., Chang, E. E. 2013. Systematic approach to determination of maximum achievable capture capacity via leaching and carbonation processes for alkaline steelmaking wastes in a rotating packed bed. *Environmental Science & Technology* 47: 13677–13685.
- Papargyropoulou, E., Preece, C., Padfield, R., Abdullah, A. A. 2011. Sustainable construction waste management in Malaysia: A contractor's perspective. Management and Innovation for a Sustainable Built Environment, June 20–23, Amsterdam, The Netherlands.
- Penilla, R. P., Bustos, A. G., Elizabe, S. G. 2003. Zeolite synthesized by alkaline hydrothermal treatment of bottom ash from combustion of municipal solid wastes. *Journal of the American Ceramic Society* 86: 1527–1533.
- Pope III, C. A., Burnett, R. T., Thun, M. J., Calle, E. E., Krewski, D., Ito, K. 2002. Lung cancer, cardiovascular mortality, and long-term exposure to fine particulate air pollution. *Journal of the American Medical Association* 287: 1132–1141.
- Rajgopal, S., Karthikeyan, T., Prakash Kumar, B. G., Miranda, L. R. 2006. Utilization of fluidized bed reactor for the production of adsorbents in removal of malachite green. *Chemical Engineering Journal* 116: 211–217.
- Ramakrishnan, G., Orlov, A. 2014. Development of novel inexpensive adsorbents from waste concrete to mitigate NO_x emissions. *Building and Environment* 72: 28–33.

- Rashidi, N. A., Yusup, S., Ahmad, M. M., Mohamed, N. M., Hameed, B. H. 2012. Activated carbon from the renewable agricultural residues using single step physical activation: A preliminary analysis. *APCBEE Procedia* 3: 84–92.
- Rezaei, F., Rownaghi, A. A., Monjezi, S., Lively, R. P., Jones, C. W. 2015. SO_x/NO_x removal from flue gas streams by solid adsorbents: A review of current challenges and future directions. *Energy & Fuels* 29: 5467–5486.
- Sahu, R. C., Patel, R., Ray, B. C. 2011. Removal of hydrogen sulfide using red mud at ambient conditions. *Fuel Processing Technology* 92: 1587–1592.
- Sarmah, M., Baruah, B. P., Khare, P. 2013. A comparison between CO₂ capturing capacities of fly ash based composites of MEA/DMA and DEA/DMA. *Fuel Processing Technology* 106: 490–497.
- Sumathi, S., Bhatia, S., Lee, K. T., Mohamed, A. R. 2010. Selection of best impregnated palm shell activated carbon (PSAC) for simultaneous removal of SO₂ and NO_x. *Journal of Hazardous Materials* 176: 1093–1096.
- Sun, Y., Yao, M. S., Zhang, J. P., Yang, G. 2011. Indirect CO₂ mineral sequestration by steelmaking slag with NH₄Cl as leaching solution. *Chemical Engineering Journal* 173: 437–445.
- Sushil, S., Batra, V. S. 2008. Catalytic applications of red mud, an aluminium industry waste: A review. *Applied Catalysis B: Environmental* 81: 64–77.
- Sushil, S., Batra, V. S. 2012. Modification of red mud by acid treatment and its application for CO removal. *Journal of Hazardous Materials* 203–204: 264–273.
- Tsai, I. T., Ali, M. A., Waddi, S. E., Zarzour, O. A. 2013. Carbon capture regulation for the steel and aluminum industries in the UAE: An empirical analysis. *Energy Procedia* 37: 7732–7740.
- Turmuzi, M., Daud, W. R. M., Tasirin, S. M., Takriff, M. S., Iyuke, S. E. 2004. Production of activated carbon from candlenut shell by CO₂ activation. *Carbon* 42: 423–460.
- U.S. Department of Energy. 2011. U.S. billion-ton update: Biomass supply for a bioenergy and bio-products industry. R. D. Perlack and B. J. Stokes (Leads), ORNL/TM-2011/224. Oak Ridge National Laboratory, Oak Ridge, Tennessee.
- Vasudevan, G. 2015. Study on the demolition waste management in Malaysia construction industry. *International Journal of Scientific Engineering and Technology* 4: 131–135.
- Wu, J., Iizuka, A., Kumagai, K., Yamasaki, A., Yanagisawa, Y. 2008. Desulfurization characteristics of waste cement particles as a sorbent in dry desulfurization. *Industrial and Engineering Chemistry Research* 47: 9871–9877.
- Xuan, X. P., Yue, C. T., Li, S. Y., Yao, Q. 2003. Selective catalytic reduction of NO by ammonia with fly ash catalyst. *Fuel* 82: 575–579.
- Yadav, V. S., Prasad, M., Khan, J., Amritphale, S. S., Singh, M., Raju, C. B. 2010. Sequestration of carbon dioxide (CO₂) using red mud. *Journal of Hazardous Materials* 176: 1044–1050.
- Yang, J., Xiao, B. 2008. Development of unsintered construction materials from red mud wastes produced in the sintering alumina process. *Construction and Building Materials* 22: 2299–2307.
- Yao, Z. T., Ji, X. S., Sarker, P. K., Tang, J. H., Ge, L. Q., Xia, M. S., Xi, Y. Q. 2015. A comprehensive review on the applications of coal fly ash. *Earth-Science Reviews* 141: 105–121.
- Yi, H., Xu, G., Cheng, H., Wang, J., Wan, Y., Chen, H. 2012. An overview of utilization of steel slag. *Procedia Environmental Sciences* 16: 791–801.
- Yu, J., Wang, K. 2011. Study on characteristics of steel slag for CO₂ capture. *Energy & Fuels* 25: 5483–5492.
- Zhang, T., Yu, Q., Wei, J., Li, J., Zhang, P. 2011. Preparation of high performance blended cements and reclamation of iron concentrate from basic oxygen furnace steel slag. *Resources, Conservation and Recycling* 56: 48–55.
- Zhuang, G. L., Tseng, H. H., Wey, M. Y. 2016. Feasibility of using waste polystyrene as a membrane material for gas separation. *Chemical Engineering Research and Design* 111: 204–217.



Taylor & Francis

Taylor & Francis Group

<http://taylorandfrancis.com>

2

Solid Waste Adsorbents for Volatile Organic Compounds Removal by Biofiltration

Hussein Znad, Benjamin Alliss, and Hari Vuthaluru

CONTENTS

2.1 Introduction: Background and Driving Factors.....	21
2.2 Biofiltration Process.....	21
2.3 Key Parameters Affecting Biofilter Performance	22
2.4 Solid Waste Adsorbents and the Biofiltration Process	27
2.5 Modeling Solid Phase Adsorption	31
2.6 Conclusions and Recommendations.....	31
References.....	32

2.1 Introduction: Background and Driving Factors

Volatile organic compounds (VOCs) are waste gases from many industrial processes, and pose a serious health and environmental risk. Many researchers have found that VOCs can contribute to the formation of smog, cause sharp declines in crop yields of surrounding areas, and devastate forests and ecosystems near the emission source (Yang et al., 2010), as well as often being described as carcinogenic. As urban sprawl continues due to population increases, the buffer distances between industrial complexes that produce VOCs and residential areas will gradually be decreased. These factors create a demand for efficient treatment of these VOCs and other odorous compounds to ensure the surrounding population has limited exposure to them, and that the forever-tightening emission limits are met.

2.2 Biofiltration Process

Biofilters are a form of reactor/packed-bed filter. They can be open or closed, depending on the available area for the unit and the amount of pollutant to be processed. In an open biofilter, the gases move upward through the filter bed. In closed biofilters, the gases to be treated are either blown or drawn through the packed bed (Metcalf & Eddy et al., 2013). The bed is ideally a porous material on which organisms are immobilized. As the pollutant gases flow through the packed bed, they are transported from the gaseous phase, into the microbial film. It is in this biofilm that the microbial oxidation of VOCs occurs (Mudliar et al., 2010). Figure 2.1 shows a schematic of a standard biofilter. Biofilters can

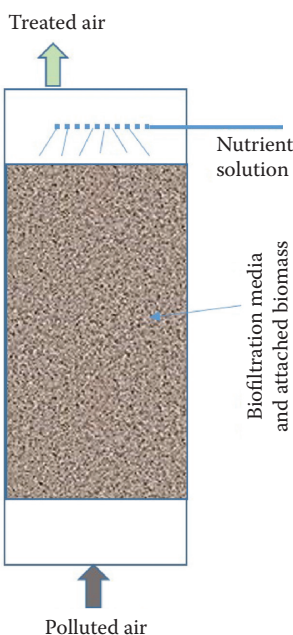


FIGURE 2.1
Schematic of a typical biofilter system.

TABLE 2.1
Advantages and Disadvantages of Biofiltration

Advantages	Disadvantages
<ul style="list-style-type: none"> • It is cost effective, having low capital costs and cheap to operate. • Low pressure drop across reactor. • Treat large volumes of gas with low contaminant concentration. • It does not produce any secondary waste stream. 	<ul style="list-style-type: none"> • The medium can get clogged by particulate matter. • Medium may deteriorate if not under proper conditions. • Treatment efficiency for high contaminant concentration streams is reduced. • There can be difficulty in moisture and pH control.

be used to treat a wide range of pollutants, from odorants such as hydrogen sulfide and ammonia, to VOCs like propane and butane. Studies have shown that so far, 60 out of 189 hazardous air pollutants (HAPs) can be treated successfully using biofiltration processes (Mudliar et al., 2010). Several of the key advantages to choosing biofilters over other methods for VOC removal can be seen in Table 2.1.

2.3 Key Parameters Affecting Biofilter Performance

Many different materials have been used as the media for biofiltration, and there is no perfect solution. This is due to the different natures of VOCs, and the different combinations

and unit requirements. One of the key considerations when selecting the media is the ability to promote biomass growth, so the selection should possess favorable conditions for microorganisms. The media will also play a role in maintaining the optimal operating conditions, such as moisture content, temperature, pH, nutrients, and oxygen levels. The common characteristics that the ideal media selections exhibit are

- Suitable particle size, void fraction, and specific surface area
- High nutritive capacity
- High moisture-retention capacity
- High buffering capacity
- Mechanically resistant, chemically inert, and stable
- Adsorption capability of the media

Some examples of media that have been commonly applied are compost, polyurethane, peat, and soil. Some common values of key parameters of common media can be seen in Table 2.2. Other applications require a mixture of different media to take the advantages of both selections. Some media may greatly promote microorganism growth and have good adsorption capability, but may lack strength and rigidity. The solution is to mix in a more rigid material that provides support to the bed.

The other key factors that can influence a biofiltration process are the temperature, pH, moisture content, the specific VOC, oxygen levels, nutrients, the microorganisms used, and loading rates. Clearly, since the media can impact on a large number of these parameters, it is a very important consideration.

The biofilm thickness plays an important part in the overall effectiveness of the biofilter. The biofilm can be described as a mass of organisms that are growing on the surface of the media/solid support. It is essentially where the bulk of the conversion of the target contaminant to harmless product takes place.

TABLE 2.2

Characterization of Different Biofilter Media

Media	Density (kg/m ³)	Porosity (%)	Water Holding Capacity	Average Pore Size (mm)	Surface Area (m ² /g)	pH	Reference
Compost/perlite (75%/25%)	220	64.4	41%			5.6	Lebrero et al., 2011
Coconut coir		72					Das et al., 2011
Polyurethane	15	98.8	57 kg-H ₂ O/ kg-PU	0.8	76.81		Ryu et al., 2010
Matured compost and coal (2:1)							Raghuvaran and Babu, 2009
Compost	600–700	40			2750 (total area)		Nikiema et al., 2009
Peat	133	31–74	88%		13.4	4.8	Alvarez et al., 2009
Soil	900		61.2%		1.3	6.2	Alvarez et al., 2008
Granular activated carbon	480			2.2 × 10 ⁻⁴			Ho et al., 2008

The thickness of the biofilm can have both positive and negative effects on the efficiency. As the thickness increases, the biological activity will also increase, up until a certain level. This level is known as the "active thickness," and is essentially the optimal thickness for the best performance. Once the thickness starts growing beyond this point, there will be inhibitory effects. The diffusion/mass transfer of nutrients will become more difficult and eventually become a rate limiting factor. Devinny and Ramesh (2005) discuss how the thickening of the biofilm will reduce the pore size and eventually plug them. This will eventually lead to an increase in pressure drop and a reduction in surface area available. When modeling, the penetration profile of the substrate, oxygen, and nutrients in the biofilm, as well as the evaluation of overall biofilm effectiveness factor, will need to be considered (Mudliar et al., 2010).

In an overview of general biofiltration modeling, Fulazzaky et al. (2014) states that since the solubility of oxygen in water is often lower than that of the contaminant, the oxygen concentration can limit the rate of biodegradation, instead of the contaminant concentration. The work done by Mudliar et al. (2010) somewhat disagrees with this view, suggesting that the effect of oxygen levels on biofiltration is case specific. It is agreed that oxygen limitation can definitely impact the overall performance, but there is a question as to how much in each different scenario. The research seems to find that once the oxygen reaches a certain point, increasing it further will yield no more benefits. The importance of avoiding anaerobic conditions was also discussed in the work of Mudliar et al. (2010). Research found that any small anaerobic zone could lead to the formation of different compounds during operation, which are odorous, and obviously goes against the goal of common biofilters of removing odorants and VOCs from the air.

The pH of a system can have severe effects on the overall efficiency of a biofiltration process if it is outside of the optimal range. A pH that is too high and a pH that is too low can both be damaging to the process. According to the research completed by Mudliar et al. (2010), the majority of microorganisms employed in biofilters are neutrophilic, which means the optimum pH is commonly around 7. This was supported by the work of Das et al. (2011) and Ho et al. (2008), who required pH levels of 6.8 and 6 to 8, respectively. During operation, the pH needs to always be considered and monitored, particularly while certain VOCs are being treated. Certain VOCs will produce acidic by-products, which will in turn lower the pH of the system and effect the microorganisms' efficiency.

To help control the pH, other parameters, such as the media or the nutrient solutions, may be altered or selected to achieve the desired result. Mudliar et al. (2010) summarizes previous works to suggest that of all the possible organic materials used as media, soil had the best pH buffering capacity, followed by compost and wood chips. Other researchers have suggested inserting buffer materials into the filter bed itself to control the pH, while others have added pH buffers to the nutrient solutions going through the biofilter.

Water is an essential component for microbial activity in the biofilm. Delhom nie and Heitz (2005) states that if the moisture content in the bed is too low, it can lead to bed desiccation and gas flow channeling. If the beds undergo dry conditions for a long period of time, they can go from hydrophilic to hydrophobic, making them difficult to bring back to optimal moisture levels. Shareefdeen and Singh (2005) reiterated these findings, describing a bed at suboptimal moisture content that could lead to the development of fissures that cause channeling and short circuiting. Delhom nie and Heitz (2005) and Mudliar et al. (2010) also consider that if the bed moisture content is allowed to go too high, the specific surface area that is normally available for the exchange between gas and biofilm is reduced, which inhibits the transfer of oxygen and

hydrophobic pollutants, and can lead to an increase in pressure drop and the creation of anaerobic zones. The ideal bed moisture content is described by Delhoménie and Heitz (2005) as being between 40% and 60%, whereas Mudliar et al. (2010) believe the optimal content is between 30% and 60%. Chen and Hoff (2009) found it to be 40% to 65%, which varies with different filtering media. The experimental research reported in Table 2.2 is relatively similar to these optimal conditions, with the work done by Nikiema et al. (2009) going slightly lower, using 25% to 50%, and others slightly higher, such as Raghuvanshi and Babu (2009) who used 60.2%. Ho et al. (2008) selected 38% to 40% as their optimal condition. Based on the research and results from others, the generally accepted range seems to be more like 25% to 60% or relatively close to that. The common range does not necessarily mean the exact range for every process, so it is still acceptable. This is an essential parameter in modeling, as if the moisture level is not maintained within the required range, the model will need to consider how channeling can alter the removal efficiency of the overall process. Table 2.3 is adapted from the review by Chen and Hoff (2009), and generally summarizes/supports the preceding findings, while adding to it.

When attempting to control or monitor the moisture content, there are several main factors that need to be considered:

- The inlet gas relative humidity
- The capacity of the selected media to hold water
- Water stripping effects monitored by the gas flow rate through the bed

Research completed by Mudliar et al. (2010) discussed some of the common methods to control the water content. Many processes involve prehumidification of the inlet gas stream, and some processes also find it necessary to add a sprinkler to provide direct

TABLE 2.3

Issues Relating to Moisture Content

Low Moisture Content	High Moisture Content	Maintenance Difficulties	Methods to Maintain Optimal Condition
Decrease in microbial activity	Larger pressure drop and low EBRT due to filling of the pore space with water	High velocity, nonsaturated gas flows that strip moisture from filter bed	Direct water supply using sprinklers or soaker hoses
Contraction leading to filter bed cracking, reducing EBRTs	Creation of anaerobic zones, resulting in odor formation and slow degradation rates	Exothermic reactions that increase temperature	Humidification of inlet gas stream
Difficulty to rewet dry media, due to hydrophobicity	Oxygen limitation		A combination of humidification and direct water supply
Channeling	Nutrient washing from biofilter media		Covers to limit evaporation and maintain moisture content
Low absorption capacity	Low pH leachate produced, requiring disposal		

application of water to the filter bed. More advanced and long-term biofilters could use load cells to determine the weight of the filter bed, and then control a sprinkler system to operate when required. Shareefdeen and Singh (2005) supported the need for a supplemental moisture supply due to the biooxidation process being an exothermic reaction, which can lead to drying of the bed. Aside from the implications listed earlier, such as fissures and channeling, the formation of dry spots can result in nonuniform gas distribution, as well as reduction in the microorganism activity.

There is a wide range of microorganisms that can be used, and each different type can affect the optimal conditions of the other parameters, such as optimal temperature and pH ranges. Microorganisms cannot just be added to a process and expected to perform right away. This will more often than not shock the system, and will greatly stunt the growth and development of the microorganisms. To overcome this, they need to be acclimatized. Different microorganisms and different operating conditions will require different acclimatization processes. For example, Rene et al. (2015) used a mixed microbial consortium that was acclimatized for 18 days in the biofilter, whereas Raghuvanshi and Babu (2009) used a sample of activated sludge and acclimatized it for 15 days, gradually increasing the amount of pollutant from 160 to 480 mg/L and decreasing the amount of glucose from 1000 to 0 mg/L.

The type of pollutant and the concentration of the pollutants can have an effect on the overall biofiltration efficiency. The biodegradation rate is largely related to the microbial strains established on the filter bed, as well as the concentration and overall chemical configuration of the VOC. If the pollutant is slightly soluble and at a low concentration, the removal is limited by the pollutant's transfer rate into the biofilm. If soluble pollutants are introduced at high concentrations, they are easily absorbed into the biofilm, and the removal is limited by the biodegradation rate, as mentioned by Delhoménie and Heitz (2005). This is an important parameter for modeling, as the rate-limiting step will change at different compositions.

Delhoménie and Heitz (2005) state that if the concentration of the pollutant is too high, it can inhibit the microbial growth and activity. Treating mixtures of different pollutants can have positive and negative effects on the overall removal efficiency of the biofiltration process, particularly in how they inhibit the growth. Some different pollutants may inhibit the biodegradation of another pollutant, whereas some may improve the biodegradation by promoting biomass growth.

Within a biofilter, the pollutants are able to act as the nutrients for the bacteria. Bacteria require carbon and energy sources to increase the microbial activity, and according to the review by Mudliar et al. (2010), the common pollutants are able to meet the demand. The required hydrogen and oxygen are commonly found in the air, with excess often in the growth media and even in the VOCs being treated. There is still a need for other nutrients, which depends on the microorganisms being used more than anything. The other common nutrients include nitrogen, phosphorous, potassium, and sulfur, as well as vitamins and metals, and they can generally be found in the biofilter media used.

Mudliar et al. (2010) cited studies that supported the need for the addition of nutrients, either by aqueous solution or in a solid form, even if the media bed is able to provide the desired nutrients. Using a media, such as compost, for a long period of time can lead to the eventual depletion of the intrinsic nutrients. Without the constant addition of these nutrients, the process would eventually be left with insufficient nutrients to operate, which may become a limiting factor.

Shareefdeen et al. (2009) shines light on the impact temperature can have on a biofiltration process, due to its effect on the growth rate of the microbial population and on the

biodegradation kinetics. There will be heat transfer between air, media, and the surroundings based on the temperature differences that will need to be considered. This work found that the majority of microorganisms used have an optimum temperature range of 20°C to 40°C, which was also supported in the review by Chen and Hoff (2009), who specified the most common optimal temperature to be 35°C for the majority of aerobic microorganisms used. The work completed in the review by Chen and Hoff (2009) found several examples that demonstrate the robust nature of the microorganisms, which allows them to recover rapidly from nonoptimal temperatures. The overall efficiency of the biofilter will generally continue to increase with temperature, until a certain point that it has inhibitory effects, commonly after reaching 40°C.

Dorado et al. (2012) have looked into how biomass growth/accumulation can impact on the operating conditions of the process, and the pressure drop was especially effected. The research found that as biomass grows, the thickness of the biofilm will grow and fill the void volume of the bed, reducing the empty bed section for air circulation. This causes an overall decrease in porosity, which in turn causes an increase in the system pressure drop.

For biodegradation of the pollutant by the microorganisms to occur, the pollutant must be transferred from the gas phase to the liquid phase, which is essentially the biofilm. According to the review of Chen and Hoff (2009), this makes the empty bed residence time (EBRT) a critical parameter for biofilter performance. EBRT is described as a relative measure of gas residence time within the biofilter media. Different pollutants/contaminants will have different characteristics, as previously discussed. These characteristics will affect how fast the transfer from gas phase to liquid phase can occur, creating the need for a different EBRT that is specific for each process. The EBRT is commonly related to the moisture content and the pollutant loading, with a high moisture content and lower pollutant loading resulting in a shorter EBRT. Chen and Hoff (2009) suggest an EBRT between 4 and 10 seconds should be suitable for a biofilter that is removing VOCs from agricultural sites. Their research also concludes that determining the absolute minimum EBRT for practical biofilter sizing should be a future consideration.

2.4 Solid Waste Adsorbents and the Biofiltration Process

Finding a new use for waste products is a growing concern in today's world, and the use of these waste products to provide environmental benefits has gathered a lot of interest over the last few years. Aside from the obvious benefits of reducing solid waste to be disposed of by making it useful, it is also considered a very cost-effective approach, as the wastes are commonly very cheap. Many researchers have applied solid adsorbents to a biofiltration process in many forms, such as the main media, as a mixture with other commonly used media as a bulking media, and to provide pretreatment of the inlet stream.

When applied as the bulking media, obviously the main goal is to increase the efficiency of the process. If, however, the results are constant while using a waste product, it may still be considered successful. It is also important to consider how the addition of the solid waste can negatively impact the process, instead of just focusing on the positives it can bring. Alvarez-Hornos et al. (2011) tested ground tire rubber (GTR) as an adsorptive material mixed into the media with fibrous peat at a 1:3 volume. GTR is described as

being a low-cost waste material that is both an economical and environmentally friendly alternative to other bulking materials. Over 4 months, it was tested against another biofilter under the same conditions that was using an entirely fibrous peat media. Previous research by Alvarez-Hornos et al. (2008) highlighted that an increase of 50% to the inlet concentration resulted in a 200% increase in pollutant emissions, showing the adverse impact a changing concentration of pollutant can have on the effectiveness of the biofiltration process. Since the majority of chemical processes that produce VOCs will not consistently produce equal concentrations of VOCs, the need for the addition of an adsorptive material to the packing media to enhance the buffering ability of the biofilter exists. The results from Alvarez-Hornos et al. (2011) observed that the addition of GTR, although the available surface area for biofilm development was decreased, did not negatively impact the biofilter performance under steady-state conditions with constant inlet concentration. It was also found that the penetration of the aromatic VOCs, in this case toluene and m-xylene, was reduced in the biofilter containing the GTR. The most significant finding from this research was during the shock loading tests, where there was a reduction greater than 60% in the biofilter containing GTR, when compared to the peat-only biofilter. This demonstrates that GTR is suitable to be used as a bulking material that can increase the buffering capacity of biofilters undergoing short-term peaks in inlet concentration.

The work of Oh et al. (2009) also investigated the addition of GTR, this time to a compost media. The work also considered other adsorptive materials, including granular activated carbon (GAC). It is suggested that another benefit of adding solid adsorbents as bulking material to media can help to improve the mass transfer rate of hydrophobic VOCs from the gas to the biofilm, increasing their effectiveness. The findings of Oh et al. (2009) can relate to that of Alvarez-Hornos et al. (2011), as the major advantage of adding solid adsorptive materials to packing media as a bulking material was found to be the enhanced buffering capacity of the biofilters to different unsteady loadings. The results obtained also showed that increasing the bulking material to compost ratio too high slowed the biodegradation activity. The main conclusions from this research were that it is important to balance biodegradation activity with adsorption capacity when determining which solid waste adsorbent to mix as the bulking material and what amount. This will require understanding of the process the biofilter is being applied to, such as what is the expected range of operating conditions.

Another method to negate the impact that changing influent concentrations can have on the overall process is to add an adsorption unit before the biofilter to pretreat the inlet air. The work of Kim et al. (2007) tested a two-bed cyclic adsorption and desorption unit, which was installed before the biofilter. The contaminant being used was toluene and the adsorption beds were made using GAC. The results were mostly positive and concluded that the integrated treatment process was able to achieve the goal of coping with fluctuating toluene loading, while maintaining a high removal efficiency. This method does naturally, however, require larger area and costs.

A similar piece of research by Cai and Sorial (2009) once again used a dual-fixed adsorption system, with a two-step cycle of adsorption and desorption. This work extended on the research of Kim et al. (2007) by considering more contaminants, in this case toluene, styrene, methyl ethyl ketone, and methyl isobutyl ketone, while using activated carbon as the packing material of the adsorption beds. The results arrived at the same conclusion as that of Kim et al. (2007), and agreed that the use of cyclic beds was successful in acting as

a buffering unit for fluctuating inlet loadings. The results did however provide some new findings, and suggested that the cyclic beds may have acted as a feeding source during starvation periods (low to no inlet contaminant concentration), which would allow for an enhanced reacclimation time for the biofilter while simultaneously regenerating the adsorption beds.

Using a solid waste product as the biofilter media is a desired option for future biofiltration processes for both environmental and economic reasons. Ramirez-Lopez et al. (2010) experimented using as the media peanut shells without any previous treatment or inoculation. The peanut shells, from a local peanut factory, were available in large quantities and at low prices. The peanut shells were found to be successful for treating methanol over a 6-month period, and it was observed that they achieved good resistance to shock loads. This is most likely due to the adsorption capabilities, as there was evidence of desorption occurring at lower inlet methanol concentrations. This would have helped ensure the biodegradation rate is only required to be relatively constant throughout operation, as the desorption capability would help the process during periods of low inlet loading. When the inlet loading of contaminants decreases, it can lead to starvation of microorganisms within the biofilm. This results in an inactive area forming, which leads to inhibitors to the diffusion of contaminant from the gas phase to the biofilm when the inlet load increases again. By maintaining the carbon source, which is the contaminant, through the use of desorption at low inlet loadings, the biofilter will be more resistant to changes in operating conditions and be able to operate as desired for longer.

Other work completed by Singh et al. (2010) used wood charcoal as the media with a toluene contaminant. The wood charcoal was used in conjunction with a layer of small glass beads to improve the air distribution. The media was tested to determine the impact that adsorption would have on the effectiveness on the biofilter, and it was determined that the biodegradation was primarily responsible for the removal of toluene. It was still suggested that the adsorption capabilities may have been useful during acclimation, as it could adsorb and slowly release the toluene to the microorganisms present on the surface of the wood charcoal. From other research, it seems unlikely that the claim that the adsorption capacity of the biofilter would have been exhausted within 3 to 4 days of operation is valid, especially when considering that Singh et al. (2010) suggested the media would "slowly release the substrate," which seems to imply desorption is occurring. The final results showed successful operation under transient and high loading conditions, which again suggests that the adsorption/desorption quality of the media was able to act as a buffer, similar to other researchers' findings, such as Alvarez-Hornos et al. (2011) and Oh et al. (2009).

Sugarcane bagasse is another promising waste material that has been applied to biofilters successfully in the past. It is an agricultural waste produced as a by-product of the industrial sugar extraction process. It is commonly used as a fuel source within the plant for the boilers, however more is produced than required, which commonly builds up onsite. This makes sugarcane bagasse an inexpensive and abundant media selection. Due to its composition of approximately 50% cellulose, 25% hemicellulose, and 25% lignin, it provides suitable nutrients for microorganism growth, without being easily biodegraded. Sene et al. (2002) experimented sugarcane bagasse mixed with glass beads as the media for the biofiltration of benzene. It was tested under two different forms: raw sugarcane bagasse and ground sugarcane bagasse. The results indicate that sugarcane bagasse could be an

effective packing media, and although it was less efficient than other alternatives available, it would be a desirable selection as it is a waste product. The results of both biofilters began with a removal efficiency of almost 100% due to the initial adsorption of the contaminant to the sugarcane bagasse, which allows high efficiency during the acclimatization of the microorganisms at the startup of processes, and will help the biofilter maintain sufficient removal at periods of high inlet loading.

Other researchers compared coconut coir, compost from the digested sludge from a wastewater treatment plant, pine leaves, and peat for the biodegradation of toluene (Maestre et al., 2007). These are a mixture of commonly available agricultural wastes and naturally occurring materials, compared to commonly used media types. Coconut coir has been tried by other researchers and has been found to be suitable (Das et al., 2011). The results showed that the adsorption of toluene to coconut coir, peat, and pine leaves was more evident than the compost. It was suggested that the higher specific surface area and deeper pores portrayed in compost would result in excess biomass growth over the surface of the media, limiting the sorption capabilities of the compost. This resulted in the compost media biofilter having less resistance to transient inlet loads, although there was a larger presence of microorganisms, meaning the efficiency is highly dependent on the stability of the operating conditions. Coconut coir was found to have the highest moisture content and a high organic matter in comparison, but had a smaller pore size. The results indicated that all four of the media options tested were suitable to be used for toluene treatment and showed high elimination capacities. The best results were shown by the coconut coir, followed by the compost, in terms of the elimination capacity, pressure drop, and ability to maintain steady operating conditions. The study considered how a shut-down period of 5 days would impact the performance of the biofilter, and it was found that all biofilters were able to quickly return to their previous efficiencies after startup began. The adsorption and desorption capabilities of the media would have supplied the microorganisms with some of the desired nutrients, while the other nutrients present in the media already would have provided the rest of the nutrients desired to avoid starvation. Although all biofilters were able to return to the desired performance quickly, the results indicated that the biofilters containing compost and pine leaves had a better capacity to withstand short shutdown periods compared to the coconut coir and peat biofilters. Overall, all of the media tested were found to be robust and able to handle different conditions. Table 2.4 indicates the characteristics of the media investigated to help better understand the phenomena observed.

TABLE 2.4

Characteristics of Different Media Used for Biofiltration

Parameter	Coconut Coir	Compost	Peat	Pine Leaves
Water content (%)	78	46	73	68
Organic matter (% dry weight)	81	38	59	87
Bed porosity	0.55	0.43	0.51	0.71
Specific surface area (m ² /g)	0.75	5.12	1.21	0.23
Carbon (% dry weight)	47.32	28.65	31.62	46.42
Hydrogen (% dry weight)	5.69	3.29	3.38	5.32
Nitrogen (% dry weight)	0.52	2.87	1.17	0.57
Sulfur (% dry weight)	–	0.52	0.10	0.11
Phosphorous (% dry weight)	0.23	–	0.05	0.02

2.5 Modeling Solid Phase Adsorption

When modeling solid phase, it completely depends on the packing material being used. Some materials will have a very low adsorption capacity of the pollutant, meaning the adsorption is negligible and does not need to be considered, whereas in other cases it does. Regardless of what media is being used, the solid phase adsorption will only need to be considered for unsteady state/dynamic models, as at steady state it is irrelevant. There is far less literature covering solid phase adsorption, so less models are available for discussion, as many are able to greatly simplify the model by assuming the adsorption is negligible, while still meeting the needs of the model.

The dynamic model developed by Baquerizo et al. (2007) considers that the adsorption of the pollutant into the solid phase is only possible once the pollutant has diffused along the entire biofilm thickness. In the solid phase, it was assumed that the mass transfer coefficient was equal to that in the biofilm.

There seems to be a common gap in the ability of models to predict the solid adsorption stage of the process. This is due mostly to the ability of models to avoid the extra complexity by only considering steady state, or when modeling for a solid with a low adsorption capacity. Further experimental work should be considered to attempt to find a correlation or new method to help model different packing materials. As the pollutant comes into contact with the “carrier material,” it is no longer seen, as the accuracy of predicting the concentration decreases within the solid phase for many researchers. The “nonreactive area” identified is also an important consideration, as it shows that the biofilm can be thicker than required, which will eventually result in that portion of the biofilm “starving” and becoming inactive. As the microorganisms begin to die, they will become inhibitors of the diffusion process if the inlet concentration increases again, as previously discussed.

2.6 Conclusions and Recommendations

The adsorption capability of the media can be very beneficial for situations where the inlet load is subject to change. Although the actual biofiltration process relies on the biodegradation of the pollutant using microorganisms, adsorption will ensure that the outlet contaminant concentration does not reach dangerous levels or go over the specified target. The use of solid waste adsorbents can also provide nutrients to the microorganisms at periods of low inlet loading, as the contaminant is desorbed from the media back into the biofilm. This will ensure that the microorganisms do not starve, and the risk of a nonreactive area forming can be reduced.

The different parameters that impact the efficiency of the biofilter were discussed, such as the empty bed residence time, the moisture content, and the media properties. The focus on the media properties highlighted what characteristics are desired for the optimal biofiltration process and what to look for when selecting a suitable media. Some of the solid waste materials that have been discussed include GTR, coconut coir, and peanut shells, and each proved to be effective under the required circumstances.

The use of solid waste adsorbents in a biofiltration process can vary. Some researchers used them as a bulking material, where different mixtures of these materials were tested with other more commonly used media to see how it might impact the process, both

positively and negatively, and to arrive at the optimal ratio of solid waste adsorbent used. Other researchers used them as a pretreatment to ensure the biofilter was subjected to a fairly constant inlet loading, which used two beds utilizing the adsorption and desorption phenomena of the media. The third approach was to use a media made entirely from an adsorptive material, which also portrayed the other desired characteristics of media.

Due to the varying conditions and the many different types of VOCs that need to be treated using biofilters, there is a need for further work to determine where solid waste adsorbents can be positively utilized. The most promising application seems to be when the solid waste adsorbents are added to a commonly used media as a bulking material, but this will always require extensive testing to ensure the mixture is at the optimal composition. The ideal solid waste will vary for each application, and the choice should depend heavily on the availability of the solid waste in the surrounding area, and ensure it is the best use for it. Further consideration will be needed as to how to dispose of the solid waste adsorbents after being used in the biofiltration process, as well as what life expectancy the media can offer.

References

- Álvarez-Hornos, F. J., C. Gabaldón, V. Martínez-Soria, M. Martín, P. Marzal, and J. M. Peña-Roja. 2008. "Biofiltration of ethylbenzene vapours: Influence of the packing material." *Bioresource Technology* 99(2):269–276.
- Álvarez-Hornos, F. J., M. Izquierdo, V. Martínez-Soria, J. M. Peña-Roja, F. Sempere, and C. Gabaldón. 2011. "Influence of ground tire rubber on the transient loading response of a peat biofilter." *Journal of Environmental Management* 92(8):1978–1985.
- Álvarez-Hornos, F. J., C. Gabaldón, V. Martínez-Soria, P. Marzal, and J.-M. Peña-Roja. 2009. "Mathematical modeling of the biofiltration of ethyl acetate and toluene and their mixture." *Biochemical Engineering Journal* 43(2):169–177.
- Álvarez-Hornos, F. J., C. Gabaldón, V. Martínez-Soria, P. Marzal, and J.-M. Peña-Roja. 2008. "Biofiltration of toluene in the absence and the presence of ethyl acetate under continuous and intermittent loading." *Journal of Chemical Technology & Biotechnology* 83(5):643–653. doi: 10.1002/jctb.1843.
- Baquerizo, G., X. Gamisans, D. Gabriel, and J. Lafuente. 2007. "A dynamic model for ammonia abatement by gas-phase biofiltration including pH and leachate modelling." *Biosystems Engineering* 97(4):431–440.
- Cai, Z., and G. A. Sorial. 2009. "Treatment of dynamic VOC mixture in a trickling-bed air biofilter integrated with cyclic adsorption/desorption beds." *Chemical Engineering Journal* 151(1–3):105–112.
- Chen, L., and S. J. Hoff. 2009. "Mitigating odors from agricultural facilities: A review of literature concerning biofilters." *Applied Engineering in Agriculture* 25(5):751–766.
- Das, C., R. Chowdhury, and P. Bhattacharya. 2011. "Experiments and three phase modelling of a biofilter for the removal of toluene and trichloroethylene." *Bioprocess and Biosystems Engineering* 34(4):447–458. doi: 10.1007/s00449-010-0487-6.
- Delhoménie, M. C., and M. Heitz. 2005. "Biofiltration of air: A review." *Critical Reviews in Biotechnology* 25(1):53–72.
- Devanny, J. S., and J. Ramesh. 2005. "A phenomenological review of biofilter models." *Chemical Engineering Journal* 113(2–3):187–196.
- Dorado, A. D., J. Lafuente, D. Gabriel, and X. Gamisans. 2012. "Biomass accumulation in a biofilter treating toluene at high loads—Part 2: Model development, calibration and validation." *Chemical Engineering Journal* 209:670–676.

- Fulazzaky, M. A., A. Talaiekhozani, M. Ponraj, and M. Z. Abd Majid. 2014. "An overview of biofiltration modeling."
- Ho, K.-L., Y.-C. Chung, Y.-H. Lin, and C.-P. Tseng. 2008. "Biofiltration of trimethylamine, dimethylamine, and methylamine by immobilized *Paracoccus* sp. CP2 and *Arthrobacter* sp. CP1." *Chemosphere* 72(2):250–256.
- Kim, D., Z. Cai, G. A. Sorial, H. Shin, and K. Knaebel. 2007. "Integrated treatment scheme of a biofilter preceded by a two-bed cyclic adsorption unit treating dynamic toluene loading." *Chemical Engineering Journal* 130(1):45–52.
- Lebrero, R., E. Rodríguez, P. A. García-Encina, and R. Muñoz. 2011. "A comparative assessment of biofiltration and activated sludge diffusion for odour abatement." *Journal of Hazardous Materials* 190(1–3):622–630.
- Maestre, J. P., X. Gamisans, D. Gabriel, and J. Lafuente. 2007. "Fungal biofilters for toluene biofiltration: Evaluation of the performance with four packing materials under different operating conditions." *Chemosphere* 67(4):684–692.
- Metcalf & Eddy Inc., G. Tchobanoglous, H. D. Stensel, R. Tsuchihashi, and F. Burton. 2013. *Wastewater Engineering: Treatment and Resource Recovery*. New York: McGraw-Hill Education.
- Mudliar, S., B. Giri, K. Padoley, D. Satpute, R. Dixit, P. Bhatt, R. Pandey, A. Juwarkar, and A. Vaidya. 2010. "Bioreactors for treatment of VOCs and odours—A review." *Journal of Environmental Management* 91(5):1039–1054.
- Nikiema, J., G. Payre, and M. Heitz. 2009. "A mathematical steady state model for methane bioelimination in a closed biofilter." *Chemical Engineering Journal* 150(2–3):418–425.
- Oh, D. I., J. Song, S. J. Hwang, and J. Y. Kim. 2009. "Effects of adsorptive properties of biofilter packing materials on toluene removal." *Journal of Hazardous Materials* 170(1):144–150.
- Raghuvanshi, S., and B. V. Babu. 2009. "Experimental studies and kinetic modeling for removal of methyl ethyl ketone using biofiltration." *Bioresource Technology* 100(17):3855–3861.
- Ramirez-Lopez, E. M., J. Corona-Hernandez, F. J. Avelar-Gonzalez, F. Omil, and F. Thalasso. 2010. "Biofiltration of methanol in an organic biofilter using peanut shells as medium." *Bioresource Technology* 101(1):87–91.
- Rene, E. R., S. Kar, J. Krishnan, K. Pakshirajan, M. Estefanía López, D. V. S. Murthy, and T. Swaminathan. 2015. "Start-up, performance and optimization of a compost biofilter treating gas-phase mixture of benzene and toluene." *Bioresource Technology* 190:529–535.
- Ryu, H. W., K.-S. Cho, and D. J. Chung. 2010. "Relationships between biomass, pressure drop, and performance in a polyurethane biofilter." *Bioresource Technology* 101(6):1745–1751.
- Sene, L., A. Converti, M. G. A. Felipe, and M. Zilli. 2002. "Sugarcane bagasse as alternative packing material for biofiltration of benzene polluted gaseous streams: A preliminary study." *Bioresource Technology* 83(2):153–157.
- Shareefdeen, Z., A. A. Shaikh, and Adeeb Ahmed. 2009. "Steady-state biofilter performance under non-isothermal conditions." *Chemical Engineering and Processing: Process Intensification* 48(5):1040–1046.
- Shareefdeen, Z., and A. Singh. 2005. *Biotechnology for Odor and Air Pollution Control*. Berlin: Springer.
- Singh, K., R. S. Singh, B. N. Rai, and S. N. Upadhyay. 2010. "Biofiltration of toluene using wood charcoal as the biofilter media." *Bioresource Technology* 101(11):3947–3951.
- Yang, C., H. Chen, G. Zeng, G. Yu, and S. Luo. 2010. "Biomass accumulation and control strategies in gas biofiltration." *Biotechnology Advances* 28(4):531–540.



Taylor & Francis

Taylor & Francis Group

<http://taylorandfrancis.com>

3

Carbon Dioxide (CO₂) Capture from Industrial Flue Gas: A Review

Dipa Das and B. C. Meikap

CONTENTS

3.1	Introduction	35
3.2	Carbon Dioxide (CO ₂) Capture Technology.....	36
3.2.1	Postcombustion Capture.....	36
3.2.2	Precombustion Capture	37
3.2.3	Oxy-Fuel Combustion	38
3.3	CO ₂ Separation Technology.....	38
3.3.1	Adsorption.....	40
3.3.1.1	Physical Adsorption	40
3.3.1.2	Chemical Adsorption	43
3.4	Effect of Amine Functional Groups, and Structural Properties of Adsorbents on CO ₂ Adsorption	47
3.5	Advantages and Disadvantages of Adsorption.....	48
3.6	Treatment and Disposal of Spent Adsorbent (Activated Carbon)	49
3.7	Conclusions.....	49
	References.....	50

3.1 Introduction

Rapid industrialization and lots of human activities cause the emission of greenhouse gas to the atmosphere. Global warming and climate change are the two main effects due to more concentration of greenhouse gases in the atmosphere. To control the greenhouse gas emission and the public concern about this issue, a meeting was organized in 1992 by the United Nations Framework Convention on Climate Change (UNFCCC). The main purpose and objective of the meeting were to discuss methods for stabilization of greenhouse gas concentration in the atmosphere at a level that the climate system was not affected by anthropogenic emission. Outgoing infrared radiation from the earth atmosphere is getting absorbed by the greenhouse gas like methane, carbon dioxide (CO₂), water vapor, and other gases by which earth's temperature increases (Solomon, 2007). Due to an increase in the level of greenhouse gas, various effects like rise in the sea level, ocean storms, and severe flooding occur. The Intergovernmental Panel on Climate Change (IPCC) predicts that by the year 2100, the CO₂ concentration of the atmosphere will reach up to 570 ppm by which the mean temperature of the earth surface rises to around 1.9°C and the mean sea level increases by 3.8 m. The most important greenhouse gas (GHG) is CO₂. Most of the gas emitted to the atmosphere is from the combustion of fossil fuel, which is the main energy

source. Most of the energy demand is supplied by fossil fuels like coal, oil, and natural gas. The total CO₂ emission from coal-fired power plant is nearly 40% (Yang et al., 2008). There are different approaches to mitigate global climate change. They are improving energy efficiency and conservation; using renewably energy like solar, wind, hydropower and bioenergy; using fuels such as natural gas, hydrogen, or nuclear power; geoengineering approaches; and carbon capture and storage (CCS). Among the different methods, CCS can reduce CO₂ emissions (85%–90%) from large point emission sources (Leung et al., 2014). CO₂ separation cost is much more than the total cost of carbon capture and storage (Selma et al., 2014). To minimize the cost regarding growing demand for energy, a cost-effective technique for CO₂ capture from the flue gas followed by sequestration is to be found (Gupta et al., 2003). Available CO₂ separation technologies are absorption, adsorption, membrane separation, and cryogenic distillation. Among this, solid adsorption processes are suggested to overcome the problems arising due to the absorption process (Sayari et al., 2011). The main focus of this chapter is based on the capture of CO₂ by using solid sorbents and modification of the sorbents by impregnation or grafting of amines solution.

3.2 Carbon Dioxide (CO₂) Capture Technology

A large amount of CO₂ emits from fossil fuel-based power plants, and then it goes to the environment. So it should be separated and captured before sequestration. Capturing CO₂ from flue gases is the most important parameter for carbon management. Capture processes are based on the following technologies.

- Postcombustion capture
- Precombustion capture
- Oxy-fuel combustion

3.2.1 Postcombustion Capture

Figure 3.1 shows the postcombustion capture from flue gas, which comes from combustion of fossil fuels from thermal power plants. Postcombustion CO₂ capture is applicable mainly for pulverized coal (PC), oil or gas-fired power plants, but it can also be applied to cases of natural gas combined cycle (NGCC) (Zaman and Lee, 2013) flue gas capture. The concentration of CO₂ in a coal-based power plant is 7%–8% and 13%–15% from power plant flue gas. For natural gas plants, thermal efficiency is higher in the case of postcombustion

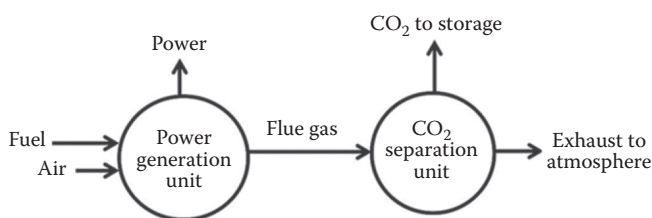


FIGURE 3.1

Principle of postcombustion CO₂ capture.

capture than precombustion technology (Blomen et al., 2009; Damen et al., 2006; Figueroa et al., 2008; Gibbins and Chalmers, 2008). Postcombustion capture is used for separation of CO₂ from a flue gas stream of low concentration of CO₂ capture (4%–15% by volume), and the regeneration energy to release CO₂ is more (Mondal et al., 2012). The volume of gas is more, so equipment sizes have to be very large. Capital costs are high. As CO₂ concentrations are low, to carry out regeneration for release of CO₂, powerful chemical solvents are used and it requires a large amount of energy. By taking into consideration different separation technologies like chemical absorption, gas separation, membranes, and low temperature distillation are used.

3.2.2 Precombustion Capture

Figure 3.2 represents precombustion capture from flue gas. In the precombustion process, fuel is reacted with air or oxygen to form carbon monoxide (CO) and hydrogen (H₂) by means of the process called gasification. The CO and H₂ mixture is passed through a catalytic reactor called the shift convertor, where CO reacts with steam to form CO₂ and a higher amount of H₂. CO₂ is separated, and H₂ is used as fuel in gas turbine combined-cycle plant.

Typical reactions are



In precombustion capture, the transformation of carbon fuel to carbon-less fuel occurs. The CO₂ concentration and pressure are much higher in this type of capture process than that of postcombustion capture. The capture equipment for CO₂ is small, and solvents like rectisol and selexol are used (Mondal et al., 2012). CO₂ can be dissolved when the pressure is high, and when the pressure is reduced it gets released. No heat is required for the regeneration process, and CO₂ is released at above the atmospheric pressure. So the regeneration cost is very low (Figueroa et al., 2008). Physical absorption can be used due to high partial pressure. One disadvantage of this technology is the capital cost of generating the facility is very high.

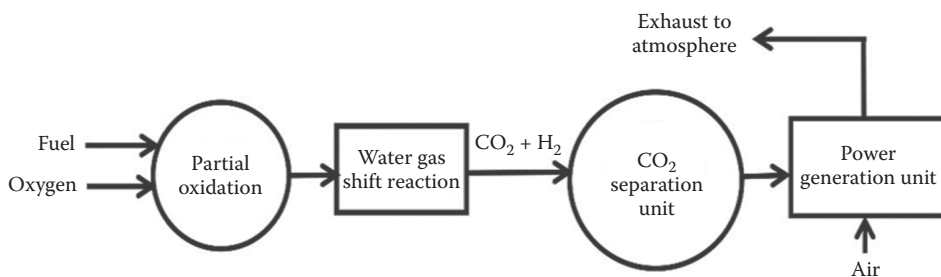


FIGURE 3.2
Principle of precombustion CO₂ capture.

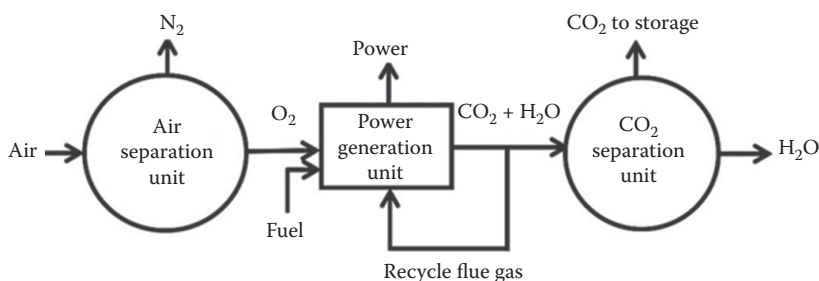


FIGURE 3.3
Principle of oxy-fuel combustion CO₂ capture.

3.2.3 Oxy-Fuel Combustion

Figure 3.3 represents oxy-fuel combustion capture from flue gas. In oxy-fuel combustion, the combustion of fuel occurs in the presence of pure oxygen instead of air. As a result, a high concentration of CO₂ is present in the flue gas. So simple purification is required. For high purity of oxygen, cryogenic separation is used. This high purity oxygen is mixed with recycle flue gas to maintain the combustion condition similar to the air-fired configuration, and then fed to the combustion chamber, because the material of construction cannot withstand high temperature resulting from the coal combustion in the presence of pure oxygen. Depending upon the fuel and process used, the CO₂ concentration varies from 70% to 95%. In oxy-fuel combustion, carbon capture cost is less due to higher concentration of CO₂. NO_x is not formed as pure oxygen is used. So compared to an air-fired unit, 60% to 70% of NO_x is reduced (Blomen et al., 2009). Less CO₂ compression energy is required due to the operation at high pressure. Oxy-fuel combustion is mainly based on the physical separation process for O₂ capture and CO₂. No solvents are used, so operating costs are reduced and no environmental disposal problems arise related to solid and liquid waste. The products from oxy-fuel combustion are CO₂ and water vapor. CO₂ is separated and water is easily removed by condensation at relatively low cost. The main disadvantage of this process is that the cost of recycling flue gas is very high. To withstand high temperature, the cost of material of construction should be high. Due to the large amount of oxygen needed, the power requirement for the cryogenic air separation is very high and the capital cost is also very high.

3.3 CO₂ Separation Technology

Figure 3.4 shows the classification of CO₂ separation technology. Various technologies are available for CO₂ separation from fossil fuel combustion power plants. They are absorption, adsorption, membrane separation, and cryogenic distillation. Among which, separation of CO₂ by adsorption techniques is very cost effective. A detailed description of adsorption separation is described in the following sections.

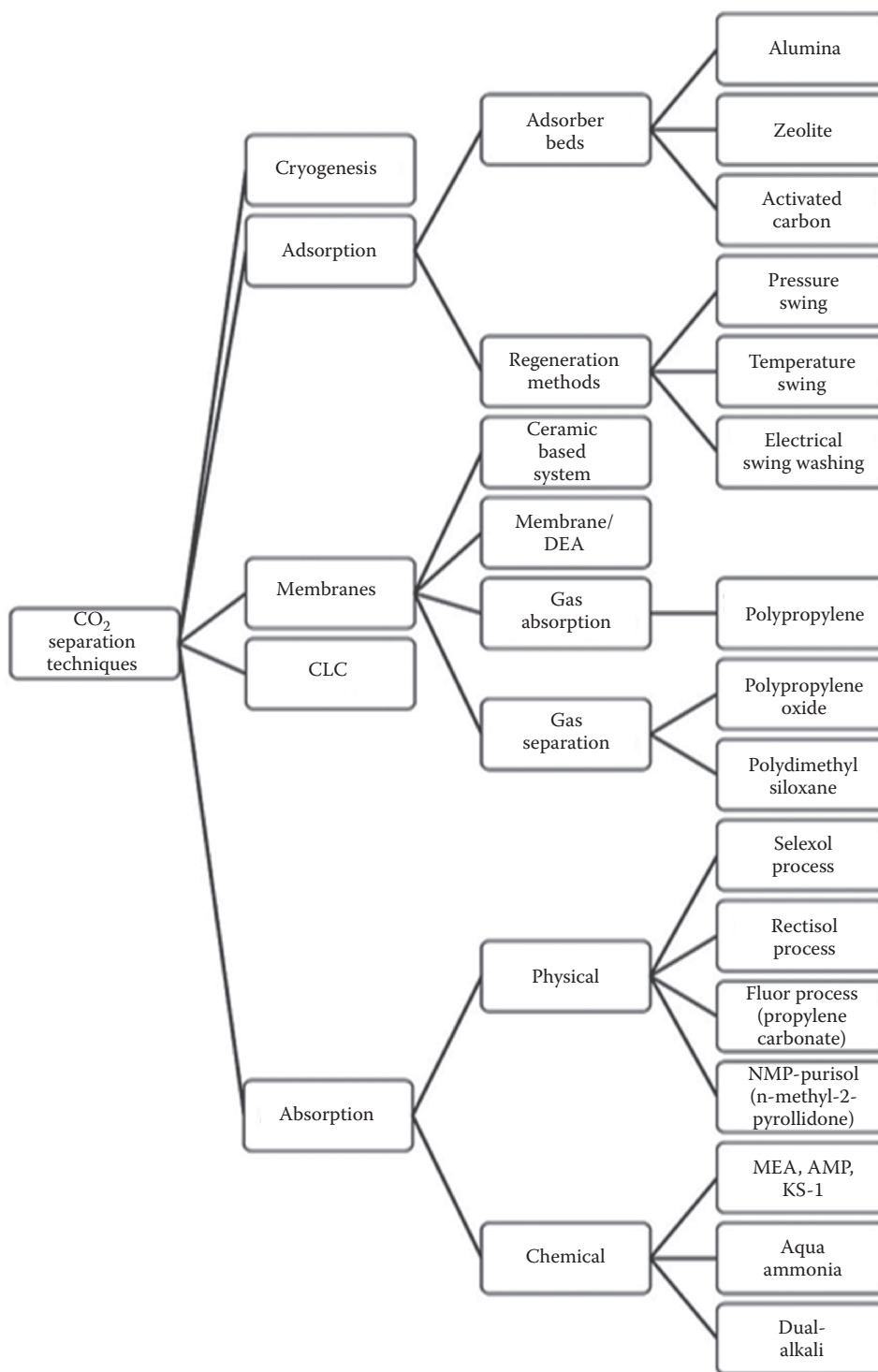


FIGURE 3.4
Classification of CO₂ separation techniques.

3.3.1 Adsorption

Adsorption is defined as the process by which molecules contained in the liquid and gaseous mixture adhere to the solid surface (i.e., the adsorbent) until equilibrium is reached. Adsorption is a surface-based process where a film of adsorbate is created on the surface. Adsorption is generally classified into physisorption (weak van der Waals force) and chemisorption (covalent bonding). It can also be caused by electrostatic attraction. Adsorption and regeneration are the two steps of the adsorption process operated on a repeated cycle. The advantages of the adsorption process are low regeneration energy requirements and no liquid waste. The process can be operated from ambient temperature to 700°C (Harrison, 2004). The advantages of an adsorption process are high as compared to absorption. Adsorption is the most important technique for CO₂ capture at an industrial scale (Drage et al., 2009; Metz et al., 2005). The adsorption phenomena is affected by the adsorbed properties of particles like molecular weight, molecular size, and polarity, and also depends on pore spacing, pore size, and polarity of the adsorbent. Fixed bed, moving bed, and fluidized beds are the three types of adsorption beds. The adsorbents are filled inside a packed column, and flue gas that contains CO₂ is passed through the column. CO₂ gas molecules attach to the adsorbent and get adsorbed on the surface of the adsorbent. To get CO₂ in pure form and to regenerate the adsorbents, desorption takes place. The fresh adsorbent can be reused further. The gases can be adsorbed on the surface of the adsorbent by a single layer and multiple layers depending on surface force, temperature, adsorbent pore sizes, and partial pressure (Meisen and Shuai, 1997).

3.3.1.1 Physical Adsorption

Physical adsorption is also called physisorption and it is based on weak Van der Waals forces. In this case the electronic structure of the atom or molecule is not much disturbed upon adsorption. In physical adsorption, no chemical bond is formed, and at high pressure CO₂ is separated by solid adsorbents from flue gas. The adsorbent materials can capture CO₂ even if at very low concentrations and by changing the pressure. By steam stripping, the process can be reversed. The major physical adsorbents reported for CO₂ adsorption from flue gas are porous carbonaceous material, zeolite, alumina, silica gel, molecular sieve, and metal-organic frameworks. The structural properties of the adsorbents are shown in Table 3.1.

TABLE 3.1

Structural Properties of Adsorbents

Adsorbents	Pore Size (nm)	Pore Volume (cm ³ g ⁻¹)	Specific Surface Area (m ² g ⁻¹)	Reference
AC	1.5–2.2	0.6–0.8	1300	Na et al., 2001
CNT	8.9	0.91	394	Lu et al., 2008
NaX	1	0.201	508	Zhang et al., 2008
Zeolite 13X	1.1	0.454	515	Bezerra et al., 2011
Silica gel KC	2	0.35	750	Berlier and Frere, 1997
MCM-41	3.6	1.03	11.38	Franchi et al., 2005
SBA-15	21		200–300	Gray et al., 2005
PMMA	17	1.2	470	Filburn et al., 2005

The main operating parameters for the adsorption process are operating pressure, temperature, adsorbent pore size, and surface forces. With higher partial pressure of CO₂ and lower temperature, the capacity of the adsorption process increases. The main advantages of physical adsorptions are low time for regeneration and low heat of adsorption of CO₂. Also high selectivity materials for CO₂/N₂ are required and H₂O adsorption is preferred over CO₂ adsorption (Miller, 2011). In this type of adsorption, drying of flue gas must be done before contact with the physical adsorbent.

Carbon-Based Material

Carbon-based material have high surface area, low cost, and are easy for surface functionalization and pore structure modification. The regeneration of the sorbents is easier. Carbon-based material adsorbents are sensitive to temperature, and their selectivity is relatively poor. So less CO₂ adsorption on carbon materials occurs. The selectivity for CO₂ over N₂ gas is very good. Due to the presence of hydrophobic core in the adsorbent material, it is very efficient for CO₂ capture (Parshetti et al., 2015).

Activated Carbon

Activated carbon materials are widely used due to their large area surface and high CO₂ adsorption capacity (Plaza et al., 2010). Activated carbon can be converted into different shapes like monolith, bead, fiber, and granular (Shen et al., 2010). It is resistant to water and cheaper than zeolites. The CO₂ adsorption capacity for porous activated carbon decreases with the increase in temperature (Berlier and Frere, 1996; Do and Wang, 1998). At low partial pressures of CO₂, as water gets completely absorbed by activated carbon, the capacity to adsorb CO₂ decreases (Wang, 2008). The CO₂ adsorption capacity decreases in the presence of contaminants in the flue gas. So researchers have focused on improving CO₂ adsorption capacity and selectivity. Modified carbon adsorbents are single-walled carbon nanotubes (Cinke et al., 2003), multiwalled carbon nanotubes (Su et al., 2009), ordered mesoporous carbon (Saha and Deng, 2010), microporous carbon, and graphene (Ghosh et al., 2008). The big challenges in applying activated carbon materials are related to their long-term stability, regeneration ability, kinetics analysis, energy input, environmental impacts, and their capability in real flue gas conditions. Rashidi and Yusup (2016) studied the activated carbon production via the chemical and physical approach for the CO₂ adsorption at an ambient pressure and low temperature (<100°C). The ability to tune and design activated carbon materials to achieve superior CO₂ separation from flue gas in the postcombustion field makes these carbon materials outstanding compared to other adsorbents, apart from their lower preparation costs.

Carbon Molecular Sieves

CNTs are a type of microporous carbon material. Due to its unique textural characteristics, it is studied for CO₂ capture. Its pore size distribution (PSD) is narrow. It also contains pore mouths of molecular size for gas separation. The micro pore volume is high. These features help to increase capacity and selectivity (Foley, 1995).

Carbon Nanotube-Based Solid Sorbent

Carbon nanotubes (CNTs) are the new generation materials for separation of gas mixtures. CNTs are suitable adsorbents for CO₂ separation and sequestration (Huang et al., 2007; Razavi et al., 2011). CNTs are classified as single-walled carbon nanotubes (SWCNTs) and multiwalled carbon nanotubes (MWCNTs). CNTs are a sheet of graphite that has been rolled into a tube. They possess excellent adsorption ability. CNTs exhibit similar or higher

adsorption capacity than silica-based sorbents or macroporous resins. CNTs usually have a diameter within a tenth to tens of nanometers and a length of up to centimeters and the ends capped by a fullerene-like structure. They exhibit limited solubility. CNTs allow a strong interaction with organic molecules via noncovalent forces. The presence of functionalized carbon nanotubes allows interactions, which increase the selectivity and the stability of the system.

Zeolites

Zeolites are physical adsorbents for CO₂ capture. They have high surface area and a crystalline structure. The pore structures are three dimensional. Their adsorption capacities are largely affected by their charge density, pore size, and chemical composition of cations in their porous structures (Wang et al., 2011). Zeolites have high hydrophilic character, which results in the decrease of CO₂ adsorption capacity when moisture is present in gas. So a higher regeneration temperature is needed. The temperature may be above 300°C.

Metal-Organic Frameworks (MOFs)

Metal-organic frameworks (MOFs) have high surface area; their pore structures are controllable, have tunable pore surface properties, and can be easily adjusted by changing the metallic clusters or the organic ligands. CO₂ capture at room temperature was first reported by Yaghi's group (Millward and Yaghi, 2005). New types of MOFs for CO₂ capture was developed after that (Banerjee et al., 2008; Wang et al., 2008). The progress of MOFs for CO₂ capture from experimental to molecular simulation was reviewed by Zhou's group (Kuppler et al., 2009; Li et al., 2009). In their review, MOFs showed an exceptional CO₂ adsorption capacity to deal with pure CO₂ at high pressures. When exposed to a gas mixture, adsorption capacities are reduced. Carbonaceous and MOF materials exhibit relatively higher CO₂ adsorption capacity. The operations are at low temperatures and high pressures. Due to abundant surface OH groups of silica materials, they can facilitate chemical modification to improve their CO₂ adsorption capacity and selectivity, and have lower adsorption capacity and selectivity toward CO₂, so that they can be used to treat a flue gas with low CO₂ partial pressure.

Graphene-Based Material

Graphene is a type of synthetic carbon allotrope that has many superior properties. Before 2011, graphite/graphene was not developed for CO₂ capture. Due to the high specific surface area and low cost of production, lots of effort has been made to explore its application in CO₂ capture. The three aspects of graphite-/graphene-based materials for CO₂ capture are based on the formation of new structures, modification of the surface by a suitable functional group, and synthesis of hybrid materials (Wang et al., 2014). Graphene or its derivatives are suitable for CO₂ adsorption (Ghosh et al., 2008). Graphene has high mechanical strength, excellent thermal conductivity, good chemical stability, large surface area, and wide porosity. Addition of the surface functional group leads to advanced CO₂ adsorbents for next-generation adsorption (Balasubramanian and Chowdhury, 2015; Chowdhury and Balasubramanian, 2016). Due to the hydrophobic nature of the 3D graphene material, it was used for capturing CO₂ from wet flue gas. Due to a strong van der Waals force between the large and planar basal planes of graphene material, it has the tendency to form agglomerates and also behaves as particulate graphite platelets. Due to agglomeration, there is a decrease of the high surface area graphene sheets (Jiang and Fan, 2014). The introduction of nanopores into graphene sheets has been identified as one of

the most effective methods to improve the adsorption performance of graphene materials (Ning et al., 2012; Yuan et al., 2014). At high pressures, graphene nanomesh is a novel type of graphene structure with pores and excellent adsorbent material for capture of CO₂. Graphene nanosheet material is used as advanced solid adsorbents for postcombustion CO₂ capture. When graphene is heated at 800°C under N₂ atmosphere for 2 h, it showed the highest surface area of 484 m²g⁻¹ and largest pore volume of 0.68 cm³g⁻¹ with a narrow distribution of pores leading to a high CO₂ capacity of 2.19 mmol g⁻¹. High CO₂/N₂ adsorption selectivity is at 25°C and 1 bar. Highly ordered graphene layers with interconnected hierarchical pore networks are used for enhanced CO₂ removal from power plant exhaust and large industrial sources (Chowdhury and Balasubramanian, 2016).

3.3.1.2 Chemical Adsorption

In chemical adsorption, a chemical bond is formed by the gas molecule on the adsorbent surface to form surface compounds. The reaction is reversible, and it is defined as the process in which chemical reaction is occurring at the exposed surface. The reaction can be reversed at high temperature. Immobilization of the sorbent on the solid support surface forms a solid regenerable sorbent by different chemicals like amines, sodium carbonates, and potassium carbonates. Alumina or silica is a high surface area support material. Polyethylenimine (PEI) and an amine sorbent called molecular basket sorbent (MBS) have high selectivity and sorption capacity for CO₂. The major advantages of this process are high stability during the adsorption and desorption cycles, high adsorption and desorption rates, good regeneration, and low energy consumption. This process is implemented for the temperature swing adsorption process, which produces pure CO₂ and water, and can be further separated by compression and cooling. Chemical adsorbents have a high heat of reaction with CO₂. The recovery of heat from an adsorbent is more difficult than that from a liquid solvent. Different chemical adsorbents are metal oxide (CaO, MgO), hydrotalcite, double salt and metal salt from alkali metal compounds like lithium silicate, lithium zirconate, to alkaline earth metal compound (Helwani et al., 2012; Lee et al., 2012). Physisorbents such as zeolites, ACs, CMSs, and CNTs suffer from low CO₂ adsorption capacities at relatively low CO₂ partial pressure and lower selectivity toward CO₂. Surface modification is done by incorporating a basic group on the porous materials that strongly interacts with acidic CO₂, and CO₂ adsorption capacity increases. Modifying functional groups are alkaline carbonates and various amine groups for high selectivity of CO₂. The sorbents can be classified as natural sorbents and synthetic sorbents. Natural sorbents are CaCO₃, NaHCO₃, and MgCO₃. The reaction kinetics of these sorbents is high and they have low cost. Synthetic sorbents are LiZrO₃, LiSiO₄, and K₂CO₃. They have lower carbonation kinetics, and production costs and durability are high (Lee et al., 2012). There are two types of sorbents: high temperature sorbents (CaCO₃, 930°C) and low temperature sorbents (NaHCO₃, 120°C–170°C; K₂CO₃, 70°C–140°C). The more suitable for the capture process are high temperature sorbents. The materials are Al₂O₃, activated carbons, TiO₂, MgO, ZrO, and SiO₂ (Kim et al., 2012; Lara et al., 2009; Lee et al., 2006, 2011).

Lithium-Based Sorbents

Lithium zirconates (Iwan et al., 2009; Ochoa-Fernandez et al., 2006) and lithium silicate (Essaki et al., 2004) are found to be suitable for CO₂ capture because absorption based on these materials can be operated as temperature swing adsorption (TSA), and the operating temperature is nearer to the syngas temperature. In the temperature range of 450°C to 590°C, the reaction of lithium zirconate is reversible. So the absorbent can be regenerated

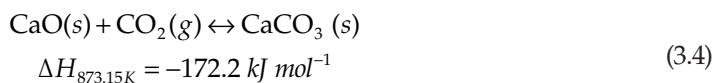
during TSA. Lithium silicate-based technology is one of the competing CO₂ capture technologies, due to its large capacity, high rates of absorption, operating temperature range, good stability, and attrition resistance.

Potassium-Based Sorbents

Various studies have been conducted using dry potassium-based sorbents (Lee et al., 2009) at Kyungpook National University (KNU). The Korea Electric Power Research Institute (KEPRI) and Korea Institute of Energy Research (KIER) have also tested absorption and regeneration properties of K₂CO₃ and support materials such as activated carbons, TiO₂, Al₂O₃, MgO, SiO₂, and zeolites (Kim et al., 2012). Several advantages of the potassium-based sorbent process are steady operation, good gas–liquid contact for sorbent particles, and good control of carbonation temperature.

Calcium-Based Sorbents

Calcium-based materials are good adsorbents for capturing CO₂ due to their high reactivity with CO₂, high capacity, and low material cost (Florin and Harris, 2009). The reversible reaction between CaO and CO₂, as shown in the following reaction (3.4), offers great potential for reducing CO₂ from various clean energy systems, such as precombustion carbon capture from gasification processes and postcombustion carbon capture from zero emission coal (ZEC) processes. The carbonation temperature for CaO-based adsorbents is between 600°C and 700°C, and the regeneration temperature is normally above 950°C (Steenneveldt et al., 2006).



The carbonation reaction (3.4) is highly exothermic and it is possible to efficiently recover the large amount of energy released during the CO₂ capture. Preliminary economic analyses suggest that this process is economically attractive because limestone (CaCO₃) is abundant and inexpensive when used at the industrial scale. Despite the simple chemistry involved, the main problem for calcium-based materials is the loss of reversibility for the carbonation reaction due to the sintering of the adsorbent particles. This is because the carbonation process is highly exothermic. CO₂ adsorption capacity of different solid sorbents is shown in Table 3.2.

Amine-Functionalized Solid Sorbents

The solid sorbents with the amine-functionalized group are formed when microporous or mesoporous materials are loaded with basic nitrogen functionality. There are three types of supported amine sorbents (Jones, 2011; Li et al., 2010):

1. Amine loading by impregnation method into the porous support of the sorbents.
2. Amine and amine-containing silane is covalently attached to a solid support, that is, binding amines to oxides via the use of silane chemistry.
3. A hybrid of the other two classes (Li et al., 2010). In this case, supported adsorbents are based on porous supports upon which amino polymers are polymerized in situ.

Amine-Based Solid Sorbents

Some organics or polymers containing the NH_x group can attract toward acidic CO₂ molecules by forming a chemical bond, and thus they are suitable for CO₂ capture at low

TABLE 3.2CO₂ Adsorption Capacity of Different Solid Sorbents

Adsorbent	Temperature (K)	Pressure, P _{CO₂} (atm)	Capacity (mmol g ⁻¹)	Process	Reference
AC	298	1	2.07	PSA	Kikkinides et al., 1993
AC	298	0.1	0.57	GC-TCD	Wong and Bioletti, 2002
Bamboo-derived AC	275	2	3.00	Volumetric analysis	Berlier and Frere, 1996
Anthracite-based AC	303	1	1.38	TGA	Maroto-Valer et al., 2005
SWNT	308	1	2.07		Cinke et al., 2003
Graphene	195	1	0.80		Ghosh et al., 2008
CMS	303	1	2.43		Burchell et al., 1997
Zeolite 13X	298	1	4.66		Cavenati et al., 2004
Silicate	303	0.15	0.48	Calorimeter-volumetric apparatus	Dunne et al., 1996
Molecular sieve 13X	293	0.15	2.18		Kamiuto and Abe, 2002
Molecular sieve 5A		0.1	2.33	Fluidized bed	Lee et al., 2004
Mordenite	290	1	1.8		Hernández-Huesca et al., 1999
HY-5	295	1	1.13		Harlick and Tezel, 2004
Erionite	290	1	2.8		Hernández-Huesca et al., 1999

reaction temperatures. Aqueous amines like methyl diethanolamine (MDEA), diethanolamine (DEA), and monoethanolamine (MEA) have been used for CO₂ removal from flue gas by absorption and believed to be a suitable technology (Jones, 2011; Rochell, 2009). Amine is corrosive in nature, due to which the drawbacks like fouling of the process equipment occurs and this process requires high regeneration energy (Mandal and Bandyopadhyay, 2006). To avoid the disadvantages associated with the liquid amine, various efforts have been made by immobilizing organic amines on certain support materials for the preparation of amine-based solid adsorbents (Lee et al., 2008; Schladt et al., 2007; Siriwardane et al., 2001). Methods used for the improvement of the CO₂ capture of amine-based solid adsorbents are amine immobilization, high amine loading support, generation of high amine density sorbent (i.e., impregnation), postsynthesis grafting, and direct condensation and hydrolysis methods. The advantages of adsorbents of solid amine are lower capital cost, low energy consumption for regeneration, and low gas recovery pressure (Khatri et al., 2006). The supports should have high mechanical strength, high surface area, proper porosity, hydrothermal stability, and a good affinity for the amine molecules. Materials that are porous are preferred due to their high surface areas and large pore size and volume compared to carbon, silica, polymers such as resin, metal oxides, and glass. Microporous materials and nonporous material are rarely selected for this purpose. The main advantage of mesoporous silicas (SBA-15, MCM-41, etc.) is their “silane chemistry”; that is aminosilanes can react with the silica surface via alkyl–silyl linkages by which

amine molecules are loaded onto the supports. The reaction of carbon surface carboxylic groups with halogenated amine molecules is also reported (Gray et al., 2004) and carbon surface carboxylic groups are suitable to aqueous media. Different amines treated for CO₂ captures are monoamino polymers such as polyethyleneimine (PEI), di- and triaminosilanes, alkanolamines (Chew et al., 2010), and hyperbranched amino silica (Hicks et al., 2008). Molecules that contain multiple amine groups and having higher amino group densities are superior. On triaminosilane/SBA-15, the CO₂ capture capacity is 2.4–2.7 mmol g⁻¹ at 60°C (Chang et al., 2009), and on TRI-PE-MCM-41, the CO₂ capture capacity is a value of 2.65 mmol g⁻¹ at 25°C (Harlick and Sayari, 2007). In tetraethylenepentaamine (TEPA)-grafted mesocellular silica foam (MSF), the CO₂ capture capacity is as high as 4.5 mmol g⁻¹ adsorbent and was achieved at 75°C (Liu et al., 2010) and also for polyethyleneimine-coated glass (Liang et al., 2008) synthesized in various generations (G₀, G₁, G₂, G₃, and G₄) of melamine-based dendrimers on SBA-15. The highest CO₂ capture capacity observed was 5.55 mmol g⁻¹ on hyperbranched amino silica (HAS) on SBA-15 at 25°C (Hicks et al., 2008), and there formation is by polymerization of aziridine on SBA-15 (Drese et al., 2009). By impregnation techniques, amine samples are prepared and have high loading. It is not good for recycling. Grafting of aminosilane molecules onto silica-based supports takes place in anhydrous solutions to reduce self-polymerization behavior of the aminosilane molecules in the postsynthesis grafting method (Simon et al., 2002). In the direct condensation and hydrolysis method, the amino groups can be incorporated into the matrix of the synthesized material and includes an aminosilane, a surfactant (template), and the silica precursor that are mixed and reacted directly. Bis((triethoxysilyl)propyl)ethylenediamine (BTEPED) was incorporated into a porous silica, and a CO₂ capture capacity of 2.3 mmol g⁻¹ was obtained in a recent work (Tang and Landskron, 2010). The amino groups that are used for capture of CO₂ molecules are trapped in the silica matrix. Grafted amines with CO₂ are similar to that between amines in aqueous solution and CO₂ (Vaidya and Kenig, 2008). Due to the presence of H₂O, the formation of bicarbonate and carbonate occurs. So there is consumption of more CO₂ molecules, by which CO₂ capture capacity increases. That is why moisture can be tolerated by CO₂ adsorbents, and CO₂ capture occurs due to the presence of moisture (Schladt et al., 2007). Since the reaction runs at a fast rate, the CO₂ capture process is getting faster. Below 140°C and under atmospheric pressure, degradation of aqueous alkanolamines occurs (Lepaumier et al., 2009).

Amine-Functionalized Activated Carbonaceous Materials

The adsorption capacity of carbonaceous materials can be improved by the incorporation of amine functional groups into their porous structure. The CO₂ adsorption capacity for different amine-supported solid sorbents is shown in Table 3.3.

Activated carbons, biochar, fly ash containing unburnt carbon, CNTs, and solid resins are carbonaceous materials that are impregnated/grafted with amine functional groups. Adsorbent prepared from biomass residue and preactivated with CO₂ show differences in texture and surface chemistry, which leads to higher capacities as compared to starting char (Plaza et al., 2009). This happens because the CO₂ capture capacity depends upon nitrogen functionalities that are responsible for increasing the CO₂-adsorbent affinity (Pevida et al., 2008). Tertiary amidine derivatives (N-methyltetrahydropyrimidine) (MTHP) are supported on activated carbon in the temperatures ranging from 290°C to 500°C (Alesi et al., 2010) for CO₂ capture and regeneration. In the presence of moisture, CO₂ capture on the amidines occurred. Fifield (2004) studied the introduction of pyrene methyl picolinimide (PMP) as an anchor on CNT as the support to increase the affinity of the carbon structure for amine-impregnated sorbents. Lu et al. (2008) reported a comparative study

TABLE 3.3CO₂ Adsorption Capacity of Different Amine-Supported Solid Sorbents

Support	Amine	Amine Content (wt. %)	Adsorption Capacity (mmol g ⁻¹)	P _{CO₂} (atm)	T (°C)	Reference
MCM-41	PEI	50	2.05	0.1	75	Xu et al., 2002
MCM-41	TEPA	50	4.54	0.05	75	Yue et al., 2008
PE-MCM-41	DEA	77	2.93	0.05	25	Bezerra et al., 2011
SBA-15	PEI	50	3.18	0.15	75	Ma et al., 2009
KIT-6	PEI	50	1.95	0.05	75	Son et al., 2008
PMMA	TEPA	41	14.03	0.15	70	Rochelle, 2009
Monolith	PEI	65	3.75	0.05	75	Chen et al., 2009
SiO ₂	PEI	40	2.40	0.10	45	Gray et al., 2009
Zeolite 13X	MEA	10	1	0.15	30	Jadhav et al., 2007

of CO₂ capture by CNT. They observed that CO₂ adsorption capacity of CNT modified with 3-aminopropyltriethoxysilane (APTES) was 2.59 mmol g⁻¹ at 20°C. The adsorption capacities of CO₂ of CNTs and CNT (APTES) increased with water content and decreased with temperature and found that the CNT (APTES) could be a suitable low-temperature adsorbent for CO₂ capture.

Novel Structured Sorbents

Sorbents such as monolithic sorbents and hollow fiber can be used for both physical and chemical sorption processes. Hollow fiber sorbents reduce the thermal effects associated with fixed-bed sorption (Lively et al., 2011). In fixed-bed sorption the energy consumption is low, recovery and purity of product and throughput is high, there is a low-pressure drop with sensible sorption capacity, and mass transfer resistance is low. The polymeric fibers that are hollow have been used with sorbent particles embedded in the porous fiber wall. This is used for postcombustion capture in a rapid temperature swing adsorption process. To prevent temperature rise due to the heat of absorption, cooling water is circulated during absorption. During desorption, steam or hot water is circulated to quickly desorb CO₂. Systems' kinetic limitations can be overcome by increasing the superficial gas velocity and packing of fiber. Hollow fiber sorbent systems are well-suited for use with amine absorbents (PEI) (Rezaei et al., 2013).

3.4 Effect of Amine Functional Groups, and Structural Properties of Adsorbents on CO₂ Adsorption

There are two types of interactions between an adsorbate and adsorbent (Aburub and Wurster, 2006) during adsorption from the fluid phase: specific interaction and nonspecific interaction. The interaction of adsorbate molecules with a particular functional group on the adsorbent surface is called a specific interaction, and the interaction between adsorbate molecules with the basal plane of an adsorbent is termed a nonspecific interaction. High adsorption capacity

will be attained when there is good compatibility between the sizes of the adsorbate molecule and the pores of the adsorbent (El-Sayed and Bandosz, 2004). In case of CO₂ adsorption by activated carbon, both specific and nonspecific interactions are important (Arenillas et al., 2005; Maroto-Valer et al., 2005). Nitrogen functional groups attached to an AC for improvement of CO₂ adsorption capacity have been studied by many researchers (Arenillas et al., 2005; Drage et al., 2007; Maroto-Valer et al., 2005; Pevida et al., 2008). The basicity of nitrogen groups attracts CO₂ for adsorption (Arenillas et al., 2005; Somy et al., 2009). As different nitrogen groups have different basicity, care must be taken to consider that how much nitrogen is incorporated (Arenillas et al., 2005; Xu et al., 2003). Due to impregnation blocking of AC occurs. As a result of which physisorption decreases and chemisorption effect appears (Plaza et al., 2007). For PEI-impregnated AC, the CO₂ adsorption capacity increased from 2.1 wt.% to 2.5 wt.%, and the surface area decreased due to the impregnation. Pelvida et al. (2008) reported that when the ammonia was treated at low temperature (i.e., 400°C), the CO₂ adsorption capacity increased from 2.7 wt.% to 3.2 wt.% at 75°C due to creation of an amide group. By anchoring a halogenated amine on the carbon surface, the CO₂ adsorption capacity of carbon increased from 0.072 mmol/g to 0.174 mmol/g (Gray et al., 2004). The hydrophobicity of the adsorbents are increased by modification of the amine group, making them more selective for CO₂ adsorption in the presence of water vapor (Hiyoshi et al., 2004b, 2005; Wei et al., 2009). In the dynamic test for amino propyltriethoxysilane, trimethoxysilylpropyl, and diethylenetriamine, the adsorption capacity increased from 0.52 mmol/g in dry conditions to 0.56 mmol/g in wet conditions. The adsorption of CO₂ leads to the formation of alkyl ammonium carbamate (Chaffee et al., 2007; Contarini et al., 2003). In the presence of water vapor, the CO₂ adsorption capacity increases (one mole of CO₂ per mole of NH₂) (Knowles et al., 2005). For unmodified activated carbon, with increasing temperature, CO₂ adsorption capacity decreases due to physical adsorption that governs the process (Maroto-Valer et al., 2005). When the temperature increases, the diffusion rate and surface adsorption energy increases (Maroto-Valer et al., 2008). In the case of activated carbon modified with amine groups, the CO₂ capacity may rise with temperature due to chemical but reversible adsorption (Maroto-Valer et al., 2008). In other words, for modified activated carbon, the adsorption capacity is dependent on two factors. The first one is the inherent capacity of the unmodified activated carbon that decreases with increasing temperature. The second factor is the chemical adsorption that increases with increasing the temperature. Arenillas et al. (2005) reported that the chemical adsorption of CO₂ is enhanced in the presence of hydroxyl groups. With an increasing size of the silylation reagent, the CO₂ adsorption decreases, as reported by Hiyoshi et al. (2004a, 2004b, 2005). The SBA-15 was silylated by three different silylation agents: 3-aminopropyltriethoxysilane (APTES) (having one amine group per reagent molecule), N-(2-aminoethyl)-3-aminopropyltrimethoxysilane (AEAPS) (with two amine groups per molecule), and (3-trimethoxysilylpropyl) diethylenetriamine (TA) (three amine groups). At the same amine density, the amine efficiency of the silylation reagents decreased in the order APTES > AEAPS > TA. This phenomenon is due to the steric hindrance of the aliphatic backbone of aminosilane, which hinders CO₂ molecules from accessing the amine groups.

3.5 Advantages and Disadvantages of Adsorption

The adsorption process has some advantages over other processes including low investment and low energy cost for regeneration. The molecules are held loosely on the surface

of the adsorbent and can be easily removed. The inherent advantage of adsorption processes is due to their relatively simple and unsteady state operation. The unsteady operation means at any particular point the extent of adsorption within the fixed bed vary with time. Adsorption only occurs in a particular region of the bed known as the mass transfer zone, which moves through the bed. As the fluid is passed through the bed of solid adsorbents, the transfer of molecules from the fluid to the solid occurs at the entrance of the bed. When the adsorbent region becomes saturated, then the mass transfer zone moves through the bed. Then at any instant of time the adsorbent particles upstream and downstream of the mass transfer zone do not participate in the mass transfer process at the equilibrium condition. Adsorption needs lower energy than that of absorption (Drage et al., 2009). There are two drawbacks in the adsorption process that make it unfavorable. The first one is that the system cannot handle large concentrations of CO₂ (Audus, 1997). The second is that the sorbent ability is usually based on pore size. So gases smaller than CO₂ can also penetrate inside the pores. N₂ is the gas that most commonly fills up pore space in sorbents, as a result of which the process becomes less efficient and the CO₂ separation rate decreases. Another drawback is that adsorption is a slow process. It is an acceptable rate for small-scale application due the cost of making this system large enough to accommodate a typical power plant. For typical materials, the residence time for maximum adsorption depends on the sorbent (Satyapal et al., 2001). For large volumes of flue gas in a power plant, this is just too slow to be practical. The adsorption processes for CO₂ capture has not yet been commercialized. Also it is not a highly attractive approach for CO₂ removal in the large-scale industrial treatment of flue gases because of higher energy consumption in comparison to the absorption method, and also the capacity and CO₂ selectivity of available adsorbents are low. Researchers are working on adsorbents and optimizing cyclic adsorption units to decrease the required energy for CO₂ capture, and the surface modification of the adsorbents should be done by suitable amine groups by different modification techniques to increase the capacity and CO₂ selectivity. So in near future, adsorption would require less energy consumption than other capture processes.

3.6 Treatment and Disposal of Spent Adsorbent (Activated Carbon)

There are three primary methods for the treatment of spent activated carbon. First, laboratory tests must determine whether the spent activated carbon is hazardous. By heating the spent activated carbon in a high temperature furnace, the contaminants are vaporized, restoring the carbon's original pore structure, allowing for its reuse. The second method of disposal of activated carbon involves reusing the carbon as a fuel in fire cement kilns. Coprocessing the carbon in cement kilns burns up the spent carbon. The third method of disposal of spent activated carbon is in an industrial landfill, but only if the material is nonhazardous.

3.7 Conclusions

Large amounts of flue gases are emitted to the environment. Various technologies exist for CO₂ capture. Chemical absorption is most effective at low CO₂ partial pressure for

flue gas from postcombustion power plants. The drawback of this process is that more than 60% of total energy consumed in the stripper for thermal regeneration of CO₂-rich chemical absorbents. So it is energy intensive. Adsorption is the most efficient technology. Physical adsorption is applicable for postcombustion CO₂ capture. Chemically modified adsorbents are feasible for CO₂ adsorption. Amine-based chemical adsorbents that have large surface area and high amine content have been extensively used due to their large CO₂ adsorption capacity. Amine-based adsorbents have high selectivity toward CO₂ over other gases, high adsorption and desorption rates, and high tolerance to moisture. To capture CO₂ using amine-impregnated adsorbents, the amines used must have high nitrogen content. The effective methods are developed for loading amine to support and to produce the amine-based chemical adsorbents with high thermal stability. Activated carbon and other carbon-based adsorbents are considered to be the most suitable adsorbents for large-scale industrial application of the adsorption process. Modification of the sorbent is done to improve the selectivity as well as the capacity of the adsorbents. Amine-modified sorbents are the most effective sorbents for CO₂ capture. Depending on the flue gas stream composition, different separation/capture technologies are used for separation of CO₂. We can now better identify the suitable technology for CO₂ capture and the cost for CO₂ separation and energy requirements.

References

- Aburub, A., Wurster, D. E. 2006. Phenobarbital interactions with derivatized activated carbon surfaces. *J Colloid Interface Sci* 296: 79–85.
- Alesi, W. R., Gray, M., Kitchin, J. R. 2010. CO₂ adsorption on supported molecular amidine systems on activated carbon. *ChemSusChem* 3: 948–956.
- Arenillas, A., Rubiera, F., Parra, J. B., Ania, C. O., Pis, J. J. 2005. Surface modification of low cost carbons for their application in the environmental protection. *Appl Surf Sci* 252: 619–624.
- Audus, H. 1997. Greenhouse gas mitigation technology: An overview of the CO₂ capture and sequestration studies and further activities of the IEA greenhouse gas R&D programme. *Energy* 22: 217–221.
- Balasubramanian, R., Chowdhury, S. 2015. Recent advances and progress in the development of graphene-based adsorbents for CO₂ capture. *J Mater Chem* 3: 21968–21989.
- Banerjee, R., Phan, A., Wang, B., Knobler, C., Furukawa, H., O’Keeffe, M., Yaghi, O. M. 2008. High-throughput synthesis of zeolitic imidazolate frameworks and application to CO₂ capture. *Science* 319: 939–943.
- Berlier, K., Frere, M. 1996. Adsorption of CO₂ on activated carbon: Simultaneous determination of integral heat and isotherm of adsorption. *J Chem Eng Data* 41: 1144–1148.
- Berlier, K., Frere, M. 1997. Adsorption of CO₂ on microporous materials on activated carbon and silica gel. *J Chem Eng Data* 42: 533–537.
- Bezerra, D. P., Oliveira, R. S., Vieira, R. S., Cavalcante, C. L. Jr., Azevedo, D. C. 2011. Adsorption of CO₂ on nitrogen-enriched activated carbon and zeolite 13X. *Adsorption* 17: 235–246.
- Blomen, E., Hendriks, C., Neele, F. 2009. Capture technologies: Improvements and promising developments. *Energy Procedia* 1: 1505–1512.
- Burchell, T. D., Judkins, R. R., Rogers, M. R., Williams, A. M. 1997. A novel process and material for the separation of carbon dioxide and hydrogen sulfide gas mixtures. *Carbon* 35: 1279–1294.
- Cavenati, S., Grande, C. A., Rodrigues, A. E. 2004. Adsorption equilibrium of methane, carbon dioxide, and nitrogen on zeolite 13X at high pressures. *J Chem Eng Data* 49: 1095–1101.
- Chaffee, A. L., Knowles, G. P., Liang, Z., Zhang, J., Xiao, P., Webley, P. A. 2007. CO₂ capture by adsorption: Materials and process development. *Int J Greenhouse Gas Con* 1: 11–18.

- Chang, F. Y., Chao, K. J., Cheng, H. H., Tan, C. S. 2009. Adsorption of CO₂ onto amine-grafted mesoporous silicas. *Sep Purif Technol* 70: 87–95.
- Chen, C., Yang, S. T., Ahn, W. S., Ryoo, R. 2009. Amine-impregnated silica monolith with a hierarchical pore structure: Enhancement of CO₂ capture capacity. *Chem Commun* 24: 3627–3629.
- Chew, T. L., Ahmad, A. L., Bhatia, S. 2010. Ordered mesoporous silica (OMS) as an adsorbent and membrane for separation of carbon dioxide (CO₂). *Adv Colloid Interface Sci* 153: 43–57.
- Chowdhury, S., Balasubramanian, R. 2016. Highly efficient, rapid and selective CO₂ capture by thermally treated graphene nanosheets. *J CO₂ Utilization* 13: 50–60.
- Cinke, M., Li, J., Bauschlicher, C. W., Ricca, A., Meyyappan, M. 2003. CO₂ adsorption in single-walled carbon nanotubes. *Chem Phys Lett* 376: 761–766.
- Contarini, S., Barbini, M., Del Piero, G., Gambarotta, E., Mazzamurro, G., Riocci, M. 2003. Solid sorbents for the reversible capture of carbon dioxide. *Int J of Greenhouse Gas Control* 1: 169–174.
- Damen, K., van Troost, M., Faaij, A., Turkenburg, W. A. 2006. Comparison of electricity and hydrogen production systems with CO₂ capture and storage. Part A: Review and selection of promising conversion and capture technologies. *Prog Energy Combust Sci* 32: 215–246.
- Do, D., Wang, K. A. 1998. New model for the description of adsorption kinetics in heterogeneous activated carbon. *Carbon* 36: 1539–1554.
- Drage, T. C., Arenillas, A., Smith, K. M., Pevida, C., Piippo, S., Snape, C. E. 2007. Preparation of carbon dioxide adsorbents from the chemical activation of urea–formaldehyde and melamine–formaldehyde resins. *Fuel* 86: 22–30.
- Drage, T. C., Smith, K. M., Pevida, C., Arenillas, A., Snape, C. E. 2009. Development of adsorbent technologies for post-combustion CO₂ capture. *Energy Procedia* 1: 881–884.
- Drese, J. H., Choi, S., Lively, R. P., Koros, W. J., Fauth, D. J., Gray, M. L., Jones, C. W. 2009. Synthesis–structure–property relationships for hyperbranched aminosilica CO₂ adsorbents. *Adv Funct Mater* 19: 3821–3832.
- Dunne, J. A., Rao, M., Sircar, S., Gorte, R. J., Myers, A. L. 1996. Calorimetric heats of adsorption and adsorption isotherms. 2. O₂, N₂, Ar, CO₂, CH₄, C₂H₆, and SF₆ on NaX, H-ZSM-5, and Na-ZSM-5 zeolites. *Langmuir* 12: 5896–5904.
- El-Sayed, Y., Bandosz, T. J. 2004. Adsorption of valeric acid from aqueous solution onto activated carbons: Role of surface basic sites. *J Colloid Interface Sci* 273: 64–72.
- Essaki, K., Nakagawa, K., Kato, M., Uemoto, H. 2004. CO₂ absorption by lithium silicate at room temperature. *J Chem Eng Jpn* 37: 772–777.
- Fifield, L. S. 2004. Carbon dioxide capture using amine-based molecular anchors on multi wall carbon nanotubes. *Prepr Pap-Am Chem Soc, Div Fuel Chem* 49: 296.
- Figueroa, J. D., Fout, T., Plasynski, S., McIlvried, H., Srivastava, R. D. 2008. Advances in CO₂ capture technology—The US Department of Energy’s Carbon Sequestration Program. *Int J Greenhouse Gas Con* 2: 9–20.
- Filburn, T., Helble, J. J., Weiss, R. A. 2005. Development of supported ethanolamines and modified ethanolamines for CO₂ capture. *Ind. Eng. Chem. Res* 44: 1542–1546.
- Florin, N. H., Harris, A. T. 2009. Reactivity of CaO derived from nano-sized CaCO₃ particles through multiple CO₂ capture-and-release cycles. *Chem Eng Sci* 64: 187–191.
- Foley, H. C. 1995. Carbogenic molecular sieves: Synthesis, properties and applications. *Microporous Mater* 4: 407–433.
- Franchi, R. S., Harlick, P. J., Sayari, A. 2005. Applications of pore-expanded mesoporous silica. 2. Development of a high-capacity, water-tolerant adsorbent for CO₂. *Ind Eng Chem Res* 44: 8007–8013.
- Ghosh, A., Subrahmanyam, K. S., Krishna, K. S., Datta, S., Govindaraj, A., Pati, S. K., Rao, C. N. R. 2008. Uptake of H₂ and CO₂ by graphene. *J Phys Chem* 112: 15704–15707.
- Gibbins, J., Chalmers, H. 2008. Carbon capture and storage. *Energy Policy* 36: 4317–4322.
- Gray, M. L., Hoffman, J. S., Hreha, D. C., Fauth, D. J., Hedges, S. W., Champagne, K. J., Pennline, H. W. 2009. Parametric study of solid amine sorbents for the capture of carbon dioxide. *Energy Fuels* 23: 4840–4844.

- Gray, M. L., Soong, Y., Champagne, K. J., Baltrus, J., Stevens, R. W., Toochinda, P., Chuang S. S. C. 2004. CO₂ capture by amine-enriched fly ash carbon sorbents. *Sep Purif Technol* 35: 31–36.
- Gray, M. L., Soong, Y., Champagne, K. J., Pennline, H., Baltrus, J. P., Stevens, R. W., Filburn, T. 2005. Improved immobilized carbon dioxide capture sorbents. *Fuel Process Technol* 86: 1449–1455.
- Gupta, M., Coyle, I., Thambimuthu, K. 2003. CO₂ capture technologies and opportunities in Canada. 1st Canadian CC&S Technology Roadmap Workshop.
- Harlick, P. J., Sayari, A. 2007. Application of pore expanded mesoporous silica. 5. Triamine grafter material with exceptional CO₂ dynamic and equilibrium adsorption performance. *Ind Eng Chem Res* 46: 446.
- Harlick, P. J., Tezel, F. H. 2004. An experimental adsorbent screening study for CO₂ removal from N₂. *Microporous Mesoporous Mater* 76: 71–79.
- Harrison, D. P. 2004. The role of solids in CO₂ capture: A mini review. 7th International Conference on Greenhouse Gas Control Technologies, Vancouver, Canada.
- Helwani, Z., Wiheeb, A. D., Kim, J., Othman, M. R. 2012. Improved carbon dioxide capture using metal reinforced hydrotalcite under wet conditions. *Int J Greenhouse Gas Con* 7: 127–136.
- Hernández-Huesca, R., Díaz, L., Aguilar-Armenta, G. 1999. Adsorption equilibria and kinetics of CO₂, CH₄ and N₂ in natural zeolites. *Sep Purif Technol* 15: 163–173.
- Hicks, J. C., Drese, J. H., Fauth, D. J., Gray, M. L., Qi, G., Jones, C. W. 2008. Designing adsorbents for CO₂ capture from flue gas-hyperbranched aminosilicas capable of capturing CO₂ reversibly. *J Am Chem Soc* 130: 2902–2903.
- Hiyoshi, N., Yogo, K., Yashima, T. 2004a. Adsorption of carbon dioxide on amine modified SBA-15 in the presence of water vapor. *Chem Lett* 33: 510–511.
- Hiyoshi, N., Yogo, K., Yashima, T. 2004b. Adsorption of carbon dioxide on modified mesoporous materials in the presence of water vapor. *Surf Sci Catalysis* 154: 2995–3002.
- Hiyoshi, N., Yogo, K., Yashima, T. 2005. Adsorption characteristics of carbon dioxide on organically functionalized SBA-15. *Microporous Mesoporous Mater* 84: 357–365.
- Huang, L., Zhang, L., Shao, Q., Lu, L., Lu, X., Jiang, S., Shen, W. 2007. Simulations of binary mixture adsorption of carbon dioxide and methane in carbon nanotubes: Temperature, pressure, and pore size effects. *J Phys Chem* 111: 11912–11920.
- Iwan, A., Stephenson, H., Ketchie, W. C., Lapkin, A. A. 2009. High temperature sequestration of CO₂ using lithium zirconates. *Chem Eng J* 146: 249–258.
- Jadhav, P. D., Chatti, R. V., Biniwale, R. B., Labhsetwar, N. K., Devotta, S., Rayalu, S. S. 2007. Monoethanol amine modified zeolite 13X for CO₂ adsorption at different temperatures. *Energy Fuels* 21: 3555–3559.
- Jiang, L., Fan, Z. 2014. Design of advanced porous graphene materials: From graphene nanomesh to 3D architectures. *Nanoscale* 6: 1922–1945.
- Jones, C. W. 2011. CO₂ capture from dilute gases as a component of modern global carbon management. *Annu Rev Chem Biomol Eng* 2: 31–52.
- Kamiuto, K., Abe, S. 2002. Effect of desorption temperature on CO₂ adsorption equilibria of the honeycomb zeolite beds. *Applied Energy* 72: 555–564.
- Khatiri, R. A., Chuang, S. S., Soong, Y., Gray, M. 2006. Thermal and chemical stability of regenerable solid amine sorbent for CO₂ capture. *Energy Fuels* 20: 1514–1520.
- Kikkinides, E., Yang, R., Cho, S. 1993. Concentration and recovery of carbon dioxide from flue gas by pressure swing adsorption. *Ind Eng Chem* 32: 2714–2720.
- Kim, K., Yang, S., Lee, J. B., Eom, T. H., Ryu, C. K., Jo, S. H., Yi, C. 2012. Analysis of K₂CO₃/Al₂O₃ CO₂ sorbent tested with coal-fired power plant flue gas: Effect of SO_x. *Int J Greenhouse Gas Con* 9: 347–354.
- Knowles, G. P., Graham, J. V., Delaney, S. W., Chaffee, A. L. 2005. Aminopropyl-functionalized mesoporous silicas as CO₂ adsorbents. *Fuel Proc Tech* 86: 1435–1448.
- Kuppler, R. J., Timmons, D. J., Fang, Q. R., Li, J. R., Makal, T. A., Young, M. D., Zhou, H. C. 2009. Potential applications of metal-organic frameworks. *Chem Rev* 253: 3042–3066.
- Lara, Y., Lisbona, P., Martínez, A., Romeo, L. M. 2009. Comparative study of optimized purge flow in a CO₂ capture system using different sorbents. *Energy Procedia* 1: 1359–1366.

- Lee, S., Filburn, T. P., Gray, M., Park, J. W., Song, H. J. 2008. Screening test of solid amine sorbents for CO₂ capture. *Ind Eng Chem Res* 47: 7419–7423.
- Lee, S. C., Chae, H. J., Lee, S. J., Park, Y. H., Ryu, C. K., Yi, C. K., Kim, J. C. 2009. Novel regenerable potassium-based dry sorbents for CO₂ capture at low temperatures. *J Molec Catalysis B: Enzymatic* 56: 179–184.
- Lee, S. C., Choi, B. Y., Lee, T. J., Ryu, C. K., Ahn, Y. S., Kim, J. C. 2006. CO₂ absorption and regeneration of alkali metal-based solid sorbents. *Catalysis Today* 111: 385–390.
- Lee, S. C., Kwon, Y. M., Ryu, C. Y., Chae, H. J., Ragupathy, D., Jung, S. Y., Kim, J. C. 2011. Development of new alumina-modified sorbents for CO₂ sorption and regeneration at temperatures below 200°C. *Fuel* 90: 1465–1470.
- Lee, S. S., Yoo, J. S., Moon, G. H., Park, S. W., Park, D. W., Oh, K. J. 2004. CO₂ adsorption with attrition of dry sorbents in a fluidized bed. *Prepr Pap-Am Chem Soc, Div Fuel Chem* 49: 314.
- Lee, Z. H., Lee, K. T., Bhatia, S., Mohamed, A. R. 2012. Post-combustion carbon dioxide capture: Evolution towards utilization of nanomaterials. *Renew Sust Renew Rev* 16: 2599–2609.
- Lepaumier, H., Picq, D., Carrette, P. L. 2009. New amines for CO₂ capture. II. Oxidative degradation mechanisms. *Ind Eng Chem Res* 48: 9068–9075.
- Leung, D. Y., Caramanna, G., Maroto-Valer, M. M. 2014. An overview of current status of carbon dioxide capture and storage technologies. *Renew Sustain Energy Rev* 39: 426–443.
- Li, J. R., Kuppler, R. J., Zhou, H. C. 2009. Selective gas adsorption and separation in metal–organic frameworks. *Chem Soc Rev* 38: 1477–1504.
- Li, W., Choi, S., Drese, J. H., Hornbostel, M., Krishnan, G., Eisenberge, P. M., Jones, C. W. 2010. Steam stripping for regeneration of supported amine based CO₂ adsorbents. *ChemSusChem* 3: 899–903.
- Liang, Z., Fadhel, B., Schneider, C. J., Chaffee, A. L. 2008. Stepwise growth of melamine-based dendrimers into mesopores and their CO₂ adsorption properties. *Microporous Mesoporous Mater* 111: 536–543.
- Liu, S. H., Wu, C. H., Lee, H. K., Liu, S. B. 2010. Highly stable amine-modified mesoporous silica materials for efficient CO₂ capture. *Top Catal* 53: 210–217.
- Lively, R. P., Leta, D. P., DeRites, B. A., Chance, R. R., Koros, W. J. 2011. Hollow fiber adsorbents for CO₂ capture: Kinetic sorption performance. *Chem Eng J* 171: 801–810.
- Lu, C., Bai, H., Wu, B., Su, F., Hwang, J. F. 2008. Comparative study of CO₂ capture by carbon nanotubes, activated carbons, and zeolites. *Energy Fuels* 22: 3050–3056.
- Ma, X., Wang, X., Song, C. 2009. “Molecular basket” sorbents for separation of CO₂ and H₂S from various gas streams. *J Am Ceram Soc* 131: 5777–5783.
- Mandal, B., Bandyopadhyay, S. 2006. Absorption of carbon dioxide into aqueous blends of 2-amino-2-methyl-1-propanol and monoethanolamine. *Chem Eng Sci* 61: 5440–5447.
- Maroto-Valer, M. M., Lu, Z., Zhang, Y., Tang, Z. 2008. Sorbents for CO₂ capture from high carbon fly ashes. *Waste Manage* 28: 2320–232.
- Maroto-Valer, M. M., Tang, Z., Zhang, Y. 2005. CO₂ capture by activated and impregnated anthracites. *Fuel Process Technol* 86: 1487–1502.
- Meisen, A., Shuai, X. 1997. Research and development issues in CO₂ capture. *Energy Convers Manage* 38: S37–S42.
- Metz, B., Davidson, O., de Coninck, H., Loos, M., Meyer, L. (eds.). 2005. *Carbon Dioxide Capture and Storage*. Cambridge, UK: Cambridge University Press.
- Miller, B. G. 2011. *Clean Coal Engineering Technology*. Burlington, MA: Elsevier.
- Millward, A. R., Yaghi, O. M. 2005. Metal-organic frameworks with exceptionally high capacity for storage of carbon dioxide at room temperature. *J Amer Chem Soc* 127: 17998–17999.
- Mondal, M. K., Balsora, H. K., Varshney, P. 2012. Progress and trends in CO₂ capture/separation technologies: A review. *Energy* 46: 431–441.
- Na, B. K., Koo, K. K., Eum, H. M., Lee, H., Song, H. K. 2001. CO₂ recovery from flue gas by PSA process using activated carbon. *Korean J Chem Eng* 18: 220–227.
- Ning, G., Xu, C., Mu, L., Chen, G., Wang, G., Gao, J., Wei, F. 2012. High capacity gas storage in corrugated porous graphene with a specific surface area-lossless tightly stacking manner. *Chem Eng Commun* 48: 6815–6817.

- Ochoa-Fernandez, E., Rønning, M., Grande, T., Chen, D. 2006. Nanocrystalline lithium zirconate with improved kinetics for high-temperature CO₂ capture. *Chem Mater* 18: 1383–1385.
- Parshetti, G. K., Chowdhury, S., Balasubramanian, R. 2015. Biomass derived low-cost microporous adsorbents for efficient CO₂ capture. *Fuel* 148: 246–254.
- Pevida, C., Plaza, M. G., Arias, B., Feroso, J., Rubiera, F., Pis, J. J. 2008. Surface modification of activated carbons for CO₂ capture. *Appl Surf Sci* 254: 7165–7172.
- Plaza, M. G., Pevida, C., Arenillas, A., Rubiera, F., Pis, J. J. 2007. CO₂ capture by adsorption with nitrogen enriched carbons. *Fuel* 86: 2204–2212.
- Plaza, M. G., García, S., Rubiera, F., Pis, J. J., Pevida, C. 2010. Post-combustion CO₂ capture with a commercial activated carbon: Comparison of different regeneration strategies. *Chem Eng J* 163: 41–47.
- Plaza, M. G., Pevida, C., Arias, B., Feroso, J., Rubiera, F., Pis, J. J. 2009. A comparison of two methods for producing CO₂ capture adsorbents. *Energy Procedia* 1: 1107–1113.
- Rashidi, N. A., Yusup, S. 2016. An overview of activated carbons utilization for the post-combustion carbon dioxide capture. *J CO₂ Utilizat* 13: 1–16.
- Razavi, S. S., Hashemianzadeh, S. M., Karimi, H. 2011. Modeling the adsorptive selectivity of carbon nanotubes for effective separation of CO₂/N₂ mixtures. *J Mol Model* 17: 1163–1172.
- Rezaei, F., Lively, R. P., Labreche, Y., Chen, G., Fan, Y., Koros, W. J., Jones, C. W. 2013. Aminosilane-grafted polymer/silica hollow fiber adsorbents for CO₂ capture from flue gas. *Appl Mater Inter* 5: 3921–3931.
- Rochelle, G. T. 2009. Amine scrubbing for CO₂ capture. *Science* 325: 1652–1654.
- Saha, D., Deng, S. 2010. Adsorption equilibrium and kinetics of CO₂, CH₄, N₂O, and NH₃ on ordered mesoporous carbon. *J Colloid Interface Sci* 345: 402–409.
- Satyapal, S., Filburn, T., Trela, J., Strange, J. 2001. Performance and properties of a solid amine sorbent for carbon dioxide removal in space life support applications. *Energy Fuels* 15: 250–255.
- Sayari, A., Belmabkhout, Y., Serna-Guerrero, R. 2011. Flue gas treatment via CO₂ adsorption. *Chem Eng J* 171: 760–774.
- Schladt, M. J., Filburn, T. P., Helble, J. J. 2007. Supported amine sorbents under temperature swing absorption for CO₂ and moisture capture. *Ind Eng Chem Res* 46: 1590–1597.
- Selma, L., Seigo, O., Dohle, S., Siegrist, M. 2014. Public perception of carbon capture and storage (CCS): A review. *Renew Sustain Energy Rev* 38: 848–863.
- Shen, C., Grande, C. A., Li, P., Yu, J., Rodrigues, A. E. 2010. Adsorption equilibria and kinetics of CO₂ and N₂ on activated carbon beads. *Chem Eng J* 160: 398–407.
- Simon, A., Cohen-Bouhacina, T., Porté, M. C., Aimé, J. P., Baquey, C. 2002. Study of two grafting methods for obtaining a 3-aminopropyltriethoxysilane monolayer on silica surface. *J Colloid Interface Sci* 251: 278–283.
- Siriwardane, R. V., Shen, M. S., Fisher, E. P., Poston, J. A. 2001. Adsorption of CO₂ on molecular sieves and activated carbon. *Energy Fuels* 15: 279–284.
- Solomon, S., Qin, D., Manning, M., Chen, Z., Marquis, M., Averyt, K. B., Tignor, M., Miller, H. L. (eds.). 2007. *Climate Change 2007: The Physical Science Basis*. Contribution of Working Group I to the Fourth Assessment Report of the Intergovernmental Panel on Climate Change. Cambridge, UK: Cambridge University Press.
- Somy, A., Mehrnia, M. R., Amrei, H. D., Ghanizadeh, A., Safari, M. 2009. Adsorption of carbon dioxide using impregnated activated carbon promoted by zinc. *Int J Greenhouse Gas Con* 3: 249–254.
- Son, W. J., Choi, J. S., Ahn, W. S. 2008. Adsorptive removal of carbon dioxide using polyethyleneimine-loaded mesoporous silica materials. *Microporous Mesoporous Mater* 113: 31–40.
- Steenneveldt, R., Berger, B., Torp, T. A. 2006. CO₂ capture and storage: Closing the knowing–doing gap. *Chem Eng Res Des* 84: 739–763.
- Su, F., Lu, C., Cnen, W., Bai, H., Hwang, J. F. 2009. Capture of CO₂ from flue gas via multi walled carbon nanotubes. *Sci Total Environ* 407: 3017–3023.
- Tang, Y., Landskron, K. 2010. CO₂-sorption properties of organosilicas with bridging amine functionalities inside the framework. *J Phys Chem* 114: 2494–2498.

- Vaidya, P. D., Kenig, E. Y. 2008. Acceleration of CO₂ reaction with N,N-diethylethanolamine in aqueous solutions by piperazine. *Ind Eng Chem Res* 47: 34–38.
- Wang, J., Huang, L., Yang, R., Zhang, Z., Wu, J., Gao, Y., Zhong, Z. 2014. Recent advances in solid sorbents for CO₂ capture and new development trends. *Eng Environ Sci* 7: 3478–3518.
- Wang, Q., Luo, J., Zhong, Z., Borgna, A. 2011. CO₂ capture by solid adsorbents and their applications: Current status and new trends. *Eng Environ Sci* 4: 42–55.
- Wang, Y., Guan, C., Wang, K., Guo, C. X., Li, C. M. 2011. Nitrogen, hydrogen, carbon dioxide, and water vapor sorption properties of three-dimensional graphene. *J Chem Eng Data* 56: 642–645.
- Wang, Y., Zhou, Y., Liu, C., Zhou, L. 2008. Comparative studies of CO₂ and CH₄ sorption on activated carbon in presence of water. *Colloids Surfaces A: Physicochem Eng Aspects* 322: 14–18.
- Wei, J., Shi, J., Pan, H., Su, Q., Zhu, J., Shi, Y. 2009. Thermal and hydrothermal stability of amino-functionalized SBA-16 and promotion of hydrophobicity by silylation. *Microporous Mesoporous Mater* 117: 596–602.
- Wong, S., Bioletti, R. 2002. Carbon dioxide separation technologies. Alberta Research Council.
- Xu, X., Song, C., Andresen, J. M., Miller, B. G., Scaroni, A. W. 2002. Novel polyethylenimine-modified mesoporous molecular sieve of MCM-41 type as high-capacity adsorbent for CO₂ capture. *Energy Fuels* 16: 1463–1469.
- Xu, X., Song, C., Andresen, J. M., Miller, B. G., Scaroni, A. W. 2003. Preparation and characterization of novel CO₂ “molecular basket” adsorbents based on polymer-modified mesoporous molecular sieve MCM-41. *Microporous Mesoporous Mater* 62: 29–45.
- Yang, H., Xu, Z., Fan, M., Gupta, R., Slimane, R. B., Bland, A. E., Wright, I. 2008. Progress in carbon dioxide separation and capture: A review. *J Environ Sci* 20: 14–27.
- Yuan, W., Chen, J., Shi, G. 2014. Nanoporous graphene materials. *Mater Today* 17: 77–85.
- Yue, M. B., Sun, L. B., Cao, Y., Wang, Y., Wang, Z. J., Zhu, J. H. 2008. Efficient CO₂ capturer derived from as synthesized MCM41 modified with amine. *Chemistry A Eur J* 14: 3442–3451.
- Zaman, M., Lee, J. H. 2013. Carbon capture from stationary power generation sources: A review of the current status of the technologies. *Korean J Chem Eng* 30: 1497–1526.
- Zhang, J., Webley, P. A., Xiao, P. 2008. Effect of process parameters on power requirements of vacuum swing adsorption technology for CO₂ capture from flue gas. *Energy Convers Manage* 49: 346–356.



Taylor & Francis

Taylor & Francis Group

<http://taylorandfrancis.com>

Carbon Dioxide (CO₂) Capture by Calcium-Based Industrial Solid Wastes in Calcium Looping Process

Yingjie Li, Xiaotong Ma, Lunbo Duan, and Chunmei Lu

CONTENTS

4.1	Introduction	57
4.2	Calcium-Based Industrial Solid Wastes as Carbon Dioxide (CO ₂) Sorbents in Calcium Looping Process	58
4.2.1	Calcium Looping Process	58
4.2.2	Value of Calcium-Based Industrial Solid Wastes as CO ₂ Sorbents	59
4.2.3	CO ₂ Capture Performance of Calcium-Based Industrial Solid Wastes in Calcium Looping Process	60
4.3	Effects of Reaction Conditions on CO ₂ Capture Performance of Calcium-Based Industrial Solid Wastes in Calcium Looping Process	61
4.3.1	Reaction Temperature	61
4.3.2	Reaction Atmosphere	62
4.3.3	Particle Size	65
4.4	Enhancing CO ₂ Capture Performance of Calcium-Based Industrial Solid Wastes....	65
4.4.1	Organic Calcium Precursors	65
4.4.2	Inert Supports	66
4.4.3	Improvement of Pore Structure	67
4.5	Coadsorption of CO ₂ and Other Pollutants by Calcium-Based Industrial Solid Wastes	70
4.5.1	CO ₂ and SO ₂ Adsorption	70
4.5.2	CO ₂ /HCl Adsorption	70
4.6	Conclusions	73
	Acknowledgments	74
	References	74

4.1 Introduction

Lots of calcium-based industrial solid wastes such as carbide slag from the chlor-alkali industry, lime mud from the paper industry, and steel slag from the steel industry containing Ca(OH)₂, CaCO₃, or xCaO·SiO₂ and so on are generated every year. It is an interesting and challenging topic to recycle these calcium-based industrial solid wastes to reduce environmental pollution and save valuable resources.

The calcium looping process, namely, calcination–carbonation cycles of calcium-based sorbent, is a promising method to capture carbon dioxide (CO₂) from coal-fired power plants and hydrogen production. The calcium-based industrial solid wastes have

been recently proposed to capture CO_2 and SO_2 (sulfur dioxide) in the calcium looping process (CLP). CO_2 capture capacities of calcium-based industrial solid wastes decrease with the number of calcium looping cycles. Thus, the research to develop novel CO_2 sorbents, which possess high and cyclically stable CO_2 capture capacities using calcium-based industrial solid wastes as raw materials, is also presented. It shows that calcium-based industrial solid wastes used in CLP have great prospects for CO_2 capture, industrial solid waste utilization, and calcium resources conservation.

This chapter of the book aims to provide the state-of-the-art studies on the use of industrial solid wastes as potential candidates for CO_2 capture at the large scales. Comprehensive summary about reaction conditions affecting the CO_2 capture performance of calcium-based industrial solid wastes, methods enhancing the CO_2 capture performance of calcium-based industrial solid wastes, and the coadsorption performance of CO_2 and other pollutants by calcium-based industrial solid wastes are also discussed in this chapter.

4.2 Calcium-Based Industrial Solid Wastes as Carbon Dioxide (CO_2) Sorbents in Calcium Looping Process

4.2.1 Calcium Looping Process

It is believed that anthropogenic CO_2 emission due to the combustion of fossil fuels has become a major contributor to global climate warming. The calcium looping process (CLP), that is, carbonation–calcination cycles of the CaO -based sorbent, has attracted increasing attention as one of the most effective ways to capture CO_2 from flue gas streams at high temperature (Asiedu-Boateng et al. 2016).

The basic concept of CLP is based on the reversible reaction between CaO and CO_2 according to Equations 4.1 and 4.2, and the process is illustrated in Figure 4.1.

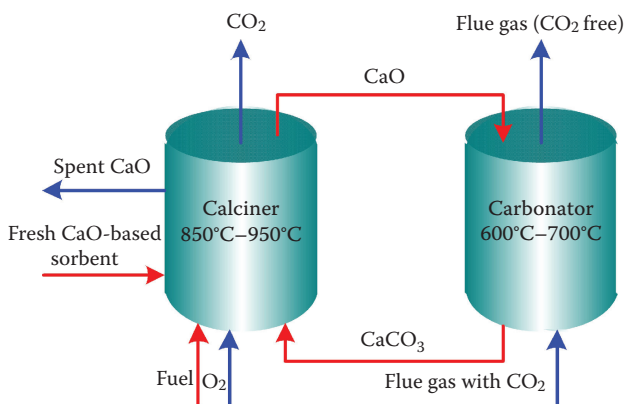


FIGURE 4.1
Schematic diagram of CLP.

The CO₂-containing flue gas stream is sent into a carbonator and CO₂ is captured by the sorbent, CaO. As a result, CaO changes into CaCO₃ and the CO₂-free gas leaves the carbonator. CaCO₃ is then transported to a calciner for the decomposition of CaCO₃, that is, regeneration of the sorbent. CaO is sent back to the carbonator for the recapture of CO₂. The high concentration of CO₂ (>95%) released from the regenerator can be compressed and sequestered.

In the CLP process, the sorbent is supposed to be utilized for multiple carbonation–calcination cycles under practical conditions. However, it has been discovered that all tested CaO-based sorbents suffer a problem of loss in capacity, that is, the CO₂ capture capacity decreases sharply with cycles (Hu et al. 2015). The problem causes a large amount of fresh sorbent makeup required to maintain the overall efficiency of CO₂ capture and thus adds extra costs, which becomes one of the major barriers limiting the widespread application of the CLP. Therefore, a large portion of efforts has focused on good solutions (Hu et al. 2015; Sun et al. 2016a).

4.2.2 Value of Calcium-Based Industrial Solid Wastes as CO₂ Sorbents

Every year, lots of calcium-based industrial wastes such as carbide slag, white mud, and steel slag are produced. The chemical components of calcium-based industrial solid wastes compared with limestone are analyzed by x-ray fluorescence (XRF), as shown in Table 4.1. All of them are primarily composed of calcined limestone calcium oxide (CaO), implying that calcium compounds are the dominant constituents for CO₂ capture.

Carbide slag is a by-product from the hydrolysis process of calcium carbide (CaC₂) for acetylene (C₂H₂) production. CaC₂ is produced through the reaction of CaO and coal char (C). Then CaC₂ reacts with water to produce C₂H₂ gas and waste, namely, carbide slag, which is mainly composed of Ca(OH)₂. The reaction mechanism is as in

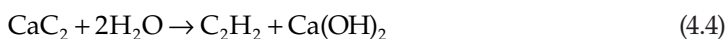
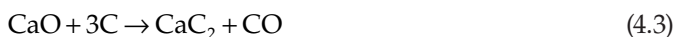


TABLE 4.1

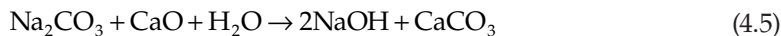
Chemical Components of Calcium-Based Industrial Solid Wastes and Limestone (wt.%)

Category	Carbide Slag	White Mud	Steel Slag	Limestone
CaO	69.52	52.39	46.83	52.08
MgO	0.02	0.7	4.61	1.32
SiO ₂	2.34	2.52	14.83	3.32
Al ₂ O ₃	1.52	1.49	11.52	0.53
Fe ₂ O ₃	0.17	0.29	17.61	0.03
SrO	0.03	0.31	–	–
TiO ₂	0.03	0.056	–	–
K ₂ O	–	0.013	–	–
Na ₂ O	–	0.14	–	0.02
Cl	–	0.88	–	–
MnO	–	–	1.25	–
Others	0.57	0.049	3.35	0.47
Loss on ignition	25.8	41.16	–	42.23

Source: Data from Ma, X. T. et al., 2016, *Appl Energy*, 168: 85–95; Sun, R. Y. et al., 2013, *Chem Eng J*, 221: 124–132; and Tian, S. C. et al., 2015, *Environ Sci Technol*, 49 (12): 7464–7472.

C_2H_2 is the raw material of polyvinyl chloride (PVC). About 1.5 to 1.9 tons of carbide slag is produced along with 1 ton of PVC in a chlor-alkali plant (Cheng et al. 2009).

White mud is the waste material that results from the sodium hydroxide recovery unit (causticization reaction) in alkali recycling process of pulp and paper manufacture industry, as shown in Equation 4.5. The major chemical component of white mud is $CaCO_3$. Approximately 1.03 tons of white mud is generated per ton of pulp (A. H. Ma et al. 2016).



Steel slag is a byproduct generated during the steel production process and obtained from the separation of the molten steel from impurities using limestone in the steel-making furnaces. Steel slag is a kind of alkaline mixture and it's mainly composed of $xCaO \cdot SiO_2$. About 0.13 to 0.2 tons of steel slag is produced per ton of steel (Yu and Wang 2011). Currently, resource utilization of steel slag is mainly for asphalt aggregate, phosphate fertilizer production, cement production and construction. Moreover, the carbonation product is more stable than the raw steel slag, so it can be reused in construction.

Considerable amounts of the aforementioned calcium-based industrial solid wastes are usually disposed in landfills, resulting in land occupation, waste of calcium resources, and environmental pollution. Converting those high calcium content wastes into useful products has attracted considerable interest from both an economic and environmental points of view. A novel process that can combine effective reuse of the calcium-based industrial wastes and low-cost CO_2 capture together is hoping to be achieved.

4.2.3 CO_2 Capture Performance of Calcium-Based Industrial Solid Wastes in Calcium Looping Process

The cyclic CO_2 capture capacities of calcium-based industrial solid wastes are depicted in Figure 4.2. Here, the CO_2 capture capacity refers to the CO_2 adsorption amount per unit

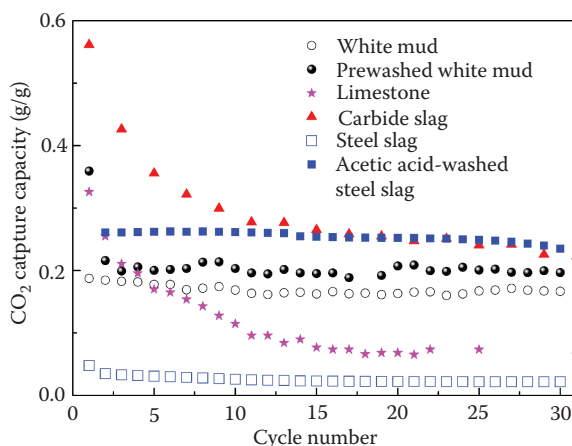


FIGURE 4.2

Comparison between cyclic CO_2 capture capacities of CaO derived from different calcium-based industrial solid wastes. (Data from Sun, R. Y. et al., 2013, *Chem Eng J*, 221: 124–132; Sun, R. Y. et al., 2013, *Int J Hydrogen Energy*, 38 (31): 13655–13663; Tian, S. C. et al., 2015, *Environ Sci Technol*, 49 (12): 7464–7472.)

mass of sorbent, g (CO₂)/g (sorbent). Carbide slag as a CO₂ sorbent was reported in relation to CLP in an investigation carried out by Li et al. (2012a), who found the increase in CO₂ capture performance using carbide slag instead of limestone. In subsequent cycles, although the CO₂ capture capacity of carbide slag decreased, it maintained a value constantly higher than that of limestone. The authors reported that the difference in pore structure distribution resulted in the difference in CO₂ capture performance. Work by Sun et al. (2013a) demonstrated that the CO₂ capture performance of white mud is lower than that of limestone in the previous 10 cycles, while it gets higher than that of limestone after 15 cycles. Moreover, the white mud after a prewash process with distilled water to eliminate impurities showed better CO₂ capture capacity than white mud, 36% after 100 cycles, which were 1.8 and 4.8 times as high as white mud and limestone, respectively. Tian et al. (2015) investigated the CO₂ capture by steel slag. The data showed that steel slag had a limited CO₂ capture capacity; only 0.05 g/g in the first cycle. Although steel slag contained considerable calcium (Table 4.1), it was mostly in the form of inert phases such as Ca₁₂Al₁₄O₃₃ and Ca₂SiO₄, which are not available to capture CO₂. However, this inert calcium was effectively converted into an activated state after mixed with acetic acid. The CO₂ capture capacity remained around 0.25 g/g, with a total decay of 12% during 30 cycles. Thus, in order to obtain CaO suitable for CO₂ capture from steel slag, a pretreatment with acetic acid has been proposed as a possible technique.

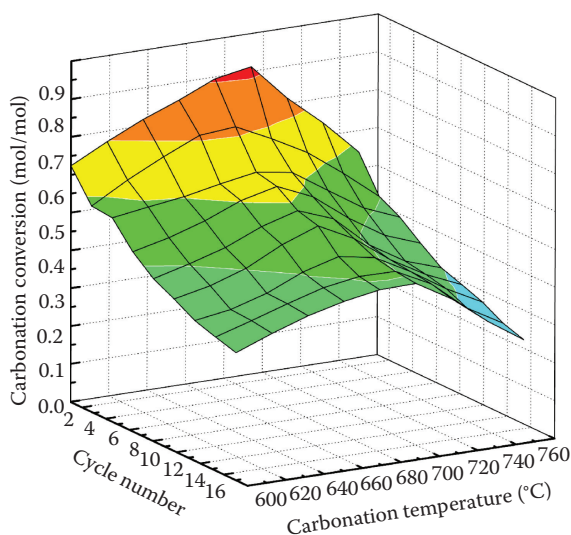
4.3 Effects of Reaction Conditions on CO₂ Capture Performance of Calcium-Based Industrial Solid Wastes in Calcium Looping Process

Optimizing the reaction conditions for in situ CO₂ capture represents a compromise between thermodynamic and kinetic limitations. The summaries of reaction conditions affecting CO₂ capture performance of calcium-based industrial solid wastes in calcium looping process are listed here.

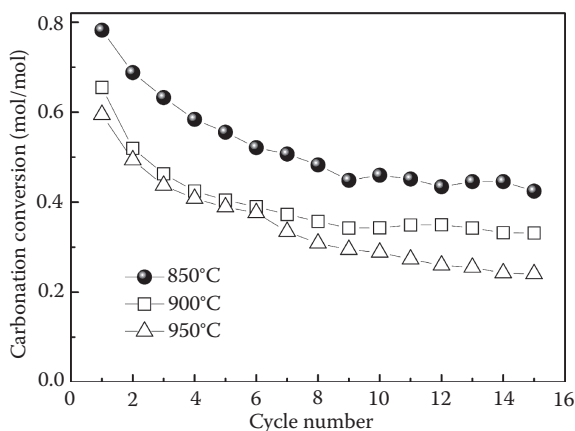
4.3.1 Reaction Temperature

The carbonation temperature has been shown to affect the cyclic CO₂ capture capacity of the calcium-based sorbents (Chen and Zhao 2011). Increasing the carbonation temperature favors a higher reaction rate. However, higher temperature does not favor the exothermic CO₂ capture reaction. Figure 4.3 shows the cyclic carbonation conversions (the fractional conversion of CaO derived from sorbent to CaCO₃) of carbide slag at various carbonation temperatures at the range of 600°C to 760°C investigated by Li et al. (2012b) in a dual fixed-bed reactor. The carbonation conversions of carbide slag carbonated at range of 650°C to 700°C are 0.41 to 0.44 after 15 cycles, which are higher than those at other temperatures. Thus, the optimum carbonation temperature range for carbide slag is about 650°C to 700°C. The temperature range is similar to that of limestone reported by Grasa et al. (2008).

The cyclic carbonation conversions of carbide slag at various calcination temperatures at the range of 850°C to 950°C are shown in Figure 4.4. Higher calcination temperature is conducive to the decomposition of CaCO₃, according to Baker (1962), but an excessively high temperature above 950°C aggravates sintering of calcium-based sorbents (Grasa and Abanades 2006). From Figure 4.4, carbide slag exhibits a decrease in cyclic carbonation conversion with the calcination temperature increasing from 850°C to 950°C.

**FIGURE 4.3**

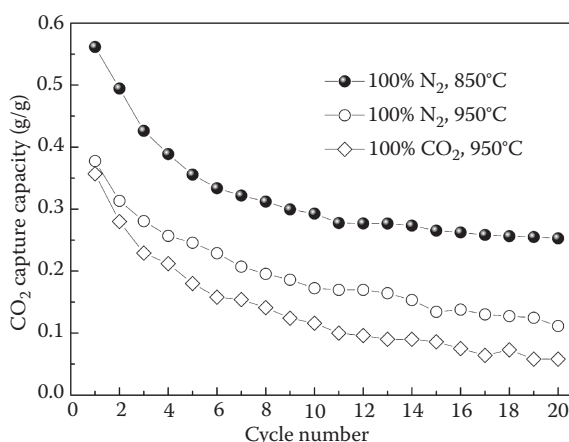
Effect of carbonation temperature on cyclic carbonation conversions of carbide slag (carbonation in 15% CO₂/N₂ for 20 min, calcination in N₂ at 850°C for 15 min). (Adapted from Li, Y. J. et al., 2012, *Int J Greenhouse Gas Con*, 9: 117–123.)

**FIGURE 4.4**

Effect of calcination temperature on cyclic carbonation conversions of carbide slag (carbonation in 15% CO₂/N₂ balance for 20 min, calcination in N₂ for 15 min). (Adapted from Li, Y. J. et al., 2012, *Int J Greenhouse Gas Con*, 9: 117–123.)

4.3.2 Reaction Atmosphere

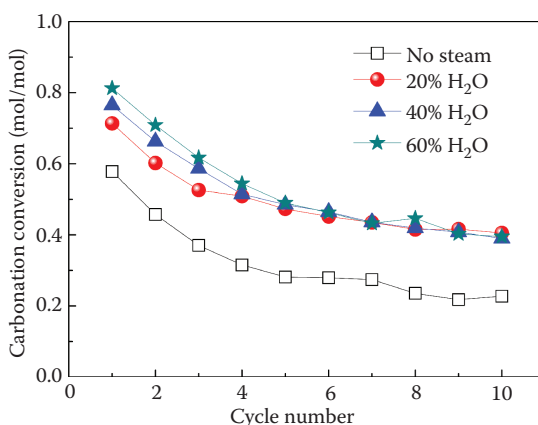
The required calcination temperature for calcium-based sorbent depends on CO₂ concentration in the calcination atmosphere. Smaller CO₂ concentration in the calcination atmosphere leads to a lower calcination temperature. To ensure the complete and rapid decomposition of calcium-based sorbent under pure CO₂, the calcination temperature of 950°C is often chosen. The high CO₂ concentration in the calcination is prone to intensify sintering of the sorbent (Manovic et al. 2009b; Valverde et al. 2014). Figure 4.5 displays CO₂

**FIGURE 4.5**

Effect of calcination atmosphere on cyclic carbonation conversions of carbide slag (carbonation in 15% CO₂/N₂ balance at 700°C for 30 min, calcination for 10 min). (Adapted from Li, Y. J. et al., 2015, *Appl Energy*, 145: 60–68.)

capture performance of carbide slag calcined in pure N₂ and pure CO₂. The CO₂ capture capacity of carbide slag calcined in pure CO₂ is 48% and 78% lower than those calcined in pure N₂ at 850°C and 950°C after 20 cycles, respectively.

In many practical systems, the gas atmosphere naturally contains steam, which is one of the factors affecting calcium conversion during the carbonation reaction of calcium oxide. Figure 4.6 shows the carbonation conversions of carbide slag carbonated for 20 min under 0%, 20%, 40%, and 60% steam in the carbonation stage during the cycles. It is found that the presence of steam promotes the carbonation reaction, especially in the situation of severe calcination condition, for example, calcination in CO₂ at 950°C. Moreover, higher steam concentration results in significantly higher carbonation conversion of carbide slag for short carbonation duration (e.g., 5 min), because higher steam

**FIGURE 4.6**

Effect of steam concentration on carbonation conversions of carbide slag for 20 min carbonation (carbonation in 20% CO₂/0%–60% steam/N₂ balance at 650°C calcination in CO₂ at 950°C for 10 min). (Adapted from He, Z. R. et al., 2016, *Int J Hydrogen Energy*, 41 (7): 4296–4304.)

concentration leads to a greater accelerating effect on CO_2 diffusion through the product layer, as shown in Figure 4.7.

The presence of steam in a calcination atmosphere also affects the CO_2 capture performance of calcium-based sorbent mainly by reducing the CO_2 partial pressure during decomposition of CaCO_3 . The temperature 850°C is high enough for the complete and rapid decomposition of calcium-based sorbent under pure N_2 and pure steam. Figure 4.8 illustrates the CO_2 capture capacities of carbide slag calcined under steam and N_2 at 850°C during 10 carbonation–calcination cycles. The CO_2 capture capacity of carbide slag calcined under pure steam is slightly lower than that under pure N_2 . It is also found that carbide slag calcined under pure steam retains much higher cyclic CO_2 capture capacity and obviously better durability than that calcined under pure CO_2 during the cycles shown in Figure 4.5. For example, the CO_2 capture capacity of carbide slag calcined under

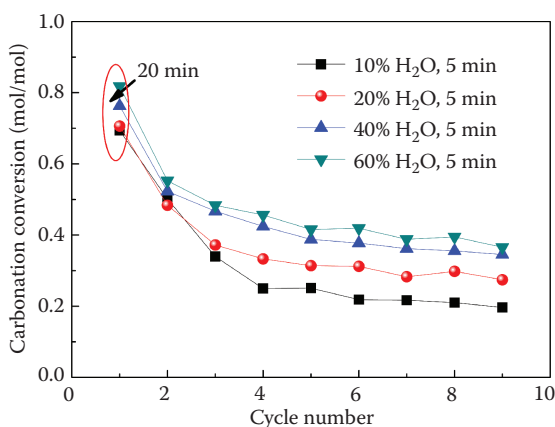


FIGURE 4.7

Effect of steam concentration on carbonation conversions of carbide slag for 5 min carbonation (carbonation at 20% CO_2 /10%–60% steam/ N_2 balance at 650°C , calcination in CO_2 at 950°C for 10 min). (Adapted from He, Z. R. et al., 2016, *Int J Hydrogen Energy*, 41 (7): 4296–4304.)

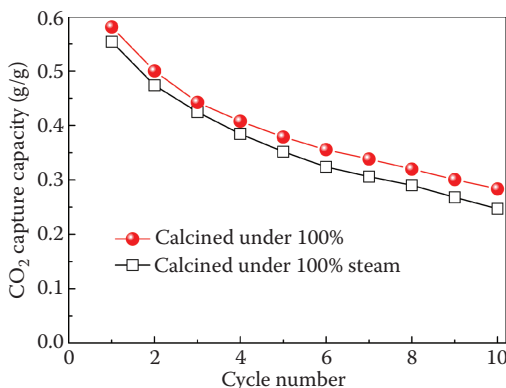
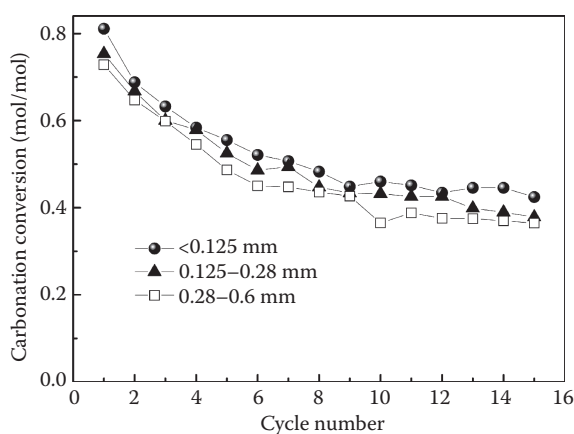


FIGURE 4.8

Effect of steam in calcinations atmosphere on CO_2 capture capacities of carbide slag (carbonation in 15% CO_2 / N_2 balance at 700°C for 20 min, calcination at 850°C for 10 min). (Adapted from Ma, X. T. et al., 2016, *Appl Energy*, 168: 85–95.)

**FIGURE 4.9**

Cyclic carbonation conversions of carbide slag with different particle sizes (carbonation in 15% CO₂/N₂ balance at 700°C for 20 min, calcination at 850°C for 15 min). (Adapted from Li, Y. J. et al., 2012, *Int J Greenhouse Gas Con*, 9: 117–123.)

pure steam is 1.7 times as high as that of carbide slag calcined under pure CO₂. Compared to the calcination under the high concentration of CO₂, the calcination under the high concentration of steam decreases the calcination temperature and the corresponding energy consumption. Even though steam would cause attrition problems, acoustic streaming around small particles typically employed in a fluidized bed is available to make use of fragile particles. Therefore, the high concentration of steam as a calcination atmosphere is more feasible and promising than the high concentration of CO₂.

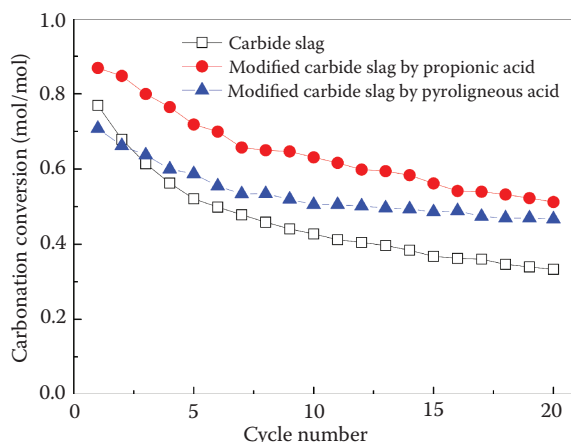
4.3.3 Particle Size

The cyclic carbonation conversions of carbide slag at three particle size fractions (<0.125, 0.125–0.28, and 0.28–0.6 mm) are shown in Figure 4.9. The cyclic carbonation conversion of carbide slag decreases slightly with the particle size increasing due to an increased CO₂ diffusion resistance. It indicates that the particle size has a slight effect on the CO₂ capture capacity of carbide slag. The particle size only affects the reaction rate of CaO at the initial fast carbonation stage that lasts for 1 to 3 min (Grasa and Abanades 2006; Grasa et al. 2008). Because the carbonation time in each cycle (20 min) is long enough during the experiments to ensure the full carbonation, diffusion resistance inside the particles does not influence the final carbonation conversion of carbide slag.

4.4 Enhancing CO₂ Capture Performance of Calcium-Based Industrial Solid Wastes

4.4.1 Organic Calcium Precursors

It has been proved that some of the organic calcium-based sorbents such as calcium magnesium acetate and calcium acetate show greater CO₂ capture capacities than limestone

**FIGURE 4.10**

Cyclic carbonation conversions of CaO from different organic calcium precursors (carbonation in 15% CO₂/N₂ balance at 700°C, calcination at 850°C for 10 min). (From Sun, R. Y. et al., 2013b, *Int J Hydrogen Energy*, 38 (31): 13655–13663; and Liu, C. T. et al., 2014, *Asia-Pac J Chem Eng*, 9 (5): 678–685.)

(Liu et al. 2010; Lu et al. 2008). These organic calcium sorbents can release organic substances such as acetone at 380°C to 400°C, as shown in Equation 4.6, and generate calcium carbonate with porous structure. And then calcium carbonate can further decompose into CaO and CO₂ at higher temperature, leaving porous CaO.

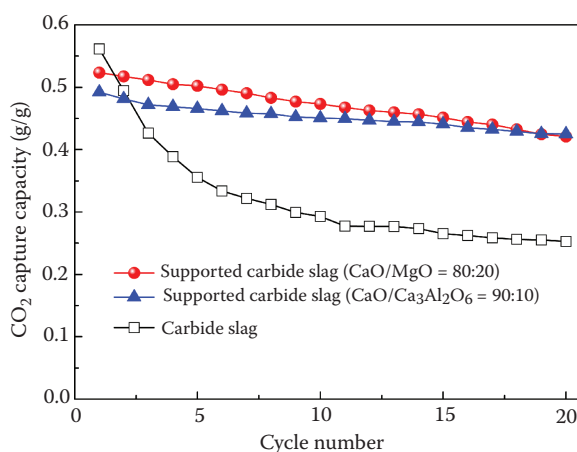


Carbide slag modified by propionic acid and pyrolygneous acid were proposed as CO₂ sorbents at high temperature, as shown in Figure 4.10. It can be seen that the modifications enhance CO₂ capture capacity of carbide slag. The carbonation conversions of carbide slag modified by propionic acid after the 1st and 20th cycles are 0.87 and 0.51, which are 13% and 53.7% higher than those of carbide slag, respectively. The carbonation conversion of carbide slag modified by pyrolygneous acid is 0.47 after 20 cycles, which is 40% higher than that of carbide slag. In addition, the modified of carbide slag by pyrolygneous acid is effective to improve the cyclic CO₂ capture durability of carbide slag, which may be attributed to the stable pore structure formed after high temperature calcination (up to 980°C) supplied by the combustion of the flammable organic substances.

4.4.2 Inert Supports

Enhancements in CO₂ capture performances of calcium-based sorbents by dispersing CaO in the various support materials, such as Ca₁₂Al₁₄O₃₃ (Barelli et al. 2014), Ca₃Al₂O₆ (Angeli et al. 2014), Ca₉Al₆O₁₈ (Radfarnia and Sayari 2015), MgO (Luo et al. 2013), SiO₂ (Valverde et al. 2012), CaTiO₃ (Wu and Zhu 2010), Y₂O₃ (Zhang et al. 2014), and ZrO₂ (Antzara et al. 2015), have been widely investigated. The supports can effectively stabilize the pore structure and thus increase the sintering resistance of the synthetic sorbents.

A comparison in CO₂ capture capacity is made between carbide slag and supported carbide slag, as shown in Figure 4.11. The two supported sorbents—one containing CaO derived from carbide slag and Al₂O₃ derived from aluminum nitrate hydrate with a mass

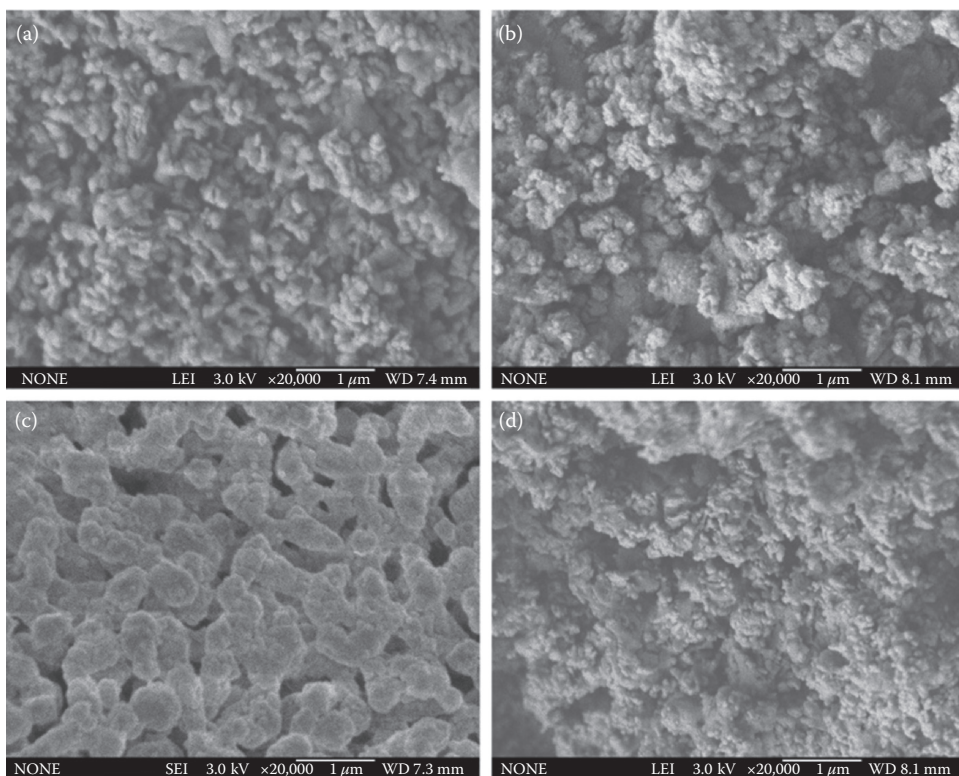
**FIGURE 4.11**

CO₂ capture capacities of carbide slag and supported carbide slag (carbonation in 15% CO₂/N₂ balance at 700°C, calcination at 850°C for 10 min). (From Ma, X. T. et al., 2016, *Appl Energy*, 168: 85–95; and Li, Y. J. et al., 2015, *Appl Energy*, 145: 60–68.)

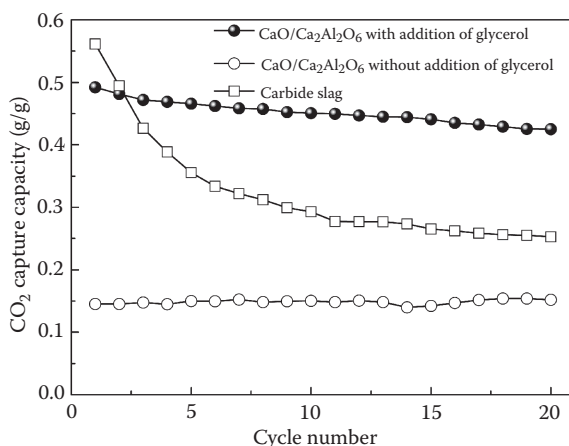
ratio of 90:10, and one containing CaO derived from carbide slag and MgO derived from magnesium nitrate hydrate—exhibit higher CO₂ capture capacities and greater cyclic durabilities than carbide slag. It reveals that CaO reacts with all Al₂O₃ to generate Ca₃Al₂O₆, while CaO and MgO exist in the free states. The supports of Ca₃Al₂O₆ and MgO sustain the high sintering resistance against high-temperature condition and thus result in the stable CO₂ capture performances of the supported carbide slag. The comparison in microstructure morphologies between the supported sorbent, CaO/Ca₃Al₂O₆, and carbide slag detected by a scanning electron microscope (SEM) are shown in Figure 4.12. It appears that the surfaces of both original CaO/Ca₃Al₂O₆ and calcined carbide slag possess a porous structure, as shown in Figure 4.12a and b. However, a dramatic pore decrease and grain growth of carbide slag after 50 cycles due to severe sintering are observed, as in Figure 4.12c. The nanosized pores of CaO/Ca₃Al₂O₆ are present to the large extent in the residue, as illustrated in Figure 4.12d.

4.4.3 Improvement of Pore Structure

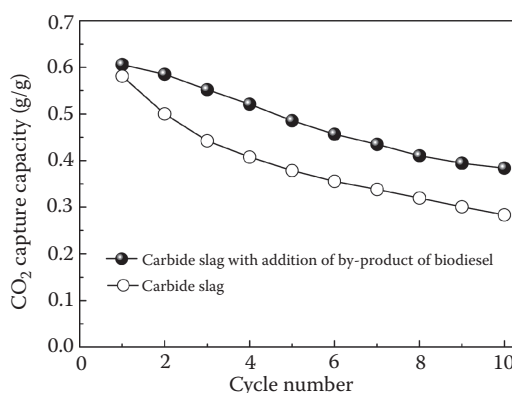
It is found that the addition of pore-forming reagent (e.g., glycerol and biomass-based materials) is able to enhance the cyclic CO₂ capture capacity of the CO₂ sorbent. Figure 4.13 shows the CO₂ capture capacity of CaO/Ca₃Al₂O₆ with and without the addition of glycerol in the preparation process. The CO₂ capture capacity of CaO/Ca₃Al₂O₆ with the addition of glycerol is much greater than that without the addition of glycerol in 20 cycles. As seen in Figure 4.14, it is also applicable to the situation where glycerol is replaced by the by-product of biodiesel (>90 wt.% glycerol content) obtained from the transesterification process of peanut oil reacted with methanol (transesterification conditions: CaO as catalyst of 6%, reaction temperature of 64°C, molar ratio of methanol to peanut oil of 12:1 and reaction time of 2 h) (Li et al. 2014). The replacement would further cut the cost for the industrial utilization of synthetic CO₂ sorbents. The porous structure is formed due to the release of CO₂ and H₂O during the rapid combustion of glycerol or by-product of biodiesel at the high temperature. Based on the results obtained from Chi et al. (2016) by a

**FIGURE 4.12**

SEM images of $\text{CaO}/\text{Ca}_3\text{Al}_2\text{O}_6$ and carbide slag: (a) calcined carbide slag, (b) $\text{CaO}/\text{Ca}_3\text{Al}_2\text{O}_6$, (c) carbide slag after 50 cycles, (d) $\text{CaO}/\text{Ca}_3\text{Al}_2\text{O}_6$ after 50 cycles (carbonation in 15% CO_2/N_2 balance at 700°C for 30 min, calcination in N_2 at 850°C for 10 min). (From Li, Y. J. et al., 2015, *Appl Energy*, 145: 60–68.)

**FIGURE 4.13**

Effect of glycerol addition in preparation of synthetic sorbent on CO_2 capture (carbonation in 15% CO_2/N_2 balance at 700°C for 30 min, calcination in N_2 at 850°C for 10 min). (Adapted from Li, Y. J. et al., 2015, *Appl Energy*, 145: 60–68.)

**FIGURE 4.14**

Effect of by-product of biodiesel addition on CO₂ capture by carbide slag (carbonation in 15% CO₂/N₂ balance at 700°C for 20 min, calcination in N₂ at 850°C for 10 min). (Adapted from Ma, X. T. et al., 2016, *Appl Energy*, 168: 85–95.)

nitrogen adsorption analyzer, the volumes of pores in the range of 2 to 10 nm ($V_{2-10\text{ nm}}$) and 10 to 150 nm ($V_{10-150\text{ nm}}$) of composite carbide slag (CaO/MgO with by-product of biodiesel) increase compared with those of carbide slag. These are the important pore areas for CO₂ capture (Sun et al. 2007).

Sun et al. (2016b) investigated doping two types of biomass-based pore-forming materials—microcrystalline cellulose and rice husk—with carbide slag as a way of overcoming the loss of specific surface area and, consequently, the inferior CO₂ capture performance. The addition of microcrystalline cellulose is effective in improving the CO₂ sorption of carbide slag pellets, and the pellets with 20 wt.% microcrystalline cellulose display the highest conversion of 52.64% after 25 cycles. This is mainly ascribed to the thermal degradation of microcrystalline cellulose (releasing large amounts of pyrolysis gases) at high temperature, resulting in the improved pore structure. A larger specific surface area and smaller average pore diameter are obtained after 25 cycles than carbide slag pellets, as shown in Table 4.2. In addition, the pellet with 20 wt.% prewashed rice husk (most K removed) displays the highest carbonation conversion of 51.02% after 25 cycles, which is 1.46 times than that with raw rice husk. It can be illustrated by the new eutectics with a low melting temperature after the reaction between potassium and aluminosilicate (Jenkins et al. 1998; Werther et al. 2000). The eutectics accelerate the sintering of CaO-based sorbent during high temperature cycles. It should also be noted that the addition of pore-forming materials weakens the mechanical strength, which is a notable problem for its application in a fluidized bed reactor.

TABLE 4.2

Specific Surface Area and Average Pore Diameter of the Pellets

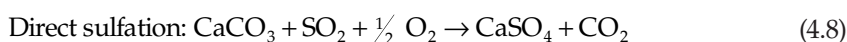
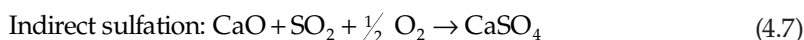
Sorbent	Surface Area (m ² /g)	Average Pore Diameter (nm)
Calcined carbide slag pellet	11.78	16.64
Carbide slag pellet after 25th cycle	3.53	74.91
Carbide slag pellet with 20% microcrystalline cellulose after 25th cycle	5.09	12.28

Source: Data from Sun, J. et al., 2016, *Chem Eng J*, 285: 293–303.

4.5 Coadsorption of CO₂ and Other Pollutants by Calcium-Based Industrial Solid Wastes

4.5.1 CO₂ and SO₂ Adsorption

Calcium-based sorbents are also used for the control of SO₂ emitted from the combustion of sulfur-containing fuels. SO₂ and CO₂ can be simultaneously absorbed by calcium-based sorbents in the CLP when SO₂ presents in the flues gas. CaCO₃ and CaSO₄ are generated after the adsorption step. CaSO₄ is thermally stable during cycles, which leads to a drop in CO₂ adsorption capacity of CaO. The related reactions are as follows:

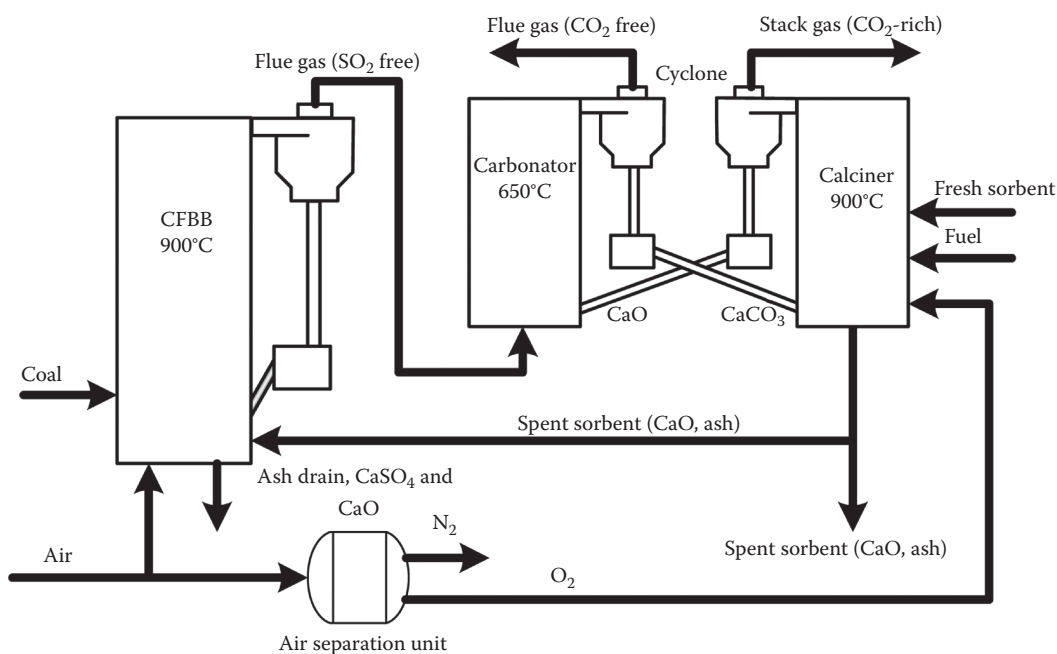


Wu et al. (2016) investigated the simultaneous CO₂/SO₂ adsorption performance of carbide slag in multiple adsorption/desorption cycles in a dual fixed-bed reactor. The presence of SO₂ is adverse to the cyclic CO₂ capture by carbide slag. Higher SO₂ concentration in the range of 0.0005–0.002 L/L and longer adsorption duration lead to more rapid decay in CO₂ capture capacity of carbide slag drops with the number of cycles. The carbonation conversions of carbide slag in the presence of 0.0005 and 0.002 L/L SO₂ decrease by 63% and 89% after eight cycles, respectively. It may be attributed to the formation of a thermally stable and compact CaSO₄ product layer, which causes an increase in the CO₂ diffusion resistance.

To avoid the adverse effect of SO₂ on CO₂ capture of carbide slag, the calcium looping technology can realize the sequential SO₂/CO₂ capture for coal-fired power plants. Li et al. (2012c) proposed the sequential SO₂/CO₂ capture operated on a coal-fired circulated fluidized bed boiler (CFBB), as shown in Figure 4.15. The residues (highly sintered CaO) after being cycled in the CLP for CO₂ capture are sent for SO₂ capture to the CFBB. Therefore, the sorbents are maintained and the overall calcium utilization can be maximized after SO₂ capture. The cost for both SO₂ and CO₂ can be saved by the reutilization of calcium-based sorbents. In addition, the negative effect of the sulfation on the cyclic CO₂ capture of CaO is minimized. Manovic et al. (2009a) proved that the spent CaO after CO₂ capture could be reused as SO₂ sorbents when significant porosity loss did not happen during CO₂ capture cycles. Grasa et al. (2008) reported that the CaO after 100 carbonation/calcination cycles exhibited a higher sulfation conversion than the fresh CaO at 850°C–950°C tested on a thermogravimetric analyzer (TGA).

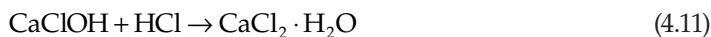
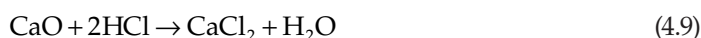
4.5.2 CO₂/HCl Adsorption

The utilization of biomass and recovered fuels in combustion and gasification leads to excessive HCl emission above limitations. Calcium-based sorbents are usually used to remove HCl, which is a poisonous air pollutant. There has been a dispute about the reaction product between CaO and HCl. Many investigations on HCl absorption by calcium-based sorbent assumes that the reaction product is CaCl₂ (Shemwell et al. 2001; Wang et al.

**FIGURE 4.15**

Schematic diagram of sequential SO₂/CO₂ capture in the CFBB. (From Li, Y. J. et al., 2012, *Ind Eng Chem Res*, 51 (49): 16042–16048.)

1996), which occurred as in Equation 4.9. Gullett et al. (1992) proposed that CaCl₂ is just the final product and there are probably various intermediate reactions, as shown in



Jozewicz et al. (1995) referred CaClOH as the product of the reaction between CaO and HCl in the temperature range of 100°C to 600°C. Chin et al. (2005) and Partanen et al. (2005) found that the chlorination product of CaO was CaClOH for shorter reaction time, but it ultimately converted to CaCl₂, which was the only chlorination product after complete reaction.

The cycled calcium-based industrial solid waste, carbide slag, from the CLP for CO₂ capture was proposed by Xie et al. (2014) to remove HCl in the flue gas from the biomass-fired and RDF (refuse-derived fuel)-fired boilers, and thus the cost for HCl removal and

CO₂ capture will be reduced further. In their later work, the enhancement in HCl adsorption performance of carbide slag by doping Ca₃Al₂O₆ as the inert support was explored (Xie et al. 2015). Figures 4.16 and 4.17 show the HCl adsorption capacities of carbide slag and synthetic CaO/Ca₃Al₂O₆ prepared using carbide slag, aluminum nitrate, and glycerol water solution by the combustion method with different chlorination temperatures and carbonation/calcination cycles. It can be seen from Figure 4.16 that carbide slag after two cycles and CaO/Ca₃Al₂O₆ after five cycles exhibit the highest HCl absorption capacities. The cycled CaO/Ca₃Al₂O₆ remains higher HCl absorption capacity than the cycled carbide

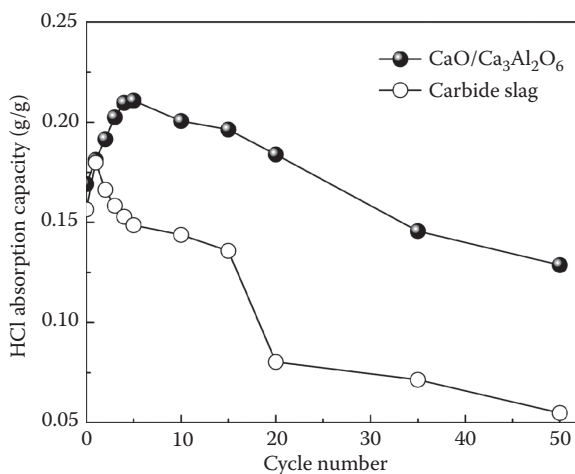


FIGURE 4.16

Effect of cycle number on HCl absorption capacities of carbide slag and CaO/Ca₃Al₂O₆ sorbent after carbonation–calcination cycles (chlorination: 700°C, 1500 ppm HCl/N₂ balance, 60 min). (Adapted from Xie, X. et al., 2015, *Fuel Process Technol.*, 138: 500–508.)

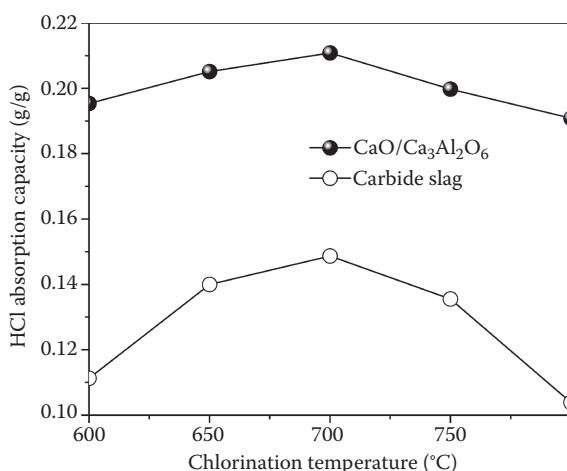
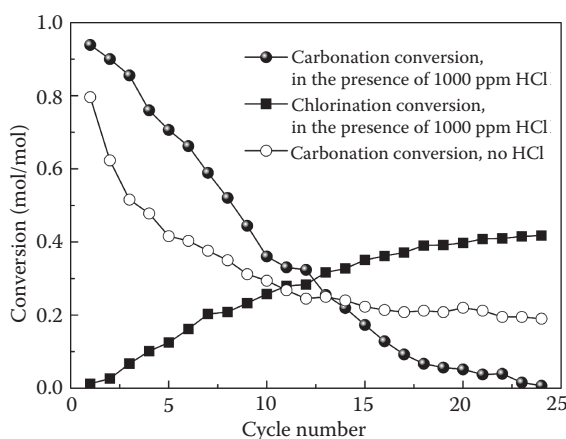


FIGURE 4.17

Effect of chlorination temperature on HCl absorption capacities of carbide slag and CaO/Ca₃Al₂O₆ sorbent after five carbonation/calcination cycles (chlorination: 1500 ppm HCl/N₂ balance). (Adapted from Xie, X. et al., 2015, *Fuel Process Technol.*, 138: 500–508.)

**FIGURE 4.18**

Carbonation and chlorination conversions of limestone in the presence of HCl (carbonation in 15% CO₂/N₂ at 700°C for 20 min, calcination in N₂ at 850°C for 10 min). (Adapted from Wang, W. J. et al., 2014, *Appl Energy*, 125: 246–253.)

slag from CO₂ capture. The HCl absorption capacity of CaO/Ca₃Al₂O₆ is 0.13 g/g after 50 cycles, which is 2.6 times higher than that of carbide slag. Ca₃Al₂O₆ as a stable inert support formed during the combustion synthesis inhibits the severe sintering of CaO. Based on Figure 4.17, the optimum chlorination temperatures for carbide slag and CaO/Ca₃Al₂O₆ are the same, which is 700°C in the temperature range of 600°C to 800°C.

It can be found that the feasible temperature for HCl adsorption is similar to CO₂ capture by calcium-based sorbents. Therefore, HCl and CO₂ can simultaneously react with calcium-based sorbents in the CLP in theory when HCl is present in the carbonation atmosphere. Thus, the competitive reactions between carbonation and chlorination of CaO occur. Currently, the theory has only been proved by Wang et al. (2014) using limestone as sorbents tested in a dual fixed-bed reactor. As depicted in Figure 4.18, the presence of HCl in the carbonation atmosphere improves CO₂ capture capacity of limestone in the previous dozen cycles, but sharply hinders its reactivity with the further increasing cycle number. It may be because that HCl destroys the compact CaCO₃ product layer, which is beneficial for CO₂ diffusion through the layer with holes in the initial cycles. However, a new molten CaCl₂-CaCO₃ product layer in the presence of HCl is formed, which corresponds to the increasing chlorination conversion (the cumulative fractional conversion of CaO to CaCl₂) with cycles. The increase of the newly formed molten areas confirmed by the SEM and energy dispersive x-ray (EDX) analysis severely aggravates the sintering of limestone as the cycle proceeds.

4.6 Conclusions

Calcium-based industrial solid wastes have been proposed to capture CO₂ in the calcium looping process. This chapter reviewed the new progress of the researches on industrial solid wastes as potential candidates for CO₂ capture in the calcium looping. A comprehensive summary about reaction conditions affecting the CO₂ capture performance of

calcium-based industrial solid wastes, methods enhancing the CO₂ capture performance of calcium-based industrial solid wastes as well as the coadsorption performance of CO₂ and other pollutants such as SO₂ and HCl by calcium-based industrial solid wastes were introduced. However, there are still problems to overcome before the calcium-based industrial solid wastes can be used in practical applications. The attrition performance of the calcium-based industrial solid wastes in the fluidized bed reactor will be investigated in the future.

Acknowledgments

The authors are grateful for research funding from the National Natural Science Foundation of China (51376003) in support of their research activities in the area of carbon capture.

References

- Angeli, S. D., C. S. Martavaltzi, and A. A. Lemonidou. 2014. Development of a novel-synthesized Ca-based CO₂ sorbent for multicycle operation: Parametric study of sorption. *Fuel*, 127 (7): 62–69.
- Antzara, A., E. Heracleous, and A. A. Lemonidou. 2015. Improving the stability of synthetic CaO-based CO₂ sorbents by structural promoters. *Appl Energy*, 156: 331–343.
- Asiedu-Boateng, P., R. Legros, and G. S. Patience. 2016. Attrition resistance of calcium oxide-copper oxide-cement sorbents for post-combustion carbon dioxide capture. *Adv Powder Technol*, 27 (2): 786–795.
- Baker, E. H. 1962. 87. The calcium oxide-carbon dioxide system in the pressure range 1–300 atmospheres. *J Chem Soc*, 70: 464–470.
- Barelli, L., G. Bidini, A. D. Michele, F. Gallorini, C. Petrillo, and F. Sacchetti. 2014. Synthesis and test of sorbents based on calcium aluminates for SE-SR. *Appl Energy*, 127: 81–92.
- Chen, H. C., and C. S. Zhao. 2011. Development of a CaO-based sorbent with improved cyclic stability for CO₂ capture in pressurized carbonation. *Chem Eng J*, 171 (1): 197–205.
- Cheng, J., J. H. Zhou, J. Z. Liu, X. Y. Cao, and K. F. Cen. 2009. Physicochemical characterizations and desulfurization properties in coal combustion of three calcium and sodium industrial wastes. *Energy Fuels*, 23 (5): 2506–2516.
- Chi, C. Y., Y. J. Li, R. Y. Sun et al. 2016. HCl removal performance of Mg-stabilized carbide slag from carbonation/calcination cycles for CO₂ capture. *Rsc Adv*, 6.
- Chin, T., R. Yan, and D. T. Liang. 2005. Study of the reaction of lime with HCl under simulated flue gas conditions using X-ray diffraction characterization and thermodynamic prediction. *Ind Eng Chem Res*, 44 (23): 8730–8738.
- Grasa, G. S., M. Alonso, and J. C. Abanades. 2008. Sulfation of CaO particles in a carbonation/calcination loop to capture CO₂. *Ind Eng Chem Res*, 47 (5): 1630–1635.
- Grasa, G. S., and J. C. Abanades. 2006. CO₂ capture capacity of CaO in long series of carbonation/calcination cycles. *Ind Eng Chem Res*, 45 (26): 8846–8851.
- Grasa, G. S., J. C. Abanades, M. Alonso, and B. Gonzalez. 2008. Reactivity of highly cycled particles of CaO in a carbonation/calcination loop. *Chem Eng J*, 137 (3): 561–567.

- Gullett, B. K., W. Jozewicz, and L. A. Stefanski. 1992. Reaction kinetics of Ca-based sorbents with HCl. *Ind Eng Chem Res*, 31 (11): 2437–2446.
- He, Z. R., Y. J. Li, X. T. Ma, W. Zhang, C. Chi, and Z. Wang. 2016. Influence of steam in carbonation stage on CO₂ capture by Ca-based industrial waste during calcium looping cycles. *Int J Hydrogen Energ*, 41 (7): 4296–4304.
- Hu, Y. C., W. Q. Liu, J. Sun, M. Li, X. Yang, Y. Zhang, and M. Xu. 2015. Incorporation of CaO into novel Nd₂O₃ inert solid support for high temperature CO₂ capture. *Chem Eng J*, 273: 333–343.
- Jenkins, B. M., L. L. Baxter, T. R. Miles, and T. R. Miles. 1998. Combustion properties of biomass. *Fuel Process Technol*, 54 (1–3): 17–46.
- Jozewicz, W., and B. K. Gullett. 1995. Reaction mechanisms of dry Ca-based sorbents with gaseous HCl. *Ind Eng Chem Res*, 34 (2): 607–612.
- Li, H., S. L. Niu, C. M. Lu, M. Q. Liu, and M. J. Huo. 2014. Use of lime mud from paper mill as a heterogeneous catalyst for transesterification. *Sci China Technological Sc*, 57 (2): 438–444.
- Li, Y. J., H. L. Liu, R. Y. Sun, S. M. Wu, and C. M. Lu. 2012a. Thermal analysis of cyclic carbonation behavior of CaO derived from carbide slag at high temperature. *J Therm Anal Calorim*, 110 (2): 685–694.
- Li, Y. J., R. Y. Sun, C. T. Liu, H. L. Liu, and C. M. Lu. 2012b. CO₂ capture by carbide slag from chlor-alkali plant in calcination/carbonation cycles. *Int J Greenhouse Gas Con*, 9: 117–123.
- Li, Y. J., C. T. Liu, R. Y. Sun, H. Liu, S. Wu, and C. Lu. 2012c. Sequential SO₂/CO₂ capture of calcium-based solid waste from the paper industry in the calcium looping process. *Ind Eng Chem Res*, 51 (49): 16042–16048.
- Li, Y. J., M. Y. Su, X. Xie, S. M. Wu, and C. T. Liu. 2015. CO₂ capture performance of synthetic sorbent prepared from carbide slag and aluminum nitrate hydrate by combustion synthesis. *Appl Energy*, 145: 60–68.
- Liu, C. T., Y. J. Li, R. Y. Sun, and S. M. Wu. 2014. Cyclic CO₂ capture of carbide slag modified by pyro-ligneous acid in calcium looping cycles. *Asia-Pac J Chem Eng*, 9 (5): 678–685.
- Liu, W. Q., N. W. L. Low, B. Feng, G. X. Wang, and J. C. Diniz da Costa. 2010. Calcium precursors for the production of CaO sorbents for multicycle CO₂ capture. *Environ Sci Technol*, 44 (2): 841–847.
- Lu, H., A. Khan, and P. G. Smirniotis. 2008. Relationship between structural properties and CO₂ capture performance of CaO-based sorbents obtained from different organometallic precursors. *Ind Eng Chem Res*, 47 (16): 6216–6220.
- Luo, C., Y. Zheng, J. J. Yin, S. Wu, and C. Liu. 2013. Effect of support material on carbonation and sulfation of synthetic CaO-based sorbents in calcium looping cycle. *Energy Fuels*, 27 (8): 4824–4831.
- Ma, A. H., Q. M. Jia, H. Y. Su, Y. F. Zhi, N. Tian, J. Wu, and S. Y. Shan. 2016. Study of CO₂ cyclic absorption stability of CaO-based sorbents derived from lime mud purified by sucrose method. *Environ Sci Pollut Res Int*, 23 (3): 2530–2536.
- Ma, X. T., Y. J. Li, L. Shi, Z. R. He, and Z. Y. Wang. 2016. Fabrication and CO₂ capture performance of magnesia-stabilized carbide slag by by-product of biodiesel during calcium looping process. *Appl Energy*, 168: 85–95.
- Manovic, V., E. J. Anthony, and D. Loncarevic. 2009a. SO₂ retention by CaO-based sorbent spent in CO₂ looping cycles. *Ind Eng Chem Res*, 48 (14): 6627–6632.
- Manovic, V., J. P. Charland, J. Blamey, P. S. Fennell, D. Y. Lu, and E. J. Anthony. 2009b. Influence of calcination conditions on carrying capacity of CaO-based sorbent in CO₂ looping cycles. *Fuel*, 88 (10): 1893–1900.
- Partanen, J., P. Backman, R. Backman, and M. Hupa. 2005. Absorption of HCl by limestone in hot flue gases. Part II: Importance of calcium hydroxychloride. *Fuel*, 84 (12–13): 1674–1684.
- Radfarnia, H. R., and A. Sayari. 2015. A highly efficient CaO-based CO₂ sorbent prepared by a citrate-assisted sol-gel technique. *Chem Eng J*, 262: 913–920.
- Shemwell, B., Y. A. Levendis, and G. A. Simons. 2001. Laboratory study on the high-temperature capture of HCl gas by dry-injection of calcium-based sorbents. *Chemosphere*, 42 (5–7): 785–796.
- Sun, P., J. R. Grace, C. J. Lim, and E. J. Anthony. 2007. The effect of CaO sintering on cyclic CO₂ capture in energy systems. *AIChE J*, 53 (9): 2432–2442.

- Sun, J., W. Q. Liu, H. Q. Chen, Y. Hu, W. Wang, X. Li, and M. Xu. 2016a. Stabilized CO₂ capture performance of extruded-spheronized CaO-based pellets by microalgae templating. *Proc Combust Instit*, 36 (3): 3977–3984.
- Sun, J., W. Q. Liu, Y. C. Hu, J. Wu, M. Li, X. Yang, W. Wang, and M. Xu. 2016b. Enhanced performance of extruded-spheronized carbide slag pellets for high temperature CO₂ capture. *Chem Eng J*, 285: 293–303.
- Sun, R. Y., Y. J. Li, C. T. Liu, X. Xie, and C. M. Lu. 2013a. Utilization of lime mud from paper mill as CO₂ sorbent in calcium looping process. *Chem Eng J*, 221: 124–132.
- Sun, R. Y., Y. J. Li, J. L. Zhao, C. T. Liu, and C. M. Lu. 2013b. CO₂ capture using carbide slag modified by propionic acid in calcium looping process for hydrogen production. *Int J Hydrogen Energy*, 38 (31): 13655–13663.
- Tian, S. C., J. G. Jiang, F. Yan, K. M. Li, and X. Chen. 2015. Synthesis of highly efficient CaO-based, self-stabilizing CO₂ sorbents via structure-reforming of steel slag. *Environ Sci Technol*, 49 (12): 7464–7472.
- Valverde, J. M., A. Perejon, and L. A. Perez-Maqueda. 2012. Enhancement of fast CO₂ capture by a nano-SiO₂/CaO composite at Ca-looping conditions. *Environ Sci Technol*, 46 (11): 6401–6408.
- Valverde, J. M., P. E. Sanchez-Jimenez, and L. A. Perez-Maqueda. 2014. Calcium-looping for post-combustion CO₂ capture. On the adverse effect of sorbent regeneration under CO₂. *Appl Energy*, 126: 161–171.
- Wang, W. J., Y. J. Li, X. Xie, and R. Y. Sun. 2014. Effect of the presence of HCl on cyclic CO₂ capture of calcium-based sorbent in calcium looping process. *Appl Energy*, 125: 246–253.
- Wang, W. Y., Z. C. Ye, and I. Bjerle. 1996. The kinetics of the reaction of hydrogen chloride with fresh and spent Ca-based desulfurization sorbents. *Fuel*, 75 (2): 207–212.
- Werther, J., M. Saenger, E. U. Hartge, T. Ogada, and Z. Siagi. 2000. Combustion of agricultural residues. *Prog Energ Combust*, 26 (1): 1–27.
- Wu, S. F., and Y. Q. Zhu. 2010. Behavior of CaTiO₃/Nano-CaO as a CO₂ reactive adsorbent. *Ind Eng Chem Res*, 49 (6): 2701–2706.
- Wu, S. M., Y. J. Li, J. L. Zhao, C. M. Lu, and Z. Y. Wang. 2016. Simultaneous CO₂/SO₂ adsorption performance of carbide slag in adsorption/desorption cycles. *Can J Chem Eng*, 94 (1): 33–40.
- Xie, X., Y. J. Li, C. T. Liu, and W. J. Wang. 2015. HCl absorption by CaO/Ca₃Al₂O₆ sorbent from CO₂ capture cycles using calcium looping. *Fuel Process Technol*, 138: 500–508.
- Xie, X., Y. J. Li, W. J. Wang, and L. Shi. 2014. HCl removal using cycled carbide slag from calcium looping cycles. *Appl Energy*, 135: 391–401.
- Yu, J., and K. Wang. 2011. Study on characteristics of steel slag for CO₂ capture. *Energy Fuels*, 25 (11): 5483–5492.
- Zhang, X. Y., Z. G. Li, Y. Peng, W. Su, X. Sun, and J. Li. 2014. Investigation on a novel CaO-Y₂O₃ sorbent for efficient CO₂ mitigation. *Chem Eng J*, 243: 297–304.

Section II

Industrial and Agricultural Solid Wastes-Based Adsorbents in Water Purification



Taylor & Francis

Taylor & Francis Group

<http://taylorandfrancis.com>

5

Current Progress on the Removal of Hazardous Pollutants from Water Using Agricultural Wastes

Suryadi Ismadji, Felycia Edi Soetaredjo, and Yi Hsu Ju

CONTENTS

5.1	Introduction.....	79
5.2	Modification of Agricultural Wastes for Adsorbents	80
5.2.1	Methods of Modification	80
5.2.1.1	Physical Treatment.....	81
5.2.1.2	Thermal Treatment	81
5.2.1.3	Chemical Treatment.....	82
5.2.2	Characterization.....	84
5.2.2.1	Nitrogen Sorption	85
5.2.2.2	Fourier Transform Infrared (FTIR) Spectroscopy	86
5.2.2.3	Scanning Electron Microscopy	87
5.3	Environmental Application.....	87
5.3.1	Heavy Metals Removal	87
5.3.2	Dye Removal.....	89
5.3.3	Biocides and Other Organic Contaminant Removal.....	90
5.4	Equilibrium, Kinetics, and Thermodynamic Studies.....	91
5.4.1	Adsorption Isotherm Models.....	92
5.4.1.1	Single Component.....	92
5.4.1.2	Single Component: Temperature-Dependent Forms	96
5.4.1.3	Binary Components	97
5.4.2	Adsorption Kinetic Models	99
5.4.3	Thermodynamic of Adsorption.....	101
5.5	Future Perspective	102
5.6	Conclusions.....	103
	References.....	103

5.1 Introduction

Water pollution is one of the more severe environment problems that the world faces. The sources of clean and safe water for human consumption are becoming scarce due to improper disposal of city sewage and industrial waste discharge. Contamination of water with toxic and hazardous chemicals can cause serious health problems to human. A number of technologies are currently available for the treatment of contaminated water such as reverse osmosis, ion exchange, biological treatment, and adsorption. Some of these techniques (reverse osmosis and ion exchange) require high capital investment and

operational cost, whereas others are considered as low-value processes (adsorption and biological treatment).

The adsorption process is known as a versatile method for the removal of hazardous pollutants from water and wastewater. The biggest obstacle to this process is the price of the adsorbent. Currently, most of the industrial adsorption processes for water and wastewater treatment processes use activated carbons as the adsorbents. Commercial activated carbons are expensive, and to reduce the operational cost of the process, it is necessary to find alternative adsorbents to substitute activated carbons. The alternative adsorbents should meet the following criteria: have high adsorption capacities, low cost, available in large quantities in one location, and be easily regenerated (Febrianto et al., 2009). One of the potential candidates as the alternative adsorbent is agricultural wastes.

Hundreds or even thousands of adsorption studies on the utilization of agricultural wastes as alternative adsorbents for water and wastewater treatment purposes have been conducted in the last three decades. A number of review articles on the use of biomass materials for the hazardous substances removal are available (Abdolali et al., 2014; Arief et al., 2008; Bhatnagar et al., 2010; Febrianto et al., 2009; Lesmana et al., 2009; Nguyen et al., 2014). Various aspects of the utilization of low-cost adsorbents including agricultural wastes have been discussed in those review papers. However, with the growing numbers of articles published on this subject, new proposed ideas, and complexity of the adsorption process, it is necessary to provide up-to-date information and comprehensive discussions on the utilization of agricultural wastes as alternative adsorbents. This chapter of the book aims to provide some recent information about the current studies on the use agricultural wastes as alternative adsorbents for water or wastewater treatments. Comprehensive discussions about modification of the adsorbents as well as the use of various adsorption isotherms and kinetic models to represent the equilibria and kinetic data are also given in this chapter of the book.

5.2 Modification of Agricultural Wastes for Adsorbents

Agricultural wastes are lignocellulosic materials, and they are the most abundantly available renewable materials on the earth that can be used as the raw materials for different kinds of applications. Its main composition is cellulose, hemicellulose, and lignin. Since it is abundantly available and renewable materials, the agricultural wastes are considered as low-cost materials. Based on the concept of waste for the treatment of waste, thousands of studies have been carried out to search the potential applications of these low-cost materials as the adsorbents for water and wastewater. However, the main obstacle of the direct use of these materials as the adsorbent is it has low adsorption capacity for most of the hazardous contaminants. Therefore, further treatments or modification processes to increase its adsorption capacity are required.

5.2.1 Methods of Modification

In general, the currently available modification methods of agricultural wastes to improve their adsorption capability can be classified into physical, chemical, thermal treatment, or a combination of them. The physical treatment has the purpose of breaking down the crystallinity of biomass by size reduction. Size reduction of the particle increases the specific

surface area of the biomass and reduces the degree of polymerization. Thermal treatment is the most efficient way to enhance the adsorption capacity of the biomass; however, the drawback of this method is in the cost of the process, since it is conducted at high temperature. Depending on the chemical used, the chemical modification is also very useful in increasing the adsorption performance of the adsorbent. The biggest problem associated with this method is it creates another problem to the environment since the excess chemical agent used in the process will also end up as hazardous waste.

5.2.1.1 Physical Treatment

The physical treatment is the environmental-friendly method of modification of agricultural waste as the adsorbent. However, the success of this treatment depends on the agricultural waste characteristic such as the moisture content or lignin composition. A suitable particle size will obviously have an impact on the adsorption capacity of the biomass. The energy required for the size reduction depends on the input and output size as well as the chemical characteristic of the biomass. Usually, the physical pretreatment is conducted as the first step in the subsequent processes.

Kurniawan et al. (2011a) studied the effect of particle size of cassava peel on the adsorption kinetic of Ni(II) from aqueous solution. Their results indicate that particle size has a significant effect on the time constant (k) and Ni(II) equilibrium uptake (q_e). The smaller the particle size, the faster the system reaches equilibrium. Reducing the size of the particle, increases the surface area of the cassava peels, and the crystallinity of the cellulose is disrupted, and the internal hydroxyl groups of the biomass are more exposed and accessible to the Ni(II) ions. Therefore, there is more chance for Ni(II) ions to bind to the hydroxyl groups of the surface of cassava peel, therefore it will increase the amount of Ni(II) uptake.

The removal of Cr(VI) from the aqueous solution using durian shells as the adsorbent was conducted by Kurniawan et al. (2011b). Their experimental results indicate that smaller particle size of the durian shell gave higher removal of Cr(VI). For the same amount of durian shell, smaller particle size has larger surface area so more active binding sites on the adsorbent surface were exposed and available for Cr(VI) adsorption (Kurniawan et al., 2011b). They found that the maximum biosorption capacity of durian shell was 117 mg/g at solution pH of 2.5 and temperature of 60°C.

Studies of the physical treatment as the only process of the preparation of agricultural wastes as biosorbents have been carried out by many researchers. These studies include the use of pomegranate peels to investigate the removal of Pb(II) and Acid Blue 40 (Ay et al., 2012), malt bagasse as the biosorbent for adsorption of orange solimax dye (Fontana et al., 2016), *Lansium domesticum* peel biosorbent for removal of Ni(II) (Lam et al., 2016), rice husk and palm leaf for removal of several heavy metals (Sadeek et al., 2015), and *Cucumis sativus* peel for efficient removal of Acid Blue 113 (Lee et al., 2016). The results from most of the studies indicate that the physical pretreatment process is sufficient enough for the treatment of agricultural wastes as the adsorbents for hazardous substances removal from aqueous solutions.

5.2.1.2 Thermal Treatment

The well-known thermal treatment processes of agricultural wastes to increase their adsorption capability are carbonization and pyrolysis. In the carbonization process, the agricultural waste reacts with a control amount of oxygen or steam at high temperature without the combustion process. In this carbonization process, the structure of lignin,

hemicellulose, and cellulose will be broken down into carbon monoxide, carbon hydroxide, and hydrogen. Unreacted carbon together with inorganic matters will remain as the solid residue called biochar. This biochar possesses a porous structure; with the presence of micropore and mesopore in this structure, it will enhance the adsorption capability of the solid.

Pyrolysis is thermal decomposition of organic material in the absence of oxygen and other oxidizing gases. In the pyrolysis of agricultural waste, cellulose, hemicellulose and lignin will be decomposed into smaller molecular organic compounds and gases, and the solid residue from this process is a porous solid called biochar. This biochar has a much higher adsorption capacity compared to the original agricultural waste; however, to improve the adsorption ability, an activation process using chemicals and gases is carried out. The result from this activation process is a porous solid carbon called activated carbon.

Table 5.1 summarizes several thermal treatments or conversion of agricultural wastes into activated carbon. In most cases, the combination with chemical treatment is necessary to improve the adsorption performance. The improvement of the adsorption ability of the resulting product of the thermal treatment of agricultural waste is mainly due to the release of volatile matter and pore development within the solid material. Thermal treatment can significantly increase the BET (Brunauer–Emmett–Teller) surface area of the resulting product, hundreds or even thousand times larger than the initial BET of agricultural residue (Koseoglu and Akmil-Basar, 2015; Li et al., 2016).

In the thermal treatment of agricultural waste, the temperature plays a significant role in the yield of biochar or activated carbon. In most cases, the yield of biochar or activated carbon decreases with an increase in temperature. Koseoglu and Akmil-Basar (2015) studied the preparation of activated carbon using orange peel as the precursor. To enhance the pore development, they used potassium carbonate (K_2CO_3) and zinc chloride ($ZnCl_2$) as activating agents. The increase in thermal treatment temperature led to a decrease in the yields of both K_2CO_3 and $ZnCl_2$ activated carbons. The yield of $ZnCl_2$ activated carbon was higher than that of K_2CO_3 activated carbon.

The use of K_2CO_3 and $ZnCl_2$ as the activating agents significantly improved the pore development; however, both of these activating agents acted differently in widening and creating the pore during thermal treatment. Potassium has strong alkaline properties; therefore, it will catalyze the oxidation reaction (Sudaryanto et al., 2006). With the increase in temperature, the oxidation of the carbon becomes severer, and in most cases, the yield of biochar or activated carbon is less than fixed carbon in the initial precursor. In the case of $ZnCl_2$, the zinc metal can retard the release of volatile matters; therefore, the yield of activated carbon activated with $ZnCl_2$ is higher than activated carbon impregnated with potassium salts.

5.2.1.3 Chemical Treatment

The adsorption of hazardous substances from aqueous solution to agricultural wastes is based on the binding mechanism between the pollutant molecules and the surface functional groups of biomass. Cellulose, hemicellulose, and lignin are the main constituents in the agricultural wastes. Therefore, most of the functional groups of the surface of biomass belong to those constituents. Cellulose has a general formula $(C_6H_{10}O_5)_n$ and is a crystalline polymer that consists of a linear chain of hundreds or even thousands of β -linked D-glucose units. Hemicellulose is an amorphous polymer with complex structure. Its structure consisted of xylose, mannose, arabinose, galactose, glucose, and some sugar acids. Chemically and structurally, hemicellulose is

TABLE 5.1

Thermal Treatment or Conversion of Several Agricultural Wastes into Activated Carbons and Their Application for the Removal of Hazardous Substances from Aqueous Solution

Agricultural Waste	Condition of Thermal Treatment	Adsorbate	Maximum Adsorption Capacity	Reference
Apricot stones	H ₃ PO ₄ + HNO ₃ activation; T = 700°C for 1 h	Methylene blue and methyl orange	36.68 mg/g for methylene blue and 32.25 mg/g for methyl orange	Djilani et al., 2015
Avocado seed	Impregnation with methanesulfonic acid; T = 700°C for 1.5 h	NH ₄ ⁺	5.4 mg/g	Zhu et al., 2016
Coconut shell	T = 800°C–1000°C; steam activation	Sulfamethoxazole	130.73 mg/g	Tonucci et al., 2015
Fig sawdust	H ₃ PO ₄ activation; T = 150°C for 24 h	Pb(II)	80.64 mg/g	Ghasemi et al., 2014
Hazelnut husk	Activating agent ZnCl ₂ ; T = 700°C for 4 h	Methylene blue	476.19 mg/g	Karacetin et al., 2014
Langsat empty fruit bunch	H ₃ PO ₄ activation; T = 500°C for 2 h	2,4-Dichloro-phenoxyacetic acid	261.2 mg/g	Njoku et al., 2015
Mug bean husk	Steam activation; T = 650°C	Ibuprofen	62.5 mg/g	Mondal et al., 2016
Orange peel	T = 500°C–1000°C; activating agents: ZnCl ₂ and K ₂ CO ₃	Methylene blue	150 mg/g	Koseoglu and Akmil-Basar, 2015
Pineapple waste	Impregnated with ZnCl ₂ ; T = 500°C for 1 h	Methylene blue	288.34 mg/g	Mahamad et al., 2015
Pomelo peel	Activating agent KOH; T = 450°C for 1.5 h, and 800°C for 2.5 h	Methyl orange	680.2 mg/g	Li et al., 2016
Potato peel	KOH activation; T = 600°C for 2 h	Pramipexole dihydrochloride and dorzolamide	89 mg/g for pramipexole and 70 mg/g for dorzolamide	Kyzas and Deliyanni, 2015
<i>Prosopis africana</i> seed hulls	CH ₃ COONa as activating agent; T = 795°C for 62 min	<i>p</i> -Chlorophenol and 2,4-Dichlorophenol	347.47 mg/g for <i>p</i> -Chlorophenol and 380.75 mg/g for 2,4-Dichlorophenol	Garba and Rahim, 2016
Rambutan peel	KOH activation, microwave heating for activation, time 12 min	Acid yellow 17	215.05 mg/g	Njoku et al., 2014a
Sky fruit husk	T = 500°C for 2 h	Herbicide bentazon	166.67 mg/g	Njoku et al., 2014b
Wild olive cores (<i>Oleaster</i>)	H ₃ PO ₄ activation; T = 805°C for 2 h	Basic red 46	781.25 mg/g	Kaouah et al., 2013

similar to cellulose. Lignin is an amorphous polymer matrix that consists of three basic units: p-hydroxyphenyl (H), guaiacyl (G), and syringyl (S) (Putro et al., 2016).

Chemical treatment is conducted to improve agricultural waste accessibility; during the adsorption process, the adsorbates should be able to penetrate the internal structure of the adsorbent to increase the adsorption capability. Mostly lignin will act as the barrier to prevent the penetration of adsorbate molecules into the structure of cellulose and hemicellulose. Chemical pretreatment process will remove some lignin and hemicellulose from the structure of agricultural waste. Lignin is chemically connected to the hemicellulose through covalent bonding; therefore, the lignin removal also will remove some of the hemicellulose (Putro et al., 2016). The chemicals used for chemical pretreatment of agricultural wastes can be classified as alkaline, dilute acid, organic solvent, ionic liquid, and surfactant. Table 5.2 lists the use of chemicals for the treatment of agricultural wastes as the adsorbents for the removal of various hazardous substances from an aqueous solution.

Ding et al. (2014) have conducted modification of peanut hull using various kinds of chemicals. The chemicals used in their experiment were 17.5% aqueous sodium hydroxide (NaOH), 0.6 M of citric acid, and 1 M of nitric acid. The purpose of impregnation with sodium hydroxide solution was to break down the structure of the peanut hull. Sodium hydroxide at this concentration can solubilize the polyoses and hydrolyze the ether bonds in the structure of biomass. With the breakdown of the ether bonds due to the hydrolysis reaction, the lignin structure is degraded. Since lignin is chemically bonded with hemicellulose through covalent bonding, some of the hemicelluloses will also be removed as mentioned in the previous paragraph. The removal of lignin and some part of hemicellulose will decrease the crystallinity of the biomass and led to the exposure of the internal hydroxyl groups of the biomass (Ding et al., 2014). The impregnation of biomass with sodium hydroxide solution increased the carboxyl groups in the surface of modified peanut hull. The addition of citric acid and nitric acid to delignified peanut shell increased the oxygen-containing surface functional groups on the surface of modified peanut hull. In the adsorption process using biomass as the adsorbent, the primary mechanism of adsorbate removal is the chemical bonding between surface functional groups and adsorbate molecules. Therefore, the increase in the surface functional groups also increases the adsorption capability. The maximum adsorption capacity of modified peanut hull is around 18.41–69.5 mg/g for Pb(II) and 28.9–49.6 mg/g for methylene blue (MB).

5.2.2 Characterization

After pretreatment process, the characterization of the modified agricultural waste should be conducted to understand the change of physical and chemical properties of the solids. Understanding of the chemical as well as the physical properties of agricultural wastes is very crucial in knowing the mechanisms of the adsorption of the hazardous pollutant on the biomass. Characterization of agricultural wastes and their modified forms as the adsorbents is usually conducted using nitrogen sorption, Fourier transform infrared (FTIR) spectroscopy, scanning electron microscopy (SEM), x-ray photo electron spectroscopy (XPS), energy dispersive x-ray (EDX) fluorescence spectrophotometry, x-ray diffraction, or thermal gravimetric analysis (TGA). To collect complete information about the physical as well as the chemical properties of the agricultural waste, these methods are usually utilized together.

TABLE 5.2

Chemical Treatment of Several Agricultural Wastes as the Adsorbents for the Removal of Hazardous Substances from Aqueous Solution

Agricultural Waste	Chemical and Operating Condition	Adsorbate	Maximum Adsorption Capacity	Reference
Barley straw	Citric acid; $T = 60^{\circ}\text{C}$ for 24 h	Cu(II)	31.71 mg/g	Pehlivan et al., 2012
Citrus peel	HCl, HNO_3 , NaOH, EDTA, SDS, CTAB, and NH_4OH	Zr(IV)	42.02 mg/g	Bhatti et al., 2016
Cottonwood	KOH; $T = 25^{\circ}\text{C}$ for 4 h	Pb(II)	7.28 mg/g	Mosa et al., 2016
Guava seed	NaOH; $T = 150^{\circ}\text{C}$ for 8 min	Methylene blue	40.9 mg/g	Pezoti et al., 2016
Maize husk leaf	$\text{Ca}(\text{OH})_2$; $T = 25^{\circ}\text{C}$ for 24 h	Malachite green	81.5 mg/g	Jalil et al., 2012
Maize spathe	HNO_3 ; $T = 25^{\circ}\text{C}$ for 2 h	Cu(II)	44.9 $\mu\text{mol/g}$	Djemmo et al., 2016
Olive stone	H_2SO_4 , HNO_3 , and NaOH	Pb(II)	–	Ronda et al., 2015
Orange peel	Citric acid; $T = 80^{\circ}\text{C}$ for 2 h	Cu(II) and phenol	32.51 mg/g for phenol and 106.91 mg/g for Cu(II)	Romero-Cano et al., 2016
Peanut hulls	NaOH, HNO_3 , and citric acid; $T = 25^{\circ}\text{C}$ for 72 h	Pb(II) and methylene blue	18.41–69.5 mg/g for Pb(II) and 28.9–49.6 mg/g for MB	Ding et al., 2014
Rice husk	Hydroxyethylidenedi-phosphonic acid and nitrilotrimethylenetri-phosphonic acid; $T = 120^{\circ}\text{C}$ for 4 h	Au(III), Hg(II), Cu(II), Co(II), and Zn(II)	0.02–1.15 mmol/g	Xu et al., 2013
Rice husk	HCl, HNO_3 , NaOH, EDTA, SDS, CTAB, and NH_4OH	U(VI)	For native biomass 29.56 mg/g at pH 4; SDS-treated rice husk 28.08 mg/g at pH 5	Kausar et al., 2013
Tomato waste	HCl	Cu(II)	34.48 mg/g	Yargic et al., 2015

5.2.2.1 Nitrogen Sorption

In the characterization of agricultural waste, the nitrogen sorption measurement is usually conducted to obtain the surface area of the solid. Nitrogen measurement is carried out at the boiling point of nitrogen gas (-196°C). The surface area of the solid is calculated by applying the BET equation to nitrogen adsorption isotherm data at a relative pressure in the range of 0.05 to 0.25. Due to the nonporous structure of the biomass, a low BET surface area is the characteristic of these kinds of materials (Chao et al., 2014; Koseoglu and Akmil-Basar, 2015; Li et al., 2016). With a low BET surface area and nonporous structure, the physical adsorption does not play any significant role in the adsorption of hazardous substances onto agricultural wastes.

5.2.2.2 Fourier Transform Infrared (FTIR) Spectroscopy

The presence of surface functional groups of agricultural wastes is the most important characteristic as the adsorbent. These surface functional groups can be determined qualitatively using FTIR spectroscopy. Using this instrument, the surface functional groups of agricultural wastes can be determined through monitoring of the vibrations of the functional groups. These vibrations characterize molecular structure of organic molecules. Since the FTIR method is very powerful, this technique is widely used for the characterization of surface functional groups of the adsorbents derived from the biomass or agricultural wastes.

The agricultural wastes are lignocellulosic materials, which contain cellulose, hemicellulose, and lignin. The cellulose chains contain both ordered (crystalline) and less ordered (amorphous) regions. The typical absorption wavenumbers for amorphous cellulose are 699 cm^{-1} (OH out of phase bending), 894 cm^{-1} (nonsymmetric out-phase ring), 1040 cm^{-1} (C–O), 1070 cm^{-1} (skeletal vibrations C–O), 1159 cm^{-1} (nonsymmetric bridge C–O–C), 1374 cm^{-1} (CH bending), 1420 cm^{-1} (CH₂ symmetric bending), 2892 cm^{-1} (CH), and 3420 cm^{-1} (OH) (Fan et al., 2012). The amount of crystalline versus amorphous structure of the cellulose is indicated at the absorption wavenumbers 1420 cm^{-1} and 894 cm^{-1} . If the bands of these wavenumbers are broad, the cellulose contains more disordered structure (Fan et al., 2012).

Lignin is an amorphous polymer, which has a more complex structure than cellulose or hemicellulose. The chemical structure of lignin distinctly differs from cellulose and hemicellulose. Lignin polymer contains carbonyl groups, phenolic hydroxyl groups, methoxyl groups, aliphatic hydroxyl groups, benzyl alcohol groups, and some terminal aldehyde groups. The wavenumbers of functional groups in lignin are as follow: 3431 cm^{-1} (hydroxyl groups in phenolic and aliphatic structures), 2937 cm^{-1} (CH stretching in aromatic methoxyl groups, and methyl and methylene groups of the side chains), 2848 cm^{-1} (C=O stretching in conjugated *p*-substituted aryl ketones), 1700 cm^{-1} (C=C stretching of the aromatic ring [syringyl], CH deformation), 1602 cm^{-1} (C=C stretching of the aromatic ring [guaiacyl], CH deformation), 1512 cm^{-1} (C–H asymmetric deformation in CH₂ and CH₃), 1460 cm^{-1} (C–H asymmetric deformation in –OCH₃), 1425 cm^{-1} (C–O stretch in lignin, C–O linkage in guaiacyl aromatic methoxyl groups), 1357 cm^{-1} (syringyl ring breathing with C–O stretching), 1328 cm^{-1} (aromatic C–H in-plane deformation, typical of guaiacyl units), 1267 cm^{-1} (aromatic C–H in-plane deformation [typical of S units] plus secondary alcohols plus C=O stretching), 1219 cm^{-1} (C–O deformation in secondary alcohols and aliphatic ethers), and 1086 cm^{-1} (deformation vibrations of the C–O bands in primary alcohols) (Todorceuc et al., 2009).

As mentioned in the previous section, hemicellulose is a complex amorphous polymer of C₅, C₆, and acid sugars. Due to the vast structural diversity, numerous absorption bands are possible for this amorphous polymer (Sim et al., 2012). FTIR absorbance bands of hemicellulose are as follows: 1750 cm^{-1} (free ester), 1730 cm^{-1} (ketone/aldehyde C=O stretch), 1440 cm^{-1} (O–H in-plane bending), 1380 cm^{-1} (C–H bending), 1335 cm^{-1} (C–H vibration, O–H in-plane bending), 1200 cm^{-1} (O–H bending), 1160 cm^{-1} (C–O–C asymmetrical stretching), 1035 cm^{-1} (C–O, C=C, C–C–O stretching), and 930 cm^{-1} (glycosidic linkage).

Due to the complex structure of agricultural wastes, the FTIR analysis of these biomasses showed many peaks and mostly are the functional groups of cellulose, hemicellulose, and lignin (Ay et al., 2012; Bhatti et al., 2016; Blazquez et al., 2011; Fontana et al., 2016; Gilbert et al., 2011; Kurniawan et al., 2011a, 2011b; Mosa et al., 2016; Pezoti et al., 2016; Sadeek et al., 2015; Safa and Bhatti, 2011; Santos et al., 2015; Soetaredjo et al., 2013; Yargic et al., 2015;

Zhao and Zhou, 2016). Several peaks belonging to minor constituents such as waxes, volatile oils, water-soluble components, and pectin were also detected in the FTIR spectra of agricultural wastes (Blazquez et al., 2011; Gilbert et al., 2011; Safa and Bhatti, 2011; Santos et al., 2015).

The surface functional groups of the agricultural wastes are believed to be involved in various metal-binding mechanisms in the adsorption process. Blazquez et al. (2011) studied the biosorption of Pb(II) from aqueous solutions using olive tree pruning waste. Based on the FTIR analysis and the results of the adsorption equilibria and kinetic studies, they found that the carboxyl, amide, and carboxylate groups participated in Pb(II) uptake. The FTIR spectra were also used to investigate the binding mechanism of Pb(II) and Cd(II) on defatted *C. Papaya* seed (Gilbert et al., 2011). Based on the assessment of the FTIR spectra, they found that some functional groups such as enolic esters, lactones, amide, quinones, and carbocyclic acid are involved in the binding of Pb(II) and Cd(II).

5.2.2.3 Scanning Electron Microscopy

Scanning electron microscopy (SEM) is one of the most widely used techniques to characterize the surface topography or morphology of agricultural wastes. This method offers direct observation of the surface structure of solids. Modern SEM also provides elemental information about the solids. The capability to provide an actual image of the surface of solids makes this method very useful for obtaining the topographical aspects of the agricultural wastes (Kurniawan et al., 2011a; Mosa et al., 2016; Safa and Bhatti, 2011; Soetaredjo et al., 2013; Yuvaraja et al., 2014).

5.3 Environmental Application

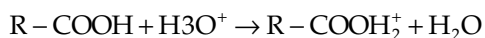
Many studies have been conducted for the removal of hazardous substances from water using agricultural wastes. In several cases, the adsorption capacity of some agricultural wastes toward some dangerous substances is small; however, many scientists still try to explore the potential application of these agricultural wastes as alternative biosorbents. Reasons for using agricultural residue as biosorbent is that it is an abundantly available and renewable resource. In this section, the use of agricultural residues for the removal of heavy metals, dyes, biocides, and other organic contaminants will be discussed.

5.3.1 Heavy Metals Removal

The presence of heavy metals in a water environment is known to be harmful to human and aquatic biota. Heavy metals can cause severe health effects on humans, and each metal leads to different health effects. Some heavy metals commonly found in water environments as pollutants are As(V), Cd(II), Cr(III), Cr(VI), Cu(II), Hg(II), Mn(II), Ni(II), Pb(II), and Zn(II). The primary targets for the poisoning of As(V) are skin, liver, and eyes. At a certain level, the As(V) may also cause cancer. Impacts of Cr(VI) on human health are headache, nausea, severe diarrhea, vomiting, epigastric pain, hemorrhage, provokes cancer, and an adverse potential to modify the DNA transcription process. The poisoning of Hg(II) on a human can cause damage to the nervous system, kidneys, and eyes, and protoplasm poisoning (Arief et al., 2008; Febrianto et al., 2009; Ismadji et al., 2015).

Natural elimination of heavy metals from the environment is tough due to the persistent properties of the heavy metals. Hence, the removal of heavy metals from wastewater is imperative to protect the environment and human health (Ghasemi et al., 2014). One of the most efficient methods of the removal of heavy metals from water and wastewater is the adsorption process. Thousands of studies for the removal of heavy metals from aqueous solutions using various kinds of adsorbents have been conducted in the last of 30 years. The results of the studies indicate that agricultural wastes are potential adsorbents for removal of heavy metals from aqueous solutions (Bhatti et al., 2016; Ding et al., 2014; Djemmoe et al., 2016; Kurniawan et al., 2011a, 2011b; Mosa et al., 2016; Pehlivan et al., 2012; Romero-Cano et al., 2016; Ronda et al., 2015; Xu et al., 2013; Yargic et al., 2015; Zhao and Zhou, 2016).

The adsorption of heavy metal onto agricultural wastes is strongly affected by the pH of the solution. Kurniawan et al. (2011a) studied the influence of pH on the uptake of Ni(II) on cassava peel. They found that the amount of Ni(II) uptake by the cassava peel increased with the increase of pH and reached a maximum at pH 4.5. At higher pH, the formation of Ni(OH)₂ occurred, and the removal of Ni(II) increased due to precipitation of Ni(II) as a metal hydroxide. However, the uptake of Ni(II) by adsorption process decreased, and some of the Ni(II) ions in the solution have been converted to its hydroxide and this phenomenon reduced the concentration of Ni(II) ions in the solution. Low Ni(II) uptake at low pH is possibly due to the competition for the active adsorption sites between hydronium ions (H₃O⁺) and Ni(II) ions. At low pH, the carboxylic groups (R-COOH) are protonated by hydronium ion according to the following reaction:



The surface charge of some functional groups of the cassava peel became positive at low pH. Therefore, the repulsion force is more dominant than the attraction force, since Ni(II) ions also have positive charge resulting in a decrease of the Ni(II) uptake (Kurniawan et al., 2011a).

The influence of pH on the Pb(II) adsorption onto *Solanum melongena* leaf was studied by Yuvaraja et al. (2014). The adsorption study was conducted within the pH range of 2.0 to 8.0. At low pH, the protonation of some functional groups occurred, and these functional groups become unavailable for binding with Pb(II). At a pH higher than 5, the formation of Pb(OH)₂ from Pb(II) occurred, and the mechanisms of Pb(II) removal were adsorption and precipitation. Several possible complexation mechanisms between Pb(II) and surface functional groups (carboxyl, hydroxyl, and amino functional groups) in *Solanum melongena* leaf were also proposed by the authors (Yuvaraja et al., 2014).

The effect of pH on the adsorption of heavy metals onto agricultural wastes also can be explained in terms of pH_{pzc} (pH at point zero charges) (Kurniawan et al., 2011b; Soetaredjo et al., 2013; Srivastava et al., 2015; Yuvaraja et al., 2014). The pH_{pzc} is one of the important characteristics of the adsorbents, especially for agricultural wastes. If the pH of the aqueous solution is below the pH_{pzc} of the adsorbents, the protonation of some functional groups of the surface of adsorbent occurs, resulting in the positive charge in the surface of adsorbents, and the repulsive force is more dominant than the attraction force; therefore, less metal ions are adsorbed. If the pH of the aqueous solution is higher than pH_{pzc}, the surface charge of the adsorbents is negative and more metal ions in the solution are attracted in the surface of agricultural wastes (Yuvaraja et al., 2014).

Temperature is also one important process parameter on the adsorption of heavy metals onto agricultural wastes (Blazquez et al., 2011; Kurniawan et al., 2011a; Soetaredjo et al., 2013). Temperature has quite a significant effect on the adsorption capacity of agricultural wastes. If the physical adsorption controls the adsorption mechanism, the temperature has a negative effect on the uptake of heavy metals (Bhatti et al., 2016; Lam et al., 2016). When chemisorption is the control mechanism, the uptake of heavy metals increases with the increase in temperature (Kumar et al., 2016; Kurniawan et al., 2011a, 2011b; Soetaredjo et al., 2013; Srivastava et al., 2015; Yuvaraja et al., 2014; Zhao et al., 2016).

5.3.2 Dye Removal

Since the beginning of human civilization, dyes have been used in coloring many things. All the dyes used at those times came from natural sources. However, beginning in late of 19th and early 20th centuries, synthetic dyes began to replace natural colorants. Currently, thousands of synthetic dyes are available on the market. The classification of synthetic dyes usually is made according to their structure. Currently, synthetic dyes are classified into 30 groups, such as anthraquinone, azine, azo, diarylmethane, indamine, indigoid, methine, and thiazole (Ismadji et al., 2015).

Some synthetic dyes are highly toxic and carcinogenic, and the direct discharge of wastewater containing these dyes into a water environment will damage the aquatic ecosystems and life. Even in a small amount, the presence of dyes in aquatic environment can disrupt the process of photosynthesis due to blocking of the penetration of sunlight into water (Ay et al., 2012; Deniz and Kepecki, 2016; Fontana et al., 2016; Lee et al., 2016; Pathania et al., 2016; Qi et al., 2011; Safa and Bhatti, 2011). Most of the synthetic dyes are designed to be stable chemically or photolytically, therefore, once they are released to the environment, they will present as a pollutant for a long time. Bioaccumulation of dyes into aquatic biota is a potential danger to humans. Through the food chain, it will be transferred into the human body causing health problems such as an allergic reaction, or severe damage to the kidney, central nervous system, reproductive system, and liver.

Several technologies are available for the removal of dyes from a water environment or wastewater. For polluted water with a high concentration of dye, the most suitable removal technologies are chemical oxidation, membrane separation, coagulation, and aerobic and anaerobic microbial degradation. For a medium to low concentration of dye, the adsorption process using various kinds of adsorbents is the best choice for the treatment of water or wastewater. Some adsorption studies for the removal of dyes from aqueous solution have been conducted to find adsorbents with high adsorption capacity and cheap production cost. Agricultural wastes are believed to be the best candidates as the adsorbents for the removal of dyes from water or wastewater. Similar to the adsorption of heavy metals, the factors affecting the removal of dyes by agricultural wastes are the pH of solution, temperature, and initial concentration (Ay et al., 2012; Deniz and Kepecki, 2016; Fontana et al., 2016; Lee et al., 2016; Pathania et al., 2016; Qi et al., 2011; Safa and Bhatti, 2011). Safa and Bhatti (2011) studied Everdirect Orange-3GL and Direct Blue-67 dyes from aqueous solution on rice husk. The maximum removal of Everdirect Orange-3GL was 27.72 mg/g obtained at pH 1, whereas for Direct N Blue-106 it was 54.39 mg/g at pH 3.

The effect of pH on the adsorption of neutral red onto spent cottonseed hull substrate was studied by Qi et al. (2011). The adsorption experiments were conducted at a range

of pH from 2.0 to 7.0. The uptake of neutral red onto spent cottonseed hull substrate increased with an increase of pH from 2.0 to 4.0. A further increase of the solution pH to 7.0 did not much change the amount of neutral red adsorbed by the biomass. The surface of spent cottonseed hull substrate has some active functional groups such as carboxyl and hydroxyl groups. At a low pH, these functional groups were protonated and had positive charges. Since neutral red is a cationic dye, in the solution this colorant will exist in the form of positively charged ions. Since both of the surface functional groups and the dye ions were positively charged, the repulsion force was more dominant than the attraction force. Therefore, fewer dye ions were adsorbed onto the surface of the biomass. Qi et al.'s (2011) experimental results show that in the first 5 minutes, rapid uptake of dye was observed, and equilibrium time was achieved after 240 min. They also found that the final equilibrium pH was higher than the initial pH; this phenomenon is possibly due to the release of some basic functional groups into the solution during the adsorption process.

5.3.3 Biocides and Other Organic Contaminant Removal

Biocides are defined as chemical substances or microorganisms to control or inhibit the growth or to prevent any harmful activities of bacteria. Biocides are widely used in medicine, aquaculture, agriculture, foods, and various kinds of industries. Some of the biocides possess a broad spectrum of antimicrobial activity (Ong et al., 2014). Due to the massive use of biocides, the disposal of waste or wastewater containing these substances cannot be avoided. Since the purpose of using biocides is to inhibit the growth or to kill bacteria or living microorganisms, the presence of these substances in the environment can cause severe damage to the ecosystem, especially the water ecosystem.

Adsorption has proven to be one of the best methods for the removal of biocides from water and wastewater. Table 5.3 summarizes several studies on the adsorption of some biocides onto agricultural wastes and their modified forms. The use of herbicide in the modern agriculture system cannot be avoided. However, one of the main problems is some parts of the herbicides will enter the aquatic ecosystem through the irrigation or rainfall water (Ouyang et al., 2016). Atrazine is a herbicide of the triazine class, which is widely used to control or to stop the growth of broadleaf and grassy weeds in crops. This biocide has been known to have negative effects on humans and animals; it causes hormone imbalance. Ouyang et al. (2016) studied the sorption properties of this biocide onto biochar derived from four agricultural wastes (corn cob, corn stalk, soybean straw, and corn stalk paralyzed with 5% of ammonium dihydrogen phosphate). For the adsorption study, they mixed the biochar with a high organic matter content of soil. Their experimental results indicated that the soil amended with rice straw and corn stalk biochar had the biggest removal rate. The soil amended with biochar was the effective way to prevent leakage of diffuse herbicide loss.

In some cases, the agricultural wastes have better adsorption performance than soil for the removal of pesticides from water environment (Rojas et al., 2014). In their study, Rojas et al. (2014) used atrazine, alachlor, endosulfan sulfate, and trifluralin as the adsorbates for adsorption experiments. The adsorbents used for the study were sunflower seed shells, rice husk, composted sewage sludge, and soil. The solubility of the pesticides had a significant influence on the uptake of pesticides by the adsorbents. The more soluble the pesticides were in water, the more difficult it was to be adsorbed onto the adsorbents (Rojas et al., 2014).

TABLE 5.3

Studies on the Adsorption of Some Biocides onto Agricultural Wastes and Their Modified Forms

Agricultural Waste	Biocide	Performance	Reference
Corn straw	Atrazine	Corn straw was converted into biochar at 450°C. Pretreatment using ammonium dihydrogen phosphate improved the adsorption capacity of biochar.	Zhao et al., 2013
Corn cob, corn stalk, and soybean straw	Atrazine	The agricultural wastes were converted into biochar at 450°C. Results showed that biochar amendment is the effective way to prevent leakage of diffuse atrazine loss.	Ouyang et al., 2016
Guava seeds	Isoproturon	Guava seed was carbonized and combined with TiO ₂ . Carbonization was conducted at a temperature of 500°C. 99% of isoproturon was removed and degraded.	Davila-Jimenez et al., 2016
<i>Phragmites australis</i> (reed)	Pentachlorophenol	Reed biomass was carbonized at 300°C to 600°C. The resulting chars were washed with 1 M of HCl solution. Acid washed biochars have higher adsorption capacity than pristine biochars.	Peng et al., 2016
Rice husk	Glyphosate	Rice husk was carbonized at slow heating rate and activated by steam activation. Maximum glyphosate removal was 82.0% at pH 4.	Herath et al., 2016
Rice straw	Clofibric acid and carbamazepine	The maximum adsorption capacity for clofibric was 126.3 mg/g while for carbamazepine was 40.0 mg/g.	Liu et al., 2013
Soybean, corn stalks, and rice stalks	Atrazine	Biomasses were converted into biochar at 450°C. Physical adsorption mechanism controlled the adsorption process of atrazine into biochars.	Liu et al., 2015
Sunflower seed shells and rice husk	Atrazine, alachlor, endosulfan sulfate, and trifluralin	Rice husk gave maximum removal efficiency (73.9%).	Rojas et al., 2014

5.4 Equilibrium, Kinetics, and Thermodynamic Studies

The study of equilibrium, kinetics, and thermodynamic in the adsorption system perhaps can provide a clear picture of the adsorption process itself. Different adsorption systems give different adsorption phenomenas, therefore, even though a large number of adsorption studies have been conducted and the results are available in the literature, the study of equilibrium, kinetic, and thermodynamic of adsorption is still required for a new adsorption system.

5.4.1 Adsorption Isotherm Models

The relevant adsorption equilibria data are some of the most important information required for the proper analysis and design of the adsorption process. Usually, the adsorption equilibria data are represented in terms of the mathematical model known as the adsorption isotherm equation. Currently, there are some adsorption isotherm models available to represent the adsorption experimental data. Most of the models initially were developed to represent the gas phase adsorption data, and later on these models were adopted to correlate liquid phase adsorption data by just changing the term of pressure with concentration. Some of the available models are purely empirical with two or three adjustable parameters, and others possess thermodynamic backgrounds in the model development. Some of the well-known adsorption isotherm equations that are widely used to correlate the liquid phase adsorption data are Langmuir, Freundlich, Sips, Toth, Dubinin–Radushkevich, and Redlich–Peterson. The applications of these models to correlate the adsorption of various hazardous substances on agricultural wastes are discussed in subsequent sections.

5.4.1.1 Single Component

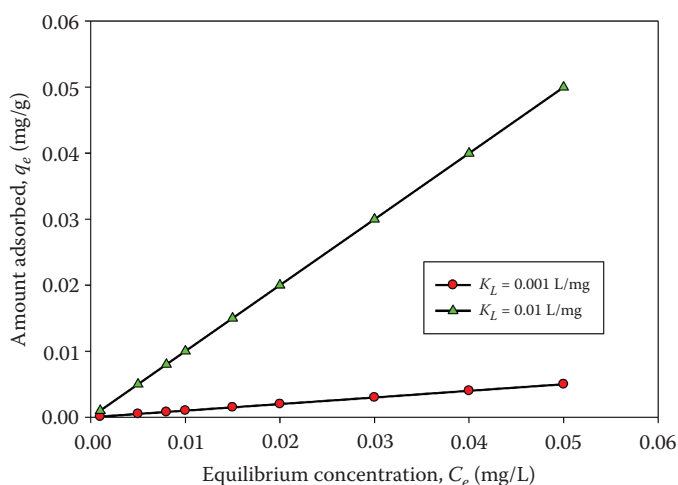
The Langmuir equation probably is one of the most widely used adsorption models to correlate the liquid phase adsorption equilibria of hazardous substances on agricultural wastes. This equation was developed according to three basic assumptions: the surface is homogeneous, adsorption on the surface is localized, and each site can only accommodate one molecule (Do, 1998). This equation has the mathematical form as follows:

$$q_e = q_{\max} \frac{K_L C_e}{1 + K_L C_e} \quad (5.1)$$

where q_e and q_{\max} are the amount of adsorbate adsorbed at equilibrium condition (mg/g or mmol/g) and adsorption capacity of the adsorbate (mg/g or mmol/g), respectively. The equilibrium concentration is indicated by the symbol C_e (mg/L or mmol/L), and K_L is the Langmuir constant that represents the adsorption affinity.

The Langmuir equation is perhaps the only equation that could well represent the adsorption experimental data for many systems including the adsorption of hazardous substances onto agricultural wastes. When the concentration of adsorbate is very low ($K_L C_e \ll 1$), the Langmuir equation reduces to the Henry law isotherm (Do, 1998), whereby the uptake of the adsorbate increases linearly with concentration, as indicated by Figure 5.1. In most cases, the adsorptions of hazardous pollutants onto agricultural wastes were conducted at medium concentration, therefore, the representation of this Henry law isotherm to adsorption equilibria data is rarely found in the literature.

At high equilibrium concentration, all of the active adsorption sites completely filled with adsorbate molecules and this phenomenon corresponds to the adsorption capacity of the adsorbent, therefore, this model is widely used for the determination of the adsorption capacity of agricultural wastes as the adsorbents (Blazquez et al., 2011; Djemmoe et al., 2016; Kurniawan et al., 2011a; Lee et al., 2016; Mahajan and Sud, 2012; Mushtaq et al., 2016; Sadeek et al., 2015; Santos et al., 2015; Soetaredjo et al., 2013; Sun et al., 2015; Wang et al., 2015; Yargic et al., 2015; Zhao and Zhou, 2016). Low values of adsorption capacities of several agricultural wastes indicate that these low-cost adsorbents do not have any potential application for industrial wastewater treatment (Liu et al., 2013; Santos et al., 2015).

**FIGURE 5.1**

Henry law in Langmuir isotherm.

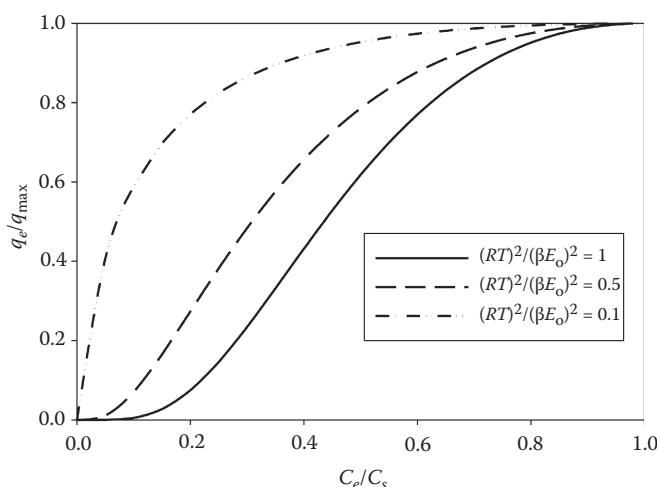
The Freundlich equation was the first empirical model to describe the liquid phase adsorption equilibria:

$$q_e = K_F C_e^{1/n} \quad (5.2)$$

where K_F ((mg/g)(L/mg) $^{-n}$ or (mmol/g)(L/mmol) $^{-n}$) is the Freundlich characteristic constant that relates to the adsorption capacity of the adsorbent, and n is the characteristic constant that relates to the heterogeneity of the system or adsorption intensity. The Freundlich equation is one of the most widely used adsorption isotherms to correlate the adsorption of hazardous pollutants onto agricultural wastes (Blazquez et al., 2011; Djemmoe et al., 2016; Kurniawan et al., 2011a; Lee et al., 2016; Mahajan and Sud, 2012; Mushtaq et al., 2016; Sadeek et al., 2015; Santos et al., 2015; Soetaredjo et al., 2013; Sun et al., 2015; Yargic et al., 2015; Zhao and Zhou, 2016).

Since the parameter K_F is related to the adsorption capacity, the numerical value of this parameter must be a positive number. The Freundlich model was employed to correlate the adsorption experimental data of several heavy metals, including (Zn(II), Cd(II), Al(III), Cu(II), Ni(II), and Pb(II)), onto heat-treated orange peel waste (Santos et al., 2015). Negative values of parameter K_F for all heavy metal adsorbent systems indicate that the Freundlich model failed to represent the adsorption experimental data.

Parameter n characterizes the system heterogeneity; the more heterogeneous the system the more deviate the value this parameter from unity. Usually the value of parameter n is 1 to 10. The influence of parameter n on the amount uptake is given in Figure 5.2. From this figure it can be seen that the adsorption isotherm becomes “rectangular” when the value of n is equal to 10. If the value of n approaches 10, the adsorption becomes irreversible, since the adsorbate molecules are strongly attached to the surface of the adsorbate. For the adsorption of hazardous pollutants from water or wastewater onto agricultural wastes, the value of n is mostly in the range of 1 to 5 (Blazquez et al., 2011; Kurniawan et al., 2011a; Qi et al., 2011; Reddy et al., 2010; Mahajan and Sud, 2012; Mondal et al., 2016).

**FIGURE 5.2**

Theoretical calculation of the effect of parameter n in Freundlich model on the amount of solute uptake.

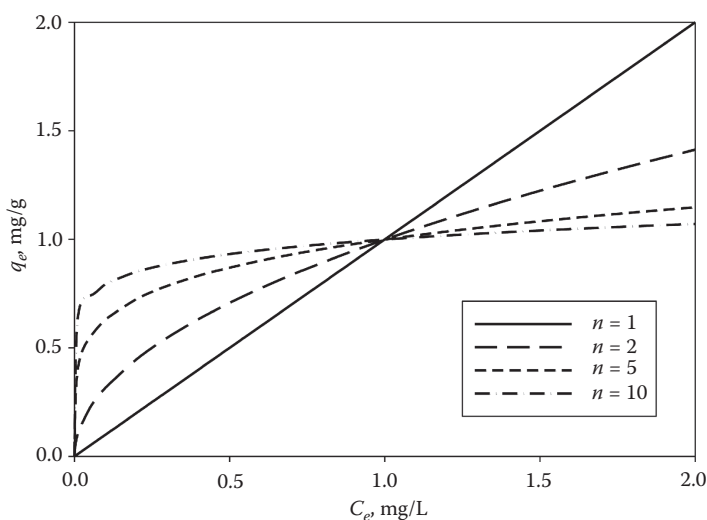
In many cases, the Freundlich model failed to correlate the adsorption experimental data of many systems, especially at high equilibrium concentration (Djemmo et al., 2016; Kurniawan et al., 2011a; Mushtaq et al., 2016). The failure of the Freundlich isotherm to correlate the experimental data at high equilibrium concentration is due to the absence of the saturation capacity term in the Freundlich equation.

Dubinin–Raduskevich (DR) is a semi-empirical model for the adsorption of subcritical vapors in microporous solids, in which a pore-filling mechanism controls the adsorption process (Do, 1998). The DR equation for liquid phase adsorption can be written as

$$q_e = q_{\max} \exp \left[-\frac{1}{(\beta E_o)^2} \left(RT \ln \frac{C_e}{C_s} \right)^2 \right] \quad (5.3)$$

The parameter β represents affinity coefficient of adsorbate and is proportional to the liquid molar volume. Parameter E_o represents the characteristic energy toward a reference adsorbate (Do, 1998). The theoretical plots of the DR equation are given in Figure 5.3. As we can see in the figure, as the characteristic energy increases, the uptake of adsorbate become higher due to the stronger interaction between adsorbate molecules and the surface of the adsorbent.

Pezoti et al. (2016) used this model to correlate the adsorption of methylene blue onto modified guava seeds. Visually, the DR equation can relate the adsorption equilibrium data quite well. From the fitting of the experimental results, the adsorption characteristic energy for the adsorption of methylene blue onto modified guava seeds using the conventional method was 19.39 kJ/mol, and for the adsorption onto modified guava seeds using the percolation method was 18.26 kJ/mol. It is widely known that the characteristic energy of adsorption can be used to determine the type of adsorption. For physical adsorption, the characteristic energy does not usually exceed 80 kJ/mol, whereas for chemisorption the value of the characteristic energy is between 80 and 800 kJ/mol. With those values of the characteristic energy, the physical adsorption was the predominant mechanism of

**FIGURE 5.3**

Theoretical plot of Dubinin–Radushkevich adsorption isotherm.

the adsorption of methylene blue onto modified guava seeds. The DR equation was also employed by other researchers to correlate the adsorption experimental data of hazardous substances onto agricultural wastes (Ay et al., 2012; Fontana et al., 2016; Kausar et al., 2013; Lam et al., 2016; Lee et al., 2016; Pehlivan et al., 2012; Reddy et al., 2010; Srivastava et al., 2015; Wang et al., 2015; Zhao and Zhou, 2016). In most cases, this equation cannot represent the experimental data well. As mentioned in the previous paragraph, the DR equation was developed to represent the adsorption data in microporous materials; agricultural wastes, especially nontreated forms, mostly have nonporous structures. Therefore, the use of the DR equation to account for the adsorption of hazardous substances onto agricultural residues is not recommended. Furthermore, as mentioned by Do (1998), in order to check the applicability of the model to represent the experimental data, that is, the plots of adsorption data of different temperatures as the logarithm of the amount adsorbed versus the square of adsorption potential, all the suitable data shall in general lie on the same curve, called the characteristic curve (Do, 1998). Since most of the experiments were conducted at a single temperature, it is hard to check the validity of the DR equation to represent the experimental data.

Another empirical equation that is used to describe the adsorption of hazardous substances onto agricultural wastes is the Temkin equation. The Temkin isotherm originally was developed by Slygin and Frumkin (1935) to describe the adsorption of hydrogen on platinum electrodes within acidic solutions (Febrianto et al., 2008). So actually, this equation was proposed to describe the chemisorption system. Temkin isotherm has the form as follows:

$$q_e = \frac{RT}{b} \ln(aC_e) \quad (5.4)$$

where a and b are characteristic constants of the Temkin equation. The Temkin isotherm is also one of the frequently used adsorption models to represent the adsorption of

hazardous substances from aqueous solution using agricultural wastes as the adsorbents (Djemmo et al., 2016; Ghasemi et al., 2014; Lee et al., 2016; Mashhadi et al., 2016; Pathania et al., 2016; Reddy et al., 2010). In many cases, this equation failed to represent the adsorption experimental data. The Temkin model may be superior in describing the adsorption in the gas phase, which in general is a much simpler phenomenon than liquid phase adsorption. However, in liquid phase adsorption, the many factors affecting the uptake of the adsorbate, such as the pH of the solution, temperature, the formation of micelles from adsorbed molecules, the interaction between solute and solvent, and interaction between adsorbate and adsorbent, are considered in the development of Temkin model, and as a result, this equation is not suitable for adsorption in a complex system.

The Sips equation, which is also known as the Langmuir-Freundlich equation, was developed to fix the problem of the Freundlich isotherm. This equation has a similar form of the Freundlich isotherm, but it has a finite limit when the concentration is sufficiently high (Do, 1998). The Sips equation has the following form:

$$q_e = q_{\max} \frac{(b_s C_e)^{1/ns}}{1 + (b_s C_e)^{1/ns}} \quad (5.5)$$

where b_s is the adsorption affinity of the Sips equation, similar to the parameter n in the Freundlich equation; the parameter ns also characterizes the system heterogeneity. If the parameter ns is equal to 1, Equation 5.5 becomes Equation 5.1.

Compared to the other two-parameter adsorption equations, this three-parameter isotherm is seldom used to correlate the adsorption equilibria data of hazardous substances onto agricultural wastes. In many occasions, this equation gives better performance in representing the adsorption equilibria data compared to the Langmuir and Freundlich equations (Blazquez et al., 2011; Deniz and Kepekci, 2016; Kosasih et al., 2010). The main reason is simple: this equation contains one more parameter than the Langmuir and Freundlich isotherms.

5.4.1.2 Single Component: Temperature-Dependent Forms

The use of temperature-dependent forms of the adsorption equations to correlate liquid phase adsorption data for the first time was conducted by Ismadji and Bhatia (2000). They used the temperature-dependent forms isotherms to correlate the adsorption data of flavor esters onto activated carbons. These temperature-dependent forms isotherms were subsequently employed by Ismadji and coworkers to correlate the adsorption data of many hazardous substances onto low-cost adsorbents including agricultural wastes (Chandra et al., 2013; Kurniawan et al., 2011a; Nathaniel et al., 2011; Maramis et al., 2012; Rahardjo et al., 2011; Soetardji et al., 2015; Yesi et al., 2010).

Parameter q_{\max} in Equation 5.1 is a function of temperature and can be expressed as

$$q_{\max} = q_{\max}^0 \exp[\delta(T_o - T)] \quad (5.6)$$

Here q_{\max}^0 is the adsorption capacity of the adsorbent at reference temperature T_o , while δ is a coefficient expansion of the adsorbate. Parameter δ is independent of the type of

adsorbents. The adsorption affinity in the Langmuir equation is also temperature dependent and can be expressed by the following equation:

$$K_L = K_L^o \exp \left[\frac{-Q_{ad}}{RT} \right] \quad (5.7)$$

where K_L^o is the adsorption affinity at a reference temperature and Q_{ad} is the heat of adsorption.

Parameters K_F and n in the Freundlich equation are temperature dependent and can be written as follows:

$$K_F = K_F^o \exp \left[\frac{-\Phi RT}{A_o} \right] \quad (5.8)$$

$$\frac{1}{n} = \frac{RT}{A_o} \quad (5.9)$$

Parameter K_F^o is the Freundlich adsorption capacity at a reference temperature T_o . Parameters Φ and A are Freundlich constants.

The Sips equation also has a temperature-dependent form as follows:

$$b_s = b_s^o \exp \left[\frac{Q_{ad}}{RT_o(T/T_o - 1)} \right] \quad (5.10)$$

$$ns = \frac{1}{(1/ns_o) + \lambda(1 - T_o/T)} \quad (5.11)$$

where b_s^o and ns_o are the adsorption affinity and parameter characterizing the system heterogeneity at reference temperature T_o , respectively. Parameter λ is a constant.

Kurniawan et al. (2011a) used these temperature-dependent forms of Langmuir, Freundlich, and Sips to correlate their adsorption experimental data of Ni(II) onto cassava peel waste. The parameters of those temperature-dependent forms of adsorption isotherms were obtained by nonlinear regression method. All of the models could fit the adsorption equilibrium data well ($r^2 > 0.998$). However, to decide the suitability and applicability of the model to represent the experimental results, they examined the physical meaning of the value of each parameter. They found that the Sips model gave the best representation of the experimental data with reasonable values of the parameters.

5.4.1.3 Binary Components

Compared to single-component adsorption, binary or multicomponent adsorption of hazardous substances into agricultural residues is seldom studied due to its complexity. In real or industrial wastewater treatment systems, the presence of the pollutant in a single component does not exist. Therefore, the adsorption equilibria for the multicomponent system are required for the correct design of the adsorption system.

There are several adsorption isotherms for a single solute that can be extended into the multicomponent system. The classical extended Langmuir model for the multicomponent system has the following form:

$$q_{e,i} = q_{\max,i} \frac{K_{L,i} C_{e,i}}{1 + \sum_{i=1}^n K_{L,i} C_{e,i}} \quad (5.12)$$

In industrial practice, the adsorption process always involves more than one or two compounds; however, to reduce the complexity of the studies, most of the adsorption experiments found in the literature used the binary component as the representative of multicomponent systems. For a binary component system, Equation 5.12 becomes

$$q_{e,1} = q_{\max,1} \frac{K_{L,1} C_{e,1}}{1 + K_{L,1} C_{e,1} + K_{L,2} C_{e,2}} \quad (5.13)$$

$$q_{e,2} = q_{\max,2} \frac{K_{L,2} C_{e,2}}{1 + K_{L,1} C_{e,1} + K_{L,2} C_{e,2}} \quad (5.14)$$

where $q_{\max,1}$ and $q_{\max,2}$ are the adsorption capacity of adsorbent toward single component 1 and 2, respectively, while $K_{L,1}$ and $K_{L,2}$ are the adsorption affinity of single components 1 and 2, respectively.

To represent the binary adsorption data using the extended Langmuir model, the parameters of the Langmuir model for the single component system are required. The procedure of using single parameters of the Langmuir model to represent the binary adsorption data is simple and provides satisfactory results. The adsorption of binary components has different mechanisms with a single component. In binary components, competition between adsorbate molecules for the active adsorption sites occurs, and this competition should be taken into the calculation to get correct theoretical results. Soetaredjo et al. (2013) proposed a modified form of extended Langmuir for binary components by taking into account the selectivity factor. This selectivity factor describes the competition between the adsorbates during the adsorption process. Soetaredjo et al. incorporated this selectivity factor in parameters q_{\max} and K_L . For the binary system, these parameters can be written as follows:

$$q_{\max,bin} = q_{\max,1} \left(C_{o,1} S_{21} / (C_{o,1} S_{2,1} + C_{o,2} S_{1,2}) \right) + q_{\max,2} \left(C_{o,2} S_{1,2} / (C_{o,1} S_{2,1} + C_{o,2} S_{1,2}) \right) \quad (5.15)$$

$$K_{L,1-bin} = K_{L,1} \exp(-S_{21}) \quad (5.16)$$

$$K_{L,2-bin} = K_{L,2} \exp(-S_{12}) \quad (5.17)$$

where $C_{o,i}$ is the initial concentration of adsorbates. S_{12} is the affinity of adsorbate 1 relative to the affinity of adsorbate 2, and S_{21} is the affinity of adsorbate 2 relative to the affinity of

adsorbate 1. This model can represent the binary data of the adsorption of Cu(II) and Pb(II) onto rice straw.

5.4.2 Adsorption Kinetic Models

The ability to predict the rate of adsorption of hazardous pollutants onto agricultural wastes is crucial for the correct design of the industrial adsorption system. Different adsorption kinetic models have been developed for that purpose, and the most widely used models to predict the kinetic of adsorption of hazardous pollutants onto agricultural wastes are pseudo-first and pseudo-second order models.

The pseudo-first-order kinetic was originally proposed by Lagergren in late of 19th century (Lagergren, 1898). The concept of chemical reaction occurring on the surface of a solid has been employed in the development of this model (Plazinski et al., 2009). This model is known as the first model to describe the adsorption rate in the liquid phase system. This model is also known as Lagergren's first-order rate equation, which has the following form:

$$\frac{dq}{dt} = k_1(q_e - q) \quad (5.18)$$

The integration of Equation 5.18 gives

$$q_t = q_e \left(1 - \exp(-k_1 t) \right) \quad (5.19)$$

Here k_1 is the time scaling factor. The higher the value of k_1 , the shorter the time required to reach the equilibrium condition (Figure 5.4).

The initial concentration of the adsorbate gives significant effect on the value of the time scaling factor k_1 . The higher the value of initial concentration, then the higher the value of

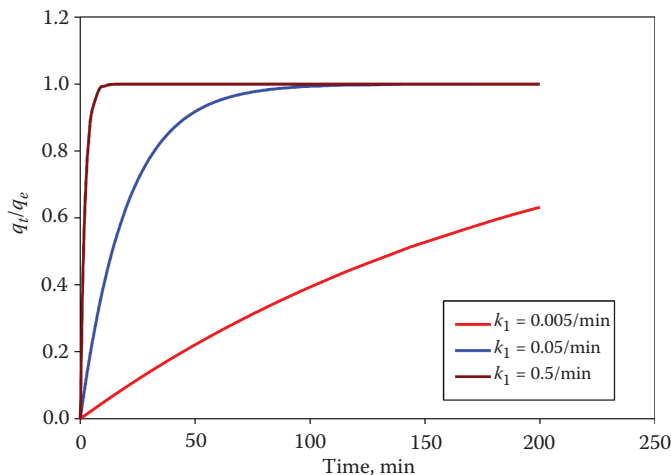


FIGURE 5.4

The effect of time scaling k_1 on the performance of the pseudo-first-order model.

the uptake amount at equilibrium condition (q_e). When a longer time is required to reach equilibrium, then the value of k_1 will decrease (Plazinski et al., 2009). In some cases, the values of this time scaling factor were independent of initial concentration (Garba and Rahim, 2016; Lam et al., 2016; Lee et al., 2016; Reddy et al., 2010; Yuvaraja et al., 2014; Zhao and Zhou, 2016). In most studies of the adsorption of hazardous pollutants onto agricultural wastes, the pseudo-first-order equation is usually not able to represent the kinetic data equally as well as the pseudo-second-order equation (Garba and Rahim, 2016; Lam et al., 2016; Lee et al., 2016; Reddy et al., 2010; Yuvaraja et al., 2014; Zhao and Zhou, 2016).

Similar to pseudo-first-order equation, the pseudo-second-order equation was developed based on the concept of chemical reaction occurring on the surface of solid. According to Plazinski et al. (2009), the pseudo-second-order kinetic is commonly associated with the condition when the rate of direct adsorption/desorption process controls the overall sorption kinetics. Blanchard et al. (1984) proposed a mathematical form of the pseudo-second-order kinetic model as follows:

$$\frac{dq}{dt} = k_2 (q_e - q)^2 \quad (5.20)$$

Solving Equation 5.20 gives

$$q_t = \frac{q_e^2 k_2 t}{1 + q_e k_2 t} \quad (5.21)$$

Parameter k_2 is a time scaling factor, and the value of this parameter strongly depends on the initial concentration of the solute. The higher the initial solute concentration, the longer the time required to reach equilibrium (time scaling factor k_2 decreases with the increasing of initial concentration). The theoretical effect of parameter k_2 on the amount of solute uptake by the adsorbent is given in Figure 5.5. It is evident that the equilibrium condition

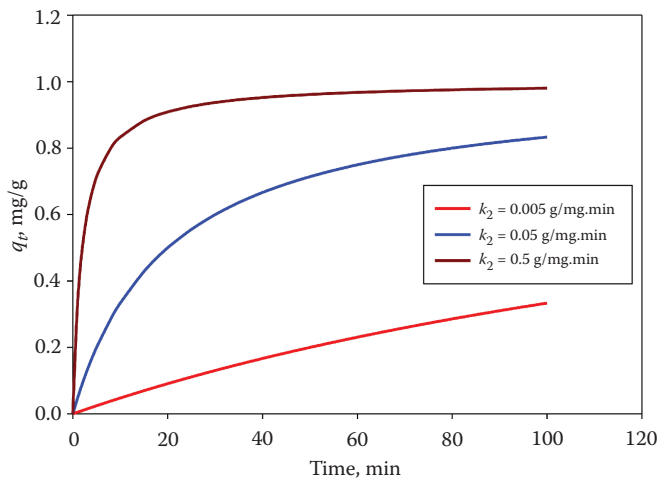


FIGURE 5.5

The effect of time scaling k_2 on the performance of pseudo-second order model.

is strongly affected by the value of k_2 ; the time required to achieve the equilibrium state is shorter at a higher value of k_2 . Several studies on the adsorption of hazardous pollutants onto agricultural wastes confirm that the increase of initial concentration decreases the value of k_2 . However, in several studies, the values of k_2 were independent with the initial concentration (Lam et al., 2016; Mondal et al., 2016; Yuvaraja et al., 2014).

Other kinetic models such as Bangham's equation (Gilbert et al., 2011), the Weber-Morris intraparticle diffusion theory (Ay et al., 2012; Djemmoe et al., 2016; Santos et al., 2015; Srivastava et al., 2015; Sun et al., 2015; Yuvaraja et al., 2014; Zhao and Zhou, 2016), and the Elovich kinetic equation (Srivastava et al., 2015; Sun et al., 2015) were also used to correlate the adsorption kinetic data of hazardous pollutants onto agricultural wastes.

5.4.3 Thermodynamic of Adsorption

To obtain complete features of the adsorption hazardous pollutants onto agricultural waste, a correct assessment of some thermodynamic properties of the adsorption systems is usually also conducted during the adsorption experiments. These thermodynamic properties—standard

Gibb's free energy change (ΔG°), standard enthalpy change (ΔH°), and standard of entropy change (ΔS°)—are used as an additional tool to confirm the nature of the adsorption process and to evaluate the thermodynamic feasibility of the process (Kurniawan et al., 2011b; Yuvaraja et al., 2014).

The standard Gibb's free energy change is an important criterion to measure the spontaneity of an adsorption process, and can be determined by the following equation:

$$\Delta G^\circ = -RT \ln K_D \quad (5.22)$$

where K_D is the linear sorption distribution coefficient. This distribution coefficient can be defined as the ratio between the equilibrium surface concentration of adsorbed solute and the equilibrium solute concentration in the liquid phase. The value of K_D is obtained by plotting $\ln(q_e/C_e)$ versus C_e and then extrapolating to C_e equal to zero (Anggraini et al., 2014). The following equation gives the correlation between the linear sorption distribution coefficient with other thermodynamic properties:

$$\ln K_D = \frac{\Delta S^\circ}{R} - \frac{H^\circ}{RT} \quad (5.23)$$

The values of ΔS° and ΔH° are obtained through logarithm plotting of $\ln K_D$ versus $1/T$. The slope and intercept point give the value of ΔH° and ΔS° , respectively. To get a valid representation of the thermodynamic properties of the adsorption process, at least three adsorption isotherms at three different temperatures are required.

The standard Gibb's free energy change measures the spontaneity of the adsorption process. The negative values of ΔG° suggest the adsorption process is thermodynamically feasible and spontaneous (Bhatti et al., 2016; Blazquez et al., 2011; Fontana et al., 2016; Kausar et al., 2013; Kurniawan et al., 2011a, 2011b; Lam et al., 2016; Mashhadi et al., 2016; Mondal et al., 2016; Srivastava et al., 2015; Yuvaraja et al., 2014). Standard enthalpy change (ΔH°) measures exothermic or endothermic nature of the adsorption process. Positive ΔH° indicates that the process is endothermic and suggests the possibility of strong binding between the adsorbate and adsorbent (Fontana et al., 2016; Kurniawan et al., 2011a, 2011b;

Mashhadi et al., 2016; Srivastava et al., 2015; Yuvaraja et al., 2014), while negative ΔH° indicates that the adsorption process is exothermic, and the uptake of adsorbate decreases with an increase of temperature (Bhatti et al., 2016; Blazquez et al., 2011; Kausar et al., 2013; Lam et al., 2016; Mondal et al., 2016). The value of ΔH° also shows whether the adsorption mechanism is physisorption or chemisorption.

The randomness of the adsorption system is measured with ΔS° . The positive value of this thermodynamic property indicates high affinity of solutes into the active adsorption sites on the surface of agricultural wastes (Blazquez et al., 2011; Fontana et al., 2016; Kausar et al., 2013; Kurniawan et al., 2011a, 2011b; Lam et al., 2016; Srivastava et al., 2015; Yuvaraja et al., 2014). The higher the positive value of ΔS° reveals the increase of randomness at the interface of solute and adsorbent. In a few studies, the adverse values of ΔS° were obtained (Bhatti et al., 2016; Mashhadi et al., 2016; Mondal et al., 2016). Negative values of ΔS° mean an increase of orderliness of the adsorption system, and this phenomenon is contrary to the actual conditions. The liquid phase adsorption in agricultural biomass is a disordered process due to the nature of the solid adsorbent, solvent, and solute. The biomass has a complex structure with different surface chemistry, pore structure, and chemical compounds; this complexity will increase the randomness of the adsorption system.

5.5 Future Perspective

Thousands of adsorption studies have been conducted in the last 30 years to search for renewable and low-cost adsorbents for the removal of hazardous pollutants from water and wastewater. Most of the agricultural wastes used in the studies have the capability to remove contaminants from water with high removal efficiency. Even intensive studies have been carried out, however, currently there is no commercial or industrial wastewater treatment facility using agricultural wastes as the adsorbents for their adsorption processes, and we are possibly still far from industrial-scale applications. Several problems still need to be addressed to make these laboratory studies become a reality.

The characteristic and chemical compositions of agricultural wastes strongly depend on the season, geographical location, condition of soils, and so forth. These properties strongly influence the adsorption capacity of the agricultural residues. With the variation of the characteristic and chemical compositions of these biomasses, it is hard to maintain the adsorption capacity at a constant value. The adsorption system at industrial scale is designed for a narrow range of the adsorption capacity fluctuation; therefore, significant variation of the adsorption capacity will significantly reduce its performance in the removal of hazardous substances.

The second challenge is to improve the adsorption performance of this biomass without creating another problem in the environment. Some agricultural residues have low adsorption capacity and can be enhanced through pretreatment or modification using physical, chemical, or thermal treatment processes. The physical pretreatment process seems to be the best solution for the environment; however, this pretreatment process only slightly increases the adsorption capacity of biomass. In the physical pretreatment process, the chemical characteristic of the agricultural waste as well as the input and output size of the final product strongly influences the energy requirement. The chemical pretreatment process can significantly enhance the adsorption performance of agricultural wastes, but this method is not favorable due to environmental concerns. Most

of the chemicals used in this treatment method are a potential hazard to the environment. The chemical in an excess amount is usually required for the chemical pretreatment process and the unused chemical often creates more severe problems and more expenses. The thermal treatment of agricultural wastes produces adsorbents with an adsorption capacity comparable to commercial adsorbents such as activated carbons; however, this process is expensive due to the high use of energy. Therefore, thermal treatment is also not a good choice in terms of capital investment and operational cost.

Another problem is the capability of these agricultural wastes for the treatment of real wastewater. All of the adsorption studies used synthetic wastewater with only a single chemical as the solute. Few of the studies used the binary solution as representative of industrial wastewater. In general, industrial wastewater is a complex mixture of chemicals with water as the solvent; it contains more than two components or even hundreds of chemical compounds are present in the system. In a single-component system, there is no competition with other solute molecules for the adsorption sites, and simple adsorption isotherm models can be used to represent the adsorption experimental data. Using simple linear regression of the adsorption experimental data, the value of adsorption capacity of the adsorbent can be obtained. In real wastewater, the competition for active adsorption sites between adsorbates occurs, and simple adsorption models are not adequate to correlate the experimental data, and the actual adsorption capacity of the adsorbent is more difficult to predict. Without any data on the adsorption capacity of the adsorbent, properly designing the adsorption system is difficult.

More effort is required to implement agricultural wastes as adsorbents for industrial wastewater treatment. The adsorption studies should be directed in multicomponent systems rather than single-component systems. Real wastewater should be used in order to get more information about the adsorption process, and an appropriate mathematical model should be developed. If sufficient data have been obtained, the capability of biomass as the adsorbent should be verified in a pilot scale experiment.

5.6 Conclusions

Reliable adsorption equilibria and kinetic data on the adsorption of hazardous pollutants from water and wastewater onto agricultural wastes are still needed for the proper design of the adsorption process. The search of high adsorption capacity of agricultural wastes for the treatment of water and wastewater is still the priority of current adsorption studies. Most of the adsorption studies focused on a single system using synthetic wastewater. The application of agricultural wastes as the adsorbent for the treatment of industrial wastewater is still some distance from reality.

References

- Abdolali, A., W. S. Guo, H. H. Ngo et al. 2014. Typical lignocellulosic wastes and by-products for bio-sorption process in water and wastewater treatment: A critical review. *Bioresource Technology* 160: 57–66.

- Anggraini, M., A. Kurniawan, L. K. Ong et al. 2014. Antibiotic detoxification from synthetic and real effluents using a novel MTAB surfactant montmorillonite (organoclay) sorbent. *RSC Advances* 4: 16298–16311.
- Arief, V. O., K. Trilestari, J. Sunarso, N. Indraswati, and S. Ismadji. 2008. Recent progress on biosorption of heavy metals from liquids using low cost biosorbents: Characterization, biosorption parameters and mechanism studies. *Clean* 36: 937–962.
- Ay, C. O., A. S. Oscan, Y. Erdogan, and A. Ozcan. 2012. Characterization of *Punica granatum* L. peels and quantitatively determination of its biosorption behavior towards lead(II) ions and Acid Blue 40. *Colloid and Surfaces B: Biointerfaces* 100: 197–204.
- Bhatnagar, A., V. J. P. Vilar, C. M. S. Botelho, and R. A. R. Boaventura. 2010. Coconut-based biosorbents for water treatment—A review of the recent literature. *Advances in Colloid and Interface Science* 160: 1–15.
- Bhatti, H. N., Q. Zaman, A. Kausar, S. Noreen, and M. Iqbal. 2016. Efficient remediation of Zr(IV) using citrus peel waste biomass: Kinetic, equilibrium and thermodynamic studies. *Ecological Engineering* 95: 216–228.
- Blazquez, G., M. A. Martin-Lara, G. Tenorio, and M. Calero. 2011. Batch biosorption of lead(II) from aqueous solutions by olive tree pruning waste: Equilibrium, kinetics and thermodynamic study. *Chemical Engineering Journal* 168: 170–177.
- Chao, H. P., C. C. Chang, and A. Nieva. 2014. Biosorption of heavy metals on Citrus maxima peel, passion fruit shell, and sugarcane bagasse in a fixed-bed column. *Journal of Industrial and Engineering Chemistry* 20: 3408–3414.
- Chandra, I. K., Y. H. Ju, A. Ayucitra, and S. Ismadji. 2013. Evans blue removal from wastewater by rarasaponin–bentonite. *International Journal of Environmental Science and Technology* 10: 359–370.
- Davila-Jimenez, M. M., M. P. Elizalde-Gonzalez, E. Garcia-Diaz, and A. M. Santes-Aquino. 2016. Assessment of the effectiveness of combined adsorption and photocatalysis for removal of the herbicide isoproturon. *Physics and Chemistry of the Earth* 91: 77–86.
- Deniz, F., and R. A. Kepecki. 2016. Dye biosorption onto pistachio by-product: A green environmental engineering approach. *Journal of Molecular Liquids* 219: 194–200.
- Ding, Z., X. Hu, A. R. Zimmerman, and B. Gao. 2014. Sorption and cosorption of lead (II) and methylene blue on chemically modified biomass. *Bioresource Technology* 167: 569–573.
- Djemmo, L. G., T. E. Njanja, M. C. N. Deussi, and K. I. Tonle. 2016. Assessment of copper(II) biosorption from aqueous solution by agricultural and industrial residues. *Comptes Rendus Chimie* 19: 841–849.
- Djilani, C., R. Zaghdoudi, F. Djazi et al. 2015. Adsorption of dyes on activated carbon prepared from apricot stones and commercial activated carbon. *Journal of the Taiwan Institute of Chemical Engineers* 53: 112–121.
- Do, D. D. 1998. *Adsorption analysis: Equilibria and kinetics*. Imperial College Press, London.
- Fan, M., D. Dai, and B. Huang. 2012. Fourier transform infrared spectroscopy for natural fibres. In *Fourier Transform—Materials Analysis*, S. M. Salih (Ed.), chap. 3. InTech.
- Febrianto, J., A. N. Kosasih, J. Sunarso et al. 2009. Equilibrium and kinetic studies in adsorption of heavy metals using biosorbent: A summary of recent studies. *Journal of Hazardous Materials* 162: 616–645.
- Fontana, K. B., E. S. Chaves, J. D. S. Sanchez et al. 2016. Textile dye removal from aqueous solutions by malt bagasse: Isotherm, kinetic and thermodynamic studies. *Ecotoxicology and Environmental Safety* 124: 329–336.
- Garba, Z. N., and A. A. Rahim. 2016. Evaluation of optimal activated carbon from an agricultural waste for the removal of para-chlorophenol and 2,4-dichlorophenol. *Process Safety and Environment Protection* 102: 54–63.
- Ghasemi, M., M. Naushad, N. Ghasemi, and Y. Khosravi-fard. 2014. A novel agricultural waste based adsorbent for the removal of Pb(II) from aqueous solution: Kinetics, equilibrium and thermodynamic studies. *Journal of Industrial and Engineering Chemistry* 20: 454–461.
- Gilbert, U. A., U. Emmanuel, A. A. Adebajo, and G. A. Olalere. 2011. Biosorptive removal of Pb(II) and Cd(II) onto novel biosorbent: Defatted Carica papaya seeds. *Biomass and Bioenergy* 35: 2517–2525.

- Herath, I., P. Kumarathilaka, M. I. Al-Wabel et al. 2016. Mechanistic modeling of glyphosate interaction with rice husk derived engineered biochar. *Microporous and Mesoporous Materials* 225: 280–288.
- Ismadji, S., F. E. Soetaredjo, and A. Ayucitra. 2015. *Clay Materials for Environmental Remediation*. Springer International Publishing AG, Switzerland.
- Ismadji, S., and S. K. Bhatia. 2000. Adsorption of flavour esters on granular activated carbon. *Canadian Journal of Chemical Engineering* 78: 892–901.
- Jalil, A. A., S. Triwahyono, M. R. Yaakob et al. 2012. Utilization of bivalve shell-treated *Zea mays* L. (maize) husk leaf as a low-cost biosorbent for enhanced adsorption of malachite green. *Bioresource Technology* 120: 218–224.
- Kaouah, F., S. Boumaza, T. Berrama, M. Trari, and Z. Bendjama. 2013. Preparation and characterization of activated carbon from wild olive cores (oleaster) by H_3PO_4 for the removal of Basic Red 46. *Journal of Cleaner Production* 54: 296–306.
- Karacetin, G., S. Sivrikaya, and M. Imamoglu. 2014. Adsorption of methylene blue from aqueous solutions by activated carbon prepared from hazelnut husk using zinc chloride. *Journal of Analytical and Applied Pyrolysis* 110: 270–276.
- Kausar, A., H. N. Bhatti, and G. MacKinnon. 2013. Equilibrium, kinetic and thermodynamic studies on the removal of U(VI) by low cost agricultural waste. *Colloids and Surfaces B: Biointerfaces* 111: 124–133.
- Kosasih, A. N., J. Febrianto, J. Sunarso, Y. H. Ju, N. Indraswati, and S. Ismadji. 2010. Sequestering of Cu(II) from aqueous solution using cassava peel (*Manihot esculenta*). *Journal of Hazardous Materials* 180: 366–374.
- Koseoglu, E., and C. Akmil-Basar. 2015. Preparation, structural evaluation and adsorptive properties of activated carbon from agricultural waste biomass. *Advanced Powder Technology* 26: 811–818.
- Kumar, B., K. Smita, E. Sanchez, C. Stael, and L. Cumbal. 2016. Andean Sacha inchi (*Plukenetia volubilis* L.) shell biomass as new biosorbents for Pb^{2+} and Cu^{2+} ions. *Ecological Engineering* 93: 152–158.
- Kurniawan, A., A. N. Kosasih, J. Febrianto, Y. H. Ju, J. Sunarso, N. Indraswati, and S. Ismadji. 2011a. Evaluation of cassava peel waste as lowcost biosorbent for Ni-sorption: Equilibrium, kinetics, thermodynamics and mechanism. *Chemical Engineering Journal* 172: 158–166.
- Kurniawan, A., V. O. A. Sisnandy, K. Trilestari, J. Sunarso, N. Indraswati, and S. Ismadji. 2011b. Performance durian shell waste as high capacity biosorbent for Cr(VI) removal from synthetic wastewater. *Ecological Engineering* 37: 940–947.
- Kyzas, G. Z., and E. A. Deliyanni. 2015. Modified activated carbons from potato peels as green environmental-friendly adsorbents for the treatment of pharmaceutical effluents. *Chemical Engineering Research and Design* 97: 135–144.
- Lagergren, S. 1898. Zur theorie der sogenannten adsorption gelöster stoffe. *Kungliga Svenska Vetenskapsakademiens Handlingar* 24: 1–39.
- Lam, Y. F., L. Y. Lee, S. J. Chua, S. S. Lim, and S. Gan. 2016. Insights into the equilibrium, kinetic and thermodynamics of nickel removal by environmental friendly *Lansium domesticum* peel biosorbent. *Ecotoxicology and Environmental Safety* 127: 61–70.
- Lee, L. Y., S. Gan, M. S. Y. Tan, S. S. Lim, X. J. Lee, and Y. F. Lam. 2016. Effective removal of Acid Blue 113 dye using overripe *Cucumis sativus* peel as an eco-friendly biosorbent from agricultural residue. *Journal of Cleaner Production* 113: 194–203.
- Lesmana, S. O., N. Febriana, F. E. Soetaredjo, J. Sunarso, and S. Ismadji. 2009. Studies on potential applications of biomass for the separation of heavy metals from water and wastewater. *Biochemical Engineering Journal* 44: 19–41.
- Li, H., Z. Sun, L. Zhang et al. 2016. A cost-effective porous carbon derived from pomelo peel for the removal of methyl orange from aqueous solution. *Colloids and Surfaces A: Physicochemical and Engineering Aspects* 489: 191–199.
- Liu, N., A. B. Charrua, C. H. Weng, X. Yuan, and F. Ding. 2015. Characterization of biochars derived from agriculture wastes and their adsorptive removal of atrazine from aqueous solution: A comparative study. *Bioresource Technology* 198: 55–62.

- Liu, Z., X. Zhou, X. Chen, C. Dai, J. Zhang, and Y. Zhang. 2013. Biosorption of clofibric acid and carbamazepine in aqueous solution by agricultural waste rice straw. *Journal of Environmental Sciences* 25: 2384–2395.
- Mahajan, G., and D. Sud. 2012. Modified agricultural waste biomass with enhanced responsive properties for metal-ion remediation: A green approach. *Applied Water Science* 2: 299–308.
- Mahamad, M. N., M. A. A. Zaini, and Z. A. Zakaria. 2015. Preparation and characterization of activated carbon from pineapple waste biomass for dye removal. *International Biodeterioration & Biodegradation* 102: 274–280.
- Maramis, V., A. Kurniawan, A. Ayucitra, J. Sunarso, and S. Ismadji. 2012. Removal of copper ions from aqueous solution by adsorption using LABORATORIES-modified bentonite (organo-bentonite). *Frontiers of Chemical Science and Engineering* 6: 58–66.
- Mashhadi, S., R. Sohrabi, H. Javadian et al. 2016. Rapid removal of Hg (II) from aqueous solution by rice straw activated carbon prepared by microwave-assisted H₂SO₄ activation: Kinetic, isotherm and thermodynamic studies. *Journal of Molecular Liquids* 215: 144–153.
- Mondal, S., K. Bobde, K. Aikat, and G. Halder. 2016. Biosorptive uptake of ibuprofen by steam activated biochar derived from mung bean husk: Equilibrium, kinetics, thermodynamics, modeling and eco-toxicological studies. *Journal of Environmental Management* 182: 581–594.
- Mosa, A., A. El-Ghamry, P. Truby et al. 2016. Chemo-mechanical modification of cottonwood for Pb²⁺ removal from aqueous solutions: Sorption mechanisms and potential application as biofilter in drip-irrigation. *Chemosphere* 161: 1–9.
- Mushtaq, M., H. N. Bhatti, M. Iqbal, and S. Noreen. 2016. Eriobotrya japonica seed biocomposite efficiency for copper adsorption: Isotherms, kinetics, thermodynamic and desorption studies. *Journal of Environmental Management* 176: 21–33.
- Nathaniel, E., A. Kurniawan, F. E. Soetaredjo, and S. Ismadji. 2011. Organo-bentonite for the adsorption of Pb(II) from aqueous solution: Temperature dependent parameters for several adsorption equations. *Desalination and Water Treatment* 36: 280–288.
- Njoku, V. O., K. Y. Foo, M. Asif, and B. H. Hameed. 2014a. Preparation of activated carbons from rambutan (*Nephelium lappaceum*) peel by microwave-induced KOH activation for acid yellow 17 dye adsorption. *Chemical Engineering Journal* 250: 198–204.
- Njoku, V. O., M. A. Islam, M. Asif, and B. H. Hameed. 2014b. Utilization of sky fruit husk agricultural waste to produce high quality activated carbon for the herbicide bentazon adsorption. *Chemical Engineering Journal* 251: 183–191.
- Njoku, V. O., M. A. Islam, M. Asif, and B. H. Hameed. 2015. Adsorption of 2,4-dichlorophenoxyacetic acid by mesoporous activated carbon prepared from H₃PO₄-activated langsat empty fruit bunch. *Journal of Environmental Management* 154: 138–144.
- Nguyen, T. A. H., H. H. Ngo, W. S. Guo et al. 2014. Modification of agricultural waste/by-products for enhanced phosphate removal and recovery: Potential and obstacles. *Bioresource Technology* 169: 750–762.
- Ong, L. K., F. E. Soetaredjo, A. Kurniawan, A. Ayucitra, J. C. Liu, and S. Ismadji. 2014. Investigation on the montmorillonite adsorption of biocidal compounds incorporating thermodynamical based multicomponent adsorption isotherm. *Chemical Engineering Journal* 241: 9–18.
- Ouyang, W., X. Zhao, M. Tysklind, and F. Hao. 2016. Typical agricultural diffuse herbicide sorption with agricultural waste derived biochars amended soil of high organic matter content. *Water Research* 92: 156–163.
- Pathania, D., A. Sharma, and Z. M. Siddiqi. 2016. Removal of congo red dye from aqueous system using *Phoenix dactylifera* seeds. *Journal of Molecular Liquids* 219: 359–367.
- Pehlivan, E., T. Altun, and S. Parlayici. 2012. Modified barley straw as a potential biosorbent for removal of copper ions from aqueous solution. *Food Chemistry* 135: 2229–2234.
- Peng, P., Y. H. Lang, and X. M. Wang. 2016. Adsorption behavior and mechanism of pentachlorophenol on reed biochars: pH effect, pyrolysis temperature, hydrochloric acid treatment and isotherms. *Ecological Engineering* 90: 225–233.
- Pezoti, O., A. L. Cazetta, K. C. Bedin et al. 2016. Percolation as new method of preparation of modified biosorbents for pollutants removal. *Chemical Engineering Journal* 283: 1305–1314.

- Plazinski, W., W. Rudzinski, and A. Plazinska. 2009. Theoretical models of sorption kinetics including a surface reaction mechanism: A review. *Advances in Colloid and Interface Science* 152: 2–13.
- Putro, J. N., F. E. Soetaredjo, S. Y. Lin, Y. H. Ju, and S. Ismadji. 2016. Pretreatment and conversion of lignocellulose biomass into valuable chemicals. *RSC Advances* 6: 46834–46852.
- Qi, Z., G. Wenqi, X. Chuanxin et al. 2011. Removal of Neutral Red from aqueous solution by adsorption on spent cottonseed hull substrate. *Journal of Hazardous Materials* 185: 502–506.
- Rahardjo, A. K., M. J. J. Susanto, A. Kurniawan, N. Indraswati, and S. Ismadji. Modified pacitan bentonite for the removal of ampicillin from wastewater. *Journal of Hazardous Materials* 190: 1001–1008.
- Reddy, D. H. K., K. Sessaiah, A. V. R. Reddy, M. M. Rao, and M. C. Wang. 2010. Biosorption of Pb^{2+} from aqueous solutions by Moringa oleifera bark: Equilibrium and kinetic studies. *Journal of Hazardous Materials* 174: 831–838.
- Rojas, R., E. Vanderlinden, J. Morillo, J. Usero, and H. El Bakouri. 2014. Characterization of sorption processes for the development of low-cost pesticide decontamination techniques. *Science of the Total Environment* 488–489: 124–135.
- Romero-Cano, L. A., L. V. Gonzalez-Gutierrez, and L. A. Baldenegro-Perez. 2016. Biosorbents prepared from orange peels using Instant Controlled Pressure Drop for Cu(II) and phenol removal. *Industrial Crops and Products* 84: 344–349.
- Ronda, A., M. A. Martin-Lara, M. Calero, and G. Blazquez. 2015. Complete use of an agricultural waste: Application of untreated and chemically treated olive stone as biosorbent of lead ions and reuse as fuel. *Chemical Engineering Research and Design* 104: 740–751.
- Sadeek, S. A., N. A. Negm, H. H. H. Hefni, and M. M. A. Wahab. 2015. Metal adsorption by agricultural biosorbents: Adsorption isotherm, kinetic and biosorbents chemical structures. *International Journal of Biological Macromolecules* 81: 400–409.
- Safa, Y., and H. N. Bhatti. 2011. Adsorptive removal of direct textile dyes by low cost agricultural waste: Application of factorial design analysis. *Chemical Engineering Journal* 167: 35–41.
- Santos, C. M., J. Dweck, R. S. Viotto, A. H. Rosa, and L. C. de Moraes. 2015. Application of orange peel waste in the production of solid biofuels and biosorbents. *Bioresource Technology* 196: 469–479.
- Sim, S. F., M. Mohamed, N. A. L. M. I. Lu, N. S. P. Sarman, and S. N. S. Samsudin. 2012. Computer-assisted analysis of Fourier transform infrared (FTIR) spectra for characterization of various treated and untreated agriculture biomass. *Bioresources* 7: 5367–5380.
- Soetardji, J. O., J. C. Claudia, Y. H. Ju et al. 2015. Ammonia removal from water using sodium hydroxide modified zeolite mordenite. *RSC Advances* 5: 83689–83699.
- Soetaredjo, F. E., A. Kurniawan, L. K. Ong, and S. Ismadji. 2013. Incorporation of selectivity factor in modeling binary component adsorption isotherms for heavy metals-biomass system. *Chemical Engineering Journal* 219: 137–148.
- Srivastava, S., S. B. Agrawal, and M. K. Mondal. 2015. Biosorption isotherms and kinetics on removal of Cr(VI) using native and chemically modified Lagerstroemia speciosa bark. *Ecological Engineering* 85: 56–66.
- Sudaryanto, Y., S. B. Hartono, W. Irawaty, H. Hindarso, and S. Ismadji. 2006. High surface area activated carbon prepared from cassava peel by chemical activation. *Bioresource Technology* 97: 734–739.
- Sun, L., D. Chen, S. Wan, and Z. Yu. 2015. Performance, kinetics, and equilibrium of methylene blue adsorption on biochar derived from eucalyptus saw dust modified with citric, tartaric, and acetic acids. *Bioresource Technology* 198: 300–308.
- Todorciuc, T., A. M. Capraru, I. Kratochvilova, and V. I. Popa. 2009. Characterization of non-wood lignin and its hydroxymethylated derivatives by spectroscopy and self-assembling investigation. *Cellulose Chemistry and Technology* 43: 399–408.
- Tonucci, M. C., A. V. A. Gurgel, and S. F. de Aquino. 2015. Activated carbons from agricultural byproducts (pine tree and coconut shell), coal, and carbon nanotubes as adsorbents for removal of sulfamethoxazole from spiked aqueous solutions: Kinetic and thermodynamic studies. *Industrial Crops and Products* 74: 111–121.

- Wang, F., L. Tan, Q. Liu et al. 2015. Biosorption characteristics of Uranium(VI) from aqueous solution by pollen pini. *Journal of Environmental Radioactivity* 150: 93–98.
- Xu, M., P. Yin, X. Liu et al. 2013. Utilization of rice husks modified by organomultiphosponic acids as low-cost biosorbents for enhanced adsorption of heavy metal ions. *Bioresource Technology* 149: 420–424.
- Yargic, A. S., R. Z. Y. Sahin, N. Ozbay, and E. Onal. 2015. Assessment of toxic copper(II) biosorption from aqueous solution by chemically-treated tomato waste. *Journal of Cleaner Production* 88: 152–159.
- Yesi, F. P. Sisnandy, Y. H. Ju, F. E. Soetaredjo, and S. Ismadji. 2010. Adsorption of acid blue 129 from aqueous solutions onto raw and surfactant modified bentonite: The application of temperature dependent form of adsorption isotherms. *Adsorption Science and Technology* 28: 847–868.
- Yuvaraja, G., N. Krishnaiah, M. V. Subbaiah, and A. Krishnaiah. 2014. Biosorption of Pb(II) from aqueous solution by Solanum melongena leafpowder as a low-cost biosorbent prepared from agricultural waste. *Colloids and Surfaces B: Biointerfaces* 114: 75–81.
- Zhao, S., and T. Zhou. 2016. Biosorption of methylene blue from wastewater by an extraction residue of *Salvia miltiorrhiza* Bge. *Bioresource Technology* 219: 330–337.
- Zhao, X., W. Ouyang, F. Hao et al. 2013. Properties comparison of biochars from corn straw with different pretreatment and sorption behaviour of atrazine. *Bioresource Technology* 147: 338–344.
- Zhu, Y., P. Kolar, S. B. Shah, J. J. Cheng, and P. K. Lim. 2016. Avocado seed-derived activated carbon for mitigation of aqueous ammonium. *Industrial Crops and Products* 92: 34–41.

6

Biosorption of Divalent Heavy Metal Ions by Rice Husk: A Review

Anteneh Mesfin Yeneneh, Tushar Kanti Sen,
Murugesan Thanabalan, and Eugene Hong

CONTENTS

6.1	Introduction	109
6.2	Studies on Chemically and Thermally Modified Rice Husk for Biosorption of Heavy Metals	111
6.3	Studies on Impact of Various Parameters on Sorption Capacity of Rice Husk	115
6.3.1	Impact of pH	115
6.3.2	Impact of Concentration of Sorbent	116
6.3.3	Effect of Use of Mixture of Rice Husk and Other Sorbents on Sorption Performance	116
6.3.4	Impact of Metal Dose on Sorption Performance	117
6.4	Sorption Isotherms	117
6.5	Studies on Kinetics of Biosorption Process by Activated Rice Husk	121
6.6	Thermodynamics of Sorption	123
6.7	Studies of Co-Ion Effect	124
6.8	Studies on Column Experiment	124
6.9	Studies on Mechanism of Sorption	126
6.10	Studies on Elution or Recovery of Sorbate (Metal Ions)	127
6.11	Conclusion	128
	References	129

6.1 Introduction

Toxic heavy metals are released into the environment from a number of industries, including petroleum, petrochemical, mining, plating, dyeing, automobile manufacturing, and metal processing. The presence of heavy metals in the environment resulted in a number of environmental problems. In order to meet the water quality standards, the concentration of heavy metals in wastewater must be controlled. Moreover, metal as a kind of resource, is becoming rare (Raju and Naidu 2013). Heavy metals are toxic and have multiple deleterious effects on the ecosystem and can last for a long time in nature; some heavy metals even could be transformed from relatively low toxic species into more toxic forms in a certain environment. Mercury is such a case; the bioaccumulation and bioaugmentation of heavy metal in the food chain could damage normal physiological activity and endanger human life. Metals can only be transformed and changed in valence and species, but cannot be degraded by any methods including biotreatment; and the toxicity of

heavy metals occurs even in low concentration. Conventional methods for removing metal ions from aqueous solution have been studied in detail, such as chemical precipitation, ion exchange, electrochemical treatment, membrane technologies, adsorption on activated carbon, and clay (Bailey et al. 1999). However, chemical precipitation and electrochemical treatment are ineffective, especially when the metal ion concentration in aqueous solution is as low as 1 to 100 mg/L. These methods also produce a large amount of sludge to be treated with great difficulties. Ion exchange, membrane technologies, and the activated carbon adsorption process are extremely expensive, especially when treating a large amount of water and wastewater containing heavy metal in low concentration, so they cannot be used at large scale. Biosorption is an alternative process that utilizes various low cost natural materials of biological origin, as the removal of toxic metal ions from water is a very difficult task involving high cost of treatment. Other methods for the removal of toxic metal ions from aqueous solutions include reverse osmosis, ion exchange, chemical precipitation, electrodialysis, lime coagulation, adsorption using activated carbon and fly ash (Gupta et al. 2015; Huang and Wu 1977; Juang and Shiau 2000; Kalderis et al. 2008; Lalwani et al. 1998; Leppert 1990; Mohan and Sreelakshmia 2006; Ouki and Kavannagh 1997; Yang and Lin 1998). In this respect, biosorption is an ideal candidate for the treatment of high volume and low concentration complex wastewaters (Veglio and Beolchini 1997; Volesky 1990, 2007; Volesky and Holan 1995). Heavy metal removal by biosorption has been extensively investigated during the last several decades (Volesky 2007). Some reviews have been published focusing on different aspects of heavy metal biosorption (Davis et al. 2003; Kapoor and Viraraghavan 1995; Kratochvil and Volesky 1998; Malik 2004; Tsezos 2001; Veglio and Beolchini 1997; Volesky and Holan 1995). According to studies conducted on biosorption, most of the research activities focus on the following three major fields:

1. Biosorbents—It is necessary to continue to search for and select the most promising types of biomass from an extremely large pool of readily available and inexpensive biomaterials (Kratochvil and Volesky 1998).
2. Mechanism of biosorption—The mechanism involved in metal biosorption is only understood to a very limited extent to date. It is necessary to identify the mechanism of metal uptake by biosorbents and understand sorbent–metal interactions.
3. Biosorption research is basically at the laboratory-scale—There are great challenges to developing large commercial scale biosorption processes and most attempts have failed when applying the biosorption process into practice (Tsezos 2001).

Recently, attention is diverted toward the biomaterials that are byproducts or waste from large-scale industrial operations and agricultural waste materials. The major advantages of biosorption over conventional treatment methods include low cost, high efficiency, minimization of chemical or biological sludge, no additional nutrient requirement, and regeneration of biosorbents, and possibility of metal recovery. Agricultural materials, particularly those containing cellulose, show potential metal biosorption capacity. The basic components of the agricultural waste materials biomass include hemicellulose, lignin, extractives, lipids, proteins, simple sugars, water hydrocarbons, and the starch-containing variety of functional groups that facilitate metal complexation which helps in the sequestering of heavy metals (Bailey et al. 1999; Hashem et al. 2005).

Agricultural waste materials that are economical and ecofriendly due to their unique chemical composition, abundance, renewable nature, low cost, and efficiency seem to be

viable options for heavy metal remediation. Studies reveal that various agricultural waste materials such as rice bran, rice husk, wheat bran, wheat husk, sawdust of various plants, bark of trees, groundnut shells, coconut shells, black gram husk, hazelnut shells, walnut shells, cotton seed hulls, waste tea leaves, *Cassia fistula* leaves, maize corn cob, jatropha deoiled cakes, sugarcane bagasse, apple, banana, orange peels, soybean hulls, grapes stalks, water hyacinth, sugar beet pulp, and sunflower have been tried and were found to have significant metal sorption capacity (Raju and Naidu 2013). These promising agricultural waste materials are used in the removal of metal ions either in their natural form or after some physical or chemical modification (Sud et al. 2008).

Among the most available and low cost lignocellulosic wastes, studies on rice husk have been reviewed in this specific research. The selection of this specific agriwaste is based on the various advantages that are obtainable in using raw and modified forms of this material for the removal of heavy metals especially cadmium and lead which are considered to have the highest environmental resource depletion impacts. Several reviews concentrating on the sorption capacity of agriwastes that are chemically or thermally modified have already been published. The removal of heavy metals by rice husk has been extensively reviewed by Chuah et al. (2005) and Ngah (2007). The heavy metal ions studied include Cd, Pb, Zn, Cu, Co, Ni, and Au. Rice husk can be used to treat heavy metals either in untreated or modified form using different modification methods. Such reviews discussed the pretreatment and modification techniques used, sorption capacity, equilibrium characteristics using appropriate sorption isotherms, kinetics and thermodynamics of sorption, mechanism of sorption, impact of various factors on sorption capacity, and to a limited extent options for recovery of sorbate and column sorption of heavy metals. However, the attention given to studies of thermodynamics and kinetic of sorption, elution of sorbate, mechanism of sorption, column experiments based on independent and mixtures of sorbents is very scattered and limited. Moreover, the future direction of the research in the area needs to be well depicted in order to avoid duplication of efforts and achieve the goal of designing and developing industrial-scale biosorption columns based on modified natural biosorbents.

This review chapter intends to investigate research conducted on biosorption of heavy metals by agriwastes, particularly by rice husk and identify the research gaps to recommend future research directions.

6.2 Studies on Chemically and Thermally Modified Rice Husk for Biosorption of Heavy Metals

Rice husk is an abundantly available agriwaste that consists of cellulose (32.24%), hemicellulose (21.34%), lignin (21.44%), and mineral ash (15.05%) (Rahman et al. 1997), as well as a high percentage of silica in its mineral ash, which is approximately 96.34% (Rahman and Ismail 1993). Rice husk is insoluble in water, has good chemical stability, has high mechanical strength, and possesses a granular structure, making it a good adsorbent material for treating heavy metals from wastewater. Pretreatment of rice husk can remove lignin and hemicellulose, reduce cellulose crystallinity, and increase the porosity or surface area (Akhtar et al. 2009). In general, several studies have well proven the fact that chemically and/or thermally modified or treated rice husk exhibited a higher adsorption capacity of

heavy metal ions than unmodified rice husk. Rice husk can be used to treat heavy metals in the form of either untreated or modified forms using different modification methods. Hydrochloric acid, sodium hydroxide, sodium carbonate, epichlorohydrin (Kumar and Bandyopadhyay 2006a, 2006b), and tartaric acid (Wong et al. 2003) are commonly used in the chemical treatment of rice husk. Pretreatment of rice husks can remove lignin or result in separation of structural linkage or decrease the degree of polymerization, reduce or remove hemicellulose, or reduce cellulose crystallinity. The heavy metal ions studied include Cd, Pb, Zn, Cu, Co, Ni, and Au (Kumar and Bandyopadhyay 2006b).

Akhtar et al. (2009) investigated the biosorption capacity of rice husk for the removal of Pb(II), Cd(II), Zn(II), and Cu(II) ions from aqueous solutions using nitric acid-modified rice husk, which was later thermally treated and later by potassium carbonate. After the modification, the surface area was significantly increased. The pore area was found to be greater than previously reported values of pore area with average pore diameter (51.3 ± 1.5 nm) of rice husk. The increase in pore area may be attributed to a different activation (chemical and thermal) methodology, which may have significantly affected the pore area, pore volume, and micropore structure of the rice husk. According to this study, rice husk activated by chemical (HNO_3 and K_2CO_3) and thermal activation (473K for 8h) exhibited significant sorption (99 ± 0.5 , 97 ± 0.6 , 96 ± 0.8 , and $95 \pm 0.9\%$) for the removal of Pb, Cd, Zn, and Cu ions, respectively, from low concentration aqueous solutions. The sorbed amount can be recovered with 20 mL of 0.1 M HCl solution. The chemical activation of sorbent with HNO_3 and K_2CO_3 increased the surface area and pore volume of sorbent. Thermal treatment of the sorbent at 473K for 8 h may also contribute to the formation of microporous material with many additional pores on the surface of the sorbent (Mahvi et al. 2004).

Munaf and Zein (1997) studied the ability of rice husk to remove chromium, zinc, copper, and cadmium from wastewater. Several parameters that can affect the uptake of metals, such as particle size, pH, and temperature, were described. At the optimal conditions, the chromium, zinc, copper, and cadmium ions removal from aqueous solution are 79%, 85%, 80%, and 85%, respectively.

Abdel-Ghani et al. (2007) found out that removal of the poisonous lead ions from solutions was possible using rice husk, maize cobs, and sawdust as adsorbents; rice husk being the most effective. The removal reached 98.15% of Pb at room temperature. Bansal (2009) observed that rice husk can be used for the removal of nickel from dilute wastewater. The effect of various process parameters showed that percent adsorption decreased with an increase in initial metal ion concentration, while it increased with an increase in adsorbent dose. Maximum nickel removal by adsorbent was at pH 6.0. Equilibrium adsorption showed that the system followed both the Langmuir and Freundlich models. According to the Dubinin-Raduskevich model, the adsorption of nickel was physical in nature. The kinetic studies concluded that nickel removal followed the pseudo-second-order rate equation. Desorption studies indicated the possibility of reusing the adsorbent.

Kumar and Bandyopadhyay (2006a, 2006b) tried three different modification methods for cadmium uptake using water-washed, HCl-treated, and NaOH-treated rice husk (NRH). Furthermore, they investigated epichlorohydrin-treated rice husk (ERH), and sodium-bicarbonate-treated rice husk (NCRH). The chemical modification resulted in an increase of the Cd(II) uptake of RRH from 75% to 97%, 80% and 97% for NRH, ERH and NCRH respectively, whereas it resulted in the decrease of the uptake from 75% to 65% for acid-treated rice husk (ARH).

Low (2000) reported that treatment with NaOH greatly enhanced sorption, whereas HCl-treated spent grain showed lower sorption than the water-washed spent grain. However, Xie et al. (1996) reported that a strong base (0.1 M NaOH) could dissolve biomass and

destroy metal binding sites. Chemical improvement by partial alkali digestion in autoclave has enhanced surface area and facilitation of transport of metal ions to the binding sites onto biomatrix (Krishnani 2008). Tarley et al. (2004) studied the potential of rice husk as a natural adsorbent in the unmodified form and after it was modified with 0.75 mol l⁻¹ NaOH solution. Furthermore, based on adsorption studies and adsorption isotherms applied to the Langmuir model, they verified that modified rice husk presents a higher adsorption capacity for both metals. Kumar and Bandyopadhyay (2006a, 2006b) found that the chemical modification on rice husk by ERH, NRH, and NCRH resulted in enhancing the sorption capacity of RRH for Cd(II) uptake, from 8.58 mg/g to 11.12, 20.24, and 16.18 mg/g, respectively. Though both NRH and NCRH had high uptake capacity, NCRH seemed to be the best because it offered two more important advantages: low cost of sodium bicarbonate (three times less than NaOH) and rapid uptake, which was favorable in column or continuous operation, where the contact time between the metal solution and the sorbent was generally short. Shamohammadi et al. (2008) studied the effect of different molarities of sodium bicarbonate on enhanced absorption capacity of rice husk to remove cadmium in low concentrations. Maximum absorption efficiency was achieved at a pH of 6 and the absorption equilibrium time was 1.5 hours. El-Shafey (2007), studied the removal of Cd(II) and Se(IV) from aqueous solution by sulfuric-acid-modified rice husk with later further thermal treatment for varying time, pH, metal concentration, temperature, and sorbent status (wet and dry). Cd(II) sorption quickly reached equilibrium within 2 h.

The formation of black (carbon fixed) particles in rice husk silica ash has been studied in detail by Krishnarao et al. (2001). The formation of black particles in the silica obtained by calcination of raw untreated rice husk is higher than that in acid-treated rice husk. The tendency to form black particles increases with an increase in the heating rate and the temperature of calcination of the untreated rice husk. Potassium has been shown to cause the formation of black particles in rice husk silica. Chemical impregnation with KOH and NaOH of pyrolyzed rice husk followed by activation at 650°C–800°C resulted in activated carbon with extremely high surface area (1413–3014 m²/g) (Ahmedna et al. 2004; Guo and Liu 2011; Guo et al. 2003). Pyrolysis of rice husk followed by H₃PO₄ impregnation and activation at high temperature (700°C–900°C) produced activated carbon with a surface area of 450 m²/g (Kennedy et al. 2004). Activated carbon produced by chemical activation with KOH or H₃PO₄ achieved high yield and removal efficiencies comparable to those of commercial products (Lozano-Castello et al. 2001). Kalderis et al. (2008) examined the production of activated carbon from bagasse and rice husk by a single-stage chemical activation method in short retention times (30–60 min). The raw materials were subjected to chemical pretreatment and were fed to the reactor in the form of a paste (75% moisture). Chemicals examined were ZnCl₂, NaOH, and H₃PO₄, for temperatures of 600°C, 700°C, and 800°C. Of the three chemical reagents under evaluation, only ZnCl₂ produced activated carbon with high surface area. The effect of impregnating agents ZnCl₂, NaOH, and H₃PO₄ on the carbon surface area was investigated at ratios of agent to raw material of 0.25, 0.5, 0.75, and 1. Activation was performed at temperatures of 400°C, 600°C, 700°C, and 800°C.

The optimum activation temperature was 700°C. The carbons produced at the optimum conditions had a surface area of 674 and 750 m²/g when bagasse and rice husk were used as precursors, respectively. At higher temperatures, more tars were formed as well as pore collapse occurred, resulting in a decrease of the surface area. It was also shown that increasing time had a negative effect on the development of the surface area, probably due to the blocking of the pores from the formation of tars. Physical activation tests were also performed at the optimum temperature. The surface areas obtained were lower compared to those obtained from the ZnCl₂ activation process. This was associated with

low temperature/low retention times, as well the uninhibited formation of tars. Girgis et al. (2002) compared three activating agents—KOH, H_3PO_4 , and ZnCl_2 —for the activation of rice hull. Of the three, H_3PO_4 produced carbon with the highest surface area of $1177 \text{ m}^2/\text{g}$. KOH after pyrolysis and 3 h heating at 500°C resulted in activated carbon with $268 \text{ m}^2/\text{g}$ surface area, and ZnCl_2 after 6 h pyrolysis at 300°C and 3 h heating at 750°C resulted in $420 \text{ m}^2/\text{g}$ surface area. All chemicals performed better than steam activation alone. Bansal (2009) studied the effect of pretreatments (boiling and formaldehyde treatment) on rice husk and various process parameters (pH, adsorbent dose, initial chromium concentration, and contact time has been studied in batch systems). To immobilize the color and water-soluble substances the ground rice husk was treated with 1% formaldehyde in the ratio of 1:5 (rice husk:formaldehyde, w/v) at room temperature ($27 \pm 3^\circ\text{C}$) for 24 h. The removal of chromium was found to be dependent on the physicochemical characteristics of the adsorbent, adsorbate concentration, and other studied process parameters. Maximum metal removal was observed at pH 2.0. The efficiencies of boiled and formaldehyde-treated rice husk for Cr(VI) removal were 71.0% and 76.5%, respectively, for dilute solutions at 20 g l^{-1} adsorbent dose. The experimental data were analyzed using Freundlich, Langmuir, and DR isotherm models. Bansal found that Freundlich and DR models fitted well. Naiya (2009) studied the effect of chemical treatment of sawdust and neem bark by sodium hydroxide and later by sulfuric acid. In these tests, washed sawdust and neem bark were soaked in 0.1N NaOH to remove lignin-based color materials followed by 0.1N H_2SO_4 (Bhattacharya et al. 2008), which was again washed several times and dried in an air oven at $105 \pm 5^\circ\text{C}$ for 6 h and cooled to room temperature in desiccators. Various physicochemical parameters such as pH, initial metal ion concentration, adsorbent dosage level, and equilibrium contact time were studied. The optimum pH for adsorption was 5 for Zn(II) and 6 for Cd(II). Kinetics data were best described by pseudo-second-order model. Mass transfer coefficients were also determined for individual adsorbents for removal of Zn(II) and Cd(II) ions from aqueous solutions. The equilibrium adsorption data were fitted to Langmuir and Freundlich isotherm models for Zn(II) and Cd(II) adsorption, respectively. Lu et al. (2009) studied various chemically modified orange peels (raw orange peel, orange peel modified with different alkali saponification, orange peel modified with different acids after saponification, orange peel modified with citric acid, and orange peel modified with citric acid after alkali saponification) for the removal of Cu^{2+} from dilute chloride solutions. The optimal material was obtained after pretreatment with 0.6 mol/L citric acid at 80°C and adsorbed a maximum of 1.22 mol/kg Cu^{2+} . The results of all the different chemically modified orange peel celluloses showed reasonable maximum adsorption capacities for Cu^{2+} compared to untreated orange peel. A comparison of different isotherm models revealed that a combination of the Langmuir and Freundlich (L-F) isotherm models fitted the experimental data best. The copper adsorption was strictly pH dependent, and maximum sorption was found to occur at around pH 4.5 and 5.5. The kinetic equilibrium was rapidly established in about 30 min. Results indicate that the chemically modified orange peel cellulose increases the number of functional groups on the cellulose and can provide an efficient and cost-effective technology for eliminating copper from wastewater and effluent solutions. On another study, adsorbent has been prepared by treatment of rice husk and sawdust with acrylamide. Removal has been studied at various pH values for different times of contact and adsorbate concentrations and is found to be pH-dependent. Maximum removal occurs at pH 9 and at a contact time of 180 min for both the adsorbents. The results were found to be consistent with both the Langmuir and Freundlich isotherm models (Sharma et al. 2008). Sharma et al. (2008) showed that the effect of chemical grafting is comparable to that of activated carbon. A comparison of the removal efficiency for

polymer-grafted rice husk, for rice husk prior to grafting, and for activated carbon shows that the removal efficiency of polymer-grafted rice husk is almost the same as that for activated carbon. However, the use of grafted rice husk is much more economical in terms of adsorbent cost as well as adsorbent regeneration. The results suggest that both polyacrylamide grafted rice husk and sawdust can be used as efficient and cost effective adsorbents for cadmium ion removal. Rice husk or sawdust is activated by treating three parts of rice husk with one to two parts of chemicals (EDTA or activated carbon) and keeping it in an oven maintained at a temperature of 140°C to 160°C for a period of 24 hours. The carbonized material was washed well with water to remove free acid and then dried at 105°C to 110°C for 1 h. The dried material was subjected to thermal activation in an atmosphere of carbon dioxide at a temperature of 800°C to 850°C for a period of 30 minutes. The material was then ground to produce particles of average diameter 170 and 1300 micrometer for sawdust and rice husk, respectively (Saravanane et al. 2001). Chand et al. (2009) studied Au(III) sorption capacity of activated carbon from rice husk and barley straw. According to Chand et al. (2009), Das (2010), and Chen et al. (2011), rice husk carbon is highly selective for Au(III), and barley straw carbon is highly selective for Au(III) and other precious metals over various base metals. The adsorption of Au(III) on both adsorbents is nearly independent of hydrochloric acid concentration, which is advantageous in practical applications. The very fast metal ion adsorption rate of barley straw carbon is an additional advantage. The enhanced adsorption capacity as a result of Au(III) to Au(0) reduction, high selectivity, and very fast adsorption rate for carbons generated from discarded agriwaste can make rice husk carbon and barley straw carbon a promising alternative adsorbent for precious metals and Au(III) recovery from industrial waste using chloride solution.

6.3 Studies on Impact of Various Parameters on Sorption Capacity of Rice Husk

According to studies conducted by different researchers, pH, contact time, sorbent dose, metal dose, particle size, temperature, presence of co-ions, and chemical or thermal pre-treatment were found to be the major factors that significantly affect heavy metal sorption capacity of rice husk and other agriwastes (Jain et al. 2016).

6.3.1 Impact of pH

It was proven by numerous research work that pH is one of the major factors affecting the biosorption capacity of rice husk, as it affects the solution chemistry and ion-exchange rate (Amer 2015). Abdel-Ghani et al. (2007) found that the optimum pH for removal was found to be in the range from 4.5 to 6.5, at which Pb removal reaches 99% for the three adsorbents they investigated. The effect of pH can be explained by the availability of negatively charged groups at the biosorbent surface that are necessary for the sorption of metals to proceed (Krishnani et al. 2008). According to Akhtar et al. (2009), the impact of PH, contact time, particle size, and sorbent dose was determined and showed maximum performance at particle size of 100 µm, agitation time of 20 min, and sorbent dose of 0.2 g of sorbent dose and pH of 6. Sorption capacity tends to increase with an increase in pH. At higher pH, the oxygen of each negatively charged binding sites available onto rice husk matrix (C=O or O-H groups of polyphenols) behaves as strong Lewis base and

may result in complexation of metal ions but a further increase may decrease the sorption capacity due to the formation of the metal hydroxides. According to Kumar and Bandyopadhyay (2006a, 2006b), adsorption by rice husk modified with epichlorohydrin, sodium bicarbonate, and sodium hydroxide, pH adsorption edge was 3 to 5. After pH 5, the sorption increased gradually up to pH 9. The optimum uptake of 86.2%, 97.0%, and 97.2% by ERH, NRH and NCRH, respectively, were observed at pH 9. A decreasing trend in uptake was observed above pH 9 due to formation of soluble hydroxyl complexes. Krishnani (2008) demonstrated that metal binding is strongly pH dependent with more metal cations bound at higher pH and the maximum uptake of metal ion took place at pH $5.5-6 \pm 0.1$. The pH of the solutions has been identified as the most important variable governing metal adsorption. This is partly due to the fact that hydrogen ions themselves are strong competing ions and partly that the solution pH influences the chemical speciation of the metal ions as well as the ionization of the functional groups onto the adsorbent surfaces. Removal of Pb(II) increases with increasing solution pH and a maximum value was reached at an equilibrium pH of around 5 (Naiya 2009). El-Shafey (2007) found that Cd(II) sorption was extremely low at low pH values (pH 1.5–2) and increased with pH rising with a decrease in the final pH due to proton release indicating an ion exchange mechanism. On the other hand, Se(IV) sorption was high at low pH, and as the pH increased, Se(IV) uptake decreased with a rise in the final pH due to proton consumption indicating a reduction process of Se(IV). Sorption of Cd(II) and Se(IV) follows the Langmuir equation with an increase in metal uptake as temperature rises due to an expected increase in the swelling of the sorbent allowing more active sites to become available for metal ions.

6.3.2 Impact of Concentration of Sorbent

Concentration is another major factor that influences heavy metal sorption capacity of rice husk (Lata and Samadder 2014). The percentage adsorption of Cd(II) by rice husk increased from 18% to 99% when the adsorbent dose was increased from 0.5 to 3.0 g, but at the same time adsorption density decreased from 90 to 16.5 mg g^{-1} (Ajmal et al. 2002). Bansal (2009) observed that the percentage removal of Ni(II) increases with the increase in the adsorbent dosage. According to Abdel-Ghani et al. (2007), an increase in mass of adsorbent and contact time resulted in an increase of the percentage removal of Pb, while the increase in the initial lead concentration resulted in the decrease of the removal efficiencies of the different adsorbents.

6.3.3 Effect of Use of Mixture of Rice Husk and Other Sorbents on Sorption Performance

Utilization of a mixture of sorbents instead of a single sorption agent like rice husk is more beneficial and effective (Hegazi 2013; Sobhanardakani et al. 2013; Xu et al. 2013).

Boonamnuyvitaya et al. (2004) investigated the preparation and utilization of coffee residues bounded with clay as an adsorbent for removal of heavy metal ions in solution. Factors affecting the adsorption such as pH, pyrolysis temperature, weight ratio of coffee residue to clay, and particle size were investigated. A particle size diameter of 4 mm, pyrolysis temperature of 500°C , and coffee residue-to-clay weight ratio of 80:20 were found to be optimum. Sorption capacity was observed to increase with increasing pH and

temperature; the heat of adsorption was found to be ($\Delta H = -1.11$ kcal/g) indicating the exothermic nature of the sorption process. Hence, the sorption capacity can be improved more than what can be achieved by chemically or thermally treated independent sorbents. Sumathi et al. (2005) observed that biosorbents and vermiculite in columns were found to be very effective in removing Cr from the tannery effluent. A mixed column of coir pith and vermiculite was found to be most effective in removing Cr. This study has, therefore, demonstrated that easily available low-cost biosorbents could be used to reduce chromium present in the tannery effluent either independently or in mixed form where sorption tests in mixed setup were conducted for different proportions of rice husk, sawdust, and vermiculite, and were found to give a better sorption capacity than experiments with individual sorbents. The presence of vermiculite notably improved the sorption capacity of the column, with a maximum sorption recorded for a sawdust:vermiculite ratio of 3:1, and sorption capacity for independent sorbents goes in the order of sawdust > coir pith > rice husk > vermiculite.

6.3.4 Impact of Metal Dose on Sorption Performance

The concentration of metal ions in solution is one other important factor that should be considered when conducting sorption studies by any agriwaste like rice husk (Amer 2015). Abdel-Ghani et al. (2007) observed that the percentage of lead(II) uptake was found to be highly dependent on the initial concentration of the sorbate, and the sorbent fractional adsorption is dependent on initial metal concentration. For fixed adsorbent dose, the total available adsorption sites are limited resulting in the decrease of percentage removal of the adsorbate corresponding to the increase of initial sorbate concentration (Krishnan and Anirudhan 2003). Removal percentages of Zn(II) as well as Cd(II) from aqueous solution decreases as the concentration increases from 3 to 100 mg/L at constant pH. As the metal ion to adsorbent ratio increases, the higher energy sites are saturated and adsorption begins on lower energy sites, resulting in the decrease of the adsorption efficiency (Bhattacharya et al. 2006; Kadirvelu and Namasivayam 2003; Zouboulis et al. 2002). The amount of metal ion adsorbed increases with concentration; however, percentage removal increases with a decrease in the concentration of Cd(II) ions. The increase in percentage adsorption with dilution may be attributed to the availability of a larger number of surface sites of the adsorbent for a relatively small number of adsorbing species at higher dilution (Raji and Anirudhan 1996; Sharma et al. 2008).

6.4 Sorption Isotherms

Several isotherm models including Langmuir, Freundlich, Dubinin-Radushkevich (DR), Redlich-Peterson, and Temkin isotherm equilibriums have been used to determine how sorbate (heavy metal) is distributed in the solid sorbent (rice husk) and liquid phase (Dada et al. 2012). The partitioning behavior between solid and liquid phases was determined by employing Freundlich, Langmuir, and DR sorption equilibrium models for the estimation of the sorption capacity of sorbent. Kinetic and thermodynamic parameters were also evaluated for applied sorption system (Akhtar et al. 2009, 2010).

The Langmuir isotherm determines the sorption of sorbates onto saturated monolayers of sorbent at specific homogeneous sites with the help of the linearized relationship form (Dada et al. 2012):

$$\frac{C_e}{q_e} = \frac{1}{Qb} + \frac{C_e}{Q} \quad (6.1)$$

The isotherm constants Q and b are calculated from the slope and intercept of the plot between C_e/q_e and C_e .

The Freundlich isotherm presumes the uptake of sorbate on a heterogeneous surface by multilayer sorption and may be tested using the linearized equation form (Dada et al. 2012)

$$\log q_e = \log K_F + \frac{1}{n} \log C_e \quad (6.2)$$

The isotherm constants n and K_F were calculated from the slope and intercept of the plot $\log q_e$ versus $\log C_e$.

The DR isotherm assumes a fixed volume or “sorption space” close to the sorbent surface and determines the heterogeneity of sorption energies within the sorption space (Dubinin 1947; Kaman et al. 2017):

$$\ln q_e = \ln X_m - \beta \epsilon^2 \quad (6.3)$$

where ϵ is the Polanyi constant and is given by

$$\epsilon = RT \ln \left(1 + \frac{1}{C_e} \right) \quad (6.4)$$

and where q_e is the amount of sorbate sorbed by sorbent and C_e is the concentration at equilibrium.

The constant (β) and X_m are obtained from the slope and intercept of the plot of $\ln q_e$ against ϵ^2 . The mean sorption energy, E , which is defined as the free energy transfer of 1 mol of solute from infinity of the surface of the sorbent, can be calculated using the calculated value of β , from

$$E = \frac{1}{\sqrt{-2\beta}} \quad (6.5)$$

If the magnitude of E is between 8 and 16 kJ mol⁻¹, the sorption process is supposed to proceed via chemisorption, while for values of $E < 8$ kJ mol⁻¹, the sorption process is of physical nature (Mohan and Pittman 2006).

The Redlich–Peterson isotherm can be described as follows (Ho 2003):

$$q_e = \frac{AC_e}{1 + BC_e^q} \quad (6.6)$$

where A , B , and q all representing isotherm constants. At low concentrations, the Redlich–Peterson isotherm approximates to Henry's law and at high concentrations its behavior approaches that of the Freundlich isotherm.

The Temkin isotherm assumes that the fall in the heat of sorption is linear rather than logarithmic, as implied in the Freundlich equation. The Temkin isotherm has generally been applied in the following form (Dada et al. 2012; Halbus et al. 2017; Schneider and Rubio 1999):

$$q_e = \frac{RT}{b_t} \ln(a_t C_e) \quad (6.7)$$

where R is the general gas constant, T is absolute temperature (K), and b_t and a_t represent isotherm constants (Wang and Qin 2005). Wang and Qin (2005) analyzed the applicability of the aforementioned four models and found that the data fit better to Langmuir, Redlich–Peterson, and Temkin models than Freundlich. In another study, for the removal of several heavy metals by rice husk biomatrix (Krishnani 2008), adsorption follows both Langmuir and Freundlich isotherms, probably due to the real heterogeneous nature of the surface sites involved in the metal uptake. In the preparation and utilization of coffee residues bounded with clay as adsorbent for removal of heavy metal ions in solution, the adsorption capacities of the CC-adsorbent for Cd^{2+} , Cu^{2+} , Pb^{2+} , Zn^{2+} , and Ni^{2+} were determined by the Langmuir isotherm model. The adsorption increased in the order of $\text{Cd}^{2+} > \text{Cu}^{2+} > \text{Pb}^{2+} > \text{Zn}^{2+} > \text{Ni}^{2+}$ (Boonamnuyvitaya et al. 2004). In the study of adsorption of Cd(II) by rice husk, the Langmuir isotherm is obeyed better than the Freundlich isotherm. The adsorption of Cd(II) increased with an increase in temperature. The Langmuir model is an indicator of surface homogeneity of the adsorbent. The thermodynamic parameters ΔG° , ΔS° , and ΔH° have also been determined (Ajmal et al. 2002). Abdel-Ghani et al. (2007) observed that the equilibrium time was attained after 120 min and the maximum removal percentage was achieved at an adsorbent loading weight of 1.5 g. The equilibrium adsorption capacity of adsorbents used for lead were measured and extrapolated using linear Freundlich, Langmuir, and Temkin isotherms, and the experimental data were found to fit the Temkin isotherm model. The adsorption behavior of Ni(II), Zn(II), Cd(II), and Cr(VI) on untreated and phosphate-treated rice husk (PRH) showed that adsorption of Ni(II) and Cd(II) was greater when PRH was used as an adsorbent. Sorption of Cd(II) was dependent on contact time, concentration, temperature, adsorbent doses, and pH of the solution. The Langmuir constants and thermodynamic parameters were calculated at different temperatures (Ajmal et al. 2002). Table 6.1 shows a summary of the maximum sorption capacity calculated using the most relevant sorption isotherm for chemically and thermally modified rice husk and other agriwaste-based adsorbents.

TABLE 6.1

Sorption Capacity of Chemically and Thermally Modified Rice Husk and Other Agriwastes for Different Heavy Metals

Sorbent	Metal Sorbed	Q max (mg/g)	Reference
Epichlorohydrin-modified rice husk	Cd(II), Pb(II), Cu(II)	11.12	Kumar and Bandyopadhyay (2006a)
Sodium hydroxide-modified rice husk	Cd(II)	20.24	Kumar and Bandyopadhyay (2006)
Sodium hydroxide-modified rice husk	Cd(II), Ni(II), Zn(II), Mn(II), Co(II), Cu(II), Hg(II), Pb(II)	0.149, 0.094, 0.124, 0.151, 0.162, 0.172, 0.18, 0.28 mmol/g	Krishnani (2008)
Sodium bicarbonate-modified rice husk	Cd(II)	16.8	Kumar and Bandyopadhyay (2006b)
Sulfuric acid-modified rice husk	Zn(II), Hg(II)	(Wet) 19.38, 384.62; (dry) 18.9, 303	El-Shafey (2007), El-Shafey et al. (2016)
Tartaric acid-modified rice husk	Pb(II), Cu(II)	120.48, 31.85	Wong et al. (2003)
Formaldehyde-modified rice husk	Cr(VI)	10.4	Bansal (2009)
Nitric acid-modified rice husk	Cu(II), Cd(II)	9.36, 11.03	Soon-An et al. (2007)
Nitric acid and potassium carbonate-modified rice husk	Cu(II), Zn(II), Pb(II), Cd(II)	2.2, 2.4, 12, 4.9	Akhtar et al. (2010)
Fixed bed of sodium carbonate-treated rice husk	Cd(II)	0.889 mg/cm ³	Kumar and Bandyopadhyay (2006b)
Fixed bed of phosphate-treated rice husk	Pb(II), Cu(II), Zn(II), Mn(II)	0.52, 0.98, 1.36, 0.81 mg/cm ³	Mohan and Sreelakshmia (2008)
Polyacrylamide-grafted rice husk/saw dust	Cu(II)	0.889, 0.291	Sharma et al. (2008)
Nanoparticles of low-value by-product rice husk	Pb(II)	93.45	Masoumi et al. (2016)
Orange peel citric acid-modified after alkali saponification	Cu(II)	78.52	Lu et al. (2009)
Orange peel phosphoric acid modified after alkali saponification	Cu(II)	54.35	Lu et al. (2009)
Orange peel oxalic acid modified after alkali saponification	Cu(II)	61.82	Lu et al. (2009)
CTAB-modified <i>Moringa oleifera</i>	Pb(II)	98.89%	Nadeem et al. (2006)
Acrylonitrile, hydroxylamine (amidoxime)-modified wood sawdust	Cu(II), Ni(II)	246, 188	Saliba et al. (2005)
Wood pulp succinic anhydride (carboxyl)	Cd(II)	169	Marchetti et al. (2000)

(Continued)

TABLE 6.1 (CONTINUED)

Sorption Capacity of Chemically and Thermally Modified Rice Husk and Other Agriwastes for Different Heavy Metals

Sorbent	Metal Sorbed	Q max (mg/g)	Reference
Mangium bark	Cu(II), Ni(II), Pb2(II), Hg(II)	0.75–5.18	Khabibi et al. (2016)
Cuscuta-based adsorbent	Fe(II)	27.0314	Dhanik et al. (2016)
Pyrolized coffee residue and clay	Cd, Cu, Ni, Pb, Zn	39.6, 31.2, 11.0, 19.5, 13.4	Boonamnuyvitaya et al. (2004)
Sunflower stalks: (1) acrylonitrile, (2) hydroxylamine (amidoxime)	Cu(II)	39 3.0–5.0 F	Hashem et al. (2005)
Mixture of sawdust and rice husk and coir pith and vermiculite clay	Cr(VI)	1482 mg/g for sawdust, 159 mg/g for coir pith	Sumathi et al. (2005)
Sugar cane bagasse with sodium bicarbonate	Cu(II), Pb(II), Cd(II)	114, 196, 189	Junior et al. (2006)
Sugarcane bagasse with ethylenediamine	Cu(II), Pb(II), Cd(II)	139, 164, 189	Junior et al. (2006)
Sugarcane bagasse with triethylenetetramine	Cu(II), Pb(II), Cd(II)	133, 313, 313	Junior et al. (2006)

6.5 Studies on Kinetics of Biosorption Process by Activated Rice Husk

A significant number of studies have been published on the kinetics of sorption of heavy metals by lignocellulosic waste materials including rice husk. Different kinetic models were proposed to represent the trend. As most studies show, the sorption kinetic behavior of most physical sorption processes follow pseudo-second-order rate kinetics (Swami and Gupta 2016).

Abdel-Ghani et al. (2007) observed that the sorption process proceeded in two distinct phases. The rates of adsorption were fast initially, and then the rate of metal removal declined appreciably as contact time increased before attaining equilibrium. The fast-phase sorption may be explained as the passive uptake through physical adsorption or the biosorbent surface ion exchange (Ting et al. 1989). Since the adsorption phenomenon characteristically tends to attain instantaneous equilibrium and many agricultural wastes act as natural ion exchange agents, equilibrium data fit well to the mostly used Langmuir and Freundlich models with coefficient of determination close to unity in most studies (Bajpai and McDonald 2008). Kinetic studies revealed that first-order rate kinetics and intraparticle diffusion mechanism were applicable. Thermodynamic parameters illustrate exothermic, feasible, and spontaneous nature of sorption process. The kinetic study (rate constant and rate of intraparticle diffusion) for the uptake of metal ions onto rice husk was carried out by applying the linearized form of the Lagergren equation

$$\ln(q_e - q_t) = \ln(q_e - k_t) \quad (6.8)$$

and the Morris–Weber equation (Dakiky et al. 2002; Weber and Morris 1963)

$$q_t = R_{id} \sqrt{t} \quad (6.9)$$

where k is the first-order rate constant, while q_e and q_t are the equilibrium and sorbed concentrations of metal ions at time t , and R_{id} is the intraparticle diffusion rate constant in linear plots of $\ln(q_e - q_t)$ versus t .

According to Kumar and Bandyopadhyay (2006b), it was observed that the chemical pretreatments resulted in reducing the equilibrium time from 10 h for raw rice husk to 2, 4, and 1 h for ERH, NRH, and NCRH, respectively. It was observed that uptake of metal ion occurred in two stages: an initial rapid uptake within 15 and 20 min followed by subsequent slow uptake from 20 to 240 min.

Ho et al. (1999) observed that most of the sorption systems followed a pseudo-second-order kinetic model as also reported by

$$t/q = 1/kq_e^2 + t/q_e \quad (6.10)$$

where t is the contact time (min); q and q_e are the quantities of sorbate, sorbed at time t and at equilibrium (mg/g); and k is the rate constant (g/mg min). The initial sorption rate can be obtained as q/t approaches zero:

$$h_o = kq_e^2 \quad (6.11)$$

The Reichenberg model (Banerjee and Chattopadhyaya 2013; Reichenberg and McCauley 1955) was applied to check that sorption proceeds via film diffusion or intraparticle diffusion, and can be written in the following form:

$$x = \left(1 - \frac{6}{\pi^2}\right) e^{Bz} \quad (6.12)$$

where $x = q_t/q_e$, and B_t is a mathematical function of X , which can be evaluated from each value of X as

$$B_t = -0.4977 \ln(1 - X) \quad (6.13)$$

If the plots of B_t versus t do not pass through the origin then it is concluded that intraparticle diffusion is not the sole rate controlling step (Ranjan et al. 2009).

The Elovich equation is commonly used to determine the kinetics of chemisorption of gases onto heterogeneous solids, and in recent years, this equation has also been used to describe the sorption of pollutants from aqueous solutions (Namasivayam and Sureshkumar 2008; Pokhrel and Viraraghavan 2007). The Elovich equation can be written in the following form:

$$\frac{dq_t}{dt} = a \exp(-bq_t) \quad (6.14)$$

where a represents the rate of chemisorption at zero coverage (mg/(g min)), and b is related to the extent of surface coverage and activation energy for chemisorption (g/mg). These constants were calculated from the slope and intercept of the plots of q_t versus $\ln(t)$.

Application of Equation 6.14 is usually tested by converting it to the integrated form, namely,

$$q_t = \frac{1}{b} \ln(ab) + \frac{1}{b} \ln\left(t + \frac{1}{ab}\right) \quad (6.15)$$

and assuming $q_t = 0$, $t = 0$ as the lower limit of integration. For large values of t , that is, $t \gg 1/ab$, the plots of q_t versus $\ln(t)$ should be linear.

Mass transfer analysis for the removal of Zn(II) and Cd(II) from aqueous solutions by the selected adsorbents were carried out using the following equation as proposed by McKay et al. (1981). According to McKay et al., the three steps involved in the sorption process according to this model are as follows:

1. Mass transfer of the solids from the aqueous phase onto the solid surface
2. Adsorption of solute onto the surface sites
3. Internal diffusion of solute via a pore diffusion model

$$\ln\left(\frac{C_t}{C_i} - \frac{1}{1 + mk}\right) = \ln\left(\frac{mk}{1 + mk}\right) - \left(\frac{1 + mk}{mk}\right)\beta S_s t \quad (6.16)$$

The plot of $\ln((C_t/C_i) - (1/(1 + mk)))$ versus t resulted a straight line of slope $[(1 + mk)/mk]\beta S_s$ and the values of mass transfer coefficients (β) calculated from the slopes of the plots. The values of mass transfer coefficients (β) obtained from the study indicated that the velocity of the adsorbate transport from bulk to the solid phase were quite fast (Naiya et al. 2008).

In connection to this, Ranjan et al. (2009) showed that the rate of transfer of mass from bulk solution to the biosorbent surface was rapid enough to use rice polish as sorbent for the treatment of wastewater rich in arsenic and it also suggests that mass transfer cannot be the rate controlling step.

6.6 Thermodynamics of Sorption

Thermodynamics is a very important parameter in sorption processes to determine the energy requirement and mechanism of sorption (Jaman et al. 2009).

Thermodynamic parameters—enthalpy ΔH (kJ mol⁻¹), entropy ΔS (J mol⁻¹ K⁻¹), and standard free energy of activation ΔG (kJ mol⁻¹)—were investigated by different researchers under the optimized conditions chosen by applying Equations 6.17, 6.18, and 6.19:

$$\ln K_c = \frac{-\Delta H}{RT} + \frac{\Delta S}{R} \quad (6.17)$$

$$\Delta G = -RT \ln K_c \quad (6.18)$$

where R is a gas constant, T is the temperature in kelvins, and K_c is the equilibrium constant estimated as

$$K_c = \frac{C_{Ae}}{C_e} \quad (6.19)$$

The heat of adsorption ($H = -1.11$ kcal/g) implied that the adsorption was physical exothermic adsorption (Boonamnuyvitaya et al. 2004).

The adsorption capacity (q_{\max}) of rice husk ash for Pb(II) ions in terms of monolayer adsorption was 91.74 mg/g. The change of entropy (ΔS^0) and enthalpy (ΔH^0) were estimated at 0.132 kJ/(mol K) and 28.923 kJ/mol, respectively. The negative value of Gibbs free energy (ΔG^0) indicates feasible and spontaneous adsorption of Pb(II) on rice husk ash (Naiya et al. 2008).

6.7 Studies of Co-Ion Effect

Investigating the impact of the presence of other ions in solution on the sorption or removal of a particular metal ion is very essential. As many ions tend to adsorb on similar active sites, the interference effect or co-ion interaction is another important aspect of heavy metal sorption research (Guo et al. 2003).

Sengil and Özacar (2009) stated that although a significantly high number of research data is available on single-metal biosorption, relatively less attention has been paid to the biosorption in multimetal ion solutions. In multicomponent systems, sorption of heavy metal ions depends not only on the specific surface properties of the biomass and on the physicochemical parameters of the solution, like temperature, pH, initial metal ion concentration, and biomass concentration, but also on features of those components, as well as the number of those different metal ions competing for binding sites, metal combination, levels of metal concentration, residence time, and test criteria (Özacar et al. 2008; Sengil and Özacar 2008).

6.8 Studies on Column Experiment

The applicability of sorption technology at industrial or commercial scale requires established understanding of continuous column heavy metal sorption process performance. Different researchers have investigated the sorption capacity of rice husk in continuous column setup (Kumar and Bandyopadhyay 2006a; Mohan and Sreelakshmia 2008; Qaiser et al. 2009; Sharma and Singh 2013).

Krishnani (2008) used the results obtained from batch experiments adsorption to remove metal ions using continuous packed columns. Continuous column adsorption

experiments were conducted to evaluate biomatrix for the removal of eight different metal ions (Pb, Hg, Cd, Cu, Ni, Co, Mn, and Zn) in combination. There was no leakage of Pb^{2+} throughout the bed volumes with an initial concentration of 12.5 mg/L. In the case of Cu^{2+} , Hg^{2+} , and Cd^{2+} , there was no leakage of 25 to 33 bed volumes with an initial concentration of 12.5 mg/L, whereas in the case of Ni^{2+} , Zn^{2+} , Mn^{2+} , and Co^{2+} , there was no leakage of 8 to 10 bed volumes. The biomatrix exhibited greater adsorption capacity due to higher initial concentration and optimum pH. About 65% to 100% of metal ions were removed at lower flow rates (0.2–1.0 mL/min), while this decreases with increased flow rate (1.0–2.0 mL/min). The higher column capacity is attributed to continuously high concentration gradient, which occurred at the interface as the concentrate passes through the column, while the concentration gradient decreased with time in the batch experiment. A column flow experiment with multiple ions revealed the clear sorption preference for Pb^{2+} and Cu^{2+} . Similar results were obtained by Gerente et al. (2004) on biosorption of Pb^{2+} , Cu^{2+} , and Ni^{2+} on sugar beet pulp, and it was also reported that Ni^{2+} has very less competitive effect.

From this it is evident that the unique ability of the biomatrix from rice husk to bind as many as eight metals can be attributed to the presence of sufficient Ca^{2+} and Mg^{2+} ions for ion exchange and functional groups that attract and sequester metal ions (Baig et al. 1999). The release of Na^{+} ions was in continuous decreasing order up to 4 bed volumes and thereafter there was no release, which indicates that initial release of Na^{+} ions are in the same decreasing order of magnitude and seem to be independent of the metal ion concentrations.

According to Kumar and Bandyopadhyay (2006b), a fixed bed of sodium carbonate treated rice husk was used for the removal of Cd(II) from a water environment. The material as adopted was found to be an efficient media for the removal of Cd(II) in continuous mode using a fixed bed column. The column having a diameter of 2 cm, with different bed depths such as 10, 20, and 30 cm could treat 2.96, 5.70, and 8.55 l of Cd(II) bearing wastewater with Cd(II) concentration 10 mg/l and flow rate 9.5 ml/min. Different column design parameters, including depth of exchange zone, adsorption rate, and adsorption capacity, were calculated. Effect of flow rate and initial concentration was studied.

Mohan and Sreelakshmia (2008) studied the performance of low-cost adsorbent such as raw rice husk (RRH) and phosphate treated rice husk (PRH) in removing the heavy metals such as lead, copper, zinc, and manganese. The adsorbent materials adopted were found to be efficient media for the removal of heavy metals in continuous mode using fixed bed column. The columns studies were conducted with 10 mg/l of individual and combined metal solution with a flow rate of 20 ml/min with different bed depths such as 10, 20, and 30 cm.

Batch and column experiments were used to assess the effectiveness of selected biosorbents (sawdust, rice husks, coir pith, and charcoal) and a naturally occurring mineral (vermiculite) in removing Cr from the tannery effluent. The adsorption capacities of the biosorbents were evaluated by using isotherm tests and by computing the distribution coefficient. The sawdust exhibited a higher adsorption capacity ($k \frac{1}{4}$ 1482 mg/kg), followed by coir pith ($k \frac{1}{4}$ 159 mg/kg). The biosorbent and mineral vermiculite in columns were observed to be very effective in removing Cr from tannery effluent. About 94% removal of Cr was achieved by a column of coir pith and equally (93%) by a column containing a mixture of coir pith and vermiculite (Sumathi et al. 2005).

Column studies have been carried out for grafted rice husk as adsorbent in order to study the adsorption capacity for dynamic adsorption. The breakthrough time has been found to be 4 h for a flow rate of 3 L h^{-1} and at feed concentration 300 mg L^{-1} at pH 9. Studies have been carried out at different flow rates, and it was observed that at higher flow rates due to

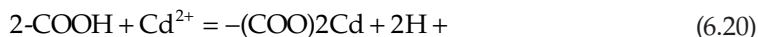
shorter residence time of solution in bed, the mass transfer and adsorption capacity were reduced (Sharma et al. 2008).

6.9 Studies on Mechanism of Sorption

Sorption study on heavy metals by agriwastes, particularly by rice husk, requires established understanding of the mechanism of the process. Most sorption processes by lignocellulosic waste involves ion exchange mechanism with some chemisorption via complexation and chelation with the ligands on the surface of the sorbent (Elhafez et al. 2016).

Increased sorption capacity was recorded for the treated rice husk because of the formation of stretching bands of –OH, C-H or deformation of –CH₂ and –CH₃ bonds. Scanning electron microscopy results show the significant change in morphology of biosorbent after activation with increased number of cavities on activated surfaces responsible for more sorption potential of rice husk (Akhtar et al. 2010; Elhafez et al. 2016; Krishnani 2008).

El-Shafey (2007) concluded that Cd(II) was sorbed via ion exchange. The carbon possesses acidic functional groups on the surface such as –COOH and –OH that are responsible for the cation exchange property as expressed in



The main species of Cd(II) is Cd²⁺ up to pH 8, and above pH 8 Cd(II) forms Cd(OH)⁺ (Baes and Mesmer 1976; Srivastava et al. 2004). But the sorption experiment was conducted under a pH of 6 to prevent precipitation of the hydroxide.

For the study of the mechanism of sorption, Krishnani (2008) obtained native rice husk (lignocellulosic substrate) from agroindustry and subjected it to 1.5% alkali treatment (300 g in 1 L) and then autoclaved it at 121°C for 30 min in order to remove the low molecular weight lignin compounds. After filtration, this material was washed with deionized water until the pH reached a constant value close to neutrality. In order to study the metal removal mechanism, metal solution was allowed to equilibrate with the biomatrix in an incubator agitated at 200 rpm for 180 min. After equilibration, the metal ion solution was filtered using a 0.45 µm filter, and filtrate was analyzed for the concentrations of metals and for the Ca²⁺, Mg²⁺, and Na⁺ ions released by the biomatrix using inductively coupled plasma (ICP) emission spectrometer (Varian Liberty-200, Palo Alto, California). Studies revealed that biomatrix has sufficient calcium, magnesium, and many OH and COOH groups in the lignocellulosic moieties, which are the sites for ion exchange with metal cations.

The functional groups studied by FTIR (Fourier transform infrared spectroscopy) indicated that hydroxyl, carboxyl, and amine groups were the main functional groups. Electrical potential study showed that the pyrolyzed coffee and clay (CC-adsorbent) exhibited negative charge that was favorable to attract metal ions. The surface and pore study implied that the high fraction mesopores in the granular CC-adsorbent contributed to the adsorption capacity (Boonamnuyvitaya et al. 2004). According to Abdel-Ghani et al. (2007) rice husk IR spectrum showed four intense bands, at 3379.1, 2920, 1604, and

1076.2 cm^{-1} . The band at 3379.1 cm^{-1} was attributed to the surface hydroxyl groups and chemisorbed water. The bands at 2920 and 2850.6 were assigned to C-H stretches of methylene groups on the surface and to chelated H-bridges. Bands at 1604 and 1076.2 cm^{-1} can be assigned to C=O stretching frequencies, and to phosphate and silicate groups, respectively. Small peaks observed at 1438–1396 cm^{-1} were attributed to carboxylate groups, and the band at 466.7 is due to the metal–halogen bond (Stuart 2004). The FTIR spectra of the polymer-coated adsorbents studied as KBr pellets show peaks at 3412 cm^{-1} (broad band) due to OH and stretching NH group; a peak 2925 cm^{-1} is attributed to stretching CH_2 ; a band at 1522 cm^{-1} indicates NH group; C=O stretching is observed at 1669 cm^{-1} ; and another band at 1420 cm^{-1} is due to stretching C=O which shows the presence of COOH group (Sharma et al. 2008). An FTIR test was conducted for the sake of understanding the mechanism of sorption and the FTIR spectra show a number of absorption peaks, indicating the complex nature of the examined adsorbents. In native raw rice husk the absorption peak around 3660.6 cm^{-1} indicates the existence of free and intermolecular bonded hydroxyl groups. The peaks observed at 3076.2 cm^{-1} can be assigned to stretching vibration of the C-H group. The peaks around 1664.4 cm^{-1} correspond to the C=O stretching that may be attributed to the lignin aromatic groups. The additional peaks at 848.6 and 750.2 cm^{-1} can be assigned to bending modes of aromatic compounds. The C=O absorption peak was observed to shift to 1589.2 cm^{-1} when raw rice husk is loaded with Cr(VI). It seems that this functional group participates in the metal binding process. In native formaldehyde-treated rice husk, a broad adsorption band observed around 3438.8 cm^{-1} can be attributed to the bonded OH groups present in the structure. The other prominent peaks are due to C-H, C=O, and C-O (2908.4, 1554.5, and 1026.0 cm^{-1} , respectively) groups. The additional peak at 862.1 and 686.6 cm^{-1} can be assigned to bending modes of aromatic compounds. However, in case of Cr(VI)-loaded formaldehyde-treated rice husk, there is a remarkable shift in positions and shapes of OH and C=O group peaks indicating Cr(VI) binding mostly with OH and CO groups. Similarly, the bending modes of aromatics have also shifted, which is indicative of association with the aromatic ring. The possible adsorption on these adsorbents may be due to physical adsorption, complexation with functional groups, ionic exchange, surface precipitations, and chemical reaction with surface sites. The changes in FTIR spectra confirm the complexation of Cr(VI) with functional groups present in the adsorbents (Bansal 2009).

6.10 Studies on Elution or Recovery of Sorbate (Metal Ions)

Regeneration and recovery of the column and recovery of the metal is an important aspect of the wastewater treatment process and, therefore, desorption of lead and chromium was tried with a number of eluents (Gupta and Ali 2004). Desorption studies were carried out by batch and column operation under similar conditions. It was observed that the column can be used for at least 10 runs without any problem. After the removal of metal ions from waters, bound metal ions were recovered by treatment with HCl or HNO_3 . Regeneration, though technically feasible, there is no need to regenerate the adsorbent, rice husk (Ajmal et al. 2002). Akhtar et al. (2009) carried out desorption via 0.1 M aqueous solutions of HCl, H_2SO_4 , HNO_3 , KCl, Na_2CO_3 , and NaHCO_3 for the recovery of sorbed amount of sorbates from the sorbent surface and the best performance was achieved with 0.1 M HCl. In the desorption study on fused pyrolyzed coffee and clay as adsorbent, desorption was easily

achieved by leaching with distilled water, which gave the recovery yield of 88% to 92% (Boonamnuyvitaya et al. 2004).

Kalderis et al. (2008) found that HCl 0.1 N was more efficient in removing Zn from the activated carbon than distilled water. Results showed that Zn recovery from bagasse activated carbon was 15.8% when distilled water was used, and 33.8% when HCl acid was used. The removal for rice husk activated carbon was 6.5% and 30.2% for water and HCl as eluents, respectively. The result indicates that a substantial amount of Zn is irreversibly bound within the activated carbon structure. It was found that recovery of Cd(II) from synthetic wastewater by column operation was better than a batch process. The desorption of Cd(II) started when a solution of 0.1 M HCl was passed through the column. The desorption was fast and 83.9% Cd(II) could be eluted in 50 ml of effluent from the column. However, the desorption of Cd(II) by batch process was slow and incomplete. The desorption of Cd(II) from wastewater containing 20 mg l⁻¹ Cd(II) by batch process was 53.9% (Ajmal et al. 2002). The adsorbed Cd²⁺ can be eluted with the help of 0.5 M HCl. The recovery of the metal was to the extent of 98% in the first cycle and is reduced to 90% in the third cycle. The decrease in recovery may be attributed to the fact that some of the metal ions may be held to the adsorbent by stronger interactions and which resulted in the reduction of removal efficiency (Sharma et al. 2008).

6.11 Conclusion

Biosorption of heavy metals by agriwastes is currently attracting significant attention due to availability, low cost, and the potential for chemical and thermal modification to achieve enhanced metal sorption. The most abundant and effective low-cost sorbents studies on the sorption of metals by rice husk are reviewed in this particular chapter. Sorption capacity of rice husk along with other agriwastes were studied by several workers in raw unmodified, or chemically and thermally modified form. Mechanism of sorption, sorption kinetics, and thermodynamics and equilibrium characteristics were also investigated. Several studies have been conducted on the impacts of different operational parameters like pH, contact time, metal dose, sorbent dose, temperature, particle size, co-ion effect, and agitation speed on sorption capacity. Optimum working conditions have also been recommended. A limited number of studies were also conducted on sorbent recovery, column (fixed) tests, and tests based on rice husk mixed with other sorbents like clay. The analysis and assessment of research published on biosorption of heavy metals shows that future research on rice husk and other agricultural waste-based sorbents should be directed toward

- Studying impact of chemical modification in the presence of two or more modifiers or chemical and thermal modification
- Impact of concentration of chemical modifiers
- Using column experiment for design of industrial scale systems based on continuous through columns refers to packed bed of the adsorbent column for continuous operation
- Mechanism of sorption, as it is not deeply understood
- Both experimental and model-based study of sorption equilibrium, thermodynamics, kinetics, and mass transfer of the process

- Sorbent recovery and optimization
- Mixture of sorbents
- Research on co-ion (ion interference effect) since actual wastewater involves multi-ion environment where interference between ions significantly influences the efficiency of the biosorption process and tests should also be conducted on actual industrial effluents laden with heavy metals and other ions instead of artificial or synthetic samples prepared in the lab

References

- Abdel-Ghani, N. T., M. Hefny, G. A. F. El-Chaghaby. 2007. "Removal of lead from aqueous solution using low-cost abundantly available adsorbents." *Int. J. Environ. Sci. Tech.* 4 (1):67–73.
- Ahmedna, M., W. E. Marshall, A. A. Hussein, R. M. Rao and, and I. Goktepe. 2004. "The use of nutshell carbons in drinking water filters for removal of trace metals." *Water Res.* 38:1062–1068.
- Ajmal, M., R. A. K. Rao, S. Anwar, J. Ahmad, and R. Ahmad. 2002. "Adsorption studies on rice husk: Removal and recovery of Cd(II) from wastewater." *Bioresour. Technol.* 86 (2):147–149.
- Akhtar, M., S. Iqbal, M. I. Bhangar, M. Zia-Ul-Haq, and M. Moazzam. 2009. "Sorption of organophosphorous pesticides onto chickpea husk from aqueous solutions." *Colloids Surf. B: Biointerf.* 69 (1):63–70.
- Akhtar, M., S. Iqbal, A. Kausar, M. I. Bhangar, and M. A. Shaheen. 2010. "An economically viable method for the removal of selected divalent metal ions from aqueous solutions using activated rice husk." *Colloids Surf. B: Biointerf.* 75 (1):149–155.
- Amer, H. A. T. 2015. "Removal of lead from industrial wastewater using a low cost waste material." Master's thesis, American University in Cairo, Egypt.
- Baes, C. F., and R. E. Mesmer. 1976. *The Hydrolysis of Cations*. New York: Wiley.
- Baig, T. H., A. E. Garcia, K. J. Tiemann, and T. J. L. Gardea. 1999. "Adsorption of heavy metal ions by the biomass of *Solanum elaeagnifolium* (Silverleaf nightshade)." Paper presented at Proceedings of the 10th Annual EPA Conference on Hazardous Waste Research, Washington, DC.
- Bailey, T. J. Olin, R. M. Bricka, and D. D. Adrian. 1999. "A review of potentially low-cost sorbents for heavy metals." *Water Res.* 33:2469–2479.
- Bajpai, D. N., and G. McDonald. 2008. "Binding of heavy metal ions by formaldehyde polymerised peanut skins by a single-stage chemical activation method at low retention times." *Bioresour. Technol.* 99:6809–6816.
- Banerjee, S., and M. C. Chattopadhyaya. 2013. "Adsorption characteristics for the removal of a toxic dye, tartrazine from aqueous solutions by a low cost agricultural by-product." *Arabian J. Chem.* doi: <http://dx.doi.org/10.1016/j.arabjc.2013.06.005>.
- Bansal, M. 2009. "Removal of Cr(VI) from aqueous solutions using pre-consumer processing agricultural waste: A case study of rice husk." *J. Hazard. Mater.* 162:312–320.
- Bhattacharya, A. K., S. N. Mandal, and S. K. Das. 2006. "Adsorption of Zn(II) from aqueous solutions by using different adsorbents." *Chem. Eng. J.* 123:43–51.
- Bhattacharya, A. K., T. K. Naiya, S. N. Mondal, and S. K. Das. 2008. "Adsorption, kinetics and equilibrium studies on removal of Cr(VI) from aqueous solutions using different low-cost adsorbents." *Chem. Eng. J.* 137:529–541.
- Boonamnuyvitaya, V., C. Chaiya, W. Tanthapanichakoon, and S. Jarudilokkul. 2004. "Removal of heavy metals by adsorbent prepared from pyrolyzed coffee residues and clay." *Separat. Purificat. Technol.* 35 (1):11–22.
- Chand, R., T. Watari, K. Inoue, H. Kawakita, H. N. Luitel, D. Parajuli, T. Torikai, and M. Yada. 2009. "Selective adsorption of precious metals from hydrochloric acid solutions using porous carbon prepared from barley straw and rice husk." *Miner. Engin.* 22 (15):1277–1282.

- Chen, X., K. F. Lam, S. F. Mak, and K. L. Yeung. 2011. "Precious metal recovery by selective adsorption using biosorbents." *J. Hazard. Mater.* 186 (1):902–910.
- Chuah, T. G., A. Jumariah, I. Azni, S. Katayon, and S. Y. T. Choong. 2005. "Rice husk as a potentially low-cost biosorbent for heavy metal and dye removal: An overview." *Desalination* 175 (3):305–316.
- Dada, A. O., A. P. Olalekan, A. M. Olatunya, and O. Dada. 2012. "Langmuir, Freundlich, Temkin and Dubinin–Radushkevich isotherms studies of equilibrium sorption of Zn²⁺ onto phosphoric acid modified rice husk." *IOSR J. Applied Chem.* 3 (1):38–45.
- Dakiky, M., M. Khamis, A. Manassra, and M. Mer'eb. 2002. "Selective adsorption of chromium(VI) in industrial wastewater using low-cost abundantly available adsorbents." *Adv. Environ. Res.* 6 (4):533–540. doi: [http://dx.doi.org/10.1016/S1093-0191\(01\)00079-X](http://dx.doi.org/10.1016/S1093-0191(01)00079-X).
- Das, N. 2010. "Recovery of precious metals through biosorption—A review." *Hydrometallurgy* 103 (1):180–189.
- Davis, T. A., B. Volesky, and A. Mucci. 2003. "A review of the biochemistry of heavy metal biosorption by brown algae." *Water Res.* 37:4311–4330.
- Dhanik, J., and S. Kumar. 2016. "Low cost cuscutea based adsorbent for removal of iron from its aqueous solution." *Asian J. Chem.* 28 (9):2077.
- Dubinin, M. 1947. "Equation of the characteristic curve of activated charcoal." *Proc. Acad. Sci. Phys. Chem. Sec.* 331–333:875–890.
- El-Shafey, E. I. 2007. "Sorption of Cd(II) and Se(IV) from aqueous solution using modified rice husk." *J. Hazard. Mater.* 147 (1–2):546–555.
- El-Shafey, E.-S. I., H. A. J. Al-Lawati, S. Al-Busafi, and B. Al-Shiraiqi. 2016. "Removal of Zn²⁺ and SO₄²⁻ from aqueous solutions on acidic and chelating dehydrated carbon." *Environ. Sci. Pollut. Res.* 24 (2):11066–11077.
- Elhafez, S. E. A., H. A. Hamad, A. A. Zaatout, and G. F. Malash. 2016. "Management of agricultural waste for removal of heavy metals from aqueous solution: Adsorption behaviors, adsorption mechanisms, environmental protection, and techno-economic analysis." *Environ. Sci. Pollut. Res.* 24 (2):1397–1415.
- Gerente, C., Z. Reddad, Y. Abdres, and P. Le Cloirec. 2004. "Competitive adsorption of metals and organics onto a low cost natural polysaccharide." *Environ. Technol.* 25:219–225.
- Girgis, B. S., S. S. Yunis, and A. M. Soliman. 2002. "Adsorption of polluting substances on activated carbons prepared from rice husk and sugarcane bagasse." *Mater. Lett.* 57:164.
- Guo, B., and G. Liu. 2011. *Applied Drilling Circulation Systems: Hydraulics, Calculations, and Models*. Burlington, MA: Gulf Professional.
- Guo, Y., K. Yu, Z. Wang, and H. Xu. 2003. "Effects of activation conditions on preparation of porous carbon from rice husk." *Carbon* 41 (8):1645–1648.
- Gupta, V. K., and I. Ali. 2004. "Removal of lead and chromium from wastewater using bagasse fly ash—A sugar industry waste." *J. Colloid Interface Sci.* 271:321–328.
- Gupta, V. K., A. Nayak, B. Bhushan, and S. Agarwal. 2015. "A critical analysis on the efficiency of activated carbons from low-cost precursors for heavy metals remediation." *Crit. Rev. Environ. Sci. Technol.* 45 (6):613–668.
- Halbus, A. F., J. M. Salman, A. J. Lafta, Z. H. Athab, F. M. Hasan, A. M. Kamil, and F. H. Hussein. 2017. "Equilibrium, isotherms and thermodynamic studies of congo red adsorption onto *Ceratophyllum Demersum*." *Indian J Chem Tech* 24:82–87.
- Hashem, A., E. S. Abdel-Halim, K. F. El-Tahlawy, and A. Hebeish. 2005. "Enhancement of adsorption of Co(II) and Ni(II) ions onto peanut hulls through esterification using citric acid." *Adsorp. Sci. Technol.* 23:367–380.
- Hegazi, H. A. 2013. "Removal of heavy metals from wastewater using agricultural and industrial wastes as adsorbents." *HBRC J* 9 (3):276–282.
- Ho, Y. S. 2003. "Removal of copper ions from aqueous solution by tree fern." *Water Res.* 37:2323–2330.
- Ho, Y. S., and G. McKay. 1999. "Pseudo-second order model for sorption processes." *Process Biochem.* 34 (5):451–465. doi: [http://dx.doi.org/10.1016/S0032-9592\(98\)00112-5](http://dx.doi.org/10.1016/S0032-9592(98)00112-5).

- Huang, C. P., and M. H. Wu. 1977. "The removal of chromium(VI) from dilute aqueous solution by activated carbon." *Water Res.* 11:673–679.
- Jain, C. K., D. S. Malik, and A. K. Yadav. 2016. "Applicability of plant based biosorbents in the removal of heavy metals: A review." *Environ. Process.* 3 (2):495–523.
- Jaman, H., D. Chakraborty, and P. Saha. 2009. "A study of the thermodynamics and kinetics of copper adsorption using chemically modified rice husk." *CLEAN: Soil, Air, Water* 37 (9):704–711.
- Juang, R. S., and R. C. Shiau. 2000. "Metal removal from aqueous solutions using chitosan enhanced membrane filtration." *J. Membr. Sci.* 165:159–167.
- Junior, O. K., L. V. A. Gurgel, J. C. P. de Melo, V. R. Botaro, T. M. S. Melo, R. P. de Freitas Gil, and L. F. Gil. 2006. "Adsorption of heavy metal ion from aqueous single metal solution by chemically modified sugarcane bagasse." *Bioresour. Technol.* 98:1291–1297.
- Kadirvelu, K., and C. Namasivayam. 2003. "Activated carbon from coconut coir pitch as metal adsorbent: Adsorption of Cd(II) from aqueous solution." *Adv. Environ. Res.* 7:471–478.
- Kalderis, D., S. Bethanis, P. Paraskeva, and E. Diamadopoulos. 2008. "Production of activated carbon from bagasse and rice husk by single stage chemical activation method at low retention times." *Bioresour. Technol.* 99:6809–6816.
- Kaman, S. P. D., I. A. W. Tan, and L. L. P. Lim. 2017. "Palm oil mill effluent treatment using coconut shell-based activated carbon: Adsorption equilibrium and isotherm." Paper presented at MATEC Web of Conferences.
- Kapoor, A., and T. Viraraghavan. 1995. "Fungi biosorption—An alternative treatment option for heavy metal bearing wastewaters: A review." *Bioresour. Technol.* 53:195–206.
- Kennedy, L. J., J. J. Vijaya, and G. Sekaran. 2004. "Effect of two-stage process on the preparation and characterization of porous carbon composite from rice husk by phosphoric acid activation." *Indust. Engin. Chem. Res.* 43 (8):1832–1838.
- Khabibi, J., W. Syafii, and R. K. Sari. 2016. "Reducing hazardous heavy metal ions using mangium bark waste." *Environ. Sci. Pollut. Res.* 23 (16):16631–16640. doi: 10.1007/s11356-016-6776-0.
- Kratochvil, D., and B. Volesky. 1998. "Advances in the biosorption of heavy metals." *Trends Biotechnol.* 16 (7):291–300.
- Krishnan, K. A., and T. S. Anirudhan. 2003. "Removal of cadmium(II) from aqueous solutions by steam activated sulphurised carbon prepared from sugar-cane bagasse pith: Kinetics and equilibrium studies." *Water SA* 29 (2):147–156.
- Krishnani, K. K., X. Meng, C. Christodoulatos, and V. M. Boddu. 2008. "Biosorption mechanism of nine different heavy metals onto biomatrix from rice husk." *J. Hazard. Mater.* 153:1222–1234.
- Krishnarao, R. V., J. Subrahmanyam, and T. J. Kumar. 2001. "Studies on the formation of black particles in rice husk silica ash." *J. Eur. Ceramic Soc.* 21 (1):99–104.
- Kumar, U., and M. Bandyopadhyay. 2006a. "Fixed bed column study for Cd(II) removal from wastewater using treated rice husk." *J. Hazard. Mater.* 129 (1–3):253–259.
- Kumar, U., and M. Bandyopadhyay. 2006b. "Sorption of cadmium from aqueous solution using pre-treated rice husk." *Bioresour. Technol.* 97:104–109.
- Lalwani, S. B., T. Wiltowski, A. Hubner, A. Weston, and N. Mandich. 1998. "Removal of hexavalent chromium and metal cations by a selective and novel carbon adsorbent." *Carbon* 36:1219–1226.
- Lata, S., and S. R. Samadder. 2014. "Removal of heavy metals using rice husk: A review." *Int. J. Environ. Res. Develop.* 4 (2):165.
- Leppert, D. 1990. "Heavy metal sorption with clinoptilolite zeolite: Alternatives for treating contaminated soil and water." *Mining Eng.* 42:604–608.
- Low, K. S., C. K. Lee, and S. C. Lie. 2000. "Sorption of cadmium and lead from aqueous solution by spent grain." *Process Biochem.* 36:59–64.
- Lozano-Castello, D., M. A. Lillo-Rodenas, D. Cazorla-Amorós, and A. Linares-Sola. 2001. "Preparation of activated carbons from Spanish anthracite: I. Activation by KOH." *Carbon* 39 (5):741–749.
- Lu, D., Q. Cao, X. Li, X. Cao, F. Luo, and W. Shao. 2009. "Kinetics and equilibrium of Cu(II) adsorption onto chemically modified orange peel cellulose biosorbents." *Hydrometallurgy* 95 (1–2):145–152. doi: <http://dx.doi.org/10.1016/j.hydromet.2008.05.008>.

- Mahvi, A. H., A. Maleki, and A. Eslami. 2004. "Potential of rice husk and rice husk ash for phenol removal in aqueous systems." *Am. J. Appl. Sci.* 1:321–326.
- Malik, A. 2004. "Metal bioremediation through growing cells." *Environ. Int.* 30:261–278.
- Marchetti, V., A. Clément, P. Gérardin, and B. Loubinoux. 2000. "Synthesis and use of esterified sawdusts bearing carboxyl group for removal of cadmium(II) from water." *Wood Sci. Technol.* 34 (2):167–173. doi: 10.1007/s002260000040.
- Masoumi, A., K. Hemmati, and M. Ghaemy. 2016. "Low-cost nanoparticles sorbent from modified rice husk and a copolymer for efficient removal of Pb(II) and crystal violet from water." *Chemosphere* 146:253–262. doi: <http://dx.doi.org/10.1016/j.chemosphere.2015.12.017>.
- McKay, G., M. S. Otterburn, and A. G. Sweeny. 1981. "Surface mass transfer process during colour removal from effluents using silica." *Water Res.* 15:321–331.
- Mohan, D., and C. U. Pittman Jr. 2006. "Activated carbons and low cost adsorbents for remediation of tri- and hexavalent chromium from water." *J. Hazard. Mater.* 137 (2):762–781.
- Mohan, S., and G. Sreelakshmia. 2008. "Fixed bed column study for heavy metal removal using phosphate treated rice husk." *J. Hazard. Mater.* 153 (1–2):75–82.
- Munaf, E., and R. Zein. 1997. "The use of rice husk for removal of toxic metals from waste water." *Environ. Technol.* 18:359–362.
- Nadeem, M., A. Mahmood, S. A. Shahid, S. S. Shah, A. M. Khalid, and G. McKay. 2006. "Sorption of lead from aqueous solution by chemically modified carbon adsorbents." *J. Hazard. Mater.* 138 (3):604–613. doi: <http://dx.doi.org/10.1016/j.jhazmat.2006.05.098>.
- Naiya, T. K. 2009. "Saw dust and neem bark as low-cost natural biosorbent for adsorptive removal of Zn(II) and Cd(II) ions from aqueous solutions." *Chem. Engin. J.* 148:68–79.
- Naiya, T. K., A. K. Bhattacharya, S. Mandal, and S. K. Das. 2008. "The sorption of lead(II) ions on rice husk ash."
- Namasivayam, C., and M. V. Sureshkumar. 2008. "Removal of chromium(VI) from water and wastewater using surfactant modified coconut coir pith as a biosorbent." *Bioresour. Technol.* 99:2218–2225.
- Ngah, W. S. W., and M. A. K. M. Hanafiah. 2007. "Removal of heavy metal ions from wastewater by chemically modified plant wastes as adsorbents: A review." *Bioresour. Technol.* 99 (10):3935–3948.
- Ouki, S. K., and M. Kavannagh. 1997. "Performance of natural zeolites for the treatment of mixed metal-contaminated effluents." *Waste Manage. Res.* 15:383–394.
- Özacar, M., I. A. Sengil, and H. Turkmenler. 2008. "Equilibrium and kinetic data, and adsorption mechanism for adsorption of lead onto valonia tannin resin." *Chem. Eng. J.* 143:32–42.
- Pokhrel, D., and T. Viraraghavan. 2007. "Arsenic removal from an aqueous solution by modified A. niger biomass: Batch kinetic and isotherm studies." *J. Hazard. Mater.* 150:818–825.
- Qaiser, S., A. R. Saleemi, and M. Umar. 2009. "Biosorption of lead from aqueous solution by *Ficus religiosa* leaves: Batch and column study." *J. Hazard. Mater.* 166 (2):998–1005.
- Rahman, I. A., and J. Ismail. 1993. "Preparation and characterization of a spherical gel from a low cost material." *J. Mater. Chem.* 3 (9):931–934.
- Rahman, I. A., J. Ismail, and H. Osman. 1997. "Effect of nitric acid digestion on organic materials and silica in rice husk." *J. Mater. Chem.* 7 (8):1505–1509.
- Raji, C., and T. S. Anirudhan. 1996. "Preparation and metal adsorption properties of the polyacrylamide grafted saw dust having carboxylate functional group." *Indian J. Chem. Technol.* 3:345–350.
- Raju, K. S., and S. V. Naidu. 2013. "A review on removal of heavy metal ions from wastewater by rice husk as an adsorbent." *J. Chem. Bio. Phys. Sci.* 3 (2):602.
- Ranjan, D., M. Talat, and S. H. Hasan. 2009. "Biosorption of arsenic from aqueous solution using agricultural residue 'rice polish.'" *J. Hazard. Mater.* 166:1050–1059.
- Reichenberg, D., and D. J. McCauley. 1955. "Properties of ion-exchange resins in relation to their structure. Part VII. Cation-exchange equilibria on sulphonated polystyrene resins of varying degrees of cross-linking." *J. Chem. Soc.*:2741–2749.
- Saliba, R., H. Gauthier, and R. Gauthier. 2005. "Adsorption of heavy metal ions on virgin and chemically-modified lignocellulosic materials." *Adsorption Sci. Technol.* 23 (4):313–322.

- Saravanane, R., T. Sundararajan, and S. S. Reddy. 2001. "Chemically modified low cost treatment for heavy metal effluent management." *Environ. Manage. Health* 12 (2):215–224.
- Schneider, I. A. H., and J. Rubio. 1999. "Sorption of heavy metal ions by the nonliving biomass of freshwater macrophytes." *Environ. Sci. Technol.* 33 (13):2213–2217.
- Sengil, I. A., and M. Özacar. 2008. "Biosorption of Cu(II) from aqueous solutions by mimosa tannin gel." *J. Hazard. Mater.* 157:277–285.
- Sengil, I. A., and M. Özacar. 2009. "Competitive biosorption of Pb²⁺, Cu²⁺ and Zn²⁺ ions from aqueous solutions onto valonia tannin resin." *J. Hazard. Mater.* 166 (2–3):1488–1494. doi: 10.1016/j.jhazmat.2008.12.071.
- Shamohammadi, H. Z., H. Moazed, H. N. E. Jaafarzadeh, and J. P. Haghighat. 2008. "Removal of low concentrations of cadmium from water using improved rice husk."
- Sharma, N., K. Kaur, and S. Kaur. 2008. "Kinetic and equilibrium studies on the removal of Cd²⁺ ions from water using polyacrylamide grafted rice (*Oryza sativa*) husk and (*Tectona grandis*) saw dust." *J. Hazard. Mater.* 163 (1–2):1338–1344.
- Sharma, R., and B. Singh. 2013. "Removal of Ni(II) ions from aqueous solutions using modified rice straw in a fixed bed column." *Bioresour. Technol.* 146:519–524.
- Sobhanardakani, S., H. Parvizimosaed, and E. Olyaie. 2013. "Heavy metals removal from wastewaters using organic solid waste—Rice husk." *Environ. Sci. Pollut. Res.* 20 (8):5265–5271.
- Soon-An, O., S. Chye-Eng, and L. Poh-Eng. 2007. "Kinetics of adsorption of Cu(II) and Cd(II) from aqueous solution on rice husk and modified rice husk." *Electron. J. Environ. Agri. Food Chem.* 6 (2):764–1774.
- Srivastava, P., B. Singh, and M. J. Angove. 2004. "Competitive adsorption of cadmium(II) onto kaolinite as affected by pH." Paper presented at Australian New Zealand Soils Conference, December 5–9.
- Stuart, B. H. 2004. *Infrared Spectroscopy: Fundamentals and Applications*. Chichester, UK: Wiley.
- Sud, D., G. Mahajan, and M. P. Kaur. 2008. "Agricultural waste material as potential adsorbent for sequestering heavy metal ions from aqueous solutions: A review." *Bioresour. Technol.* 99 (14):6017–6027.
- Sumathi, K. M. S., S. Mahimairaja, and R. Naidu. 2005. "Use of low-cost biological wastes and vermiculite for removal of chromium from tannery effluent." *Bioresour. Technol.* 96:309–316.
- Swami, D. N., and S. K. Gupta. 2016. "Adsorption kinetics for the removal of chromium(VI) from synthetic waste water using adsorbent derived from saw dust, bark and rice husk." In *Recent Advances in Chemical Engineering*, I. Regupathi, K. V., Shetty, and M. Thanabalan (eds.), 153–163. Singapore: Springer.
- Tarley, T., C. Ricardo, Z. Arruda, and M. Aurélio. 2004. "Biosorption of heavy metals using rice milling by-products. Characterisation and application for removal of metals from aqueous effluents." *Chemosphere* 54 (7):987–995.
- Ting, Y. P., F. Lawson, and I. G. Prince. 1989. "Uptake of cadmium and zinc by the alga *Chlorella vulgaris*: II. Multi-ion situation." *Biotechnol. Bioeng.* 34:990.
- Tsezos, M. 2001. "Biosorption of metals. The experience accumulated and outlook for technology development." *Hydrometallurgy* 59:241–243.
- Veglio, F., and F. Beolchini. 1997. "Removal of metals by biosorption: A review." *Hydrometallurgy* 44:301–316.
- Volesky, B. 1990. "Biosorption by fungal biomass." In *Biosorption of Heavy Metals*, 139–172. Boca Raton, FL: CRC.
- Volesky, B. 2007. "Biosorption and me." *Water Res.* 41 (18):4017–4029.
- Volesky, B., and Z. R. Holan. 1995. "Biosorption of heavy metals." *Biotechnol. Prog.* 11:235.
- Wang, X.-S., and Y. Qin. 2005. "Equilibrium sorption isotherms of CU(II) on rice bran." *Process Biochem.* 40:677–680.
- Weber, W. J., and J. C. Morris. 1963. "Kinetics of adsorption carbon from solutions." *Am. Soc. Civ. Eng.* 89:31–60.
- Wong, K. K., C. K. Lee, K. S. Low, and M. J. Haron. 2003. "Removal of Cu and Pb from electroplating wastewater using tartaric acid modified rice husk." *Process Biochem.* 39:437–445.

- Xie, J. Z., H.-L. Chang, and J. J. Kilbane. 1996. "Removal and recovery of metal ions from wastewater using biosorbents and chemically modified biosorbents." *Bioresour. Technol.* 57 (2):127–136.
- Xu, X., X. Cao, and L. Zhao. 2013. "Comparison of rice husk-and dairy manure-derived biochars for simultaneously removing heavy metals from aqueous solutions: Role of mineral components in biochars." *Chemosphere* 92 (8):955–961.
- Yang, G. C. C., and S. Lin. 1998. "Removal of lead from a silt loam soil by electrokinetic remediation." *J. Hazard. Mater.* 58:285–299.
- Zouboulis, A., K. N. Lazaridis, and K. A. Matis. 2002. "Removal of toxic metal ions from aqueous systems by biosorptive flotation." *J. Chem. Technol. Biotechnol.* 77:958–964.

Utilization of Red Mud for Environmental Applications

Manoj Kumar Sahu and Raj Kishore Patel

CONTENTS

7.1	Introduction	135
7.2	Utilization of Red Mud for Wastewater Treatment.....	136
7.2.1	Utilization of Red Mud for the Removal of Anions from Water and Wastewater	136
7.2.2	Utilization of Red Mud for the Removal of Heavy Metal Ions from Aqueous Solution	140
7.2.3	Utilization of Red Mud for the Removal of Dyes from Aqueous Solution ...	145
7.2.4	Utilization of Red Mud for the Removal of Organic Pollutants from Aqueous Solution	149
7.2.5	Utilization of Red Mud to Purify Toxic Waste Gases	152
7.2.6	Utilization of Red Mud for Preparation of Catalyst.....	153
7.3	Conclusion	155
	References.....	155

7.1 Introduction

Red mud is an industrial waste material generated as a by-product during the processing of bauxite for the production of alumina by the Bayer process. It is generated when bauxite ores are subjected to caustic leaching at a temperature between 106°C and 230°C and under pressure of 1 to 6 atm for the extraction of alumina (Kurniawan et al. 2006; Newson et al. 2006). After separation of alumina, red mud is released as slurry that is highly alkaline having a pH > 12, due to the presence of residual caustic soda (Genc-Fuhrman et al. 2004a; Fois et al. 2007). The composition of the red mud is a mixture of solid metallic and nonmetallic oxide. The red color of red mud is due to the presence of oxidized iron. Approximately 60% of the mass of red mud is due to the presence of oxidized iron (Chandra et al. 1996; Schmitz et al. 2006). Red mud consists mostly of the mixtures of hematite, goethite, quartz, gibbsite, boehmite, anatase, calcite, and desilication product. Annual production of smelter grade and chemical grade alumina in 2015 was around 115 million tons. The global average generation of red mud is between 1 and 1.5 tons per ton of alumina extraction. Hence, it is estimated that around 150 million tons of bauxite residue is produced annually. A huge amount of red mud is released globally to the environment (Piga et al. 1993; Prasad et al. 1985; Wagh and Desai 1987). Red mud is a serious problem to the environment because of its chemical composition and the amount generated every year. Voluminous research and development work is being carried out all over the world for the storage, disposal,

and utilization of red mud. Red mud is disposed as slurry or dry or semidry material in red mud ponds or abandoned bauxite mines. Slurry has a high ionic strength and a solid concentration of 30% to 60%. The environmental concerns relate to two major aspects: the very large quantity of red mud generated and its causticity. Problems associated with the disposal of red mud waste include its high pH, safety in storage, alkali seepage into underground water, alkaline airborne dust emissions, and the vast area of land required for disposal.

Although red mud appears to be consolidated, it has a muddy consistency with colloidal nature because of the fineness of the material and presence of caustic soda. Many efforts are being made globally to find suitable uses for red mud so that the alumina industry may end up with no residue at all. Neutralization is required to convert the highly caustic state of red mud to a state that is no longer caustic and is less hazardous. Neutralization of red mud will help to reduce the environmental impact caused by the adverse storage behavior of the residue and also significantly lower the effort needed during ongoing management of the red mud. It will also open new opportunities for utilization of the residue, which to date have been prevented because of the high pH. After neutralization, red mud can be used as a low-cost environment-friendly adsorbent for removal of hazardous inorganic metal ions and organic pollutants from water, besides other uses. As a consequence of the variation in the composition and different pretreatment process, reported adsorption capacities for heavy metals on red mud have a wide variation. Different utilization of red mud has been reported to minimize the environmental impact of red mud. Some of the methods reported are removal of toxic inorganic and organic species like fluoride (Tor et al. 2009a), Cr(VI) (Costa et al. 2010), arsenic (Genc-Fuhrman et al. 2004b, 2004c, 2005), cadmium (Zhu et al. 2007), lead (Apak et al. 1998), vanadate and molybdate (Palmer et al. 2010), copper (Nadaroglu et al. 2010), phosphate (Yue et al. 2010; Zhao et al. 2009), nickel (Smiljanić et al. 2010), organic dyes (Namasivayam and Arasi 1997), pollutants, and gas from water and wastewater.

In recent years, using red mud as an adsorbent for wastewater treatment as well as development of catalysts for purification of gas and liquid cleaning have also been reported. Utilization of one industrial waste for the treatment of another waste imparts many benefits in terms of the economy and environment. In this chapter, the different utilizations of red mud are reviewed and summarized, including the development of low-cost adsorbents from red mud for the adsorption of toxic gas, wastewater treatment, and catalyst for the treatment of solid waste and gas. A summary of relevant published data in terms of adsorption capacities of red mud-based adsorbents for the removal of various pollutants with some of the latest important findings and a source of up-to-date literature are presented with discussion of the results.

7.2 Utilization of Red Mud for Wastewater Treatment

7.2.1 Utilization of Red Mud for the Removal of Anions from Water and Wastewater

Contamination of groundwater and surface water by anions coming out from nonpoint sources has become a growing environmental problem for both developed and developing countries. The increase of anion concentration in water occurs due to the widespread use of fertilizers containing nitrate and phosphate, and owing to poorly treated or untreated

human and animal wastes. Nitrate is a by-product of many industrial processes, including paper, explosives manufacturing, and the production of nitro-organic and pharmaceutical compounds. The increasing anion concentration in the groundwater causes a serious health risk.

Magnetic nanoparticles were synthesized from red mud and performed the removal of pentavalent arsenic (As(V)) from underground water (Akin et al. 2012). The synthesized Fe_3O_4 -NPs were sphere-shaped with an average particle size of 9 nm. The maximum removal of As(V) was obtained at pH 2.5 of the solution. The sorption of As(V) can be attributed to interaction between the positive charge of Fe_3O_4 -NPs surface and H_2AsO_4^- . The maximum adsorption capacities was 15.30 $\mu\text{g/L}$ (removal: 99.2%) at 25°C. The Freundlich isotherm was fitted to the experimental data and followed second-order-type reaction kinetics. The results showed that synthesized Fe_3O_4 -NPs from red mud have satisfactory magnetic properties and As(V) sorption capacity, especially at low equilibrium arsenate concentrations. Activated CO_2 -neutralized red mud (ANRM) was synthesized and used for the removal of arsenate from the aqueous solutions in a laboratory scale (Sahu et al. 2010). The percentage removal of arsenate increased gradually with a decrease in pH, and maximum removal were found to be 55.55 mg/g at pH ~4. Arsenic removal from aqueous solution on seawater-neutralized red mud (Bauxsol) have been investigated (Genç et al. 2003). The adsorption capability of Bauxsol for arsenate was in the range of 6.08 to 14.43 $\mu\text{mol/g}$ with a wide range of pH 6.3 to 10.0. The adsorption of arsenate on Bauxsol may be due to the inner-sphere complex reported in the literature. In another work, Genc-Fuhrman et al. (2005) investigated the removal of arsenic from water by using a number of different sorbents, namely, seawater-neutralized red mud (Bauxsol), acid-treated Bauxsol (ATB), activated Bauxsol (AB), Bauxsol-coated sand (BCS), and activated Bauxsol-coated sand (ABCS). The adsorption of arsenic on the developed sorbents decreases in the order $\text{AB} > \text{ATB} > \text{ABCS} > \text{BCS} > \text{Bauxsol}$. The authors reported that the adsorption of arsenate on seawater-neutralized red mud was favorable at a slightly alkaline pH of 8.5. Modified Bauxsol and activated Bauxsol both were mixed with sand and prepared BCS and ABCS grains, respectively, and the adsorption of arsenate from water by both batch and column experiment were studied (Genc-Fuhrman et al. 2005). The maximum adsorption capacities of arsenate for ABCS and BCS were 2.14 mg/g and 1.64 mg/g at pH 7.1 respectively.

The removal of fluoride ions (F^-), and pentavalent and trivalent arsenic (As(V) and As(III)) from aqueous solution using activated red mud (ARM) was investigated (Guo et al. 2014b). The red mud was activated by calcination in a muffle furnace at 800°C for 3 h, and then pretreated by 1.0 mol/L HCl with a liquid-to-solid ratio of 20 mL/g for 24 h at room temperature. The maximum adsorption capacities for F^- , As(V), and As(III) was found to be 3.96, 5.16, and 1.47 mg/g, respectively, at pH 7 and 25°C. The pseudo-second-order kinetic model better described the adsorption of F^- , As(V), and As(III) on ARM. The Langmuir isotherm described well the F^- adsorption in the absence or presence of As(III)/As(V). Modified red mud (RM) has been developed by mixing red mud with FeCl_3 and used for the removal of arsenate from water (Zhang et al. 2008). The adsorption capability of modified red mud was reported to be 68.5 mg/g, 50.6 mg/g, and 23.2 mg/g at pH 6, 7, and 9, respectively. The NO_3^- ion had little effect on the adsorption, whereas Ca^{2+} enhanced the adsorption and HCO_3^- decreased the adsorption.

Granular acid-activated neutralized red mud (AaN-RM) was prepared by mixing with powdered AaN-RM, powdered straw, and hydroxypropyl methylcellulose (HPMC) for adsorption of phosphate (Ye et al. 2015a). The maximum adsorption capacity for phosphate on granular AaN-RM was found to be 86.69 mg/g. Ye et al. (2015a) reported that the high phosphate adsorption capacity of granular AaN-RM was mainly attributed to a

high specific surface area caused by complex mineralogy of iron and aluminum, and the addition of powdered straw, but they found that when the mass ratio of powdered straw increased from 0% to 33%, the total pore volume of granular AaN-RM increased from 0.0056 to 0.0375 cm³/g. The optimal mass ratio of powdered AaN-RM, powdered straw, and HPMC was chosen as 71:22:7 with sintering temperature and time were 225°C and 30 min, respectively, for the better adsorption of phosphate. In another work, Ye et al. (2015b) prepared powdered-acid-activated-neutralized red mud (Aan-RM) by employing the activated red mud with hydroxypropyl methylcellulose and powdered straw, and used for the adsorption of phosphate. They reported that the maximum phosphate adsorption capacity of granular Aan-RM reached 153.227 mg/g with the optimal granular Aan-RM dosage of 3.0 g/L, adsorption temperature of 40°C, and initial solution pH of 6.0. The kinetics and isotherm studies showed that the phosphate adsorption process was well described by the Ritchie *n*th-order kinetic model and Langmuir–Freundlich isotherm, which demonstrated that the phosphate adsorption onto granular Aan-RM could be governed by multiple mechanisms. From the XPS (x-ray photon spectroscopy) analysis of P 2p peak on granular Aan-RM after phosphate adsorption confirmed that 79.01% of the phosphate was adsorbed onto granular Aan-RM through the precipitation and ion exchange mechanisms with strong chemical bonds, and 20.99% of the phosphate was adsorbed through the surface deposition mechanism with weak chemical bonds. Later, the same authors attributed the excellent adsorption performance of AaN-RM for removal of phosphate (Ye et al. 2015c). The maximum phosphate adsorption capacity of AaN-RM reached 492.46 mg/g at pH 4.5 and adsorption temperature 50°C. They reported that phosphate adsorption was best fitted with the pseudo-second-order kinetic model and Langmuir–Freundlich isotherm, which suggested that the chemisorption occurred between the phosphate and AaN-RM, and the phosphate adsorption was governed by heterogeneous processes. Furthermore, the phosphate complexes of Fe–P, Al–P, Fe–P–H₃PO₄, and Al–P–H₃PO₄ were formed on AaN-RM surface through ion exchange, precipitation, and surface deposition mechanisms. They concluded from the XPS analysis that the P 2p peak showed that 59.78% of the phosphate was adsorbed through the ion exchange and precipitation with strong chemical bonds, and 40.22% was adsorbed through the surface deposition with weak chemical bonds.

Artificial neural network (ANN) modeling was applied for the adsorption of phosphate onto AaN-RM (Ye et al. 2016a). Ye et al. demonstrated that the phosphate adsorption capacity of AaN-RM decreased with the enhancement of adsorbent dosage and the concentration of the competing ion (carbonate), while it increased with an increase of initial phosphate concentration and contact time. The optimal adsorption temperature and initial solution pH for phosphate adsorption onto AaN-RM were 50°C and 4.0, respectively. Acid-activated Bauxsol was applied to treat wastewater with high phosphate concentration (Ye et al. 2016b). The response surface methodology with central composite design was employed to obtain the interaction of initial solution pH and adsorption temperature on phosphate adsorption onto acid-activated Bauxsol. The maximum phosphate adsorption capacity of 192.94 mg/g was reported with an initial solution pH of 4.19 and an adsorption temperature of 52.18°C.

A novel composite red mud (RM)/polyaluminum chloride (PACl) coagulant (RMPACl) was prepared for effective removal of phosphate from aqueous solution (Ni et al. 2015). A phosphate removal efficiency of 94.9% was achieved at the RMPACl dosage of 147.5 mg/L, and the dosage of RMPACl was economized by having residual RM particles in the coagulant. RMPACl was considered to be a cost-effective coagulant for the effective removal of phosphate from natural water. Also, heat activated and acid-heat activated red mud was synthesized to enhance the phosphate sorption capacity (Liu et al. 2007). The red mud was

calcined at 700°C for 2 h to make heat-activated red mud and the red mud was activated at 80°C with 0.25 mol/L HCl for 2 h in an acid heat active process. The optimum pH for phosphate removal was at pH 7 in which 31.0 and 30.7 mg P/g of phosphate was removed from solution by acid-heat activated red mud and heat-activated red mud, respectively, with the initial phosphate concentration of 155 mg P/L. The Langmuir isotherm model fitted well and indicated that the maximum sorption capacity of phosphate by the acid-heat activated red mud and heat-activated red mud was 202.9 mg P/g and 155.2 mg P/g, respectively.

The acid and acid-thermal process were employed to activate the raw red mud using different acids such as HCl and HNO₃ (Huang et al. 2008). The HCl-treated red mud showed the highest adsorption capacity (0.58 mgP/g at pH 5.5 and 40°C) because of the high surface area for phosphate removal. The adsorption capacity of the red mud decreases with increasing pH. The HCl-treated red mud having pH 2 showed adsorption 0.8 mg P/g, whereas the adsorption was reduced to 0.05 mg P/g at pH 10. The adsorption was increased by 25% while increasing the temperature from 30°C to 40°C because of the existence of two acidic phosphorus species, H₂PO₄⁻ and HPO₄²⁻. The adsorption of phosphorous on the red mud showed first-order kinetics. Two activated red mud samples were prepared by (1) stirring red mud with 0.25 M HCl for 2 h (RM 0.25) and (2) heating the red mud at 700°C for 2 h (RM700) and used for the removal of phosphate from aqueous solution (Li et al. 2006). Both samples showed the maximum removal of phosphate (99%) at pH 7.0 and 25°C with initial phosphate concentration of 155 mg/L. The acid-sintered red mud RM0.25 had higher phosphate removal capacity of 24.67 mg/g as compared to the heat-treated red mud RM700.

The activated red mud was prepared by treating red mud with sulfuric acid and used to adsorb phosphorus from dilute aqueous solution (Mohanty et al. 2004). The optimum removal of phosphate was achieved at pH 4.5 at an equilibrium time of 60 min. Lower adsorbent dose and higher initial phosphorus concentration preferred higher loading capacity. The equilibrium adsorption process fitted well with the Freundlich isotherm and Lagergren first-order kinetics. The effect of different anions on phosphorus removal was explained on the basis of the changing affinity of anions for the surface and their relative concentrations. Bauxsol and acid-treated Bauxsol were used for phosphate removal from aqueous solution (Akhurst et al. 2006). It was reported that the adsorption of PO₄³⁻ increases with decreasing pH, and the maximum adsorption efficiencies were obtained at pH 5.2 ± 0.1. The adsorption capacity of Bauxsol and acid-treated Bauxsol was 0.21 and 0.48 mmol/g at pH 9.0 and 5.2, respectively. The PO₄³⁻ adsorption by Bauxsol decreases in the presence of HCO₃⁻ ions, whereas SO₄²⁻ and Cl⁻ ions had little effect and the adsorption efficiency increases in case of Ca²⁺ and Mg²⁺ ions. The adsorption process followed a ligand-exchange mechanism.

Red mud granular adsorbent (RMGA) has been prepared using dewatered red mud as the main raw material, bentonite, and starch with some natural additives for the removal of phosphate from aqueous solution (Zhao et al. 2012). Initially, the phosphate removal rate decreases with an increase in the initial pH. The maximum phosphate removal capacity was reported to be 6.64 mg/g at pH 5. Granular red mud (GRM) was synthesized for the removal of fluoride from water by mixing fly ash (2 g), sodium carbonate (1 g), powder quick lime (0.8 g), and sodium silicate (1.2 g) with red mud (15 g) and roasted at 400°C for 2 h followed by calcination at 900°C for 0.5 h (Tor et al. 2009a). The maximum fluoride removal of 0.644 mg/g was obtained at pH 4.7 with an equilibrium time of 6 h. Heat-activated AlCl₃ modified red mud (MRMAH) was used for the removal of fluoride from aqueous solution (Wei et al. 2009). The adsorption capability was reported to be 68.07 mg/g for AlCl₃-modified red mud (MRMA) and 91.28 mg/g for MRMAH, which were much higher than that of red mud (13.46 mg/g). The Langmuir adsorption isotherm model was

well fitted to the experimental data and the highest removal efficiency was achieved at pH 7 to 8.

Mechanochemical-activated red mud was used to improve the nitrate adsorption from aqueous solution (Alighardashi et al. 2016). High-energy milling and acidification were selected for mechanical and chemical activation methods, respectively. Experimental data were analyzed with two-way ANOVA (analysis of variance) and Kruskal–Wallis methods for verification and accuracy, and to reveal any probable errors. A best condition (acceptable removal percentage > 75) was 17.6% w/w for acid concentrate and 19.9 min for acidification and 8 h for milling. Red mud and HCl-activated red mud was synthesized and used for the removal of nitrate from aqueous solution in the batch adsorption technique (Cengeloglu et al. 2006). The adsorption capacity of the red mud and activated red mud was reported to be 1.86 and 5.86 mmol/g, respectively, at pH 7. The adsorption mechanism was described on the basis of the chemical nature and specific interaction with metal oxide surfaces and nitrate ions. Nitrate removal was enhanced from groundwater samples containing 2.52 mM nitrate by using untreated and acid-treated red mud combined with zero-valent iron (Fe(0)) (Cho et al. 2011). The nitrate removal increased with an increasing dose of acid-treated red mud resulting in a 164% increase in the first-order rate constant (k_{obs}) as compared to Fe(0).

Multifunction red mud granule (RMGM) material was prepared and modified by Fe(II)-akaganeite (β -FeOOH) for the removal of bromate from aqueous solution (S. Chen et al. 2016). The results showed that Fe(II)-akaganeite/RMGM exhibits higher bromate removal capacity than raw red mud granule material due to its higher isoelectric point, rich mesoporous, and multifunction surface. Bromate removal capacity was enhanced by addition of Fe(II) and akaganeite on RMGM. The reaction mechanism included four effects:

1. Electrostatic adsorption, in which bromate could be attached on the surface of Fe(II)-akaganeite/RMGM
2. Ligand exchange, in which bromate could react with metal oxide of Fe(II)-akaganeite/RMGM
3. Ion exchange, in which BrO_3^- could exchange with the Cl^- in the akaganeite channel
4. Redox, in which the electrons from Fe(II) could transfer to bromate and get bromate reduced to bromide

The RMGM with 5.3% Fe loading exhibited the highest removal capacity. A summary of the adsorption capacity of red mud for different anions is presented in Table 7.1.

7.2.2 Utilization of Red Mud for the Removal of Heavy Metal Ions from Aqueous Solution

Metal ions are one of the important classes of aquatic pollutants. In recent years, the rapid growth of industries, especially fertilizer, metal plating, tanneries, mining, and textile, have increased the discharge of toxic heavy metals into water streams, particularly in developing countries. Elements with atomic weights in the range 63.5 to 200.6 and specific gravity greater than 5.0 come under the purview of heavy metals. Unlike organic contaminants, heavy metals are not biodegradable and tend to accumulate in living organisms. Many heavy metal ions are known to be toxic and carcinogenic, and cause various diseases and disorders in human, animals, and aquatic life. Hence, they need to be removed

TABLE 7.1

Summary of the Adsorption Capacity of Red Mud for Different Anions

Adsorbent	Adsorbate	Temperature (°C)	pH	Amount Adsorbed/% Removal	Reference
Fe ₃ O ₄ -NPs from red mud	As(V)	25	2.5	15.30 µg/L	Akin et al. 2012
CO ₂ -neutralized red mud (ANRM)	As(V)	–	4	55.55 mg/g	Sahu et al. 2010
Seawater-neutralized red mud (Bauxsol)	As(V)	–	6.3–10.0	6.08–14.43 µmol/g	Genç et al. 2003
Bauxsol-coated sand	As(V)	–	4.5	3.32 mg/g	Genc-Fuhrman et al. 2005
Activated Bauxsol-coated sand	As(V)	–	7.1	1.64–2.14 mg/g	Genc-Fuhrman et al. 2005
Activated red mud (ARM)	As(V)	25	7	5.16 mg/g	Guo et al. 2014a
Activated red mud (ARM)	As(III)	25	7	1.47 mg/g	Guo et al. 2014a
FeCl ₃ -coated red mud	As(V)	–	6–9	23.2–68.5 mg/g	Zhang et al. 2008
Granular acid-activated neutralized red mud (AaN-RM)	Phosphate	–	–	86.69 mg/g	Ye et al. 2015a
Powdered acid-activated neutralized red mud (Aan-RM)	Phosphate	6	40	153.227 mg/g	Ye et al. 2015b
Acid-activated neutralized red mud (AaN-RM)	Phosphate	4.5	50	492.46 mg/g	Ye et al. 2015c
Acid-activated neutralized red mud (AaN-RM)	Phosphate	4	50	24.64%	Ye et al. 2016a
Acid-activated Bauxsol		4.19	52.18	192.94 mg/g	Ye et al. 2016b
Red mud polyaluminum chloride coagulant (RMPACl)	Phosphate	7	–	92.3%	Ni et al. 2015
Red mud activated by HCl	Phosphorous	–	7	202.9 mgP/g	Liu et al. 2007
Acid-treated red mud	Phosphorous	40	5.5	0.58 mgP/g	Huang et al. 2008
Red mud-activated HCl	Phosphorous	25	7	24.67 mgP/g	Li et al. 2006
Red mud activated by H ₂ SO ₄	Phosphorous	40	4.5	7.4 mg/g	Mohanty et al. 2004
Bauxsol acid treated	Phosphorous	23	9.0	0.21 mmol/g	Akhurst et al. 2006
Bauxsol	Phosphorous	23	5.2	0.48 mmol/g	Akhurst et al. 2006

(Continued)

TABLE 7.1 (CONTINUED)

Summary of the Adsorption Capacity of Red Mud for Different Anions

Adsorbent	Adsorbate	Temperature (°C)	pH	Amount Adsorbed/% Removal	Reference
Red mud-granular (RMGA)	Phosphorous	–	5	6.64 mg/g	Zhao et al. 2012
Activated red mud (ARM)	Fluoride	25	7	3.96 mg/g	Guo et al. 2014b
Red mud-granular (GRM)	Fluoride	–	4.7	0.644 mg/g	Tor et al. 2009a
Red mud	Fluoride	–	7–8	13.46 mg/g	Wei et al. 2009
Red mud AlCl ₃ (MRMA)	Fluoride	–	7–8	68.07 mg/g	Wei et al. 2009
Heated red mud (MRMAH)	Fluoride	–	7–8	91.28 mg/g	Wei et al. 2009
Red mud	Nitrate	–	7	1.86 mmol/g	Cengeloglu et al. 2006
HCl-activated red mud	Nitrate	–	7	5.86 mmol/g	Cengeloglu et al. 2006

prior to their discharge into water streams. In the treatment of industrial wastewaters, the toxic heavy metals of utmost concern are chromium (Cr), cadmium (Cd), lead (Pb), zinc (Zn), copper (Cu), and nickel (Ni). Therefore, different organizations have set the maximum limits for the discharge of toxic heavy metals into natural water bodies. The effective treatment of wastewater contaminated with toxic heavy metal ions has grown into an important research area. Therefore, red mud has been exploited as a low-cost adsorbent by many researchers for the removal of toxic heavy metals from wastewater due to their constituents (silica, alumina, calcium, iron, titanium oxides, and hydroxides) and high surface reactivity.

Rinsed Bosnian red mud (RBRM) was used for the adsorption of divalent nickel (Ni(II)) ion from aqueous solution (Smiljanić et al. 2010). The mineral mixture has a high acid-neutralizing capability, and at pH range of 2 to 8 the mixture showed the highest cation immobilization. The accumulation of 5 g/L of RBRM affected 100% removal from the solutions of 1×10^{-4} to 5×10^{-4} mol/L, which decreases to 26% with an increase in Ni(II) concentration to 8×10^{-3} mol/L. The maximum sorption capacity by Langmuir model was 0.372 mmol/g at pH 5. The maximum sorption of Ni(II) by red mud was reported at pH 5, 30°C, and contact time of 4 h (Hannachi et al. 2010). The adsorption process followed the first-order rate mechanism with an adsorption capacity of 13.69 mg/g.

Copper was removed from aqueous solution by using red mud, sea nodule residue (SNR), and fly ash separately (Agrawal et al. 2004). The maximum adsorption capacity of divalent copper (Cu(II)) on red mud was reported to be 2.28 mg/g at pH 5.5. Red mud and activated red mud were employed for sorption of copper from aqueous solution (Nadaroglu et al. 2010). The maximum adsorption of copper occurred at an initial solution concentration of 3 mmol, pH 5.5, 30°C, and adsorbent dose of 1 g/ml. The activated red mud has a higher level of adsorption capacity for Cu(II) than normal red mud.

Granular red mud (GRM) was prepared and used for the removal of cadmium ions from aqueous solutions (Zhu et al. 2007). The granular red mud adsorbent exhibited a high capability to adsorb cadmium ions from aqueous solutions. The adsorption of cadmium

on GRM was a spontaneous, feasible, and endothermic process as confirmed from thermodynamic parameters. The maximum adsorption capacity for GRM was reported to be 38.2 mg/g at 20°C, 43.4 mg/g at 30°C, and 52.1 mg/g at 40°C. The experimental adsorption kinetics at initial pH 3.0 and pH 6.0 were fairly fitted by the pseudo-second-order kinetics model. The granular red mud (GRM) mixed with cement and used as an adsorbent for the removal of cadmium ions from aqueous solutions (Ju et al. 2012). The GRM showed good adsorption capacity. The equilibrium adsorption increases with the increase of temperature during the adsorption process, indicating the adsorption of cadmium ions onto GRM was an endothermic process. The Langmuir adsorption isotherm model matched the experimental adsorption isotherm well. The adsorption capacity of adsorbent for Cd(II) was more than 9 mg/g at 30°C and 6.5 pH of the solution. The pseudo-second-order model matched the experimental data well.

Activated red mud has been prepared by the acid dilution and ammonia precipitation process, and used for the removal of Cd(II) from aqueous solution by batch mode of experiment (Sahu et al. 2015). The maximum adsorption capacities of Cd(II) on activated red mud (ARM) were reported to be 12.046 and 12.548 mg/g at pH 6 and of 293 K and 303 K, respectively. The mass transfer study revealed that the adsorption of cadmium ions was faster at lower temperature. Bacteria-modified red mud was used for the removal of cadmium from aqueous solutions (Kalkan et al. 2013). A red mud sample of 1 g having 200 mesh sieves was shaken with 10 mL, 108 CFU (colony-forming units)/mL *Staphylococcus cohnii* GC sub-group A solution for approximately 1 h, and then the separated particles were stored and named as bacteria-modified red mud from the adsorption of cadmium from aqueous solutions. The uptake capacity of bacteria-modified red mud was 83.034 mg/g at the optimum condition of pH 4.0, contact time of 60 min, temperature of 30°C, and an adsorbent dose of 1 mg/mL. The adsorption data best correlated with the Langmuir adsorption model and the kinetic data obeyed pseudo-second-order rate equations. The removal process was spontaneous and endothermic in nature.

Iron oxide-activated red mud (IOARM) was effectively used to adsorb cadmium ions from aqueous solution (Khan et al. 2015). The optimized adsorption parameters were dose 6.0 g/L, pH 6.0, contact time 90 min, initial concentration 400 µg/L, and temperature 300 K. Cd(II) adsorption followed the Freundlich isotherm model. Langmuir monolayer adsorption capacities was 117.64, 116.28, and 107.53 µg/g, while Freundlich adsorption capacities were 3.83, 3.68, and 3.07 µg/g at 293, 298, and 308 K, respectively. The adsorption capacities in both isotherms decreased with an increase in temperature, showing the exothermic nature of the process. The negative value of change in Gibb's free energy indicated spontaneity and feasibility of the process. The enthalpy change was found to be 7.27 kJ/mol, indicating physical adsorption of Cd(II) onto IOARM. The pseudo-second-order kinetics model was best fitted with the adsorption data. The removal of cadmium from aqueous solutions on red mud, acidified red mud, and ball milling nanoparticle red mud was investigated (Luo et al. 2011). The maximum sorption capacity of cadmium was 0.16, 0.19, and 0.21 mol/kg for the original, acidified, and nanoparticle red mud, respectively, at pH 6.5. Both acidification and ball milling treatments considerably enhanced cadmium sorption and facilitated conversion of cadmium into less extractable fractions. The formation of inner-sphere complexes of cadmium similar to XCdOH (X represents surface groups on red mud) on the red mud surfaces is the mechanism of cadmium sorption, although outer-sphere complexes of cadmium were the primary species.

Acid-activated red mud was prepared to investigate the removal efficiency of lead ions from aqueous solutions (Sahu et al. 2013). The percentage removal was found to gradually increase with a decrease in pH, with maximum removal at pH 4. The adsorption isotherm

was better described by the Langmuir isotherm model. The maximum adsorption capacity of ARM was 6.0273 mg/g at 30°C. The adsorption kinetics were found to follow the pseudo-second-order rate equation and equilibrates within 30 min. The authors reported that the material have not only a high adsorption capacity for the lead ion but is also capable of lowering the metal ion concentration to a great extent. The metal ion concentration gradient is a fundamental force that transfers metal ion from solution to adsorbent surface and diffuses metal ion inside of adsorbent.

Removal of lead and chromium ions from aqueous solutions using red mud was reported (Gupta et al. 2001). It was reported that the adsorption capacity of red mud for lead was 64.79 mg/g at pH 4 to 6, and for chromium was 35.66 mg/g at pH 2. ARM was prepared by the treatment of red mud with hydrogen peroxide and used for the adsorption of cadmium and zinc from aqueous solution in the batch and column process (Gupta and Sharma 2002). The removal of hexavalent chromium Cr(VI) from aqueous solutions by using red mud activated with cetyltrimethylammonium bromide (CTAB) was studied (Li et al. 2015). The best concentration of CTAB for modifying red mud was reported to be 0.50%. The lower pH (<2) was found to be much more favorable for the removal of Cr(VI). The adsorption of Cr(VI) on activated red mud fitted well to the Langmuir isotherm model, and the maximum adsorption capacity was estimated as 22.20 mg/g. The adsorption process was well described using the pseudo-second-order kinetic model.

The heavy metals lead, cadmium, and zinc ions have been removed using nontreated red mud (RM_{nt}) and acid-treated red mud (RM_a) (Santona et al. 2006). The adsorption capacity of RM_{nt} for these metals were in the order of zinc ≥ lead > cadmium. Seawater-neutralized red mud (SWN-RM) having hydrotalcite structure has been prepared by taking magnesium and aluminum with the ratio between 3.5:1 and 4:1, and used for the adsorption of arsenate, vanadate, and molybdate separately as well as mixed solutions, and compared with several synthetic hydrotalcite minerals (Palmer et al. 2010). The percentage of anions removed from solution increased with an increasing Mg:Al ratio to 4:1. The increasing affinity adsorption was in the order of arsenate > vanadate > molybdate.

The effectiveness of the red mud for the removal of inorganic mercury ions from aqueous solutions was investigated (Rubinos and Barral 2015). The red mud exhibited high Hg(II) removal efficiency for the whole pH range studied (3.5–11.5), being optimal at pH ~6 and decreasing slightly at both lowest and highest pH. The ability of red mud to tightly retain Hg(II) may be useful in engineering applications such as for the decontamination of Hg-rich industrial effluents or acid mine drainage. The removal of manganese ions Mn(II) from aqueous solution using annealed red mud was studied (H. Chen et al. 2016). The annealing temperature (105°C–900°C) changed the mineralogical components and the point of zero charge of red mud. The removal efficiency of Mn(II) by annealed red mud at 700°C (ARM700) was ~56.5% with initial Mn(II) concentration 385 mg/L at initial pH > 5. The pseudo-second-order model better predicted the kinetics process. The Langmuir isotherm displayed a better fitting model than the Freundlich isotherm and the maximum adsorption capacity of ARM700 was reported to be 88.3 mg/g. Sorption kinetics of cobalt and strontium ions was investigated using red mud as a low-cost sorbent (Milenković et al. 2015). Different total concentrations of mixtures and different molar ratios of two cations Co(II) and Sr(II) were taken for the investigation. Kinetics of metal sorption from binary systems was found to be well described by the pseudo-second-order rate model. Equilibrium adsorbed amounts and equilibrium times for Co(II) sorption increased with an increase of its total concentration in the mixture, whereas pseudo-second-order rate constants exhibited the opposite trend. Sr(II) sorption was strongly suppressed in the presence of Co(II) ions, and the removal efficiency decreased with an increasing concentration

TABLE 7.2

Summary of Adsorption Capacity of Red Mud for Different Metal Ions

Adsorbent	Adsorbate	Temperature (°C)	pH	Amount Adsorbed/% Removal	Reference
Rinsed Bosnian red mud	Ni(II)	–	5	0.372 mmol/g	Smiljanić et al. 2010
Red mud	Ni(II)	30	5	13.69 mg/g	Hannachi et al. 2010
Red mud	Cu(II)	–	5.5	2.28 mg/g	Agrawal et al. 2004
Granular red mud (GRM)	Cd(II)	40	6	52.1 mg/g	Zhu et al. 2007
Granular red mud (GRM)	Cd(II)	30	6.5	9 mg/g	Ju et al. 2012
Activated red mud	Cd(II)	30	6	12.548 mg/g	Sahu et al. 2015
Bacteria-modified red mud	Cd(II)	30	4	83.034 mg/g	Kalkan et al. 2013
Red mud	Cd(II)	–	6.5	0.16 mol/kg	Luo et al. 2011
Acidified red mud	Cd(II)	–	6.5	0.19 mol/kg	Luo et al. 2011
Nanoparticles red mud	Cd(II)	–	6.5	0.21 mol/kg	Luo et al. 2011
Activated red mud	Cd(II)	30	4	1.16×10^4 mol/g	Gupta and Sharma 2002
Activated red mud	Zn(II)	30	4	2.22×10^4 mol/g	Gupta and Sharma 2002
Red mud	Pb(II)	–	4–6	64.79 mg/g	Gupta et al. 2001
Acid-activated red mud	Pb(II)	30	4	6.0273 mg/g	Sahu et al. 2013
Red mud	Cr(VI)	–	2	35.66 mg/g	Gupta et al. 2001
Red mud activated with cetyltrimethylammonium bromide (CTAB)	Cr(VI)	–	<2	22.20 mg/g	Li et al. 2015
Annealed red mud (ARM700)	Mn(II)		>5	88.3 mg/g	H. Chen et al. 2016

and mole fraction of Co(II). Milenković et al. (2015) concluded that red mud can be used for simultaneous Co(II) and Sr(II) removal from mixtures of lower initial concentration; otherwise Co(II) sorption is dominant. The utilization of zeolite synthesized from red mud for the adsorption of ammonium from aqueous solution was investigated (Zhao et al. 2016). The adsorption dynamics was described by Ho's pseudo-second-order kinetic model to understand the exchange process of ammonium by the synthesized zeolite. The Koble–Corrigan isotherm model was best fit to the equilibrium isotherm data. The maximum ammonium adsorption capacity obtained was 17.5 mg/g. A summary of adsorption capacity of red mud for different metal ions is shown in Table 7.2.

7.2.3 Utilization of Red Mud for the Removal of Dyes from Aqueous Solution

Dyes are basically chemical compounds that can connect themselves to surfaces or fabrics to impart color. Synthetic dyestuffs, one group of organic pollutants, are used extensively in textile, paper, and printing industries, and dye houses. It is reported that there are over 100,000 commercially available dyes with a production of over 7×10^5 metric tons per year. The total dye consumption in the textile industry worldwide is more than 10,000 tons/year, and approximately 100 tons/year of dyes is discharged into water streams. However,

wastewater containing dyes is very difficult to treat, since the dyes are recalcitrant organic molecules, resistant to aerobic digestion, and are stable to light, heat, and oxidizing agents.

H₂O₂-activated red mud has been used for the removal of some basic dyes like rhodamine B, fast green, and methylene blue from wastewater (Gupta et al. 2004a). The percentage removals were 92.5%, 94.0%, and 75.2% for rhodamine B, fast green, and methylene blue dyes at optimum pH 1.0, 7.0, and 8.0, respectively. The adsorption of the three dyes on H₂O₂-activated red mud was reported to be exothermic in nature. The suitability of acetone for desorption of rhodamine B, fast green, and methylene blue dyes were described. Red mud was chemically treated and the surface was modified by sodium dodecyl sulfate anionic surfactant for the removal of safranin-O dye from aqueous solution (Sahu and Patel 2015). The maximum adsorption of safranin-O was found to be 8.9471 mg/g at pH 4 with an equilibrium time of 45 min and temperature of 35°C. The pseudo-second-order kinetics model was found to be best fitted to the experimental data and the equilibrium data were found to follow the Langmuir isotherm model for the adsorption of safranin-O dye onto sodium dodecyl sulfate-modified red mud (SDS/RM). The adsorption of safranin-O onto SDS/RM was determined to be faster at lower temperature and the process was regulated by mass transfer.

The adsorption potential of red mud for the removal of acid blue 15 (AB15) dye from aqueous solutions was investigated (Balarak et al. 2015). Maximum adsorption capacity of the red mud was found to be 29.44 mg/g when 73.6% of the AB15 dye was removed at pH 3 and initial concentration 25 mg/L, with red mud dosage of 5 g/L and contact time of 60 min. The Langmuir isotherm models and pseudo-second-order kinetic models best fit the experimental data. Acid-treated red mud was used as an adsorbent for removal of Remazol Brilliant Blue (RBB) dye from dye synthetic aqueous solution (Ratnamala et al. 2013). The maximum percentage adsorption of 26.7 mg/g or 94% was obtained at pH 2 with initial concentration 10 mg/L and with red mud dosage of 3.2 g/L. The optimum conditions were obtained by 2⁴ factorial central composite design for red mud treated with concentrated acid were pH of 1, initial concentration of 100 mg/L, red mud dosage of 4.8 g/L, and temperature of 33°C. In another work, concentrated sulfuric acid activated red mud (CATRM) was used for removal of RBB dye from dye-contaminated aqueous solution (Ratnamala et al. 2016). Acidic pH favored adsorption and 300 min contact time was found to be suitable for attainment of equilibrium under shaking conditions of 145 rpm. The Langmuir isotherm model was found to represent the equilibrium data better for RBB–CATRM adsorption system. The adsorption capacity of CATRM was found to increase with an increase in temperature to 40°C, and it was found to be 125 mg dye/g of CATRM. The adsorption kinetics was represented by second-order kinetic model. The factors affecting the adsorption process were optimized by response surface methodology based on experiments designed as per the central composite design. The results of the study showed that dye removal efficiency of almost 100% can be obtained with optimal conditions of initial dye concentration of 105 mg/L, red mud dosage of 2.05 g/L, initial pH 1, and temperature of 31.65°C. pH and temperature were found to have a high interaction effect on adsorption.

Sulfuric acid-treated red mud was used as an adsorbent for the removal of RBB from aqueous solution (Ratnamala et al. 2012). The adsorption capacity of red mud was found to be 27.8 mg dye/g at 40°C and pH 2 to 6. The Langmuir isotherm model was found to be better fitted with the equilibrium data for the RBB–red mud adsorption system. Adsorption kinetics was represented by the second-order kinetic model for the sorption of RBB onto red mud. The intraparticle diffusion kinetic model suggested that among the mass transfer processes, pore diffusion was the controlling step, and not the film diffusion.

Thermodynamic analysis confirmed that RBB–red mud adsorption was an endothermic process. Polystyrene-modified red mud (MRM-PS) with a hierarchical macroporous–mesoporous structure was prepared via a template synthesis method by using polystyrene (PS) microspheres and waste red mud to be used for the removal of rhodamine B dye (Cao et al. 2014). It was reported that the maximum adsorption capacity of MRM-PS was 59.37 mg dye/g of adsorbent at 25°C, pH 1, and equilibrium time of 10 min.

Removal of acid blue 113 (AB113) and reactive black 5 (RB5) dyes from aqueous solutions using nitric acid-activated red mud was investigated (Shirzad-Siboni et al. 2014). The activated red mud has higher removal efficiency for AB113 than that for RB5 due to the greater molecular size of RB5 than that of AB113. The equilibrium data was best fitted with the Freundlich isotherm model and the kinetic data followed a pseudo-second-order model for both dyes. The maximum adsorption capacity was reported to be 83.33 mg/g and 35.58 mg/g at pH 3 and 25°C for AB113 and RB5, respectively. Removal of two cationic dyes, malachite green (MG) and crystal violet (CV), from aqueous solution was investigated (Zhang et al. 2014) using acid-activated sintering process red mud (ASRM) as an adsorbent. The solution pH higher than 3.2 was found to be favorable for the adsorption of MG and CV on the ASRM. Adsorption data was better fitted with the Langmuir isotherm model for both the dyes, and the maximum adsorption capacities were found to be 336.4 mg/g and 60.5 mg/g for MG and CV at 25°C, respectively. The kinetic data were better described by a pseudo-second-order kinetic model. The thermodynamic data show that the adsorption of MG onto ASRM was endothermic, whereas the adsorption of CV was exothermic.

Granular red mud (GRM) was prepared by mixing the red mud with cement, and its efficiency for the removal of methylene blue (MB) from aqueous solutions was evaluated (Sadler et al. 2013). The maximum removal percentage and uptake capacity was found to be 86.89% and 2.6040 mg/g, respectively, with dosage of 150 mg/L, pH 11, and temperature of 303 K. The Freundlich isotherm model was better fitted with the adsorption data, which was attributed to successive multilayer adsorption. The thermodynamic data depicted the endothermic nature of adsorption and the process was spontaneous. Thermal treatment on the adsorbent increased the surface area, which results in an increase in adsorption capacity due to more available adsorption sites. In order to obtain reasonable adsorption, Reactive Blue dye 19 (RB 19) on thermal treatment of seawater-neutralized red mud (SWRM) was investigated (De Souza et al. 2013). SWRM was thermally treated at 400°C and 500°C for the removal of RB 19 from aqueous solution. The Langmuir isotherm was more appropriate to describe the phenomenon of the removal of RB 19 using SWRM, SWRM400, and SWRM500, with a maximum adsorption capacity of 250.0 mg/g, 416.7 mg/g, and 384.6 mg/g, respectively. De Souza et al. (2013) also reported that the pseudo-second-order reaction mechanism was responsible for the adsorption of RB 19 using SWNRM, in which adsorption was occurs by electrostatic interactions.

Removal of RB 19 from aqueous solution was evaluated using thermally treated red mud at 500°C (RM 500°C) (De Costa et al. 2015). The Langmuir isotherm model was more fit for describing adsorption phenomenon in acidic conditions, with a maximum adsorption capacity of 178.4 mg/g. Kinetics studies showed that pseudo-second-order reaction mechanism was responsible for the adsorption of RB 19, which indicated that the adsorption of RB 19 dyes onto RM 500°C occurs through electrostatic interactions. Red mud was modified with laccase from Russulaceae (*Lactarius volemus*) and used for the removal of acid red 37 (AR37) from aqueous solutions (Nadaroglu et al. 2014). The optimum pH for efficient adsorption of AR37 was found to be 4 with contact time of 60 min and temperature of 30°C. The adsorption capacity was strongly dependent on the temperature and found to be increase significantly with an increase in temperature from 20°C to 30°C. Freundlich

adsorption isotherm model was fitted very well with the experimental data. The thermodynamic parameters indicated that the adsorption of AR37 onto laccase modified-RM adsorbent was feasible, spontaneous, and exothermic.

Bagasse carbon-red mud (BCRM) was prepared from solid red mud and bagasse and applied as a low-cost adsorbent for the disposal of organic methylene blue (MB) dyes from wastewater (Wang et al. 2016). The adsorption results showed that the pseudo-second-order kinetic model was better fitted with experimental data. The Langmuir model was a better fit isotherm for MB adsorption on BCRM. It was reported that MB adsorption on BCRM was a monolayer adsorption, and the adsorption occurred at specific homogeneous sites on the adsorbent. The results of adsorption thermodynamics indicated MB adsorption on BCRM was a spontaneous, endothermic, and physical process. Column absorption and regeneration behavior of a granular red mud (GRM) for absorbing MB dye from wastewater was investigated (Le et al. 2016). The breakthrough time was found to be as high as 330 min, when 20.5 cm GRM column was used, with initial concentration and flow rate of MB wastewater being 150 mg/L and 4 mL/min, respectively, for effective removal of MB from wastewater. The Thomas model was capable of describing the adsorption kinetics. For the regeneration, the MB-loaded column with dilute nitric acid solution, whose pH value was about 3.0, was conducted.

Nitric acid-activated red mud was used for the removal of reactive red 198 dye (RR198) from aqueous solution (Zazouli et al. 2013). They reported that the adsorption efficiency was reduced by increasing the initial dye concentration, but an increasing of time and adsorbent dose can lead to an increased removal efficiency. The maximum removal efficiency occurred at pH between 2 to 3. The removal data were best fitted with Freundlich and Temkin isotherms models. The removal of acid orange 7 dye from aqueous solution was studied through Fenton and photo-Fenton oxidation processes using Portuguese common clay, Fe-impregnated clay, red mud, and clay-red mud mixtures as catalysts (Hajjaji et al. 2016). A 38% discoloration was observed after 420 min of reaction time by untreated red mud due to the presence of high iron and aluminum compounds in the adsorbent. The removal rate was higher when red mud was calcined at 400°C (RM400). It was reported that the acid orange 7 removal approached 300% in the Fenton-type process when H₂O₂ was added. With the introduction of natural clay (Bo) to the red mud catalyst preparation (to improve the degradation), the quantitative removal of the dye was upgraded to 38% at pH 7, and at a more acidic pH value of 3, high dye removal efficiencies were obtained of >80% removal after 240 min for RM-Bo 400 under photo-Fenton conditions. The removal data was good fitting with a pseudo-second-order expression with high R² value of 0.99.

Red mud was used for the removal of Indosol dark-blue (IDB) from textile effluents (De Oliveira et al. 2016). The maximum amount adsorbed by the red mud (0.110 mg/g) was obtained in the case of high concentration of the adsorbent mass and high pH ranges. From the factorial experimental planning, it was found that the adsorption process was influenced by the amount of mass of the adsorbent, the pH, and the by interaction between pH and mass. Red mud was modified by HCl leaching and used for photodegradation of methyl orange dye (MO) from aqueous solution under UV irradiation (Ma et al. 2015). The results showed that the specific surface area of modified red mud was 317.14 m²/g, which was about 40 times higher than that of the normal red mud. After ultraviolet irradiation for 50 min and the concentration of modified red mud 0.7 g/L, the removal percentage of MO reached 94.2%, indicating that modified red mud possessed a better dispersibility and more photoactive sites, causing an enhanced photodegradation of MO molecules. Red mud was modified with ethanol via chemical vapors deposition process (RM/C) and applied in the heterogeneous photo-Fenton process for the degradation of the reactive black 5 (RB 5)

textile dye (Dias et al. 2016). The RM/C catalyst reached 100% efficiency in the dye degradation after 60 min of photo-Fenton reaction at pH 3 and 11 in presence of 1 mM of H_2O_2 . The kinetic data related to RB5 dye degradation were well fitted to the Langmuir–Hinshelwood model. The H_2O_2 was activated by surface Fe(II) sites on red mud-based catalyst, especially in the presence of light to produce $\bullet\text{OH}$ radicals in a heterogeneous photo-Fenton-like mechanism to oxidize the organic pollutant RB 5.

Cobalt-doped neutralized red mud (Co/NRM) nanocomposite materials were prepared by the impregnation method for the photodegradation of methylene blue dye under solar light irradiation (Sahu and Patel 2016). Different Co/NRM catalysts were prepared by varying the weight ratio of Co and NRM, that is, 10:90, 20:80, 30:70, 40:60, and 50:50. Under solar light, 97.21% degradation was observed in the presence of 0.08 g of Co/NRM (Co:NRM::20:80) photocatalyst within 150 min at pH 9. A summary of the adsorption capacity of red mud for different dyes is presented in Table 7.3.

7.2.4 Utilization of Red Mud for the Removal of Organic Pollutants from Aqueous Solution

Chemical contamination of water from a wide range of toxic pollutants, especially aromatic molecules, is a serious environmental problem due to its toxicity on human health and environment. Phenol and its derivatives appear to be the major organic pollutants of this century. They are released from many chemicals, pesticides, and dye manufacturing, and cause serious threat to human health and to natural water.

The removal of phenol, 2-chlorophenol, 4-chlorophenol, and 2,4-dichlorophenol from wastewater were studied by using red mud (Gupta et al. 2004b). The maximum adsorption of phenol and 2-chlorophenol was reported to be 50% to 81% at pH 6.0, whereas the maximum adsorption of 4-chlorophenol and 2,4-dichlorophenol was 94% to 97% at pH 5.0 and 4.0, respectively. Gupta et al. (2004b) described the removal of phenol and its derivatives by particle diffusion mechanism and the order of removal was 2,4-dichlorophenol > 4-chlorophenol > 2-chlorophenol > phenol. The adsorption process was endothermic in nature and fitted well with both Langmuir and Freundlich models. Red mud has also been used for the removal of 2,4-dinitrophenol (Gupta and Ali 2006). About 95% of 2,4-dinitrophenol was sorbed by the developed adsorbent and the removal efficiency reached up to 96% in column experiments at the flow rate of 0.5 mL/min. The removal of phenol from aqueous solution was investigated using neutralized red mud by the batch process (Tor et al. 2006). The maximum monolayer sorption ability for the adsorption of phenol by neutralized red mud was found to be 4.12 mg/g at the pH range of 1 to 9 with an equilibrium time of 10 h. Tor and coworkers reported that the adsorption of phenol decreased from 66% to 32% and 15% in the presence of nitrate and sulfate ions, respectively, but there was no negative effect on adsorption by the chloride ion. HCl-activated red mud was used for the removal of phenol from aqueous solution (Tor et al. 2009). The maximum adsorption capacity of activated red mud was 8.156 mg/g at pH 6 and temperature $25^\circ\text{C} \pm 1^\circ\text{C}$ with an equilibrium time of 10 h. The adsorption kinetics followed pseudo-second-order reaction and followed both Langmuir and Freundlich isotherms models.

Activated red mud (ARM) was used as a supporting material with Zn/Al oxide catalysts by the hot wet impregnation method and investigated the conversion of glycerol and urea to glycerol carbonate (GC) (Nguyen-Phu et al. 2016). ARM-supported Zn/Al oxide catalysts exhibited higher GC yields. Nguyen-Phu et al. (2016) reported that the catalyst with 50% of Zn/Al loaded on ARM attained a GC yield of 58.1%, which was higher than that (49.6%) of the unsupported catalyst, $\text{Zn}_7\text{Al}_3\text{O}_x$. The FTIR analysis revealed the ARM-supported

TABLE 7.3

Summary of the Adsorption Capacity of Red Mud for Different Dyes

Adsorbent	Adsorbate	Temperature (°C)	pH	Amount Adsorbed/% Removal	Reference
H ₂ O ₂ -activated red mud	Rhodamine B	30–50	1	$(1.01\text{--}1.16) \times 10^{-5}$ mol/g	Gupta et al. 2004a
H ₂ O ₂ -activated red mud	Fast Green	30–50	7	$(7.25\text{--}9.35) \times 10^{-6}$ mol/g	Gupta et al. 2004a
H ₂ O ₂ -activated red mud	Methylene blue	30–50	8	$(4.35\text{--}5.23) \times 10^{-5}$ mol/g	Gupta et al. 2004a
Sodium dodecyl sulfate-modified red mud	Safranin-O	35	4	8.9471 mg/g	Sahu and Patel 2015
Red mud	Acid blue 15 (AB15)	–	3	29.44 mg/g	Balarak et al. 2015
Concentrated sulfuric acid-activated red mud	Remazol Brilliant Blue (RBB)	33	2	26.7 mg/g	Ratnamala et al. 2013
Concentrated sulfuric acid-activated red mud (CATRM)	Remazol Brilliant Blue (RBB)	40	1	125 mg/g	Ratnamala et al. 2016
Sulfuric acid-treated red mud	Remazol Brilliant Blue (RBB)	40	2–6	27.8 mg/g	Ratnamala et al. 2012
Modified red mud with polystyrene (MRM-PS)	Rhodamine B	25	1	59.37 mg/g	Cao et al. 2014
Nitric acid-activated red mud	Acid blue 113 (AB113)	25	3	83.33 mg/g	Shirzad-Siboni et al. 2014
Nitric acid-activated red mud	Reactive black 5 (RB5)	25	3	35.58 mg/g	Shirzad-Siboni et al. 2014
Acid-activated sintering process red mud (ASRM)	Malachite green (MG)	25	>3	336.4 mg/g	Zhang et al. 2014
Acid-activated sintering process red mud (ASRM)	Crystal violet (CV)	25	>3	60.5 mg/g	Zhang et al. 2014
Granular red mud (GRM)	Methylene blue (MB)	25	11	2.60 mg/g	Sadler et al. 2013
Seawater-neutralized red mud	Reactive blue dye 19	–	–	250.0 mg/g	De Souza et al. 2013
Seawater-neutralized red mud thermally treated with 400°C	Reactive blue dye 19	–	–	416.7 mg/g	De Souza et al. 2013
Seawater-neutralized red mud thermally treated with 500°C	Reactive blue dye 19	–	–	384.6 mg/g	De Souza et al. 2013
Thermally treated red mud at 500°C (RM 500°C)	Reactive blue 19 (RB 19)	–	3	178.4 mg/g	Jesus et al. 2015

Zn/Al oxide catalysts to be more selective, resulting in higher GC yield. The balance of active sites from ARM and Zn/Al oxide was related to rates of each reaction step in GC synthesis, which eventually influenced the selectivity and yield of GC. The adsorption of bisphenol by red mud modified with nitric acid has been studied and found that increasing the contact time from 10 to 210 min increased the adsorption of bisphenol from 43% to 84% (Ali et al. 2013). Also, increasing the adsorbent dosage from 2 to 20 g/l increased the adsorption bisphenol from 40% to 82%. The best pH for bisphenol removal was found to be 3. The adsorption data's were best fitted to the Freundlich isotherm and pseudo-second order kinetic model.

The removal of phenol from aqueous solution was investigated by using activated and nonactivated red mud (Soldán et al. 2014). The maximum removal was obtained at dosage of 0.5 g of red mud and initial concentration of phenol 40 mg/L. It was reported that the activation had no positive effect on adsorption effectiveness. Red mud-based porous materials (RMPM) were prepared and applied for the adsorption of polyvinyl alcohol (PVA) from simulated textile wastewater (Zhang et al. 2012). Zhang et al. (2012) reported that the best mass ratio of RMPM to PVA solution was 50:100 with a removal maximum of 25.8% after they were in contact for 50 min. The adsorption rate and kinetics could be better described by Lagergren's pseudo-second-order model in comparison with the pseudo-first-order model. Acid-modified red mud (RM6.0) showed more significant catalytic activity for the removal of nitrobenzene (Kang et al. 2013). It was reported that when the ozone concentration increased from 0.4 mg/L to 1.7 mg/L, the removal efficiency of nitrobenzene increased from 45% to 92%. The variation of the removal efficiency depended on the initial aqueous solution pH because the concentration of OH^- led to ozone decomposition to generate hydroxyl radicals. The higher water pH value led to the quenching of hydroxyl radicals, resulting in the reduction of catalytic activity of RM6.0.

Cerium-modified red mud (Ce/RM) catalysts were prepared by the doping method, and applied for the degradation and detoxification of bezafibrate (BZF) in the aqueous phase (Xu et al. 2016a). Xu et al. (2016a) reported two findings: (1) surface texture (specific surface area and mesoporous volume) influenced the catalytic reaction pathway; and (2) the Ce(III) species and oxygen vacancies were generated on the surface of the catalyst after cerium modification, which played an important role in the development of the catalytic activity of cerium-modified red mud. Cerium-modified red mud exhibited better activity and 96.0% removal efficiency was achieved in less than 5.0 min oxidation. Xu et al. (2016b) again prepared cobalt-modified red mud (Co/RM) by impregnation method and used for bezafibrate (BZF) degradation. The kinetics analysis showed that the BZF degradation was due to quenching of HO^- in solution, and not the surface chelation reaction. The BZF degradation and mineralization performances of a red mud catalyst doped with cobalt (Co/RM) during the ozonation reaction have been evaluated (Li et al. 2014). The decomposition ability of Co/RM was reported to be over 83.3% in 10 min.

Waste red mud was used to develop an effective catalyst by heating activation to enhance nitrobenzene (NB) removal from aqueous solution by ozonation (Qi et al. 2014). Qi et al. (2014) reported that the catalyst prepared by heating red mud at 400°C for 4 h showed the highest activity in catalytic ozonation of NB. Removal of phenol from aqueous solutions by nitric acid-activated red mud has also been examined (Shirzad-Siboni et al. 2013). The removal percentage of phenol was initially increased, as the solution pH increased from 3 to 7, and then decreased above neutral pH. The adsorption result showed that equilibrium data followed the Freundlich isotherm, and kinetic data was well described by a pseudo-second-order kinetic model. The removal of organ chlorine pesticides (OCPs) from aqueous solutions using neutralized red mud was studied (Ozcan et al. 2011). Approximately

TABLE 7.4

Summary of Adsorption Capacity of Red Mud for the Removal of Different Phenolic Pollutants

Adsorbent	Adsorbate	Temperature (°C)	pH	Amount Adsorbed/% Removal	Reference
Red mud	Phenol	30–50	6	0.63–0.74 mol/g	Gupta et al. 2004b
Red mud	2-chlorophenol	30–50	6	0.72–0.79 mol/g	Gupta et al. 2004b
Red mud	4-chlorophenol	30–50	5	0.78–0.82 mol/g	Gupta et al. 2004b
Red mud	2,4-dichlorophenol	30–50	4	0.80–0.85 mol/g	Gupta et al. 2004b
Neutralized red mud	Phenol	–	–	4.12 mg/g	Tor et al. 2006
HNO ₃ -modified red mud	Bisphenol	–	3	84%	Ali et al. 2013
HCl-activated red mud	Phenol	25 ± 1	6	8.156 mg/g	Tor et al. 2009

0.2 g of red mud was able to remove 99% of aldrin from 100 mL of aqueous samples (10 mg/L) at pH 1. The adsorption of aldrin was explained according to the electrostatic interaction between the positively charged $\equiv \text{MOH}_2^+$ groups on the surface of the red mud and negatively charged (d[–]) chlorine atoms of the aldrin molecule. The kinetic study showed that the pseudo-second-order kinetic model was found to be well suited for the adsorption process and mainly controlled by the film diffusion mechanism. Removal of benzene from aqueous solution was examined using red mud as the adsorbent (Souza et al. 2011). The benzene adsorption process took 1 h to attain equilibrium and followed the pseudo-second-order model. The maximum amount of benzene removal was found to be 98%. A summary of adsorption capacity of red mud for the removal of different phenolic pollutants is presented in Table 7.4.

7.2.5 Utilization of Red Mud to Purify Toxic Waste Gases

Treatment of waste gases is very important in modern industrialization practices. Various methods (biological, chemical, and physical) are available for removal of solute gases from waste gas streams. Toxic waste gases such as H₂S, SO_x, NO_x, CO₂, and CO obtained from fossil fuel and different industrial processes have numerous deleterious effects on human health and the environment. Thus, treatment of waste streams from the chemical plants is a major challenge to technological advancement. However, it is beneficial to use bauxite residues as a low-cost raw material for the absorption and purification of toxic waste gases.

The concentration of nitrogen oxides (NO_x) in engines that use biodiesel as fuel is higher compared to conventional diesel engine exhaust. The utilization of red mud with dielectric barrier discharge plasma generated by high frequency alternating current (AC) in cascade to enhance the efficiency of NO_x removal in biodiesel run engine exhaust was investigated (Bhattacharyya and Rajanikanth 2015a). It was reported that the first reactor, having a gap length of 3.11 mm, achieved an NO_x removal efficiency of 61%, and the other, having a gap length of 2.8 mm, displayed an efficiency of 72%, more or less similar to the first reactor. In another work, Bhattacharyya and Rajanikanth (2015b) used red mud as an adsorbent for the removal of NO_x. It was reported that the plasma–bauxite residue combination showed good synergistic properties and enhanced the NO_x removal up to about 90%. Red mud was used as catalyst for the conversion of associated petroleum gas (APG) into carbon that can be stored, transported, and then converted to syngas by oxidation with H₂O (Teixeira et al. 2014). It was reported that red mud waste reduced and decomposed CH₄ to produce H₂ fuel and 27 wt% of carbon deposits.

Ce–Fe mixed metal oxide sorbent (C2F3B850) was prepared by using cerium oxide and red mud. Its desulfurization activity in a simulated coal-derived gas and regenerability through successive sulfurization–regeneration cycles was tested (Guo et al. 2014a). It was found that the addition of red mud in CeO_2 could decrease the sulfurization temperature, and 500°C is the best temperature for sulfurization in the range of 500°C to 700°C . After eight successive sulfurization–regeneration cycles over C2F3B850, the regenerated sorbent still performed well with no apparent deterioration. The average breakthrough sulfur capacity corresponding to H_2S concentrations below 50 ppmv is 9.97 (g S/100 g sorbent). In an investigation, red mud was activated by hydrochloric acid digestion and ammonia reprecipitation, and used as the support for preparation of copper oxide modified activated red mud (CuO/ARM) catalysts for carbon monoxide oxidation (Hu et al. 2016). The catalyst calcined at 200°C with 20% CuO loading amount demonstrated the highest catalytic activity with complete conversion of CO at 170°C , and good stability after 12 h of reaction without deactivation. In conclusion it was suggested that CuO/ARM was a promising catalyst for the CO oxidation reaction. The red mud modified by acid digestion and alkali reprecipitation method and used as the support to prepare the CuO/MRM nanocatalysts for carbon monoxide oxidation (Cao et al. 2015). In another work, Cao et al. (2014a) prepared modified red mud and employed it as the support for preparation of Ni/MRM catalysts by the impregnation method and investigated it for ammonia decomposition. It was reported that the content of Ni and the precalcination temperature can affect the catalytic properties of the catalysts remarkably, with the 12 wt.% nickel modified red mud (Ni/MRM) catalyst calcined at 600°C showing the highest activity. Furthermore, the same group reported that the Ni/MRM catalysts prepared by homogeneous precipitation method and used for ammonia decomposition (Cao et al. 2014b). The results of the catalytic activity measurements showed that these mesoporous nanostructured Ni/MRM catalysts were very active for ammonia decomposition. The catalyst with 15% Ni loading and calcined at 600°C exhibited the highest catalytic activity. It was shown that in both the cases (i.e., Ni/MRM prepared by impregnation method and the homogeneous precipitation method) the synergistic effect between Ni and nanostructure MRM support, the highly dispersed Ni species and high surface area of the catalysts were responsible for the high catalytic activity and hydrogen production.

7.2.6 Utilization of Red Mud for Preparation of Catalyst

In many industries, catalytic processes are widely used. Development of effective catalysts is the key issue for any catalytic reaction. In recent years, development of catalysts based on waste materials has drawn great interest. As red mud contains an important component, iron oxide, that can be employed as an iron metal precursor. In the past decades, some investigations have been carried out to use red mud as catalysts.

Modified red mud (MRM) was prepared by the sol-gel method and utilized for catalytic methane decomposition (CMD) to produce hydrogen (Fang et al. 2016). The catalytic performances of the catalysts have been tested at 800°C and the peak methane conversion was found to be 25.99%. ZrO_2 -impregnated macro-mesoporous red mud catalysts were successfully prepared for the catalytic cracking of vacuum residue (VR) in a steam atmosphere under a fixed-bed reaction condition at 500°C for 2 h (Nguyen-Huy and Shin 2016). It was found that the ZrO_2 -impregnated macro-mesoporous red mud catalysts exhibited better catalytic behavior for the steam catalytic cracking of VR as compared to the ZrO_2 -impregnated mesoporous red mud. The ZrO_2 -impregnated macro-mesoporous red mud catalyst showed excellent regenerability due to its large pore volume, good recovery of the hematite structure

in the iron oxide phase, and good stability of the macroporous structure after regeneration. ZrO_2 -impregnated red mud was prepared and applied as a novel catalyst for catalytic cracking of vacuum residue with steam (Lee et al. 2016). Under the batch reaction condition at 470°C for 2 h with superheated steam, 3 wt% ZrO_2 -impregnated red muds exhibited the best performance for catalytic cracking of vacuum residue. The better catalytic performance of 3 wt% ZrO_2 -impregnated red mud was due to large surface area and high catalyst stability. The large surface area of 3 wt% ZrO_2 -impregnated red mud could generate more active sites for hydrogenation, which induced a higher H/C ratio in liquid product.

Acidified/calcined red mud (ACRM) was prepared by acidification and calcination, and used as a catalyst for the degradation of butyl xanthate in Fenton-like process (Shao et al. 2016). In order to reduce the alkalinity of red mud, 0.5 mol/L mineral acid was added during stirring. After achieving the appropriate pH of red mud, the red mud was dried at 378 K. The dried residue (i.e., acidified red mud) was calcined at a predetermined temperature for a different time. After the acidification and calcination, ACRM was obtained. The degradation ratio of butyl xanthate reached 90.2% at 40 min under the following conditions: $[\text{H}_2\text{O}_2]_0 = 5 \text{ mmol/L}$, $[\text{ACRM}]_0 = 0.2 \text{ g/L}$. The degradation of butyl xanthate was well fitted by the second-order kinetic model, and ACRM showed an excellent long-term stability in the Fenton-like process. Red mud residue was used for the preparation of amphiphilic catalyst by mixing with carbon nanostructures and applied for the biphasic oxidation reactions of organic contaminants with H_2O_2 (Oliveira et al. 2014). The prepared amphiphilic catalysts were tested in oxidation of different model molecules, such as Sudan IV lipophilic dye, thiophene, dibenzothiophene, and quinolone, and showed very good removal, reaching 100% of contaminants oxidation. It was reported that the amphiphilic catalysts acted in two steps of biphasic oxidation: (1) favor the formation of a reversible emulsion between the organic contaminated phase and the aqueous oxidized phase, and (2) catalyze Fenton reaction. After reaction, the emulsion was easily separated by a magnetic process into two phases: decontaminated organic phase and aqueous phase with oxidized contaminants. In another work, gold nanoparticles were supported on the surface of three different matrixes based on red mud waste—pure red mud (Au/Rm), reduced red mud (Au/Rm H_2), and partially carbon coated red mud (Au/RmEt)—in order to produce different catalysts for desulfurization reactions (Oliveira et al. 2015). The catalysts were applied in biphasic desulfurization reactions with H_2O_2 and the catalyst Au/RmEt showed a remarkable efficiency in comparison with the other red mud-based catalysts.

A composite poly(ethylene terephthalate) modified red mud (RM/PET) material was prepared using red mud and poly(ethylene terephthalate) (PET) by mechanical mixture (10, 15, and 20 wt.% of PET powder/red mud) followed by a controlled thermal treatment at 400°C under air and used as a catalyst for the organic oxidation of the methylene blue dye (Bento et al. 2016). The catalytic tests showed that the composites presented higher capacity to remove methylene blue dye, presenting about 90% of removal after 24 h of reaction. The RM/PET catalysts showed to be stable during reaction and can be used for at least four reaction cycles. The physical properties and engine performance of biodiesel was investigated using conventional KOH and red mud in Mahua oil (Senthil et al. 2016). The author's used red mud as a catalyst for biodiesel to improve the economics of biodiesel processes. It was reported that a B50 blend of red mud biodiesel could be the best blending option in terms of its physical properties such as specific gravity, calorific value, pour point, and specific fuel consumption that decreased compared to KOH biodiesel. The red mud biodiesel possessed a lower fuel consumption of 0.6 kJ/kWh for a 25% blend. The engine performance was also at its optimum in comparison to diesel. Red mud biodiesel from Mahua oil could be a potential biodiesel blend for the future.

The feasibility of red mud powders (RMPs) as catalysts was studied for persulfate activation, and development of an effective, cost-efficient oxidation system for both wastewater treatment and in situ soil remediation, with sulfadiazine as the target contaminant was sought (Feng et al. 2016). Under the conditions of 2 g/L red mud powders and 1.75 mM persulfate, approximately 100% of the sulfadiazine could be degraded. Meanwhile, less than 10% of the persulfate was consumed after 180 min under the same conditions. Sulfate radicals were probably generated through the interactions between the red mud powders and persulfate and were responsible for degrading sulfadiazine. Feng reported that the red mud powders have a high stability and a persistent catalytic efficiency, with degradation rates of 94.0%, 92.5%, 92.1%, 87.5%, and 87.6% for the first, second, third, fourth, and fifth runs, respectively.

7.3 Conclusion

In this chapter, different processes for the utilization of red mud were discussed to solve problems related to the management of waste red mud. Each constituent of red mud is useful in isolation but is treated as waste in combination. Red mud consists of a wide range of fine particles and contains many metal oxides with porous structures. Because of surface reactivity and stability, researchers have widely investigated the adsorption capacity of red mud for different types of contaminants in both the liquid and solid phases and have found them to be efficient for the removal of anions, heavy metals, and organic pollutants (dyes and phenols) from water and wastewater. Furthermore, red mud has also been used for gas cleaning and as a catalyst for some industrial processes. The neutralization or modification of raw red mud with acid or heat treatment was found to considerably improve the sorption capacity of red mud. The utilization of red mud, an industrial solid waste, as a catalyst for wastewater treatment contributes to the betterment of the environment, as red mud itself creates a lot of problems for the environment. The utilization of red mud for a value-added process or product not only solves the problems of red mud but also creates a pathway to utilize the other industrial waste. It is clear from the preceding discussions that red mud is a novel low-cost material that represents a promising green technology for the future. Red mud can be used as an adsorbent for full-scale wastewater treatment, a photocatalyst for degradation of persistent organic pollutant, and a catalyst for synthesis of organic compounds. However, most of the published studies referred to experimentations at lab-scale. Furthermore, the majority of the studies focused on synthetic solutions with only a few studies reporting using real wastewater. More extensive research is required to convert the lab-scale reaction to commercial scale.

References

- Agrawal, A., K. K. Sahu, and B. D. Pandey. 2004. "A Comparative Adsorption Study of Copper on Various Industrial Solid Wastes." *AIChE Journal* 50 (10): 2430–2438.
- Akhurst, D. J., G. B. Jones, M. Clark, and D. McConchie. 2006. "Phosphate Removal from Aqueous Solutions Using Neutralised Bauxite Refinery Residues (Bauxsol™)." *Environmental Chemistry* 3: 65–74.

- Akin, I., G. Arslan, A. Tor, M. Ersoz, and Y. Cengeloglu. 2012. "Arsenic(V) Removal from Underground Water by Magnetic Nanoparticles Synthesized from Waste Red Mud." *Journal of Hazardous Materials* 235–236: 62–68.
- Ali, Z. Md., B. Davoud, M. Yousef, B. Mansour, and E. Masoumeh. 2013. "Adsorption of Bisphenol from Industrial Wastewater by Modified Red Mud." *Journal of Health and Development* 2 (1): 1–11.
- Alighardashi, A., H. Gharibi, Sh. Raygan, and A. Akbarzadeh. 2016. "Study of Novel Mechano-Chemical Activation Process of Red Mud to Optimize Nitrate Removal from Water." *Water Science and Technology* 73 (4): 899–908.
- Apak, R., E. Tutem, M. Hugul, and J. Hizal. 1998. "Heavy Metal Cation Retention by Unconventional Sorbents (Red Mud and Fly Ashes)." *Water Research* 32 (2): 430–440.
- Balarak, D., M. Yousef, and S. Sadeghi. 2015. "Adsorptive Removal of Acid Blue 15 Dye (AB15) from Aqueous Solutions by Red Mud: Characteristics, Isotherm and Kinetic Studies." *Scientific Journal of Environmental Sciences* 4 (5): 102–112.
- Bento, N. I., P. S. C. Santos, T. E. De Souza, L. C. A. Oliveira, and C. S. Castro. 2016. "Composites Based on PET and Red Mud Residues as Catalyst for Organic Removal from Water." *Journal of Hazardous Materials* 314: 304–311.
- Bhattacharyya, A., and B. S. Rajanikanth. 2015a. "Biodiesel Exhaust Treatment with HFAC Plasma Supported by Red Mud: Study on DeNO_x and Power Consumption." *Energy Procedia* 75: 2371–2378.
- Bhattacharyya, A., and B. S. Rajanikanth. 2015b. "Discharge Plasma Combined with Bauxite Residue for Biodiesel Exhaust Cleaning: A Case Study on NO_x Removal." *IEEE Transactions on Plasma Science* 43 (6): 1974–1982.
- Cao, J. L., Y. Wang, Z. Yan, and G. Li. 2014. "Polystyrene Microspheres-Templated Preparation of Hierarchical Porous Modified Red Mud with High Rhodamine B Dye Adsorption Performance." *Micro and Nano Letters* 9 (4): 229–231.
- Cao, J. L., Y. Wang, G. Li, K. Li, Y. Wang, and M. Ma. 2015. "Mesoporous Modified Red Mud Supported CuO Nanocatalysts for Carbon Monoxide Oxidation." *Current Nanoscience* 11 (4): 413–418.
- Cao, J. L., Z. L. Yan, Q. F. Deng, Y. Wang, Z. Y. Yuan, G. Sun, T. K. Jia, X. D. Wang, H. Bala, and Z. Y. Zhang. 2014a. "Mesoporous Modified-Red-Mud Supported Ni Catalysts for Ammonia Decomposition to Hydrogen." *International Journal of Hydrogen Energy* 39 (11): 5747–5755.
- Cao, J. L., Z. L. Yan, Q. F. Deng, Z. Y. Yuan, Y. Wang, G. Sun, X. D. Wang, B. Hari, and Z. Y. Zhang. 2014b. "Homogeneous Precipitation Method Preparation of Modified Red Mud Supported Ni Mesoporous Catalysts for Ammonia Decomposition." *Catalysis Science & Technology* 4: 361–368.
- Cengeloglu, Y., A. Tor, M. Ersoz, and G. Arslan. 2006. "Removal of Nitrate from Aqueous Solution by Using Red Mud." *Separation and Purification Technology* 51 (3): 374–378.
- Chandra, S. 1996. "Red Mud Utilization." In *Waste Materials Used in Concrete Manufacturing*, 292–295. Westwood, NJ: Noyes.
- Chen, H., J. Zheng, Z. Zhang, Q. Long, and Q. Zhang. 2016. "Application of Annealed Red Mud to Mn²⁺ Ion Adsorption from Aqueous Solution." *Water Science and Technology* 73 (11): 2761–2771.
- Chen, S., L. Fang, Q. Zhu, L. Li, and Z. Xing. 2016. "Bromate Removal by Fe(II)-akaganeite (β-FeOOH) Modified Red Mud Granule Material." *RSC Advances* 6 (34): 28257–28262.
- Cho, D. W., R. A. I. Abou-Shnab, Y. Kim, B. H. Jeon, and H. Song. 2011. "Enhanced Reduction of Nitrate in Groundwater by Zero-Valent Iron with Activated Red Mud." *Geosystem Engineering* 14: 65–70.
- Costa, R. C. C., F. C. C. Moura, P. E. F. Oliveira, F. Magalhaes, J. D. Ardisson, and R. M. Lago. 2010. "Controlled Reduction of Red Mud Waste to Produce Active Systems for Environmental Applications: Heterogeneous Fenton Reaction and Reduction of Cr(VI)." *Chemosphere* 78: 1116–1120.
- De Costa, J. C. P., M. L. P. Antunes, F. T. da Conceição, G. R. B. Navarro, and R. B. Moruzzi. 2015. "Removal of Reactive Dye from Aqueous Solution Using Thermally Treated Red Mud." *Desalination and Water Treatment* 55 (4): 1040–1047.

- De Oliveira, E. H. C., E. T. R. Mendonça, O. S. Barauna, J. M. Ferreira, and M. A. da Motta-Sobrinho. 2016. "Study of Variables for Optimization of the Dye Indosol Adsorption Process Using Red Mud and Clay as Adsorbents." *Adsorption* 22 (1): 59–69.
- De Souza, K. C., M. L. P. Antunes, S. J. Couperthwaite, F. T. da Conceição, T. R. de Barros, and R. Frost. 2013. "Adsorption of Reactive Dye on Seawater-Neutralised Bauxite Refinery Residue." *Journal of Colloid and Interface Science* 396: 210–214.
- Dias, F. F., A. A. S. Oliveira, A. P. Arcanjo, F. C. C. Moura, and J. G. A. Pacheco. 2016. "Residue-Based Iron Catalyst for the Degradation of Textile Dye via Heterogeneous Photo-Fenton." *Applied Catalysis B: Environmental* 186: 136–142.
- Fang, X., Q. Liu, P. Li, H. Li, F. Li, and G. Huang. 2016. "A Nanomesoporous Catalyst from Modified Red Mud and Its Application for Methane Decomposition to Hydrogen Production." *Journal of Nanomaterials* 2016: 1–8.
- Feng, Y., D. Wu, C. Liao, Y. Deng, T. Zhang, and K. Shih. 2016. "Red Mud Powders as Low-Cost and Efficient Catalysts for Persulfate Activation: Pathways and Reusability of Mineralizing Sulfadiazine." *Separation and Purification Technology* 167: 136–145.
- Fois, E., A. Lallai, and G. Mura. 2007. "Sulfur Dioxide Absorption in a Bubbling Reactor with Suspensions of Bayer Red Mud." *Industrial & Engineering Chemistry Research* 46: 6770–6776.
- Genc, H., J. C. Tjell, D. McConchie, and O. Schuiling. 2003. "Adsorption of Arsenate from Water Using Neutralized Red Mud." *Journal of Colloid and Interface Science* 264 (2): 327–334.
- Genc-Fuhrman, H. 2004a. "Arsenic Removal from Water Using Seawater-Neutralized Red Mud (Bauxsol)." Technical University of Denmark, Kongens Lyngby.
- Genc-Fuhrman, H., J. C. Tjell, and D. McConchie. 2004b. "Adsorption of Arsenic from Water Using Activated Neutralized Red Mud." *Environmental Science & Technology* 38: 2428–2434.
- Genc-Fuhrman, H., H. Bregnhøj, and D. McConchie. 2005. "Arsenate Removal from Water Using Sand-Red Mud Columns." *Water Research* 39 (13): 2944–2954.
- Genc-Fuhrman, H., J. C. Tjell, and D. McConchie. 2004c. "Increasing the Arsenate Adsorption Capacity of Neutralized Red Mud (Bauxsol)." *Journal of Colloid and Interface Science* 271 (2): 313–320.
- Guo, B., L. Chang, and K. Xie. 2014a. "Desulfurization Behavior of Cerium-Iron Mixed Metal Oxide Sorbent in Hot Coal Gas." *Industrial and Engineering Chemistry Research* 53 (21): 8874–8880.
- Guo, H., L. Yang, and X. Zhou. 2014b. "Simultaneous Removal of Fluoride and Arsenic from Aqueous Solution Using Activated Red Mud." *Separation Science and Technology* 49: 2412–2425.
- Gupta, V. K., M. Gupta, and S. Sharma. 2001. "Process Development for the Removal of Lead and Chromium from Aqueous Solutions Using Red Mud—An Aluminium Industry Waste." *Water Research* 35 (5): 1125–1134.
- Gupta, V. K., and S. Sharma. 2002. "Removal of Cadmium and Zinc from Aqueous Solutions Using Red Mud." *Environmental Science & Technology* 36 (16): 3612–3617.
- Gupta, V. K., S. I. Ali, and V. K. Saini. 2004a. "Removal of Rhodamine B, Fast Green, and Methylene Blue from Wastewater Using Red Mud, an Aluminum Industry Waste." *Industrial & Engineering Chemistry Research* 43 (7): 1740–1747.
- Gupta, V. K., I. Ali, and V. K. Saini. 2004b. "Removal of Chlorophenols from Wastewater Using Red Mud: An Aluminum Industry Waste." *Environmental Science & Technology* 38 (14): 4012–4018.
- Gupta, V. K., and I. Ali. 2006. "Removal of 2,4-Dinitrophenol from Wastewater by Adsorption Technology: A Batch and Column Study." *International Journal of Environment and Pollution* 27: 104–120.
- Hajjaji, W., R. C. Pullar, J. A. Labrincha, and F. Rocha. 2016. "Aqueous Acid Orange 7 Dye Removal by Clay and Red Mud Mixes." *Applied Clay Science* 126: 197–206.
- Hannachi, Y., N. A. Shapovalov, and A. Hannachi. 2010. "Adsorption of Nickel from Aqueous Solution by the Use of Low-Cost Adsorbents." *Korean Journal of Chemical Engineering* 27: 152–158.
- Hu, Z. P., Y. P. Zhu, Z. M. Gao, G. Wang, Y. Liu, X. Liu, and Z. Y. Yuan. 2016. "CuO Catalysts Supported on Activated Red Mud for Efficient Catalytic Carbon Monoxide Oxidation." *Chemical Engineering Journal* 302: 23–32.

- Huang, W., S. Wang, Z. Zhu, L. Li, X. Yao, V. Rudolph, and F. Haghseresht. 2008. "Phosphate Removal from Wastewater Using Red Mud." *Journal of Hazardous Materials* 158 (1): 35–42.
- Ju, S., S. Lu, J. Peng, L. Zhang, C. Srinivasakannan, S. Guo, and W. Li. 2012. "Removal of Cadmium from Aqueous Solutions Using Red Mud Granulated with Cement." *Transactions of Nonferrous Metals Society of China* 22: 3140–3146.
- Kalkan, E., H. Nadaroglu, N. Dikbas, E. Tasgin, and N. Celebi. 2013. "Bacteria-Modified Red Mud for Adsorption of Cadmium Ions from Aqueous Solutions." *Polish Journal of Environmental Studies* 22 (2): 417–429.
- Kang, Y., H. Li, B. Xu, F. Qi, and L. Zhao. 2013. "Catalytic Ozonation of Nitrobenzene in Water by Acidification-Activated Red Mud." *Chinese Journal of Environmental Science* 34 (5): 1790–1796.
- Khan, T. A., S. A. Chaudhry, and I. Ali. 2015. "Equilibrium Uptake, Isotherm and Kinetic Studies of Cd(II) Adsorption onto Iron Oxide Activated Red Mud from Aqueous Solution." *Journal of Molecular Liquids* 202: 165–175.
- Kurniawan, T. A., G. Y. S. Chan, W. Lo, and S. Babel. 2006. "Comparisons of Low-Cost Adsorbents for Treating Wastewaters Laden with Heavy Metals." *Science Total Environment* 366: 409–426.
- Le, X. T. Q., H. Wang, S. Ju, J. Peng, L. Zhou, and L. Dai. 2016. "Column Absorption and Regeneration Behavior of a Granular Red Mud for Treating Wastewater Containing Methylene Blue." *Desalination and Water Treatment* 57 (2): 728–737.
- Lee, H. S., C. Nguyen-Huy, T. T. Pham, and E. W. Shin. 2016. "ZrO₂-Impregnated Red Mud as a Novel Catalyst for Steam Catalytic Cracking of Vacuum Residue." *Fuel* 165: 462–467.
- Li, D., Y. Ding, L. Li, Z. Chang, Z. Rao, and L. Lu. 2015. "Removal of Hexavalent Chromium by Using Red Mud Activated with Cetyltrimethylammonium Bromide." *Environmental Technology* 36 (9–12): 1084–1090.
- Li, H., B. Xu, F. Qi, D. Sun, and Z. Chen. 2014. "Degradation of Bezafibrate in Wastewater by Catalytic Ozonation with Cobalt Doped Red Mud: Efficiency, Intermediates and Toxicity." *Applied Catalysis B: Environmental* 152–153 (1): 342–351.
- Li, Y., C. Liu, Z. Luan, X. Peng, C. Zhu, Z. Chen, Z. Zhang, J. Fan, and Z. Jia. 2006. "Phosphate Removal from Aqueous Solutions Using Raw and Activated Red Mud and Fly Ash." *Journal of Hazardous Materials* 137 (1): 374–383.
- Liu, C., Y. Li, Z. Luan, Z. Chen, Z. Zhang, and Z. Jia. 2007. "Adsorption Removal of Phosphate from Aqueous Solution by Active Red Mud." *Journal of Environmental Sciences* 19: 1166–1170.
- Luo, L., C. Ma, Y. Ma, S. Zhang, J. Lv, and M. Cui. 2011. "New Insights into the Sorption Mechanism of Cadmium on Red Mud." *Environmental Pollution* 159 (5): 1108–1113.
- Ma, M., G. Wang, Z. Yang, S. Huang, W. Guo, and Y. Shen. 2015. "Preparation, Characterization, and Photocatalytic Properties of Modified Red Mud." *Advances in Materials Science and Engineering* 2015: 1–6.
- Milenković, A., I. Smičiklas, M. Šljivić-Ivanović, and N. Vukelić. 2015. "Concurrent Co²⁺ and Sr²⁺ Sorption from Binary Mixtures Using Aluminum Industry Waste: Kinetic Study." *Russian Journal of Physical Chemistry A* 89 (13): 2461–2465.
- Mohanty, S., J. Pradhan, S. N. Das, and R. S. Thakur. 2004. "Removal of Phosphorus from Aqueous Solution Using Alumized Red Mud." *International Journal of Environmental Studies* 61: 687–697.
- Nadaroglu, H., E. Kalkan, and N. Celebi. 2010. "Removal of Copper from Aqueous Solution Using Red Mud." *Desalination* 251 (1–3): 90–95.
- Nadaroglu, H., E. Kalkan, and N. Celebi. 2014. "Azo Dye Removal from Aqueous Solutions Using Laccase-Modified Red Mud: Adsorption Kinetics and Isotherm Studies." *Annual Research & Review in Biology* 4 (17): 2730–2754.
- Namasivayam, C., and D. J. S. E. Arasi. 1997. "Removal of Congo Red from Wastewater by Adsorption onto Waste Red Mud." *Chemosphere* 34 (2): 401–417.
- Newson, T., T. Dyer, C. Adam, and S. Sharp. 2006. "Effect of Structure on the Geotechnical Properties of Bauxite Residue." *Journal of Geotechnical and Geoenvironmental Engineering* 132: 143–151.
- Nguyen-Huy, C., and E. W. Shin. 2016. "Amelioration of Catalytic Activity in Steam Catalytic Cracking of Vacuum Residue with ZrO₂-Impregnated Macro-Mesoporous Red Mud." *Fuel* 179: 17–24.

- Nguyen-Phu, H., C. Park, and W. S. Eun. 2016. "Activated Red Mud-Supported Zn/Al Oxide Catalysts for Catalytic Conversion of Glycerol to Glycerol Carbonate: FTIR Analysis." *Catalysis Communications* 85 (3): 52–56.
- Ni, F., J. He, Y. Wang, and Z. Luan. 2015. "Preparation and Characterization of a Cost-Effective Red Mud/polyaluminum Chloride Composite Coagulant for Enhanced Phosphate Removal from Aqueous Solutions." *Journal of Water Process Engineering* 6: 158–165.
- Oliveira, A. A. S., I. F. Teixeira, T. Christofani, J. C. Tristão, I. R. Guimarães, and F. C. C. Moura. 2014. "Biphasic Oxidation Reactions Promoted by Amphiphilic Catalysts Based on Red Mud Residue." *Applied Catalysis B: Environmental* 144 (1): 144–151.
- Oliveira, A. A. S., D. A. S. Costa, I. F. Teixeira, and F. C. C. Moura. 2015. "Gold Nanoparticles Supported on Modified Red Mud for Biphasic Oxidation of Sulfur Compounds: A Synergistic Effect." *Applied Catalysis B: Environmental* 162: 475–482.
- Ozcan, S., A. Tor, and M. E. Aydin. 2011. "Removal of Organochlorine Pesticides from Aqueous Solution by Using Neutralized Red Mud." *Clean: Soil, Air, Water* 39 (11): 972–979.
- Palmer, S. J., M. Nothling, K. H. Bakon, and R. L. Frost. 2010. "Thermally Activated Seawater Neutralised Red Mud Used for the Removal of Arsenate, Vanadate and Molybdate from Aqueous Solutions." *Journal of Colloid and Interface Science* 342 (1): 147–154.
- Piga, L., F. Pochetti, and L. Stoppa. 1993. "Recovering Metals from Red Mud Generated during Alumina Production." *Journal of Metals* 45 (11): 54–59.
- Prasad, P. M., J. S. Kachawha, R. C. Gupta, T. R. Mankhand, and J. M. Sharma. 1985. "Processing and Applications of Red Muds." In *Light Metals Science and Technology*, edited by C. Suryanarayana, P. M. Prasad, S. L. Malhotra, and T. R. Anantraman, 31–52. Switzerland: Trans Tech.
- Qi, F., H. Li, B. Xu, and D. Sun. 2014. "Heating Activated Red Mud Catalytic Ozonation for Degradation Nitrobenzene from Aqueous Solution: Performance and Influence of Preparation Factors." *Journal of Nanoscience and Nanotechnology* 19 (9): 6984–6990.
- Ratnamala, G. M., K. V. Shetty, and G. Srinikethan. 2012. "Removal of Remazol Brilliant Blue Dye from Dye-Contaminated Water by Adsorption Using Red Mud: Equilibrium, Kinetic, and Thermodynamic Studies." *Water, Air, & Soil Pollution* 223 (2012): 6187–6199.
- Ratnamala, G. M., K. V. Shetty, and G. Srinikethan. 2013. "Optimization Studies for Removal of Remazol Brilliant Blue Dye from Aqueous Solution Using Acid Treated Red Mud." *International Journal of Current Engineering and Technology*, 161–167.
- Ratnamala, G. M., K. V. Shetty, and G. Srinikethan. 2016. "Isotherm, Kinetics, and Process Optimization for Removal of Remazol Brilliant Blue Dye from Contaminated Water Using Adsorption on Acid-Treated Red Mud." *Desalination and Water Treatment* 57 (24): 11361–11374.
- Rubinos, D. A., and M. T. Barral. 2015. "Use of Red Mud (Bauxite Residue) for the Retention of Aqueous Inorganic mercury(II)." *Environmental Science and Pollution Research* 22: 17550–17568.
- Sadler, B. A., S. Lu, T. Le, S. Ju, J. Peng, and L. Zhang. 2013. "Removal of Methylene Blue from Aqueous Solutions Using a Novel Granular Red Mud Mixed with Cement." In *Light Metals 2013*, edited by B. A. Sadler. Hoboken, NJ: John Wiley & Sons.
- Sahu, M. K., S. Mandal, S. S. Dash, P. Badhai, and R. K. Patel. 2013. "Removal of Pb(II) from Aqueous Solution by Acid Activated Red Mud." *Journal of Environmental Chemical Engineering* 1 (4): 1315–1324.
- Sahu, M. K., S. Mandal, L. S. Yadav, S. S. Dash, and R. K. Patel. 2015. "Equilibrium and Kinetic Studies of Cd(II) Ion Adsorption from Aqueous Solution by Activated Red Mud." *Desalination and Water Treatment* 2: 1–15.
- Sahu, M. K., and R. K. Patel. 2015. "Removal of Safranin-O Dye from Aqueous Solution Using Modified Red Mud: Kinetics and Equilibrium Studies." *RSC Advances* 5 (96): 78491–78501.
- Sahu, M. K., and R. K. Patel. 2016. "Novel Visible-Light-Driven Cobalt Loaded Neutralized Red Mud (Co/NRM) Composite with Photocatalytic Activity toward Methylene Blue Dye Degradation." *Journal of Industrial and Engineering Chemistry* 40: 72–82.
- Sahu, R. C., R. K. Patel, and B. C. Ray. 2010. "Utilization of Activated CO₂-Neutralized Red Mud for Removal of Arsenate from Aqueous Solutions." *Journal of Hazardous Materials* 179 (1–s3): 1007–1013.

- Santona, L., P. Castaldi, and P. Melis. 2006. "Evaluation of the Interaction Mechanisms between Red Muds and Heavy Metals." *Journal of Hazardous Materials* 136 (2): 324–329.
- Schmitz, C. 2006. "Red Mud Disposal." In *Handbook of Aluminium Recycling*, 18. New York: McGraw Hill.
- Senthil, M. K., K. Visagavel, C. G. Saravanan, and K. Rajendran. 2016. "Investigations of Red Mud as a Catalyst in Mahua Oil Biodiesel Production and Its Engine Performance." *Fuel Processing Technology* 149: 7–14.
- Shao, L., G. Wei, Y. Wang, Z. Li, L. Zhang, S. Zhao, and M. Zhou. 2016. "Preparation and Application of Acidified/Calcined Red Mud Catalyst for Catalytic Degradation of Butyl Xanthate in Fenton-Like Process." *Environmental Science and Pollution Research* 23 (15): 15202–15207.
- Shirzad-Siboni, M., S. J. Jafari, O. Giahi, I. Kim, S. M. Lee, and J. K. Yang. 2014. "Removal of Acid Blue 113 and Reactive Black 5 Dye from Aqueous Solutions by Activated Red Mud." *Journal of Industrial and Engineering Chemistry* 20: 1432–1437.
- Shirzad-Siboni, M., S. J. Jafari, M. Farrokhi, and J. K. Yang. 2013. "Removal of Phenol from Aqueous Solutions by Activated Red Mud: Equilibrium and Kinetics Studies." *Environmental Engineering Research* 18 (4): 247–252.
- Smiljanić, S., I. D. Smičiklas, A. Perić-Grujić, B. Lončar, and M. Mitrić. 2010. "Rinsed and Thermally Treated Red Mud Sorbents for Aqueous Ni^{2+} Ions." *Chemical Engineering Journal* 162 (1): 75–83.
- Soldán, M., L. Blinová, J. Fiala, B. Galbičková, J. Ševčíková, and H. Kobetičová. 2014. "Adsorption of Phenol on Red Mud." *Advanced Materials Research* 864–867: 1759–1762.
- Souza, R. S., H. S. el Didi, and M. G. C. da Silva. 2011. "Removal of Benzene from Aqueous Solution Using Raw Red Mud." *Chemical Engineering Transactions* 24: 1225–1230.
- Teixeira, I. F., T. P. V. Medeiros, P. E. Freitas, M. G. Rosmaninho, J. D. Ardisson, and R. M. Lago. 2014. "Carbon Deposition and Oxidation Using the Waste Red Mud: A Route to Store, Transport and Use Offshore Gas Lost in Petroleum Exploration." *Fuel* 124: 7–13.
- Tor, A., Y. Cengeloglu, M. E. Aydin, and M. Ersoz. 2006. "Removal of Phenol from Aqueous Phase by Using Neutralized Red Mud." *Journal of Colloid and Interface Science* 300 (2): 498–503.
- Tor, A., Y. Cengeloglu, and M. Ersoz. 2009. "Increasing the Phenol Adsorption Capacity of Neutralized Red Mud by Application of Acid Activation Procedure." *Desalination* 242 (1–3): 19–28.
- Tor, A., N. Danaoglu, G. Arslanb, and Y. Cengeloglu. 2009a. "Removal of Fluoride from Water by Using Granular Red Mud: Batch and Column Studies." *Journal of Hazardous Materials* 164 (1): 271–278.
- Wagh, A. S., and P. Desai (eds.). 1987. "Bauxite Tailings: Red Mud." Kingston: Jamaican Bauxite Institute and the University of West Indies.
- Wang, Y., L. Zhang, Z. Yan, L. Shao, H. Kang, G. Wei, and M. Zhou. 2016. "Application of a Low-Cost Bagasse Carbon-Red Mud (BCRM) Adsorbent for Adsorption of Methylene Blue Cationic Dye: Adsorption Performance, Kinetics, Isotherm, and Thermodynamics." *Desalination and Water Treatment* 57 (15): 7109–7119.
- Wei, N., Z. K. Luan, J. Wang, L. Shi, Y. Zhao, and J. W. Wu. 2009. "Preparation of Modified Red Mud with Aluminum and Its Adsorption Characteristics on Fluoride Removal." *Chinese Journal of Inorganic Chemistry* 25: 849–854.
- Xu, B., F. Qi, D. Sun, Z. Chen, and D. Robert. 2016a. "Cerium Doped Red Mud Catalytic Ozonation for Bezafibrate Degradation in Wastewater: Efficiency, Intermediates, and Toxicity." *Chemosphere* 146: 22–31.
- Xu, B., F. Qi, J. Zhang, H. Li, D. Sun, D. Robert, and Z. Chen. 2016b. "Cobalt Modified Red Mud Catalytic Ozonation for the Degradation of Bezafibrate in Water: Catalyst Surface Properties Characterization and Reaction Mechanism." *Chemical Engineering Journal* 284: 942–952.
- Ye, J., X. Cong, P. Zhang, E. Hoffmann, G. Zeng, Y. Liu, W. Fang, Y. Wu, and H. Zhang. 2015c. "Interaction between Phosphate and Acid-Activated Neutralized Red Mud during Adsorption Process." *Applied Surface Science* 356: 128–134.
- Ye, J., X. Cong, P. Zhang, E. Hoffmann, G. Zeng, Y. Wu, H. Zhang, and W. Fan. 2015a. "Phosphate Adsorption onto Granular-Acid-Activated-Neutralized Red Mud: Parameter Optimization, Kinetics, Isotherms, and Mechanism Analysis." *Water, Air, & Soil Pollution* 226 (9): 306–316.

- Ye, J., X. Cong, P. Zhang, E. Hoffmann, G. Zeng, Y. Wu, H. Zhang, and W. Fang. 2015b. "Preparation of a New Granular Acid-Activated Neutralized Red Mud and Evaluation of Its Performance for Phosphate Adsorption." *ACS Sustainable Chemistry and Engineering* 3 (12): 3324–3331.
- Ye, J., X. Cong, P. Zhang, G. Zeng, E. Hoffmann, Y. Liu, Y. Wu, H. Zhang, W. Fang, and H. H. Hahn. 2016b. "Application of Acid-Activated Bauxsol for Wastewater Treatment with High Phosphate Concentration: Characterization, Adsorption Optimization, and Desorption Behaviors." *Journal of Environmental Management* 167: 1–7.
- Ye, J., X. Cong, P. Zhang, G. Zeng, E. Hoffmann, Y. Wu, H. Zhang, and W. Fang. 2016a. "Operational Parameter Impact and Back Propagation Artificial Neural Network Modeling for Phosphate Adsorption onto Acid-Activated Neutralized Red Mud." *Journal of Molecular Liquids* 216: 35–41.
- Yue, Q., Y. Zhao, Q. Li, W. Li, B. Gao, S. Han, Y. Qi, and H. Yu. 2010. "Research on the Characteristics of Red Mud Granular Adsorbents (RMGA) for Phosphate Removal." *Journal of Hazardous Materials* 176: 741–748.
- Zazouli, M. A., D. Balarak, Y. Mahdavi, and M. Ebrahimi. 2013. "Adsorption Rate of 198 Reactive Red Dye from Aqueous Solutions by Using Activated Red Mud." *Iranian Journal of Health Sciences* 1 (1): 36–43.
- Zhang, L., H. Zhang, W. Guo, and Y. Tian. 2014. "Removal of Malachite Green and Crystal Violet Cationic Dyes from Aqueous Solution Using Activated Sintering Process Red Mud." *Applied Clay Science* 93–94: 85–93.
- Zhang, S., C. Liu, Z. Luan, X. Peng, H. Ren, and J. Wang. 2008. "Arsenate Removal from Aqueous Solutions Using Modified Red Mud." *Journal of Hazardous Materials* 152 (2): 486–492.
- Zhang, Y., W. Chen, G. Lv, F. Lv, P. K. Chu, W. Guo, B. Cui, R. Zhang, and H. Wang. 2012. "Adsorption of Polyvinyl Alcohol from Wastewater by Sintered Porous Red Mud." *Water Science & Technology* 65 (11): 2055–2060.
- Zhao, Y., Y. Niu, X. Hu, B. Xi, X. Peng, W. Liu, W. Guan, and L. Wang. 2016. "Removal of Ammonium Ions from Aqueous Solutions Using Zeolite Synthesized from Red Mud." *Desalination and Water Treatment* 57 (10): 4720–4731.
- Zhao, Y., J. Wang, Z. Luan, X. Peng, Z. Liang, and L. Shi. 2009. "Removal of Phosphate from Aqueous Solution by Red Mud Using a Factorial Design." *Journal of Hazardous Materials* 165: 1193–1199.
- Zhao, Y., Q. Yue, Q. Li, X. Xu, Z. Yang, X. Wang, B. Gao, and H. Yu. 2012. "Characterization of Red Mud Granular Adsorbent (RMGA) and Its Performance on Phosphate Removal from Aqueous Solution." *Chemical Engineering Journal* 193–194: 161–168.
- Zhu, C., Z. Luan, Y. Wang, and X. Shan. 2007. "Removal of Cadmium from Aqueous Solutions by Adsorption on Granular Red Mud (GRM)." *Separation and Purification Technology* 57 (1): 161–169.



Taylor & Francis

Taylor & Francis Group

<http://taylorandfrancis.com>

Dolochar as a Low-Cost Adsorbent for the Removal of Pb(II) from Aqueous Solutions

Gayatree Patra and B. C. Meikap

CONTENTS

8.1	Introduction	163
8.2	Materials and Methods	165
8.2.1	Adsorbent for Lead Removal	165
8.2.2	Adsorbate	166
8.3	Pore Structure Characterization	166
8.4	Method of Experiment	167
8.5	Results and Discussion	167
8.5.1	Zero Point Charge (pH Drift Method)	167
8.5.2	Effect of Solution pH on Pb Adsorption	168
8.5.3	Effect of Contact Time	169
8.5.4	Effect of Adsorbent Dosage	169
8.5.5	Effect of Adsorption Particle Size	169
8.5.6	Kinetic Model	171
8.5.6.1	Pseudo-First-Order Model	171
8.5.6.2	Pseudo-Second-Order Model	171
8.5.7	Adsorption Isotherms	172
8.5.8	Effect of Temperature on Pb(II) Adsorption	173
8.5.9	Thermodynamic Parameters	174
8.6	Conclusions	175
	References	176

8.1 Introduction

A large amount of heavy metal usage in industrial processes and fast growing industrialization have resulted in the increase of heavy metals in industrial wastewater. Heavy metals including cadmium, chromium, mercury, arsenic, lead, and copper are toxic in nature when they enter into the ecosystem. The main sources from where lead enters into the ecosystem are lead-acid batteries, metal phosphate fertilizer, paint, electronics, mining activity, automobile emission, and wastewater from many industries. Lead (Pb) is a poisonous metal that is not essential for mammals and may cause headache, anemia, and diarrhea. It becomes toxic in human beings at a dosage of 800 mg, and causes harm to the brain, kidney, liver, central nervous system, and reproduction system (Singh et al., 2008). Hence, lead removal from wastewater is significantly important.

The higher concentrations of lead in the environment aggravates the harmful effects to the ecosystem. Therefore, the concentration must be reduced to an allowable level according to national and international health organization standards. According to the World Health Organization (WHO), the limit of lead was 0.05 mg/l in 1995, which was decreased to 0.01 mg/l in 2010. Lead restricts plant chlorophyll synthesis.

The conventional treatment methods of wastewaters containing lead are precipitation, filtration, electrochemical reduction, coagulation, ion exchange, reverse osmosis, evaporation, and membrane processes. However, these methods have many disadvantages, such as the need for more reagents and energy consumption, incomplete metal removal, high cost, and creation of secondary wastes that creates a disposal problem. For example, among the traditional methods the membrane filtration process is a useful way to remove heavy metals. But this method is not economically feasible. For high concentrations of heavy metals in wastewater, the conventional methods can be suitable, but for low concentrations the techniques are ineffective.

Among the heavy metal treatment methods, adsorption is the most proven technique because the process has significant advantages such as low cost, high selectivity, high efficiency for removal of very low concentrations of heavy metal ions from dilute solutions, easy to handle, less sludge production, and regeneration of adsorbent. However, adsorption of heavy metals using activated carbon is the most widely used treatment method. Activated carbon is an expensive adsorbent due to its high industrial demand. Replacement of the high-cost activated carbon is the main research interest. Agricultural and industrial solid wastes are used for this purpose. Some examples are activated groundnut husk carbon (Periasamy et al., 1991), hazelnut shell activated carbon (Kobya, 2004), *Terminalia arjuna* nuts activated carbon (Mohanty et al., 2005), olive cake (Doyurum and Celik, 2006), tea waste activated carbon (Amarasinghe and Williams, 2007), coconut shell (Dwivedi et al., 2008), Ceiba pentandra hulls (Madhava Rao et al., 2008), Tamarind wood activated carbon (Acharya et al., 2009; Singh et al., 2008), and rice husk carbon (Sahu et al., 2009). Issabayeva et al. (2006) worked on palm shell activated carbon. Srivastava et al. (1997) and Dimitrova and Mehandgiev (1998) worked on activated slag (a blast furnace waste) and granulated blast furnace slag, respectively. Peat (Ho and McKay, 1999), red mud from the aluminum industry (Gupta et al., 2001; Pradhan et al., 1999), heat-activated bauxite (Erdem et al., 2004), and fly ash (Rastogi et al., 2008) are used for removal of heavy metals. Dolochar is a carbonaceous material and has a porous nature that makes it ideal for adsorption. This material can be used for removal of heavy metal ions like Pb(II) from wastewater.

Rotary kiln during direct reduction of iron (DRI) produces large quantities of solid waste materials such as coal fines and dolochar. Coal fines having higher calorific value are generally used in coal-fired furnaces as fuel, but dolochar having low calorific value creates serious environmental problems. Dolochar (black dust) is a waste that is generated from the sponge iron industry. Dolochar, which comes out of the system as a by-product, poses serious environmental and disposal problems. Dolochar generally consists of unburnt coal fused with iron oxide and calcium oxide. DRI units have spread over the Indian states of Odisha, Jharkhand, Chhattisgarh, West Bengal, Karnataka, Tamil Nadu, Andhra Pradesh, and Goa. A 100 tons capacity DRI plant produces 40 tons of dolochar per day, resulting in 14,600 tons in a year. Annually, India produces 32 million tons of sponge iron. However, the waste generated (dolochar) poses a serious disposal problem (Dwari et al., 2012). Very few plants in India have come forward for utilization of dolochar as a fuel for captive power generation. Generally, boiler plants accept dolochar having more than 20% fixed carbon by weight and having a gross calorific value of 1800 to 2000 kcal/kg (Panda et al., 2011). However, in India, most of the sponge iron industries generate dolochar

containing less than 19% fixed carbon and 1% to 7% volatile matter. The dolochar samples contain 70% to 80% of ash with the absence of volatile matter (very small), and hence cannot be reused as a fuel substitute.

Dolochar can be used as an adsorbent because of its requisite porosity, which makes it favorable for adsorption. In this study, dolochar is used as an adsorbent for removal of Pb(II) from aqueous solution. Our main objective is to utilize dolochar as an adsorbent and possibility of replacing high-cost adsorbent.

8.2 Materials and Methods

8.2.1 Adsorbent for Lead Removal

The sample required for the experiment was collected from a sponge iron plant located in Rourkela, Odisha, India. The sample was washed with distilled water several times to remove contaminant and dried at 100°C for 2 hours. The material was ground with the help of a laboratory ball mill with 50 balls. The powder form of dolochar, size ranging from 40 μm to 250 μm , was used. This powder dolochar was stored in airtight bottles for the experiment. The proximate analysis of the dolochar sample was conducted following the standard method for coal sample. The proximate analysis data and the x-ray fluorescence (XRF) data of the sample are given in Tables 8.1 and 8.2, respectively.

TABLE 8.1

Proximate Analysis of Dolochar Sample

Constituents	Composition (mass%)
Ash	74.5
Moisture	4.5
Volatile matter	2
Fixed carbon	19

TABLE 8.2

XRF Data of Dolochar

Compound	Concentration (%)	Compound	Concentration (%)
Na	0.0657	Fe	11.8629
Mg	2.42	Ni	0.0633
Al	29.7	Cu	0.0347
Si	42.8	Zn	0.0346
P	0.336	Ga	0.00865
S	2.96	Se	0.00667
Cl	0.207	Rb	0.0910
K	1.23	Sr	0.0499
Ca	5.25	Y	0.0170
Ti	2.41	Zr	0.119
Cr	0.0727	Nb	0.0107
Mn	0.219	Pb	0.0181

8.2.2 Adsorbate

Distilled water and $\text{Pb}(\text{NO}_3)_2$ is required for the stock preparation. One liter of 1000 mg/l stock was prepared. The concentrated solution (1000 mg/l) was diluted to 10–100 mg/l with distilled water. The solution pH was adjusted by adding the required amount of either NaOH or H_2SO_4 . Merck (India) analytical grade chemicals are required for this study.

8.3 Pore Structure Characterization

Scanning electron microscopy (SEM) was conducted on the dolochar sample to analyze its surface structure and porosity under the optimum condition. In this analysis, JEOL-JSM field emission SEM images were recorded. During SEM imaging, a gold coating was required for charge dissipation. The SEM image of the dolochar sample is shown in Figure 8.1.

BET (Brunauer–Emmett–Teller) analysis gives the precise specific surface area of the sample using a fully automated BET analyzer (Flowsorb 2300). The basic principle of this analyzer is monolayer adsorption. A mixture of nitrogen and helium nearly 30% to 35% was used to form the monolayer. First, the sample quantity is optimized so that the surface area falls in the range of 0.5 to 2.5 m^2 . The sample free from any gases or vapors is dried in an air oven at 105°C. This analysis determines the surface area of the sample contained in the sample tube holder and the displayed number is converted to the specific surface area by dividing the weight of the sample. The BET surface area of dolochar was measured and found to be 208.59 m^2/g .

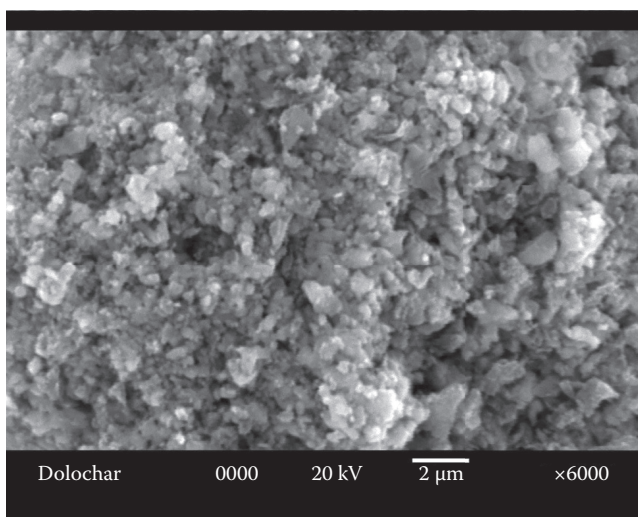


FIGURE 8.1
SEM image of dolochar sample.

8.4 Method of Experiment

Batch adsorption experiments were carried out by contacting 0.5 g of dolochar samples with 100 ml of aqueous solution of three different initial lead(II) concentrations: 10, 30, 50 mg/l. Batch experiments were conducted, as volume correction is not required for the batch process. Erlenmeyer flasks of 250 ml containing 100 ml of different Pb(II) concentrations were kept in a thermal shaker for a period of 1 hr. The experiments were performed at control temperature ($30^{\circ}\text{C} \pm 2^{\circ}\text{C}$). Continuous mixing was done during the whole experimentation with a constant agitation speed of 120 rpm. At this agitation speed, the interfacial area of contact is high, hence the mass transfer rate is high. At regular interval, the samples were taken from the shaker and filtered using Whatman filter paper. The carbon-free solution was analyzed by using atomic absorption spectroscopy (AAS).

The adsorbent phase retaining the Pb(II) concentration was calculated by using the equation

$$q_e = \frac{C_i - C_e}{w} V_i \quad (8.1)$$

where C_i is the initial concentrations (mg/l) of Pb(II) solution, C_e is the equilibrium concentrations (mg/l) of Pb(II) solution, v is the volume in liters, and w is the weight of the adsorbent in grams. Three replicates per sample were performed and the average results recorded.

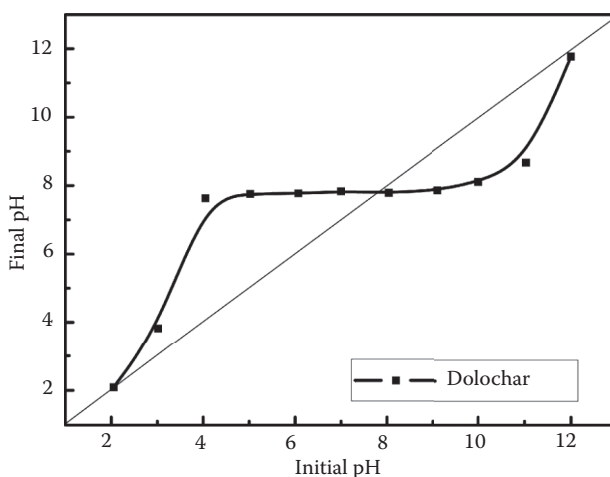
Sample concentration analysis was done using an atomic absorption spectrophotometer, which measures the concentration of metals present in the water sample. It detects the concentration of metals at the parts per million (ppm) level and only 1 ml of sample is required for one analysis. In this study, the concentration of Pb(II) at the ppm level was detected.

8.5 Results and Discussion

8.5.1 Zero Point Charge (pH Drift Method)

The zero point charge (ZPC) is the equilibrium pH value of a solution with a particle whose net charge from all sources is zero. Batch equilibrium methods were applied to determine the ZPC of the sample. For the analysis, 100 ml of 0.1 M NaCl solution was taken in a container. The pH was adjusted with NaOH and HCl to a value between 2 and 12. The initial pH was recorded. A 0.3 g dolochar sample was added into the 100 ml pH-adjusted solution and then sealed. The sealed containers were placed on a shaker for 24 hours, and then the final pH was measured. A graph of initial and final pH was plotted. The result is shown in Figure 8.2.

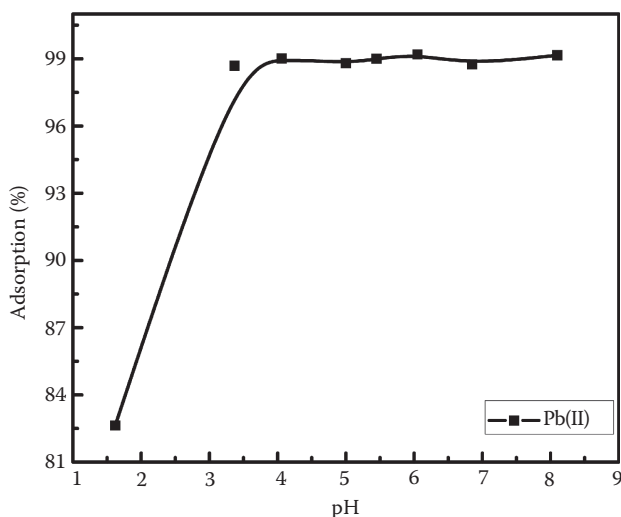
The ZPC occurs where there is no change in the pH after contact with the adsorbent. In this case, ZPC values were 2 and 7.8. Greater adsorption occurs when pH is above ZPC.

**FIGURE 8.2**

Initial pH verses final pH.

8.5.2 Effect of Solution pH on Pb Adsorption

The pH of the solution is one of the important parameters that affects the adsorption process. The effect of pH on Pb(II) adsorption was investigated by varying the pH of the sample. Adsorption (%) was calculated as a function of pH for the initial concentration of 10 mg/l for the adsorbent dose of 5 g/l, and the result is shown in Figure 8.3. From Figure 8.3 it is shown that the adsorption percentage of Pb(II) increases with an increase in pH from 1.5 to 3, and after 3 the adsorption was almost constant.

**FIGURE 8.3**

Effect of pH on adsorption of Pb(II) at initial feed concentration of 10 mg/l at constant temperature 30°C and adsorbent dose of 5 g/l.

8.5.3 Effect of Contact Time

The effect of contact time for initial Pb(II) concentrations of 10, 30, and 50 mg/l with the dolochar dose of 5 g/l at solution pH of 6 is shown in Figure 8.4. The lead adsorption increases with time up to 15 min, then it becomes almost constant as equilibrium is attained. The plot of time versus adsorption shows that the adsorption of Pb(II) increases with time from 0 to 15 min and then becomes almost constant up to the end of the experiment. The fast adsorption occurs at the initial stage due to the higher concentration gradient between the adsorbate in solution and the adsorbate in the adsorbent, as more vacant sites are available at the beginning.

8.5.4 Effect of Adsorbent Dosage

A comparison of different adsorbent (dolochar) doses with a constant pH of 6 at three different initial concentrations has been studied. The effect of adsorbent dosage on the adsorption efficiency is shown in Figure 8.5. It is clearly shown from Figure 8.5 that the adsorption initially increases sharply with the increase in adsorbent dose. The adsorption for Pb(II) increases from 83.6% to 99.45%, 60% to 92.2%, and 35% to 97.34% at 10, 30, and 50 mg/l initial Pb(II) concentration, respectively, with the increase in the adsorbent dosages from 1 to 5 g/l, for solution pH of 6, and at constant temperature of 30°C. Adsorption occurs more in higher dosage because more adsorbent sites are available for adsorption with an increase in adsorbent dose.

8.5.5 Effect of Adsorption Particle Size

The effect of adsorbent particle size was studied for initial Pb(II) concentrations of 10, 30, and 50 mg/l of Pb(II) at a constant temp of 30°C and pH of 6. The adsorbent size varied from 63 to 210 μm . Figure 8.6 shows the adsorption of Pb(II) at different particle sizes of adsorbent. The adsorption of Pb(II) decreases from 99.2% to 82.6%, 97.34% to 82.6%, and 97.34% to 82.6% at 10, 30, and 50 mg/l initial Pb(II) concentration, respectively, with the increase in the adsorbent particle size from 63 to 210 μm .

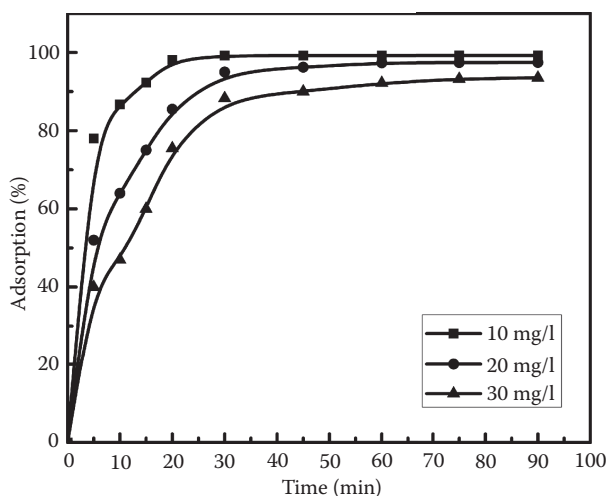
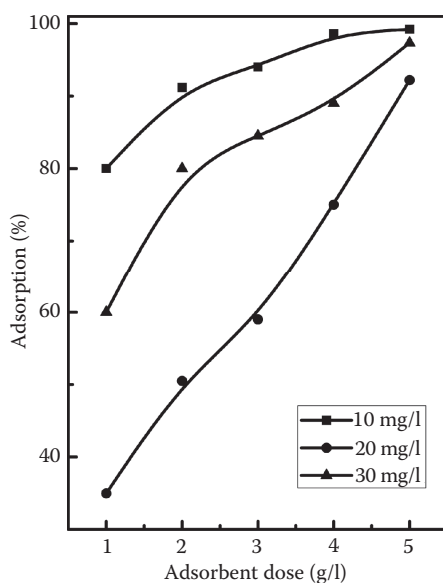
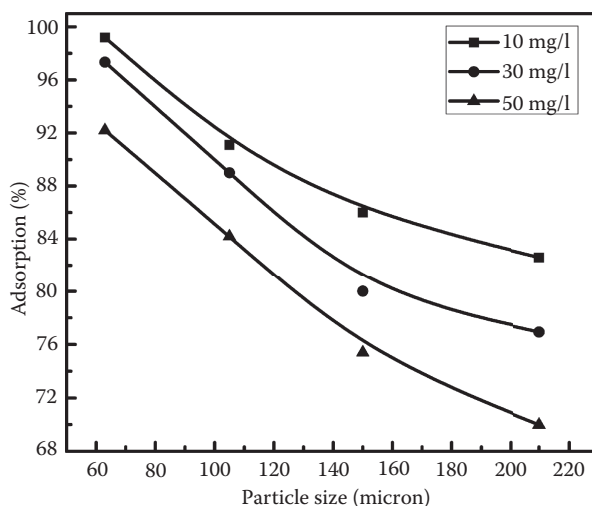


FIGURE 8.4

Effect of contact time on adsorption of Pb(II) at three different initial feed concentrations.

**FIGURE 8.5**

Effect of adsorbent doses on adsorption of Pb(II) at different initial feed concentrations.

**FIGURE 8.6**

Effect of particle size on adsorption of Pb(II).

to 82%, and 92.2% to 70% at 10, 30, and 50 mg/l initial Pb(II) concentration, respectively, with the increase in the particle size from 63 to 210 μm due to the decrease in surface area. Adsorption is a surface phenomenon. As the particle size increases, the surface area decreases, hence adsorption capacity decreases. In this case, adsorption capacity is highest on 63 μm particle sizes.

8.5.6 Kinetic Model

The pseudo-first-order and pseudo-second-order kinetic models were applied for the investigation of the controlling mechanism of the adsorption process.

8.5.6.1 Pseudo-First-Order Model

Lagergren proposed the pseudo-first order kinetic model. The model equation is

$$\log(q_e - q) = \log q_e - \frac{K_{ad}}{2.303} t \quad (8.2)$$

where q_e and q are the amount of Pb(II) adsorbed (mg/g) at equilibrium and at any time t (min) respectively, and K_{ad} is the pseudo-first-order equilibrium rate constant of adsorption (min^{-1}).

8.5.6.2 Pseudo-Second-Order Model

Pseudo-second-order kinetic model was used to fit the experimental data. The model equation is

$$\frac{t}{q} = \frac{1}{q_e^2 k_2} + \frac{t}{q_e} \quad (8.3)$$

where k_2 is the rate constant for the pseudo-second-order kinetic model. The applicability of the aforementioned two models can be examined by plotting $\log(q_e - q)$ versus time (min) and $\frac{t}{q}$ versus time (min), respectively, and are presented in Figures 8.7 and 8.8.

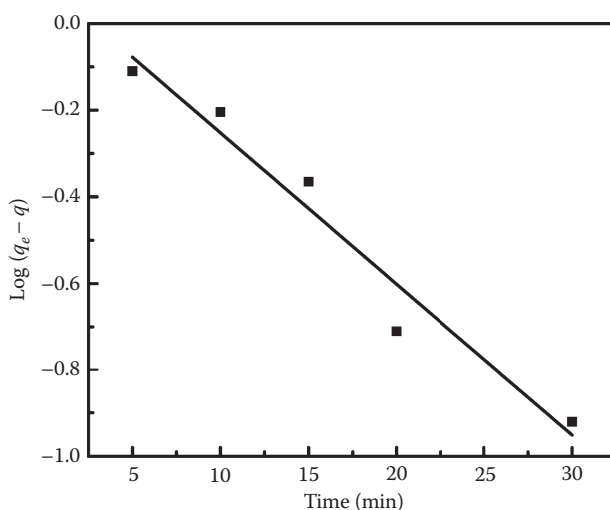
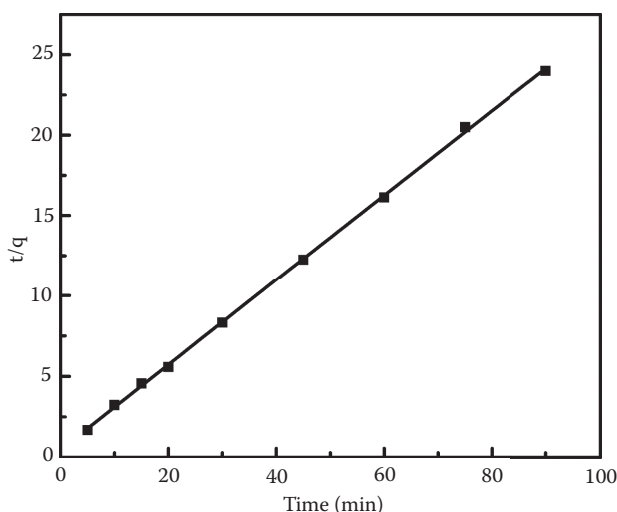


FIGURE 8.7

Kinetic of lead removal according to the pseudo-first-order model.

**FIGURE 8.8**

Kinetic of lead removal according to the pseudo-second-order model.

The correlation coefficient (R^2) is the measure of the applicability of these models and it was calculated from these plots. The correlation coefficients were 0.94 for and 0.99 for the pseudo-first-order model and pseudo-second-order model, respectively. This result indicated that the experimental data fits better for the pseudo-second-order model, hence indicating the chemisorption mechanism.

8.5.7 Adsorption Isotherms

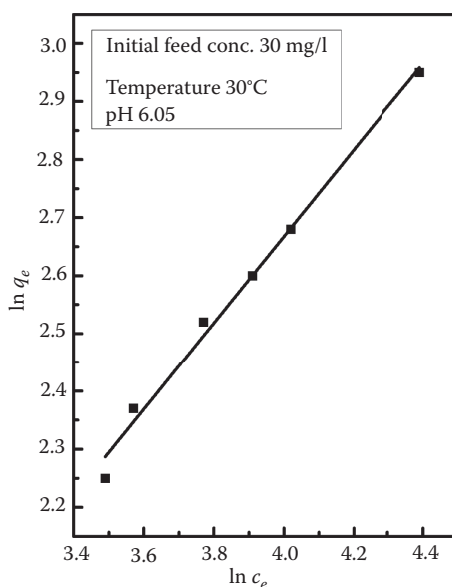
The equilibrium adsorption isotherm study is very much useful for the understanding of the adsorption mechanism. In the literature, several models have been used to describe the experimental data of adsorption isotherms. In this study, the equilibrium data for the Pb(II) adsorption on dolochar was applied for both the Freundlich and Langmuir models, because these models can be applied to a large variation of concentrations and, hence, are frequently used.

The Freundlich adsorption isotherm is expressed mathematically as

$$\ln q_e = \ln k + \frac{1}{n} \ln c_e \quad (8.4)$$

where q_e is the adsorbent capacity (mg/g), c_e is the equilibrium residual metal ion concentration (mg/l), the intercept $\ln k$ is a measure of adsorbent capacity, and $1/n$ is the adsorption intensity. The Pb(II) adsorption following the Freundlich model is shown in Figure 8.9.

The isotherm data fits well for the Freundlich model ($R^2 = 0.989$). The values of the constants k and $1/n$ were calculated to be 0.72 and 0.745. Since the value of $1/n$ is less than 1, it indicates a favorable adsorption.

**FIGURE 8.9**

Freundlich adsorption isotherm.

In the Langmuir adsorption isotherm, the solid phase adsorbate concentration (q_e) relates with the equilibrium liquid concentration (c_e) and is expressed as

$$q_e = \frac{k_l b c_e}{1 + b c_e} \quad (8.5)$$

where k_l and b are the Langmuir constant and the energy constant. k_l represents the maximum adsorption capacity and b is related to the heat of adsorption. The Pb(II) adsorption followed the Langmuir model is shown in Figure 8.10. From Figure 8.10 it can be understood that the isotherm data fits well for the Langmuir equation ($R^2 = 0.98$). The values of k_l and b were found from Figure 8.10 as 62.5 mg/g and 0.005 l/mg, respectively. The adsorption capacities of a few adsorbents are given in Table 8.3.

8.5.8 Effect of Temperature on Pb(II) Adsorption

Experiments were conducted for the temperature dependence of Pb(II) at five different temperatures—10°C, 20°C, 30°C, 40°C, and 50°C—with a constant adsorbent dose of 5 g/l for three different initial feed concentrations. The experimental results are shown in Figure 8.11. The adsorption increases from 96% to 99.34%, 85% to 98.1%, and 72% to 93.2% for three different initial feed concentrations of 10, 30, and 50 mg/l, respectively, with the increase in temperature from 10°C to 40°C. It can be seen from the Figure 8.11 that the adsorption percentage increases with the rise in temperature from 30°C to 40°C. After that, the adsorption remains almost constant. As adsorption increases with a rise in temperature, and the adsorbent is porous in nature, indicating that the sorption may be diffusion control. The increase of temperature is suitable for the transport of sorbate within the pores

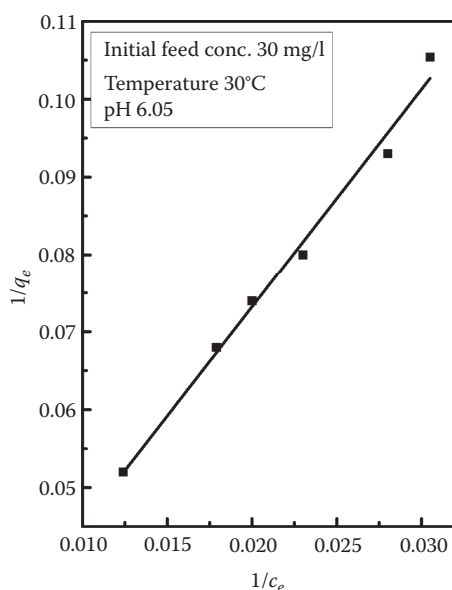


FIGURE 8.10
Langmuir adsorption isotherm.

TABLE 8.3
Adsorption Capacity of Pb(II) by Various Adsorbent

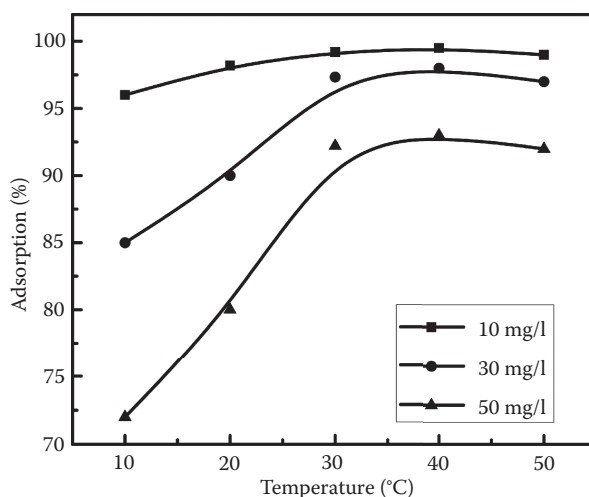
Adsorbent	Adsorption Capacities (mg/g)	Reference
Coir	18.9	Conrad and Hansen, 2007
Olive cake	18.14	Doyurum and Celik, 2006
Fly ash	15.08	Cho et al., 2005
Waste mud from copper mines	24.4	Ozdes et al., 2009
<i>Ceiba pentandra</i> hulls	25.5	Madhava Rao et al., 2008
Coconut shell activated carbon	21.88	Goel et al., 2005
Dolochar	62.5	Present study

of the sorbent. Adsorption with diffusion control is endothermic in nature, which showed that the sorption is endothermic in nature.

8.5.9 Thermodynamic Parameters

Free energy (ΔG°), enthalpy (ΔH°), and entropy (ΔS°) are the three important thermodynamic parameters. These parameters were determined from the Van't Hoff equation. The Van't Hoff equation is expressed as

$$\text{Log } k_c = \frac{\Delta S^\circ}{2.303} - \frac{\Delta H^\circ}{2.303RT} \quad (8.6)$$

**FIGURE 8.11**

Effect of temperature for different initial feed concentration at constant dose 5g/l and pH 6.

Change in free energy of adsorption, ΔG° , was calculated by using the following equation:

$$\Delta G^\circ = -RT \ln k_c \quad (8.7)$$

where R and T are the gas constant and temperature (kelvins), respectively, and k_c is the equilibrium constant which is evaluated from

$$K_c = \frac{C_{Ae}}{C_e} \quad (8.8)$$

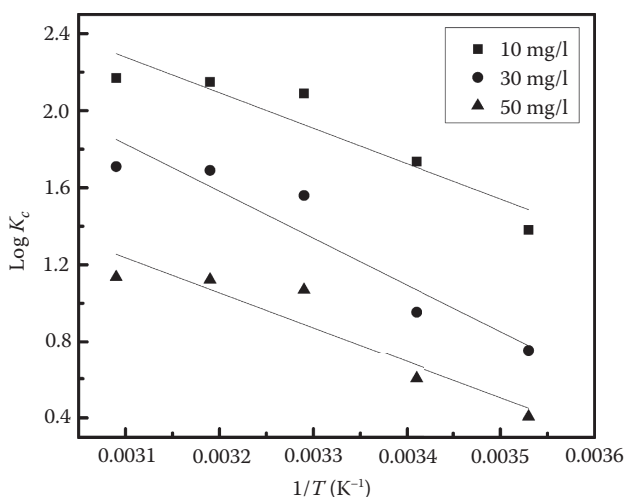
where C_{Ae} and C_e (mg/l) are the equilibrium concentration for the solute on the adsorbent and in the solution, respectively. A plot of $\log k_c$ versus $1/T$ for Pb(II) is shown in Figure 8.12.

The enthalpy (ΔH°) was calculated from the slope of the plot and the entropy (ΔS°) was obtained from the intercept of the plot, and both values are found to be positive. The thermodynamic parameters are given in Table 8.4.

The enthalpy of chemical adsorption should be greater than 21 kJ mol^{-1} (Ozdes et al., 2009). Hence, the values of enthalpy (ΔH°) indicate the chemisorption process. The positive values of entropy suggest an irreversible and stable process. The change in free energy (ΔG°) was found to be negative, indicating that the process is spontaneous in nature and also feasible.

8.6 Conclusions

Pb(II) removal from wastewater is possible by using abundantly available low-cost adsorbents. The present study shows that dolochar can be used as a low-cost adsorbent.

**FIGURE 8.12**

A plot against $\log k_c$ to $1/T$ for estimation of thermodynamic parameters for Pb(II) adsorption.

TABLE 8.4

Thermodynamic Parameter for the Adsorption of Pb(II)

C_i (mg/l)	ΔH° (kJ mol ⁻¹)	ΔS° (J mol ⁻¹ K ⁻¹)	ΔG° (kJ mol ⁻¹)				
			10°C	20°C	30°C	40°C	50°C
10	33	18.4	-7.48	-9.74	-12.13	-12.88	-13.48
30	46	21.6	-4.07	-5.35	-9.05	-10.13	-10.5
50	34	15.8	-2.21	-3.37	-6.21	-6.7	-7.02

Experiments on dolochar samples were carried out for initial Pb(II) concentrations of 10, 30, and 50 mg/l. At room temperature, a 99% removal of Pb(II) was possible. It was observed from the experimental data that adsorption of Pb(II) is very fast at the initial stage and almost constant while approaching equilibrium, and the experimental data fits well for the pseudo-second-order rate expression. The adsorption capacity of dolochar is greater than that of many adsorbents from industrial and agricultural wastes. The positive values of entropy and negative values of free energy indicate that the process is stable and spontaneous.

References

- Acharya, J., J. N. Sahu, B. K. Sahoo, C. R. Mphanty, B. C. Meikap. 2009. Removal of chromium(VI) from wastewater by activated carbon developed from Tamarind wood activated with zinc chloride. *Chemical Engineering Journal* 150: 25–39.
- Amarasinghe, B. M. W. P. K., R. A. Williams. 2007. Tea waste as a low cost adsorbent for the removal of Cu and Pb from waste water. *Chemical Engineering Journal* 132: 299–309.

- Cho, H., D. Oh, K. Kim. 2005. A study on removal characteristics of heavy metals from aqueous solutions by fly ash. *Journal of Hazardous Materials* B127: 187–195.
- Conrad, K., H. C. B. Hansen. 2007. Sorption of zinc and lead on coir. *Bioresource Technology* 98: 89–97.
- Dimitrova, S. V., D. R. Mehandgiev. 1998. Lead removal from aqueous solutions by granulated blast furnace slag. *Water Research* 32: 3289–3292.
- Doyurum, S., A. Celik. 2006. Pb(II) and Cd(II) removal from aqueous solutions by olive cake. *Journal of Hazardous Materials* 138: 22–28.
- Dwari, R. K., D. S. Rao, A. K. Swar, P. S. R. Reddy, B. K. Mishra. 2012. Characterization of dolochar wastes generated by the sponge iron waste. *International Journal of Minerals, Metallurgy and Materials* 19: 992–1003.
- Dwivedi, C. P., J. N. Sahu, C. R. Mohanty, B. Raj Mohan, B. C. Meikap. 2008. Column performance of granular activated carbon packed bed for Pb(II) removal. *Journal of Hazardous Materials* 156: 596–603.
- Erdem, M., H. S. Altundogan, F. Tumen. 2004. Removal of hexavalent chromium by using heat activated bauxite. *Minerals Engineering* 17: 1045–1052.
- Goel, J., K. Kadirvelu, C. Rajagopal, V. K. Garg. 2005. Removal of lead(II) by adsorption using treated granular activated carbon: Batch and column studies. *Journal Hazardous Materials* 125: 211–220.
- Gupta, V. K., M. Gupta, S. Sharma. 2001. Process development for the removal of lead and chromium from aqueous solutions using red mud—An aluminium industry waste. *Water Research* 35: 1125–1134.
- Ho, Y. S., G. McKay. 1999. The sorption of lead(II) ions on peat. *Water Research* 33: 578–584.
- Issabayeva, G., M. K. Aroua, N. M. N. Sulaiman. 2006. Removal of lead from aqueous solutions on palm shell activated carbon. *Bioresource Technology* 97: 2350–2355.
- Koby, M. 2004. Adsorption, kinetic and equilibrium studies of Cr(VI) by hazelnut shell activated carbon. *Adsorption Science & Technology* 22: 51–64.
- Madhava Rao, M., G. P. Chandra Rao, K. Seshiah, N. V. Choudary, M. C. Wang. 2008. Activated carbon from Ceiba pentandra hulls, an agricultural waste, as an adsorbent in the removal of lead and zinc from aqueous solutions. *Waste Management* 28: 849–858.
- Mohanty, K., M. Jha, B. C. Meikap, M. N. Biswas. 2005 Removal of chromium(VI) from dilute aqueous solutions by activated carbon developed from Terminalia arjuna nuts activated with zinc chloride. *Chemical Engineering Science* 60: 3049–3059.
- Ozdes, D., A. Gundogdu, B. Kemer, C. Duran, H. B. Senturk, M. Soylak. 2009. Removal of Pb(II) ions from aqueous solution by a waste mud from copper mine industry: Equilibrium, kinetic and thermodynamic study. *Journal of Hazardous Materials* 166: 1480–1487.
- Panda, L., B. Das, D. S. Rao, B. K. Mishra. 2011. Application of Dolochar in the removal of cadmium and hexavalent chromium ions from aqueous solutions. *Journals of Hazardous Materials* 192: 822–831.
- Periasamy, K., K. Srinivasan, P. R. Muruganan. 1991. Studies on chromium(VI) removal by activated ground nut husk carbon. *Indian Journal of Environmental Health* 33: 433–439.
- Pradhan, J., S. N. Das, R. S. Thakur. 1999. Adsorption of hexavalent chromium from aqueous solution by using activated red mud. *Journal of Colloid and Interface Science* 217: 137–141.
- Rastogi, K., J. N. Sahu, B. C. Meikap, M. N. Biswas. 2008. Removal of methylene blue from wastewater using fly ash as an adsorbent by hydrocyclone. *Journals of Hazardous Materials* 158: 531–540.
- Sahu, J. N., S. Agarwal, B. C. Meikap, M. N. Biswas. 2009. Performance of a modified multi-stage bubble column reactor for lead(II) and biological oxygen demand removal from wastewater using activated rice husk. *Journal of Hazardous Materials* 161: 317–324.
- Singh, C. K., J. N. Sahu, K. K. Mahalik, C. R. Mohanty, B. Raj Mohan, B. C. Meikap. 2008. Studies on the removal of Pb(II) from waste water by activated carbon developed from Tamarind wood activated with sulphuric acid. *Journal of Hazardous Materials* 153: 221–228.
- Srivastava, S. K., V. K. Gupta, D. Mohan. 1997. Removal of lead and chromium by activated slag—A blast furnace waste. *Journal of Environmental Engineering* 123: 461–468.



Taylor & Francis

Taylor & Francis Group

<http://taylorandfrancis.com>

A Review on Potential Reusability of Industrial Solid Wastes as Adsorbents

Gopinath Halder and Soumya Banerjee

CONTENTS

9.1	Introduction: Background and Current Scenario	179
9.2	Environmental Concerns about Industrial Wastes	180
9.3	Heavy Metal Pollution and Its Remediation	180
9.3.1	Adsorption: Exploration of Low-Cost Adsorbents	180
9.4	Industrial Solid Wastes: An Alternative Solution	181
9.4.1	Postcombustion Residue	182
9.4.2	Blast Furnace Slag, Sludge, and Flue Dust	183
9.4.3	Alumina Extraction Waste	184
9.4.4	Leather Industry Waste	185
9.4.5	Paper Industry Waste	185
9.4.6	Fertilizer Industry	186
9.4.7	Miscellaneous Industries	186
9.5	Competitive Removal of Metal Ions	187
9.6	Cost Incurred in Using Industrial Solid Wastes	189
9.7	Toxicity Analysis of Industrial Waste-Based Adsorbents	190
9.8	Comparative Analysis of Heavy Metal Removal	191
9.9	Air Pollution: Emission of Flue Gas	191
9.10	Possible Remedies in Flue Gas Treatment	191
9.11	Implementation of Industrial Solid Wastes for Flue Gas Remediation	192
9.12	Conclusion: Recommendations and Future Aspect of Industrial Solid Wastes	193
	References	194

9.1 Introduction: Background and Current Scenario

For the past few decades, unscientific dumping of industrial solid wastes has created multiple environmental nuisances. The concept of their safe disposal and reusability has attracted various researchers from around the world for finding a scientific alternative to this problem. This present chapter deals with the productive use of these industrial solid wastes as adsorbent for remediating heavy metal-contaminated aqueous solution. Apart from being a cost-effective adsorbent, their applicability in large-scale operation, maintenance, and sustainability of their adsorptivity are also included in the discussion. Other constraints like their consistent activity under competitive conditions along with interionic interference in adsorption are also included. In parallel with heavy-metal removal, application of these solid wastes as adsorbents for flue gas separation are also summarized in this chapter.

9.2 Environmental Concerns about Industrial Wastes

In general, generation of waste has been considered to be proportionally related to the ever-growing world population and its overall dependency on industrialization. Although, the latter is required in every progressive society, its mode of channelizing raw materials into waste has raised serious environmental concern. Vigorous usage of raw materials has not only created scarcity and deletion of natural resources, but at the same time created high risk of multiple contaminations in every sphere of the environment. As reported by different agencies, including the British Medical Bulletin and World Health Organization, continuous generation of industrial waste has increased the numbers of health issues due to contaminated drinking water and the air we breathe. These effluents can be categorically divided into three types: solid, liquid, and gaseous wastes. Almost every industry produces all three types of effluents, but the nature of their toxicity depends on the final product and the raw material used.

9.3 Heavy Metal Pollution and Its Remediation

In reference to the aforementioned context, application of mineral ores or heavy metals has been the backbone of industrialization. Heavy metals can be required either as raw materials or as ingredients of a process. Production of heavy metal-containing waste has concerned environmentalists about its adverse effects, which might be a reason for various diseases within the living world. As a serious consequence of heavy metal discharge, their concentrations are increasing gradually in both ground and superficial water bodies. Therefore, various regulatory bodies such as the BIS (Bureau of Indian Standards), WHO (World Health Organization), USEPA (United States Environment Protection Agency), and EU (European Union) have limited the presence of heavy metal in ground, superficial, and drinkable water (Table 9.1). Feasible technologies have been recommended from various studies for treating metal-polluted wastewater. Both biotic and abiotic techniques have been tried and few of them showed promising results even at large scale. Various methods like ion exchange, membrane separation, filtration, chemical precipitation, reverse osmosis, and bioremediation have been tested, but multiple usages of chemicals have constrained them from commercial applications under various scenarios.

9.3.1 Adsorption: Exploration of Low-Cost Adsorbents

On the contrary, consideration of adsorption as a remedial process is gradually gaining importance for its wide application and low investment. Initially it was only restricted to commercially available activated carbon as adsorbents but due to its high price and cost ineffectiveness, alternative adsorbents from different sources are being considered (Gupta and Ali, 2002). Thus, usage of solid wastes has proven to be a path-breaking finding in adsorbing various contaminants from aqueous solution. Among such wastes, kitchen and agricultural leftovers exhibited a promising role in adsorbing metal ions and other contaminants. This provided an option in reducing waste volume and channeling it into a fruitful application. Interestingly, a similar concept was used for industrial solid wastes as well. Unlike agricultural and kitchen wastes, industrial wastes were more prone to

TABLE 9.1

Metal Discharge, Permissible Limits, and Their Concentration in Natural Water Reservoir

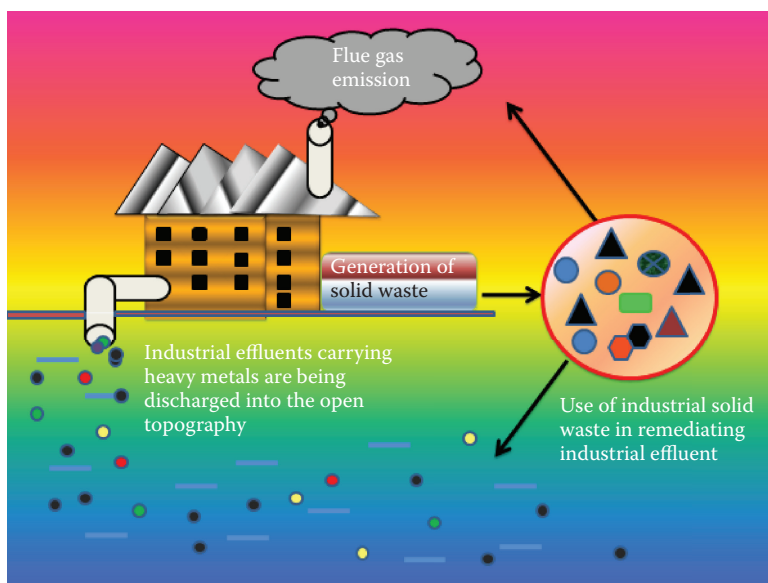
Metal Ions	Permissible Limits for Industrial Discharge (mg/L)				Permissible Limits for Drinkable Water (mg/L)			
	Indian Standard (IS)			WHO				
	Inland Superficial Water	Public Drains	Marine Littoral Areas	Inland Superficial Water	Indian Standard (IS-10500)	WHO	USEPA	EU Standards
Pb	0.1	1.0	2.0	0.1	0.05	0.01	0.015	0.01
Cd	2.0	1.0	2.0	0.1	0.01	0.003	0.005	0.005
Zn	5.0	15.0	15.0	5.0 to 15.0	5.0	3.0	5.0	–
Fe	3.0	3.0	3.0	0.1 to 1.0	0.3	0.2	0.3	0.2
Cu	3.0	3.0	3.0	0.05 to 1.5	1.5	2.0	1.3	2.0
As	0.2	0.2	0.2	–	0.01	0.01	0.01	0.01
Ni	3.0	3.0	5.0	–	0.02	0.02	0.1	0.2
V	0.2	0.2	0.2	–	–	1.4	–	–
Mn	2.0	2.0	2.0	0.05 to 0.5	0.1	0.2	0.2	0.2
Cr	2.0	2.0	2.0	–	0.05	0.05	0.1	0.05
Hg	0.01	0.01	0.01	–	0.001	0.001	0.002	0.001

Source: Data from United Nations Environment, n.d., Global Environment Monitoring System for freshwater (GEMS/Water), <http://www.gemswater.org>; Lenntech, n.d., Water treatment solutions, <http://www.lenntech.com>; Bureau of Indian Standards, 1991, Indian standard drinking water—Specification (1st rev.) IS-10500, New Delhi, India: Bureau of Indian Standards; and India Ministry of Environment, Forest and Climate Change (MoEF), 1993, May, General standards for discharge of environment pollutants: Effluent, *Gazette Notification of Ministry of Environment, Forest and Climate Change (MoEF)*.

environmental contamination due to their complicated inorganic nature. Therefore, exploration of these wastes as adsorbents is reported with few promising outcomes.

9.4 Industrial Solid Wastes: An Alternative Solution

Industrial solid wastes derived from several industries with different origin and different chemical and physical characteristics have proved to be operative, alternative, and low-cost adsorbents. Comparable lesser pretreatment and cost is incurred during processing of these wastes into appropriate adsorbents. These effluents are produced as by-products and are available locally, even at low or no cost. Industrial by-products like fly ash, blast furnace sludge, industrial slurry, black liquor, and red mud are reported to eliminate heavy metals at a maximum level from aqueous solutions. Some miscellaneous wastes like saw dust, rice husk, wheat bran, and sugar beet pulp were equally effective toward metal ions. These industrial wastes have also been converted into other compounds like zeolites and activated carbon or into some other specific compounds that adhered contaminants more effectively at cheaper expense (Shim et al., 1999; Somerset et al., 2008). Figure 9.1 shows the concept of using industrial solid wastes as potential adsorbents. Corresponding applications and triumph over decontamination of metal-laden wastewater and elimination of flue gases from air using various industrial adsorbents are explained in detail in the following sections.

**FIGURE 9.1**

Schematic representation of industrial solid waste as potential adsorbent for treating industrial effluents.

9.4.1 Postcombustion Residue

Fly ash, a postcombustion residue, has been reported in the removal of metal ions from contaminated aqueous solution (Banerjee et al., 2003; Bayat, 2002). It is an industrial solid waste produced from the incineration of fossil fuel in metric tons annually around the world. This industrial by-product being chemically versatile in nature has proved to be an effective and inexpensive adsorbent as compared to commercially available activated carbon or zeolite. Apart from an effective role as an adsorbent it was also used in brick and cement making and even in construction of roads (Namasivayam and Sumithra, 2007). A lot of its function in metal binding depends on its origin. It is mainly due to the fact that the composition of fly ash, which includes silica (>60%), alumina (>30%), and magnetite (>10%), differs from the quality of coal. Also, the physiochemical characteristics like bulk density, water-holding capacity, porosity, particle size, and surface area support its behavior in adhering metal ions from aqueous solution. Apart from being an effective metal adsorbent, it also acts as a good neutralizing agent for the same phenomenon. Metal ions such as Cr(III), Cr(VI), As(III), As(V), Cu(II), Ag(II), Mn(II), Zn(II), Cd(II), Pb(II), and Ni(II) have been successfully removed from contaminated aqueous solution using fly ash. This adsorbent can even remove metal ions from a multiple-cationic solution. Chemical composition of fly ash, as stated earlier, helps in better bonding of metal ions. For instance, the iron content of fly ash increases its efficacy toward As removal by forming a ferroarsenate bond over its surface. Fly ash originating from a Turkish province showed lower efficacy of >1 mg/g of adsorptivity. In other reports on metal removal by fly ash (of different origin), efficacy was found to rise from 10 mg/g up to 20 mg/g depending on the metal contaminant and its initial concentration. In another study, it was found that the same adsorbate varied in uptake when fly ash from a different origin was used. Apart from the usage of crude fly ash, this industrial waste can even be modified physically and chemically. In such a study, zeolite was prepared from fly ash. This industrial solid waste comprises an appreciable amount

of silica, which after a series of acid-base treatments, zeolites can be prepared. Coal fly ash-based zeolite effectively removed metal ions like Cu(II), Cd(II), and Pb(II) from aqueous solution. Development of geopolymers from fly ash has showed greater efficiency than crude fly ash. These geopolymers include aluminosilicate, which can remove Cu(II) from metal-laden solutions. A higher reaction temperature and Na:fly ash ratio helps this adsorbent to achieve greater adsorptivity (Somerset et al., 2008). As compared to fly ash and natural zeolites, whose optimum uptake reside around 0.1 and 3.5 mg/g, respectively, refined fly ash-based products exhibited adsorptivity up to 92 mg/g. Thus, this industrial solid waste can be used as a low-cost source for adsorbent development toward metal removal from aqueous solution.

9.4.2 Blast Furnace Slag, Sludge, and Flue Dust

In the metal industry, such as the steel industry, several unwanted by-products are produced as waste in huge quantity. These wastes include blast furnace slag or steel and iron slag, blast furnace slurry, and dust. This slag being granular in nature is produced in large quantity and used as filler for production of slag cement. Dimitrova (1996) reported the use of blast furnace slag for Cu(II), Ni(II), and Zn(II) removal, where its alkalizing activity created a suitable environment for adhesion by hydroxy complexes and colloid formation with silicic acid. In one study, it was concluded that a higher adsorption capacity was possible due to the formation of soluble compounds onto the internal surface of the slag (Srivastava et al., 1997). In another investigation, it was found that the optimum adsorptivity of Pb(II) and Cr(VI) were up to 40 and 7.5 mg/g, respectively, which is a considerable and comparable amount with commercially available activated carbon. In this same study, it was reported that blast furnace slag was bought for US\$38 per ton, which was cheaper than commercially available activated carbon worth US\$1000 per ton. In removal of Pb(II) from aqueous solution, it was found that the process was mostly affected by adsorbent dose since overall adsorption was compromised with increasing adsorbent dose. When similar removal was carried out with Pb(II) in a continuous process, a contradictory result was found where decreasing the slag bed reduced both rate and overall removal. Pb(II) showed greater possibilities of bond formation in presence of indigenous metal ions present on the adsorbent. Removal of Pb(II) was highly influenced by sodium and calcium. Apart from packed bed material, change in effluent pH also altered metal concentration at breakthrough. In the case of continuous adsorbate removal through a column of blast furnace slag, adsorption was found to be driven by ion exchange and precipitation. An important finding was made by Nehrenheim's research team in 2008, where it was found that this blast furnace slag was comparable with other low-cost adsorbents like pine bark (Nehrenheim and Gustafsson, 2008). In that comparison, storm water and landfill leachate were used as metal ion sources since these water drainages are enriched with toxic heavy metals like Zn, Cr, Ni, Cu, and Pb. Both adsorbents showed multiple degree of adsorption. At low metal concentration, pine bark was more efficient, but when metal ion concentration gradually increased, the efficacy of blast furnace slag was comparatively higher. This slag not only removed more metal ions, but also the time for metal removal was relatively shorter.

Industrial sludge on the other hand is a dried solid waste that is generated mainly due to electroplating. As a result of electroplating, a significant amount of metal ions are washed away as residue, which then precipitates as metal hydroxide when it comes in contact with calcium hydroxide along with other salts. A research team headed by Lopez documented a potential role of industrial sludge in removal of metal ions from contaminated aqueous

solution (Lopez et al., 1996). Metal ions, including Cu(II), Pb(II), Zn(II), Cd(II), and Cr(III), were being tested for adsorption by blast furnace sludge, which demonstrated effective metal removal. One of the driving forces toward metal removal by blast furnace sludge was examined to be the iron oxide-to-carbon ratio (Lopez et al., 1995). At a higher temperature, if the carbon content increases it will decrease the overall adsorption and vice versa. This industrial sludge encouraged easy applicability with minimal pretreatment. So far, adsorptivity of blast furnace sludge for metal ions followed was found to be in the order of Pb(II) > Ni(II) > Cd(II) > Cu(II) > Zn(II).

Another important waste from steel industry is blast furnace flue dust, which is a carbon-based waste whose ferro-alumino-silicate phase helps in adhesion of metal ions onto it. Metal ions like Cu(II) and Pb(II) have been removed by this flue dust. In a comparative study of Pb(II) removal by multiple industrial wastes, which included carbon slurry and steel plant wastes like blast furnace slag, sludge, and flue dust, it was found that the sludge was more effective than flue dust and slag and the least removal efficacy was exhibited by carbonaceous slurry. Therefore, the three aforementioned steel industrial solid wastes unveiled a promising role for removal for Pb(II), along with other metallurgical wastes, as a low-cost adsorbent for detoxification of metal-laden industrial effluent.

Sludge produced from other industries apart from blast furnace waste was also tested for metal adsorption. Distillery sludge, which is conventionally used as fertilizer, has also been used for metal removal. In one such study of metal removal it was found that dried distillery sludge removed 82% of Cr(VI) from chromium-laden water with a maximum uptake of 5.7 mg/g. As documented by Bhatnagar et al. (2008) it was found that metal sludge obtained from the electroplating industry was able to adhere vanadium(V) from aqueous solution with a maximum uptake of 24.8 mg/g. After adhesion, this metal-laden adsorbent was disposed as an immobilized constituent in cement making. This mixing was found fruitful without compromising the functional stability of cement. Thus, this conclusion was found to be a groundbreaking achievement in vanadium(V) removal. Also, this trial was able to meet the need of metal remediation and safe disposal of adsorbent, hence, bridging the need of treating metal effluent with industrial solid waste. Clarified sludge, which is also a type of steel industry waste, removed Zn(II) distinctively from aqueous solution. This waste removed more Zn(II) comparatively than other reported adsorbents like neem bark, activated alumina, and rice husk ash (Bhattacharya et al., 2006).

9.4.3 Alumina Extraction Waste

It has been investigated that red mud is an abundantly available industrial waste produced as a by-product of the Bayer process (Gupta et al., 2001). In extraction of alumina from bauxite, this principal is used where, as a consequence of caustic leaching of ore, this red mud is formed. Annually, an estimated amount of around 1 to 2 tons of red mud is produced. Due to the caustic nature, red mud has the possibility of imparting health hazard on living organism. Neutralization of this by-product enhances its reusability for other applicability, but this leaching might cause environmental contamination. Therefore, various proposals were made in transferring it to a probable adsorbent. This bauxite ore-based industrial waste is comprised of silica, aluminum, calcium, iron, and oxides and hydroxides of titanium, which creates greater adsorbing possibilities due to maximum surface reaction abilities. As a result, various remediating investigations have been conducted on various toxic contaminants, including heavy metals originating from various sources. Both industrial and acid mine drainage containing heavy metals were reported to have been removed by red mud. As(III), As(V), Cu(II), Zn(II), Cr(VI), Cd(II), and Pb(II) are some of

the metal ions that have been successfully removed by red mud. As an alternative to conventional agricultural and commercial adsorbents, red mud adheres to metal ions with a maximum uptake of 19.72 mg/g for Cu(II) within a contact time of 48 hours. Greater adhesion was seen with Cr(VI) and Pb(II) with an adsorptivity of 64.79 mg/g and 35.66 mg/g, respectively, in a batch study. When the same study was conducted on a continuous mode, then adsorptivity got increased up to 88.2 mg/g and 75 mg/g for Cr(VI) and Pb(II), respectively (Wang et al., 2008). In most studies on metal removal, it was found that among all the process parameters, effect of pH was more prominent since great divergence was visible with little change in pH. Two forms of arsenic—As(III) and As(V)—were removed but the pH varied greatly. Optimum removal of As(III) was possible when the solution pH was slightly acidic to alkaline in nature, whereas in the highly acidic condition As(V) was removed.

Various basic level technologies were used in increasing its effectiveness for better metal removal. Initially it was found that simply by acid and heat treatment, metal uptake capacity of red mud could be increased (Altundogan et al., 2000, 2002). From multiple sources on arsenic removal by various sets of activated red mud or bauxol, it was found that with preliminary treatment with acid and heat As removal went up to 100% for arsenate maintained at a pH of 4.5 without the interference of other competing anions like phosphate, sulfate, or bicarbonate. Apart from its potential of being a good adsorbent, safe disposal of metal-laden spent red mud could be an ecofriendly process. In an adsorptive trial, it was found that the bauxol or red mud, which was used to remove Cu(II), Pb(II), and Cd(II) was mixed uniformly with cement, which was then transformed into a hard-wearing concrete mass resulting in a form safe for disposal (Apak et al., 1998).

9.4.4 Leather Industry Waste

Derivation of potential heavy metal adsorbent was also obtained from leather industry solid waste. The main leather industry wastes include animal hides or skin obtained from fleshing and protein-based effluent. Among the two wastes, the leftover of fleshing is used as an adsorbent but so far study has only been conducted with As(V) and Cr(VI) removal. An overall uptake of 133 mg/g and 26 mg/g of Cr(VI) and As(V) was achieved, which was an appreciable alternate to commercial high-priced adsorbents. In one of the preliminary studies on metal adsorption by this leather industry based solid waste, it was found that Fe(II) doping increases its efficacy to a comparable higher level than its crude form. Similar investigation was made for Cr(VI) removal from aqueous solution where the instrumental analysis of the adsorbent under x-ray photoelectron spectroscopy explained that the ions of Fe(II) were attached to the protein, which provided a better ionic surface for complex formation. Another abundantly produced leather industry waste is the buffing dust, which is still in a nascent state since proper characterization, durability, and longevity under stressed condition are yet to be studied in details. So far, few adsorption-based trials have been carried out on dye removal and the results were quite supportive for its role as a newer adsorbent material.

9.4.5 Paper Industry Waste

For the past few decades, paper industry-based waste has turned into a matter of concern at multiple levels for its possible polluting where it might change the natural chemistry of water bodies as a consequence of its exposure. This includes black liquor, which contains a high amount of lignin that could substitute costlier adsorbents. It is a naturally

occurring aromatic cross-linking polymer consisting of multiple numbers of functional groups present on its surface. These include phenols, hydroxyls, carboxyls, benzyl alcohol, methoxyls, and aldehydes, which play important roles in metal adhesion (Sarkanen and Ludwig, 1971). C, N, H, S, K, Ca, Na, Fe, Mg, Al, Si, and ash are some of the important constituents of lignin. A few other elements are also present in trace amounts, but they can be easily removed by acid washing. Therefore, there are lesser possibilities of metal leaching from spent lignin, but there should be a proper evaluation of it before the lignin is used. To date only Pb(II) and Zn(II) have been removed. Unlike conventional adsorbents, this paper waste was able to adsorb Pb(II) up to 1865 mg/g and 95 mg/g of Zn(II). The concentration of phenol, which is present as nitrophenol, chlorophenol, dichlorophenol, and trichlorophenol was found to be responsible for the greater retention time. Also, it was found that structural composition of paper supports development of activated carbon from it. The adsorption capacity was found to be efficient when it was mixed in iodine (1310 mg/g) and methylene blue (326 mg/g) aqueous solutions. Heavy metal like Cu(II) was removed with this paper waste. Experimental studies showed that metal retention properties varied with the type of waste paper pulp being used. Waste paper pulp obtained from virgin pulp sludge is mostly composed of micropores, whereas mesopores are predominant in deinked pulp sludge. Although metal removal was optimum in acidic conditions, the increase in pH did not initiate metal lixiviation. However, leaching of Ca and Mg was observed. This was evident at the end of Cu(II) adsorption when there was an increase in metal ions in solution because of calcium carbonate generation. Deinked paper pulp was more active for adsorption of heavy metal because due to this deinking process elevation of oxygenated groups was found. Also, pore diameter and surface charge were intensified with exchange of Mg and Ca into the solution.

9.4.6 Fertilizer Industry

It has been found in some studies that adsorption of metal ions from aqueous solution can be achieved using metal hydroxides as adsorbents. A similar concept was applied on metal hydroxide waste from the fertilizer industry. Like various other industrial pollutants, waste from fertilizer industry has also contributed to environmental contamination. Thus, the Fe(III)/Cr(III) hydroxide produced as a by-product has been cleverly used in the removal of Cr(VI), Pb(II), As(V), Cd(II), and Ni(II) from metal-laden waste water (Namasivayam and Ranganathan, 1993, 1995, 1998). In Cr(VI) removal, it was found that this industrial waste was able to remove up to 0.47 mg/g. In another study, Cr(III) was removed from aqueous solution where intraparticle diffusion through pores was found to be the rate-limiting step. Ligands like ethylenediaminetetraacetic acid (EDTA), acetate, and citrate interfere in metal adsorption by reducing adsorptivity. The impact of these ligands on Pb(II) adsorption was found to be profound over a wide range of pH from 3.8 to 8.5. In Ni(II) adsorption, citrate along with EDTA reduced the overall uptake, whereas acetate increased its adsorptivity. Cd(II) adsorption on the other hand was increased with the use of both citrate and acetate.

9.4.7 Miscellaneous Industries

In this pollution-driven human civilization, a diverse section of government agencies from all over the world are planning for a variety of environmental schemes on the industrial scale so as to reduce the pollution level from every stratum of nature. Therefore, ways to cope with the pollutants has intrigued researchers for the past couple of decades.

As already mentioned, industrialization has been the cause of several environmental casualties in terms of hazardous activity. Consequently, effluent treatment at its very source using cheap resources has become an important issue in the scientific arena. Thus, more attention has been given to developing industrial wastes as a useful commodity. Hence, newer industrial by-products coming out as wastes are being studied for removing heavy metals. Wastes like textile waste, grape stalk, sour orange residue, sea nodule residue, waste pomace olive oil factory waste, sugar beet pulp, tea factory waste, areca waste, coffee husk, waste slurry, biogas residue slurry, and battery waste have been reported to remove metal ions from aqueous solution. In one recent study, textile industry-based wastes were assessed for heavy metal removal (Ahmaruzzaman, 2011). In this context lyocell fabric was treated, modified, and then used as an adsorbent for Cd(II) removal. Cheap chemical treatment with sodium chloroacetate and sodium hydroxide were used in surface modification of the waste textile material. Initially sodium chloroacetate was used for etherification of the hydroxyl groups, which produced carboxymethyl cellulose. It was followed by a cross-linking reaction with epichlorohydrin, which formed an intra- and interlocking of hydroxyl groups. This provided hydro stability to the adsorbent. Removal of Cd(II) was optimized by response surface methodology, which concluded that the adsorbent adhered up to 137.81 mg/g of metal ions. Since the cost incurred was only restricted with the chemicals used, it made it an effective low-cost adsorbent that could remove Cd(II) up to six cycles without its efficiency being compromised. Sour orange residue, on the other hand, removed Cu(II) in a considerable amount when pretreated with sodium hydroxide. Slurry obtained from combustion of liquid fuel was treated with hydrogen peroxide followed by an intermediate phase of air activation at 450°C adsorbed Cu(II), Cr(II), Hg(II), and Pb(II) metal solution (Srivastava et al., 1988). Several other wastes collected from different food processing industries including seafood waste, coffee husks, tea factory industry, sugar beet pulp, and olive oil waste also showed compatibility for metal bonding. Metal ions like Cu(II), Cr(VI), Pb(II), and Zn(II) were used as test contaminants for determining efficiency of these adsorbents. Manufacturing polymetallic sea nodules generates a residue that could remove inorganic metal contaminants like Zn(II) from aqueous solution (Agrawal et al., 2004). Slurry derived as biogas residue adsorbed 28 mg/g of Pb(II) ions from aqueous solution. Solid waste obtained as grape stalk from the wine industry forms ionic bonds when mixed in a metal solution of Cu(II) and Ni(II), which was evident from the release of alkaline earth metal in the solution and active response of the lignin present in it. Olive mill residue could remove Cu(II) from aqueous solution, and it was reported to have effective removal if properly regenerated. Regeneration with hydrochloric acid and calcium chloride sustained its efficacy, whereas EDTA and other acids damaged its active sites leading to a decrease in its metal adsorption <40%. Battery waste was able to adsorb Pb(II), Cu(II), Cr(II), and Zn(II) from metallic solution at an appreciable level up to 64 mg/g.

9.5 Competitive Removal of Metal Ions

Industrial effluents are rarely composed of single metal ion; thus, a system should be fabricated to support cation removal from a multiple-metal solution. Hence, elimination of a target metal ion from a competitive metal solution is an important issue in treating industrial effluent or contaminated wastewater. So far, few systems have been developed which supported metal removal from a competitive ion solution. Industrial wastes have been used

in few studies were metal like Cu(II), Cd(II), and Pb(II) were removed both from binary and tertiary metal ion solutions (Mohan et al., 2006). Black liquor lignin has been used to remove Cu(II) and Cd(II) from binary and tertiary solutions, which were reported as Cu-Cd, Cu-Zn, and Cd-Cu-Zn with an adsorptivity of more than 30 mg/g for both metal ions.

Similarly, fly ash, anaerobic sludge, cellulose pulp waste, and carboxymethylated lignin were used to remove Pb(II), Cu(II), and Cd(II) from competitive metal solutions. At the industrial level an adsorption process is considered to be the convenient treatment if it can sustain its efficacy at a continuous mode rather than its corresponding laboratory-based batch approach. Various factors are taken into account, which plays an important role in considering the importance of industrial wastes as adsorbents. Factors include available cations, ionic size, and the bonding stability formed between metal ions and adsorbents. It has been found that industrial-based adsorbents have been able to remove more Pb(II) and Cu(II) in a bimetal solution than from an individual metal solution. Adsorbents such as activated sludge removed both phenol and Cr(VI) from an aqueous solution from a continuous mode packed bed reactor. The study also revealed an interesting finding where it was seen that among both adsorbates, adsorptivity of activated sludge was more toward the metal ion than phenol. The rate of removal increased with an increase in their initial concentration, although the presence of phenol gradually decreased both of their adsorptions as compared to the single removal study. The competitive interference of metal ions was predicted by the Yoon and Nelson model with single and binary conditions to determine the breakthrough point for each of the adsorbates using response surface methodology. This comparison helped in determining the rate of adsorption in an unknown experimental condition. Turkish tea waste derived from different tea industries was also used as an alternative adsorbent for competitive removal of metal ions (Cay et al., 2004). Cd(II) and Cu(II) were treated with tea waste fibers from both noncompetitive and competitive conditions where adsorption of the former metal ion increased in a competitive state from 8.64 mg/g to 11.29 mg/g. Unlike Cd(II), removal of Cu(II) decreased from 6.65 mg/g to 2.59 mg/g in the same competitive condition.

In industrial effluents, heavy metals are sometimes accompanied with either acids or alkali, which proposes other possibilities in defining metal adsorption processes under challenging conditions. In such a condition, removal of Pb(II) and Cu(II) along with humic acid were tested, where the presence of this acid as the contaminant promoted greater metal adsorption along with its own adsorption onto fly ash (Wang et al., 2008). Humic acid increased metal adsorptivity up to 37 mg/g and 28 mg/g for Pb(II) and Cu(II), respectively, in the system at a constant pH of 5 and temperature of 30°C. Being an accelerator of metal adsorption on fly ash, removal of humic acid on the other hand gradually decreased at greater metal concentration. Apart from acids and alkali industrial dyes which are also found in industrial effluent can interfere metal adsorption. Thus, an anion-cation system with Gemazol turquoise blue-G dye and Cu(II) were formulized to determine their individual effect on removal (Aksu and Isoglu, 2007). The adsorbent dried sugar beet pulp removed Cu(II) from single and binary solutions under a batch adsorptive condition. In a binary condition, removal of dye was not compromised at elevated Cu(II) concentration, whereas with an increase in initial dye concentration the overall cationic removal diminished. Both Cu(II) and dye imparted contradictory effect on each other while the cation showed synergetic consequences, and the anion revealed an antagonistic effect. Among various parametric effects, the pH value differed in the single and dual systems, but in each case, it followed a nonlinear monolayer adsorption. Similar exploration with rice husk for Cd(II) and Zn(II) removal was executed under a competitive atmosphere (Srivastava et al., 2008).

9.6 Cost Incurred in Using Industrial Solid Wastes

Applicability of an adsorbent toward adsorbate removal depends on its availability, adsorption efficiency, and preparation cost effectiveness. Also, it has to be considered that the removal capability of an adsorbent is optimized in respect to various factors that define its need in a large-scale operation. In general, it can be seen that most of these adsorbents were not always used in their original state; instead multiple technologies were employed in changing their forms for better adsorptivity. Therefore, the precursor undergoes a series of experimented trials before it is modified into an effective adsorbent, which eventually increases its price depending on the agents that have been used.

The precursors that are modified into an adsorbent are derived from a wide array of sources. In most cases, process leftovers from industries, agricultural, municipal, and even crude natural unwanted plant sources are used as adsorbents for contaminant removal purposes (Ahmaruzzaman, 2011). Since these waste materials are accompanied with other unwanted materials, proper modification becomes an important factor in material development. Cost efficacy of an adsorbent is a cumulative representation of material development, removal efficiency, regeneration, and reusability. Industrial solid wastes are abundant in nature. Therefore, the cost incurred in adsorbent collection is negligible or free. In one such case, fly ash is easily obtained and does not involve any charge, but additional charges like transportation, laying, and rolling are included which increases the preliminary charges. Likewise, bagasse fly ash, which costs about US\$0.002 is made into a fine adsorbent at a cost of US\$0.007. Eventually the same material turns expensive when fine products are deduced from it. Works have been reported where final products like activated carbon, zeolites are produced whose price was found to be depending more on the purity of the precursor. A list of commercially available adsorbents along with adsorbent derived from industrial wastes are shown in Table 9.2. In most of the cases the waste-based adsorbents cost around US\$0.1/Kg, which makes it quite affordable as compared to

TABLE 9.2

Variance in Cost of Adsorbents Obtained from Industrial Waste and Commercial Adsorbents

Industrial Waste	State of Usage	Price (\$US/Kg)	Reference
Commercial activated carbon	Finer grade	20	Atun et al., 2003
	Granular grade	3.30	Toles et al., 2000
Postcombustion residue	Bagasse fly ash	0.009	Srivastava et al., 1995
Fertilizer industry waste	Carbonaceous adsorbent	0.1	Jain et al., 2003
Blast furnace waste	Unmodified	0.038	Srivastava et al., 1997
	Carbonaceous adsorbent	0.052	Srivastava et al., 1997
Metal sludge	Slag	0.04	Atun et al., 2003
	Carbonaceous adsorbent	0.1 to 0.2	Bhatnagar et al., 2008
	Unmodified	0.004 to 0.005	Bhatnagar et al., 2008

commercial adsorbents where the price may vary from US\$3/Kg to US\$5/Kg depending on its grade.

The actual price involved in an overall water treatment process also consists of the apparatus, energy consumption for pumping, and maintenance. Also, the duration of a process varies with variation in the metal concentration in the wastewater, which depends on demand versus supply. Thus, a wholesome knowledge of a complete wastewater treatment process by adsorption is quite scarce. Consequently, this leaves a greater area of research completely dedicated to the cost efficacy of a process where both adsorbents and operational costs are analyzed. On a large scale, where crude wastewater is treated, additional costs like pretreatment and separation of other solid wastes removal from the effluent also increases the cost. The manpower included along with this process varies from country to country. As a result, precise investigation is required before commercialization of an adsorbent as suggested from laboratory-scale analysis. Hence, for a proper estimation of operational and maintenance cost, a pilot scale study is needed to provide a greater factual estimate on how much the cost might be on a commercial scale. Although other conventional technologies have already been reported to be more effective than adsorption, their monetary constraints have always been a question of their feasibility. On the contrary, adsorption in most of the cases has not been effective in lowering heavy metal contaminants below the permissible limit but its reusable possibilities have invested more thoughts in developing this process. Therefore, more funds are being invested on developing suitable low-cost adsorbents from wastes that can work in a wider range of wastewater effluents containing heavy metals.

9.7 Toxicity Analysis of Industrial Waste-Based Adsorbents

Interestingly, usage of industrial wastes as adsorbents has curtailed the cost of disposing these wastes. Also, it has lowered the environmental risk, where in a variety of dumping zones these wastes were found to alter the ecology and chemistry of adjoining soil and water. Unfortunately, there has always been a question of additional toxicity that might occur due to the usage of these industrial adsorbents. Reports on metal removal from unwanted industrial solid wastes have been documented, but the possibility of toxicity due to these wastes is hardly reported. Secondary toxicity has always been a concern, since it has restrained the use of waste-transformed adsorbents. In a few cases, it was seen that with little change in solution pH, the adsorbents instead of removing heavy metals added more metal ions into the aqueous medium, thus increasing the unsuitability of the treated water. Second, a major concern lies with imparting of toxic chemical complexes during adsorption, which apparently have been considered to be the crucial criterion on unsuitability of an adsorbent derived from waste.

When using industrial wastes, which vary widely both chemically and physically, there might be chances of releasing toxic elements when metal-laden acidic or basic solutions are passed. This can be seen in case of raw or crude adsorbents since preliminary treatments might enhance their adsorptivity but the chance of toxicity remains a matter of concern. Eventually in many studies, these wastes were further transferred into specific forms, namely, activated carbon or zeolite, which are already used in various water treatments with no further reports on secondary toxicity.

9.8 Comparative Analysis of Heavy Metal Removal

Apart from commercial and standard adsorbents, applicability of an adsorbent under the trial laboratory phase can only be justified if it meets the basic requirements. An adsorbent prepared from least value material can only be considered for valorization if it meets the following criterion:

- Efficient adsorptivity toward a wide array of heavy metals
- Greater amount of removal efficiency
- Higher rate of adsorptivity
- Lower cost of production
- Usable for multiple cycles and easy regenerable
- Low fluctuation rate in a competitive environment

Industrial wastes like postcombustion waste, industrial slag and sludge, and red mud have been used by different workers and recommended for adsorption. Again, it has to be considered that the chemical and physical characteristics vary in each case, which reflects the adsorbent morphology. As a result, these adsorbents encountered various challenges. One such disadvantage is their fluctuating behavior toward metal removal where their performance changes with the solution condition. In contrast to these shortcomings, they support easy application in removal of heavy metals from aqueous solution.

9.9 Air Pollution: Emission of Flue Gas

Industrialization and modernization of new age human civilization have not only introduced heavy metal ions into our food chain, but serious degradation of atmospheric (gas) composition is occurring at a steady rate. Effluents from fossil fuel combustion from energy-driven industries have introduced CO_2 , NO_x , and SO_x into the atmosphere. In this respect, an increase in flue gas has been fueling atmospheric degradation for the past few years. Melting of glaciers, increase of global temperature, smog generation, and acid rain are some of the results of gaseous pollution. Eventually, these changes in environmental conditions have infested the living world, which can be evident from skin irritation, breathing disorders, blurred vision, sclerosis in plants, destruction of agricultural crops, and change in water pH, for example, have raised social remarks over unscientific emission of these gases into the environment.

9.10 Possible Remedies in Flue Gas Treatment

At present, few recommended technologies are being implemented to eradicate harmful gases from the atmosphere. So far, large-scale CO_2 capturing was mainly based on

chemical absorption, which includes use of chemical complexes. Aqueous solvents like alkanolamine, monoethanolamine, and piperazine are some of the frequently used chemical agents for absorption. Consequently, use of these solvents makes the process expensive for both purchasing and maintenance. It has been estimated that the overall energy consumption of an industry was found to accelerate from 15% to 37% for elimination of flue gas via absorption. Also, this technique turns ineffective with an increase in CO₂ concentration, which leads to counteremission of CO₂ into the atmosphere making the entire sequestering process ineffective.

9.11 Implementation of Industrial Solid Wastes for Flue Gas Remediation

Interestingly, recent studies showed that adsorption of CO₂ can be commercialized since it overcomes a lot of shortcomings that were the key restraining factors in chemical absorption. Usefulness of gaseous adsorption onto solid adsorbent depends largely on the molecular configuration of the solid substance where pore size, surface area, and polarity are considered to be the governing factors (Kaithwas et al., 2012). Thus, unlike solvent absorption where a significant amount of energy is consumed, adsorption by solid adsorbent reduced such consumption. Again, in terms of adsorbent regeneration, alteration of temperature could rejuvenate the solid adsorbent for multiple procedures. It has been comparatively analyzed that capturing of CO₂ from a postcombustion stage can be effectively organized with solid adsorbents due to its lower energy requirement, which is less complex as compared to the use of aqueous-absorbing solvents (Aaron and Tsouris, 2005). Adsorption of contaminating gaseous agents can be achieved with zeolites and carbonaceous materials. Although adsorbent prepared from commercially available activated carbon and zeolites have proved to be highly effective, the surplus in demand has made various industries reconsidering its application with low-cost materials. As stated earlier, adsorption of heavy metals was achieved with different adsorbents prepared from low-cost materials in which industrial and other solid wastes are included; unfortunately, there is not a similar scenario gas capturing. CO₂ capturing is quite a sophisticated procedure since it requires great precision and a leak-proof environment for better capture. Also, it demands purity and greater thermal stability in the case of adsorbent material in order to survive the process.

Accordingly, among various industrial wastes, fly ash has been used for separation of CO₂ from industrial gaseous effluent. Activated carbon prepared from fly ash enhanced its active sites via chemical adsorption. In such cases, activated carbon of desired amounts were doped with alcohol amines solvents such as monoethanolamine, diethanolamine, 2-amino-2-methyl-1-propanol, piperazine, and methyldiethethanolamine, which have already been reported to have CO₂ capturing efficiency (Khan et al., 2015, 2016a, 2016b). Differences in adsorbents after chemical treatment were evident where the surface area increased up to 1138 m²/g with a total pore volume of 1.03 mL/g. Apart from alcohol amines, chemical solvents like 3-chloropropylamine-hydrochloride salts with potassium hydroxide (optional) have been used to prepare chemically treated active carbon from fly ash. It was found that this activated carbon prepared from fly ash was able to capture CO₂ up to 174.5 mg/g of the adsorbent, which after regeneration retained at 140.6 mg/g (Kaithwas et al., 2012). In comparison to commercially available activated carbon, the maximum CO₂ uptake ranges from 1800 to 2000 mg/g, whereas fly ash-derived activated carbon was able to capture only 9% of the CO₂.

Other gas contaminants like SO_x and NO_x have also been studied for their adsorptive removal using low-cost adsorbents derived from industrial solid wastes. Along with CO_2 , SO_x and NO_x have been persistent in the atmosphere due to continuous emission of flue gas produced from combustion of fossil fuel. Firing of fossil fuel alone is responsible for 67% and 87% of global NO_x and SO_x emission. Among these oxide species of SO_x and NO_x , SO_2 , NO , and NO_2 have been recognized to be toxic.

Various methodologies, mostly classified as regenerable and nonregenerable, have been used where both are based on the application of sorbing of SO_x and NO_x by suitable sorbents. Among them wet flue gas desulfurization (regenerable) and selective catalytic reduction (nonregenerable) have been widely used. On the contrary, more attention has been given to regenerable methodology, since its efficacy lies both in terms of cost and waste generation. Consequently, development of regenerable adsorbents has led to the formation of various solid complexes, which includes traditional activated carbon and zeolites, Ca-based adsorbents, and metal oxides. These adsorbents have given remarkable results. Similarly, industrial waste-derived regenerable adsorbents like fly ash have also given fruitful removal of SO_x and NO_x from flue gas before they are emitted into the atmosphere. Some advanced approaches have been made where metal–organic frameworks and organic–inorganic fusions recently have gained interest for their application in flue gas treatment.

A variety of fly ash-derived zeolites have been developed that removed SO_2 with a maximum capacity varying from 0.11 mmol/g to 2.66 mmol/g. Although fly ash has been invested in flue treatment where CO_2 and SO_x have been removed, no effort has been made so far in removing NO_x from flue gas. Several other technologies have already been used for NO_x removal with synthetic and natural zeolites, but the industrial-waste based adsorbents, mainly activated carbon or zeolites, are still untouched.

9.12 Conclusion: Recommendations and Future Aspect of Industrial Solid Wastes

Generation of industrial effluent and utilization of industrial wastes for countertreatment are gaining tremendous interest. Remediation of harmful contaminants using industrial solid wastes as the “tool” for removal have forced researchers into further exploration of industrial solid wastes. From the preceding review, it is evident that the variation and number of studies about decontamination of industrial solid wastes have paved the path for future investigation in exploring their potential role in adsorption as adsorbents. Among the reported industrial waste-based adsorbents, fly ash has been one of the most promising and versatile in removing toxic heavy metals and gas. Surface modification has led this solid waste to retain its efficacy in a wide array of contaminant environments. Heavy metals like Pb, Cu, Zn, Hg, Cr, Cd, Ni, and As have been studied in detail for their removal from contaminated wastewater. However, modification of these industrial solid wastes into specific components like zeolites and activated carbon have proved to be a boon for this ever-growing environmental crisis. An alternative to expensive commercial activated carbon or zeolite extraction and preparation from industrial solid wastes could curtail the operation cost, which would affect the overall procedure. These adsorbents were effective in terms of selectivity, since their adsorptivity were not compromised in binary and tertiary metal solution or with acids and alkalis or even in the presence of dyes. In some

cases, it was observed that adsorption of metal ions has influenced simultaneous removal of other toxic components from aqueous solution. Along with heavy metals, postcombustion-derived fly ash has also extended its adsorptivity to removal of individual components from flue gas, namely, CO_2 and SO_x . Although the efficiency was not so promising in comparison to commercial adsorbents, it showed latent possibilities for future research.

It can be summarized that instead of accepting the fact of industrial solid wastes as a nuisance, it can be technically turned into a fruitful applicant in remedial techniques, which provides a lesser chance of dumping and environmental degradation. As far as the literature is concerned, most of the studies are found to be concentrated only on finding suitable adsorbents from wastes. On the contrary, the concept of material science in developing a material that can withstand multiple studies without desorbing any contaminants is still infrequent in its documentation. Being a complex of several elements and complicated organic structures, there are chances of releasing harmful compounds while treating contaminant effluents. Thus, a search for less harmful and better compatible adsorbents is required. As frequently shown in various studies, the cost of adsorbent development and its extended efficacy for multiple cycles have questioned their use in terms of commercial feasibility. Thus, there has always been a need for developing an adsorbent that is cost efficient with greater adsorptivity rate obtained from the waste. Also, more detailed study on their use in removing heavy metals from aqueous solution under competitive conditions is required. In conclusion, much more attention is required in treating flue gas using other industrial wastes.

References

- Aaron, D, Tsouris, C. 2005. Separation of CO_2 from flue gas: A review. *Separation Science and Technology*. 40: 321–348.
- Agrawal, A, Sahu, KK, Pandey, BD. 2004. Removal of zinc from aqueous solution using sea nodules residue. *Colloids and Surfaces A: Physicochemical and Engineering Aspects*. 237: 133–140.
- Ahmaruzzaman, M. 2011. Industrial wastes as low-cost potential adsorbents for the treatment of wastewater laden with heavy metals. *Advances in Colloid and Interface Science*. 166: 36–59.
- Aksu, Z, Isoglu, IA. 2007. Use of dried sugar beet pulp for binary biosorption of Gemazol Turquoise Blue-G reactive dye and copper(II) ions: Equilibrium modelling. *Chemical Engineering Journal*. 127: 177–188.
- Altundogan, HS, Altundogan, S, Tumen, F, Bildik, M. 2000. Arsenic removal from aqueous solutions by adsorption on red mud. *Waste Management*. 20: 761–767.
- Altundogan, HS, Altundogan, S, Tumen, F, Bildik, M. 2002. Arsenic adsorption from aqueous solutions by activated red mud. *Waste Management*. 22: 357–363.
- Apak, R, Tutem, E, Hugul, M, Hizal, J. 1998. Heavy metal cation retention by unconventional sorbents (red muds and fly ashes). *Water Research*. 32: 430–440.
- Atun, G, Hisarli, G, Sheldrick, WS, Muhler, M. 2003. Adsorptive removal of methylene blue from colored effluents on fuller's earth. *Journal of Colloid and Interface Science*. 261: 32–39.
- Banerjee, SS, Jayaram, RV, Joshi, MV. 2003. Removal of nickel(II) and zinc(II) from wastewater using fly ash and impregnated fly ash. *Separation Science and Technology*. 38: 1015–1032.
- Bayat, B. 2002. Comparative study of adsorption properties of Turkish fly ash: II. The case of chromium(VI) and cadmium(II). *Journal of Hazardous Materials*. 95: 275–290.
- Bhatnagar, A, Minocha, AK, Pudasainee, D, Chung, HK, Kim, SH, Kim, HS, Lee, G, Min, B, Jeon, BH. 2008. Vanadium removal from water by waste metal sludge and cement immobilization. *Chemical Engineering Journal*. 144: 197–204.

- Bhattacharya, AK, Mandal, SK, Das, SK. 2006. Adsorption of Zn(II) from aqueous solution by using different adsorbents. *Chemical Engineering Journal*. 123: 43–51.
- Bureau of Indian Standards. 1991. Indian standard drinking water—Specification (1st rev.) IS-10500. New Delhi, India: Bureau of Indian Standards.
- Çay, S, Uyanik, A, Özasiç, A. 2004. Single and binary component adsorption of copper(II) and cadmium(II) from aqueous solutions using tea-industry waste. *Separation Science and Technology*. 38: 273–280.
- Dimitrova, SV. 1996. Metal sorption on blast furnace slag. *Water Research*. 30: 228–232.
- Gupta, VK, Ali, I. 2002. Adsorbents for water treatment: Low cost alternatives to carbon. In *Encyclopedia of Surface and Colloid Science*, vol. 1, edited by AT Hubbard, pp. 136–166. New York: Marcel Dekker.
- Gupta, VK, Gupta, MS, Sharma, S. 2001. Process development for the removal of lead and chromium from aqueous solutions using red mud—An aluminium industry waste. *Water Research*. 35, 1125–1134.
- India Ministry of Environment, Forest and Climate Change (MoEF). 1993, May. General standards for discharge of environment pollutants: Effluent. *Gazette Notification of Ministry of Environment, Forest and Climate Change (MoEF)*.
- Jain, AK, Gupta, Bhatnagar, VK, Suhas, A. 2003. Utilization of industrial waste products as adsorbents for the removal of dyes. *Journal of Hazardous Materials*. 101: 31–42.
- Kaithwas, A, Prasad, M, Kulshreshtha, A, Verma, S. 2012. Industrial wastes derived solid adsorbents for CO₂ capture: A mini review. *Chemical Engineering Research and Design*. 90: 1632–1641.
- Khan, AA, Halder, GN, Saha, AK. 2015. Carbon dioxide capture characteristics from flue gas using aqueous 2-amino-2-methyl-1-propanol (AMP) and monoethanolamine (MEA) solutions in packed bed absorption and regeneration columns. *International Journal of Greenhouse Gas Control*. 32: 15–23.
- Khan, AA, Halder, GN, Saha, AK. 2016a. Comparing CO₂ removal characteristics of aqueous solutions of monoethanolamine, 2-amino-2-methyl-1-propanol, methyldiethanolamine and piperazine through absorption process. *International Journal of Greenhouse Gas Control*. 50: 179–189.
- Khan, AA, Halder, GN, Saha, AK. 2016b. Experimental investigation of sorption characteristics of capturing carbon dioxide into piperazine activated aqueous 2-amino-2-methyl-1-propanol solution in a packed column. *International Journal of Greenhouse Gas Control*. 44: 217–226.
- Lenntech. n.d. Water treatment solutions. <http://www.lenntech.com>.
- Lopez, FA, Carlos, SP, Alonso, E, Manuel, J. 1995. Adsorption of Pb²⁺ on blast furnace sludge. *Journal of Chemical Technology and Biotechnology*. 62: 200–206.
- Lopez, FA, Perez, C, Lopez-Delgado, A. 1996. The adsorption of copper(II) ions from aqueous-solution on blast-furnace sludge. *Journal of Materials Science Letters*. 15: 422–424.
- Mohan, D, Pittman Jr, CU, Steele, PH. 2006. Single, binary and multi-component adsorption of copper and cadmium from aqueous solutions on Kraft lignin. *Journal of Colloid and Interface Science*. 297: 489–504.
- Namasivayam, C, Ranganathan, K. 1993. Waste Fe(III)/Cr(III) hydroxide as adsorbent for the removal of Cr(VI) from aqueous solution and chromium plating industry wastewater. *Environmental Pollution*. 82: 255–261.
- Namasivayam, C, Ranganatha, K. 1995. Removal of Cd(II) from wastewater by adsorption on waste Fe(III)/Cr(III) hydroxide. *Water Research*. 29: 1737–1744.
- Namasivayam, C, Ranganatha, K. 1998. Effect of organic ligands on the removal of Pb(II), Ni(II), and Cd(II) by “waste” Fe(III)/Cr(III) hydroxide. *Water Research*. 32: 969–971.
- Namasivayam, C, Sumithra, S. 2007. Adsorptive removal of phenols by Fe(III)/Cr(III) hydroxide, an industrial solid waste. *Clean Technologies and Environmental Policy*. 9: 215–223.
- Nehrenheim, E, Gustafsson, JP. 2008. Kinetic sorption modelling of Cu, Ni, Zn, Pb and Cr ions to pine bark and blast furnace slag by using batch experiments. *Bioresource Technology*. 99: 1571–1577.
- Sarkanen, KV, Ludwig, CH. 1971. *Lignins: Occurrence, Formation, Structure and Reactions*. New York: Wiley-Interscience.

- Shimada, M, Hamabe, HT, Iida, K, Kawarada, T, Okayama. 1999. The properties of activated carbon made from waste newsprint paper. *Journal of Porous Materials*. 6: 191–196.
- Somerset, V, Petrik, L, Iwuoha, E. 2008. Alkaline hydrothermal conversion of fly ash precipitates into zeolites 3: The removal of mercury and lead ions from wastewater. *Journal of Environmental Management*. 87: 125–131.
- Srivastava, SK, Bhattacharjee, G, Tyagi, R, Pant, N, Pal, N. 1988. Studies of the removal of some toxic metal ions from aqueous solutions and industrial waste. Part I (Removal of lead and cadmium lead and cadmium by hydrous iron and aluminium oxide). *Environmental Technology Letters*. 9: 1173–1185.
- Srivastava, SK, Gupta, VK, Mohan, D. 1997. Removal of lead and chromium by activated slag—A blast-furnace waste. *Journal of Environmental Engineering*. 123: 461–468.
- Srivastava, SK, Gupta, VK, Yadav, IS, Mohan, D. 1995. Removal of 2,4-dinitrophenol using bagasse fly ash—A sugar industry waste material. *Indian Journal of Chemical Technology*. 4: 333–336.
- Srivastava, VC, Mall, ID, Mishra, IM. 2008. Removal of cadmium(II) and zinc(II) metal ions from binary aqueous solution by rice husk ash. *Colloids and Surfaces A: Physicochemical and Engineering Aspects*. 312: 172–184.
- Toles, CA, Marshall, WE, Wartelle, LH, McAloon, A. 2000. Steam or carbon dioxide activated carbons from almond shells: Physical, chemical and adsorptive properties and estimated cost of production. *Bioresource Technology*. 75: 197–203.
- United Nations Environment. n.d. Global Environment Monitoring System for freshwater (GEMS/Water). <http://www.gemswater.org>.
- Wang, S, Terdkiatburana, T, Tade, MO. 2008. Single and co-adsorption of heavy metals and humic acid on fly ash. *Separation and Purification Technology*. 58: 353–358.

A Review of Agricultural Solid Waste Materials as Potential Adsorbents for Copper Ions from Water and Wastewater

Mohd Rafatullah, Syed Zaghum Abbas, Akil Ahmad, and David Lokhat

CONTENTS

10.1 Introduction.....	197
10.2 Recent Literature on Activated Carbon Based on Agricultural Waste Materials	199
10.3 Recent Literature on Agricultural Waste Materials.....	203
10.4 Conclusions.....	212
Acknowledgment.....	213
References.....	213

10.1 Introduction

Water is a major source for survival on this planet. Comprising over 70% of the Earth's surface, water is undeniably the most valuable natural resource on our planet. Without this invaluable compound, the life on the Earth would be nonexistent. Water is an important and essential component of this universe and plays a vital role in the proper functioning of the earth's ecosystems. In spite of this, safe drinking water is not available in some parts of the world. The quality of water resources is deteriorating exponentially because of their contamination (Ali and Gupta, 2006; Ambashtha and Sillanpaa, 2010; Ahmad et al., 2011). The ever-growing population, unplanned urbanization, rapid industrialization, and unskilled utilization of natural water resources have led to the destruction of water quality in many parts of the world. In many developing countries, groundwater provides drinking water for more than one-half of the nation's population, and is the sole source of drinking water for many rural communities and some large cities. However, due to industrial, agricultural, and domestic activities, a variety of chemicals can pass through the soil and potentially contaminate the natural water resources and reservoirs. In recent years, various toxic chemicals have been widely detected at dangerous levels in drinking water in many parts of the world, posing a variety of serious health risks to human beings (Bhatnagar et al., 2010). Industrial waters and even natural waters are often contaminated by toxic or sometimes carcinogenic impurities causing ecological disequilibrium and severe public health problems (Karnitz et al., 2007; Gurgel et al., 2008). In general, contaminants come under two broad classes: organic and inorganic. Some organic pollutants include industrial solvents, volatile organic compounds, insecticides, pesticides, and food processing wastes. Inorganic pollutants include gaseous pollutants (such as nitrogen oxide, sulfur dioxide, hydrogen sulfide, ammonia and ammonium compounds), toxic metals, fertilizers, and industrial discharges (Vijayaraghavan and Yun, 2008). Many organic and inorganic pollutants have been

reported in water along with microbial populations. Among these, certain organic and inorganic pollutants are dangerous because of their high toxic and carcinogenic nature (Ali and Aboul-Enein, 2004). Moreover, some organics and heavy metal ions are not biodegradable or biotransformable and, hence, persist in the environment for a long time. Most toxic organic pollutants are pesticides, polynuclear aromatic hydrocarbons (PAHs), polychlorinated biphenyls (PCBs), polybrominated diphenyl ethers (PBDEs), plasticizers, phenols, and drug residues, whereas toxic metal ions include arsenic, cadmium, chromium, zinc, lead, copper, mercury, and nickel among others (Ahmad, 2015; Stiborova, 2017).

Copper is essential to human life and health, but like all heavy metals, it is potentially toxic, especially at high concentration. Copper and its compounds are ubiquitous in the environment and are thus found frequently in surface waters. Potential sources of copper bearing waste include plating baths, fertilizer industry, paints and pigments, and municipal and storm water runoffs. Intake of excessively large doses of copper by man leads to severe mucosal irritation and corrosion, widespread capillary damage, hepatic and renal damage, and central nervous system irritation followed by depression. Severe gastrointestinal irritation and possible necrotic changes in the liver and kidney could occur. The maximum recommended concentration for drinking water that is regulated in Environmental Quality Act 1974 is 0.2 mg/L (Yu et al., 2000; Acemioglu and Alma, 2004; King et al., 2006; Ahmad et al., 2009).

In developed countries, removal of heavy metals from wastewater is normally achieved by advanced technologies such as ion exchange, chemical precipitation, ultrafiltration, or electrochemical deposition (Kurniawan et al., 2006; Aziz et al., 2008; Barakat, 2011). But these technologies do not seem to be economically feasible because of their relatively high costs and that developing countries cannot afford such technologies. Therefore, there is a need to look into alternatives to investigate a low-cost method that is effective and economical. To overcome this difficulty there is a strong need to develop cheap adsorbents that can be used in developing countries.

Adsorption by natural materials is another alternative method. The natural materials form complexes with metal ions using their ligand or functional groups. As a process for metal removal, adsorption has been suggested as being cheaper and more effective than other technologies (Pehlivan et al., 2006). Adsorption was first observed by Lowitz in 1785 (Brunauer, 2007) and was soon applied as a process for removal of color from sugar during refining. In the first half of the nineteenth century, American water treatment plants used inactivated charcoal filters for water purification. Currently, adsorption on activated carbon is a recognized method for the removal of heavy metals from wastewater (Santhy and Selvapathy, 2004; Chan Jun and Jung Heon, 2005), however the high cost of activated carbon limits its use in adsorption. A search for a low-cost and easily available adsorbent has led to the investigation of materials of agricultural and biological origin as potential metal sorbents (Mohan and Singh, 2002). Agricultural by-products, such as sugar beet pulp and sawdust (Aksu and Isoglu, 2005; Ofomaja, 2010), coconut shell (Sekar et al., 2004), clay (Ladonin, 2003), red mud (Geyikçi et al., 2012), and tea leaves (Ngah and Hanafiah, 2008) have received attention. The sorption of metals by these kinds of materials might be attributed to their proteins, carbohydrates, and phenolic compounds that have carboxyl, hydroxyl, sulfate, phosphate, and amino groups that can bind metal ions. Most cases have confirmed that the use of large quantities of wastes from agricultural products for the treatment of polluted water is an attractive and promising option with a double benefit for the environment (Larous et al., 2006): (1) it reduces the residues whose disposal becomes a major, costly problem and (2) it converts the wastes into useful and inexpensive sorbents for water purification.

This chapter deals with the technical feasibility of various solid agricultural waste materials as adsorbents for copper ion removal from water and wastewater. The main aim of

this chapter is to provide a summary of recent information concerning the use of agricultural waste materials as adsorbents. For this, an extensive list of adsorbents has been compiled from recent literature. The reader is strongly encouraged to refer to the original research papers for detailed information on experimental conditions.

10.2 Recent Literature on Activated Carbon Based on Agricultural Waste Materials

Activated carbon is the generic term used to describe a family of carbonaceous adsorbents with highly crystalline forms and extensively developed internal pore structures. Activated carbon has been proven to be an effective adsorbent for the removal of a wide variety of organic and inorganic pollutants dissolved in aqueous media or from a gaseous environment (Danish et al., 2011; Rafatullah et al., 2013). Apart from that, activated carbon is known as a very effective adsorbent due to its large porous surface area, controllable pore structure, thermostability, and low acid/base reactivity. The high surface area and pore volume of activated carbon disclosed the high binding sites, and the activation process enhances this structure to make the carbon more porous. Therefore, it is assumed that there is a good chance for the adsorption and chelation of metal ions onto the binding sites of the adsorbent's surface (Chen et al., 2011). Temperature can play a role in enhancing the pore development of the agricultural waste materials. These characteristics enables its use as cleansing media in pollution control, solvent recovery, food processing, chemical and pharmaceutical industries, wastewater treatment (dyes, heavy metals, detergents, herbicides, pesticides, and polyaromatic hydrocarbons), metal recovery, catalysis, and improving of odor and taste (Chingombe et al., 2005; Crini, 2006; Foo and Hameed, 2009; Li et al., 2008; Singh et al., 2008). Despite its prolific use in adsorption processes, the biggest barrier of its application by the industries is the cost-prohibitive adsorbent and difficulties associated with regeneration (Lata et al., 2008). In recent years, however, there has been a growing interest in the production of activated carbon from different precursors such as agricultural by-products and residual wastes. In fact, cheap materials with high carbon content and low inorganic materials can be used as raw materials for the production of activated carbon. Agricultural by-products have proven to be promising raw materials for the production of activated carbons because of their availability at a low price (Zhou and Haynes, 2010). They can be used for the production of activated carbon with a high adsorption capacity, considerable mechanical strength, and low ash content (Savova et al., 2001). Agricultural by-products such as shells, kernels, fruit stones, fruit seeds, and hulls and husks, for instance, are produced during harvesting and processing of commercial crops. Depending on the crop, some of these by-products have found uses as feedstock for animals, fillers in plasterboard, additives in paper making, and as a material resource for combustion and cogeneration processes. Despite these applications, there is a large quantity of such by-products generated annually that requires disposal and thus pose an environmental problem. Agricultural by-products are rich sources of cellulosic material with an average composition of 40%–50% cellulose, 20%–30% hemicellulose, 20%–25% lignin, and 1%–5% ash making them an attractive source for activated carbon production. There have been many attempts to obtain low-cost activated carbon or adsorbent from agricultural wastes. The lists of precursor materials from different agricultural source for the production of low-cost activated carbon are presented in Table 10.1.

TABLE 10.1

Adsorption Capacities and Other Parameters for the Adsorption of Copper Ions by Activated Carbon Based on Agricultural Waste Materials

Adsorbents	Surface Area/ Particle Size of Adsorbent	Adsorption Capacity	Concentration Range	Contact Time	Temperature (°C)	pH	Percent Adsorption	Reference
Palm shell	–	30.8 mg/g	–	200 min	–	5.0	–	Issabayeva et al., 2010
<i>Moringa oleifera</i>	1.0 mm	11.534 mg/g	10–50 mg/L	15	29	7.0	–	Kalavathy and Miranda, 2010
Cassava peel	1.2 µm	55 mg/g	10–100 mg/L	120 min	–	5.0	–	Moreno-Piraján and Giraldo, 2010
Palm kernel shell	1.68–2.38 mm	1.581 mg/g	–	75 min	–	5.0	97	Onundi et al., 2010
Alga <i>Sargassum</i> sp.	0.5 mm	–	70–150 mg/L	120 min	25	4.0	95.09	Esmaili et al., 2010
Hazelnut shells; apricot stones	1–1.4 mm	0.39 mg/g; 0.53 mg/g	25–1000 ppm	480 min	25	5.0	–	Özçimen and Ersoy-Meriçboyu, 2010
Pine cone	65 mesh	15.05 mg/g	25–100 mg/L	60 min	25	5.0	–	Gegel et al., 2010
Rice hull ash	–	20.12 mg/g	200–400 mg/L	50 min	500	6.2	–	Wang et al., 2010
Potato peel	1.2 µm	74 mg/g	10–100 mg/L	–	–	7.0	–	Moreno-Piraján and Giraldo, 2011
<i>Cicer arietinum</i>	–	18.34 mg/g	20–250 mg/L	70 min	–	7.0	–	Ramana et al., 2010
Coconut shell	0.5–0.2 mm	76.66 mg/g	600 mg/L	90 min	25	5.8	–	Moreno-Piraján et al., 2011
Palm shell	1.6–2.0 mm	22 mg/g	20–350 mg/g	–	–	5.0	–	Issabayeva and Aroua, 2011
Rice husk	0.22 µm	20 mg/g	–	1440 min	30	5.5	–	Zhang et al., 2011
Waste coconut buttons	0.096 mm	73.60 mg/g	10–300 mg/L	180 min	30	7.0	95.2	Anirudhan and Sreekumari, 2011
<i>Ulva fasciata</i>	150 µm	23.64 mg/g	10–80 mg/L	60 min	28	5.0	97.53	Suresh Jeyakumar and Chandrasekaran, 2012
Tunisian date stones	<1.5 mm	31.25 mg/g	10–100 mg/L	120 min	450	5.0	–	Bouhamed et al., 2012
Kenaf fibers	1–2 mm	30.30 mg/g	50–100 mg/L	100 min	70	6.0	–	Chowdhury et al., 2012
Mangosteen peel	40–80 mesh	21.74 mg/g	5–200 ppm	–	–	–	99.6	Chen et al., 2012
Sorghum	100 µm	11.77 mg/L	–	–	–	8.0	100	Uçar et al., 2014

(Continued)

TABLE 10.1 (CONTINUED)
Adsorption Capacities and Other Parameters for the Adsorption of Copper Ions by Activated Carbon Based on Agricultural Waste Materials

Adsorbents	Surface Area/ Particle Size of Adsorbent	Adsorption Capacity	Concentration Range	Contact Time	Temperature (°C)	pH	Percent Adsorption	Reference
Mosa bamboo	150–180 µm	0.396 mg/g; 0.63 mg/g	–	1440 min	–	7.5; 9.8	96.4	Lo et al., 2012
Ma bamboo	0.075–1.14 mm	–	5–70 ppm	30 min	45	7.0	92.9	Thajeel et al., 2013
Rice husk	–	23.584 mg/g	10–30 mg/L	120	–	3.0	67.25	Hou et al., 2013
Corn cob	–	0.005 mmol/g	–	–	–	5.5	–	Zaini et al., 2013
Cattle manure compost	–	50 mg/g	0–250 mg/L	120 min	25	5.2	–	Liu et al., 2014
Fiber board	200–500 µm	0.999 mg/g	–	–	–	3.0	–	Hadjittofi et al., 2014
Cactus fiber	Width = 10 cm; length = 3 cm	498.94 mg/g	–	30 min	700–800	–	68.59	Zhang and Zhang, 2014
Wood bark	–	–	–	–	–	–	–	–
Pomegranate wood	1–3 mm	–	–	70 min	36.1	5.6	65	Ghaedi et al., 2015
Banana peel	361–764 µm	351.1 mg/g	10–30 mg/L	250 min	21	7.0	96	DeMessie et al., 2015
<i>Typha latifolia</i>	<150 µm	34.48 mg/g	50–150 mg/L	120 min	25	7.0	98.16	Song et al., 2015
Grape processing waste	177–400 µm	417 mg/g	–	240 min	600	6.0	94.61	Saygılı et al., 2015
Poplar bark	60–80 mesh	15.2 mg/g	–	–	700	–	87.3	Zhang et al., 2014
Olive stones	0.375 mm	17.780 mg/g	0.5–5.0 mM	–	30	5.5	62	Bohli et al., 2015
Potato peel charcoal	0.2 mm	0.3877 mg/g	150–400 mg/L	120 min	30	6.0	99.8	Afolabi et al., 2016
Green vegetable	25 mm	75.0 mg/g	1.5–3.0 ppm	90 min	25	3.5	–	Sabela et al., 2016
Grape bagasse	0.60–0.80 mm	43.47 mg/g	10–100 mg/L	60 min	45	5.0	71.13	Demiral and Güngör, 2016
<i>Eupatorium adenophorum</i>	–	27.62 mg/g	–	30 min	25	5.0	–	Chen et al., 2016
Softwood and hardwood biochars	<1 mm	4.39 mg/g	0.25–3.00 mM	–	25	5.5	–	Jiang et al., 2016
Capsicum straw	120 mesh	21.93 mg/g	20–50 mg/L	200 min	19	5.0	–	Shoua and Qiu, 2016
Grapeseed	–	11.350 mg/g	50–800 mg/L	–	25	5.0	–	Baylan and Meriçoğlu, 2016
Date stones	100–160 µm	16.12 mg/g	10–100 mg/L	480 min	20	5.5	–	Bouhamed et al., 2015
Milk bush kernel shells	–	0.56 mg/g	1–3	25 min	–	6.7	90	Afolabi et al., 2016

Jiang et al. (2016) studied the copper adsorption by softwood and hardwood biochars under elevated sulfate-induced salinity and acidic pH conditions. Wood-derived biochars pyrolyzed at high temperature adsorbed Cu ions from mimicked pore water of different pH and sulfate salt, but at a lower capacity than those pyrolyzed at a low-moderate temperature. The porosity and surface heterogeneity played an important role in the adsorption capacity and intensity of these biochars, compared with activated carbon. Quantitative analyses with the Langmuir adsorption model point out that hardwood jarrah biochar had advantages over the softwood pine biochar in their adsorption capacity. The adsorption capacities of these biochars were solution pH dependent: the greatest adsorption occurred at a high pH where Cu could be present as free ions in equilibrium with different hydrolysis products whose affinity for the biochars' surfaces was higher. Sulfate salinity had a generally weaker effect on the adsorption capacity, which increased with Na_2SO_4 concentration from 0 to 0.1 M, but slightly decreased at a higher ionic strength. In general, the adsorption capacity of a biochar produced from hardwood timber can be attributed to its high porosity, total surface area, pH buffering capacity, alkalinity, and cation exchange capacity. Detailed adsorption mechanisms as well as the long-term effect of biochars in direct contact with sulfidic tailings should be followed up in further studies to maximize the effect of amendment strategies on mined land and other contaminated environments.

Mosayebi and Azizian (2016) studied copper ion adsorption from aqueous solution with different nanostructured and microstructured zinc oxides and zinc hydroxide loaded on activated carbon cloth. They found that the deposited sample on activated carbon by microwave-assisted chemical bath deposition method was ZnO with a flower-like microstructure at pH 9.8. They also studied a mixture of ZnO and $\text{Zn}(\text{OH})_2$ at pH 10.8 with a flower-like and rhombic microstructures. The deposited sample on activated carbon by hydrothermal method was pure ZnO with dandelion-like nanostructure. It had been found that the number of microwave irradiation steps in the microwave-assisted chemical bath deposition method can affect the adsorption performance of ZnO for removal of Cu^{2+} from aqueous solution. All of the prepared samples in the present work behave as a superadsorbent for copper ion removal with an adsorption capacity of about 1300 mg/g, which was the highest reported value for ZnO adsorbents. The main advantages of prepared adsorbents in the present work were very high adsorption capacity and also ease of separation from solution.

Shou and Qiu (2016) reported the copper ion adsorption onto activated carbon from capsicum straw. The activated carbon contains porous structures and presents an adequate morphology for copper ion adsorption. It was shown that the pseudo-second-order kinetic model better described the sorption data. The adsorption isotherm studies showed that the Langmuir isotherm fits better than the Freundlich isotherm. The maximum adsorption capacity obtained from the Langmuir isotherm was 21.93 mg/g. The positive value of change of free energy indicated a chemical adsorption process at 293 K. As the temperature increases, the value of change of free energy decreases, which may be due to less driving force of the adsorbate molecules resulting in less adsorption capacity. Above 303 K, the thermodynamic parameters showed a spontaneous, thermodynamically favorable and endothermic adsorption.

The adsorption behavior of bentonite and grapeseed activated carbon was investigated in single (Pb^{2+} and Cu^{2+}) and binary ($\text{Pb}^{2+} + \text{Cu}^{2+}$) ion systems by Baylan and Meriçboyu (2016). The adsorption capacity values of bentonite were found to be higher than the values obtained for grapeseed activated carbon under the same conditions due to the differences in the chemical and physical properties of these adsorbents. Adsorption behavior of metal ions on activated grapeseed mainly depends on the functional groups such as phenol, carboxylic, lactone and basic groups are present in the structure. The affinity of bentonite toward the metal ions changed in the order of $\text{Pb}^{2+} > \text{Cu}^{2+}$ in all systems; however, the affinity of

grapeseed activated carbon changed in the order of $\text{Pb}^{2+} > \text{Cu}^{2+}$ in the single-ion system and $\text{Pb}^{2+} \approx \text{Cu}^{2+}$ in the binary-ion system. Adsorption capacities of the adsorbents were also changed depending on the interactions between the metal ions in the binary-ion system. The adsorption capacity values of bentonite and grapeseed activated carbon obtained for Pb^{2+} and Cu^{2+} ions were found to be lower in the binary-ion system than that in the single-ion system. The total adsorption capacity values of bentonite in a binary-ion system were lower than that of single Pb_{2+} ion system and was higher than that of single Cu^{2+} ion system. The total adsorption capacity values of grapeseed activated carbon in the binary-ion system was lower than that of the single Pb^{2+} ion system and was nearly same of the single Cu^{2+} ion system except the lowest (50 mg/L) and the highest (800 mg/L) initial concentrations. It was observed that isotherm models that provide the best fit to the experimental results were changed depending on the type of metal ion, the adsorbent used, and the system studied.

Bouhamed et al. (2016) studied the multicomponent adsorption of copper, nickel, and zinc from aqueous solutions onto activated carbon prepared from date stones. The concentration of metal ions in supernatant was close to equilibrium within 2 h and the optimal pH for the sorption was determined to be about 5.5. At lower pH, adsorption of metal was found to be less, which is due to more hydrogen ions present on the surface of adsorbent. But with an increase in pH, the adsorption capacity increases may be due to the decrease in surface charge and low electrostatic repulsion that enhance the sorption capacity. Adsorption isotherms clearly indicated competitive effects upon sorption. The order of affinity decreases for metal ions sorption on activated carbon calculated on the mass basis as follows: $\text{Cu} > \text{Ni} > \text{Zn}$. The data could be fitted by both the Freundlich and pseudo-Langmuir isotherm models, the latter giving somewhat better results. The maximum adsorption capacities calculated by the pseudo-Langmuir equation were 18.68, 16.12, and 12.19 mg/g for the Cu, Ni, and Zn ions, respectively. The increase in temperature resulted in an increase of sorption of copper, nickel, and zinc ions. The results of this study showed that the prepared activated carbon was suitable for the removal of metal ions present in a multicomponent system in contaminated wastewater.

Afolabi et al. (2016) reported the toxic heavy metals commonly found in typical dairy industrial wastewater using activated carbon produced from milk bush kernel shell produced at 400°C (MBK400) and 600°C (MBK600). The study showed that the adsorption of the heavy metals was influenced by the dose, contact time, and activation temperature. The application of the adsorbent developed in this study indicates that the use of agricultural-based adsorbents is very effective in the treatment of the dairy industrial wastewater. The selected agricultural residue (milk bush kernel shell) was readily available, thus making the method affordable and less expensive. Therefore, the use of agricultural-based adsorbent, as viable alternatives to relatively expensive commercial carbon, in the treatment of dairy industrial wastewater will be an economically competitive solution, because of their better removal efficiency in terms of their adsorption capacities.

10.3 Recent Literature on Agricultural Waste Materials

Activated carbon has been a popular choice as an adsorbent for the removal of heavy metals from aqueous as well as wastewater, but its high cost poses an economical problem. Therefore, researchers felt the need for the development of low cost and easily available materials, which can be used more economically on a large scale. It opened the doors of research interests into the production of alternative adsorbents to replace the costly

activated carbon. The waste materials and by-products from agriculture and other industries are the sources of low-cost adsorbents due to their abundance in nature and because they have processing requirements. In recent years, a new class of adsorbents and specifically cellulosic and lignocellulosic materials have been investigated for the same purposes: their attractiveness resulting from their availability, low cost, and biodegradability. Some previous studies reported their ability to quantitatively accumulate heavy metals and various other water pollutants (Ahmad et al., 2010, 2011, 2012; Rafatullah et al., 2010a; Vakili et al., 2014a, 2014b, 2015). Accumulation of these copper ions on agricultural adsorbents is generally achieved through interactions with the hydroxyl and carboxyl groups particularly abundant in polysaccharides (cellulose and hemicelluloses) and lignin, both of which constitute about 90% of dry lignocellulosic materials. Furthermore, the functionalization of this material by the grafting of organic molecules bearing active groups was carried out very successfully. Interestingly, the use of the resulting hybrid materials as an adsorbent leads to significant increases in adsorption capacity (sometimes greater than that of activated carbons) compared to raw materials. Several recent publications reported the use of low-cost and locally available adsorbents, including sawdust, rice husk, date stones, watermelon peels, rice bran, pine sawdust, oak sawdust, tea leaves, wood sawdust, chestnut shells, bamboo canes straw, mango kernel, peanut shells, and peach nut shells (Rafatullah et al., 2009, 2010b, 2011; Ahmad et al., 2009, 2016; Ibrahim et al., 2010). The sorption of metals by these kinds of materials might be attributed to their proteins, carbohydrates, and phenolic compounds that have carboxyl, hydroxyl, sulfate, phosphate, and amino groups that can bind the metal ions. Various functional groups such as carboxylic, hydroxyl, sulfhydryl, thio, aldehyde, ester, ether, ketones, and amino are present on the surface of agricultural waste materials. Mainly carboxylic and hydroxyl groups are responsible for the binding of metal ions. Binding of metal ions onto the agricultural waste may be due to the ion exchange, chelation, electrostatic attraction, and surface adsorption between the functional group of adsorbents and metal ions (Ahmad et al., 2016). Figure 10.1 shows the ion exchange and chelation between metal ions and the functional group present on adsorbents. The use of agricultural wastes for the treatment of polluted water is also an attractive and promising option for the environment. In Table 10.2, the research activities

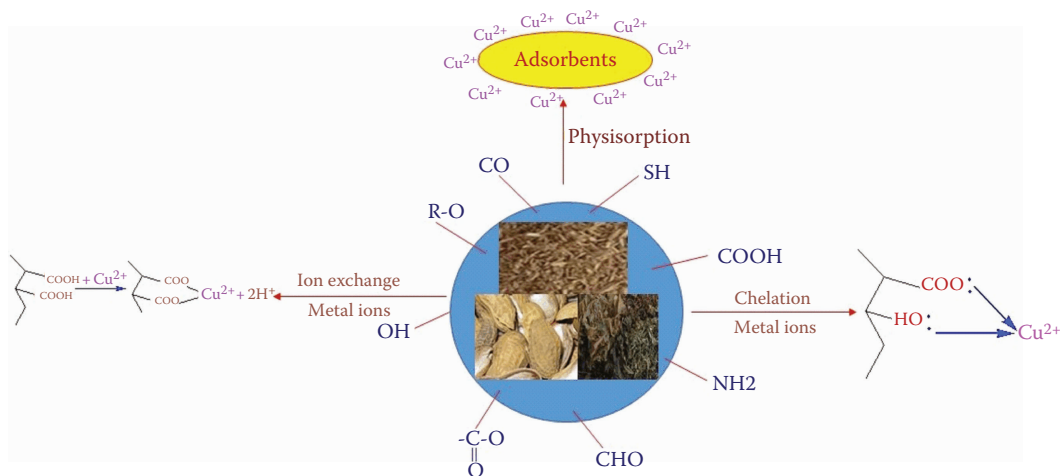


FIGURE 10.1

Mechanism of copper ions adsorption on agricultural solid waste materials.

TABLE 10.2
Adsorption Capacities and Other Parameters for the Adsorption of Copper Ions by Agricultural Wastes Materials

Adsorbents	Surface Area/ Particle Size of Adsorbent	Adsorption Capacity	Concentration Range	Contact Time	Temperature (°C)	pH	Percent Adsorption	Reference
<i>Rosa centifolia</i> waste biomass	-	42.68 mg/g	-	160 min	39	-	-	Nadeem et al., 2010
Citric acid modified wheat straw	-	39.17 mg/g	-	-	140	-	-	Han et al., 2010
<i>Cinnamomum</i> <i>camphora</i> powder	-	17.870 mg/g	-	240 min	-	2.0-4.0	-	Chen et al., 2010
Cassava peel	125-500 µm	41.77 mg/g	-	1440 min	60	4.5	-	Kosasih et al., 2010
Moringa oleifera	1 mm	11.5340 mg/g	0.05-0.7 g/ 100 mL	240 min	29	6.0	55.60	Kalavathy and Miranda, 2010
Pine cone powder	-	26.32 mg/g	60-120 mg d/m ³	15 min	73	5.0	62.06	Ofomaja et al., 2010a
Orange peel	-	77.60 mg/g	50-1000 mg/L	180 min	110	5.5	80	Liang et al., 2010a
xanthate	-	-	-	-	-	-	-	-
Mg ²⁺ /organe peel; K ⁺ /orange peel	50 mesh	40.37 mg/g; 59.77 mg/g	5.0 g/L	120 min	25	5.5	90	Liang et al., 2010b
Soybean hull	0.074 mm	18.00 mg/g	-	90 min	70	8.0	90	Xiang et al., 2010
Mansonia wood sawdust	-	57.1 mg/g	120 mg/dm ³	-	55	6.0	61.5	Ofomaja et al., 2010b
Rice hulls	-	11.83 mg/g	5.0 g	30 min	-	4.0	33	Jeon, 2011
Hazelnut shells;	0.5 mm	35.61 mg/g;	2-10 g d/m ³	10 min	99	6.0	92.11;	Turan and Mesci, 2011
almond shells;	-	23.35 mg/g;	-	-	-	-	78.55;	-
walnut shells	-	21.28 mg/g	-	-	-	-	89.70	-
Peanut shell	-	25.39 mg/g	10 g/L	60 min	20	5.0	-	Witek-Krowiak et al., 2011
Keratin/PA6 blend nanofibers	130-230 nm	103 mg/g	-	1440 min	-	5.8	-	Aluigi et al., 2011

(Continued)

TABLE 10.2 (CONTINUED)

Adsorption Capacities and Other Parameters for the Adsorption of Copper Ions by Agricultural Wastes Materials

Adsorbents	Surface Area/ Particle Size of Adsorbent	Adsorption Capacity	Concentration Range	Contact Time	Temperature (°C)	pH	Percent Adsorption	Reference
Peanut shells, nut shells, plum seeds, eucalyptus bark, olive pips, peach stones, pine sawdust	–	10–15 mg/g	–	0–1800 min	–	5.0–10.0	–	Hansen et al., 2011
Hardwood, corn straw	–	12.52 mg/g	1.0 mm		450–600	3.0–4.0	–	Chen et al., 2011
<i>Uncaria gambir</i>	–	9.950 mg/g	10–50 mg/L	180 min	59	5.0	83.78	K. Tong et al., 2011
Peanut straw, soybean straw, canola straw	0.83 mm	0.58–1.40, 0.48–0.79 mol/ kg	2.5–15.0 mM	60 min	400	4.5–5.0	–	X. Tong et al., 2011
Oil palm leaf powder	250–500 µm	75.98 mg/g	1–200 mg/L	120 min	50	6.0	98.75	Rafatullah et al., 2011
Olive stone; pine bark	<1.000 mm	11.94 mg/g; 1.97 mg/g	10–300 mg/L	100 min	20	5.0	86.9	Blázquez et al., 2011
Cashew nut shell	30–200 µm	20 mg/g	10–50 mg/L	30 min	30	5.0	86.03	Senthil et al., 2011
Banana peel	35–45 µm	20.97 mg/g	10–100 mg/L	60 min	30	3.0	98	Castro et al., 2011
Sugarcane bagasse	120 mesh	31.53 mg/g	–	1440 min	50	5.0	–	Dos Santos et al., 2011
Pineapple leaf powder	Length, 75–90 cm; width, 5–7 cm	9.28 mg/g	1×10^{-5} – 4×10^{-5} M	20 min	41	5.0	90	Weng and Wu, 2011
Chemically activated pine cone	>150 µm	16.53 mg/g	60–120 mg/dm ³	120 min	120	6.3	–	Ofomaja and Naidoo, 2011
Gooseberry fruit	100–300 µm	24.0 mg/g	10–150 mg/L	1440 min	40	3.0	97.60	Rao and Ikram, 2011

(Continued)

TABLE 10.2 (CONTINUED)
Adsorption Capacities and Other Parameters for the Adsorption of Copper Ions by Agricultural Wastes Materials

Adsorbents	Surface Area/ Particle Size of Adsorbent	Adsorption Capacity	Concentration Range	Contact Time	Temperature (°C)	pH	Percent Adsorption	Reference
Biochars	-	-	5–12.5 g/L	240 min	300	5.0–6.0	31.9–78.7	Pellera et al., 2012
Barley straw	-	31.71 mg/g	0.0001– 0.001 mol/L	120 min	120	7.0	88.1	Pehlivan et al., 2012
Pine cone shell	<1.00 mm	6.18 mg/g	10 mg/L	60 min	25	5.0	-	Blázquez et al., 2012
Palm oil fruit shells	<75 µm	60 mg/g	-	600 min	-	6.5	-	Hossain et al., 2012a
Biochars	-	-	-	1440 min	-	-	98	Inyang et al., 2012
Garden grass	150 to <75 µm	137.12 mg/g	10–100 mg/L	400 min	69	6.0	-	Hossain et al., 2012c
Sawdust	0.315 mm	19.475 mg/g	10–60 mg/L	120 min	150	6.0	97.37	Larous and Meniai, 2012
Sawdust	0.315 mm	19.475 mg/g	10–60 mg/L	120 min	23	4.1	97.37	Larous and Meniai, 2012
Activated watermelon shell	150–300 µm	111.1 mg/g	6–20 ppm	120 min	30	8.0	84	Banerjee et al., 2012
Kenaf fibers	1.0 mm	44.27 mg/g	100 mg/L	37 h	38	5.0	-	Hasfalina et al., 2012
Chemically modified cashew nut shell	30–200 mesh	455.7 mg/g	0.1–1.6 g/L	30 min	30	5.0	95	Senthil et al., 2012
Banana peel	>75 µm	27.78 mg/g	10–400 g/L	120 min	51	6.0	94	Hossain et al., 2012b
<i>Artocarpus odoratissimus</i>	355–850 µm	-	20 g/L	240 min	650	4.0	27	Lim et al., 2012
Banana peel; sugarcane bagasse; watermelon rind	>150 µm	8.24 mg/g; 9.48 mg/g; 5.73 mg/g	-	120 min	120	-	80.2; 90.1; 56.4	Liu et al., 2012
Cortex of banana; lemon; orange	1–2 mm	36 mg/g; 70.4 mg/g; 67.2 mg/g	1.5–10 mg/L	-	-	-	45; 88; 84	Kelly-Vargas et al., 2012
Rice husk biochar	-	297 mmol/kg	1–5 mM	15 min	-	-	25.6	Xu et al., 2013a
Rice husk; fly ash	-	-	20–60 mg/L	20 min	-	6.0; 7.0	98.1; 98.5	Hegazi, 2013

(Continued)

TABLE 10.2 (CONTINUED)
Adsorption Capacities and Other Parameters for the Adsorption of Copper Ions by Agricultural Wastes Materials

Adsorbents	Surface Area/ Particle Size of Adsorbent	Adsorption Capacity	Concentration Range	Contact Time	Temperature (°C)	pH	Percent Adsorption	Reference
Pinion shell	<1.000 mm	4.29 mg/g	10 mg/L	100 min	25	5.0	–	Calero et al., 2013
Chufa corm peels	0.15 mm	3.29 mg/g	10–100 mg/L	20 min	25	6.0	72.29	Lin et al., 2013
Root powder of <i>Eichhornia</i> <i>crassipes</i>	–	32.51 mg/g	100 mg/L	30 min	700	5.0	90.2	Li et al., 2013
Rice straw; rice bran; rice husk; hyacinth roots; coconut shell; neem leaves	250–350 µm	18.351 mg/g; 20.977 mg/g; 17.869 mg/g; 21.795 mg/g; 19.888 mg/g; 17.488 mg/g	5–300 mg/L	150 min	29	6.0	–	Singha and Das, 2013
Manure-derived biochar	1–50 m ² /g	48.4 mg/g	1–5 mM	–	–	6.9	62.4	Xu et al., 2013b
Soybean meal waste	1–2 mm	15.7 mg/g	25–700 mg/L	180 min	20	5.0	100	Witek-Krowiak and Reddy, 2013
Rose petals waste biomass	0.25 mm	124.21 mg/g	25–400 mg/L	14450 min	30	–	–	Manzoor et al., 2013
Oil palm shell	0.5–18 mm	1.756 mg/g	5–400 mg/L	480 min	90	8.0	–	Chong et al., 2013
Teak leaves	32 mesh	7.98 mg/g	5–25 g/L	60 min	55	–	60	Goswami et al., 2013
Wheat straw	0.4–1.0 mm	5 mg/g	0.2 g d/m ³	–	–	–	–	Gorgievski et al., 2013
Unmodified wheat straw	25 mesh	0.587 mg/g	100 mg/L	120 min	25	5.0	56.36	Anis et al., 2013
Corn stalk	–	0.325 mmol/g	–	20 min	24	4.5	–	Vafakhah et al., 2014
Wheat straw	380–500 µm	16.01 mg/g	25–300 mg/L	360 min	30	6.0	–	Zhong et al., 2014
Sulfuric acid treated sugarcane bagasse	–	–	5–20 ppm	120 min	25	5.0	94.4	Rana et al., 2014

(Continued)

TABLE 10.2 (CONTINUED)
Adsorption Capacities and Other Parameters for the Adsorption of Copper Ions by Agricultural Wastes Materials

Adsorbents	Surface Area/ Particle Size of Adsorbent	Adsorption Capacity	Concentration Range	Contact Time	Temperature (°C)	pH	Percent Adsorption	Reference
Mushroom biomass	3–5 mm	50 mg/g	0–200 mg/L	–	25	5.0	89.8	Xiao-jing et al., 2014
Olive solid waste	1–1.6 mm	2.23 mg/g	–	30 min	–	–	58	Chouchene et al., 2014
Sweet lime peels	0.355–0.71 mm	37.45 mg/g	100–500 ppm	500 min	30	6.0	–	Panadare et al., 2014
Palm tree frond sawdust	–	–	–	5 min	–	5.0	26	Nouacer et al., 2015
Waste flax meal	–	34.4 mg/g	1–10 g/L	–	–	5.0	–	Podstawczyk et al., 2015
Sugarcane bagasse	–	1.197 mmol/g	0.79 mmol/L	–	25	–	–	do Carmo Ramos et al., 2015
Tomato waste	–	–	0.2 g/50 mL	120 min	39	8.0	92.08	Yargıç et al., 2015
Adlai shell	–	17.2 mg/g	100 mg/L	240 min	24	–	–	de Luna et al., 2015
Citric acid- modified pine sawdust	0.15–0.30 mm	0.16 mmol/g	–	480	59	8.0	–	Zhang et al., 2015
<i>Acidosasa edulis</i> shoot shell	–	2.51 mg/g	20–500 mg/L	45 min	24	5.0	–	Hu et al., 2015
Tea waste	–	–	10–100 ppm	120 min	30	5.0	87	Dwivedi and Rajput, 2015
<i>Citrus maxima</i> peel; passion fruit shell; sugarcane bagasse	–	101 mg/g; 23.0 mg/g; 19.1 mg/g	–	120 min	–	6.0	–	Zhang et al., 2015
Cotton seed	–	–	300 mg/L	–	50	7.0	88	Thirugnanasambandham and Sivakumar, 2015
<i>Fumaria indica</i> biomass	0.25 mm	5.0 mg/g	25–150 mg/L	–	–	–	–	Iqbal and Kheta, 2015
<i>Sophora japonica</i> pods powder	>44 µm	35.84 mg/g	5–100 mg/L	120 min	–	6.0	–	Amer et al., 2015

(Continued)

TABLE 10.2 (CONTINUED)
Adsorption Capacities and Other Parameters for the Adsorption of Copper Ions by Agricultural Wastes Materials

Adsorbents	Surface Area/ Particle Size of Adsorbent	Adsorption Capacity	Concentration Range	Contact Time	Temperature (°C)	pH	Percent Adsorption	Reference
Groundnut shell, orange peel, banana peel, rice husk, coconut husk, wawa tree sawdust	0.5–0.8 mm	1.378 mg/g	40.7 mg/L	64 min		4.4	75	Janyasuthiwong et al., 2015
<i>Carica papaya</i> leaf powder	–	24.51 mg/g	20–30 mg/L	120 min	–	7.0	94.1	Varma and Misra, 2016a
Paddy straw powder	–	37.17 mg/g	10–30 mg/L	120 min	–	7.0	95	Varma and Misra, 2016b
<i>Eriobotrya japonica</i> seed	0.25 mm	58.87 mg/g	75 mg/L	45 min	45	5.0	–	Mushtaq et al., 2016
Cashew nutshell	20–200 nm	48.05 mg/g	20–100 mg/L	30 min	30	6.0	–	Prabu et al., 2016
Raw pomegranate peel	50–3150 µm	3012 mg/g	10–50 mg/L	120 min	39	5.8	–	Ali et al., 2016
Sesame straw	<0.5 mm	55 mg/g	0–320 mg/L	1440 min	25	–	60	Park et al., 2016
Potato peel	0.5–2 mm	84.74 mg/g	25–300 mg/L	35 min	25	5.0	–	Guechi and Hamdaoui, 2016
Wheat straw	250–850 µm	5.38 mg/g	20 mg/L	15 min	25	5.0	26.9	Rebough et al., 2016
Chemically treated potato leaf powder	100–150 µm	42.74 mg/g	5–80 mg/L	160	25	6.5	80	Rebough et al., 2016
Treated sugar beet shreds	224–1000 µm	4.7 mg/g	50 mg/dm ³	180 min	–	6.0	–	Sciban et al., 2016
<i>Jatropha curcas</i> seeds	22.910 mg/g	86.14 mg/g	5–200 mg/L	160 min	25	5.0	92	Nacke et al., 2016
Watermelon shell	–	27.027– 31.25 mg/g	1 g/L	60 min	30–40	5.0	88	Gupta and Gogate, 2016
Sugarcane bagasse	–	0.935 mmol/g	–	–	–	5.5–6.0	–	do Carmo Ramos et al., 2016

have been compiled and the relative data concerning the type of adsorbents, experimental conditions, and adsorption capacities are reported.

Nacke et al. (2016) studied the adsorption of copper ions from water by *Jatropha curcas* L. as the biosorbent. Results showed that the biosorbents obtained from jatropha biomass are capable of removing copper ions from water solutions. Various studies such as the effect of pH, contact time, effect of initial concentration, and amount of adsorbents were carried out. High adsorption capacity was reported at pH 5. pH influences the adsorption process, which may be due to change of surface properties and functional group of adsorbents. Since Langmuir's mathematical model had the best adjustment in the study of isotherms, it indicated the prevalence of chemisorption by monolayers. The biosorbents had a desorption rate that allowed the recovery after the adsorption process, with possible use in sorption/desorption flows.

Ali et al. (2016) reported the adsorption capacity of raw pomegranate peel biosorbents for copper removal. This study showed also that adsorption capacity is dependent on initial metal concentration, time contact, and the metal solution pH. The adsorption process was rapid and reaches equilibrium after 2 hours of contact with a maximum uptake of metal within the first 30 minutes. At low pH, adsorption was unfavorable due to the repulsive electrostatic interaction of both positively charged copper and the adsorbent functional group. The adsorption capacity of pomegranate peel adsorbent was maximal for pH 5.8. The experimental adsorption data showed a good correlation with the Langmuir, Temkin, and Dubinin–Radushkevich isotherm models. The Langmuir maximum adsorption capacity was 30.12 mg/g. The kinetics process followed a pseudo-second-order model. A thermodynamic study gives a positive value for enthalpy change indicating an endothermic process, and a negative value for free energy change indicating a spontaneous process, and a positive value for entropy change indicating the affinity of the adsorbent to copper ions.

Rebouch et al. (2016) used an intelligent architecture based neuro-fuzzy technique for the prediction of removal capacity of copper from aqueous solution through wheat straw as a biosorbent. The adsorption capacity of this material was enhanced using two different treatments. The biosorbent acidic treatment promotes copper adsorption. However, the wheat straw that went through an alkaline treatment better adsorbed chromium. The adsorption capacity of copper and chromium decreased with an increase in temperature, confirming the spontaneous nature of the adsorption, and the sites of adsorption are difficult to access, as it is found to be effective at lower temperatures ($T = 25^{\circ}\text{C}$).

Varma and Misra (2016a) studied the equilibrium and kinetics on the adsorption of copper onto carica papaya leaf powder. They observed that a maximum of 90% to 94.1% of copper removal from the wastewater can be obtained under optimum conditions for small initial concentrations of copper. Therefore, it can be utilized in treatments like polishing by reducing levels of copper to safe limits. When the metal's initial concentration in test solution was 10 mg/L, the equilibrium duration was about 60 min and slightly increased with higher initial concentrations. The optimum pH was found to be 7. Pseudo-second-order reaction fits the experimental data well with an R^2 value of 0.9998, whereas experimental data does not fit well with the pseudo-first-order model for batch experiments. Based on the correlation coefficients ($R^2 = 0.9328$), the Freundlich model better fit the test data and the adsorption process was demonstrated better by this model.

Guechi and Hamdaoui (2016) reported the potato peel as a novel adsorbent for the removal of copper from aqueous solution. Fourier transform infrared (FTIR) analysis confirmed that many functional groups were present on the potato peel surface. The amount of copper ions adsorbed by potato peel increased with an increase in initial concentration,

pH, adsorbent dose, and stirring speed. Maximum adsorption capacity was found at pH 5.0 and adsorption may be speculated due to ion exchange or hydrogen bonding between the copper metal and the adsorbent surface functional groups. However, the amount of copper adsorbed decreased with an increase in temperature, ionic strength, and particle size. The kinetics of the adsorption of copper ions on potato peel closely followed the pseudo-second-order kinetic model. For the diffusion mechanism studies, the results obtained reveal that intraparticle diffusion is not the only rate-limiting step; other processes may control the rate of adsorption of copper on potato peel. Equilibrium data were fitted to the Langmuir, Freundlich, Temkin, and Elovich isotherm models, and the equilibrium data were best described by both the Langmuir and Freundlich isotherm models. The maximum monolayer adsorption capacity of 84.74 mg/g was obtained at 25°C.

10.4 Conclusions

This chapter attempted to cover a wide range of solid agricultural waste materials as adsorbents so that the reader can get an idea about the various types of agricultural materials used for the removal of copper ions from water and wastewater. Inexpensive, locally available, and effective materials could be used in place of commercial activated carbon for the removal of copper ions from aqueous solution. Little effort seems to have been made to carry out a cost comparison between activated carbon and various agricultural waste adsorbents. This aspect needs to be investigated further in order to promote large-scale use of agricultural waste adsorbents. In spite of the scarcity of consistent cost information, the widespread uses of low-cost adsorbents in industries for wastewater treatment applications today are strongly recommended due to their local availability, technical feasibility, engineering applicability, and cost effectiveness. If low-cost adsorbents perform well in removing copper ions at low cost, they can be adopted and widely used in industries not only to minimize cost inefficiency but also improve profitability. Undoubtedly, agricultural waste materials adsorbents offer a lot of promising benefits for commercial purposes in the future.

Literature also reveals that in some cases the modification of the adsorbent increased the removal efficiency. However, less work has been carried out in this direction especially to understand the mechanism of adsorption. We speculate the possibility of the ion exchange mechanism to play an important role in copper ion uptake being a cationic ion. The ion exchange sites on the surface of adsorbents are converted to cationic form and cations are exchanged with copper ions, being a cationic ion, in the equilibrating solution. However, the release of H^+ ions decreases the pH of the solution and the condition becomes unfavorable for copper uptake by ion exchange and ultimately the apparent total adsorption capacity decreases. Thus uptake of copper ions is accompanied by the dual mechanism of ion exchange as well as adsorption. The process of bioadsorption requires further investigation in the direction of modeling, regeneration of bioadsorbents and recovery of copper ion, and immobilization of the waste material for enhanced efficiency and recovery. Most of the reported studies are performed in the batch process; this gives a platform for the designing of continuous flow systems with industrial applications at the commercial level as well. Further research is to be carried out to make the process economically viable at the industrial scale with focus on copper recovery and regeneration of agricultural waste.

Finally we wish to comment on the zero waste strategy of the adsorption process in treatment of wastewater. There is a bigger scope of research of utilization of used adsorbents for further treatment processes. For example, copper-adsorbed adsorbents can further be explored for their application in second-stage adsorption, which is completely an unexplored area of research. Another possibility of exploration is the recovery and reuse of adsorbed substances. All future researches might be accompanied by adsorption/desorption and/or adsorption/readsorption process so that there is no net sludge generation and, if any, it should be minimum. Such a strategy will fulfill the goal of zero waste.

Acknowledgment

The authors would like to express their appreciation to Universiti Sains Malaysia Global Fellowship (USMGF) for support and research facilities for this project.

References

- Acemioglu, B., and Alma, M. H. 2004. Sorption of copper (II) ions by pine sawdust. *Holz als Roh- und Werkstoff* 62:268–272.
- Afolabi, T. J., Alade, A. O., Jimoh, M. O., and Fashola, I. O. 2016. Heavy metal ions adsorption from dairy industrial wastewater using activated carbon from milk bush kernel shell. *Desalin Water Treat* 57:14565–14577.
- Ahmad, A., Khatoon, A., Mohd-Setapar, S.-H., Kumar, R., and Rafatullah, M. 2016. Chemically oxidized pineapple fruit peel for the biosorption of heavy metals from aqueous solutions. *Desalin Water Treat* 57:6432–6442.
- Ahmad, A., Mohd-Setapar, S. H., Chuong, C. S., Khatoon, A., Waseem, A. W., Kumar, A., and Rafatullah, M. 2015. Recent advances in new generation dye removal technologies: Novel search for approaches to reprocess wastewater. *RSC Adv* 5:30801–30818.
- Ahmad, A., Rafatullah, M., Sulaiman, O., Ibrahim, M. H., Chii, Y. Y., and Siddique, B. M. 2009. Removal of Cu (II) and Pb (II) ions from aqueous solutions by adsorption on sawdust of meranti wood. *Desalination* 247:636–646.
- Ahmad, A., Siddique, J. A., Laskar, M. A., Kumar, R., Mohd-Setapar, S. H., Khatoon, A., and Shiekh, R. A. 2015. New generation Amberlite XAD resin for the removal of metal ions: A review. *J Environ Sci* 31:104–123.
- Ahmad, T., Danish, M., Rafatullah, M., Ghazali, A., Sulaiman, O., Hashim, R., and Ibrahim, M. N. M. 2012. The use of date palm as a potential adsorbent for wastewater treatment: A review. *Environ Sci Pollut Res* 19:1464–1484.
- Ahmad, T., Rafatullah, M., Ghazali, A., Sulaiman, O., and Hashim, R. 2011. Oil palm biomass-based adsorbents for the removal of water pollutants—A review. *J Environ Sci Health, Part C* 29:177–222.
- Ahmad, T., Rafatullah, M., Ghazali, A., Sulaiman, O., Hashim, R., and Ahmad, A. 2010. Removal of pesticides from water and wastewater by different adsorbents: A review. *J Environ Sci Health, Part C* 28:231–271.
- Aksu, Z., and İsoğlu, İ. A. 2005. Removal of copper (II) ions from aqueous solution by biosorption onto agricultural waste sugar beet pulp. *Process Biochem* 40:3031–3044.
- Ali, I., and Aboul-Enein, H. Y. 2004. *Chiral Pollutants: Distribution, Toxicity and Analysis by Chromatography and Capillary Electrophoresis*. Chichester: John Wiley & Sons.

- Ali, I., and Gupta, V. K. 2006. Advances in water treatment by adsorption technology. *Nat Protoc* 1:2661–2667.
- Ali, S. B., Jaouali, I., Souissi-Najar, S., and Ouederni, A. 2017. Characterization and adsorption capacity of raw pomegranate peel biosorbent for copper removal. *J Clean Prod* 142:43809–43821.
- Aluigi, A., Tonetti, C., Vineis, C., Tonin, C., and Mazzuchetti, G. 2011. Adsorption of copper (II) ions by keratin/PA6 blend nanofibres. *Eur Polym J* 47:1756–1764.
- Ambashta, R. D., and Sillanpaa, M. 2010. Water purification using magnetic assistance: A review. *J Hazard Mater* 180:38–49.
- Amer, M. W., Ahmad, R. A., and Awwad, A. M. 2015. Biosorption of Cu (II), Ni (II), Zn (II) and Pb (II) ions from aqueous solution by *Sophora japonica* pods powder. *Int J Ind Chem* 6:67–75.
- Anirudhan, T., and Sreekumari, S. 2011. Adsorptive removal of heavy metal ions from industrial effluents using activated carbon derived from waste coconut buttons. *J Environ Sci* 23:1989–1998.
- Anis, M., Haydar, S., and Bari, A. J. 2013. Adsorption of lead and copper from aqueous solution using unmodified wheat straw. *Environ Eng Manage J* 12:2117–2124.
- Aziz, H. A., Adlan, M. N., and Ariffin, K. S. 2008. Heavy metals (Cd, Pb, Zn, Ni, Cu and Cr (III)) removal from water in Malaysia: Post treatment by high quality limestone. *Bioresour Technol* 99:1578–1583.
- Banerjee, K., Ramesh, S., Gandhimathi, R., Nidheesh, P., and Bharathi, K. 2012. A novel agricultural waste adsorbent, watermelon shell for the removal of copper from aqueous solutions. *Iran J Energy Environ* 3:143–156.
- Barakat, M. A. 2011. New trends in removing heavy metals from industrial wastewater. *Arabian J Chem* 4:361–377.
- Baylan, N., and Meriçboyu, A. E. 2016. Adsorption of lead and copper on bentonite and grapeseed activated carbon in single- and binary-ion systems. *Sep Sci Technol* 51:2360–2368.
- Bhatnagar, A., Vilar, V. J. P., Botelho, C. M. S., and Boaventura, R. A. R. 2010. Coconut-based biosorbents for water treatment: A review of the recent literature. *Adv Colloid Interface Sci* 160:1–15.
- Blázquez, G., Martín-Lara, M., Dionisio-Ruiz, E., Tenorio, G., and Calero, M. 2011. Evaluation and comparison of the biosorption process of copper ions onto olive stone and pine bark. *J Ind Eng Chem* 17:824–833.
- Blázquez, G., Martín-Lara, M., Dionisio-Ruiz, E., Tenorio, G., and Calero, M. 2012. Copper biosorption by pine cone shell and thermal decomposition study of the exhausted biosorbent. *J Ind Eng Chem* 18:1741–1750.
- Bohli, T., Ouederni, A., Fiol, N., and Villaescusa, I. 2015. Single and binary adsorption of some heavy metal ions from aqueous solutions by activated carbon derived from olive stones. *Desalin Water Treat* 53:1082–1088.
- Bouhamed, F., Elouear, Z., and Bouzid, J. 2012. Adsorptive removal of copper (II) from aqueous solutions on activated carbon prepared from Tunisian date stones: Equilibrium, kinetics and thermodynamics. *J Taiwan Inst Chem Eng* 43:741–749.
- Bouhamed, F., Elouear, Z., Bouzid, J., and Ouddane, B. 2016. Multi-component adsorption of copper, nickel and zinc from aqueous solutions onto activated carbon prepared from date stones. *Environ Sci Pollut Res* 23:15801–15806.
- Brunauer, S. 2007. *The Adsorption of Gases and Vapors, Vol I: Physical Adsorption*. London: Oxford University Press.
- Calero, M., Blázquez, G., Dionisio-Ruiz, E., Ronda, A., and Martín-Lara, M. 2013. Evaluation of biosorption of copper ions onto pinion shell. *Desalin Water Treat* 51:2411–2422.
- Castro, R. S., Laércio, C., Guilherme, F., Padilha, P. M., Saeki, M. J., Zara, L. F., Martines, M. A. U., and Castro, G. R. 2011. Banana peel applied to the solid phase extraction of copper and lead from river water: Preconcentration of metal ions with a fruit waste. *Ind Eng Chem Res* 50:3446–3451.
- Chan-Jun, M., and Jung-Heon, L. 2005. Use of curdlan and activated carbon composed adsorbents for heavy metal removal. *Process Biochem* 40:1279–1283.
- Chen, H., Dai, G., Zhao, J., Zhong, A., Wu, J., and Yan, H. 2010. Removal of copper (II) ions by a biosorbent—*Cinnamomum camphora* leaves powder. *J Hazard Mater* 177:228–236.

- Chen, J., Song, D., and Yang, P. 2016. Study on adsorption of Cu (II)–Cr (VI) binary system by carbonized *Eupatorium adenophorum*. *Sep Sci Technol* 51:749–758.
- Chen, X., Chen, G., Chen, L., Chen, Y., Lehmann, J., McBride, M. B., and Hay, A. G. 2011. Adsorption of copper and zinc by biochars produced from pyrolysis of hardwood and corn straw in aqueous solution. *Bioresour Technol* 102:8877–8884.
- Chen, Y., Huang, M., Chen, W., and Huang, B. 2012. Adsorption of Cu (II) from aqueous solution using activated carbon derived from mangosteen peel. *BioResources* 7:4965–4975.
- Chingombe, P., Saha, B., and Wakeman, R. J. 2005. Surface modification and characterization of a coal-based activated carbon. *Carbon* 43:3132–3143.
- Chong, H., Chia, P., and Ahmad, M. 2013. The adsorption of heavy metal by Bornean oil palm shell and its potential application as constructed wetland media. *Bioresour Technol* 130:181–186.
- Chouchene, A., Jeguirim, M., and Trouvé, G. 2014. Biosorption performance, combustion behavior, and leaching characteristics of olive solid waste during the removal of copper and nickel from aqueous solutions. *Clean Technol Environ Policy* 16:979–986.
- Chowdhury, Z. Z., Zain, S. M., Khan, R. A., and Islam, M. S. 2012. Preparation and characterizations of activated carbon from kenaf fiber for equilibrium adsorption studies of copper from wastewater. *Korean J Chem Eng* 29:1187–1195.
- Crini, G. 2006. Non-conventional low-cost adsorbents for dye removal: A review. *Bioresour Technol* 97:1061–1085.
- Danish, M., Hashim, R., Ibrahim, M. N. M., Rafatullah, M., Sulaiman, O., Ahmad, T., Shamsuzzoha, M., and Ahmad, A. 2011. Sorption of copper (II) and nickel (II) ions from aqueous solutions using calcium oxide activated date (*Phoenix dactylifera*) stone carbon: Equilibrium, kinetic, and thermodynamic studies. *J Chem Eng Data* 56:3607–3619.
- de Luna, M. D. G., Flores, E. D., Cenía, M. C. B., and Lu, M. C. 2015. Removal of copper ions from aqueous solution by adlai shell (*Coix lacryma-jobi* L.) adsorbents. *Bioresour Technol* 192:841–844.
- DeMessie, B., Sahle-Demessie, E., and Sorial, G. A. 2015. Cleaning water contaminated with heavy metal ions using pyrolyzed biochar adsorbents. *Sep Sci Technol* 50:2448–2457.
- Demiral, H., and Güngör, C. 2016. Adsorption of copper (II) from aqueous solutions on activated carbon prepared from grape bagasse. *J Clean Prod* 124:103–113.
- do Carmo Ramos, S. N., Xavier, A. L. P., Teodoro, F. S., Gil, L. F., and Gurgel, L. V. A. 2016. Removal of cobalt (II), copper (II), and nickel (II) ions from aqueous solutions using phthalate-functionalized sugarcane bagasse: Mono- and multicomponent adsorption in batch mode. *Ind Crops Prod* 79:116–130.
- do Carmo Ramos, S. N., Xavier, A. L. P., Teodoro, F. S., Elias, M. M. C., Goncalves, F. J., Gil, L. F., de Freitas, R. P., and Gurgel, L. V. A. 2015. Modeling mono- and multi-component adsorption of cobalt (II), copper (II), and nickel (II) metal ions from aqueous solution onto a new carboxylated sugarcane bagasse. Part I: Batch adsorption study. *Ind Crops Prod* 74:357–371.
- Dos Santos, V. C., De Souza, J. V., Tarley, C. R., Caetano, J., and Dragunski, D. C. 2011. Copper ions adsorption from aqueous medium using the biosorbent sugarcane bagasse in natura and chemically modified. *Water, Air, Soil Pollut* 216:351–359.
- Dwivedi, A., and Rajput, D. P. S. 2013. Studies on adsorptive removal of heavy metal (Cu, Cd) from aqueous solution by tea waste adsorbent. *Control Pollut* 30:85–90.
- Esmaili, A., Ghasemi, S., and Sohrabipour, J. 2010. Biosorption of copper from wastewater by activated carbon preparation from alga *Sargassum* sp. *Nat Prod Res* 24:341–348.
- Foo, K. Y., and Hameed, B. H. 2009. Recent developments in the preparation and regeneration of activated carbons by microwaves. *Adv Colloid Interface Sci* 149:19–27.
- Gecgel, U., Sezer, K., and Kolancilar, H. 2010. Removal of Cu (II) ions from aqueous solutions by the activated carbon obtained from pine cone. *Asian J Chem* 22:3936.
- Geyikçi, F., Kiliç, E., Çoruh, S., and Elevli, S. 2012. Modelling of lead adsorption from industrial sludge leachate on red mud by using RSM and ANN. *Chem Eng J* 183:53–59.
- Ghaedi, A., Ghaedi, M., Vafaei, A., Irvani, N., Keshavarz, M., Rad, M., Tyagi, I., Agarwal, S., and Gupta, V. K. 2015. Adsorption of copper (II) using modified activated carbon prepared from pomegranate wood: Optimization by bee algorithm and response surface methodology. *J Mol Liq* 206:195–206.

- Gorgievski, M., Božić, D., Stanković, V., Štrbac, N., and Šerbula, S. 2013. Kinetics, equilibrium and mechanism of Cu^{2+} , Ni^{2+} and Zn^{2+} ions biosorption using wheat straw. *Ecol Eng* 58:113–122.
- Goswami, A. K., Kulkarni, S. J., and Dharmadhikari, S. 2013. Adsorption of copper (II) ions from synthetic waste water by teak leaves. *Int J Sci Eng Technol Res* 2:1336–1339.
- Guechi, E.-K., and Hamdaoui, O. 2016. Evaluation of potato peel as a novel adsorbent for the removal of Cu (II) from aqueous solutions: Equilibrium, kinetic, and thermodynamic studies. *Desalin Water Treat* 57:10677–10688.
- Gupta, H., and Gogate, P. R. 2016. Intensified removal of copper from waste water using activated watermelon based biosorbent in the presence of ultrasound. *Ultrason Sonochem* 30: 113–122.
- Gurgel, L. V. A., de Freitas, R. P., and Gil, L. F. 2008. Adsorption of Cu (II), Cd (II), and Pb (II) from aqueous single metal solutions by sugarcane bagasse and mercerized sugarcane bagasse chemically modified with succinic anhydride. *Carbohydr Polym* 74:922–929.
- Hadjittofi, L., Prodromou, M., and Pashalidis, I. 2014. Activated biochar derived from cactus fibres—preparation, characterization and application on Cu (II) removal from aqueous solutions. *Bioresour Technol* 159:460–464.
- Han, R., Zhang, L., Song, C., Zhang, M., Zhu, H., and Zhang, L. 2010. Characterization of modified wheat straw, kinetic and equilibrium study about copper ion and methylene blue adsorption in batch mode. *Carbohydr Polym* 79:1140–1149.
- Hansen, H. K., Arancibia, F., and Gutierrez, C. 2011. Adsorption of copper onto agriculture waste materials. *J Hazard Mater* 180:442–448.
- Hasfalina, C., Maryam, R., Luqman, C., and Rashid, M. 2012. Adsorption of copper (II) from aqueous medium in fixed-bed column by kenaf fibres. *APCBEE Procedia* 3:255–263.
- Hegazi, H. A. 2013. Removal of heavy metals from wastewater using agricultural and industrial wastes as adsorbents. *HBRC J* 9:276–282.
- Hossain, M., Ngo, H. H., Guo, W., and Nguyen, T. 2012a. Palm oil fruit shells as biosorbent for copper removal from water and wastewater: Experiments and sorption models. *Bioresour Technol* 113:97–101.
- Hossain, M., Ngo, H. H., Guo, W., and Nguyen, T. 2012b. Removal of copper from water by adsorption onto banana peel as bioadsorbent. *Int J Geomate* 2:227–234.
- Hossain, M., Ngo, H. H., Guo, W., and Setiadi, T. 2012c. Adsorption and desorption of copper (II) ions onto garden grass. *Bioresour Technol* 121:386–395.
- Hou, X. X., Deng, Q. F., Ren, T. Z., and Yuan, Z. Y. 2013. Adsorption of Cu^{2+} and methyl orange from aqueous solutions by activated carbons of corncob-derived char wastes. *Environ Sci Pollut Res* 20:8521–8534.
- Hu, H., Zhang, J., Lu, K., and Tian, Y. 2015. Characterization of *Acidosasa edulis* shoot shell and its biosorption of copper ions from aqueous solution. *J Environ Chem Eng* 3:357–364.
- Ibrahim, M. N. M., Ngah, W. S. W., Norliana, M. S., Wan Daud, W. R., Rafatullah, M., Sulaiman, O., and Hashim, R. 2010. A novel agricultural waste adsorbent for the removal of lead (II) ions from aqueous solutions. *J Hazard Mater* 182(1):377–385.
- Inyang, M., Gao, B., Yao, Y., Xue, Y., Zimmerman, A. R., Pullammanappallil, P., and Cao, X. 2012. Removal of heavy metals from aqueous solution by biochars derived from anaerobically digested biomass. *Bioresour Technol* 110:50–56.
- Iqbal, M., and Khera, R. A. 2015. Adsorption of copper and lead in single and binary metal system onto *Fumaria indica* biomass. *Chem Int* 1:157b–163b.
- Issabayeva, G., and Aroua, M. K. 2011. Removal of copper and zinc ions onto biomodified palm shell activated carbon. *World Acad Sci Eng Technol* 76:259–262.
- Issabayeva, G., Aroua, M. K., and Sulaiman, N. M. 2010. Study on palm shell activated carbon adsorption capacity to remove copper ions from aqueous solutions. *Desalination* 262:94–98.
- Janyasuthiwong, S., Phiri, S. M., Kijjanapanich, P., Rene, E. R., Esposito, G., and Lens, P. N. 2015. Copper, lead and zinc removal from metal-contaminated wastewater by adsorption onto agricultural wastes. *Environ Technol* 36:3071–3083.

- Jeon, C. 2011. Removal of copper ion using rice hulls. *J Ind Eng Chem* 17:517–520.
- Jiang, S., Huang, L., Nguyen, T. A., Ok, Y. S., Rudolph, V., Yang, H., and Zhang, D. 2016. Copper and zinc adsorption by softwood and hardwood biochars under elevated sulphate-induced salinity and acidic pH conditions. *Chemosphere* 142:64–71.
- Kalavathy, M. H., and Miranda, L. R. 2010. *Moringa oleifera*—A solid phase extractant for the removal of copper, nickel and zinc from aqueous solutions. *Chem Eng J* 158:188–199.
- Karnitz, O., Gurgel, Jr., L. V. A., Perin de Melo, J. C., Botaro, V. R., Melo, T. M. S., De Freitas Gil, R. P., and Gil, L. F. 2007. Adsorption of heavy metal ion from aqueous single metal solution by chemically modified sugarcane bagasse. *Bioresour Technol* 98:1291–1297.
- Kelly-Vargas, K., Cerro-Lopez, M., Reyna-Tellez, S., Bandala, E. R., and Sanchez-Salas, J. L. 2012. Biosorption of heavy metals in polluted water, using different waste fruit cortex. *Phy Chem Earth, Pt A/B/C* 37:26–29.
- King, P., Srinivas, P., Prasanna, K. Y., and Prasad, V. S. R. K. Sorption of copper (II) ion from aqueous solution by *Tectona grandis* l.f. (teak leaves powder). *J Hazard Mater* 136:560–566.
- Kosasih, A. N., Febrianto, J., Sunarso, J., Ju, Y. H., Indraswati, N., and Ismadi, S. 2010. Sequestering of Cu (II) from aqueous solution using cassava peel (*Manihot esculenta*). *J Hazard Mater* 180:366–374.
- Kurniawan, T. A., Chan, G. Y. S., Lo, W. H., and Babel, S. 2006. Physico-chemical treatment techniques for wastewater laden with heavy metals. *Chem Eng J* 118:83–98.
- Ladonin, D. V. 2003. The effect of iron and clay minerals on the adsorption of copper, zinc, lead, and cadmium in the concretion horizon of podzolic soil. *Pochvovedenie* 10:1197–1206.
- Larous, S., and Meniai, A. 2012. Removal of copper (II) from aqueous solution by agricultural by-products-sawdust. *Energy Procedia* 18:915–923.
- Larous, S., Meniai A. H., and Lehocine, M. B. 2005. Experimental study of the removal of copper from aqueous solutions by adsorption using sawdust. *Desalination* 185:483–490.
- Lata, H., Garg, V. K., and Gupta, R. K. 2008. Adsorptive removal of basic dye by chemically activated Parthenium biomass: Equilibrium and kinetic modeling. *Desalination* 219:250–261.
- Li, W., Zhang, L. B., Peng, J. H., Li, N., and Zhu, X. Y. 2008. Preparation of high surface area activated carbons from tobacco stems with K_2CO_3 activation using microwave radiation. *Ind Crops Prod* 27:341–347.
- Li, X., Liu, S., Na, Z., Lu, D., and Liu, Z. 2013. Adsorption, concentration, and recovery of aqueous heavy metal ions with the root powder of *Eichhornia crassipes*. *Ecol Eng* 60:160–166.
- Liang, S., Guo, X., Feng, N., and Tian, Q. 2010a. Effective removal of heavy metals from aqueous solutions by orange peel xanthate transactions of nonferrous metals. *Soc China* 20:s187–s191.
- Liang, S., Guo, X., Feng, N., and Tian, Q. 2010b. Isotherms, kinetics and thermodynamic studies of adsorption of Cu^{2+} from aqueous solutions by Mg^{2+}/K^+ type orange peel adsorbents. *J Hazard Mater* 174:756–762.
- Lim, L. B., Priyantha, N., Tennakoon, D., and Dahri, M. K. 2012. Biosorption of cadmium (II) and copper (II) ions from aqueous solution by core of *Artocarpus odoratissimus*. *Environ Sci Pollut Res* 19:3250–3256.
- Lin, Q., Wang, Q., Duan, Y., Wei, X., Wu, G., Luo, Y., and Xie, Q. 2013. Removal of Cu (II), Cr (III), and Cr (VI) from aqueous solution using a novel agricultural waste adsorbent. *Sep Sci Technol* 48:2843–2851.
- Liu, C., Ngo, H. H., Guo, W., and Tung, K. L. 2012. Optimal conditions for preparation of banana peels, sugarcane bagasse and watermelon rind in removing copper from water. *Bioresour Technol* 119:349–354.
- Liu, X., Zhang, W., and Zhang, Z. 2014. Preparation and characteristics of activated carbon from waste fiberboard and its use for adsorption of Cu (II). *Mater Lett* 116:304–306.
- Lo, S. F., Wang, S. Y., Tsai, M. J., and Lin, L. D. 2012. Adsorption capacity and removal efficiency of heavy metal ions by Moso and Ma bamboo activated carbons. *Chem Eng Res Des* 90:1397–1406.
- Manzoor, Q., Nadeem, R., Iqbal, M., Saeed, R., and Ansari, T. M. 2013. Organic acids pretreatment effect on *Rosa bourbonia* phyto-biomass for removal of Pb (II) and Cu (II) from aqueous media. *Bioresour Technol* 132:446–452.

- Mohan, D., and Singh, K. P. 2002. Single and multi-component adsorption of Cd (II) and Zn (II) using activated carbon derived from bagasse an agricultural waste. *Water Res* 36:2304–2318.
- Moreno-Piraján, J., and Giraldo, L. 2010. Adsorption of copper from aqueous solution by activated carbons obtained by pyrolysis of cassava peel. *J Anal Appl Pyrol* 87:188–193.
- Moreno-Piraján, J., and Giraldo, L. 2011. Activated carbon obtained by pyrolysis of potato peel for the removal of heavy metal copper (II) from aqueous solutions. *J Anal Appl Pyrol* 90:42–47.
- Moreno-Piraján, J. C., Garcia-Cuello, V. S., and Giraldo, L. 2011. The removal and kinetic study of Mn, Fe, Ni and Cu ions from wastewater onto activated carbon from coconut shells. *Adsorption* 17:505–514.
- Mosayebi, E., Azizian, S., and Hajian, A. 2016. Synthesis of nanostructured and microstructured ZnO and Zn(OH)₂ on activated carbon cloth by hydrothermal and microwave-assisted chemical bath deposition methods. *Superlattice Microst* 81:226–232.
- Mushtaq, M., Bhatti, H. N., Iqbal, M., and Noreen, S. 2016. *Eriobotrya japonica* seed biocomposite efficiency for copper adsorption: Isotherms, kinetics, thermodynamic and desorption studies. *J Environ Manage* 176:21–33.
- Nacke, H., Affonso, C. G., Campagnolo, M. A., Coelho, G. F., Schwantes, D., dos Santos, M. G., Briesch, Jr., D. L., and Zimmermann, J. 2016. Adsorption of Cu (II) and Zn (II) from water by *Jatropha curcas* L. as biosorbent. *Open Chem* 14:103–117.
- Nadeem, R., Hanif, M. A., Riaz, M., Azhar, A. A., Iqbal, T., and Ansari, T. M. 2010. Kinetic and equilibrium modeling of Cu (II) and Ni (II) sorption onto physically pretreated *Rosa centifolia* distillation waste biomass. *Afr J Biotechnol* 9:9051–9062.
- Ngah, W. S. W., and Hanafiah, M. A. K. M. 2008. Biosorption of copper ions from dilute aqueous solutions on base treated rubber (*Hevea brasiliensis*) leaves powder: Kinetics, isotherm, and biosorption mechanisms. *J Environ Sci* 20:1168–1176.
- Nouacer, S., Hazourli, S., Despas, C., and Hébrant, M. 2015. Sorption of polluting metal ions on a palm tree frond sawdust studied by the means of modified carbon paste electrodes. *Talanta* 144:318–323.
- Ofomaja, A. E. 2010. Biosorption studies of Cu (II) onto *Mansonia* sawdust: Process design to minimize biosorbent dose and contact time. *React Funct Polym* 70:879–889.
- Ofomaja, A., and Naidoo, E. 2011. Biosorption of copper from aqueous solution by chemically activated pine cone: A kinetic study. *Chem Eng J* 175:260–270.
- Ofomaja, A., Naidoo, E., and Modise, S. 2010a. Biosorption of copper (II) and lead (II) onto potassium hydroxide treated pine cone powder. *J Environ Manage* 91:1674–1685.
- Ofomaja, A., Unuabonah, E., and Oladoja, N. 2010b. Competitive modeling for the biosorptive removal of copper and lead ions from aqueous solution by *Mansonia* wood sawdust. *Bioresour Technol* 101:3844–3852.
- Onundi, Y. B., Mamun, A., Al Khatib, M., and Ahmed, Y. M. 2010. Adsorption of copper, nickel and lead ions from synthetic semiconductor industrial wastewater by palm shell activated carbon. *Int J Environ Sci Technol* 7:751–758.
- Özçimen, D., and Ersoy-Meriçboyu, A. 2010. Adsorption of copper (II) ions onto hazelnut shell and apricot stone activated carbons. *Adsorpt Sci Technol* 28:327–340.
- Panadare, D. C., Lade, V. G., and Rathod, V. K. 2014. Adsorptive removal of copper (II) from aqueous solution onto the waste sweet lime peels (SLP): Equilibrium, kinetics and thermodynamics studies. *Desalin Water Treat* 52:7822–7837.
- Park, J. H., Ok, Y. S., Kim, S. H., Cho, J. S., Heo, J. S., Delaune, R. D., and Seo, D. C. 2016. Competitive adsorption of heavy metals onto sesame straw biochar in aqueous solutions. *Chemosphere* 142:77–83.
- Pehlivan, E., Altun, T., and Parlayici, Ş. 2012. Modified barley straw as a potential biosorbent for removal of copper ions from aqueous solution. *Food Chem* 135:2229–2234.
- Pehlivan, E., Certin, S., and Yanik, B. H. 2006. Equilibrium studies for the sorption of zinc and copper from aqueous solutions using sugar beet pulp and fly ash. *J Hazard Mater* 135:193–199.

- Pellera, F. M., Giannis, A., Kalderis, D., Anastasiadou, K., Stegmann, R., Wang, J. Y., and Gidaracos, E. 2012. Adsorption of Cu (II) ions from aqueous solutions on biochars prepared from agricultural by-products. *J Environ Manage* 96:35–42.
- Podstawczyk, D., Witek-Krowiak, A., Dawiec, A., and Bhatnagar, A. 2015. Biosorption of copper (II) ions by flax meal: Empirical modeling and process optimization by response surface methodology (RSM) and artificial neural network (ANN) simulation. *Ecol Eng* 83:364–379.
- Prabu, D., Parthiban, R., Senthil, K. P., Kumari, N., and Saikia, P. 2016. Adsorption of copper ions onto nano-scale zero-valent iron impregnated cashew nut shell. *Desalin Water Treat* 57:6487–6502.
- Rafatullah, M., Ahmad, T., Ghazali, A., Sulaiman, O., Danish, M., and Hashim, R. 2013. Oil palm biomass as a precursor of activated carbons: A review. *Crit Rev Environ Sci Technol* 43:1117–1161.
- Rafatullah, M., Sulaiman, O., Hashim, R., and Ahmad, A. 2009. Adsorption of copper (II), chromium (III), nickel (II) and lead (II) ions from aqueous solutions by meranti sawdust. *J Hazard Mater* 170:969–977.
- Rafatullah, M., Sulaiman, O., Hashim, R., and Ahmad, A. 2010a. Adsorption of copper (II) onto different adsorbents. *J Dis Sci Technol* 31:918–930.
- Rafatullah, M., Sulaiman, O., Hashim, R., and Ahmad, A. 2010b. Adsorption of methylene blue on low-cost adsorbents: A review. *J Hazard Mater* 177(1):70–80.
- Rafatullah, M., Sulaiman, O., Hashim, R., and Amini, M. 2011. Adsorption of copper (II) ions onto surfactant-modified oil palm leaf powder. *J Disper Sci Technol* 32:1641–1648.
- Ramana, D., Jamuna, K., Satyanarayana, B., Venkateswarlu, B., Rao, M. M., and Sessaiah, K. 2010. Removal of heavy metals from aqueous solutions using activated carbon prepared from *Cicer arietinum*. *Toxicol Environ Chem* 92:1447–1460.
- Rana, K., Shah, M., and Limbachiya, N. 2014. Adsorption of copper Cu²⁺ metal ion from waste water using sulphuric acid treated sugarcane bagasse as adsorbent. *Int J Adv Eng Res Sci* 1:55–59.
- Rao, R. A. K., and Ikram, S. 2011. Sorption studies of Cu (II) on gooseberry fruit (*Embllica officinalis*) and its removal from electroplating wastewater. *Desalination* 277:390–398.
- Rebouch, S., Bouhedda, M., and Hanini, S. 2016. Neuro-fuzzy modeling of Cu (II) and Cr (VI) adsorption from aqueous solution by wheat straw. *Desalin Water Treat* 57:6515–6530.
- Sabela, M. I., Kunene, K., Kanchi, S., Xhakaza, N. M., Bathinapatla, A., Mdluli, P., Sharma, D., and Bisetty, K. 2016. Removal of copper (II) from wastewater using green vegetable waste derived activated carbon: An approach to equilibrium and kinetic study. *Arabian J Chem*. doi: dx.doi.org/10.1016/j.arabjc.2016.06.001.
- Santhy, K., and Selvapathy, P. 2004. Removal of heavy metals from wastewater by adsorption on coir pith activated carbon. *Sep Sci Technol* 39:3331–3351.
- Savova, D., Apak, E., Ekinci, E., Yardim, F., Petrov, N., Budinova, T., Razvigorova, M., and Minkova, V. 2001. Biomass conversion to carbon adsorbents and gas. *Biomass Bioenerg* 21:133–142.
- Saygili, H., Güzel, F., and Önal, Y. 2015. Conversion of grape industrial processing waste to activated carbon sorbent and its performance in cationic and anionic dyes adsorption. *J Clean Prod* 93:84–93.
- Sciban, M., Vulic, T., Kukic, D., Prodanovic, J., and Klasnja, M. 2016. Characterization of raw and treated sugar beet shreds for copper ions adsorption. *Desalin Water Treat* 57:14590–14597.
- Sekar, M., Sakthi, V., and Rengaraj, S. 2004. Kinetics and equilibrium adsorption study of lead (II) onto activated carbon prepared from coconut shell. *J Colloid Interface Sci* 279:307–313.
- Senthil, K. P., Ramalingam, S., Abhinaya, R. V., Kirupha, S. D., Murugesan, A., and Sivanesan, S. 2012. Adsorption of metal ions onto the chemically modified agricultural waste. *Clean–Soil, Air, Water* 40:188–197.
- Senthil, K. P., Ramalingam, S., Sathiaselvabala, V., Kirupha, S. D., and Sivanesan, S. 2011. Removal of copper (II) ions from aqueous solution by adsorption using cashew nut shell. *Desalination* 266:63–71.
- Shou, J., and Qiu, M. 2016. Adsorption of copper ions onto activated carbon from capsicum straw. *Desalin Water Treat* 57:353–359.
- Singh, K. P., Malik, A., Sinha, S., and Ojha, P. 2008. Liquid-phase adsorption of phenols using activated carbons derived from agricultural waste material. *J Hazard Mater* 150:626–641.

- Singha, B., and Das, S. K. 2013. Adsorptive removal of Cu (II) from aqueous solution and industrial effluent using natural/agricultural wastes. *Colloids Surfaces B: Biointerfaces* 107:97–106.
- Song, J., Zhang, R., Li, K., Li, B., and Tang, C. 2015. Adsorption of copper and zinc on activated carbon prepared from *Typha latifolia* L. *Clean–Soil, Air, Water* 43:79–85.
- Stiborova, H., Kolar, M., Vrkoslavova, J., Pulkrabova, J., Hajslova, J., Demnerova, K., and Uhlik, O. 2017. Linking toxicity profiles to pollutants in sludge and sediments. *J Hazard Mater* 321:672–680.
- Sulaiman, O., Amini, M., Hazim, M., Rafatullah, M., Hashim, R., and Ahmad, A. 2010. Adsorption equilibrium and thermodynamic studies of copper (II) ions from aqueous solutions by oil palm leaves. *Int J Chem Reac Eng* 8:1.
- Suresh, J. R., and Chandrasekaran, V. 2012. Comparative studies on the removal of copper (II) by *Ulva fasciata* activated carbon and commercially activated carbon. *Pol J Chem Technol* 14:88–94.
- Thajeel, A. S., Al-Faize, M. M., and Raheem, A. 2013. Removal of Cu^{2+} & Fe^{3+} ions from oil wells by local activated carbon in batch adsorption process. *Aquat Sci Technol* 1:78–94.
- Thirugnanasambandham, K., and Sivakumar, V. 2015. An eco-friendly approach for copper (II) ion adsorption onto cotton seed cake and its characterization: Simulation and validation. *J Taiwan Inst Chem Eng* 50:198–204.
- Tong, K., Kassim, M. J., and Azraa, A. 2011. Adsorption of copper ion from its aqueous solution by a novel biosorbent *Uncaria gambir*: Equilibrium, kinetics, and thermodynamic studies. *Chem Eng J* 170:145–153.
- Tong, X. J., Li, J. Y., Yuan, J. H., and Xu, R. K. 2011. Adsorption of Cu (II) by biochars generated from three crop straws. *Chem Eng J* 172:828–834.
- Turan, N. G., and Mesci, B. 2011. Adsorption of copper (II) and zinc (II) ions by various agricultural by-products, experimental studies and modeling. *Environ Protec Eng* 37:143–161.
- Uçar, G., Bakircioglu, D., and Kurtulus, Y. 2014. Determination of metal ions in water and tea samples by flame-AAS after preconcentration using sorghum in nature form and chemically activated. *J Anal Chem* 69:420–425.
- Vafakhah, S., Bahrololoom, M., Bazarganlari, R., and Saeedikhani, M. 2014. Removal of copper ions from electroplating effluent solutions with native corn cob and corn stalk and chemically modified corn stalk. *J Environ Chem Eng* 2:356–361.
- Vakili, M., Rafatullah, M., Ibrahim, M. H., Abdullah, A. Z., and Salamatinia, B. 2014. Oil palm biomass as an adsorbent for heavy metals. *Rev Environ Cont Toxicol* 232:61–88.
- Vakili, M., Rafatullah, M., Salamatinia, B., Abdullah, A. Z., Ibrahim, M. H., Tan, K. B., Gholami, Z., and Amouzgar, P. 2014. Application of chitosan and its derivatives as adsorbents for dye removal from water and wastewater: A review. *Carbohydr Polym* 113:115–130.
- Varma, V. G., and Misra, A. K. 2016a. Equilibrium and kinetic studies on the adsorption of copper onto carica papaya leaf powder. *Membrane Water Treat* 5:403–416.
- Varma, V. G., and Misra, A. K. 2016b. Equilibrium and kinetic studies on the adsorption of copper onto paddy straw powder. *Desalin Water Treat* 57:13081–13090.
- Vijayaraghavan, K., and Yun, Y. S. 2008. Bacterial biosorbents and biosorption. *Biotechnol Adv* 26:266–291.
- Wang, L. H., Lin, C. I., and Wu, F. C. 2010. Kinetic study of adsorption of copper (II) ion from aqueous solution using rice hull ash. *J Taiwan Inst Chem Eng* 41:599–605.
- Weng, C. H., and Wu, Y. C. 2011. Potential low-cost biosorbent for copper removal: Pineapple leaf powder. *J Environ Eng* 138:286–292.
- Witek-Krowiak, A., and Reddy, D. H. K. 2013. Removal of microelemental Cr (III) and Cu (II) by using soybean meal waste—Unusual isotherms and insights of binding mechanism. *Bioresour Technol* 127:350–357.
- Witek-Krowiak, A., Szafran, R. G., and Modelski, S. 2011. Biosorption of heavy metals from aqueous solutions onto peanut shell as a low-cost biosorbent. *Desalination* 265:126–134.
- Xiang, G., Zhang, Y., Jiang, X., He, L., Fan, L., and Zhao, W. 2010. Determination of trace copper in food samples by flame atomic absorption spectrometry after solid phase extraction on modified soybean hull. *J Hazard Mater* 179:521–525.

- Xiao-jing, H., Hai-dong, G., Ting-ting, Z., Yu, J., and Juan-juan, Q. 2014. Biosorption mechanism of Cu^{2+} by innovative immobilized spent substrate of fragrant mushroom biomass. *Ecol Eng* 73:509–513.
- Xu, X., Cao, X., and Zhao, L. 2013a. Comparison of rice husk-and dairy manure-derived biochars for simultaneously removing heavy metals from aqueous solutions: Role of mineral components in biochars. *Chemosphere* 92:955–961.
- Xu, X., Cao, X., Zhao, L., Wang, H., Yu, H., and Gao, B. 2013b. Removal of Cu, Zn, and Cd from aqueous solutions by the dairy manure-derived biochar. *Environ Sci Pollut Res* 20:358–368.
- Yargıç, A., Şahin, R. Y., Özbay, N., and Önal, E. 2015. Assessment of toxic copper (II) biosorption from aqueous solution by chemically-treated tomato waste. *J Clean Prod* 88:152–159.
- Yu, B., Zhang, Y., Shukla, A., Shukla, S. S., and Dorris, K. L. 2000. The removal of heavy metal from aqueous solutions by sawdust adsorption-removal of copper. *J Hazard Mater* 80:33–42.
- Zaini, M. A. A., Che, Y. M. A., Mohd, S. S. H., Amano, Y., and Machida, M. 2013. Effect of heat treatment on copper removal onto manure-compost-activated carbons. *Desalin Water Treat* 51:5608–5616.
- Zhang, J., Fu, H., Lv, X., Tang, J., and Xu, X. 2011. Removal of Cu (II) from aqueous solution using the rice husk carbons prepared by the physical activation process. *Biomass Bioenerg* 35:464–472.
- Zhang, J., and Zhang, W. 2014. Preparation and characteristics of activated carbon from wood bark and its use for adsorption of Cu (II). *Mater Sci* 20:474–478.
- Zhang, J., Zhang, W., and Zhang, Y. 2014. Pore structure characteristics of activated carbon fibers derived from poplar bark liquefaction and their use for adsorption of Cu (II). *BioResources* 10:566–574.
- Zhang, R., Zhou, Y., Gu, X., and Lu, J. 2015. Competitive adsorption of methylene blue and Cu^{2+} onto citric acid modified pine sawdust. *Clean—Soil, Air, Water* 43:96–103.
- Zhong, Q. Q., Yue, Q. Y., Li, Q., Gao, B. Y., and Xu, X. 2014. Removal of Cu (II) and Cr (VI) from wastewater by an amphoteric sorbent based on cellulose-rich biomass. *Carbohydr Polym* 111:788–796.
- Zhou, H. F., and Haynes, R. J. 2010. Sorption of heavy metals by inorganic and organic components of solid wastes: Significance to use of wastes as low-cost adsorbents and immobilizing agents. *Crit Rev Environ Sci Technol* 40:909–977.



Taylor & Francis

Taylor & Francis Group

<http://taylorandfrancis.com>

Section III

Solid Wastes-Based Emerging Adsorbents in Gaseous/ Water Purification



Taylor & Francis

Taylor & Francis Group

<http://taylorandfrancis.com>

Mesoporous Adsorbents from Biomass: Opportunities and Challenges in Hydrothermal Treatment

Akshay Jain, Kubilay Tekin, and Madapusi P. Srinivasan

CONTENTS

11.1 Introduction.....	225
11.2 Biomass and Biomass-Based Adsorbents.....	227
11.3 Hydrothermal Carbonization: A Promising Tool for Hydrochar Synthesis.....	230
11.4 Hydrochar Formation, Properties, and Applications.....	231
11.4.1 Hydrochar for Activated Carbon Synthesis.....	235
11.4.1.1 Case Study 1: Effect of Hydrothermal Pretreatment Temperature... 235	
11.4.1.2 Case Study 2: Use of ZnCl_2 as a Catalyst.....	237
11.4.1.3 Case Study 3: Effect of Higher ZnCl_2 Amounts under Different Hydrothermal Temperatures	239
11.4.1.4 Case Study 4: Use of H_3PO_4 as a Catalyst	240
11.4.1.5 Case Study 5: Use of H_2O_2 as a Catalyst	240
11.4.1.6 Case Study 6: Use of ZnCl_2 as a Catalyst under Different Concentrations.....	244
11.5 Conclusions.....	246
References.....	246

11.1 Introduction

In recent years, waste-to-energy/-resource conversion has received considerable attention in response to substantial increase in the utilization of natural resources and the amount of solid wastes generated caused by rapid population growth (Lua and Guo 2001). Utilization of biomass waste for producing new resources, especially for environmental remediation, is attractive because it (1) offers solutions for solid waste management, (2) reduces the cost of raw materials required for production of valuable chemicals and commercial products, and (3) addresses global environmental issues in the context of sustainability. Products such as activated carbon obtained from biomass wastes have been explored for a wide range of applications, such as removal of heavy metals from contaminated water (Lesmana et al. 2009), removal of contaminants from flue gas (Khalili and Arastoopour 2002; Khalili and Perez-Luna 2004), carbon dioxide (CO_2) capture (Sevilla and Fuertes 2011), hydrogen storage (Sevilla, Fuertes, and Mokaya 2011), heterogeneous catalysis (Jain et al. 2016; Titirici et al. 2012), photocatalysis, energy storage (Sandí et al. 2003; Simon and Gogotsi 2008), bio-imaging, and drug delivery (Selvi et al. 2008).

Activated carbons with high microporosity (micropore area/total area) are used extensively for adsorption of small-sized pollutants or molecules. However, the treatment of

wastewater streams containing large molecules (high molecular weight compounds, dyes, etc.) requires adsorbents with high mesopore contents (as per IUPAC [International Union of Pure and Applied Chemistry], mesopores constitute the pore size, which lies between 2 nm and 50 nm, and micropores constitute <2 nm). Carbons with high mesopore surface areas are also of great interest in numerous applications, for example, in electrochemical capacitors, chromatography, biocatalysis (Hartmann 2005; Talapaneni et al. 2012), electrocatalysis (Calvillo et al. 2007), and lithium batteries (Ryoo et al. 2001).

Depending on the feedstocks being considered, templating methods or activation processes with suitable activating agents are primarily used to produce mesoporous carbons. Zhuang et al. (2009) showed that using commercial triblock copolymer F127 as a structure-directing agent and tetraethyl orthosilicate as a template can yield 100% mesoporosity (mesopore area/total area) with high specific surface areas up to 2580 m²/g. Despite the ability to generate high mesopore surface areas by hard templating, the process has some inherent limitations. Removal of the sacrificial component requires appropriate treatment procedures; in particular, hydrofluoric acid (HF) is used for the removal of silica templates (Vinu et al. 2006; Xia and Mokaya 2004; Zhuang et al. 2009). The carbonaceous material that constitutes the matrix may have structural defects formed during template removal (Meng et al. 2005). In the case of soft template synthesis, a constraint is imposed in terms of the availability of the right combination of carbon-yielding and pore-forming components (Liang, Li, and Dai 2008). Furthermore, the use of specific precursors as sacrificial and matrix compounds increases the cost of production.

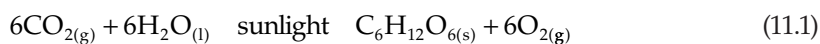
To a large extent, synthesis of mesoporous carbons from biomass-based starting material has been carried out using physical and chemical activating agents (Ania et al. 2005; Aygün, Yenisoý-Karakaş, and Duman 2003; Guo and Lua 1999; Khalili, Arastoopour, and Walhof 2000; Littrell et al. 2002; Stavropoulos and Zabaniotou 2005) or a combination of both (Hu, Srinivasan, and Ni 2000, 2001). A number of materials have been introduced as activating agents prior to or concurrently with pyrolysis, including CO₂, steam, KOH, ZnCl₂, and H₃PO₄. KOH as an activating agent is predominantly used for the preparation of microporous carbons. Chemical activating agents to produce mesoporous carbons (i.e., ZnCl₂ and H₃PO₄) are typically dehydrating agents that remove oxygen and hydrogen from the lignocellulosic material in the form of water and increase the porosity (Nakagawa, Molina-Sabio, and Rodríguez-Reinoso 2007). Additionally, the presence of oxygenated functional groups (OFGs) in the precursor enhances the activity of activating agents (Falco, Marco-Lozar et al. 2013; Jain, Balasubramanian, and Srinivasan 2015b; Jain et al. 2015; Lillo-Ródenas et al. 2004; Linares-Solano et al. 2007; Sevilla and Fuertes 2011; Sevilla, Fuertes, and Mokaya 2011) and thus yields improved porosity in the carbon. It may be advantageous to introduce pretreatment steps that enhance the positive attributes, such as OFG content, in order to deliver better products.

In the past few years, the use of hydrothermal carbonization for conversion of biomass waste into valuable carbon materials has received growing attention due to its ability to deliver excellent properties to the hydrochar products (namely, the high concentration of OFGs and the low degree of aromatization), which are used in numerous applications such as adsorption (Liu and Zhang 2009; Liu, Zhang, and Wu 2010), biological applications (Guo et al. 2008; Selvi et al. 2008), catalysis (Makowski et al. 2008; Titirici, Antonietti, and Thomas 2006; Wang, Hu et al. 2011), and activated carbon synthesis (Sevilla and Fuertes 2011; Sevilla, Fuertes, and Mokaya 2011; Sevilla, Maciá-Agulló, and Fuertes 2011). The synthesis of highly porous carbon materials based on the use of hydrochar products is of great importance since hydrochar exhibits special properties in terms of surface functionalities (Jain, Balasubramanian, and Srinivasan 2015b, 2016; Jain et al. 2014, 2015).

This chapter highlights the insights into chemical activation of hydrochars and to prepare activated carbon with high mesoporous surface area under optimal hydrothermal treatment conditions. Furthermore, a few case studies are discussed based on the use of chemical activating agents and oxidizing agents during hydrothermal carbonization for the enhancement of chemical activation, therefore achieving higher porosity in activated carbon.

11.2 Biomass and Biomass-Based Adsorbents

Biomass refers to carbon-based materials including living or recently lived organisms and their wastes. It is considered one of the most important energy sources due to its high potential to meet the world's energy demand, as it is abundant, renewable, and widespread across the globe (Dhillon and von Wuehlisch 2013; Tekin, Karagöz, and Bektaş 2014). There are a wide range of utilization areas for biomass such as production of energy, chemicals, and adsorbents. Solar energy is stored in chemical form in the structure of biomass through the photosynthesis process in which CO_2 and H_2O are converted into carbohydrates ($\text{C}_m(\text{H}_2\text{O})_n$) in the presence of sunlight, chlorophyll, and enzymes. Formation of glucose from photosynthesis is represented as



The utilization of biomass for the production of energy and chemicals is a carbon-neutral process. In other words, there is no additional CO_2 release to the atmosphere as in the fossil fuels used because the CO_2 taken from the atmosphere by plants through photosynthesis is returned to the atmosphere when biomass is utilized. Thus, biomass is a promising substitute for fossil fuels, which are finite and whose deployment cause irreversible destructive impact to the environment.

Carbonized biomass (e.g., hydrochars, activated carbons, carbon nanotubes, graphene) are generating great interest in a wide range of applications in filtration and separation technology, energy storage, batteries, catalysis, sensor, environmental remediation, and bioapplications (Dawood, Sen, and Phan 2014; Jain, Balasubramanian, and Srinivasan 2015b; Luo et al. 2014; Sen, Afroze, and Ang 2011; Wei et al. 2016; Xie et al. 2015; Xu et al. 2015; Yang et al. 2016). These diverse applications arise from the remarkable and unique properties of carbon in biomass, such as bonding ability, chemical stability, thermal and electrical conductivity, high porosity, and tunable surface chemistry (Thompson et al. 2015). Biomass content varies according to the type of the biomass, and plays a crucial role in the utilization process. The category of lignocellulosic biomass primarily comprises cellulose, hemicellulose, and lignin. A complex carbohydrate, cellulose is represented by the general formula $(\text{C}_6\text{H}_{10}\text{O}_5)_n$ with molecular masses ranging up to 500,000 u (Figure 11.1). It is a crystalline natural polymer formed by the β -1,4 glycosidic linkage of D-glucopyranose monomers. It is an important raw material due to its abundance, high energy content, and exclusive properties, such as strength, insolubility, and biodegradable structure (Klemm et al. 2005; Kobayashi and Makino 2009). Hemicellulose is an amorphous carbohydrate composed mainly of D-glucopyranose, D-xylopyranose, D-galactopyranose, D-mannopyranose, and L-arabinofuranose units with a lower degree

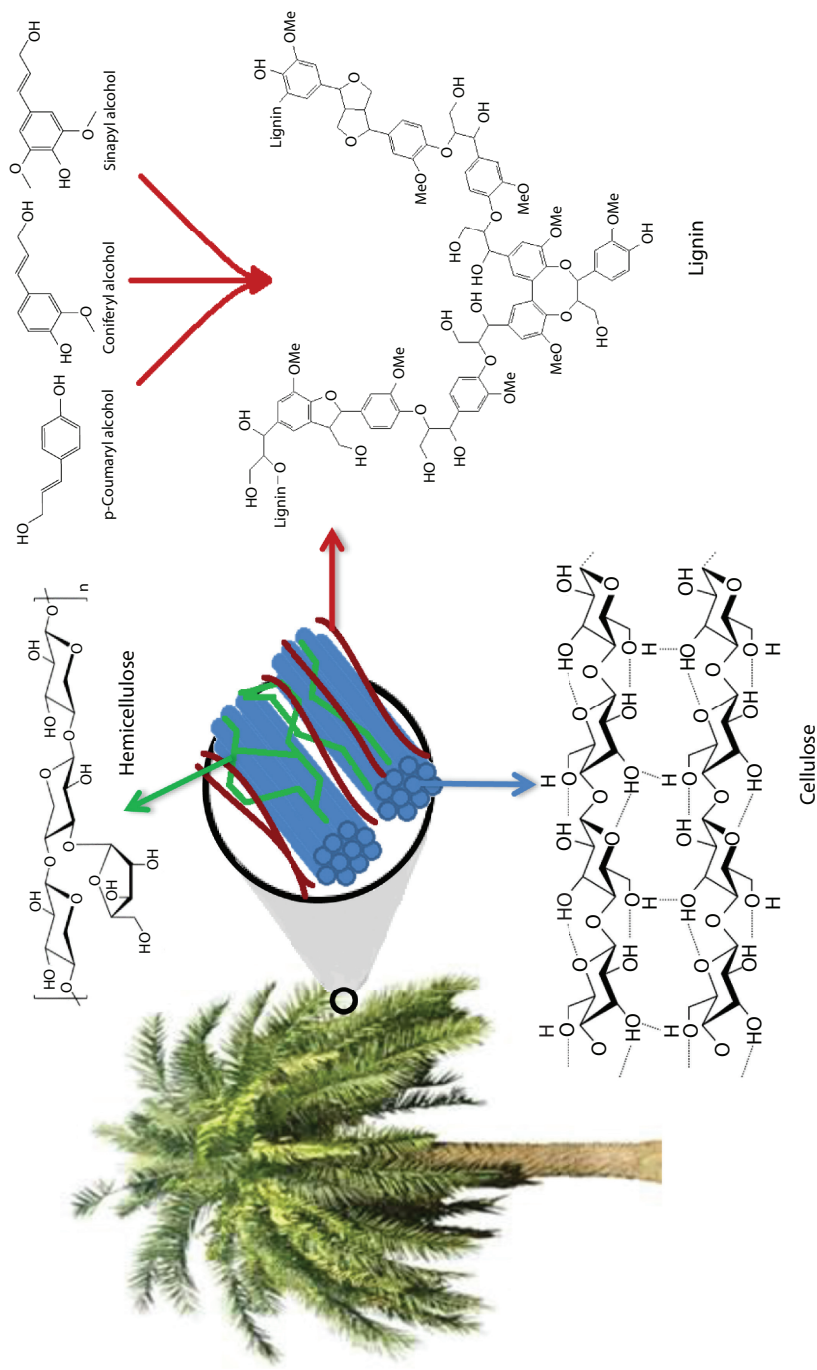


FIGURE 11.1
Structure of lignocellulosic biomass.

of polymerization than cellulose. Unlike cellulose, hemicellulose has a branched structure and due to its relatively low degree of polymerization and amorphous structure, hemicellulose can be easily degraded to its constituent components. It is soluble both in acidic (2% HCl) and alkaline (5% Na₂CO₃) solutions, and forms a viscous state or becomes a gelling agent in water depending on the concentration (Chen 2014). Lignin, the third component of lignocellulosic biomass, comprises methoxylated phenylpropane units and has amorphous, highly branched structure with very low solubility in water. *p*-Coumaryl alcohol (4-[(E)-3-hydroxyprop-1-enyl]phenol), coniferyl alcohol (4-(3-hydroxy-1-propenyl)-2-methoxyphenol), and sinapyl alcohol (4-(3-hydroxyprop-1-enyl)-2,6-dimethoxyphenol) are the three basic monomers of lignin (Liu, Jiang, and Yu 2015). It is produced in large quantities as a waste of the paper-making process (isolation of cellulose) and in the bio-ethanol production from lignocellulosic biomass (Deepa and Dhepe 2014). It can be combusted to produce heat and power in industries as a low-grade fuel, but, if depolymerized effectively, it is a valuable source of commercially important chemicals, fuel, or fuel additives. Thermochemical conversion of lignin also allows producing of functional carbon materials with various applications in the removal of pollutants, energy storage, and catalysis (Liu, Jiang, and Yu 2015).

The production of biomass-derived materials starting from waste biomass is a highly attractive prospect in the removal of environmental pollutants (Titirici et al. 2012). Biomass was traditionally deployed as-is for adsorption processes (biosorption) (Volesky and Holan 1995). However, using raw biomass has some drawbacks (i.e., low adsorption capacity, low selectivity, and so on) due to nonporosity, low surface area, and ineffective functional groups on the surface. Therefore, modification processes are frequently applied to the biomass. Adsorption gels derived from tea leaves and orange juice residue for the removal of Sr(II) and Cs(I) ions have been reported (Gurung et al. 2013; Pangeni et al. 2014). Such gel adsorbents showed high adsorption capacities and fast adsorption rates for metal ions. Panda, Das, and Guha (2008) functionalized husk of *Lathyrus sativus* with thio groups with the help of carbon disulfide treatment in alkaline condition for the adsorption of Cd(II) and Ni(II) ions. Thiol-functionalized magnetic sawdust was prepared for the separation of Cd(II), Pb(II), and Cu(II) from water by Gan et al. (2016). Modified sawdust was found effective and exhibited high stability in acidic-basic conditions. It could also be easily separated from water with the help of magnetic field. Tekin et al. (2016) attached a dye ligand (cibacron blue) to Scotch pine wood sawdust to enhance the adsorption capacity and stability of the sorbent for the removal of Pb(II) and Cd(II) ions from aquatic solutions.

Biomass is also subjected to thermal treatments to obtain high surface-area products such as activated carbons (Hameed and Rahman 2008; Jain, Balasubramanian, and Srinivasan 2016). Activated carbon can be produced from different kinds of biomass waste in different forms (Budinova et al. 2009; Malik, Ramteke, and Wate 2007; Williams and Reed 2006). They show a wide variety of pore size distribution and their application is determined according to their pore sizes. Microporosity is generally useful for the removal of small-sized species or pollutants; however, mesoporous adsorbents are needed for dye removal from water, electrochemical capacitors, lithium batteries, and in some catalysis applications (Calvillo et al. 2007; Dai et al. 2014; Ryoo et al. 2001; Zhuang et al. 2009). Porosity is dependent on the raw material, technique, and experimental conditions, and can be increased using activating agents. Hu and Srinivasan (2001) showed that while micropore formation is dominant at a low ZnCl₂-to-biomass ratio, a high ZnCl₂-to-biomass ratio led to pore widening increasing mesoporosity (Hu and Srinivasan 2001). Hydrothermal pretreatment also increases the porosity, as hydrochar has many oxygenated functional groups in

the structure. These oxygenated groups increase reactivity and improve chemical activation (Jain et al. 2014). In situ modification or postmodification also allows these materials to be modified or be combined with other materials to form composites with different properties (Hu et al. 2010).

11.3 Hydrothermal Carbonization: A Promising Tool for Hydrochar Synthesis

Hydrothermal carbonization has gained importance in recent years for energy and materials processing because of the intrinsic advantages such as benign environment, versatile chemistry, enhanced reaction rate, and economics. Basically, hydrothermal carbonization is a thermochemical conversion technique that uses subcritical water for the conversion of wet/dry biomass to carbonaceous products through fractionation of the feedstock. A typical temperature range of 150°C to 350°C is used for the carbonization which is dependent on the type of starting material and its decomposition temperature (Berge et al. 2011; Falco et al. 2012; Liu et al. 2013; Liu, Zhang, and Wu 2010; Parshetti et al. 2013; Sevilla, Maciá-Agulló, and Fuertes 2011; Titirici et al. 2012).

In general, higher temperatures result in higher rates of reaction and formation of more gaseous products, while solid products dominate at lower temperatures. With an increase in process temperatures up to 220°C and the corresponding pressures up to approximately 20 bar, about 1%–5% gas is usually generated, and most of the organics in biomass are transformed into solids. At even higher temperatures, up to nearly 400°C, more liquid hydrocarbons are formed and more gas is also generated with the use of catalysts. This “hydrothermal liquefaction” has drawn some attention, although most liquefaction work is performed using organic solvents instead of water. If the temperature and pressure are increased farther up to the supercritical state for water, the primary product is gaseous (hydrothermal gasification). Depending on the process conditions, either more methane or more hydrogen is produced.

During hydrothermal carbonization of lignocellulosic biomass, water acts as a solvent as well as a catalyst that facilitates hydrolysis and bond cleavage (Bobleter 1994; Hatcher and Clifford 1997; Masselter, Zemmann, and Bobleter 1995); water possesses high ionization constants at high temperatures and is responsible for hydrolysis of organics, which can further be catalyzed by acid or base (Bobleter 1994; Libra et al. 2011; Titirici et al. 2007, 2012). A decrease in pH during hydrothermal carbonization of biomass is typically observed and is due to formation of a variety of organic acids such as acetic, levulinic, formic, and lactic acids. The presence of these organic acids further promotes hydrolysis and decomposition of oligomers and monomers to smaller fragments (Demir-Cakan et al. 2009; Funke and Ziegler 2010; Titirici et al. 2007).

Hydrothermal carbonization for conversion of biomass into valuable carbon materials has received growing attention due to its simplicity and promise in delivering desirable properties (i.e., the high concentration of OFGs, such as carboxylic, lactonic, and phenolic groups, and the low degree of aromatization) (Baccile, Antonietti, and Titirici 2010; Kubo et al. 2010). The hydrothermal carbonization process is both energy economic and atom economic: (1) it releases one-third of the combustion energy throughout dehydration; (2) the wet condition avoids the predrying process; and (3) the carbon efficiency is close to one after adequate reaction time under proper conditions (Hu et al. 2010).

11.4 Hydrochar Formation, Properties, and Applications

Characterization and applications of biomass-derived hydrochars have been discussed extensively in the literature (Berge et al. 2011; Hoekman, Broch, and Robbins 2011; Hu et al. 2010; Parshetti et al. 2013; Sevilla and Fuertes 2009). Scanning electron microscopy (SEM) images of hydrochars reveal specific characteristics that can be attributed to the source (Figure 11.2). Water-soluble sugars such as glucose and xylose show homogenous spherical morphology after hydrothermal carbonization. The reaction occurs via the nucleation-growth mechanism from hydroxymethylfurfural (HMF) and furfural (Baccile et al. 2009; Sun and Li 2004; Titirici et al. 2012), which are the dehydration products of glucose and xylose, respectively (Baccile et al. 2013), and particle growth continues until all monomers are consumed. Long residence times and high temperatures result in larger particles (Baccile et al. 2013). The morphology of hydrochar obtained from biomass (rice husk), shown in Figure 11.2c, indicates that spherical particles are formed, but the surface is not homogenous due to the complex structure of this source. The fibrous structure of biomass and insoluble fragments formed during the hydrothermal treatment affect the surface morphology. In hydrothermal media, fibrous structure of biomass start to

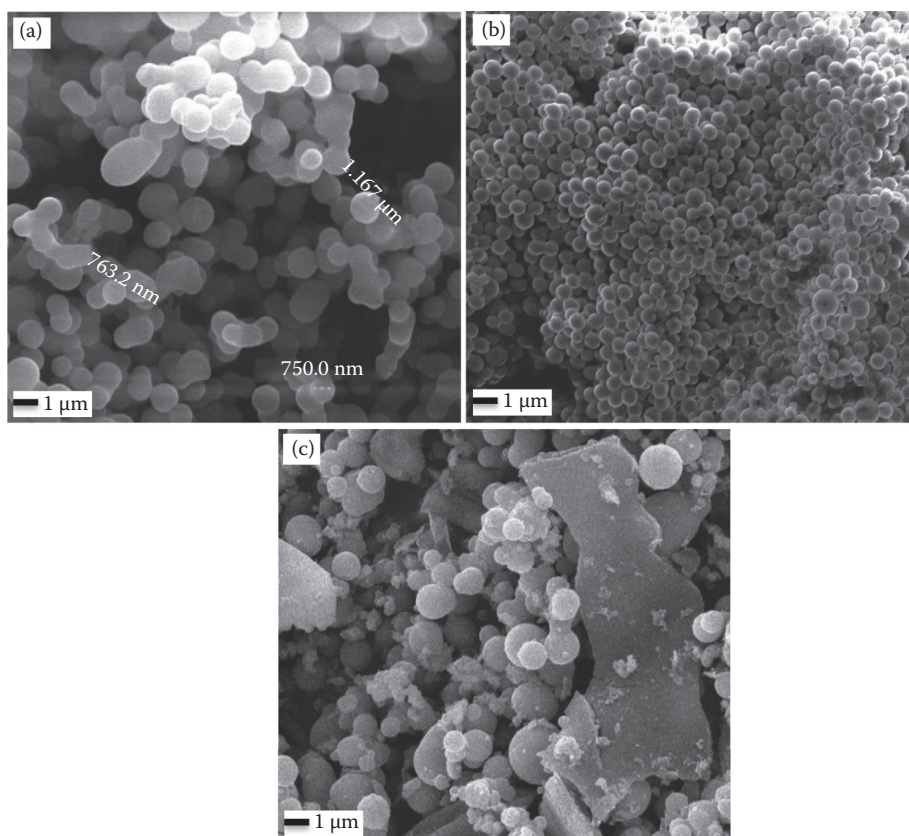


FIGURE 11.2

Scanning electron microscopy (SEM) images of hydrochars obtained from (a) glucose, (b) xylose, and (c) rice husk at 250°C.

decompose at high temperatures ($T = 240^{\circ}\text{C}$), and spherical particles occur in a similar way that has been previously described for cellulose (Falco, Baccile, and Titirici 2011).

Elemental analyses of some hydrochars obtained from different kinds of biomass are shown in Table 11.1. The heating values of the hydrochars can be determined from the elemental compositions using the Dulong formula:

$$\text{High heating value (HHV; MJ.kg}^{-1}\text{)} = 0.338\text{C} + 1.428(\text{H-O}/8) + 0.095\text{S} \quad (11.2)$$

As can be seen from Table 11.1, hydrothermal carbonization leads to an increase in carbon content and a decrease in oxygen content (Tekin, Karagöz, and Bektaş 2014) as a result of dehydration and polymerization reactions that take place during the carbonization. Also, the HHV of the hydrochars are higher than those of the raw materials. Low H/C ratios of the hydrochars indicate that hydrothermal carbonization leads to an increase in aromatic content.

Representative FTIR spectra for Scotch pine and its hydrochar obtained at 200°C is shown in Figure 11.3. The spectrum of hydrochar confirms the presence of OFGs on the surface of hydrochars. The broad absorption band between 3100 and 3600 cm^{-1} is assigned to O–H stretching vibrations. The peak between 2870 and 3000 cm^{-1} corresponds to aliphatic C–H stretching vibration. The intense bands at around 1600 and 1700 cm^{-1} represent the C=C and C=O groups, respectively (Sun and Li 2004). The presence of such groups support the hydrochar formation mechanism that involves aromatization and polymerization (Baccile et al. 2013). The peaks between 650 and 900 cm^{-1} are also assigned to aromatic C–H vibrations.

Hydrochar is comprised of condensed aromatic structures and bears high concentrations of OFGs (Liu and Zhang 2009; Liu, Zhang, and Wu 2010; Sevilla and Fuertes 2009). The presence of OFGs offers the advantage of further functionalization and makes hydrochar more hydrophilic for suitable applications including adsorption, catalysis, and as a precursor for activated carbon synthesis (Baccile et al. 2009; Titirici, Antonietti, and Baccile

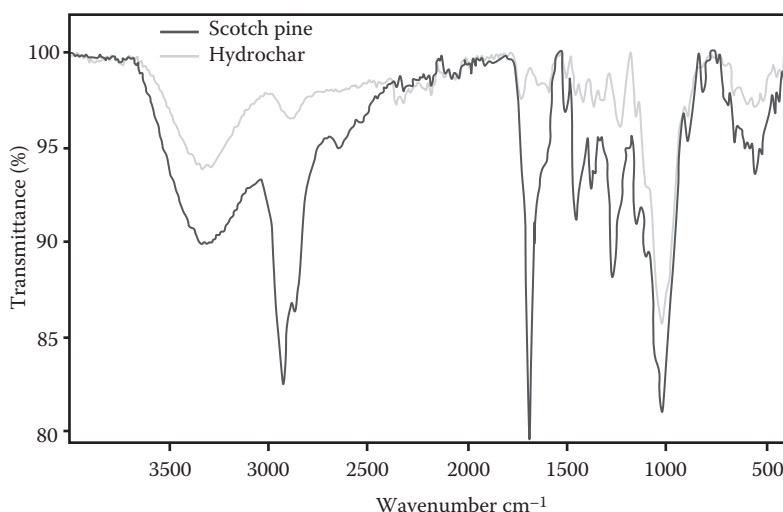
TABLE 11.1

Elemental Composition (wt.%) and High Heating Values of Hydrochars Obtained from Different Kinds of Biomass

Biomass	Temperature	C	H	N	O ^a	H/C	O/C	HHV ^b (MJ/kg)	Reference
Russian olive stone	–	43.71	6.65	1.73	47.91	1.83	0.82	15.72	Tekin 2015
Russian olive stone hydrochar	280°C	59.61	5.13	1.91	33.35	1.03	0.42	21.52	Tekin 2015
Beechwood	–	44.68	6.08	–	49.24	1.63	0.83	14.99	Tekin, Karagöz, and Bektaş 2012
Beechwood hydrochar	300°C	61.30	4.94	–	33.97	0.97	0.41	21.74	Tekin, Karagöz, and Bektaş 2012
Scotch pine	–	48.33	6.49	–	45.18	1.61	0.70	17.54	Tekin and Karagöz 2013
Scotch pine hydrochar	300°C	60.24	5.94	–	33.82	1.18	0.42	22.81	Tekin and Karagöz 2013

^a By difference.

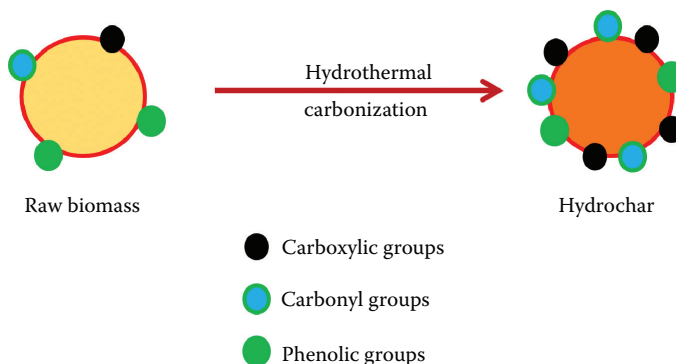
^b Calculated by Dulong formula.

**FIGURE 11.3**

FTIR spectra of Scotch pine and hydrochar obtained from Scotch pine at 200°C for 8 h.

2008; Xue et al. 2012). Mild processing conditions and simplicity of the hydrothermal carbonization process makes it even more attractive (Berge et al. 2011; Falco et al. 2012; Liu et al. 2013; Liu, Zhang, and Wu 2010; Parshetti et al. 2013; Sevilla, Maciá-Agulló, and Fuertes 2011; Titirici et al. 2012). Figure 11.4 depicts the formation of OFG by the use of hydrothermal carbonization.

Liu, Zhang, and Wu (2010) reported the formation of OFGs in the pinewood-derived hydrochar, which is found to be almost 340% higher compared to the pyrolytic char, and when employed as an adsorbent, showed a 62% higher uptake of copper ions. The higher adsorption on hydrochar was attributed to the higher OFG content since the porosity of pyrolytic char was comparatively higher. This demonstrates the importance of OFG when it comes to involvement with cationic species (Liu, Zhang, and Wu 2010). Recently, the use of amine-rich hydrothermally carbonized carbons was reported for CO₂ capture; CO₂ uptake of up to 4.3 mmol per g at -20°C along with very high (CO₂/N₂) selectivity at up to 110 at 70°C was obtained (Zhao et al. 2010). Additionally, hydrothermally carbonized

**FIGURE 11.4**

Formation of oxygenated functional groups during hydrothermal carbonization. (From Jain, A., R. Balasubramanian, and M. P. Srinivasan, 2016, *Chemical Engineering Journal* 283:789–805.)

spheres were used to load Pd nanoparticles by a one-step reaction, which was found to be promising for hydrogenation of hydroxy aromatic derivatives (Titirici, Antonietti, and Thomas 2006). Table 11.2 shows the BET (Brunauer–Emmett–Teller) surface area of hydrochars prepared under different conditions and raw materials.

Titirici et al. (2007) developed mesoporous carbon directly from hydrothermal carbonization at 200°C with orange peels, oak leaves, pinecones, and pine needles as raw materials and obtained BET surface areas of 0.2, 15.5, 34, and 12 m²/g, respectively. Fechner et al. (2013) reported the hydrothermal carbonization of glucose under hypersaline conditions to develop significant porosity (BET surface area of 673 m²/g). However, these and similar processes deliver products with relatively low surface areas compared to activated carbons. Therefore, in the absence of further processing, hydrothermal carbonization as a stand-alone process led to underdeveloped porosity. Thus, the direct use of hydrochar in various applications is not efficient compared to that of activated carbons with improved performance characteristics (Liu and Zhang 2009; Sevilla and Fuertes 2009; Titirici et al. 2007). However, the synthesis of highly porous carbon materials based on the use of hydrochar products is highly advantageous since hydrochar exhibits special properties

TABLE 11.2

BET Surface Area of Hydrochars Obtained from Different Starting Raw Materials

Biomass/Starting Material	Method or Catalyst Used (if any)	BET Surface Area (m ² /g)	Reference
Orange peels	Citric acid	0.2	Titirici et al. 2007
Oak leaf	Citric acid	15	Titirici et al. 2007
Pine cone	Citric acid	34	Titirici et al. 2007
Pine needles	Citric acid	12	Titirici et al. 2007
Glucose	LiCl/ZnCl ₂	673	Fechner et al. 2013
Glucose	NaCl/ZnCl ₂	546	Fechner et al. 2013
Glucose	KCl/ZnCl ₂	425	Fechner et al. 2013
Glucose	Template	200	Titirici, Thomas, and Antonietti 2007
Starch	Fe(NH ₄) ₂ (SO ₄) ₂	113	Cui, Antonietti, and Yu 2006
Starch	Fe ₂ O ₃	402	Cui, Antonietti, and Yu 2006
Pinewood		21	Liu, Zhang, and Wu 2010
Glucose	Borax	233	Fellinger et al. 2012
Glucose	Borax	427	Wohlgemuth et al. 2013
Walnut shell		31	Roman et al. 2013
Sunflower stem		27	Roman et al. 2013
Olive stone		22	Roman et al. 2013
Barley straw		153	Sevilla, Maciá-Agulló, and Fuertes 2011
Glucose acrylic acid		<50	Demir-Cakan et al. 2009
Ovalbumin/glucose		250	White et al. 2011
Peanut hull		1.3	Xue et al. 2012
Hazel nutshell		45	Aydincak et al. 2012
Olive oil waste		22	Aydincak et al. 2012
Palm empty fruit bunches		8	Parshetti, Kent Hoekman, and Balasubramanian 2013
<i>Sargassum horneri</i>	Citric acid	32	Xu, Qian et al. 2013
Microcrystalline cellulose	Citric acid	29	Diakité et al. 2013
Hazelnut shell	Citric acid	60	Unur et al. 2013

Source: Jain, A., R. Balasubramanian, and M. P. Srinivasan, 2016, *Chemical Engineering Journal* 283:789–805.

in terms of surface functionalities, particularly oxygenated functional groups, which promote chemical activation (Falco, Marco-Lozar et al. 2013; Lillo-Ródenas et al. 2004; Qi et al. 2014; Sevilla and Fuertes 2011; Sevilla, Fuertes, and Mokaya 2011).

11.4.1 Hydrochar for Activated Carbon Synthesis

Despite the extensive literature available on preparation techniques, few studies have investigated the effect of the reactivity of the precursor on the porosity of activated carbons. Recent works have shown that reactive carbonaceous precursors yield activated carbons with increased porosity when activated with NaOH and KOH (Falco, Marco-Lozar et al. 2013; Lillo-Ródenas et al. 2004; Linares-Solano et al. 2007; Sevilla and Fuertes 2011; Sevilla, Fuertes, and Mokaya 2011).

The presence of OFGs comprising carboxylic, lactonic, and phenolic moieties in the precursor is an important indicator of reactivity, which governs the chemical activation (Figure 11.5) (Sevilla and Fuertes 2009; Sevilla, Fuertes, and Mokaya 2011). To this end, biomass and pure carbohydrates have been hydrothermally carbonized to improve the chemical characteristics of hydrochar products by bestowing OFGs and reducing the degree of aromatization (Falco, Marco-Lozar et al. 2013; Lillo-Ródenas et al. 2004; Linares-Solano et al. 2007; Sevilla and Fuertes 2009, 2011; Sevilla, Fuertes, and Mokaya 2011).

Sevilla and Fuertes (2011) validated hydrochar as a suitable precursor for activated carbon synthesis by showing high BET surface area up to 2850 m²/g and high uptake of CO₂. More results are presented in Table 11.3, which shows the surface area of such hydrochar-derived activated carbons under different activation conditions.

Tailoring of hydrochar properties using different processing conditions and catalysts have been attempted by numerous researchers in the interest of obtaining desirable hydrochars for different end applications. Specifically, for preparing hydrochar as an activated carbon precursor, chemical activating agents or oxidizing agents can be introduced during the hydrothermal carbonization to bestow desirable surface properties on the resulting hydrochars (Jain, Balasubramanian, and Srinivasan 2015a, 2015b; Jain et al. 2013, 2014).

11.4.1.1 Case Study 1: Effect of Hydrothermal Pretreatment Temperature

Falco Marco-Lozar et al. (2013) demonstrated the role of hydrothermal temperature, which was manifested as different levels of porosities in the derived activated carbons from KOH activation (Figure 11.6). The extent of carbonization, aromatization, and carbonyl functionalities were reported to increase up to 240°C (Falco, Baccile, and Titirici 2011) which led to an increase in porosity in activated carbons. A further increase in temperatures to 280°C

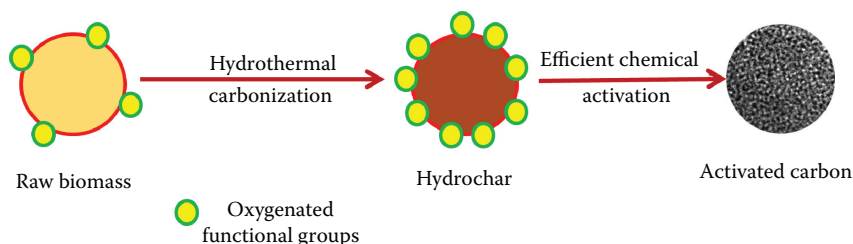


FIGURE 11.5

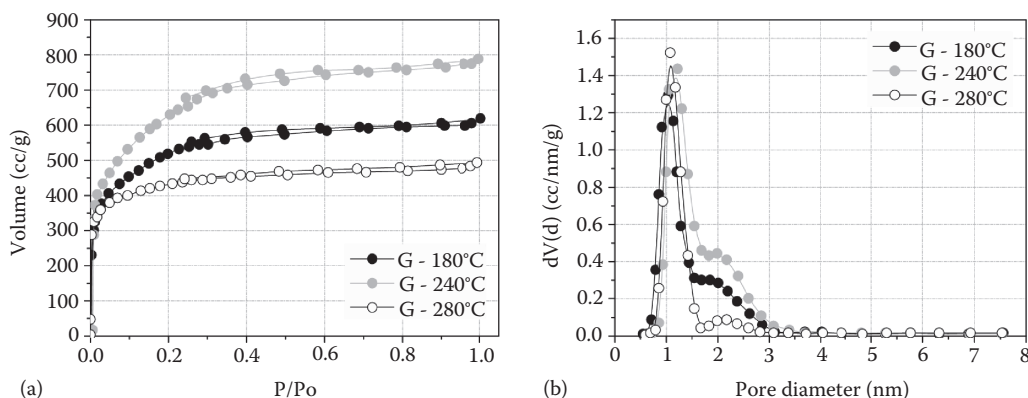
Scheme depicting the formation of hydrochar and efficient chemical activation due to high OFG content. (From Jain, A., R. Balasubramanian, and M. P. Srinivasan, 2016, *Chemical Engineering Journal* 283:789–805.)

TABLE 11.3

BET Surface Areas of Activated Carbons with Different Hydrochar Precursors as the Starting Material

Starting Material	Activation Agent	BET Surface Area (m ² /g)	Reference
Starch	KOH	2190	Sevilla and Fuertes 2011
Sawdust	KOH	2850	Sevilla and Fuertes 2011
Rice husk	H ₃ PO ₄	1498	Ding et al. 2013
Rice husk	KOH	3322	Ding et al. 2013
Rice husk	NaOH	2455	Ding et al. 2013
Hazelnut shell	KOH	1700	Unur et al. 2013
Rice husk	H ₃ PO ₄	2610	Wang, Guo et al. 2011
Pinewood	CO ₂	569	Liu and Zhang 2009
Rice husk	CO ₂	446	Liu and Zhang 2009
Eucalyptus sawdust	KOH	2252	Sevilla, Fuertes, and Mokaya 2011
Cellulose	KOH	2722	Sevilla, Fuertes, and Mokaya 2011
Walnut shell	CO ₂	379	Roman et al. 2013
Sunflower stem	CO ₂	438	Roman et al. 2013
Olive stone	CO ₂	438	Roman et al. 2013
Glucose/borax	–	614	Fellinger et al. 2012
Glucose/ovalbumin	–	476	White et al. 2011
Sucrose	H ₃ PO ₄	2120	Romero-Anaya et al. 2014
Glucose	NaOH	2129	Romero-Anaya et al. 2014
Glucose	KOH	3152	Romero-Anaya et al. 2014
Sucrose	CO ₂	2555	Romero-Anaya et al. 2014
Rye straw	KOH	2200	Falco, Marco-Lozar et al. 2013
Corn cobs	KOH	2300	Falco, Sieben et al. 2013
Eucalyptus wood sawdust	KOH	2967	Wei et al. 2011
Salix psammophila	ZnCl ₂	1351	Zhu et al. 2014
Apple pulp	H ₃ PO ₄	1022	Dolores et al. 2013
Rice husk	KOH	3362	Zhang et al. 2014

Source: Jain, A., R. Balasubramanian, and M. P. Srinivasan, 2016, *Chemical Engineering Journal* 283:789–805.

**FIGURE 11.6**

(a) N₂ adsorption isotherms and (b) pore size distribution of carbons hydrothermally pretreated at different temperatures. (From Falco, C., J. P. Marco-Lozar et al., 2013, *Carbon* 62:346–355.)

led to enhanced chemical stability and structural order in the precursor, which led to the decline of porosity in the derived carbons (Falco, Marco-Lozar et al. 2013; Linares-Solano et al. 2007).

11.4.1.2 Case Study 2: Use of ZnCl_2 as a Catalyst

ZnCl_2 was incorporated as a catalyst during hydrothermal carbonization in addition to serving as a chemical activating agent in the subsequent activation step (Jain et al. 2014). The hydrothermal carbonization of coconut shell in the presence of ZnCl_2 led to improved chemical activation and resulted in significant improvement in mesopore area by as much as 67% for the same usage of the chemical activating agent compared to conventional oven soaking (Figure 11.7).

The individual roles of ZnCl_2 and hydrothermal treatment were investigated by carrying out hydrothermal pretreatment in the absence of ZnCl_2 , followed by ZnCl_2 incorporation (soaking) and physicochemical activation. The product obtained in the absence of ZnCl_2 yielded mesopore area of $521 \text{ m}^2/\text{g}$, which was 20% less than that prepared in the presence of ZnCl_2 due to lower OFG content in the latter hydrochar that was prepared in the absence of ZnCl_2 . Thus, OFG content in hydrochar plays a crucial role in efficient chemical activation with ZnCl_2 (Jain et al. 2013, 2014).

The pore size distribution of these prepared carbons lies between those of microporous carbon and zeolites (narrow pore size distribution and small pore size in the range $0.2 \pm 1.2 \text{ nm}$) (Hu, Srinivasan, and Ni 2000), and mesoporous silica gel and mesoporous commercial carbon (larger pores [mesopores], wide distribution, small mesopore area) (Figure 11.8). The large surface areas, coupled with the narrow pore size distribution make these synthesized activated carbons highly competitive and efficient for treating adsorbates with differing molecular sizes.

The higher surface area and mesoporosity was demonstrated by the high dye uptakes (Jain et al. 2014). Results of the batch equilibrium studies shown in Figure 11.9 confirmed the higher adsorption capacity of mesoporous carbons for methylene blue and erythrosine

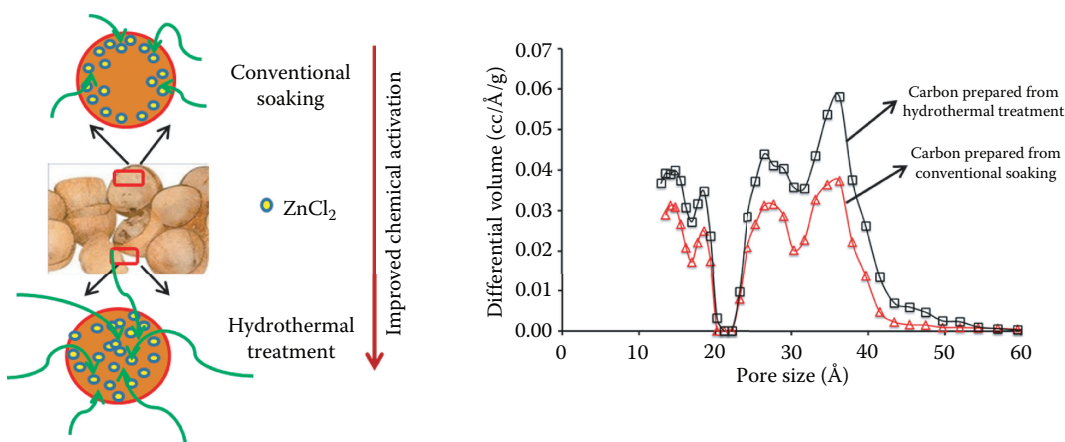
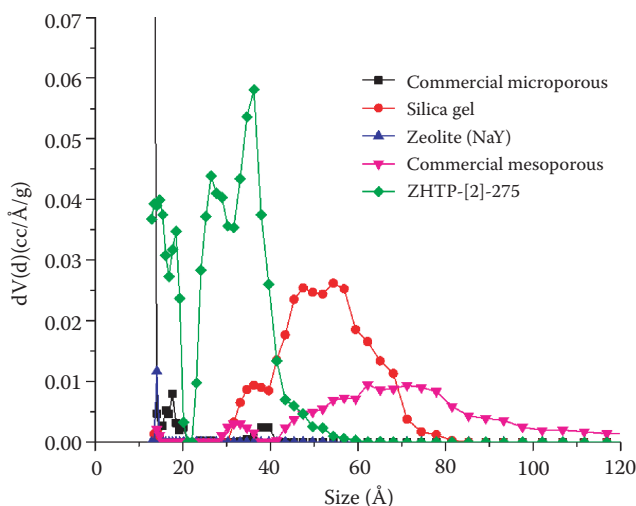
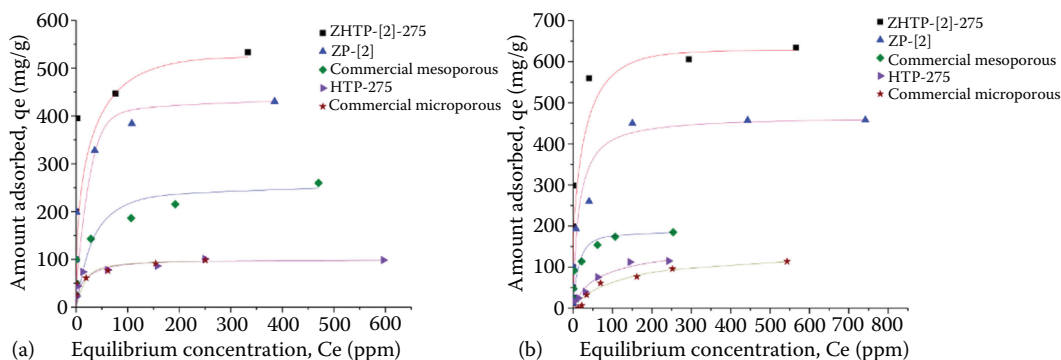


FIGURE 11.7

Hydrothermal carbonization facilitating the incorporation of chemical activating agent in the biomass and corresponding carbons with higher mesoporosity. (From Jain, A. et al. 2014, *Journal of Materials Chemistry A* 2 (2):520–528.)

**FIGURE 11.8**

Pore size distribution of different commercial adsorbents. ZHTP-[2]-275 sample that underwent hydrothermal pretreatment with ZnCl_2 (ZnCl_2 :raw shell ratio = 2:1) and subsequently activated. (From Jain, A. et al. 2014, *Journal of Materials Chemistry A* 2 (2):520–528.)

**FIGURE 11.9**

(a) Adsorption isotherms for methylene blue (1000 ppm, initial concentration) from aqueous solutions. (b) Adsorption isotherms for erythrosine red (1000 ppm, initial concentration) from aqueous solutions. C_e , equilibrium concentration of adsorbate in the liquid phase; ZP, soaking; HTP, hydrothermally pretreated sample; ZHTP, hydrothermally pretreated sample in the presence of ZnCl_2 ; [x], ZnCl_2 :biomass ratio. (From Jain, A. et al. 2014, *Journal of Materials Chemistry A* 2 (2):520–528.)

red; ZHTP-[2], ZP-[2] and commercial mesoporous carbon had greater adsorption saturation capacities when compared with the microporous adsorbents. In the case of methylene blue, the saturation capacity for mesoporous carbon, ZHTP-[2] is 21% higher compared to that for ZP-[2], while both samples were prepared with the same ZnCl_2 :shell ratio of 2:1. Similarly the capacity for erythrosine red is 36% higher for ZHTP-[2] when compared with that of ZP-[2].

This enhancement in adsorption shows the contribution of higher mesoporosity and the presence of oxygen functional groups that resulted from the ZnCl_2 -laden hydrothermal treatment prior to activation. With reference to previous literature by the same group (Hu and Srinivasan 2001), the carbons prepared with the ZnCl_2 ratio of 3:1 showed

saturation capacities for methylene blue and erythrosine red to be 465 mg/g and 540 mg/g, respectively. However, by employing hydrothermal pretreatment and ZnCl_2 ratio of 2:1, the saturation capacities for these dyes were increased to 526 mg/g and 630 mg/g, respectively.

11.4.1.3 Case Study 3: Effect of Higher ZnCl_2 Amounts under Different Hydrothermal Temperatures

The enhanced mesopore area in activated carbons prepared by hydrothermal carbonization of coconut shell is found to be strongly influenced by the hydrothermal processing conditions. Jain, Balasubramanian, and Srinivasan (2015a) reported that the mesopore area increased with hydrothermal treatment temperature up to 315°C when the ZnCl_2 :shell ratio was 1:1. However, the mesopore area decreased when the hydrothermal temperature was performed at 350°C due to reduced solubility of ZnCl_2 at these processing conditions and thus reduced availability at the time of activation. On the other hand, at higher ZnCl_2 :shell ratios of 2:1 and 3:1, mesoporosity was improved at hydrothermal treatment temperatures of 200°C and 275°C, while the porosity declined at 315°C and 350°C, suggesting that reduced solubility led to a decrease in availability of ZnCl_2 at the time of activation and outweighs the benefit of elevated temperature (Jain, Balasubramanian, and Srinivasan 2015a). Figure 11.10 shows the demarcation that identifies the effective region of hydrothermal treatment (function of temperature and ZnCl_2 content) for the synthesis of desired hydrochar in the context of activated carbon production.

Table 11.4 presents the adsorption capacities of various activated carbons for the removal of phenol red and phenol mixture. The highest and lowest adsorption capacities for phenol red and phenol were observed when the hydrothermal treatment temperatures were 275°C and 350°C, respectively, which was consistent with the mesopore areas of activated carbons obtained from hydrochars produced at those conditions. Furthermore, the higher adsorption capacity of ZHTP-[2]-200 and ZHTP-[2]-275 for phenol red (which is an anionic dye, and therefore OFG content is not favorable) even in the presence of higher OFG content showed the importance of higher mesopore area, which dominated over OFG content.

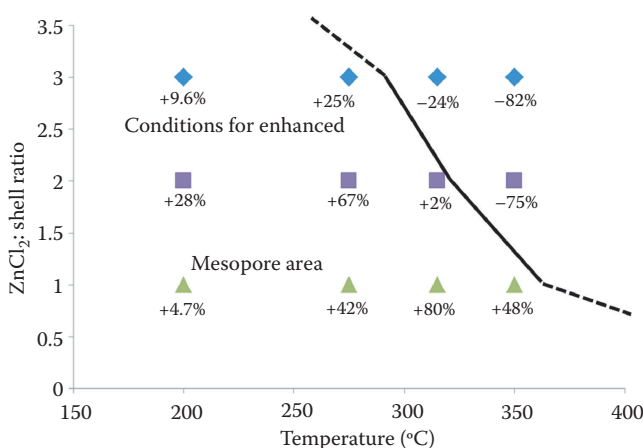


FIGURE 11.10

Favorable working range of hydrothermal treatment conditions for enhancement of mesopore area. Percentages refer to change in mesopore area relative to activated carbons prepared by conventional soaking at same ZnCl_2 :shell ratios. (From Jain, A., R. Balasubramanian, and M. P. Srinivasan, 2015, *Microporous and Mesoporous Materials* 203:178–185.)

TABLE 11.4

Adsorption Capacity for Phenol Red and Phenol (mg/g) on Mesoporous Activated Carbons

Sample	ZP-[2]	ZHTP-[2]-200	ZHTP-[2]-275	ZHTP-[2]-315	ZHTP-[2]-350	Commercial Microporous	Commercial Mesoporous
Phenol red adsorbed (mg/g)	263	306	351	294	153	95	119
Phenol adsorbed (mg/g)	221	254	264	217	132	103	51
OFG (meq/g)	0.3	0.68	0.62	0.5	0.35	0.3	0.25

Source: Jain, A., R. Balasubramanian, and M. P. Srinivasan, 2015, *Microporous and Mesoporous Materials* 203:178–185.

Note: ZP, sample prepared by ZnCl_2 soaking followed by activation; ZHTP, sample prepared by hydrothermal pretreatment at different temperatures followed by activation; [x], ZnCl_2 :biomass ratio.

Particularly, the difference in adsorption capacities between ZHTP-[2]-275 and ZHTP-[2]-315 for phenol emphasized the importance of mesopores in a competitive environment, possibly due to blockage of smaller pores by the larger molecules. Similar observations were reported by Takahashi et al. (2000) during horseradish peroxidase (HRP) immobilization and Zhuang et al. (2009) for dye adsorption.

11.4.1.4 Case Study 4: Use of H_3PO_4 as a Catalyst

Quesada-Plata et al. (2016) showed that H_3PO_4 assisted hydrothermal carbonization has an advantage over conventional method of preparation, that is, impregnation. They reported that porosity was greatly enhanced by substituting the impregnation stage of the conventional method by a hydrothermal treatment in the presence of phosphoric acid. This might be due to the fact that hydrothermal conditions favor the digestion of the different biopolymers through hydrolysis reactions that are facilitated in acidic conditions. Thus, the activating agent can reach all the fractions of the biomass facilitating an adequate development of porosity.

The largest porosity development had been achieved for almond shells (AS), a hard biomass, while a similar porosity development had been also obtained from the sawdust (SD). When phosphoric acid was added during the hydrothermal treatment, the differences derived from the different composition and structures of the pristine biomasses were minimized. However, important differences among the biomasses were found when the conventional activation route was followed (Quesada-Plata et al. 2016). In the conventional activation case, the development of porosity was more important for soft biomass such as sawdust (SD) and hemp residue (HR).

Romero-Anaya et al. (2012) reported that activation after the incipient wetness impregnation method resulted in better porosity than the activation after hydrothermal impregnation. This may be attributed to the presence of water in the hydrothermal method, which will affect the complex process (for more details refer to Romero-Anaya et al. 2012), certainly modifying the reactions. However, a definitive conclusion requires a careful, comparative study of the methods under controlled conditions.

11.4.1.5 Case Study 5: Use of H_2O_2 as a Catalyst

The use of an oxidizing agent (e.g., hydrogen peroxide) for increasing the OFG content on hydrochar was investigated for the betterment of ZnCl_2 -mediated activation (Figure 11.11). The substantial increase in the mesopore area by up to 140% was reported by the use of successive hydrothermal carbonization in the presence of H_2O_2 and ZnCl_2 .

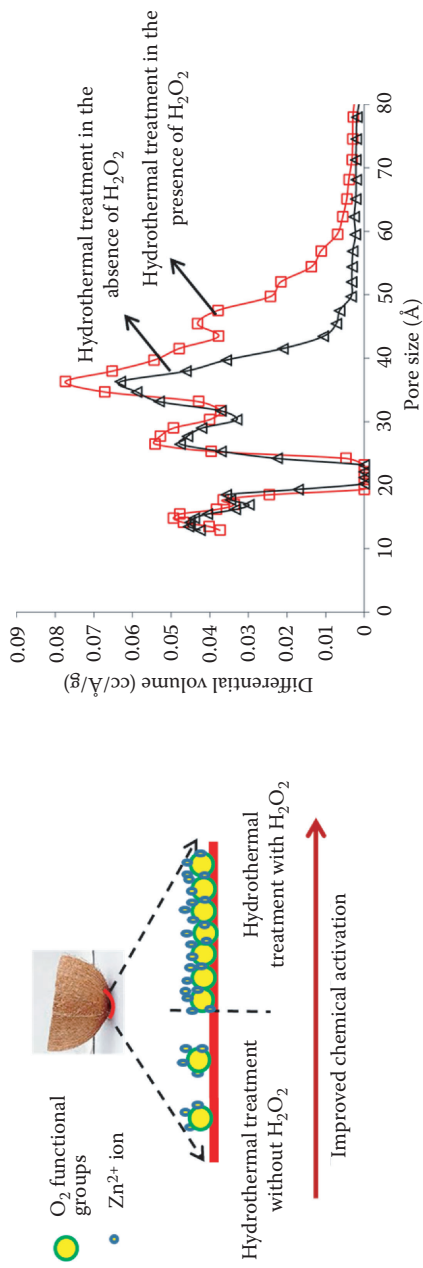


FIGURE 11.11 Scheme depicting the formation of hydrochar with more OFG content by the use of H_2O_2 and corresponding carbons with higher mesoporosity. (From Jain, A., R. Balasubramanian, and M. P. Srinivasan, 2015, *Chemical Engineering Journal* 273:622–629.)

(Jain, Balasubramanian, and Srinivasan 2015b); it was attributed to the improved chemical activation due to the increased OFG formation due to inclusion of hydrogen peroxide and extensive dehydration by ZnCl_2 at hydrothermal conditions.

Jain, Balasubramanian, and Srinivasan (2015b) reported a strong interdependence between the OFG content in hydrochar precursors and mesopore area in corresponding carbons (Figure 11.12). They also reported the important role of acids released from coconut shell on the solubility of ZnCl_2 and thus its effect on the mesoporosity formation in the activated carbons.

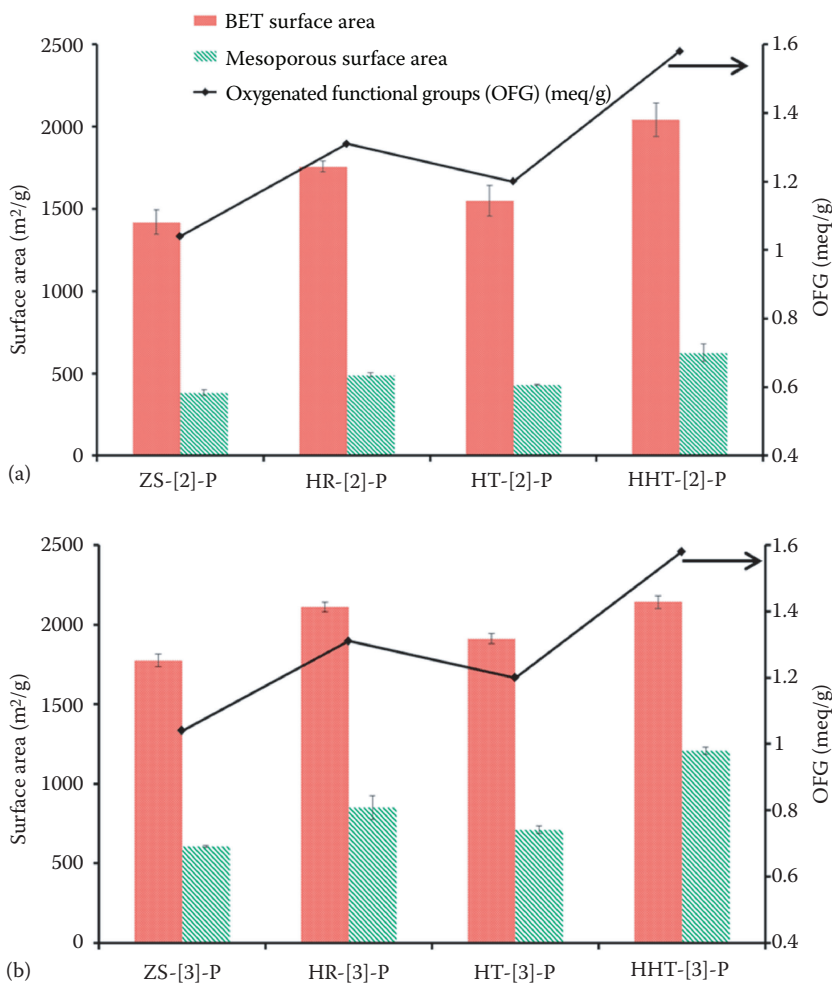


FIGURE 11.12

OFG content in precursors and surface areas of corresponding carbons: Effect of pre-treatment conditions. (a) ZnCl_2 :raw shell ratio = 2:1; (b) ZnCl_2 :raw shell ratio = 3:1. ZS, soaking; HR, reflux treatment; HT, hydrothermal treatment; HHT, H_2O_2 -mediated hydrothermal treatment; [x], ZnCl_2 :biomass ratio. (From Jain, A., R. Balasubramanian, and M. P. Srinivasan, 2015, *Chemical Engineering Journal* 273:622–629.)

TABLE 11.5

Adsorption Capacity for Rhodamine B (Initial Concentration Used Is 1000 ppm) and Surface Acidity of Activated Carbons

Activated Carbon	Rhodamine B Adsorbed (mg/g)	Surface Acidity (meq/g)
HR-[2]-P	410	0.31
HHT-[2]-P	515	0.44
HT-ZHT-[2]-P	397	0.54
HHT-ZHT-[2]-P	714	0.46

Source: Jain, A., R. Balasubramanian, and M. P. Srinivasan, 2015, *Chemical Engineering Journal* 273:622–629.

Note: HR, reflux treatment; HHT, H₂O₂-mediated hydrothermal treatment; HT-ZHT, successive hydrothermal pretreatments without H₂O₂ followed by ZnCl₂; HHT-ZHT, successive hydrothermal pretreatments with H₂O₂ followed by ZnCl₂; [x], ZnCl₂:biomass ratio.

The higher surface area and mesoporosity due to H₂O₂-mediated hydrothermal treatment was demonstrated by the high dye uptakes. Results of batch equilibrium studies (Table 11.5) show that carbon prepared by using successive hydrothermal treatment in the presence of H₂O₂ (HHT-ZHT-[2]-P) resulted in the highest adsorption capacity for rhodamine B. The trend for adsorption by the carbons was in accordance to their respective mesopore surface areas, that is, HHT-[2]-P > HR-[2]-P > HT-ZHT-[2]-P. Although HT-ZHT-[2]-P had the highest OFG content, which would normally be expected to yield the highest adsorption capacity for a cationic dye, the observed capacity for rhodamine B was the lowest, which was a clear indication of the importance of mesoporosity which dominated over the OFG content of activated carbons.

Uptake capacity of rhodamine B obtained in this work (up to 714 mg/g) was higher when compared to capacities obtained with other activated carbons. For example, Guo et al. (2005) obtained an adsorption capacity of 0.95 mmol/g (~455 mg/g) using an initial dye concentration of 1000 ppm. At the same time, it is comparable with that delivered by ordered mesoporous carbons (uptake capacity of 785 mg/g) obtained by the more onerous and expensive templating process (Zhuang et al. 2009).

The PMCR (percentage molasses color removed) obtained from molasses testing is a strong function of surface functionalities, pore size distribution, and total area, and therefore a strong indicator of the mesoporosity of the activated carbon and its ability to adsorb large molecules. Figure 11.13 pictorially depicts the relationship showing that the PMCR values were consistent with the mesopore areas, which substantiated the role of H₂O₂ pretreatment in enhancing the chemical activation and mesopore development. In particular, carbons derived from H₂O₂ pretreated precursors showed an increase in PMCR and higher removal is observed when H₂O₂ is incorporated under hydrothermal conditions compared to reflux. Similarly, successive hydrothermal treatments in the absence of H₂O₂ show lesser PMCR compared to the carbons prepared in the presence of H₂O₂. As it is known, an increase in ZnCl₂:raw shell ratio led to an increase in mesopore area and thus an increase in PMCR values; the highest obtained for the case when the ZnCl₂:raw shell ratio of 3:1 was employed along with the H₂O₂-mediated hydrothermal treatment. However, in the case of HR-[2]-P and HT-ZHT-[3]-P, HR-[2]-P resulted in higher PMCR even after having lower mesopore area because of the lower OFG content, which is favorable for high PMCR.

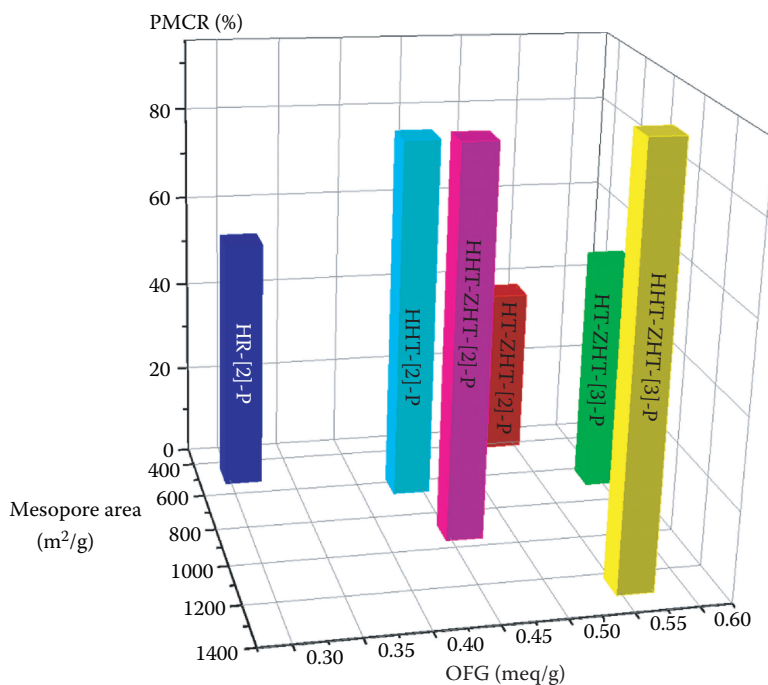


FIGURE 11.13

The PMCR (percentage molasses color removed) of activated carbons prepared under different pretreatment conditions as a function of mesopore area and OFG. HR, reflux treatment; HHT, H_2O_2 -mediated hydrothermal treatment; HT-ZHT, successive hydrothermal pretreatments without H_2O_2 followed by ZnCl_2 ; HHT-ZHT, successive hydrothermal pretreatments with H_2O_2 followed by ZnCl_2 ; [x], ZnCl_2 :biomass ratio. (From Jain, A., R. Balasubramanian, and M. P. Srinivasan, 2015, *Chemical Engineering Journal* 273:622–629.)

11.4.1.6 Case Study 6: Use of ZnCl_2 as a Catalyst under Different Concentrations

Jain et al. (2015) further investigated the tuning of the stoichiometry of reactants (biomass, ZnCl_2 , and water), which governed the formation of oxygenated functional groups on hydrochar and ZnCl_2 solubility, and thus its availability at the time of activation. Therefore, the observed dependence of surface areas on ZnCl_2 concentration was due to opposing contributions from OFG content and ZnCl_2 solubility (for more details refer to Jain et al. 2015). Moreover, the hydrothermal pretreatment using H_2O_2 followed by the treatment using ZnCl_2 at different concentrations was employed to increase the OFG content in the hydrochar for efficient utilization of ZnCl_2 (Jain et al. 2015). Successive hydrothermal treatments using H_2O_2 and ZnCl_2 (under different concentrations) resulted in an up to 39% increase in BET surface area (1753 to 2440 m^2/g) and up to a 30% increase in mesopore area (859 to 1121 m^2/g) when the ZnCl_2 :shell ratio of 3:1 was employed. When deployed in energy storage applications, these carbons delivered a high capacitance of 246 F/g between 0 to 1 V at 0.25A/g.

Jain et al. (2015) observed that the carbon obtained using the lowest biomass concentration (C_1) exhibited higher capacitance in spite of having lower mesopore area compared to carbon prepared using higher biomass concentration (C_2); this was correlated with the greater number of pores in C_1 in the mesopore range of 2 to 4 nm, as shown in Figure 11.14a, which in turn increased the storage capacity due to ease of motion of ions, thus resulting in higher capacitance and energy density (Sevilla et al. 2007). On the other

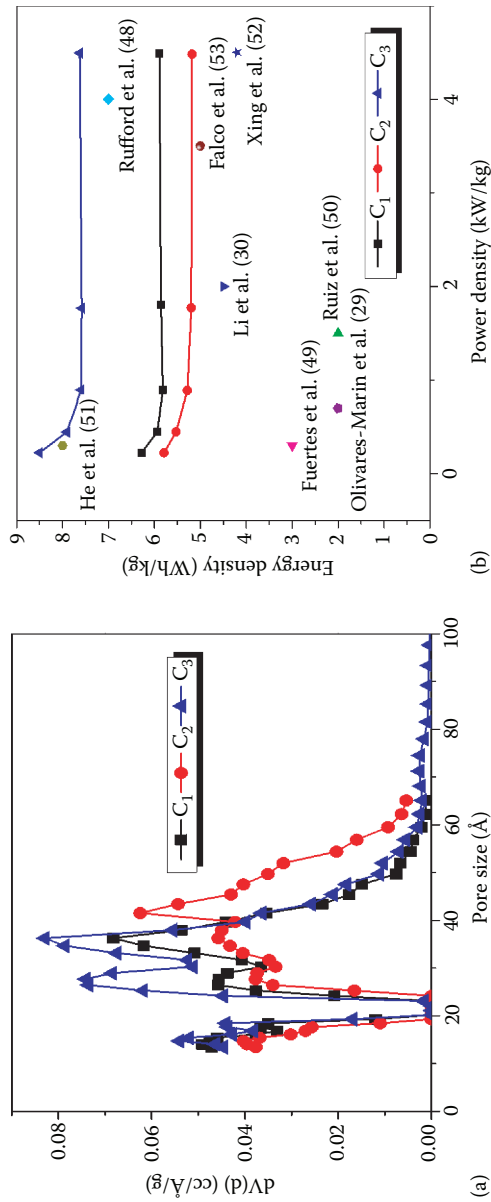


FIGURE 11.14

(a) DFT pore size distribution of the carbons. (b) Ragone plot of the carbon-derived electrodes. C_1 , C_2 , and C_3 were obtained by the process C at the concentration of 0.16, 0.33, and 0.5 g/mL and the comparison from literature.

hand, the carbon produced from a higher biomass concentration (C_2) resulted in lower capacitance despite having higher surface area and pore volume; this was because the pores in the range beyond 4 nm reduced the discharging time and led to reduction in the capacitance. C_3 resulted in the highest energy density and capacitance, as it possessed the highest BET surface area and highest pore density in the mesopore range of 2 to 4 nm. Therefore, higher surface area along with suitable pore size in the mesopore range of 2 to 4 nm is crucial to allow easy access of ions (in case of aqueous electrolytes and may vary with organic electrolytes). However, pores bigger than 4 nm might prove to be a drawback, as they will reduce the discharging time. C_3 delivers an energy density of 8.5 Wh kg^{-1} , which was much higher than that of commercial AC electrodes (Xu, Xu et al. 2013). The energy density was still as high as 7.6 Wh kg^{-1} at a power density of 4.5 kW kg^{-1} , demonstrating superior electrochemical properties. This provides the pathway to further tune the pore size distribution for specific applications by tuning of hydrothermal parameters.

11.5 Conclusions

This chapter gives a summary of the activated carbons synthesis from waste biomass. It highlights the high potential of the hydrothermal method as a means of conversion of waste or cheap biomass into value-added hydrochar. It also summarizes significant progress toward the exploitation of hydrothermal conditions for the synthesis of desirable hydrochars for production of activated carbon and understanding the role of these parameters influencing the porosity. Furthermore, it represents an important contribution to the body of knowledge in the application of hydrothermal carbonization, since it demonstrated the use of chemical activating agents and oxidizing agents during hydrothermal carbonization for the enhancement of chemical activation. The insights and highlights on biomass-based activated carbons and hydrothermal carbonization will provide an interesting and useful view of the rapidly developing area of mesoporous carbons in the field of materials science and technology.

References

- Ania, C. O., J. B. Parra, J. A. Menendez, and J. J. Pis. 2005. "Effect of microwave and conventional regeneration on the microporous and mesoporous network and on the adsorptive capacity of activated carbons." *Microporous and Mesoporous Materials* 85 (1):7–15.
- Aydincak, K., T. Yumak, A. Sinağ, and B. Esen. 2012. "Synthesis and characterization of carbonaceous materials from saccharides (glucose and lactose) and two waste biomasses by hydrothermal carbonization." *Industrial & Engineering Chemistry Research* 51 (26):9145–9152.
- Aygün, A., S. Yenisoy-Karakaş, and I. Duman. 2003. "Production of granular activated carbon from fruit stones and nutshells and evaluation of their physical, chemical and adsorption properties." *Microporous and Mesoporous Materials* 66 (2):189–195.
- Baccile, N., M. Antonietti, and M.-M. Titirici. 2010. "One-step hydrothermal synthesis of nitrogen-doped nanocarbons: Albumine directing the carbonization of glucose." *ChemSusChem* 3 (2): 246–253.

- Baccile, N., G. Laurent, Fl. Babonneau, F. Fayon, M.-M. Titirici, and M. Antonietti. 2009. "Structural characterization of hydrothermal carbon spheres by advanced solid-state MAS ^{13}C NMR investigations." *The Journal of Physical Chemistry C* 113 (22):9644–9654.
- Baccile, N., J. Weber, C. Falco, and M.-M. Titirici. 2013. "Characterization of hydrothermal carbonization materials." In *Sustainable Carbon Materials from Hydrothermal Processes*, edited by M.-M. Titirici, 151–211. Chichester: John Wiley & Sons.
- Berge, N. D., K. S. Ro, J. Mao, J. R. V. Flora, M. A. Chappell, and S. Bae. 2011. "Hydrothermal carbonization of municipal waste streams." *Environmental Science & Technology* 45 (13):5696–5703.
- Bobleter, O. 1994. "Hydrothermal degradation of polymers derived from plants." *Progress in Polymer Science* 19 (5):797–841.
- Budinova, T., D. Savova, B. Tsyntsarski, C. O. Ania, B. Cabal, J. B. Parra, and N. Petrov. 2009. "Biomass waste-derived activated carbon for the removal of arsenic and manganese ions from aqueous solutions." *Applied Surface Science* 255 (8):4650–4657.
- Calvillo, L., M. J. Lázaro, E. García-Bordejé, R. Moliner, P. L. Cabot, I. Esparbé, E. Pastor, and J. J. Quintana. 2007. "Platinum supported on functionalized ordered mesoporous carbon as electrocatalyst for direct methanol fuel cells." *Journal of Power Sources* 169 (1):59–64.
- Chen, H. 2014. "Chemical composition and structure of natural lignocellulose." In *Biotechnology of Lignocellulose*, 25–71. Dordrecht: Springer.
- Cui, X., M. Antonietti, and S.-H. Yu. 2006. "Structural effects of iron oxide nanoparticles and iron ions on the hydrothermal carbonization of starch and rice carbohydrates." *Small* 2 (6):756–759.
- Dai, Y., H. Jiang, Y. Hu, Y. Fu, and C. Li. 2014. "Controlled synthesis of ultrathin hollow mesoporous carbon nanospheres for supercapacitor applications." *Industrial & Engineering Chemistry Research* 53 (8):3125–3130. doi: 10.1021/ie403950t.
- Dawood, S., T. K. Sen, and C. Phan. 2014. "Synthesis and characterisation of novel-activated carbon from waste biomass pine cone and its application in the removal of Congo red dye from aqueous solution by adsorption." *Water, Air, & Soil Pollution* 225 (1):1–16.
- Deepa, A. K., and P. L. Dhepe. 2014. "Lignin depolymerization into aromatic monomers over solid acid catalysts." *ACS Catalysis* 5 (1):365–379.
- Demir-Cakan, R., N. Baccile, M. Antonietti, and M.-M. Titirici. 2009. "Carboxylate-rich carbonaceous materials via one-step hydrothermal carbonization of glucose in the presence of acrylic acid." *Chemistry of Materials* 21 (3):484–490.
- Dhillon, R. S., and G. von Wuehlisch. 2013. "Mitigation of global warming through renewable biomass." *Biomass and Bioenergy* 48:75–89.
- Diakité, M., A. Paul, C. Jäger, J. Pielert, and J. Mumme. 2013. "Chemical and morphological changes in hydrochars derived from microcrystalline cellulose and investigated by chromatographic, spectroscopic and adsorption techniques." *Bioresource Technology* 150:98–105.
- Ding, L., B. Zou, Y. Li, H. Liu, Z. Wang, C. Zhao, Y. Su, and Y. Guo. 2013. "The production of hydrochar-based hierarchical porous carbons for use as electrochemical supercapacitor electrode materials." *Colloids and Surfaces A: Physicochemical and Engineering Aspects* 423:104–111.
- Dolores, L.-C., P. M.-L. Juan, C. Falco, M.-M. Titirici, and C.-A. Diego. 2013. "Porous biomass-derived carbons: Activated carbons." In *Sustainable Carbon Materials from Hydrothermal Processes*, edited by M.-M. Titirici, 75–100. Chichester: John Wiley & Sons.
- Falco, C., N. Baccile, and M.-M. Titirici. 2011. "Morphological and structural differences between glucose, cellulose and lignocellulosic biomass derived hydrothermal carbons." *Green Chemistry* 13 (11):3273–3281.
- Falco, C., J. P. Marco-Lozar, D. Salinas-Torres, E. Morallon, D. Cazorla-Amoros, M.-M. Titirici, and D. Lozano-Castello. 2013. "Tailoring the porosity of chemically activated hydrothermal carbons: Influence of the precursor and hydrothermal carbonization temperature." *Carbon* 62:346–355.
- Falco, C., M. Sevilla, R. J. White, R. Rothe, and M.-M. Titirici. 2012. "Renewable nitrogen-doped hydrothermal carbons derived from microalgae." *ChemSusChem* 5 (9):1834–1840.
- Falco, C., J. M. Sieben, N. Brun, M. Sevilla, T. van der Maulen, E. Morallón, D. Cazorla-Amorós, and M.-M. Titirici. 2013. "Hydrothermal carbons from hemicellulose-derived aqueous hydrolysis products as electrode materials for supercapacitors." *ChemSusChem* 6 (2):374–382.

- Fechler, N., S.-A. Wohlgemuth, P. Jäker, and M. Antonietti. 2013. "Salt and sugar: Direct synthesis of high surface area carbon materials at low temperatures via hydrothermal carbonization of glucose under hypersaline conditions." *Journal of Materials Chemistry A* 1 (33):9418–9421.
- Fellinger, T.-P., R. J. White, M.-M. Titirici, and M. Antonietti. 2012. "Borax-mediated formation of carbon aerogels from glucose." *Advanced Functional Materials* 22 (15):3254–3260.
- Fuertes, A. B., F. Pico, and J. M. Rojo. 2004. "Influence of pore structure on electric double-layer capacitance of template mesoporous carbons." *Journal of Power Sources* 133 (2):329–336.
- Funke, A., and F. Ziegler. 2010. "Hydrothermal carbonization of biomass: A summary and discussion of chemical mechanisms for process engineering." *Biofuels, Bioproducts and Biorefining* 4 (2):160–177.
- Gan, W., L. Gao, X. Zhan, and J. Li. 2016. "Preparation of thiol-functionalized magnetic sawdust composites as an adsorbent to remove heavy metal ions." *RSC Advances* 6 (44):37600–37609.
- Guo, J., and A. C. Lua. 1999. "Textural and chemical characterisations of activated carbon prepared from oil-palm stone with H_2SO_4 and KOH impregnation." *Microporous and Mesoporous Materials* 32 (1):111–117.
- Guo, S.-R., J.-Y. Gong, P. Jiang, M. Wu, Y. Lu, and S.-H. Yu. 2008. "Biocompatible, luminescent silver@phenol formaldehyde resin core/shell nanospheres: Large-scale synthesis and application for in vivo bioimaging." *Advanced Functional Materials* 18 (6):872–879.
- Guo, Y., J. Zhao, H. Zhang, S. Yang, J. Qi, Z. Wang, and H. Xu. 2005. "Use of rice husk-based porous carbon for adsorption of Rhodamine B from aqueous solutions." *Dyes and Pigments* 66 (2):123–128.
- Gurung, M., B. B. Adhikari, S. Alam, H. Kawakita, K. Ohto, K. Inoue, and H. Harada. 2013. "Adsorptive removal of Cs (I) from aqueous solution using polyphenols enriched biomass-based adsorbents." *Chemical Engineering Journal* 231:113–120.
- Hameed, B. H., and A. A. Rahman. 2008. "Removal of phenol from aqueous solutions by adsorption onto activated carbon prepared from biomass material." *Journal of Hazardous Materials* 160 (2):576–581.
- Hartmann, M. 2005. "Ordered mesoporous materials for bioadsorption and biocatalysis." *Chemistry of Materials* 17 (18):4577–4593.
- Hatcher, P. G., and D. J. Clifford. 1997. "The organic geochemistry of coal: From plant materials to coal." *Organic Geochemistry* 27 (5):251–274.
- He, X., Y. Geng, J. Qiu, M. Zheng, S. Long, and X. Zhang. 2010. "Effect of activation time on the properties of activated carbons prepared by microwave-assisted activation for electric double layer capacitors." *Carbon* 48 (5):1662–1669.
- Hoekman, S. K., A. Broch, and C. Robbins. 2011. "Hydrothermal carbonization (HTC) of lignocellulosic biomass." *Energy & Fuels* 25 (4):1802–1810.
- Hu, B., K. Wang, L. Wu, S. H. Yu, M. Antonietti, and M. M. Titirici. 2010. "Engineering carbon materials from the hydrothermal carbonization process of biomass." *Advanced Materials* 22 (7):813–828. doi: 10.1002/adma.200902812.
- Hu, Z., and M. P. Srinivasan. 2001. "Mesoporous high-surface-area activated carbon." *Microporous and Mesoporous Materials* 43 (3):267–275.
- Hu, Z., M. P. Srinivasan, and Y. Ni. 2000. "Preparation of Mesoporous High-Surface-Area Activated Carbon." *Advanced Materials* 12 (1):62–65.
- Hu, Z., M. P. Srinivasan, and Y. Ni. 2001. "Novel activation process for preparing highly microporous and mesoporous activated carbons." *Carbon* 39 (6):877–886.
- Jain, A., V. Aravindan, S. Jayaraman, P. S. Kumar, R. Balasubramanian, S. Ramakrishna, S. Madhavi, and M. P. Srinivasan. 2013. "Activated carbons derived from coconut shells as high energy density cathode material for Li-ion capacitors." *Scientific Reports* 3. doi: 10.1038/srep03002/.
- Jain, A., R. Balasubramanian, and M. P. Srinivasan. 2015a. "Tuning hydrochar properties for enhanced mesopore development in activated carbon by hydrothermal carbonization." *Microporous and Mesoporous Materials* 203:178–185. doi: <http://dx.doi.org/10.1016/j.micromeso.2014.10.036>.
- Jain, A., R. Balasubramanian, and M. P. Srinivasan. 2015b. "Production of high surface area mesoporous activated carbons from waste biomass using hydrogen peroxide-mediated hydrothermal treatment for adsorption applications." *Chemical Engineering Journal* 273:622–629.

- Jain, A., R. Balasubramanian, and M. P. Srinivasan. 2016. "Hydrothermal conversion of biomass waste to activated carbon with high porosity: A review." *Chemical Engineering Journal* 283:789–805.
- Jain, A., S. Jayaraman, R. Balasubramanian, and M. P. Srinivasan. 2014. "Hydrothermal pre-treatment for mesoporous carbon synthesis: Enhancement of chemical activation." *Journal of Materials Chemistry A* 2 (2):520–528. doi: 10.1039/C3TA12648J.
- Jain, A., V. Ong, S. Jayaraman, R. Balasubramanian, and M. P. Srinivasan. 2016. "Supercritical fluid immobilization of horseradish peroxidase on high surface area mesoporous activated carbon." *The Journal of Supercritical Fluids* 107:513–518.
- Jain, A., C. Xu, S. Jayaraman, R. Balasubramanian, J. Y. Lee, and M. P. Srinivasan. 2015. "Mesoporous activated carbons with enhanced porosity by optimal hydrothermal pre-treatment of biomass for supercapacitor applications." *Microporous and Mesoporous Materials* 218:55–61.
- Khalili, N. R., and H. Arastoopour. 2002. "Drying, crushing, sieving, chemical activation, light and humidity treatment, pyrolyzing, cooling and rinsing of waste from paper mills; adsorption of gaseous pollutants; nitrous oxide, hydrogen sulfide and sulfur dioxide." Illinois Institute of Technology.
- Khalili, N. R., H. Arastoopour, and L. K. Walhof. 2000. "Synthesizing carbon from sludge." US Patent 6,030,922 A.
- Khalili, N. R., and V. H. Perez-Luna. 2004. "Producing low cost, efficient flue gas scrubber; surface treating activated carbon with negatively charged protein then electroless plating gold."
- Klemm, D., B. Heublein, H.-P. Fink, and A. Bohn. 2005. "Cellulose: Fascinating biopolymer and sustainable raw material." *Angewandte Chemie International Edition* 44 (22):3358–3393.
- Kobayashi, S., and A. Maki. 2009. "Enzymatic polymer synthesis: An opportunity for green polymer chemistry." *Chemical Reviews* 109 (11):5288–5353.
- Kubo, S., R. Demir-Cakan, L. Zhao, R. J. White, and M.-M. Titirici. 2010. "Porous carbohydrate-based materials via hard templating." *ChemSusChem* 3 (2):188–194.
- Lesmana, S. O., N. Febriana, F. E. Soetaredjo, J. Sunarso, and S. Ismadji. 2009. "Studies on potential applications of biomass for the separation of heavy metals from water and wastewater." *Biochemical Engineering Journal* 44 (1):19–41. doi: <http://dx.doi.org/10.1016/j.bej.2008.12.009>.
- Li, X., W. Xing, S. Zhuo, J. Zhou, F. Li, S.-Z. Qiao, and G.-Q. Lu. 2011. "Preparation of capacitor's electrode from sunflower seed shell." *Bioresource Technology* 102 (2):1118–1123. doi: <http://dx.doi.org/10.1016/j.biortech.2010.08.110>.
- Liang, C., Z. Li, and S. Dai. 2008. "Mesoporous carbon materials: Synthesis and modification." *Angewandte Chemie International Edition* 47 (20):3696–3717.
- Libra, J. A., K. S. Ro, C. Kammann, A. Funke, N. D. Berge, Y. Neubauer, M.-M. Titirici, C. Fühner, O. Bens, and J. Kern. 2011. "Hydrothermal carbonization of biomass residuals: A comparative review of the chemistry, processes and applications of wet and dry pyrolysis." *Biofuels* 2 (1):71–106.
- Lillo-Ródenas, M. A., J. Juan-Juan, D. Cazorla-Amorós, and A. Linares-Sola. 2004. "About reactions occurring during chemical activation with hydroxides." *Carbon* 42 (7):1371–1375.
- Linares-Solano, A., D. Lozano-Castelló, M. A. Lillo-Ródenas, and D. Cazorla-Amorós. 2007. "Carbon activation by alkaline hydroxides." In *Chemistry & Physics of Carbon* (vol. 30), edited by L. Radovic, 1–62. Boca Raton, FL: CRC Press.
- Littrell, K. C., N. R. Khalili, M. Campbell, G. Sandí, and P. Thiyagarajan. 2002. "Microstructural analysis of activated carbons prepared from paper mill sludge by SANS and BET." *Chemistry of Materials* 14 (1):327–333.
- Liu, W.-J., H. Jiang, and H.-Q. Yu. 2015. "Thermochemical conversion of lignin to functional materials: A review and future directions." *Green Chemistry* 17 (11):4888–4907.
- Liu, Z., A. Quek, G. Parshetti, A. Jain, M. P. Srinivasan, S. K. Hoekman, and R. Balasubramanian. 2013. "A study of nitrogen conversion and polycyclic aromatic hydrocarbon (PAH) emissions during hydrochar–lignite co-pyrolysis." *Applied Energy* 108:74–81.
- Liu, Z., and F. S. Zhang. 2009. "Removal of lead from water using biochars prepared from hydrothermal liquefaction of biomass." *Journal of Hazardous Materials* 167 (1–3):933–939.

- Liu, Z., F. S. Zhang, and J. Wu. 2010. "Characterization and application of chars produced from pine-wood pyrolysis and hydrothermal treatment." *Fuel* 89 (2):510–514.
- Lua, A. C., and J. Guo. 2001. "Microporous oil-palm-shell activated carbon prepared by physical activation for gas-phase adsorption." *Langmuir* 17 (22):7112–7117.
- Luo, P. G., F. Yang, S.-T. Yang, S. K. Sonkar, L. Yang, J. J. Broglie, Y. Liu, and Y.-P. Sun. 2014. "Carbon-based quantum dots for fluorescence imaging of cells and tissues." *RSC Advances* 4 (21):10791–10807.
- Makowski, P., R. D. Cakan, M. Antonietti, F. Goettmann, and M.-M. Titirici. 2008. "Selective partial hydrogenation of hydroxy aromatic derivatives with palladium nanoparticles supported on hydrophilic carbon." *Chemical Communications* (8):999–1001.
- Malik, R., D. S. Ramteke, and S. R. Wate. 2007. "Adsorption of malachite green on groundnut shell waste based powdered activated carbon." *Waste Management* 27 (9):1129–1138.
- Masselter, S., A. Zemmann, and O. Bobleter. 1995. "Analysis of lignin degradation products by capillary electrophoresis." *Chromatographia* 40 (1–2):51–57.
- Meng, Y., D. Gu, F. Zhang, Y. Shi, H. Yang, Z. Li, C. Yu, B. Tu, and D. Zhao. 2005. "Ordered mesoporous polymers and homologous carbon frameworks: Amphiphilic surfactant templating and direct transformation." *Angewandte Chemie* 117 (43):7215–7221.
- Nakagawa, Y., M. Molina-Sabio, and F. Rodríguez-Reinoso. 2007. "Modification of the porous structure along the preparation of activated carbon monoliths with H_3PO_4 and ZnCl_2 ." *Microporous and Mesoporous Materials* 103 (1):29–34.
- Olivares-Marín, M., J. A. Fernández, M. J. Lázaro, C. Fernández-González, A. Macías-García, V. Gómez-Serrano, F. Stoeckli, and T. A. Cente. 2009. "Cherry stones as precursor of activated carbons for supercapacitors." *Materials Chemistry and Physics* 114 (1):323–327.
- Panda, G. C., S. K. Das, and A. K. Guha. 2008. "Biosorption of cadmium and nickel by functionalized husk of *Lathyrus sativus*." *Colloids and Surfaces B: Biointerfaces* 62 (2):173–179.
- Pangeni, B., H. Paudyal, K. Inoue, H. Kawakita, K. Ohto, M. Gurung, and S. Alam. 2014. "Development of low cost adsorbents from agricultural waste biomass for the removal of Sr (II) and Cs (I) from water." *Waste and Biomass Valorization* 5 (6):1019–1028.
- Parshetti, G. K., S. Kent Hoekman, and R. Balasubramanian. 2013. "Chemical, structural and combustion characteristics of carbonaceous products obtained by hydrothermal carbonization of palm empty fruit bunches." *Bioresource Technology* 135:683–689.
- Parshetti, G. K., Z. Liu, A. Jain, M. P. Srinivasan, and R. Balasubramanian. 2013. "Hydrothermal carbonization of sewage sludge for energy production with coal." *Fuel* 111:201–210.
- Qi, X. H., L. Y. Li, Y. Wang, N. Liu, and R. L. Smith. 2014. "Removal of hydrophilic ionic liquids from aqueous solutions by adsorption onto high surface area oxygenated carbonaceous material." *Chemical Engineering Journal* 256:407–414. doi: 10.1016/j.cej.2014.07.020.
- Quesada-Plata, F., R. Ruiz-Rosas, M. Emilia, and D. Cazorla-Amorós. 2016. "Activated carbons prepared through H_3PO_4 -assisted hydrothermal carbonization from biomass wastes: Porous texture and electrochemical performance." *ChemPlusChem* 81 (12):1349–1359. doi: 10.1002/cplu.201600412.
- Roman, S., J. M. V. Nabais, B. Ledesma, J. F. González, C. Laginhas, and M. M. Titirici. 2013. "Production of low-cost adsorbents with tunable surface chemistry by conjunction of hydrothermal carbonization and activation processes." *Microporous and Mesoporous Materials* 165:127–133.
- Romero-Anaya, A. J., M. A. Lillo-Ródenas, C. Salinas-Martínez de Lecea, and A. Linares-Sola. 2012. "Hydrothermal and conventional H_3PO_4 activation of two natural bio-fibers." *Carbon* 50 (9):3158–3169. doi: <http://dx.doi.org/10.1016/j.carbon.2011.10.031>.
- Romero-Anaya, A. J., M. Ouzzine, M. A. Lillo-Ródenas, and A. Linares-Sola. 2014. "Spherical carbons: Synthesis, characterization and activation processes." *Carbon* 68:296–307.
- Rufford, T. E., D. Hulicova-Jurcakova, K. Khosla, Z. Zhu, and G. Q. Lu. 2010. "Microstructure and electrochemical double-layer capacitance of carbon electrodes prepared by zinc chloride activation of sugar cane bagasse." *Journal of Power Sources* 195 (3):912–918.

- Ruiz, V., C. Blanco, R. Santamaría, J. M. Ramos-Fernández, M. Martínez-Escandell, A. Sepúlveda-Escribano, and F. Rodríguez-Reinoso. 2009. "An activated carbon monolith as an electrode material for supercapacitors." *Carbon* 47 (1):195–200.
- Ryoo, R., S. H. Joo, M. Kruk, and M. Jaroniec. 2001. "Ordered mesoporous carbons." *Advanced Materials* 13 (9):677–681.
- Sandí, G., N. R. Khalili, W. Lu, and J. Prakash. 2003. "Electrochemical performance of carbon materials derived from paper mill sludge." *Journal of Power Sources* 119:34–38.
- Selvi, B. R., D. Jagadeesan, B. S. Suma, G. Nagashankar, M. Arif, K. Balasubramanyam, M. Eswaramoorthy, and T. K. Kundu. 2008. "Intrinsically fluorescent carbon nanospheres as a nuclear targeting vector: Delivery of membrane-impermeable molecule to modulate gene expression in vivo." *Nano Letters* 8 (10):3182–3188.
- Sen, T. K., S. Afroze, and H. M. Ang. 2011. "Equilibrium, kinetics and mechanism of removal of methylene blue from aqueous solution by adsorption onto pine cone biomass of *Pinus radiata*." *Water, Air, & Soil Pollution* 218 (1–4):499–515.
- Sevilla, M., S. Alvarez, T. A. Centeno, A. B. Fuertes, and F. Stoeckli. 2007. "Performance of templated mesoporous carbons in supercapacitors." *Electrochimica Acta* 52 (9):3207–3215.
- Sevilla, M., and A. B. Fuertes. 2009. "The production of carbon materials by hydrothermal carbonization of cellulose." *Carbon* 47 (9):2281–2289.
- Sevilla, M., and A. B. Fuertes. 2011. "Sustainable porous carbons with a superior performance for CO₂ capture." *Energy & Environmental Science* 4 (5):1765–1771.
- Sevilla, M., A. B. Fuertes, and R. Mokaya. 2011. "High density hydrogen storage in superactivated carbons from hydrothermally carbonized renewable organic materials." *Energy & Environmental Science* 4 (4):1400–1410.
- Sevilla, M., J. A. Maciá-Agulló, and A. B. Fuertes. 2011. "Hydrothermal carbonization of biomass as a route for the sequestration of CO₂: Chemical and structural properties of the carbonized products." *Biomass and Bioenergy* 35 (7):3152–3159. doi: <http://dx.doi.org/10.1016/j.biombioe.2011.04.032>.
- Simon, P., and Y. Gogotsi. 2008. "Materials for electrochemical capacitors." *Nature Materials* 7 (11):845–854.
- Stavropoulos, G. G., and A. A. Zabaniotou. 2005. "Production and characterization of activated carbons from olive-seed waste residue." *Microporous and Mesoporous Materials* 82 (1):79–85.
- Sun, X., and Y. Li. 2004. "Colloidal carbon spheres and their core/shell structures with noble-metal nanoparticles." *Angewandte Chemie International Edition* 43 (5):597–601.
- Takahashi, H., B. Li, T. Sasaki, C. Miyazaki, T. Kajino, and S. Inagaki. 2000. "Catalytic activity in organic solvents and stability of immobilized enzymes depend on the pore size and surface characteristics of mesoporous silica." *Chemistry of Materials* 12 (11):3301–3305.
- Talapaneni, S. N., G. P. Mane, A. Mano, C. Anand, D. S. Dhawale, T. Mori, and A. Vinu. 2012. "Synthesis of nitrogen-rich mesoporous carbon nitride with tunable pores, band gaps and nitrogen content from a single aminoguanidine precursor." *ChemSusChem* 5 (4):700–708.
- Tekin, K. 2015. "Hydrothermal conversion of Russian olive seeds into crude bio-oil using a CaO catalyst derived from waste mussel shells." *Energy & Fuels* 29 (7):4382–4392.
- Tekin, K., M. K. Akalin, L. Uzun, S. Karagöz, S. Bektaş, and A. Denizli. 2016. "Adsorption of Pb (II) and Cd (II) ions onto dye-attached sawdust." *CLEAN—Soil, Air, Water* 44 (4):339–344.
- Tekin, K., and S. Karagöz. 2013. "t-BuOK catalyzed bio-oil production from woody biomass under sub-critical water conditions." *Environmental Chemistry Letters* 11 (1):25–31.
- Tekin, K., S. Karagöz, and S. Bektaş. 2012. "Hydrothermal liquefaction of beech wood using a natural calcium borate mineral." *The Journal of Supercritical Fluids* 72:134–139.
- Tekin, K., S. Karagöz, and S. Bektaş. 2014. "A review of hydrothermal biomass processing." *Renewable and Sustainable Energy Reviews* 40:673–687.
- Thompson, E., A. E. Danks, L. Bourgeois, and Z. Schnepp. 2015. "Iron-catalyzed graphitization of biomass." *Green Chemistry* 17 (1):551–556.

- Titirici, M.-M., M. Antonietti, and N. Baccile. 2008. "Hydrothermal carbon from biomass: A comparison of the local structure from poly- to monosaccharides and pentoses/hexoses." *Green Chemistry* 10 (11):1204–1212.
- Titirici, M.-M., M. Antonietti, and A. Thomas. 2006. "A generalized synthesis of metal oxide hollow spheres using a hydrothermal approach." *Chemistry of Materials* 18 (16):3808–3812.
- Titirici, M.-M., A. Thomas, and M. Antonietti. 2007. "Replication and coating of silica templates by hydrothermal carbonization." *Advanced Functional Materials* 17 (6):1010–1018.
- Titirici, M.-M., A. Thomas, S. H. Yu, J. O. Müller, and M. Antonietti. 2007. "A direct synthesis of mesoporous carbons with bicontinuous pore morphology from crude plant material by hydrothermal carbonization." *Chemistry of Materials* 19 (17):4205–4212.
- Titirici, M.-M., R. J. White, C. Falco, and M. Sevilla. 2012. "Black perspectives for a green future: Hydrothermal carbons for environment protection and energy storage." *Energy & Environmental Science* 5:6796–6822.
- Unur, E., S. Brutti, S. Panero, and B. Scrosati. 2013. "Nanoporous carbons from hydrothermally treated biomass as anode materials for lithium ion batteries." *Microporous and Mesoporous Materials* 174:25–33.
- Vinu, A., M. Miyahara, T. Mori, and K. Ariga. 2006. "Carbon nanocage: A large-pore cage-type mesoporous carbon material as an adsorbent for biomolecules." *Journal of Porous Materials* 13 (3–4):379–383.
- Volesky, B., and Z. R. Holan. 1995. "Biosorption of heavy metals." *Biotechnology Progress* 11 (3):235–250.
- Wang, L., Y. Guo, B. Zou, C. Rong, X. Ma, Y. Qu, Y. Li, and Z. Wang. 2011. "High surface area porous carbons prepared from hydrochars by phosphoric acid activation." *Bioresource Technology* 102 (2):1947–1950.
- Wang, X., C. Hu, Y. Xiong, H. Liu, G. Du, and X. He. 2011. "Carbon-nanosphere-supported Pt nanoparticles for methanol and ethanol electro-oxidation in alkaline media." *Journal of Power Sources* 196 (4):1904–1908.
- Wei, J., Y. Liang, Y. Hu, B. Kong, G. P. Simon, J. Zhang, S. P. Jiang, and H. Wang. 2016. "A versatile iron–tannin-framework ink coating strategy to fabricate biomass-derived iron carbide/Fe–N–carbon catalysts for efficient oxygen reduction." *Angewandte Chemie* 128 (4):1377–1381.
- Wei, L., M. Sevilla, A. B. Fuertes, R. Mokaya, and G. Yushin. 2011. "Hydrothermal carbonization of abundant renewable natural organic chemicals for high-performance supercapacitor electrodes." *Advanced Energy Materials* 1 (3):356–361.
- White, R. J., N. Yoshizawa, M. Antonietti, and M.-M. Titirici. 2011. "A sustainable synthesis of nitrogen-doped carbon aerogels." *Green Chemistry* 13 (9):2428–2434.
- Williams, P. T., and A. R. Reed. 2006. "Development of activated carbon pore structure via physical and chemical activation of biomass fibre waste." *Biomass and Bioenergy* 30 (2):144–152.
- Wohlgemuth, S.-A., T.-P. Fellingner, P. Jäker, and M. Antonietti. 2013. "Tunable nitrogen-doped carbon aerogels as sustainable electrocatalysts in the oxygen reduction reaction." *Journal of Materials Chemistry A* 1 (12):4002–4009.
- Xia, Y. D., and R. Mokaya. 2004. "Ordered mesoporous carbon hollow spheres nanocast using mesoporous silica via chemical vapor deposition." *Advanced Materials* 16 (11):886–891.
- Xie, T., K. R. Reddy, C. Wang, E. Yargicoglu, and K. Spokas. 2015. "Characteristics and applications of biochar for environmental remediation: A review." *Critical Reviews in Environmental Science and Technology* 45 (9):939–969.
- Xing, W., C. C. Huang, S. P. Zhuo, X. Yuan, G. Q. Wang, D. Hulicova-Jurcakova, Z. F. Yan, and G. Q. Lu. 2009. "Hierarchical porous carbons with high performance for supercapacitor electrodes." *Carbon* 47 (7):1715–1722.
- Xu, C., B. Xu, Y. Gu, Z. Xiong, J. Sun, and X. S. Zhao. 2013. "Graphene-based electrodes for electrochemical energy storage." *Energy & Environmental Science* 6 (5):1388–1414. doi: 10.1039/C3EE23870A.
- Xu, G., J. Han, B. Ding, P. Nie, J. Pan, H. Dou, H. Li, and X. Zhang. 2015. "Biomass-derived porous carbon materials with sulfur and nitrogen dual-doping for energy storage." *Green Chemistry* 17 (3):1668–1674.

- Xu, Q., Q. Qian, A. Quek, N. Ai, G. Zeng, and J. Wang. 2013. "Hydrothermal carbonization of macroalgae and the effects of experimental parameters on the properties of hydrochars." *ACS Sustainable Chemistry & Engineering* 1 (9):1092–1101.
- Xue, Y. W., B. Gao, Y. Yao, M. Inyang, M. Zhang, A. R. Zimmerman, and K. S. Ro. 2012a. "Hydrogen peroxide modification enhances the ability of biochar (hydrochar) produced from hydrothermal carbonization of peanut hull to remove aqueous heavy metals: Batch and column tests." *Chemical Engineering Journal* 200:673–680. doi: 10.1016/j.cej.2012.06.116.
- Yang, T., T. Qian, M. Wang, X. Shen, N. Xu, Z. Sun, and C. Yan. 2016. "A sustainable route from biomass byproduct okara to high content nitrogen-doped carbon sheets for efficient sodium ion batteries." *Advanced Materials* 28 (3):539–545.
- Zhang, Z., Y. Qu, Y. Guo, Z. Wang, and X. Wang. 2014. "A novel route for preparation of high-performance porous carbons from hydrochars by KOH activation." *Colloids and Surfaces A: Physicochemical and Engineering Aspects* 447:183–187.
- Zhao, L., Z. Bacsik, N. Hedin, W. Wei, Y. Sun, M. Antonietti, and M.-M. Titirici. 2010. "Carbon dioxide capture on amine-rich carbonaceous materials derived from glucose." *ChemSusChem* 3 (7):840–845.
- Zhu, X., Y. Liu, G. Luo, F. Qian, S. Zhang, and J. Chen. 2014. "Facile fabrication of magnetic carbon composites from hydrochar via simultaneous activation and magnetization for triclosan adsorption." *Environmental Science & Technology* 48 (10):5840–5848.
- Zhuang, X., Y. Wan, C. Feng, Y. Shen, and D. Zhao. 2009. "Highly efficient adsorption of bulky dye molecules in wastewater on ordered mesoporous carbons." *Chemistry of Materials* 21 (4):706–716.



Taylor & Francis

Taylor & Francis Group

<http://taylorandfrancis.com>

12

Sustainable Biochar Derived from Agricultural Wastes for Removal of Methylene Green 5 from Aqueous Solution: Adsorption Kinetics, Isotherms, Thermodynamics, and Mechanism Analysis

Hai Nguyen Tran, Sheng-Jie You, Huan-Ping Chao, and Ya-Fen Wang

CONTENTS

12.1	Introduction	256
12.2	Materials and Methods	257
12.2.1	Biochar Preparation	257
12.2.2	Biochar Characterization	258
12.2.3	Adsorption Experiments	259
12.2.3.1	Batch Adsorption Experiment.....	259
12.2.3.2	Column Adsorption Experiment.....	260
12.2.4	Statistical Analysis.....	261
12.3	Results and Discussion	261
12.3.1	Characteristics of Biochar	261
12.3.2	Point of Zero Charge and Effect of Solution pH.....	265
12.3.3	Effect of Ionic Strength.....	266
12.3.4	Adsorption Kinetics	267
12.3.5	Adsorption Isotherms	272
12.3.6	Adsorption Thermodynamics	274
12.3.7	Adsorption Reversibility.....	278
12.3.8	Continuous Adsorption Experiment	279
12.3.9	Possible Adsorption Mechanisms	282
12.3.9.1	Electrostatic Attraction and Cation Exchange.....	282
12.3.9.2	Hydrogen Bonding Formation.....	283
12.3.9.3	n- π Interaction.....	284
12.3.9.4	π - π Interaction	284
12.3.9.5	Pore Filling	286
12.3.10	Comparison.....	288
12.4	Conclusions.....	288
	References.....	289

12.1 Introduction

The presence of dyes and pigments in water environments has been receiving attention recently because of the aesthetically displeasing reasons (strong and persistent color), environmentally adverse problems (oxygen deficiency), and potential health risks for humans (their toxicological, carcinogenic, and mutagenic nature). There are more than an estimated 100,000 known commercial dyes, approximately 700,000 tons of dye are produced each year, and around 10,000 tons are subsequently discharged into wastewater streams annually (Raval et al., 2016).

Among current techniques (i.e., membrane filtration, photocatalytic degradation, and chemical oxidation), adsorption is widely acknowledged as the most economically favorable technique to remove dyes from spent textile dyeing wastewater because of its relatively high removal efficiency, low operation costs, simplicity of design, ease of operation, minimal secondary by-products (i.e., harmful substances or sludge formation), low energy consumption, and feasibility to separate a wide range of contaminants from industrial effluents. In water and wastewater treatment, activated carbon (AC) with its highly porous structure, large Brunauer–Emmett–Teller (BET) specific surface area, and high total pore volume has been widely applied for removal of numerous organic and inorganic pollutants. According to a Cleveland-based industry market research report (Freedonia, 2016), the global demand for AC is estimated to increase 6% annually, and be up to 1.9 million metric tons by 2020.

However, AC is much more expensive than biochar, and therefore its use at large industrial scale is restricted by financial burden. The estimated average cost of commercial biochar (around US\$2,060 per ton) is overwhelmingly lower than that of commercially available AC (approximately US\$135,000 per ton), because biochar requires less energy than AC and can be used without further activation (chemical or physical) (Jirka and Tomlinson, 2015). The physical or thermal activation method often comprises two stages: (1) raw materials pyrolyzed to convert into a fixed carbon mass (biochar) that has rudimentary pore structures; and (2) physical activation of biochar by oxidizing gases (i.e., air, CO₂, or steam) at a high carbonization temperature (i.e., >900°C). Meanwhile, the chemical activation process can be conducted in traditional methods (one or two stages) (Tran et al., 2017c) and a new method (three stages) (Tran et al., 2017d).

Unlike lignocellulose-derived biosorbent and hydrochar, biochar is a stable carbon-enriched and porous material along with its relatively large BET specific surface area, substantially high pore volume, well-developed porous structure, moderate cation exchange capacity (CEC), and excellent thermal stability (Tran et al., 2017c). Additionally, biochar (referred to as black carbon)—considered as a by-product in the biomass-to-biofuel production process—can be synthesized using biomass produced through carbonization in an inert atmosphere (i.e., N₂ or Ar) (Huang et al., 2014), in a noncirculated air atmosphere (i.e., within lid-enclosed crucible) (Tran et al., 2016a), under a vacuum condition (Carrier et al., 2012), or under a microwave-assisted condition (Dai et al., 2017). Agricultural waste materials can be considered potential feedstocks to prepare biochar because of their abundantly available, renewable, inexpensive, and nontoxic nature. Generally, the BET specific surface area of biochar can be directly proportional to pyrolysis temperatures. However, a higher pyrolysis temperature (>800°C) can lead to a decrease in the biochar's yield and partially destroy its surface functional groups (i.e., —COOH and —OH).

Methylene green 5 (MG5) is a cationic phenothiazine dye and heterocyclic aromatic chemical compound that can be considered as a nitro derivative of methylene blue. MG5

can be classed as a nitro-aromatic contaminant because it contains polar nitro-functional groups. In addition, MG5—commonly used in various industries—shows considerable solubility in both polar organic media and water. The investigation of MG5 adsorption onto various kinds of adsorbents has been published in the literature. These adsorbents were comprised of (1) pristine biosorbents derived from coconut shell (CC), orange peel (OP), and golden shower pod (GS) (Tran et al., 2017f); (2) hydrochars prepared from CC, OP, GS, and commercial glucose through hydrothermal carbonization (Tran et al., 2017a, 2017e); (3) activated carbons synthesized from OP, GS, and commercial saccharide precursors (i.e., glucose, xylose, and sucrose) (Huang et al., 2014; Tran et al., 2017d); (4) commercial activated carbons (Huang et al., 2014; Tran et al., 2017b); (5) hydrochar and activated carbon functionalized with triethylenetetramine (Tran et al., 2017a); and (6) others (i.e., silver and zinc oxide nanostructures loaded on activated carbons, mesoporous zeolite, and collagen-g-poly(acrylamide-co-maleic anhydride) hydrogel nanocomposite) (Lee et al., 2007; Marandi et al., 2013; Ghaedi et al., 2014). However, the capacity and mechanism of MG5 adsorption onto agricultural waste-derived biochar have not yet been investigated or presented in the scientific literature.

In this chapter, the biochar samples (adsorbent) derived from various agricultural residues (i.e., coconut shell, orange peel, golden shower pod) were prepared and applied to remove MG5 molecules (adsorbate) from an aqueous solution. The biochar's characteristics—textural, physicochemical, and morphological properties, and surface chemistry—were thoroughly investigated. The effects of various operation conditions (i.e., solution pH, ionic strength, contact time, temperature, and initial MG5 concentration) on MG5 adsorption efficiency were systematically investigated in batch experiments. A continuous study was also examined in a fixed-bed column. An efficient method (oxygenation of biochar surface using a hydrothermal process with acrylic acid) was also applied to identify the presence of any π - π interaction in the MG5 adsorption process. Adsorption mechanisms were also proposed on the basis of the experimental observations (i.e., FTIR, N_2 adsorption/desorption isotherms, desorption study, and adsorption kinetics and thermodynamics).

12.2 Materials and Methods

12.2.1 Biochar Preparation

The carbohydrate precursors—golden shower pod, coconut shell, and orange peel—were collected in Taiwan. The collected samples were then washed with tap water at least thrice and then with deionized distilled water. They were then placed in an oven at 80°C for 48 h. The dried samples were ground and sieved into desirable particles (0.106–0.250 mm).

Approximately 50 g of the precursors was placed in a porcelain crucible covered with a lid. The crucible was placed in a muffle furnace (Deng Yng DF 40, Taiwan) at 800°C with a heating rate of 30°C/min for 4 h. After pyrolysis in a noncirculated air atmosphere, the biochar samples—golden shower pod (GSB), coconut shell (CCB), and orange peel (OPB)—were rinsed with 0.1 M HCl. Last, deionized distilled water was used to wash the biochar until filtrates reached a constant pH value. The biochar was then dried, sieved, and stored in airtight brown bottles.

An additional experiment was also conducted to identify the presence of any π - π interactions. The synthesized procedure has been reported in our recent studies (Tran et al.,

2017b, 2017d, 2017e). Approximately 4.0 g biochar was impregnated with 100 mL deionized distilled water containing 20 mL of acrylic acid. The mixture was vigorously stirred at 300 rpm for 1 h and transferred into a 200 mL Teflon-lined autoclave. After a 24 h hydrothermal process at 190°C formed oxygenated-biochar, the black solids were separated and washed with deionized distilled water until the pH of filtrate reached a constant value. The oxygenated biochar was then dried, sieved, and stored in tightly closed brown bottles.

12.2.2 Biochar Characterization

Textural properties were measured using N₂ adsorption–desorption isotherms (Micromeritics ASAP 2020 sorptometer) at 77 K. The BET method was employed to compute the specific surface areas (S_{BET}) in the range $0.05 < p/p_0 < 0.3$. The micropore surface area (S_{micro}) and micropore volume (V_{micro}) were determined using De Boer's t-plot (statistical thickness) method. The external (nonmicropore) surface area (S_{external}) was calculated as the difference between S_{BET} and S_{micro} . The total pore volume (V_{total}) was estimated in terms of the amount of adsorption at a relative pressure (P/P_0) of 0.99 by using the Horvath–Kawazoe method. Pore size distributions were measured using Brunauer's MP method, and the nonmicropore volume ($V_{\text{non-micro}}$) was computed by subtracting the micropore volume from the total pore volume. The characteristic energy (E_o ; kJ/mol) was derived from the nitrogen adsorption isotherm at 77 K by applying the Dubinin–Radushkevich method. The dependence of the characteristic energy on the average width (L ; nm) of the slit pore (Stoeckli and Centeno, 1997) is widely accepted by the following equation:

$$L_o(\text{nm}) = \frac{10.8(\text{nm})(\text{kJ/mol})}{E_o(\text{kJ/mol}) - 11.4(\text{kJ/mol})} \quad (12.1)$$

The morphology of the biochar was obtained using scanning electron microscopy (SEM; Hitachi S-4800, Japan). The methods applied to determine the other biochar's properties (i.e., proximate analysis, ultimate analysis, the bulk density, $\text{pH}_{1.20}$, and hardness number) have been reported elsewhere (Tran et al., 2017c).

The surface chemistry of biochar was determined by three techniques. First, the functional groups present on the adsorbent surface were detected using Fourier transform infrared spectroscopy (FTIR; FT/IR-6600 JASCO); the biochar particles were pelleted mixing with KBr. Second, the pH value of the biochar at the point of zero charge (pH_{PZC}) was determined using the “drift method.” Recently, we investigated the effects of different operation conditions on the pH_{PZC} of commercial activated charcoal determined by the drift method (Tran et al., 2017b). The results demonstrated that the pH_{PZC} of charcoal (9.81 ± 0.07) was insignificantly dependent on the operation conditions (i.e., CO₂, solid/liquid ratio, electrolyte type, electrolyte concentration, and contact time). Additionally, our previous study (Tran et al., 2016a) also indicated that the pH_{PZC} values of biochar (9.4 ± 0.13) were dependent on pyrolysis temperatures (from 400°C to 800°C) and times (2 h and 6 h). Last, the concentration of oxygen-containing functional groups on the biochar's surface (i.e., the acidic groups and basic sites) were determined through the Boehm titration procedure. The numbers of moles of adsorbent surface functionalities were calculated using the equations reported in our recent work (Tran et al., 2017c).

12.2.3 Adsorption Experiments

All MG5 solutions were consecutively diluted from the MG5 stock solution (1200 mg/L). The stock solution was prepared by dissolving the given amount of MG5 in deionized distilled water. All the chemicals were of analytical grade and used without further purification.

12.2.3.1 Batch Adsorption Experiment

Batch adsorption experiments were conducted to study the effects of different operating parameters (i.e., solution pH, contact time, NaCl concentration, initial MG5 concentration, temperature, and desorption agent) on the MG5 adsorption process. All batch adsorption experiments were undertaken at the constant solid/liquid ratio of 4.0 gram of biochar per 1.0 liter of dye. The effects of pH on the adsorption process were studied at different MG5 solutions pH; the solutions pH were adjusted from 2.0 to 10.0 \pm 0.2 by adding 1 M NaOH or 1M HCl. Similarly, the influences of ionic strength were examined in various NaCl concentrations from 0 to 0.5 M. Kinetic adsorption studies were conducted by a series of 100 mL Erlenmeyer flasks containing 50 mL of MG5 solution at 30°C and 50°C. Adsorption isotherms were investigated with MG5 concentrations from 50 to 1200 mg/L at different temperatures. Thermodynamic adsorption experiments were carried out at three different temperatures (i.e., 30°C, 40°C, and 50°C) with various MG5 concentrations (50–1200 mg/L). The MG5-biochar mixture was shaken using a water batch isothermal shaker (DKW-20; Deng Yng Co.) at 150 rpm. After predetermined intervals, the mixture was separated using glass fiber filter. The MG5-laden biochar was rinsed with deionized distilled water, dried, and stored for the further experiments (i.e., FTIR, BET analysis, and desorption). The MG5 concentration in solution was determined using ultraviolet-visible spectrophotometry (Genesys 10 UV-Vis; Thermo Scientific) at maximum absorbance wavelengths. The maximum absorbance wavelength (λ_{\max}) is approximately 655 nm at pH 1.05–11.02 (selected for this study) and 590 nm at pH 11.98–12.87 (Tran et al., 2017b, 2017d). The amount of MG5 uptake at equilibrium, q_e (mg/g), was calculated according to the mass balance equation:

$$q_e = \frac{(C_o - C_e)}{m_1} V_1 \quad (12.2)$$

where C_o (mg/L) and C_e (mg/L) are the MG5 concentrations at beginning and equilibrium, respectively; m_1 (g) is the mass of used biochar; and V_1 (L) is the volume of the MG5 solution.

Reversibility for adsorption was determined by desorption experiments. The desorbing agents used in this study comprised deionized distilled water at pH 2.0, HCl (1 M), NaCl (0.5 M), NaOH (1M), H_2O_2 (10%), hexane, methanol, ethanol, acetone, acetonitrile, ethyl glycol, toluene, 1-pentanol, 1-hexanol, and 1-heptanol. MG5 was desorbed from a given mass of MG5-loaded biochar (m_2) using 0.025 L of various desorbing agents (V_2). The amount of MG5 that remained on the biochar was estimated by a mass balance (Equation 12.3), and the percentage of desorption can be computed from Equation 12.4.

$$q_r = q_e - q_d = q_e - \left(\frac{C_d}{m_2} \times V_2 \right) \quad (12.3)$$

$$\%Desorption = \frac{q_e - q_r}{q_e - q_d} \times 100\% \quad (12.4)$$

where C_d (mg/L) is the concentration of MG5 in solution after desorption, q_r (mg/g) is the mass of MG5 that remained adsorbed after desorption, and q_d (mg/g) is the mass of MG5 desorbed if the adsorption process is reversible.

12.2.3.2 Column Adsorption Experiment

An adsorption test in fixed bed system was conducted in a glass minicolumn of 10 cm height and 1.0 cm inside diameter, which has been published in our earlier work (Chao et al., 2014). In general, breakthrough time (t_b ; min), breakthrough volume (V_b ; L), and adsorption capacity of the biochar (q_b ; mg/g) at t_b can be obtained when the effluent concentration of MG5 reached 10% of the influent value ($C_t/C_o = 0.1$). Meanwhile, exhaustion time (t_s ; min), exhaustion volume (V_s ; L), and adsorption capacity (q_s ; mg/g) at t_b can be calculated when $C_t/C_o = 0.95$.

Total effluent volume (V_{eff} ; L) and adsorption capacity at the breakthrough time (q_b ; mg/g) and at the exhausted time (q_s ; mg/g), were calculated from Equations 12.5 to 12.7, respectively. The empty-bed contact time (EBCT; min) or the residence time for an empty reactor, was estimated by Equation 12.8. The height of mass transfer zone (MTZ) (or the length of adsorption zone in the column) can be determined by Equation 12.9. The length of unused bed (LUB; cm) is relevant to the adsorption rate. In real operation, the adsorption process is often stopped at the breakthrough time. Clearly, at the breakthrough point, a fraction of the biochar adsorption capacity remains unused. The LUB (Equation 12.10) was predicted according to the experiment of breakthrough curve (Worch, 2012).

$$V_{eff} = \frac{Q}{1000} t_{total} \quad (12.5)$$

$$q_b = \frac{Q}{1000} \left(C_o - \frac{C_b}{2} \right) \frac{t_b}{m_3} \quad (12.6)$$

$$q_s = \frac{Q}{1000} \left(C_o - \frac{C_s}{2} \right) \frac{t_s}{m_3} \quad (12.7)$$

$$EBCT = \frac{V_{BV}}{Q} = \frac{A \cdot Z}{Q} = \frac{\pi \cdot r_{column}^2 \cdot Z}{Q} = \frac{Z}{u} \quad (12.8)$$

$$H_{MTZ} = Z \frac{t_s - t_b}{t_{st}} = Z \frac{t_z}{t_{st}} \quad (12.9)$$

$$LUB = \frac{t_{st} - t_b}{t_{st}} Z \quad (12.10)$$

where V_{BV} (L) is the volume occupied by the used biochar sample; Z (cm) is the depth of the used biochar mass in the column; t_{st} (min) is the stoichiometric time at the barycenter of the

breakthrough curve ($C_t/C_0 = 0.5$); t_z (min) is zone time; A (cm^2) is cross-section area of the used column; u (cm/min) is the superficial velocity or superficial flow velocity determined as the quotient of the volume flow rate (cm^3/min) and the column cross-section area (cm^2); m_3 (g) is the mass of biochar used in the column; and Q (mL/min) is the volumetric flow rate.

12.2.4 Statistical Analysis

All experiments were conducted in triplicate, and the results were expressed as mean \pm standard deviation. Blank samples without the adsorbent were also conducted simultaneously. Trial-and-error nonlinear methods were performed using the Solver Add-in of Microsoft Excel to compute parameters of the isotherm and kinetic models. The coefficient of determination (R^2) of the nonlinear method was computed using the following equation:

$$R^2 = 1 - \frac{\sum (q_{e,\text{exp}} - q_{e,\text{cal}})^2}{\sum (q_{e,\text{exp}} - q_{e,\text{mean}})^2} \quad (12.11)$$

where $q_{e,\text{exp}}$ (mg/g) is the amount of MG5 uptake at equilibrium obtained from Equation 12.2; $q_{e,\text{cal}}$ (mg/g) is the amount of MG5 uptake achieved from the model after using the Solver Add-in; and $q_{e,\text{mean}}$ (mg/g) is the mean of $q_{e,\text{exp}}$ values.

The Statgraphics Plus 3.0 statistical program was applied to statistically analyze the maximum Langmuir adsorption capacities among three biochar samples. Differences were considered to be significant at $p < 0.05$. To identify the best-fit model, calculation of the chi-squared (χ^2) value and average absolute percentage deviation (%D) is recommended in addition to calculations of the coefficient of determination (R^2):

$$\chi^2 = \sum \frac{(q_{e,\text{exp}} - q_{e,\text{cal}})^2}{q_{e,\text{cal}}} \quad (12.12)$$

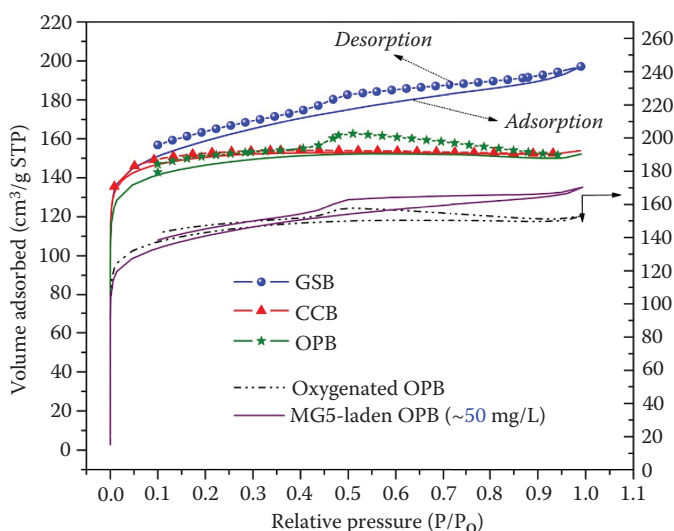
$$\%D = \frac{1}{N} \sum \left| \frac{(q_{e,\text{exp}} - q_{e,\text{cal}})}{q_{e,\text{cal}}} \right| \times 100 \quad (12.13)$$

where N is the number of experimental data point; and $q_{e,\text{exp}}$ and $q_{e,\text{cal}}$ are obtained from Equation 12.11.

12.3 Results and Discussion

12.3.1 Characteristics of Biochar

The nitrogen adsorption/desorption isotherms of biochars are portrayed in Figure 12.1. According to the IUPAC (International Union of Pure and Applied Chemistry) classification, such isotherms belong to Type I, which is a typical characteristic of micropores with a relatively small external surface area. Additionally, a wide knee (hysteresis loop) was present in the isotherms of the porous carbonaceous materials. Hysteresis appearing in the multilayer

**FIGURE 12.1**

Nitrogen adsorption/desorption isotherms of the biochar samples at 77 K.

range of physical adsorption isotherms at a relative pressure above 0.3 is usually related to the adsorbent with micropore or mesopore structures. According to the IUPAC nomenclature, porous carbonaceous materials exhibit the H4-type hysteresis loop, which is associated with narrow slit-like pores. Table 12.1 provides a summary of corresponding textural properties of the biochars. As expected, the biochars exhibit remarkably higher S_{BET} and V_{total} than their precursors. The S_{BET} and V_{total} of biochar diminished in the following order: GSB (604 m²/g and 0.308 cm³/g) > OPB (565 m²/g and 0.256 cm³/g) > CCB (536 m²/g and 0.2379 cm³/g), respectively. Meanwhile, the S_{BET} of their precursors ranged from 2.08 to 5.73 cm³/g (Tran et al., 2017f).

Several basic characteristics of the biochar are recorded in Table 12.2. As expected, the biochar exhibited relatively low percentages of moisture, total ash, and volatile matter. Generally, the low percentages of ash and moisture indicate a high quality of biochar, and

TABLE 12.1

Textural Parameters of the Pristine, MG5-Loaded, and Oxygenated Biochar Samples

	Unit	Before Adsorption			After Adsorption				Oxygenated OPB ^c
		GSB	CCB	OPB	GSB ^a	CCB ^a	OPB ^a	OPB ^b	
S_{BET}	m ² /g	603.8	535.9	565.2	48.79	13.56	13.45	528.8	548.1
S_{Langmuir}	m ² /g	772.2	660.2	658.8	57.80	3.62	44.52	645.8	657.5
S_{external}	m ² /g	262.3	188.1	236.1	~0	~0	15.54	262.4	233.5
$S_{\text{micropore}}$	m ² /g	341.1	347.9	329.1	52.64	56.79	~0	266.4	315.5
V_{total}	cm ³ /g	0.305	0.238	0.236	0.022	0.018	0.023	0.264	0.236
$V_{\text{micropore}}$	cm ³ /g	0.113	0.140	0.110	0.019	0.004	~0	0.086	0.105
$V_{\text{non-micro}}$	cm ³ /g	0.193	0.098	0.126	NA	NA	NA	0.178	0.131
$V_{\text{non-micro}}$	%	62.95	69.81	53.31	NA	NA	NA	67.36	55.54
E_{o}	kJ/mol	16.74	13.43	13.31	NA	NA	NA	13.11	13.28

^a The textural parameters obtained after MG5 adsorption ($C_0 = 300$ mg/L).

^b The textural parameters obtained after MG5 adsorption ($C_0 = 50$ mg/L).

^c The textural parameters obtained after oxygenated OPB.

TABLE 12.2

Basic Physical and Chemical Characteristics of the Biochar Samples

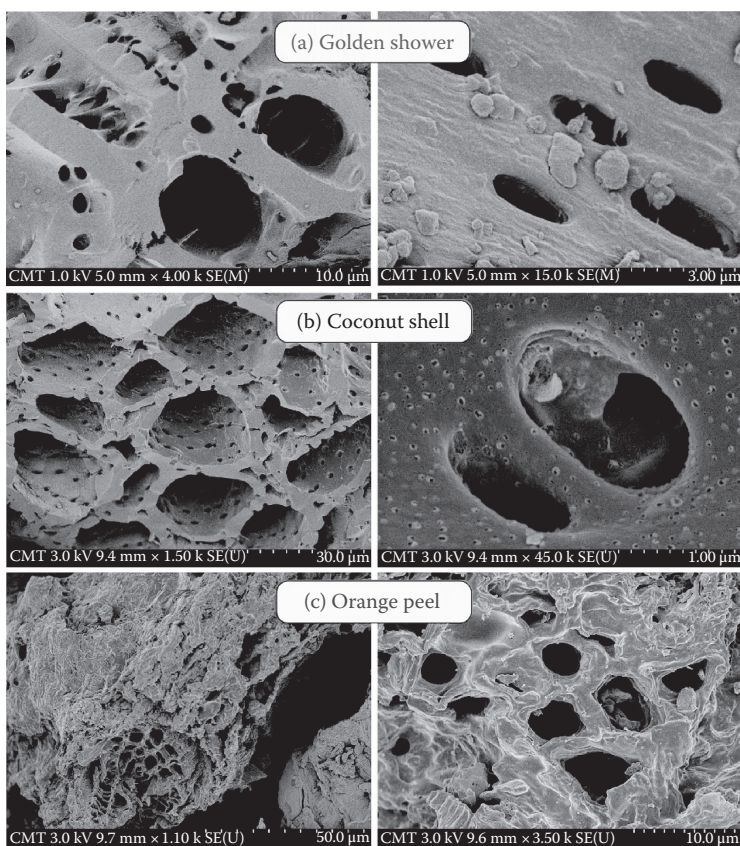
	Unit	GSB	CCB	OPB
<i>Ultimate Analysis</i>				
C	wt%	74.29	75.16	74.11
H	wt%	1.260	0.921	1.690
N	wt%	0.560	0.950	1.780
O ^a	wt%	23.86	22.97	22.42
H/C atomic ratio	–	0.201	0.146	0.272
O/C atomic ratio	–	0.241	0.229	0.227
<i>Proximate Analysis</i>				
Moisture	wt%	2.37 ± 0.21	6.32 ± 0.19	6.76 ± 0.52
Volatile	wt%	12.4 ± 2.06	0.86 ± 0.03	1.71 ± 0.83
Total ash	wt%	0.85 ± 0.03	1.34 ± 0.24	9.82 ± 0.34
Fixed carbon ^a	wt%	84.4 ± 1.13	91.5 ± 0.04	81.7 ± 0.25
<i>Physicochemical Property</i>				
Total yield	%	25.5 ± 1.54	21.5 ± 2.25	22.9 ± 0.66
Hardness	%	83.1 ± 2.99	95.8 ± 0.25	82.5 ± 0.95
Bulk density	g/cm ³	0.42 ± 0.01	0.48 ± 0.08	0.56 ± 0.04
pH _{1:20}	–	8.47 ± 0.22	7.69 ± 0.06	9.76 ± 0.13
<i>Surface Chemistry of Pristine Biochar</i>				
Total acidic groups	mmol/g	0.737 ± 0.03	0.373 ± 0.06	0.228 ± 0.02
+ Phenolic	mmol/g	0.055 ± 0.06	0.268 ± 0.17	0.145 ± 0.02
+ Lactonic	mmol/g	0.264 ± 0.17	0.077 ± 0.09	0.040 ± 0.01
+ Carboxylic	mmol/g	0.418 ± 0.24	0.028 ± 0.02	0.042 ± 0.04
Total basic sites	mmol/g	0.339 ± 0.18	1.011 ± 0.04	2.349 ± 0.02
Total groups	mmol/g	1.089	1.384	2.577
<i>Surface Chemistry of Biochar Oxygenated with Acrylic Acid</i>				
Total acidic groups	mmol/g	1.297 ± 0.17	0.917 ± 0.09	0.805 ± 0.11
+ Phenolic	mmol/g	0.085 ± 0.05	0.420 ± 0.04	0.391 ± 0.07
+ Lactonic	mmol/g	0.314 ± 0.04	0.052 ± 0.10	0.065 ± 0.06
+ Carboxylic	mmol/g	0.898 ± 0.05	0.499 ± 0.05	0.349 ± 0.05
Total basic sites	mmol/g	0.582 ± 0.15	0.664 ± 0.03	0.753 ± 0.07
Total groups	mmol/g	1.879	1.635	1.559

Note: Data are presented in mean values ± standard deviation.

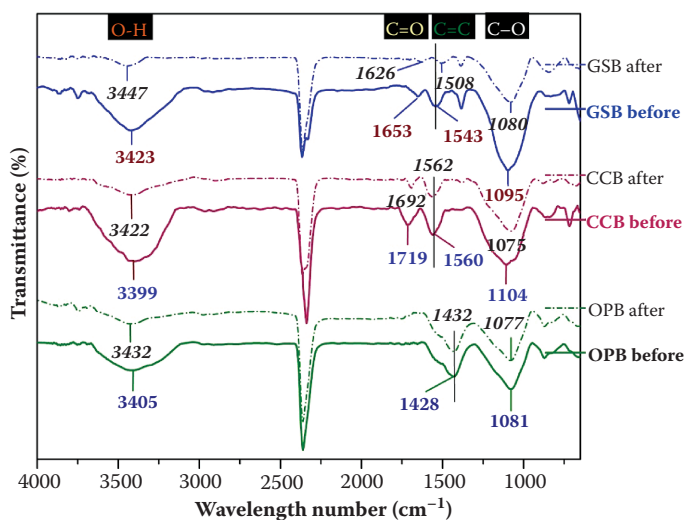
^a Data are calculated by difference.

a low volatile content reflects a high potential for industrial applications. Also, a high fixed carbon content implies that biochar consists mainly of carbon in a highly stabilized state. The scanning electron micrographs in Figure 12.2 reveal that the biochar possesses an irregular and heterogeneous surface morphology with a well-developed porous structure, which is consistent with its fairly high BET specific surface area (Table 12.1). Therefore, the biochar can serve as a potential porous carbonaceous adsorbent for wastewater treatment.

Qualitative information on functional groups present on the biochars' surfaces and their spectroscopic assignments are provided in Figure 12.3. Two peaks identified at approximately 1700 and 1100 cm⁻¹, correspond to the stretching of the C=O and C–O bonds,

**FIGURE 12.2**

Scanning electron micrographs (SEM) of (a) golden shower biochar, (b) coconut shell biochar, and (c) orange peel biochar.

**FIGURE 12.3**

FTIR spectra of the biochar samples before and after adsorption of MG5.

respectively. The observed peaks from 1430 to 1560 cm^{-1} are related to the aromatic C=C ring stretching. The presence of the surface hydroxyl group ($-\text{OH}$) is evident by the broad peaks observed at around 3400 cm^{-1} . The presence of C=O, C-O, and $-\text{OH}$ bonds are consistent with the quantitative results analyzed by Boehm titration in Table 12.2. The qualitative and quantitative information demonstrated that the biochar plentifully possesses its surface oxygen-bearing functional groups (polar characters) on its surface.

12.3.2 Point of Zero Charge and Effect of Solution pH

The pH of an aqueous solution is considered as one of the most important parameters in the adsorption process due to its great impact on the surface charge of the adsorbent and the speciation of adsorbate in solutions. Meanwhile, pH_{PZC} plays a pivotal role in selecting the optimal pH value for adsorption studies and elucidating adsorption mechanisms. The pH value at which the net total (external and internal) surface charge of the adsorbent is

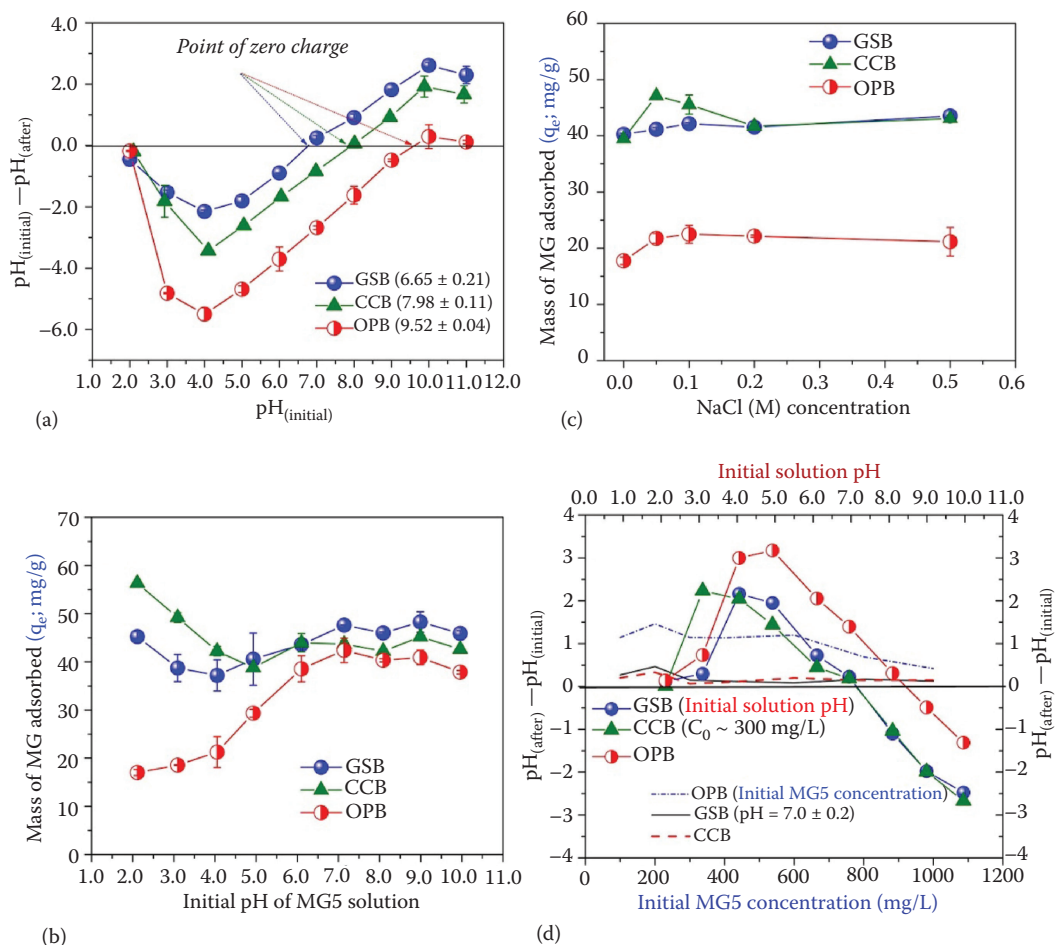


FIGURE 12.4

(a) Point of zero charge of the biochar, (b) pH dependence on adsorption capacity, (c) effect of ionic strength on adsorption capacity, and (d) pH values after adsorption. (Experimental conditions: (b) approximately 340 mg/L, 48 h, 30°C, 0 M NaCl; and (c) 340 mg/L, 48 h, 30°C, pH 7.0.)

zero is defined as pH_{PZC} . As given in Figure 12.4a, the pH_{PZC} followed the selective order OPB (9.52) > CCB (7.98) > GSB (6.65). A higher pH_{PZC} value often coincides with a lower content of acidic groups on the surface: OPB (0.228 mmol/g) < CCB (0.373 mmol/g) < GSB (0.737 mmol/g) (Table 12.2). Especially, OPB exhibited a higher pH_{PZC} than the others that might result from the presence of CaCO_3 , which has identified by thermogravimetric analysis (Tran et al., 2017f) and x-ray diffraction (Tran et al., 2016a).

The pH dependence of MG5 uptake by the biochars is observed in Figure 12.4b. Obviously, the amount of adsorbed dye was strongly dependent on the solution's pH. In essence, pH_{PZC} is indicative of the adsorbent's surface charge as a function of the solution's pH. When the pH of a solution ($\text{pH}_{\text{solution}}$) exceeds the pH_{PZC} , the biochar's surface becomes predominantly negative charged because of the deprotonation of oxygen-containing surface groups (i.e., $-\text{COOH}$ and $-\text{OH}$), favoring the adsorption of cationic ions from the solution through electrostatic attraction and vice versa.

Clearly, the MG5 adsorption on biochar still occurred when $\text{pH}_{\text{solution}} < \text{pH}_{\text{PZC}}$. Furthermore, at a low pH (approximately 2.0), the biochar was still able to adsorb MG5 molecules, although at this pH, the excess H^+ ions present in the system demonstrated strong competition with the cationic MG5 molecules for the active adsorption sites. Additionally, the $\text{pH}_{\text{solution}}$ values did not indicate a decreasing tendency after MG5 adsorption (Figure 12.4d), which means that there might not be dissociation phenomenon of the acidic oxygen-containing functionalities on the biochar's surface. These results confirmed that the MG5 adsorption mechanisms did not involve electrostatic attraction between negatively charged biochar surface sites and positively charged dye molecules, but rather than other interactions (i.e., pore filling, hydrogen bonding formation, $n-\pi$ interaction, or $\pi-\pi$ interaction). However, when the $\text{pH}_{\text{solution}}$ is higher than the pK_a of phenolic groups (~ 8.0 – 9.0), phenolic groups can be deprotonated and predominantly negatively charged, which is endorsed by a reduction of pH values after adsorption (Figure 12.4d). Correspondingly, the weak electrostatic attraction might be expected between deprotonated phenolic groups and MG5 cations within the initial $\text{pH}_{\text{solution}}$ higher than 8.0.

Because the further experiments were conducted at solution pH 7.0, the electrostatic attraction was not considered. Notably, the GSB and CCB samples shared the similarity in the adsorption tendency (Figure 12.4b), indicating that they might exhibit the identical adsorption mechanisms.

12.3.3 Effect of Ionic Strength

Various dissolved salts and dye contaminant often coexist in wastewater systems. Similar to the $\text{pH}_{\text{solution}}$, ionic strength is the factor governing the electrostatic interactions between the adsorbent and adsorbate.

Essentially, the presence of inorganic salts (i.e., NaCl or MgCl_2) has negative or positive impacts on the amounts of dye uptake. The dye adsorption capacity decreasing with increasing salt concentrations might be attributed to (1) the competition phenomenon occurring between Na^+ ions and dye cations for the active adsorbing sites on the adsorbent's surface ($-\text{COO}^-$ or $-\text{O}^-$), or (2) a screening effect (also known as electrostatic screening) existing between the positively charged adsorbent surface and dye molecules (Tran et al., 2017f). On the other hand, the adsorption capacity of adsorbent can be enhanced by the NaCl ions introduced into the solution. The enhancement might result from (1) an increase in the degree of dissociation of the dye molecules by facilitating the protonation (Doğan et al., 2009), and (2) partial neutralization of the positive charge on the adsorbent's surface and a consequent compression of the electrical double layer by anions (i.e., Cl^-) (Guo et al., 2003).

The effects of the presence of the electrolyte on the MG5 uptake are illustrated in Figure 12.4c. Clearly, an increase in ionic strength from 0 to 0.5 M NaCl resulted in a slight improvement of dye adsorption efficiency. This observation signified that the electrostatic attraction did not involve the adsorption process, which is consistent with the conclusion in Section 12.3.2. The enhanced dye adsorptive capacity in the presence of NaCl ions has been reported elsewhere (Guo et al., 2003; Doğan et al., 2009; Ghaedi et al., 2014; Song et al., 2015; Tran et al., 2017e).

12.3.4 Adsorption Kinetics

The effects of contact time toward the MG5 adsorption at two temperatures are depicted in Figure 12.5. The rate of dye removal from solution (adsorption on biochar) increased

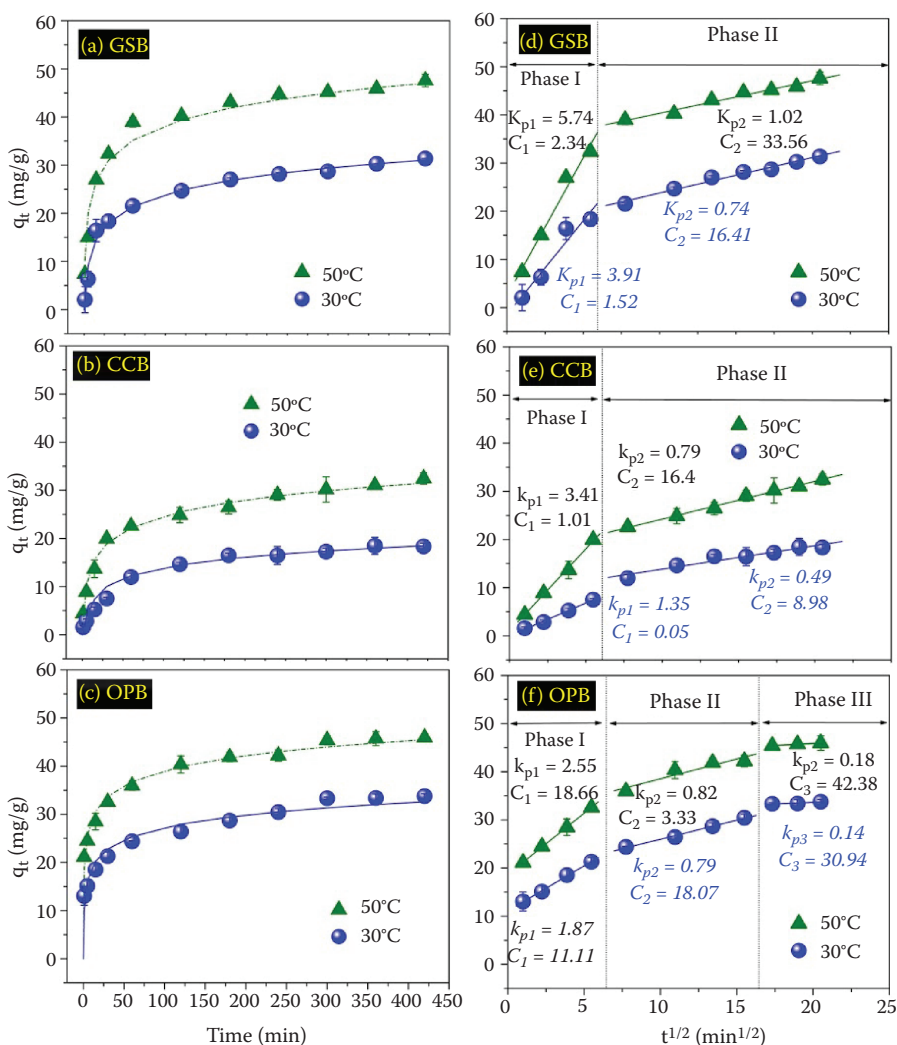


FIGURE 12.5

(a–c) The effects of contact time on the adsorption capacity of MG5 onto the biochar samples at different temperatures. (d–f) Intraparticle diffusion plots for MG5 adsorption. (Experimental conditions: approximately 340 mg/L, 0 M NaCl, and pH 7.0.)

consecutively over the first 30 min of the contact; the removal rate then decreased steadily and plateaued after approximately 120 min. The adsorption equilibrium can be rapidly achieved because low activation energy was required. Additionally, the amounts of MG5 removal was enhanced at a higher temperature, confirming that the adsorption reaction was more favorable at higher temperatures and needs supplementary (thermal) energy. The instantaneous adsorption phenomenon demonstrated that the biochar has a strong affinity for MG5 molecules. The kinetics play a significant role, facilitating scaling the process up to small reactor volumes to ensure efficiency and economy.

In this study, two reaction kinetic models, the Elovich or Roginsky–Zeldovich model, and the intraparticle diffusion model (diffusion into the pore of the biochar) were applied for the mathematical description of intrinsic kinetic adsorption constants. The nonlinearized forms of the Lagergren pseudo-first-order, Blanchard pseudo-second-order, and Elovich models are expressed in Equations 12.14, 12.15, and 12.16, respectively. The linearized form of the Weber–Morris intraparticle diffusion model is presented in Equation 12.17.

$$q_t = q_e(1 - e^{-k_1 t}) \quad (12.14)$$

$$q_t = \frac{q_e^2 k_2 t}{1 + k_2 q_e t} \quad (12.15)$$

$$q_t = \frac{1}{\beta} \ln(1 + \alpha \beta t) \quad (12.16)$$

$$q_t = k_p \sqrt{t} + C \quad (12.17)$$

where k_1 (1/min), k_2 (g/mg \times min), α (mg/g \times min), and k_p (mg/g \times min) are the rate constants of the pseudo-first-order, pseudo-second-order, Elovich, and intraparticle diffusion models, respectively; q_e and q_t are the amounts of MG5 uptake per mass of biochar at equilibrium and at any time t (min), respectively; β (mg/g) is a desorption constant during any one experiment; and C (mg/g) is the constant describing the thickness of the boundary layer. The C value is directly proportional to the boundary layer thickness—a higher value of C corresponding to a greater effect on the limiting boundary layer.

Table 12.3 lists the relative kinetic parameters for MG5 adsorption at different operating temperatures. A higher temperature generally indicated a faster removal rate because the rate constants (k_1 , k_2 , α , and k_p) of the four kinetic models increased with the increasing temperatures. Obviously, the Elovich model exhibits higher nonlinear R^2 values than the other kinetic models, implying that the surface of biochar is a heterogeneous system. However, the nonlinear χ^2 and %D values of the pseudo-second-order model (0.37–23.2 and 6.72–15.8) were sustainably lower than those of the pseudo-first-order model (2.88–56.22 and 13.23–20.85) and Elovich model (1.525–807 and 6.475–72.8), respectively. In addition, the theoretical amount of MG5 uptake at equilibrium calculated from the pseudo-second-order equation ($q_{e,ca}$) matched well with that obtained from the experiment ($q_{e,exp}$). Consequently, its rate constant (k_2) was the most appropriate for computing activation energy.

The activation energy of adsorption process (E_a ; kJ/mol) is defined as the magnitude of the energy barrier, which must be surmounted by the adsorbate molecules. The dependence

TABLE 12.3

Relative Kinetic Parameters for MG5 Sorption by the Biochar Samples at Different Temperatures

Kinetic Model	Parameter	Unit	30°C			50°C		
			GSB	CCB	OPB	GSB	CCB	OPB
Experiment	$q_{e,exp}$	mg/g	30.27	18.47	33.38	46.73	31.03	45.40
<i>Pseudo-First-Order Model</i>								
	$q_{e,cal}$	mg/g	27.97	17.45	29.47	43.61	28.69	39.96
	k_1	1/min	0.041	0.019	0.083	0.059	0.040	0.248
	R^2	–	0.937	0.982	0.535	0.943	0.914	0.429
	χ^2	–	3.818	6.044	56.22	2.879	14.12	25.13
	%D	%	13.63	15.25	20.85	13.23	16.86	17.61
<i>Pseudo-Second-Order Model</i>								
	$q_{e,cal}$	mg/g	30.53	20.11	30.83	46.50	31.28	41.79
	$k_2 (\times 10^{-3})$	mg/g \times min	1.795	1.143	4.879	1.935	1.763	8.665
	R^2	–	0.978	0.992	0.716	0.985	0.964	0.679
	χ^2	–	1.165	3.167	23.195	0.374	6.148	13.14
	%D	%	6.962	11.20	15.80	6.720	11.80	12.97
<i>Elovich Model</i>								
	β	mg/g	0.186	0.233	0.264	0.143	0.191	0.223
	α	mg/g \times min	4.417	0.865	50.58	17.39	5.526	268.8
	R^2	–	0.984	0.988	0.957	0.978	0.992	0.977
	χ^2	–	1.663	172.5	385.8	1.525	512.4	806.9
	%D	%	11.32	61.86	66.63	6.475	71.30	72.84
<i>Intraparticle Diffusion Model</i>								
	C	mg/g	7.530	2.441	14.12	16.78	8.488	23.66
	k_p	mg/g \times min ^{1/2}	1.299	0.888	1.052	1.734	1.285	1.229
	R^2	–	0.860	0.927	0.966	0.807	0.902	0.932

Note: The parameters of pseudo-first-order, pseudo-second-order, and Elovich models were calculated using the nonlinearization optimization technique.

of the adsorption rate on the temperature provides the idea for estimation of the activation energy, which can be estimated through the Arrhenius equation (Equation 12.18). Equation 12.19 describes the activation energy estimated from adsorptive kinetic experiments performed at two different operating temperatures.

$$K = Ae^{-E_a/RT} \quad (12.18)$$

$$\ln k_{2(323K)} - \ln k_{2(303K)} = \left(\ln A - \frac{E_a}{RT_{323K}} \right) - \left(\ln A - \frac{E_a}{RT_{303K}} \right) \Leftrightarrow E_a = \frac{R \ln \frac{k_{2(323K)}}{k_{2(303K)}}}{\frac{1}{T_{303K}} - \frac{1}{T_{323K}}} \quad (12.19)$$

where $k_{2(323K)}$ and $k_{2(303K)}$ are the rate constants of the pseudo-second-order model at 323 K and 303 K, respectively; A is the pre-exponential factor (frequently factor); R is the universal gas constant (8.314 J/mol \times K); and T is the absolute temperature in kelvins.

The activation energy of the MG5 adsorption process followed the decreasing order: OPB ($E_a = 23.34$ kJ/mol) > CCB (17.62 kJ/mol) > GSB (3.046 kJ/mol), which well agrees with the change of the reaction rate constant of the second-order model. The k_2 values increased by 77.6% for OPB > 54.2% for CCB > 7.79% for GSB when the temperatures increased from 30°C to 50°C. This result endorsed that the environmental temperature has a profound effect on the adsorption rate. The positive values of E_a also signified the endothermic nature of the adsorption process, and the low magnitudes of E_a (<40 kJ/mol) reflected the diffusion-controlled transport and the physical adsorption process. In contrast, chemical reaction or surface-controlled processes often exhibit higher magnitude of activation energy. Notably, a low adsorption energy is key for the rapid establishment of adsorption equilibrium.

Although the experimental data can be satisfactorily described by the pseudo-second-order model, this model cannot help to recognize the adsorption mechanisms. Similarly, the Elovich model seems to describe various reaction mechanisms, such as bulk diffusion and surface diffusion. In contrast, the intraparticle diffusion model can be useful to identify the reaction pathways and the adsorption mechanisms as well as predict the rate controlling step. In a solid-liquid sorption process, the adsorbate transfer is often characterized by film diffusion (also known as external diffusion), surface diffusion, pore diffusion, or combined surface and pore diffusion. In short, if the plot of q_t against $t^{0.5}$ is straight linear and passes through the original point (zero point), the adsorption will be entirely governed by intraparticle diffusion. Contrastingly, if the intraparticle diffusion plot gives multilinearity, the adsorption process can be controlled by multistep mechanisms.

Four steps associated with transport processes in adsorption by porous adsorbents were originally proposed by Walter (1984). The first stage is transport in the solution phase (known as “bulk transport”; occurs quickly), which can occur instantaneously after the adsorbent is transferred into the adsorbate solution; therefore, it does not control engineering design. In most cases, this stage occurs too rapidly and its contribution is considered negligible. The second stage is “film diffusion” (occurs slowly). In this stage, adsorbate molecules are transported from the bulk liquid phase to the adsorbent’s external surface through a hydrodynamic boundary layer or film. The third stage involves diffusion of the adsorbate molecules from the exterior of the adsorbent into the pores of the adsorbent, along pore-wall surfaces, or both (known as “intraparticle diffusion”; occurs slowly). The last stage, adsorptive attachment, often occurs very quickly; therefore, it is not significant for design.

Plots of q_t versus $t^{0.5}$ for the intraparticle diffusion model are presented in Figure 12.5d through f. Clearly, the GSB and CCB samples shared the similarity in the number of stages (or phases) of the adsorption process, suggesting that GSB and CCB likely have similar adsorption mechanisms. Notably, the regression curves are straight lines with relative high values of linear regression coefficient ($R^2 = 0.81$ – 0.97). Nevertheless, these straight lines did not pass through the origin, which strongly suggests that intraparticle diffusion was certainly involved in the adsorption process but was not only rate-controlling step. Moreover, the plots of intraparticle diffusion display multilinearity (Figure 12.5d–f), demonstrating that the MG5 adsorption was controlled by two or more mechanisms occurring simultaneously. Furthermore, the values of thickness of the C boundary layer increased along with the rise in temperature from 30°C to 50°C (Table 12.3 and Figure 12.5d–f), implying that more MG5 molecules were adsorbed at the boundary layer in a higher temperature (Ofomaja, 2007).

Unlike the GSB and CCB samples, the first linear plot of q_t versus $t^{0.5}$ of OPB did not pass through the original point, indicating that the intraparticle diffusion was not the first step of the adsorption process (Figure 12.5f). A similar tendency was found for

the adsorption of MG5 onto OPB at low initial dye concentration (data not shown). Analyzing the change of textural properties of OPB before and after adsorption will give more valid information on this hypothesis. At a low initial MG5 concentration (50 mg/L) with approximately 99% removal efficiency, the S_{BET} (m^2/g) and V_{total} (cm^3/g) of OPB before adsorption (565 m^2/g and 0.2356 cm^3/g) were similar to those of OPB after adsorption (529 m^2/g and 0.2635 cm^3/g) (Table 12.1 and Figure 12.6c). This observation was consistent with the analysis performance of the intraparticle diffusion model—the first straight line or first linear portion (Figure 12.5f) did not pass through the origin. Furthermore, the $\text{pH}_{\text{solution}}$ after MG5 adsorption tended to increase after adsorption (Figure 12.4d), which means that the $-\text{COOH}$ group did not dissociate into carboxylate ($-\text{COO}^-$) groups when $\text{pH}_{\text{solution}} < \text{pH}_{\text{PZC}}$. In other words, when OPB was transferred into the MG5 solution, hydrogen bonding interaction or other interactions (exception for electrostatic interactions) can occur instantaneously, which prevents the $-\text{COOH}$ groups ($\text{pK}_a = 2.0\text{--}4.0$) from dissociation into $-\text{COO}^-$. The acid dissociation constant pK_a of phenol ranged from 8.0 to 9.0, and the kinetic and isotherm studies were conducted at solution pH 7.0; therefore, the dissociation of the phenolic group ($-\text{OH}$; $\text{pK}_a = 8.0\text{--}9.0$) was not considered. However, at a higher MG5 concentration, there was a remarkable decrease regarding the S_{BET} and V_{total} of MG5-laden OPB to 13.5 m^2/g and 0.023 cm^3/g , respectively (Table 12.1 and Figure 12.6c). This means that after the active adsorbing sites

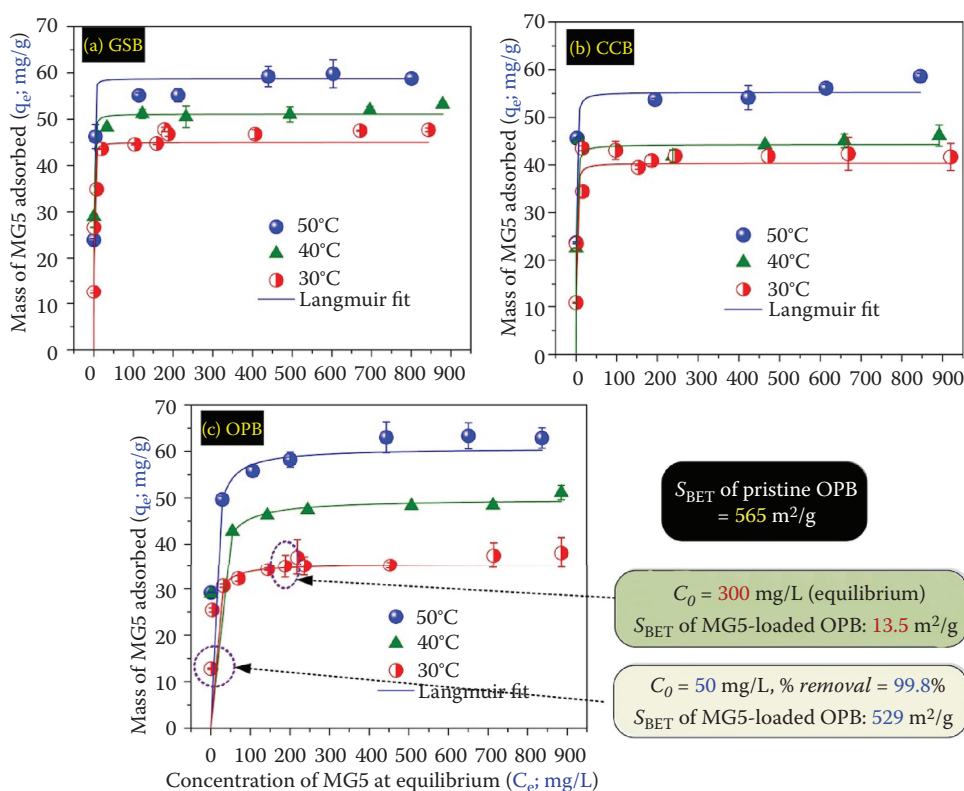


FIGURE 12.6

MG5 adsorption isotherms on the biochar samples at different temperatures. (Experimental conditions: 50–1200 mg/L, 0 M NaCl, 48 h, pH 7.0.)

on the biochar's surface (i.e., $-\text{COOH}$ and $-\text{OH}$) yielded a saturation, the MG5 molecules can diffuse into the internal pore of the biochar.

To sum up, it can be concluded that (1) there was coexistence of other interactions than pore filling in MG5 sorption mechanisms and (2) the contribution of pore filling at low initial dye concentrations was negligible.

12.3.5 Adsorption Isotherms

Although adsorption isotherms can insignificantly contribute to elucidating the adsorption mechanism, it is less helpful in this regard than adsorption kinetics and thermodynamics. However, collecting adsorption isotherms is a useful strategy to both describe the relationship between the adsorbate concentration in solution (liquid phase) and the adsorbent (solid phase) at a constant temperature under given conditions and design adsorption systems (Tran et al., 2017g). In the current study, the Langmuir, Freundlich, and Dubinin–Radushkevich models were applied to observe the MG5 adsorption behaviors of MG5 onto the biochar.

The nonlinear and linear forms of the Langmuir model are expressed in Equations 12.20 and 12.21, respectively. The nonlinear and linear forms of the Freundlich model are described in Equations 12.22 and 12.23, respectively.

$$q_e = \frac{Q_{\max}^o K_L C_e}{1 + K_L C_e} \quad (12.20)$$

$$\frac{C_e}{q_e} = \left(\frac{1}{Q_{\max}^o} \right) C_e + \frac{1}{Q_{\max}^o K_L} \quad (12.21)$$

$$q_e = K_F C_e^n \quad (12.22)$$

$$\log q_e = n \log C_e + \log K_F \quad (12.23)$$

where Q_{\max}^o (mg/g) is the maximum saturated monolayer adsorption capacity of the biochar; C_e and q_e are obtained from Equation 12.2; K_L (L/mg) is the constant related to the affinity between the MG5 and biochar; K_F (mg/g)/(mg/L)ⁿ is the Freundlich constant; and n (dimensionless) is a Freundlich intensity parameter, which indicates the magnitude of the adsorption driving force or surface heterogeneity. The adsorption isotherm becomes linear with $n = 1$, favorable with $n < 1$, and unfavorable with $n > 1$ (Worch, 2012).

The Dubinin–Radushkevich equation has been developed to account for the effects of the porous structure of an adsorbent on the adsorption amount:

$$q_e = q_{DR} e^{-K_{DR} \epsilon^2} \quad (12.24)$$

The linear form of the Dubinin–Radushkevich model is

$$\ln q_e = -K_{DR} \epsilon^2 + \ln q_{DR} \quad (12.25)$$

$$\varepsilon = RT \ln \left(1 + \frac{1}{C_e} \right) \quad (12.26)$$

By inserting Equation 12.26 into Equation 12.24, Equation 12.27 can be obtained:

$$\ln q_e = -K_{DR} R^2 T^2 \ln^2 \left(1 + \frac{1}{C_e} \right) + \ln q_{DR} \quad (12.27)$$

The parameters of q_{DR} and K_{DR} in Equation 12.27 can be obtained as follows: (1) plot of $\ln q_e$ against $\ln^2(1 + 1/C_e)$ with slope = $-K_{DR} R^2 T^2$ and intercept = $\ln q_{DR}$, and the E value can be obtained using Equation 12.28; and (2) plot of $\ln q_e$ against $R^2 T^2 \ln^2(1 + 1/C_e)$ with slope = $-K_{DR}$ and intercept = $\ln q_{DR}$, and the E value can be obtained using Equation 12.29. Noticeably, the E values obtained from Equation 12.28 and Equation 12.29 are the same (Tran et al., 2016b).

$$E = \frac{1}{\sqrt{2K_{DR}}} = \frac{RT}{\sqrt{-2slope}} \quad (12.28)$$

$$E = \frac{1}{\sqrt{2K_{DR}}} = \frac{1}{\sqrt{-2slope}} \quad (12.29)$$

where q_{DR} (mg/g) is the adsorption capacity, K_{DR} (mol²/kJ²) is a constant related to the sorption energy, ε is the Polanyi potential, E (kJ/mol) is the mean adsorption energy, R is the gas constant, T is temperature in kelvins, and q_e and C_e are calculated from Equation 12.2.

Figure 12.6 displays the complete adsorption isotherms of MG5 by the biochar samples at various temperatures. These isotherms exhibit profiles with sharp rises under low equilibrium concentrations, reaching a plateau upon increasing the equilibrium concentration continuously. Although the R^2 values (0.573–0.982) of the nonlinear methods were lower than those of the linear method (0.616–0.999), the nonlinear method can minimize error distributions (between the experimental-calculated data and model-predicted data) better than the linear method. This conclusion was additionally supported by the lower χ^2 (0.22–11.4) and %D (1.78–12.5) values of the nonlinear method compared to the linear method (0.27–351 and 1.85–227), respectively. Clearly, a higher determination coefficient (R^2) did not necessarily mean a better fit for the experiment and the model. Therefore, the accuracy parameters of adsorption isotherms can be obtained by the nonlinear optimization technique.

Furthermore, the nonlinear determination coefficient of the Langmuir model ($R^2 = 0.85$ –0.98) was generally higher than that of the Freundlich model (0.57–0.97). In contrast, its nonlinear χ^2 and %D values (0.22–2.63 and 1.78–6.85) were significantly lower than those of the Freundlich model (0.32–11.4 and 2.96–12.5), respectively. Therefore, it can be concluded that the experimental adsorption equilibrium data fitted the Langmuir model better than the Freundlich model. Additionally, the region in which the experimental data correspond to the adsorption equilibrium is undoubtedly described by the Langmuir isotherm model, which is characterized by saturation at high concentrations (Figure 12.6). Moreover, the

isotherm shapes in Figure 12.6 were classified as H-type (high affinity), which is a result of extremely strong adsorption at low adsorbate concentrations (Radovic et al., 2001). A similar H-type isotherm shape was found in the studies of MG5 adsorption onto laboratory-synthesized ACs (Tran et al., 2017d) and commercial AC (Tran et al., 2017b).

The corresponding adsorption parameters are summarized in Tables 12.4 and 12.5. The theoretical monolayer maximum adsorption capacities (Q_{\max}^0) calculated from the Langmuir model at 30°C were ordered as follows: GSB (45.54 mg/g) > CCB (41.52 mg/g) > OPB (35.20 mg/g), which well agrees with the maximum adsorption capacities computed from the Dubinin–Radushkevich model (45.0, 41.81, and 35.56 mg/g), respectively. As expected, these values indicated a statistically significant difference ($p < 0.05$).

As depicted in Figure 12.6, the MG5 adsorption was strongly dependent on the operation temperature. The amount of MG5 uptake increased dramatically with the increasing temperature, which reflects the endothermic nature of the adsorption process. More efficient adsorption at a higher temperature resulted from an increase in the adsorption energy (Table 12.5). A typical example for GSB, the (Q_{\max}^0) values increased in the following order: 45.54 mg/g at 30°C < 51.16 mg/g at 40°C < 56.31 at 50°C along with the increasing adsorption energies (E): 2.96 kJ/mol < 3.01 kJ/mol < 4.34 kJ/mol, respectively. This means that the energy increase in the adsorption systems facilitated the enhanced adsorption capacity of MG5. The low adsorption energies for the biochar samples (<8 kJ/mol) also suggested that physical adsorption plays a dominant role in adsorption mechanism.

When the experimental equilibrium data are adequately described by the Langmuir model, it is essential to calculate the separation factor. Hall et al. (1966) stated that the essential characteristics of a Langmuir isotherm model can be expressed in terms of a dimensionless constant known as the separation factor R_L , which is defined as follows:

$$R_L = \frac{1}{1 + K_L C_o} \quad (12.30)$$

where R_L is a constant separation factor (dimensionless) of the solid–liquid adsorption system; K_L (L/mg) is a Langmuir equilibrium constant; and C_o (mg/L) is the initial MG5 concentration.

The isotherm shape can be predicted whether an adsorption system is favorable ($0 < R_L < 1$), unfavorable ($R_L > 1$), linear ($R_L = 1$), or irreversible ($R_L = 0$). Alternatively, the R_L values in this study ranged from 0 to 1 and the exponent values were typical ($n < 1$) (Table 12.4), suggesting that the isotherm shape for MG5 adsorption onto biochar is a concave downward (favorable for adsorption).

12.3.6 Adsorption Thermodynamics

Thermodynamic studies are an indispensable component of predicting adsorption mechanism (i.e., physical or chemical). The thermodynamic parameters can be computed according to the thermodynamics through the following equation:

$$\Delta G^\circ = -RT \ln K_C \quad (12.31)$$

The relationship between ΔG° and ΔH° and ΔS° is described as follows:

$$\Delta G^\circ = \Delta H^\circ - T\Delta S^\circ \quad (12.32)$$

TABLE 12.4

Corresponding Isotherm Parameters of MG5 Sorption Deduced from the Langmuir and Freundlich Models

	Langmuir Parameters					Freundlich Parameters					Separation Factor (R_L) × 10 ⁻³
	Q_{\max}^o (mg/g)	K_L (L/mg)	R ²	χ ²	%D	K_F [(mg/g)/(mg/L) ⁿ]	n	R ²	χ ²	%D	
Non-linear Method											
30°C											
GSB	45.5	2.37	0.92	2.63	6.35	27.2	0.096	0.83	7.58	10.3	0.41–7.76
CCB	41.5	1.39	0.95	1.30	4.02	24.9	0.091	0.70	11.4	12.5	0.66–15.7
OPB	35.2	0.98	0.91	1.95	6.85	20.1	0.101	0.89	2.65	7.29	0.98–18.6
40°C											
GSB	51.2	3.14	0.97	0.22	1.78	34.6	0.067	0.88	1.23	5.46	0.29–2.69
CCB	45.2	1.49	0.92	0.76	4.25	30.9	0.060	0.57	5.32	10.5	0.62–6.81
OPB	47.6	1.44	0.90	0.70	3.29	30.4	0.077	0.96	0.32	2.96	0.64–5.86
50°C											
GSB	56.3	5.31	0.91	1.69	5.76	35.5	0.083	0.91	2.44	6.76	0.18–1.95
CCB	55.8	1.65	0.98	0.26	2.71	33.8	0.082	0.82	4.34	9.63	0.57–6.28
OPB	59.1	2.55	0.85	2.28	6.20	34.8	0.094	0.97	0.51	3.47	0.36–3.32
Linear Method											
30°C											
GSB	47.8	0.28	0.99	128	76.8	23.4	0.127	0.79	9.08	95.7	3.44–62.4
CCB	42.0	0.63	0.99	11.3	17.6	20.2	0.134	0.73	14.1	15.9	1.49–34.9
OPB	38.0	0.09	0.99	117	90.7	17.7	0.127	0.87	3.01	8.63	10.4–169
40°C											
GSB	52.9	0.17	0.99	191	109	33.0	0.077	0.90	1.25	5.50	5.43–48.1
CCB	45.9	0.11	0.99	131	110	28.4	0.076	0.61	5.84	11.3	8.01–82.4
OPB	50.5	0.09	0.99	146	85.9	29.7	0.082	0.96	0.32	96.3	10.6–89.9
50°C											
GSB	59.5	0.20	0.99	351	227	33.1	0.097	0.90	2.64	7.17	4.69–48.6
CCB	57.8	0.10	0.99	247	174	31.5	0.096	0.79	4.78	10.5	8.58–87.8
OPB	63.7	0.11	0.99	286	155	33.5	0.102	0.98	0.50	3.28	8.26–71.6

The well-known van't Hoff equation is obtained by substituting Equation 12.31 into Equation 12.32:

$$\ln K_C = \frac{-\Delta H^\circ}{R} \times \frac{1}{T} + \frac{\Delta S^\circ}{R} \quad (12.33)$$

where R is the universal gas constant and T is the absolute temperature in kelvins.

The Gibbs energy change (ΔG°) is directly calculated from Equation 12.31, while the enthalpy change (ΔH°) and the entropy change (ΔS°) were determined from the slope and intercept, respectively, of a plot of $\ln K_C$ against $1/T$ (Equation 12.33). It is well known that the equilibrium constant (K_C) must be dimensionless. Our previous study (Tran et al., 2016b) demonstrated that the optimal selection of K_C for the accurate calculation of thermodynamic parameters

TABLE 12.5
Corresponding Isotherm Parameters of MG5 Sorption Deduced from the Dubinin–Radushkevich Model

	Nonlinear Method					Linear Method						
	q_{DR} (mg/g)	K_{DR} (mol ² /kJ ²)	E (kJ/mol)	R^2	χ^2	%D	q_{DR} (mg/g)	K_{DR} (mol ² /kJ ²)	E (kJ/mol)	R^2	χ^2	%D
30°C												
GSB	45.0	0.061	2.96	0.90	2.92	5.63	44.8	0.060	2.88	0.95	2.85	4.84
CCB	41.8	0.165	1.74	0.97	1.60	3.94	39.9	0.078	2.54	0.93	3.61	7.63
OPB	35.6	0.963	0.72	0.80	1.36	4.49	34.0	0.104	2.19	0.89	3.36	7.37
40°C												
GSB	51.0	0.055	3.01	0.97	0.27	2.18	51.0	0.055	3.01	0.98	0.27	1.85
CCB	44.7	0.141	1.89	0.97	0.28	2.49	44.6	0.141	1.89	0.98	0.28	2.50
OPB	47.4	0.165	1.74	0.88	0.80	3.47	47.3	0.164	1.75	0.92	0.81	3.49
50°C												
GSB	55.8	0.027	4.34	0.88	2.27	7.37	55.6	0.026	4.38	0.93	2.25	6.19
CCB	54.5	0.097	2.27	0.94	1.14	5.54	54.2	0.093	2.32	0.97	1.04	4.87
OPB	58.8	0.061	2.87	0.84	2.57	6.90	58.6	0.060	2.88	0.90	2.58	6.88

was strongly dependent on the adsorption characteristics (i.e., the Henry, Freundlich, and Langmuir models) where equilibrium data are actually located. As discussed in Section 12.3.5, the adsorption equilibrium data were accurately described by the Langmuir model; therefore, in this study the K_C derived from the Langmuir constant (K_L) was employed for calculating the thermodynamic parameters— ΔG° , ΔH° , and ΔS° . The K_C can be easily obtained as a dimensionless parameter by multiplying K_L by the molecular mass of adsorbate (MG5; 433 g/mol), 1000, and then 55.5 (the number of moles of pure water per liter) (Tran et al., 2017g).

In this study, we also compared the thermodynamic parameters calculated from the K_L constant (after converted into dimensionless) derived from the nonlinear method (Equation 12.20) and linear method (Equation 12.21). The thermodynamic parameters of the MG5 removal process are listed in Table 12.6. As expected, the thermodynamic parameters calculated from the K_L constants derived from the linear method demonstrated an inconsistent result with the experimental data of adsorption equilibria. For example, Figure 12.6 shows that the MG5

TABLE 12.6

Thermodynamic Parameters of MG5 Sorption Process by the Biochar Samples

Adsorbent	T (K)	Van't Hoff Equation	K_C	ΔG° (kJ/mol)	ΔH° (kJ/mol)	ΔS° (J/mol \times K)
<i>K_L Obtained from the Nonlinear Method</i>						
Golden Shower Pod Biochar						
	303	$y = -3936x + 30.8$	56947446	-44.99	32.7	256.1
	313	$R^2 = 0.9642$	75509376	-47.21		
	323		127652925	-50.13		
Coconut Shell Biochar						
	303	$y = -716x + 19.7$	33528749	-43.65	5.95	163.7
	313	$R^2 = 0.9937$	35797564	-45.26		
	323		38818082	-46.93		
Orange Peel Biochar						
	303	$y = -4681x + 29.2$	976200	-34.74	38.9	242.8
	313	$R^2 = 0.9832$	1436600	-36.90		
	323		2546700	-39.61		
<i>K_L Obtained from the Linear Method</i>						
Golden Shower Pod Biochar						
	303	$y = 1588x + 10.4$	6687861	-39.59	-13.2	86.1
	313	$R^2 = 0.402$	4030127	-39.58		
	323		4870075	-41.35		
Coconut Shell Biochar						
	303	$y = 8669x - 12.4$	14740972	-41.58	-72.1	-102.7
	313	$R^2 = 0.7946$	2731422	-38.57		
	323		2549019	-39.62		
Orange Peel Biochar						
	303	$y = -888x + 14.3$	91319	-28.78	7.39	118.9
	313	$R^2 = 0.4967$	85751	-29.56		
	323		109867	-31.17		

adsorption capacity of MG5 by the biochar increased with the increasing temperature, signifying an endothermicity of the adsorption process; therefore the enthalpy change must obtain a positive value ($\Delta H^\circ > 0$). However, the enthalpy changes for GSB and CCB indicated negative values ($\Delta H^\circ < 0$) in the case of K_L calculated from the linear method (Table 12.6). Thus, the application of the K_L constant obtained from the linear method was not appropriate for calculating the thermodynamic parameters in this study, and a poor regression coefficient of the van't Hoff equation ($R^2 = 0.40\text{--}0.79$) was a supplementary confirmation of the inappropriateness.

Further discussions on the adsorptive thermodynamic study can be based on the K_L constants obtained from the nonlinear optimization technique. The ΔG° exhibits a negative quantity for three biochars at all investigated temperatures, suggesting that the adsorptive process occurred favorably and spontaneously. The result was in accordance with the conclusion drawn from analysis of the separation factor ($0 < R_L < 1$) and the exponent n of the Freundlich equation ($n < 1$) in Section 12.3.5. The degree of the spontaneity of the adsorption process can be determined by the Gibbs energy change. The ΔG° magnitude of GSB, CCB, and OPB significantly increased when the investigated temperatures increased from 30°C to 50°C, demonstrating a more energetically favorable adsorption at a higher temperature. The increase of ΔG° magnitude with a higher temperature was good agreement with an increase in adsorption energy (E) in Table 12.5.

The positive ΔH° demonstrated that the adsorption process is endothermic in nature, which was further indicated by an increase in both the amount of MG5 adsorbed (q_e) (Figures 12.5 and 12.6) and the equilibrium constant (K_C) (Table 12.6) at higher temperatures. The endothermicity of the adsorption process also implied the adsorbed energy in form of heat from its surroundings during the adsorptive process. The low adsorption enthalpy (less than 40 kJ/mol) also affirmed that the adsorption process was regarded as the physical adsorption (Tran et al., 2016b). The organization of the adsorbate at the solid–solution interface during the adsorption process becomes more random ($\Delta S^\circ > 0$). The positive ΔS° values also imply a dissociative mechanism and the increased degree of freedom of MG5 ions in the solution.

12.3.7 Adsorption Reversibility

To some extent, adsorption mechanisms of cationic dye can be elucidated based on desorption studies. Table 12.7 presents the percentage of desorption of MG5 by using various desorbing agents, such as deionized distilled water at pH 2.0, HCl, NaOH, NaCl, H_2O_2 with and without heat, hexane, methanol, ethanol, acetone, acetonitrile, ethyl glycol, toluene, 1-pentanol, 1-hexanol, and 1-heptanol. Undoubtedly, the adsorption process was completely irreversible in environment excess of H^+ (i.e., distilled water at low pH 2.0 and HCl). This result confirmed again that the electrostatic attraction between the negatively charged groups (i.e., $-\text{COO}^-$) on the biochar's surface and MG5 cationic molecules was not accountable for this study, which agrees with the discussion in Sections 12.3.2 and 12.3.3. Furthermore, the dye adsorption process of MG5 might not involve cation exchange because the amount of MG5 molecules adsorbed onto the biochar cannot be desorbed using NaCl.

Generally, the amount of MG5 desorbed was negligible for all desorbing agents, suggesting that the MG5 adsorption onto the biochar was an irreversible process. The irreversible process can be confirmed by the magnitude of the theoretical separation factor (R_L) in Section 12.3.5; R_L values reached nearly zero, indicating the adsorption system was irreversible. The irreversible adsorption of MG5 onto porous carbonaceous materials (i.e., synthesized AC and commercial AC) has been reported elsewhere (Tran et al., 2017b, 2017d). Notably, the MG5 adsorption was an irreversible process; therefore, the cycle of adsorption–desorption process was not examined.

TABLE 12.7

Percentage of MG5 Desorption from the Biochars Using Various Desorption Agents

Desorbing Agent	Chemical Formula	GSB	CCB	OPB
Deionized distilled water	H ₂ O (pH 2.0)	NA	NA	NA
Hydrochloric acid (1 M)	HCl	NA	NA	NA
Sodium chloride (0.5 M)	NaCl	NA	NA	NA
Sodium hydroxide (1 M)	NaOH	NA	NA	NA
Hydrogen peroxide (10%) ^a	H ₂ O ₂	NA	NA	NA
Hexane	C ₆ H ₁₄	NA	NA	NA
Methanol	CH ₃ OH	34.85 ± 1.27	8.863 ± 0.93	15.29 ± 0.92
Ethanol	C ₂ H ₆ O	8.412 ± 0.29	4.404 ± 0.71	17.13 ± 1.05
Acetone	C ₃ H ₆ O	9.242 ± 0.82	3.673 ± 0.79	7.437 ± 2.45
Acetonitrile	C ₂ H ₃ N	18.32 ± 3.04	1.417 ± 1.24	14.11 ± 1.06
Ethyl glycol	C ₂ H ₆ O ₂	8.183 ± 0.82	9.354 ± 1.75	20.59 ± 0.32
Toluene	C ₇ H ₈	10.36 ± 2.05	8.836 ± 0.31	10.80 ± 1.66
1-Pentanol	C ₅ H ₁₂ O	8.093 ± 0.69	8.891 ± 0.44	9.397 ± 0.69
1-Hexanol	C ₆ H ₁₄ O	6.63 ± 0.812	7.924 ± 0.41	8.012 ± 2.32
1-Heptanol	C ₇ H ₁₆ O	5.891 ± 0.94	7.573 ± 1.54	7.939 ± 0.95

Note: Data are presented in mean values ± standard deviation. NA means an irreversible process (% desorption ~ 0).

^a Data are represented for both no heat and heated 60°C; adsorption study was conducted at pH 7.0 for 48 h.

12.3.8 Continuous Adsorption Experiment

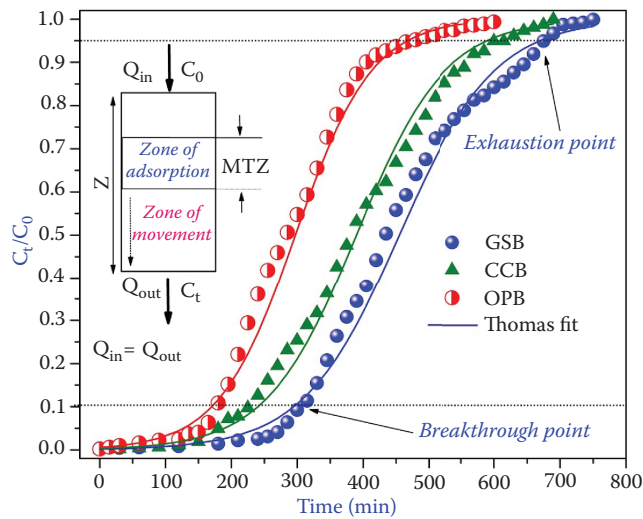
The breakthrough curves and operation parameters in a fixed-bed column are demonstrated in Figure 12.7 and Table 12.8, respectively. As expected, the breakthrough profiles exhibited a typical smooth S shape—a shape controlled by the shape and length of MTZ. The breakthrough and saturation times were ranked in the following order: GSB > OPB > CCB. The prolonged times for GSB demonstrated that a better removal performance than CCB and OPB, which corresponds with the observed results from the batch experiments.

To analyze the breakthrough profiles in the fixed-bed adsorption process, various mathematical models were applied to describe the dynamic adsorption behavior of MG5 in the fixed-bed column, such as the Thomas, Adams–Bohart, and Yoon–Nelson models. The nonlinear and linear forms of the Thomas model are described in Equations 12.34 and 12.35, respectively. The Adams–Bohart mathematical expression in the nonlinear and linear forms are given in Equations 12.36 and 12.37, respectively. Equations 12.38 and 12.39 present the nonlinear and linear forms of the Yoon–Nelson model, respectively.

$$\frac{C_t}{C_o} = \frac{1}{1 + \exp\left(k_{TH}q_o \frac{m_3}{Q} - k_{TH}C_o t\right)} \quad (12.34)$$

$$\ln\left(\frac{C_o}{C_t} - 1\right) = k_{TH}q_o \frac{m_3}{Q} - k_{TH}C_o t \quad (12.35)$$

where k_{TH} (mL/min × mg) is the Thomas adsorption rate constant; q_o (mg/g) is the column maximum equilibrium MG5 uptake per gram of biochar; and m_3 , Q , C_o , and C_t are defined in Section 12.2.3.2. The Thomas linear plot is $\ln((C_o/C_t) - 1)$ versus t .

**FIGURE 12.7**

The breakthrough curves for MG5 adsorption on the biochar samples. (Experimental conditions: $m_3 = 1.0$ g, $Q = 2.4$ mL/min, $C_o = 50$ mg/L, 30°C , pH 7.0, and 0 M NaCl)

TABLE 12.8

Corresponding Parameters in the Fixed-Bed Column for MG5 Sorption

	t_b (min)	q_b (mg/g)	V_b (L)	t_s (min)	q_s (mg/g)	V_s (L)	t_{st} (min)	t_{total} (min)	V_{eff} (L)	MTZ (cm)	LUB (cm)	EBCT (min)
GSB	300	26.17	0.60	645	32.60	1.29	435	750	1.50	0.555	0.227	0.287
CCB	240	20.33	0.48	570	28.46	1.14	375	690	1.38	0.484	0.198	0.216
OPB	180	15.50	0.36	405	20.26	0.81	285	600	1.20	0.450	0.221	0.236

Note: Breakthrough time (t_b), breakthrough volume (V_b), and adsorption capacity of the biochar (q_b) at t_b ; exhaustion time (t_s), exhaustion volume (V_s), and adsorption capacity (q_s) at t_s ; height of mass transfer zone, MTZ; length of unused bed, LUB; empty-bed contact time, EBCT; total effluent volume, V_{eff} .

$$\frac{C_t}{C_o} = \frac{\exp(k_{AB}C_o t)}{\exp\left(\frac{k_{AB}N_o Z}{u}\right) - 1 + \exp(k_{AB}C_o t)} \quad (12.36)$$

$$\ln \frac{C_t}{C_o} = k_{AB}C_o t - k_{AB}N_o \frac{Z}{u} \quad (12.37)$$

where k_{AB} (L/mg \times min) is the Adams–Bohart rate constant; N_o (mg/L) is the saturation concentration of the column; Z (cm), and u (cm/min) are defined in Section 12.2.3.2. The Bohart–Adams parameters can be predicted by a plot of $\ln(C_t/C_o)$ versus t .

$$\frac{C_t}{C_o} = \frac{\exp(k_{YN}t - \tau k_{YN})}{1 + \exp(k_{YN}t - \tau k_{YN})} \quad (12.38)$$

$$\ln\left(\frac{C_t}{C_o - C_t}\right) = k_{YN}t - \tau k_{YN} \quad (12.39)$$

$$q_{YN} = \frac{C_o Q \tau}{m_3} \quad (12.40)$$

where k_{YN} (1/min) is the Yoon–Nelson rate constant; τ (min) is the time required for 50% MG5 breakthrough (also known as the breakthrough half-breakthrough time); and q_{YN} (mg/g) is the Yoon–Nelson sorption capacity. The plot of Equation 12.39 is given as $\ln(C_t/(C_o - C_t))$ versus t .

Table 12.9 illustrates the parameters of the selected dynamic models for the fixed-bed systems. The Thomas model ($R^2 = 0.979$ – 0.986) and Yoon–Nelson model ($R^2 = 0.983$ – 0.986) exhibit higher determination coefficients than the Adams–Bohart model ($R^2 = 0.811$ – 0.895). Unlike the Thomas and Yoon–Nelson model, the Adams–Bohart model might only appropriately describe the initial part of the breakthrough curve (Aksu and Gönen, 2004); therefore, the Adams–Bohart model was less satisfactory than the others. Higher χ^2 and %D values of the Adams–Bohart model were additionally supported for this conclusion. Particularly, the maximum adsorption capacity in the column experiment calculated from the Thomas model was similar to that from the Yoon–Nelson model (Table 12.9), indicating that the breakthrough behavior was satisfactorily described by the two models.

TABLE 12.9

Constants of the Thomas, Adams–Bohart, and Yoon–Nelson Models for MG5 Sorption

Dynamic Model	Parameter	Unit	GSB	CCB	OPB
<i>Thomas Model</i>					
	q_o	mg/g	41.57	35.99	27.47
	k_{TH}	mL/min.mg ($\times 10^{-3}$)	0.302	0.328	0.378
	R^2	–	0.979	0.985	0.986
	χ^2	–	0.163	0.274	0.233
	%D	–	17.31	20.49	13.53
<i>Adams–Bohart Model</i>					
	N_o	mg/L	11,455	9,749	8,270
	k_{AB}	L/mg.min ($\times 10^{-3}$)	0.176	0.197	0.199
	R^2	–	0.895	0.822	0.811
	χ^2	–	12.34	1.039	3.098
	%D	–	103.5	33.01	49.08
<i>Yoon–Nelson Model</i>					
	q_{YN}	mg/g	42.12	36.04	27.47
	k_{YN}	1/min	0.0134	0.0150	0.0173
	τ	min	461	399	302
	R^2	–	0.983	0.985	0.986
	χ^2	–	0.219	0.282	0.233
	%D	–	17.47	20.67	13.53

Especially, the maximum adsorption capacity of the biochar calculated from the Thomas model (q_o ; the column test) was lower than that from the Langmuir model (Q_{\max}^o ; the batch test). At 30°C, the q_o and Q_{\max}^o values were as follows: 42 mg/g and 46 mg/g for GSB, 36 mg/g and 42 mg/g for CCB, and 27 mg/g and 35 mg/g for OPB, respectively. Several possible explanations for lower adsorption capacities in the column than in batch experiments have been reported elsewhere. First, the MG5 molecules flowing through the columns have not completely reached equilibrium unlike in the batch equilibrium experiment. Second, the adsorption capacity in the column test was determined at a lower MG5 concentration (i.e., 50 mg/L), whereas the MG5 adsorption capacity in the batch experiment was obtained at the higher MG5 concentrations (ranging from 50 to 1200 mg/L) (Nguyen et al., 2015). Third, the adsorption process in the fixed-bed column is a dynamic process in an unstable state. The continuous influent approximates to a fresh adsorbent when it passes through the column and tends to establish a new equilibrium of adsorption. However, a true equilibrium is never attained, because the contact time in the column system is limited, causing a decrease in adsorption capacity (Huang et al., 2009). Another explanation is due to the density decrease of packed adsorbent, which contributes to decreasing the contact surface area of the filter media in the packed column configuration. Consequently, the adsorption capacity of MG5 onto biochar will decrease (Li and Champagne, 2009). Last, a high flow is employed in the column study, which could cause short circuiting and flow through a preferred path in the column, which may preclude contact between the adsorbate molecules and several adsorbent particles in the fixed bed (Mathialagan and Viraraghavan, 2002).

Furthermore, the adsorption rate constants (k_{TH} , k_{AB} , and k_{YN}) of three models diminished in the order OPB > CCB > GSB (Table 12.9), which can estimate the exhausted time of the biochar samples: OPB > CCB > GSB (Table 12.8). This tendency is consistent with the observation of the breakthrough curves in Figure 12.7. It should be noted that the breakthrough half-breakthrough time (τ , min) estimated from the Yoon–Nelson model (Table 12.9), successfully matched with that from the experimental breakthrough curves (Table 12.8).

12.3.9 Possible Adsorption Mechanisms

In-depth understanding of adsorption mechanisms is an integral part of the study of the adsorption process. Several underlying adsorption mechanisms of aromatic pollutants have been postulated in the literature: (1) electrostatic attraction, (2) cationic exchange, (3) hydrogen bonding formation, (4) n - π interaction, (5) π - π interaction, and (6) pore filling (Xing et al., 1994; Radovic et al., 2001; Blackburn, 2004; Keiluweit and Kleber, 2009; Heibati et al., 2014; Tran et al., 2017a, 2017b, 2017c, 2017d, 2017e, 2017f). In this study, the adsorption mechanisms will be discussed according to the fixed experimental conditions (i.e., initial solution pH 7.0).

12.3.9.1 Electrostatic Attraction and Cation Exchange

Electrostatic attraction and cationic exchange have been ruled out as contributing interactions in the MG5 adsorption mechanisms (as discussed in Sections 12.3.2, 12.3.3, and 12.3.7), and thus these interactions are not further discussed. However, weak electrostatic attraction (Figure 12.8a) might occur between negatively charged groups (mainly $-\text{O}^-$ derived from the $-\text{OH}$ phenolic groups) and MG5 cations when solution pH is higher than 8.0, as discussed in Section 12.3.2.

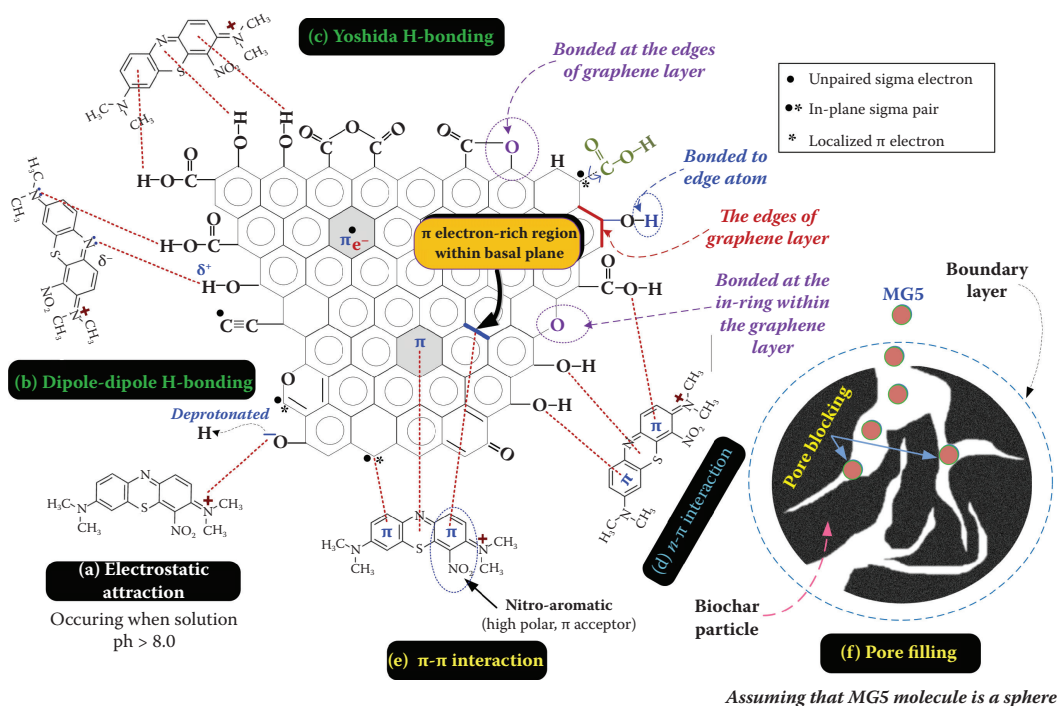


FIGURE 12.8

Schematic depiction of proposed adsorption mechanisms of MG5 by the biochar samples.

12.3.9.2 Hydrogen Bonding Formation

Hydrogen bonding interaction can be generally divided into dipole–dipole H-bonding and Yoshida H-bonding. The dipole–dipole H-bonding interaction (Figure 12.8b) occurs between surface hydrogen bonds of hydroxyl groups (i.e., —COOH or —OH that acts as the H-donors) on the biochar’s surface and the atoms (i.e., nitrogen or oxygen that acts as the H-acceptors) in MG5. Meanwhile, the Yoshida H-bonding interaction (Figure 12.8c) occurs between the hydroxyl groups on the biochar surface and the aromatic rings in MG5 molecules.

Analysis of the FTIR spectra variation before and after adsorption provides useful information on the adsorption mechanism. For example, Al-Ghouti et al. (2003) observed the variation of FTIR spectra of the diatomite samples before and after adsorption of methylene blue (MB). A shift in the peaks related to —OH groups from 3690 to 3674 cm^{−1} after MB adsorption confirmed the presence of dipole–dipole H-bonding interactions between the —OH group (activating group) on the diatomite surface and the nitrogen atoms of MB. Figure 12.3 demonstrates that the —OH peak at approximately 3400 cm^{−1} dramatically reduced in relative intensity and shifted toward higher wavenumbers after MG5 adsorption, which is also similar to observations in the adsorption of MG5 onto synthesized AC (Tran et al., 2017d) and commercial AC (Tran et al., 2017b). The results indicated that the presence of the hydrogen bonding interactions of both dipole–dipole and Yoshida (Blackburn, 2004). Also, as reported by Franz et al. (2000), the nitro (—NO₂) functional group of adsorbate might not be capable of H-bonding with carbonaceous materials, such as activated carbon.

12.3.9.3 n - π Interaction

n - π interaction (also known as n - π electron donor-acceptor interaction or donor-accepter complex) was originally proposed by Mattson et al. (1969). In this interaction, the carbonyl oxygen groups on the biochar's surface act as the electron donors, whereas the aromatic rings of MG5 molecule act as the electron acceptors (Figure 12.8d). The FTIR spectra revealed a slight shift of the C=O and C-O peaks toward lower wavenumbers after adsorption (Figure 12.4), which is an endorsement of the presence of n - π interaction. The shifts of the C=O and C-O positions after the adsorption of aromatic contaminants have been observed by other scholars (Xing et al., 1994).

It can be denied that the oxygen-containing functionalities (i.e., -COOH and -OH) on the biochar's surface play a certain role in adsorbing MG5. However, the H-bonding and n - π interactions might not be primary interactions in the MG5 adsorption process because the number of oxygen groups on the biochar's surface is limited. As shown in Table 12.2, the total concentrations of oxygen-containing acid groups available on the biochar's surface ranged from 0.228 mmol/g to 0.737 mmol/g (determined by the Boehm titration method). Likewise, Franz et al. (2000) also pointed out that the n - π interaction cannot be an effective adsorption interaction of aromatics on activated carbon. Thus, further experiments should be conducted to identify the dominated mechanisms of the dye adsorption process.

12.3.9.4 π - π Interaction

π - π interaction (also known as π - π electron donor-acceptor interactions) was initially proposed by Coughlin and Ezra (1968). In such interaction (Figure 12.8e), the aromatic rings in carbon material (i.e., activated carbon or biochar containing structures with high electron polarizability) act as π -electron donors and the aromatic rings in adsorbate (i.e., MG5 or phenol) act as π -electron acceptors. Figure 12.8 shows that every MG5 molecule possesses a polar nitro-functional group (electron-withdrawing group) on its benzene ring, which often acts as a strong electron acceptor and facilitates a decrease in π -electron density in its aromatics. Therefore, it will be expected that MG5 can be physisorbed on the biochar through the existence of a strong π - π interaction. Franz et al. (2000) highlighted that the heterogeneous surface of activated carbon was usually characterized into three main zones as follows: the carbon basal planes, heterogeneous surface groups (mainly oxygen-containing functional groups), and inorganic ash. They also pointed out that the majority of the adsorption sites for liquid organics occurred on the basal planes, which forms over 90% of the carbon surface.

To identify the presence of π - π interaction in the MG5 adsorption process, we used two pieces of experimental evidence, such as FTIR analysis before and after adsorption MG5 (qualitative analysis), and comparison on the amount of MG5 uptakes between the nonoxygenated biochar and oxygenated biochar (possibly quantitative analysis). First, the results of FTIR analysis demonstrated that the peak belonging to the vibration of biochar C=C bonds decreased in intensity and slightly shifted after MG5 adsorption (Figure 12.3). The result confirmed the presence of π - π interaction in the MG5 adsorption process, which is well consistent with the performance found in the literature (Xu et al., 2012; Tran et al., 2017b, 2017d).

Second, the effects of biochar surface oxygenation on its capacity to adsorb MG5 was additionally probed. In short, the addition of oxygen-containing functional groups (known as the electron-withdrawing groups) at the edges of the individual graphene layers within the biochar can cause a considerable drop in the biochar π -electron density. Consequently,

positive holes are created in the conductive π -band of graphene layers, and the interactions between the π -electrons of biochar and MG5 become weaker (Coughlin and Ezra, 1968; Radovic et al., 2001).

Figure 12.9 depicts the effects of biochar-surface oxygenation with acrylic acid on its capacity of MG5 adsorption. Acrylic acid has been used to synthesize carboxylate-rich carbonaceous materials through a one-step hydrothermal carbonization of glucose (Demir-Cakan et al., 2009). Our current studies (Tran et al., 2017b, 2017d) also demonstrated that carboxylate abundant activated carbon can be synthesized through two-step carbonizations (see Section 12.2.1), and we have proposed that the two-step carbonizations were a simple and effective approach for synthesizing oxygen functional groups-rich activated carbon. As expected, the oxygenated biochar samples exhibited the overwhelmingly higher concentration of oxygen-containing groups than the nonoxygenated biochar samples did (Table 12.2), which is in accordance with the conclusion of Huff and Lee (2016). The amount of oxygen-containing groups remained nearly constant upon further increasing of the acrylic acid concentrations (data not shown). Remarkably, the oxygenation process had a little impact on the BET surface area and total pore volume of biochar's textural properties (Table 12.1), which agrees with the findings of Wu et al. (2016) and our previous observations (Tran et al., 2017b, 2017d). Therefore, we emphasized that the oxygenation of biochar's surface through the hydrothermal process with acrylic acid contributed to enhancing the amount of its oxygen-containing groups without significant effects on its BET surface area and total pore volume.

Clearly, the adsorption of MG5 decreased dramatically upon the addition of oxygen-containing functionalities to the aromatic ring structure of the biochar (Figure 12.9). This drastic decrease is an undoubted endorsement for the presence of π - π interaction, which can be considered the primary mechanism of adsorption process (Coughlin and Ezra, 1968; Radovic et al., 2001; Tran et al., 2017b, 2017d). However, this result was different than our previous study (Tran et al., 2017e). In the study (Tran et al., 2017e), we prepared the hydrochar samples derived from GS, CC, and OP through a hydrothermal carbonization

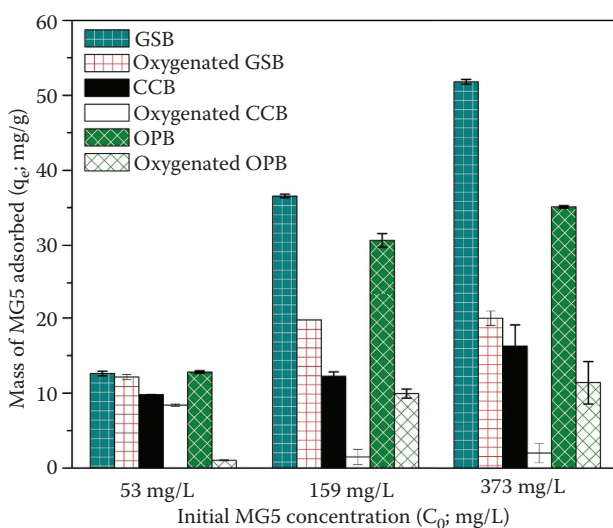


FIGURE 12.9

The comparison on adsorption capacities between the nonoxygenated biochar and the oxygenated biochar.

at 190°C for 24 h. Although the hydrochars also possessed the aromatic C=C bonds in their structures, the π - π interaction did not involve the MG5 adsorption process onto the hydrochars. This is because (1) oxygenation of the hydrochar surface through a hydrothermal process with acrylic acid contributed to increasing MG5 adsorption and identifying the negligible role of π - π interaction in the adsorption process, and (2) the analysis of FTIR demonstrated that the aromatic C=C peaks did not significantly decrease in intensity or shift toward higher/lower wavenumbers after adsorption, which further confirms the insignificant contribution of π - π interaction.

Recently, Huff and Lee (2016) examined pinewood-derived biochar-surface oxygenation with H₂O₂ and identified that methylene blue adsorption onto the biochar decreased when higher H₂O₂ concentrations were used in the treatment. They concluded that the additional oxygen groups onto the aromatic ring structure of the biochar weakened the π - π interactions that were primarily responsible for the dye adsorption onto the nonoxygenated biochar. Likewise, Guo et al. (2003) investigated the adsorption of malachite green on micro- and mesoporous rice husk-based active carbon. They also found that the adsorption capacity of activated carbons oxidized with HNO₃ and H₂O₂ was lower than that of nonoxygenated activated carbons. Therefore, after thorough inspection, we proposed that the hydrothermal treatment with carboxylate acid will be an effective method to probe the contribution of π - π interactions to the adsorption process of aromatic pollutants onto carbonaceous materials (i.e., activated carbon, biochar, graphene, and hydrochar).

Particularly, at a low initial concentration of MG5 (53 mg/L), the nonoxygenated and oxygenated GSB samples shared the similarity in the amount of MG5 adsorbed, demonstrating the important role of other interactions (H-bonding or n- π interactions) in binding MG5 rather than the π - π interactions; a similar trend was found for the nonoxygenated and oxygenated CCB samples (Figure 12.9). In contrast, the adsorption capacity of nonoxygenated OPB decreased significantly compared to oxygenated OPB. This means that the π - π interactions were responsible for the MG5 adsorption onto OPB even at a low MG5 concentration (53 mg/L). These conclusions were endorsed by (1) the insignificant change in the S_{BET} and V_{total} of MG5-laden OPB (Table 12.1), and (2) the intraparticle diffusion model in the investigation of adsorption kinetics (Section 12.3.4).

12.3.9.5 Pore Filling

Besides the π - π interactions, pore filling (Figure 12.8f) also played an additional role in the MG5 adsorption because the biochar had a relatively high porosity level. The simultaneous decrease in the specific surface area, nonmicropore volume, and total pore volume of all the biochars samples upon the MG5 adsorption (Table 12.1) confirmed that pore filling also had a great contribution to the MG5 adsorption mechanisms. This conclusion was in line with the discussions in the adsorption kinetics discussion (see Section 12.3.4) and previous literature studies (Lee et al., 2007; Tran et al., 2017b, 2017d). Notably, the large molecular size of MG5 does not favor its adsorption into the internal micropore of biochar. The noticeable decrease in micropore surface area and micropore volume of MG5-laden biochar samples (Table 12.1) was attributed to the effects of pore blocking (Figure 12.8f). In fact, the large MG5 molecules can screen the rugged biochar surface and clog some smaller pores, which inhibits nitrogen molecules from accessing the full biochar's surface and entering these pores. As a result, the micropore surface area and micropore volume of MG5-laden biochar simultaneously decreased (Lee et al., 2007; Tran et al., 2017b, 2017d).

On the basis of experimental results and aforementioned discussion, the order of interactions between MG5 and biochar can be withdrawn. For the MG5 adsorption onto GSB

TABLE 12.10

Comparison of the Maximum Capacities (Q_{\max}^0) of MG5 Sorption by the Biochars Studied Here and Those of Other Adsorbents Reported in the Literature

Adsorbent	S_{BET} (m ² /g)	pH	Temperature (°C)	Q_{\max}^0 (mg/g)	Reference
<i>Biosorbent</i>					
Golden shower	5.727	7.0	30	106	Tran et al., 2017f
Coconut shell	3.167	7.0	30	59.5	Tran et al., 2017f
Orange peel	2.086	7.0	30	92.4	Tran et al., 2017f
<i>Hydrochar</i>					
Golden shower	14.7	7.0	30	59.6	Tran et al., 2017e
Coconut shell	6.65	7.0	30	32.7	Tran et al., 2017e
Orange peel	6.99	7.0	30	15.6	Tran et al., 2017e
Commercial glucose	7.08	5.0	25	13.9	Tran et al., 2017a
<i>Biochar</i>					
Commercial glucose	677	5.0	25	119	Data unpublished
Golden shower	604	7.0	30	45.5	This study
Coconut shell	536	7.0	30	41.5	This study
Orange peel	565	7.0	30	35.2	This study
Commercial sucrose	409	5.0	25	29.6	Data unpublished
<i>Activated Carbon</i>					
Golden shower	812–1413	7.0	30	253–531	Tran et al., 2017d
Orange peel	1025	7.0	30	330	Tran et al., 2017d
Commercial glucose	335	5.0	25	175	Tran et al., 2017a
Commercial AC	768	5.0	25	178	Huang et al., 2014
Commercial xylose	1386	5.0	25	417	Huang et al., 2014
Commercial sucrose	1494	5.0	25	299	Huang et al., 2014
Commercial glucose	1612	5.0	25	444	Huang et al., 2014
Norit RB4C	1026	7.0	30	543	Tran et al., 2017b
<i>Others</i>					
Ag-NP-AC	NA	7.0	Room	167	Ghaedi et al., 2014
ZnONR-AC	NA	7.0	Room	200	Ghaedi et al., 2014
MCM-41	1004	4.0	25	137	Lee et al., 2007
GH _{1%}	NA	5.0	25	67.6	Tran et al., 2017a
GAC _{1%}	233	5.0	25	101	Tran et al., 2017a
C-g-nanocomposite	NA	7.0	30	137	Marandi et al., 2013

Note: Ag-NP-AC, silver nanoparticles-loaded activated carbon; ZnONR-AC, zinc oxide nanorods-loaded activated carbon; MCM-41, mesoporous zeolite; Norit RB4C, commercial activated-charcoal; GH_{1%}, commercial glucose hydrochar modified with 1% triethylenetetramine; GAC_{1%}, commercial glucose activated carbon modified with 1% triethylenetetramine; C-g-nanocomposite, collagen-g-poly(acrylamide-co-maleic anhydride) hydrogel nanocomposite; NA, data not reported. All biochar samples prepared through pyrolysis process at 800°C. All hydrochar samples prepared through a hydrothermal process at 190°C.

and CCB, the H-bonding or $n-\pi$ interactions can primarily occur, subsequently $\pi-\pi$ interactions and pore filling. Meanwhile, for the MG5 adsorption onto OPB, the H-bonding, $n-\pi$ interaction, and $\pi-\pi$ interaction can occur simultaneously, following by pore filling.

12.3.10 Comparison

Table 12.10 shows a comparison of the S_{BET} and Q_{max}^0 of the synthesized biochar in this study with those of the other adsorbents (e.g., biosorbent, hydrochar, activated carbon) in the previous literature. The difference in the Q_{max}^0 values among these adsorbents might result from different primary adsorption mechanisms. For example, the MG5 adsorption mechanisms onto biosorbent and hydrochar were mainly regarded as electrostatic attraction, while those for biochar and activated carbon were $\pi-\pi$ interaction and pore filling. Furthermore, the differences in the adsorbent's characteristics (i.e., textural properties and surface chemistry) disparity in Q_{max}^0 values among them. Typically, in the same feedstock (golden shower pod as a typical example), the S_{BET} values followed the sequence of activated carbon > biochar > hydrochar > biosorbent. In contrast, the amount of oxygen-containing functionalities exhibited the following order: biosorbent > hydrochar > activated carbon > biochar. According to the Q_{max}^0 parameter, MG5 sorption is produced following the sequence activated carbon > biosorbent > hydrochar > biochar. Therefore, to some extent, the amount of oxygen-containing functionalities of an adsorbent played a more critical role than its BET specific surface area. A comprehensive comparison of the properties (i.e., textural, structural, morphological, physicochemical, crystal, thermally stable properties, and surface chemistry) of activated carbons prepared from different chemical activation methods and their precursors (i.e., biosorbent, hydrochar, and biochar) has been reported in detail in our recent study (Tran et al., 2017c).

12.4 Conclusions

Laboratory-prepared biochar samples, which were porous carbonaceous materials, exhibited their relatively large specific surface area and high total pore volume, relatively abundant surface oxygen-containing functional groups. With these characteristics, along with good physiochemical properties, the biochar might be considered as a potential adsorbent for application in water treatment.

The maximum adsorption capacities toward MG5 in both batch and column experiments were in the following order: golden shower pod biochar (GSB) > coconut shell biochar (CCB) > orange peel biochar (OPB). The MG5 adsorption process was fast to reach equilibrium, favorable at a higher temperature, strongly dependent on the solution pH and ionic strength, and irreversible. The nonlinear method was more appropriate than the linear method in calculating the corresponding parameters of kinetics, isotherms, and thermodynamics.

The equilibrium constant (K_C) derived from the Langmuir constant (K_L , dimensionless) was appropriate for calculating the thermodynamic parameters. The thermodynamic investigation demonstrated that the MG5 adsorption occurred spontaneously or naturally ($-\Delta G^\circ$), in an endothermic nature ($+\Delta H^\circ$), and with increased randomness ($+\Delta S^\circ$).

The MG5 adsorption process from the aqueous solution onto the biochar involved physical adsorption. The major adsorption mechanisms were $\pi-\pi$ interactions and pore filling.

The other minor contributions in adsorption mechanisms belonged to dipole–dipole hydrogen bonding, Yoshida hydrogen bonding, and n – π interactions.

When biochar was transferred into MG5 solution, the biochar's surface interactions will occur instantaneously. After the surface active sites were occupied by MG5, the phenomenon of pore filling can subsequently occur until adsorption equilibrium was reached. At a low MG5 concentration (removal efficiency being 99%), the S_{BET} of biochar before and after adsorption was insignificantly different. However, at a higher MG5 concentration (considered as the equilibrium point in an adsorption isotherm), the S_{BET} of biochar decreased substantially, which is the endorsement of pore filling phenomenon.

Analyzing the biochar's textural properties before and after MG5 adsorption alongside the intraparticle model can endorse the presence of pore filling in adsorption mechanisms. Meanwhile, the oxygenation of the biochar's surface through the hydrothermal process with acrylic acid can be regarded as an effective method to identify the existence of π – π interaction. The oxygenation process possibly enhanced the amount of oxygen-containing groups of the biochar's surface but did not significantly alter their textural properties. A decrease in MG5 uptake upon oxygenated-biochar was due to weaken or suppressed π – π interaction. Analysis FTIR can additionally support the presence of π – π interaction. The agricultural waste-derived biochar could be a low-cost and renewable adsorbent for efficiently removing cationic dye from aqueous media.

References

- Aksu, Z. and F. Gönen. 2004. Biosorption of phenol by immobilized activated sludge in a continuous packed bed: Prediction of breakthrough curves. *Process Biochemistry* 39(5): 599–613.
- Al-Ghouti, M. A., M. A. M. Khraisheh, S. J. Allen and M. N. Ahmad. 2003. The removal of dyes from textile wastewater: A study of the physical characteristics and adsorption mechanisms of diatomaceous earth. *Journal of Environmental Management* 69(3): 229–238.
- Blackburn, R. S. 2004. Natural polysaccharides and their interactions with dye molecules: Applications in effluent treatment. *Environmental Science & Technology* 38(18): 4905–4909.
- Carrier, M., A. G. Hardie, Ü. Uras, J. Görgens and J. Knoetze. 2012. Production of char from vacuum pyrolysis of South-African sugar cane bagasse and its characterization as activated carbon and biochar. *Journal of Analytical and Applied Pyrolysis* 96: 24–32.
- Chao, H.-P., C.-C. Chang and A. Nieva. 2014. Biosorption of heavy metals on Citrus maxima peel, passion fruit shell, and sugarcane bagasse in a fixed-bed column. *Journal of Industrial and Engineering Chemistry* 20(5): 3408–3414.
- Coughlin, R. W. and F. S. Ezra. 1968. Role of surface acidity in the adsorption of organic pollutants on the surface of carbon. *Environmental Science & Technology* 2(4): 291–297.
- Dai, L., L. Fan, Y. Liu, R. Ruan, Y. Wang, Y. Zhou, Y. Zhao and Z. Yu. 2017. Production of bio-oil and biochar from soapstock via microwave-assisted co-catalytic fast pyrolysis. *Bioresource Technology* 225: 1–8.
- Demir-Cakan, R., N. Baccile, M. Antonietti and M.-M. Titirici. 2009. Carboxylate-rich carbonaceous materials via one-step hydrothermal carbonization of glucose in the presence of acrylic acid. *Chemistry of Materials* 21(3): 484–490.
- Doğan, M., H. Abak and M. Alkan. 2009. Adsorption of methylene blue onto hazelnut shell: Kinetics, mechanism and activation parameters. *Journal of Hazardous Materials* 164(1): 172–181.
- Franz, M., H. A. Arafat and N. G. Pinto. 2000. Effect of chemical surface heterogeneity on the adsorption mechanism of dissolved aromatics on activated carbon. *Carbon* 38(13): 1807–1819.
- Freedonia. 2016. World activated carbon. Industry Studies and Freedonia Focus Report.

- Ghaedi, M., H. Karimi and F. Yousefi. 2014. Silver and zinc oxide nanostructures loaded on activated carbon as new adsorbents for removal of methylene green. *Human & Experimental Toxicology* 33(9): 956–967.
- Guo, Y., S. Yang, W. Fu, J. Qi, R. Li, Z. Wang and H. Xu. 2003. Adsorption of malachite green on micro- and mesoporous rice husk-based active carbon. *Dyes and Pigments* 56(3): 219–229.
- Hall, K. R., L. C. Eagleton, A. Acrivos and T. Vermeulen. 1966. Pore- and solid-diffusion kinetics in fixed-bed adsorption under constant-pattern conditions. *Industrial & Engineering Chemistry Fundamentals* 5(2): 212–223.
- Heibati, B., S. Rodriguez-Couto, A. Amrane, M. Rafatullah, A. Hawari and M. A. Al-Ghouti. 2014. Uptake of Reactive Black 5 by pumice and walnut activated carbon: Chemistry and adsorption mechanisms. *Journal of Industrial and Engineering Chemistry* 20(5): 2939–2947.
- Huang, F.-C., C.-K. Lee, Y.-L. Han, W.-C. Chao and H.-P. Chao. 2014. Preparation of activated carbon using micro-nano carbon spheres through chemical activation. *Journal of the Taiwan Institute of Chemical Engineers* 45(5): 2805–2812.
- Huang, X., X. Liao and B. Shi. 2009. Adsorption removal of phosphate in industrial wastewater by using metal-loaded skin split waste. *Journal of Hazardous Materials* 166(2–3): 1261–1265.
- Huff, M. D. and J. W. Lee. 2016. Biochar-surface oxygenation with hydrogen peroxide. *Journal of Environmental Management* 165: 17–21.
- Jirka, S. and T. Tomlinson. 2015. State of the biochar industry: A survey of commercial activity in the biochar field. International Biochar Initiative.
- Keiluweit, M. and M. Kleber. 2009. Molecular-level interactions in soils and sediments: The role of aromatic π -systems. *Environmental Science & Technology* 43(10): 3421–3429.
- Lee, C.-K., S.-S. Liu, L.-C. Juang, C.-C. Wang, K.-S. Lin and M.-D. Lyu. 2007. Application of MCM-41 for dyes removal from wastewater. *Journal of Hazardous Materials* 147(3): 997–1005.
- Li, C. and P. Champagne. 2009. Fixed-bed column study for the removal of cadmium (II) and nickel (II) ions from aqueous solutions using peat and mollusk shells. *Journal of Hazardous Materials* 171(1–3): 872–878.
- Marandi, G. B., Z. P. Kermani and M. Kurdtabar. 2013. Fast and efficient removal of cationic dyes from aqueous solution by collagen-based hydrogel nanocomposites. *Polymer-Plastics Technology and Engineering* 52(3): 310–318.
- Mathialagan, T. and T. Viraraghavan. 2002. Adsorption of cadmium from aqueous solutions by perlite. *Journal of Hazardous Materials* 94(3): 291–303.
- Mattson, J. A., H. B. Mark, M. D. Malbin, W. J. Weber and J. C. Crittenden. 1969. Surface chemistry of active carbon: Specific adsorption of phenols. *Journal of Colloid and Interface Science* 31(1): 116–130.
- Nguyen, T. C., P. Loganathan, T. V. Nguyen, S. Vigneswaran, J. Kandasamy and R. Naidu. 2015. Simultaneous adsorption of Cd, Cr, Cu, Pb, and Zn by an iron-coated Australian zeolite in batch and fixed-bed column studies. *Chemical Engineering Journal* 270: 393–404.
- Ofomaja, A. E. 2007. Sorption dynamics and isotherm studies of methylene blue uptake on to palm kernel fibre. *Chemical Engineering Journal* 126(1): 35–43.
- Radovic, L. R., C. Moreno-Castilla and J. Rivera-Utrilla. 2001. Carbon materials as adsorbents in aqueous solutions. *Chemistry and Physics of Carbon* 27: 227–406.
- Raval, N. P., P. U. Shah and N. K. Shah. 2016. Adsorptive amputation of hazardous azo dye Congo red from wastewater: A critical review. *Environmental Science and Pollution Research* 23(15): 14810–14853.
- Song, S., Y. Ma, H. Shen, M. Zhang and Z. Zhang. 2015. Removal and recycling of ppm levels of methylene blue from an aqueous solution with graphene oxide. *RSC Advances* 5(35): 27922–27932.
- Stoeckli, F. and T. A. Centeno. 1997. On the characterization of microporous carbons by immersion calorimetry alone. *Carbon* 35(8): 1097–1100.
- Tran, H. N., S.-J. You and H.-P. Chao. 2016a. Effect of pyrolysis temperatures and times on the adsorption of cadmium onto orange peel derived biochar. *Waste Management & Research* 34(2): 129–138.

- Tran, H. N., S.-J. You and H.-P. Chao. 2016b. Thermodynamic parameters of cadmium adsorption onto orange peel calculated from various methods: A comparison study. *Journal of Environmental Chemical Engineering* 4(3): 2671–2682.
- Tran, H. N., F.-C. Huang, C.-K. Lee and H.-P. Chao. 2017a. Activated carbon derived from spherical hydrochar functionalized with triethylenetetramine: Synthesis, characterizations, and adsorption application. *Green Processing and Synthesis*. doi: 10.1515/gps-2016-0178.
- Tran, H. N., Y.-F. Wang, S.-J. You and H.-P. Chao. 2017b. Insights into the mechanism of cationic dye adsorption on activated charcoal: The importance of π - π interactions. *Process Safety and Environmental Protection* 107: 168–180.
- Tran, H. N., S.-J. You and H.-P. Chao. 2017c. Activated carbons from golden shower upon different chemical activation methods: Synthesis and characterizations. *Adsorption Science & Technology*. doi: 10.1177/0263617416684837.
- Tran, H. N., S.-J. You and H.-P. Chao. 2017d. Fast and efficient adsorption of methylene green 5 on activated carbon prepared from new chemical activation method. *Journal of Environmental Management* 188: 322–336.
- Tran, H. N., S.-J. You and H.-P. Chao. 2017e. Insight into adsorption mechanism of cationic dye onto agricultural residues-derived hydrochars: Negligible role of π - π interaction. *Korean Journal of Chemical Engineering* 34(6): 1708–1720.
- Tran, H. N., S.-J. You and H.-P. Chao. 2017f. Insight into adsorption mechanism of cationic dye onto biosorbents derived from agricultural wastes. *Chemical Engineering Communications*. DOI: 10.1080/00986445.2017.1336090.
- Tran, H. N., S.-J. You, A. Hosseini-Bandegharai and H.-P. Chao. 2017g. Mistakes and inconsistencies regarding adsorption of contaminants from aqueous solutions: A critical review. *Water Research* 120: 88–116.
- Walter, W. J. 1984. Evolution of a technology. *Journal of Environmental Engineering* 110(5): 899–917.
- Worch, E. 2012. *Adsorption Technology in Water Treatment: Fundamentals, Processes, and Modeling*. Berlin: Walter de Gruyter.
- Wu, W., J. Li, N. K. Niazi, K. Müller, Y. Chu, L. Zhang, G. Yuan, K. Lu, Z. Song and H. Wang. 2016. Influence of pyrolysis temperature on lead immobilization by chemically modified coconut fiber-derived biochars in aqueous environments. *Environmental Science and Pollution Research* 23(22): 22890–22896.
- Xing, B., W. B. McGill, M. J. Dudas, Y. Maham and L. Hepler. 1994. Sorption of phenol by selected biopolymers: Isotherms, energetics, and polarity. *Environmental Science & Technology* 28(3): 466–473.
- Xu, J., L. Wang and Y. Zhu. 2012. Decontamination of bisphenol A from aqueous solution by graphene adsorption. *Langmuir* 28(22): 8418–8425.



Taylor & Francis

Taylor & Francis Group

<http://taylorandfrancis.com>

13

Impact of Surface Modification of Activated Carbon on BTEX Removal from Aqueous Solutions: A Review

Hirra Anjum, Fareeda Chemat, Nirmala Gnanasundaram,
Appusami Arunagiri, and Murugesan Thanabalan

CONTENTS

13.1 Introduction	293
13.2 Activated Carbon and Its Sources	294
13.2.1 Activation Process.....	295
13.2.2 Governing Properties for Activation Process.....	299
13.2.3 Kinetic Models for Activation Process.....	300
13.2.4 Adsorption Mechanism	301
13.2.5 Effect of Textural Properties of Activated Carbon without Modification	302
13.2.6 Effect of Textural Properties of Modified Activated Carbon	303
13.3 Conclusion and Way Forward	307
References.....	308

13.1 Introduction

Environmental contamination caused by primary pollutants endangers human health, therefore, contemporaneous research has been conducted to annihilate its detrimental effects. Polycyclic aromatic compounds along with benzene, toluene, xylene, aniline, and phenol have attracted much attention, since they constitute some of the most common and serious threats to the environment (Zhang and Somasundaran, 2006). This abundant class of organic compounds is usually presupposed in chemical processes as raw materials or as solvents in paints and thinners. These hydrophobic volatile organic compounds represent 20% to 30% of gasoline, which predominately encompasses benzene, toluene, and xylene. The maximum solubility of benzene, toluene, and xylene in water is in the range of 1740 to 1800 mg/l (Ray and Engelhardt, 2012), 515 to 540 mg/l (Alonso et al., 2007), and 178 to 220 mg/l, respectively. They are the source of long-term pernicious effects on biological organisms even in small concentrations; they penetrate into the body cells and cause respiratory disease, reduced lung development, cardiovascular complications, and longtime impairment to the nervous system.

These dissolved contaminants, even at low concentration on account of their pernicious effects and solubility, infiltrate the environment through insufficient oxidation, industrial sewage dumping, gasoline leakage, transportation exhaust (75%–85% benzene emissions) (Kerbachi et al., 2006), surface spills, the petrochemical wastes infiltrate BTEX

(Benzene, Toluene, Ethylbenzene, and Xylenes) in the soil, water and pipeline leaks, and so forth. Benzene and toluene usually represent an average concentration value of $14.7 \pm 2.4 \mu\text{g.m}^{-3}$ and $8.1 \pm 1.2 \mu\text{g.m}^{-3}$, respectively, while the mean concentration of p-xylene and o-, m-xylene is found to be $5.1 \pm 1.2 \mu\text{g.m}^{-3}$ and $2.1 \pm 0.8 \mu\text{g.m}^{-3}$, respectively (Singla et al., 2012).

The removal of these mutagenic pollutants (BTEX) is critical and stimulating due to the close range of boiling points and numerous azeotropic combinations. Substantial endeavors have been devoted to the abatement of these flammable and carcinogenic compounds during the recent past. Many well-established and developed methods have been employed to reduce the costs of current treatments, including liquid extraction, extractive distillation, chemical clarification, membrane filtration, advanced oxidation, photocatalytic oxidation, bubble separation, adsorption, photoremediation, biofiltration, and membrane technology, to remediate contaminated effluents. Removal with standard techniques/processes are not economically viable, as they do not result in appropriate uptake. Nevertheless, novel technologies are continually being developed through constant efforts of researchers. Each of these processes has its own pros and cons; however, adsorption proves to be one of the most effective of these processes to purify the effluent such that it is suitable for the environment (Hackbarth et al., 2014). This unit operation removes surface active material by interphase transfer. Thus, carbonaceous sorbents, among all the available adsorbents, present superior performance due to their profound specific surface area, well-developed microporosity, pore size distribution, the presence of surface functional groups, degree of modification, frequency of regeneration of adsorbent, and, above all, the complex heterogeneous nature of carbon.

Extensive work on carbon-based adsorbents opened the doors to nanotechnology that is flourishing with every passing day. It is, nonetheless, the situation that practical applications of these adsorbents remain limited due to some unresolved problems, including cost-effective production, dispersion, and regeneration techniques. Therefore, activated carbon is still the best choice for researchers, because of its economic viability, easy accessibility, and environmental friendly nature. Hence, in order to obtain the desired physicochemical properties of the activated carbon, it is very important to perceive the chemistry of BTEX to be removed. In this review, a detailed comparison of raw and modified activated carbon, and their physicochemical properties and the adsorption capabilities before and after modification that was exploited for the removal of BTEX is presented.

13.2 Activated Carbon and Its Sources

Activated carbon (AC) is the most implicit form of amorphous carbon for the removal of different organic/inorganic compounds dissolved in the aqueous/gaseous environment. The exceptionally high surface areas ($500\text{--}3000 \text{ m}^2/\text{g}$), established microporosity ($0.7\text{--}1.8 \text{ cm}^3\text{g}^{-1}$), significant characteristics of surface chemistry, and prodigious surface reactivity cause the adsorption capacity to be enhanced (Yin et al., 2007). The carbon matrix is comprised of bonded heteroatoms, having a strong influence on the surface chemistry of graphitic surfaces. It can distribute the organic/inorganic molecule on its hydrophobic surface because of its inert porous structure.

The conventional forms of activated carbon, exploited for purification and separation purposes are powdered AC, granular AC, AC fiber (ACF), and molded AC. Powdered AC

comprises crushed carbon particles whose average size varies from 15 to 25 μm . The biological regeneration of this form is quite difficult. Granular AC is found either in crushed or pellet form (manufactured through agglomeration of pulverized powder with coal tar pitch that acts as a binder) and the particle sizes are usually of the 8/20, 8/30, 20/40, and 12/42 mesh size. Nevertheless, the thin carbon fibers are preferred because of ease of handling and fast intraparticle adsorption kinetics that result in the reduction of the size of adsorption unit. They demand high strength and elasticity. Therefore, the source of high-strength ACF is polyacrylonitrile (PAN) and high elasticity is produced by utilizing coal tar as a primary source of production.

Additionally, activated carbons are either manufactured from heterogeneous materials (bituminous coal, lignite, coconut shells and wood, wheat, bagasse, miscanthus, rapeseed, grape seeds, rice husk, rice hulls, sunflower shell, almond shell, peanut hulls, hazelnut shells, pecan shells, apricot stones, peach stones, almond stones, etc.) or homogenous polymeric materials (polyacrylonitrile, phenolic resin, cellulose, etc.), depending upon the appreciable mechanical strength and minimal ash contents. General compositions of the source materials for the preparation of AC are presented in Table 13.1.

Generally, if the moisture content in agricultural waste is around 50% and C/N >30, then direct combustion, pyrolysis, and gasification processes are to be followed for further polishing of charcoal; otherwise, biochemical treatment is the process to be selected. Furthermore, the rise in temperature leads to an increase in the percentage of ash as well as the percentage of carbon and reduces the volatile matter. Thus, higher temperature leads toward the production of high-quality charcoal. On the other hand, reduction in the yield of charcoal may result, due to the excessive primary or secondary decomposition of agricultural waste, at a higher temperature.

13.2.1 Activation Process

The process of activation is comprised of physical and chemical activation. The production of AC through the physical process encompasses two steps: carbonization and activation. This thermal treatment (the temperature range lies between 400°C and 800°C and sometimes reaches to 1000°C) creates a nongraphitizing structure via cross-linking reactions (carbonization) (Jia and Lua, 2008), and to make incipient pores more accessible and to create new active sites, treatment (activation) at much higher temperature in the presence of air, CO_2 , or steam is required (Daud et al., 2007). The most frequently used oxidizing agent is CO_2 because its handling is quite easy and the slow reaction rate at $\sim 800^\circ\text{C}$ makes it able to control the activation process (Girgis et al., 2002; Lua and Yang, 2004; Lua et al., 2004; Zhang et al., 2004). The duration of activation in physical mode also affects the specific surface area and pore volumes of AC. Zhang et al. (2004) showed that the surface area and pore volume of corn stover and corn hulls were plausibly higher after 1 hour activation as compared to that of 2 hours. The physical activation process does not give satisfactory results to make the commercial adsorbent, because physical activation either results in undesired widening of pores or diffusion issues (Ioannidou and Zabaniotou, 2007).

Chemical activation usually carried out as one-step, two-step, and three-step processes. It is preferred over physical activation because of high surface area, pore volume, percent yield, and low activation temperature (low energy cost) with pronounced adsorption capacity (Kennedy et al., 2004; Tran et al., 2017). The single-stage process commences with impregnation using conventional oxidizing agents (e.g., KOH , ZnCl_2 , H_3PO_4 , K_2CO_3). Among these H_3PO_4 is the preferred activating agent compared to ZnCl_2 , due to the corrosion and inefficient chemical recovery issues encountered with the latter. Bansode et al. (2003) activated

TABLE 13.1
Compositions of Various Raw Materials Used for the Preparation of Activated Carbon

Agricultural Waste	Moisture %	Ash %	Volatiles %	Carbon %	Hydrogen %	Oxygen %	Nitrogen %	Sulfur %	Gross Calorific Value (kcal/kg)	Reference
Apricot tree pruning	40	0.2	80.4	51.4	6.29	41.2	0.8	0.1	4971	Skoulou and Zabaniotou, 2007
Almond tree pruning	40	–	–	–	–	–	–	–	4398	Skoulou and Zabaniotou, 2007
Barley straw	15	4.9	–	46.8	5.53	41.9	0.41	0.06	4489	L. Sun et al., 1997
Cherry tree pruning	40	1	84.2	–	–	–	–	–	5198	Skoulou and Zabaniotou, 2007
Corn cob	7.1	5.34	–	46.3	5.6	42.19	0.57	0	4300	Sun et al., 1997
Corn straw	0	6.4	–	45.53	6.15	41.11	0.78	0.13	4253	Sun et al., 1997
Cotton gin waste	6	13.3	–	41.23	5.03	34	2.63	0	3772	Zabaniotou et al., 2000b
Durum wheat straw	40	–	–	–	–	–	–	–	4278	Sun et al., 1997
Oat straw	15	4.9	–	46	5.91	43.5	1.13	0.015	4321	Skoulou and Zabaniotou, 2007
Olive residues	7.1	4.75	–	49.9	6	43.4	0.7	–	4500	Zabaniotou et al., 2000a
Peach tree pruning	40	1	79.1	53	5.9	39.1	0.32	0.05	4500	Skoulou and Zabaniotou, 2007
Rice husk	0	15.5	39.8	38.5	5.7	39.8	0.5	–	3757	L. Sun et al., 1997
Soft wheat straw	15	13.7	69.8	–	–	–	–	–	4278	L. Sun et al., 1997
Sugar beet leaves	75	4.8	–	44.5	5.9	42.8	1.84	0.13	4230	Skoulou and Zabaniotou, 2007
Sunflower straw	40	3	–	52.9	6.58	35.9	1.38	0.51	4971	Skoulou and Zabaniotou, 2007
Vineyard pruning	40	3.8	–	47.6	5.6	41.1	1.8	0.08	4011	Skoulou and Zabaniotou, 2007

pecan and almond shell-based carbon with steam (900°C for 6 hours) and H_3PO_4 (50 wt%) to study their effectiveness for the removal of benzene. The steam activated carbon showed better adsorption profile than that of H_3PO_4 activated carbon, although the surface area with phosphoric acid treatment was much higher (AL: 1340 m^2/g , PS: 902 m^2/g) than that of steam activated carbon. This may be attributed to high negative surface charge of carbon and efficient removal is ascribed by the zero dipole moment of benzene. However, Adinata et al. (2007) deduced that H_3PO_4 showed commendable results of activation at 500°C, for 2 hours but the resultant surface area was a little lower than that of ZnCl_2 activated product. Moreover, KOH, although it develops large microspores (at higher temperature), results in low yield and less carbon content (Prahas et al., 2008). These reagents result in the generation of fine pores over the surface of carbon after sufficient soaking time.

This single-step process has an edge over the physical process in that the added chemicals can be recovered easily as it is performed at lower temperature, providing much higher surface area, higher yield, and better pore characteristics (pore size, pore volume, etc.) (Lillo-Ródenas et al., 2003). They also compared NaOH and KOH as activating agents for anthracite at 730°C and proposed that KOH results in higher yield (90%) and surface area as compared to that of NaOH. Mohammed et al. (2015) initially activated the coconut shell-based carbon with KOH followed by the treatment with ammonia and examined the effect of activation temperature and duration on percentage yield. Their results showed that, with the increase of activation temperature from 600°C to 700°C for 1 to 2 hours, the yield increased to 32% and after that a decreasing trend was observed. Moreover, the removal efficiency of benzene and toluene after treatment with ammonia increased from 82.5% to 91% and 85.6% to 92.3%, respectively, and removal is observed to be efficient only at lower initial concentrations. Similarly, Gong et al. (2016) activated coal-based carbon with KOH and studied the effect of activation temperature, duration, and dosage of the activating agent as inducing factors responsible for uptake. They proved that with the increase of activation temperature (950°C) for the duration of 3 hours with KOH (dose of 2.5%), the sorption capacity of benzene improved remarkably. Table 13.2 compares the carbonization and activation conditions for the production of AC using different raw materials.

Moreover, ZnCl_2 is a strong oxidizing agent that produces high-quality ACs with high specific surface area and porosity, as compared to other activating agents, namely, ZnCl_2 , NaOH, and H_3PO_4 at various temperatures (600°C, 700°C, and 800°C). Kalderis et al. (2008) concluded that ACs produced with ZnCl_2 showed higher surface area at 700°C. On the other hand, the studies showed that the activation product of KOH showed better results as compared to that of K_2CO_3 . Sudaryanto et al. (2006) inferred that the maximum textural properties (1378 m^2/g , 0.583 cm^3/g) were obtained with an impregnation ratio of 5:2 of cassava peel and KOH at 750°C, while the activated carbon (palm shell) with K_2CO_3 showed a maximum specific surface area around 1170 m^2/g at 800°C. However, Akpa and Nmegbu (2014) activated coconut shell, bamboo and palm kernel at 300°C to 400°C with trioxo nitrate acid and proved that with the increase of adsorbent dose, the sorption of benzene increases, while it had opposite effect on the increase of initial concentration of benzene and particle size of adsorbate. The two-stage process encompasses the precarbonization (pyrolysis/hydrolysis) and activation steps. The process of pyrolysis occurs at a high temperature (400°C to 1200°C) in an inert environment. However, the raw material is dispersed in an autoclave with controlled temperature (150°C to 350°C) for about 2 to 24 hours, in case of hydrolysis (Tran et al., 2017). In another study, activated carob bean seed husk (CBSH) by two stage chemical activation by utilizing ZnCl_2 with air was reported (Şahin et al., 2016), and they concluded that the highest BET surface area (1002 m^2/g) with pore volume (0.52 cm^3/g) can be obtained through this procedure. Similarly, Saka (2012) proposed that ZnCl_2 activation

TABLE 13.2

Carbonization and Activation Conditions for the Preparation of Activated Carbon from Several Raw Materials

Raw Material	Carbonization Temperature (°C)	Activation Temperature (°C)	Type of Activation (Physical/Chemical)	Reference
Sunflower shell	1000	1000	Steam	Haykiri et al., 2006
Sugarcane bagasse	750	900	CO ₂ /N ₂	Ahmedna et al., 2000
Apricot stones	800	800	Steam	Savova et al., 2001
Coconut shell	300–400	300–400	Trioxo nitrate acid	Akpa and Nmegbu, 2014
Bamboo	300–400	300–400	Trioxo nitrate acid	Akpa and Nmegbu, 2014
Palm kernel	300–400	300–400	Trioxo nitrate acid	Akpa and Nmegbu, 2014
Cassava peel	750	750	KOH	Sudaryanto et al., 2006
Palm shell	800	800	K ₂ CO ₃	Sudaryanto et al., 2006
Pecan shell	900	900	Steam	Bansode et al., 2003
Almond shell	900	900	Steam	Bansode et al., 2003
Coal-based carbon	950	950	KOH	Gong et al., 2016
Coconut shell	600–700	600–700	KOH	Mohammed et al., 2015
Apricot stones	800	800	ZnCl ₂	Aygün et al., 2003
Rice husk	400	600	Steam	Malik, 2003
Olive seed	800	800	KOH	Stavropoulos and Zabaniotou, 2005
Corn cob	500–800	–	K ₂ CO ₃	Tsai et al., 2001
Almond shells	400	850	Physical	Marcilla et al., 2000
Pecan shells	700–800	800	Physical	Ahmedna et al., 2000

at 600° in N₂ atmosphere improves the surface area to 1289 m²/g. Furthermore, (Adinata et al., 2007; Prahas et al., 2008; Sudaryanto et al., 2006) proposed that with an increase in temperature and impregnation ratio, the percent yield tended to decrease due to the dehydration of phosphoric acid, and degrades the activation product (jack fruit peel waste), which in turn releases the gaseous products and decrease the percent yield of carbon. Also, they concluded that with activation temperature of 550°C maximum structural properties (1260 m²/g, 0.733 cm³/g) can be achieved. Tongpoothorn et al. (2011) proposed that increase in impregnation ratio of *Jatropha curcas* fruit shell with NaOH lead to the widening of pores (pore volume 1.312 cm³/g). In addition to this, the amount of NaOH plays an important role in micropore development that in turn increases the surface area (1873 m²/g). Nonetheless, a new three-stage activation process was recently introduced. It comprises hydrothermal carbonization (190°C), pyrolysis (800°C), and chemical activation. Tran et al. (2017) studied the activation of golden shower in three different stages and deduced that the textural properties (903 m²/g and 0.46 cm³/g) improve with the introduction of additional activation step.

Hence, the selection of an appropriate precursor, method of activation, and activation conditions influence the surface chemistry and sorption capacity of the activated carbon (Li et al., 2002). Recently, the research on modification of activated carbon with different functional groups for the removal of VOCs (volatile organic compounds) and BTEX in particular is gaining prominence.

13.2.2 Governing Properties for Activation Process

Among the physical, surface, and textural properties of activated carbon, specific surface area, pore volume, and pore size distribution have their own specific role in determining the adsorption properties of AC. The literature exhibits that the specific surface areas of AC tend to increase at elevated temperatures (650°C–700°C), therefore the probable reason for increase in surface area is the opening of the restricted pores (Ioannidou and Zabaniotou, 2007).

Furthermore, pore volume and pore size distribution are important in deciding the adsorption capacity in such a way that smaller pores are incapable of capturing larger adsorbate molecules, and the larger pores cannot retain the smaller molecules (Ahmedna et al., 2004). The pore volume (micropore and mesopore volume) of carbon plays a vital role on the percentage removal of aromatic compounds (Tham et al., 2011). According to Lillo-Ródenas et al. (2005), micro-, meso-, and macropores take part in the uptake of toluene. This transport through the pores play a significant role in enhancing adsorption capacity when all available micropore sites saturate quickly (Branton et al., 2009). On the other hand, Bansode et al. (2003) concluded that AC with high surface area does not always results in better aromatic adsorption.

The selection of raw material plays a vital role, as the literature reveals that raw material that has abundant lignin content in it yields the microporous structure, while macropores are being developed by the utilization of raw materials with high cellulosic content. The studies depict that the activation temperature and soaking time are two major factors that has an immense impact on total pore volume of AC, as an increase in temperature and soaking time results in the fall of pore volume (Hu and Srinivasan, 2001; Hu et al., 2001; Ioannidou and Zabaniotou, 2007). On the contrary, the total pore volume exponentially increases with the elevation of activation temperature.

The range of surface area and the pore volumes obtained after the activation of different raw materials used for the preparation of ACs are compiled in Table 13.3.

It is apparent that corn cob and macadamia nutshell showed a high pore volume, however, the highest yield (76%) is obtained from olive seeds. Correspondingly, the higher surface area of activated carbon can be obtained from rice husk, corn cob, olive seed, and cassava peel that are activated with KOH.

TABLE 13.3

Textural Properties of Activated Carbon Prepared from Agricultural Waste

Raw Material	Surface Area (m ² /g)	Micropore Volume (cm ³ /g)	Reference
Apricot stones	1190	0.50	Savova et al., 2001
Macadamia nutshell	1718	0.723	Minkova et al., 2000
Corn cob	960	0.629	El-Hendawy et al., 2001
Olive seed	1339	–	Stavropoulos and Zabaniotou, 2005
Olive waste cakes	514–1271	0.217–0.557	Baçaoui et al., 2001
Rice straw	2410	1.4	Oh and Park, 2002
Cassava peel	1378	0.583	Sudaryanto et al., 2006
Waste tire rubber	1000	0.44	Lehmann et al., 1998
Waste tires	1031	0.28	Lehmann et al., 1998
Scrap tires	1031	0.28	J. Sun et al., 1997
Waste tires	1177	0.54	Ariyadejwanich et al., 2003
Waste tire rubber	1070	0.55	Miguel et al., 2002

13.2.3 Kinetic Models for Activation Process

The kinetic study of the complex activation process has become a significant characteristic in optimizing this procedure. These models can be classified into three categories: kinetic equation models, semiempirical models, and models including transport phenomenon as well as kinetics. The fluid–solid first-order reaction has momentous importance in interpreting the laboratory data for the production of activated carbon. Therefore, various models—volume reaction model, the grain model, random pore model, simple model, direct method model, and nucleation model—are specifically utilized for porous solid structure. On the other hand, some numerical models involve partial differential equations, including the finite volume model, finite element model, Crank–Nicholson model, line method model, and collocation model. The shrinking core model depicts that the reduction of carbon structure (occupied and free volume of carbon structure) directly affects the physical and textural properties. Selected kinetic models reported for the activation of carbon from the agricultural raw material are summarized in Table 13.4.

TABLE 13.4

Summary of Selective Kinetic Models Used for the Preparation of Activation of Carbon

Kinetic Model	Equation	Significance	Reference
Volume reaction model	$\frac{dX}{dt} = K_v(1-X)C_{A0}$ $-\ln(1-X) = (k_v C_{A0})t$	A reaction is assumed to take place all over the volumetric structure, and diffusional gradients cause the rate of reaction to be lowered down at the interior points.	Bhat et al., 2001
Shrinking core model	$\rho \left(-\frac{dr_c}{dt} \right) = K_r C_{A0}$ $t = \left(\frac{\rho R_p}{k_r C_{A0}} \right) [1 - (1-X)^{\frac{1}{3}}]$	Describes the state in which solid particles are expended either by dissolution or chemical reaction and the amount of the raw material consumed is the shrinking core.	Bhat et al., 2001
Random pore model	$\frac{1}{1-X} \left(\frac{dx}{dt} \right) = K_0 e^{\frac{E_a}{RT}}$	A kinetic model that encapsulates the deviations in physical assembly during the activation process.	Zolin et al., 2002
<i>n</i> th Order kinetic model	$R_{50} = K P_{CO_2}^n$ $R_{50} = K_0 e^{\frac{E}{RT}}$	Often utilized when CO is preoccupied in the activation process and reactivity depends upon the temperature.	Ollero et al., 2002
Langmuir–Hinshelwood model	$R_{50} = \frac{k_1 p_{CO_2}}{1 + \alpha p_{CO} + \beta p_{CO_2}}$	According to this model the reactant is adsorbed over the surface active sites to form a complex. Thus, the rate of reaction is governed by the adsorbed molecule.	Ollero et al., 2002
Pseudo-steady-state model	$\frac{\partial X}{\partial t} = (1-X)R$	Includes convection flow and neglects the diffusion and pressure driven flow.	Ollero et al., 2002
Reaction diffusion model	$R(X) = f(X) R_{50}$	The heterogeneous reaction takes place on the inner surface of the carbon to be activated.	Ollero et al., 2002
Nonequimolar model	$\eta_{cal}(t) = \frac{\iiint v_{C_{co}}(1-X)R dV}{\iiint v_{C_{co}}(1-X)R_G dV}$	It determines the effectiveness factor at any time that is a measure of heat and mass transfer during the process of activation.	Ollero et al., 2002

The isothermal procedures follow first-order reaction in the first phase and decomposition rate in the next stage. On the other hand, it has been observed that under dynamic conditions, the heating rate affects the overall kinetics in such a way that the lower rate of heating causes a series of redundant reactions and vice versa. Thus, in order to circumvent these complicated reactions, the path of fast rate of heating should be followed. The n th order model utilizes the Arrhenius equation to determine the kinetic parameters from thermogravimetric analysis. Hence, only a small amount of data is essential for the support of kinetics from the first-order model, and it considers autonomous parallel reactions in order to describe the overall decomposition process.

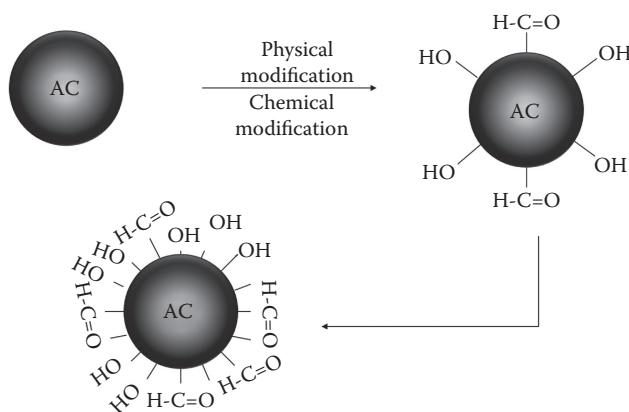
Furthermore, the pseudo-steady-state model lies in the last category that incorporates transport phenomena and kinetics. The effects of heat of reaction, internal and external heat transfer, and heat generation are incorporated in the coupling model to predict the impacts of varying physical properties of the raw material. They introduced empirical correlations between conversion and temperature.

13.2.4 Adsorption Mechanism

The fundamental issue for the aqueous solution adsorption is the understanding of adsorption mechanism of activated carbon. The major mechanism by which activated carbon adsorbs organic compounds vary, depending upon the polar or nonpolar nature of that species. Thus, several possible interactions, such as electrostatic, hydrogen bonding, and electron donor–acceptor, might act individually or simultaneously.

The dispersive interactions between BTEX and carbon basal planes define the process of physisorption on activated carbon (Franz et al., 2000). Thrower (1993) reported that the functional groups on carbon basal planes localize the surface electrons, rendering the surface partially positively charged, while the activating group on the benzene ring creates a partial negative charge. It means that methyl and ethyl groups ($-\text{CH}_3$, $-\text{C}_2\text{H}_5$) being activating groups, localize the ring structure by creating a partially negative charge. Hence, the oxygen-bearing functional groups over the basal planes attract the negatively charged ring structure, ultimately increasing the adsorption capacity. Additionally, Radovic et al. (1997) explained that the dispersive interactions are dominant over the electrostatic forces at the pH values near the point of zero charge because of the negligible electrostatic interactions. However, it was proposed that when weak acidic or nonacidic oxygen bearing groups interact with the localized ring structure, resulting in more electrostatic interactions and thereby leading to higher adsorption capacity (Yakout, 2014). Furthermore, these dispersive interactions are not solely responsible for the enhancement of adsorption capacity; hydrogen bonding is thought to be a significant mechanism as well (Rossner Campos, 2008). Moreover, oxygen-bearing groups affect the density of delocalized π electrons and affect the surface charge of activated carbon. These groups (acidic or basic) have an impact on the surface of the carbon. The increased acidity is primarily explained by carboxylic acid, lactonic, phenolic, and carboxylic anhydride groups, whereas the basic oxygen-bearing functionalities of activated carbon at the boundary of crystallitic structure of carbon are pyrone, chromene, and carbonyl structures. Thus, oxygen sites develop on the polychromatic sheet, giving rise to the basic character to delocalized π electrons of graphitic structure.

Nevertheless, most of the literature reported that by increasing the oxygen-bearing groups on the exterior of the carbon structure reduces the sorption of compounds that form a hydrogen bond on the surface of carbon (Zhu et al., 2005). These opposite results imply that detailed research should be conducted on the hydrogen-bonding mechanism. Furthermore, hydrogen bonds formed by water molecules with the oxygen-bearing groups

**FIGURE 13.1**

Impact of water cluster formation.

on the outer surface of AC compete either with the ring structure for active sorption sites (Ahnert et al., 2003) or configure a three-dimensional cluster that causes the occlusion of the adsorption sites by a water cluster formation (Ania et al., 2007). The formation of a water cluster is shown in Figure 13.1.

Therefore, the configuration of a hydrogen bond between functional groups and water molecules could effectively reduce the adsorption of organic molecules (Pan and Xing, 2008). Thus, the relative strength of the hydrogen bond (water-activated carbon/organic molecule-activated carbon) decides the extent of sorption. Consequently, the size exclusion phenomena results in a dramatic fall of organic uptake, as the inner pores and interstitial channels hinder the infiltration of comparatively bigger molecules (Beless et al., 2014; Kilduff et al., 1996).

It is observed that the carboxylic functional groups over the basal planes of carbon act as the electron donor and BTEX act as the electron acceptor, resulting in π - π electron donor-acceptor interactions, which is responsible for BTEX sorption in aqueous solution (Daifullah and Girgis, 2003; Yakout, 2014). The presence of carbonyl groups over the surface of carbon leads to an increased sorption capacity via donor-acceptor mechanism as the surface oxygenation transforms the carbonyl groups to other oxygen-bearing moieties (Franz et al., 2000).

On the other hand, the mechanism of mass transport controls the adsorption rate depending upon the properties of the AC and BTEX. The adsorbates in the form of BTEX first approach the boundary layer through dispersion, from the bulk liquid, and it is called as advection. Additionally, the mass transport through hydrodynamic boundary layer arises from molecular diffusion for which concentration difference is the dominating factor, and this step is called external diffusion. Internal diffusion encompasses the relocation of BTEX from the exterior of activated carbon to the internal sites, depending upon the size and porosity of the particle. It may occur by molecular diffusion of solutes. The later one occurs along the surface of activated carbon after occurrence of adsorption and is substantial only in porous adsorbents carrying high surface area and narrow porosity.

13.2.5 Effect of Textural Properties of Activated Carbon without Modification

The studies have shown that physiochemical properties and surface chemistry (surface functional groups, pore structure, composition, elemental analyses, and ash content) of AC

mainly relies upon the type of raw material and the activation process (Najm et al., 1991). Thus, these factors can be altered to their particular physical and chemical attributes to inflate their affinities toward inorganic/organic moieties in aqueous solutions with particular reference to BTEX. Based on the available literature, it is clear that even without surface modification, the coal-based sorbents have many folds of high surface area than that of other precursors, which might be due to high carbon (55% to 95%) and ash (0.3% to 2.15%) content.

Similarly, oxygen contents play an important role in sequestering BTEX. It is revealed that oxygen contents over the surface of catalyst (Pt or Pd) cause the sticking coefficient to be large enough for abatement of hydrocarbons, as the catalyst is oxidized to give rise to a oxygen-containing functional groups over the graphitic planes (Liu et al., 2013; Vesper et al., 1999). The adsorption capacity of activated carbon is expected to increase with an increase in surface area available for sorption. But, the studies reported that finely divided activated carbon with high porous structure ($1292.10 \text{ m}^2/\text{g}$) (Su et al., 2010) yields less sorption capacity as compared to that of activated carbon with low surface area ($923 \text{ m}^2/\text{g}$). Hindarso et al. (2001) indicated that the specific surface area is not the only governing factor to decide the adsorption capacity. Thus, the sources of activated carbon play a vital role in deciding the efficacy of the particular adsorbent. It is apparent from the literature that the coal-based activated carbons (305 mg/g) result in higher adsorption capacity than that of commercial (274.7 mg/g) or coconut shell-based (114.77 mg/g) activated carbon. Nonetheless, polarity is another imperative aspect to be focused on. Activated carbon is known to attract nonpolar (BTEX) molecules more comfortably than that of polar molecules. But, it solely relies on the solubility of adsorbate in solution.

On the other hand, Nouri and Haghseresht (2005) carried out the adsorption experiments for the removal of benzene and toluene at varying pH (2, 8, and 12) and proved that the adsorption capacity of activated carbon is not significantly influenced by changing the solution pH. Additionally, Souza et al. (2012) verified that the initial concentration of xylene is not affected, as compared to that of benzene and toluene. This may be explained by the fact that toluene and benzene have almost similar molecular configurations that help them in adsorption in micropores of AC and exhibit resistance with the change in initial concentration. Whereas xylene, being bigger in size, normally adsorbs on mesopores of AC manifesting lower resistance to diffusion. Moreover, they explained that in the preferential adsorption, the sorption of benzene is inhibited in the presence of toluene and o-xylene because of the rapid saturation of the available active sites. The competition among benzene, toluene, and o-xylene to occupy these sites commences with much higher affinity. In another study, Wang et al. (2015) evaluated the effect of temperature on the adsorption capacity of benzene. They revealed that with the increase of temperature from 27°C to 57°C , the sorption capacity of benzene decreases. This may be attributed to the fact that with at 27°C , the nondissociating, planner molecules of benzene begin to stack because of structural rearrangements (higher π - π interactions), whereas at higher temperatures the molecular movement is so random that it weakens the interactions between adsorbent and adsorbate, ultimately reducing the sorption capacity. Table 13.5 summarizes the characteristics of raw activated carbon without modification for the removal of BTEX from aqueous solution.

13.2.6 Effect of Textural Properties of Modified Activated Carbon

The abundantly available sorption sites are mostly responsible for remarkable uptake of organic molecules, whereas the composition of the activated carbon, the type of source

TABLE 13.5

Summary of the Characteristics of Raw Activated Carbon without Modification Used for the Removal of BTEX from Aqueous Solution

Adsorbent	Pollutant	Surface Area (m ² /g)	Pore Volume (cm ³ /g)	Adsorption Capacity, <i>q_e</i> (mg/g)	pH/ Temperature	Reference
AC (commercial)	Benzene/ toluene	790	0.44	–	–	Schüth et al., 2003
ACF (polyacrylonitrile precursor)	Toluene	1224	0.582	–	–	Liu et al., 2013
AC (fuel oil residue)	o-Xylene	72.32	75.75	–	pH: 5.53	Mohammed and Haider, 2013
AC (coal)	Benzene/ toluene	877.82	0.342	B: 219.42 T: 230.53	pH: 7 T: 30°C	Wibowo et al., 2007
AC (coconut shell)	BTX	724	0.39	B: 114.77 T: 125.09 o-X: 141.30	pH: 6.4 T: 30°C	Souza et al., 2012
OMAC (resol)	Benzene	1762	1.75	148.2	T: 25°C 35°C 45°C pH: 7	Wang et al., 2015
AC (commercial)	Benzene	1118	0.618	B: 274.7 T: 285	pH: 2, 8, 12	Nouri and Haghseresht, 2005
AC (commercial)	Benzene	923	0.46	380	–	Zhao et al., 1998
AC (bituminous coal)	Benzene/ toluene	850	–	B: 305.18, T: 361.14	T: 30°C 40°C 50°C pH: 7	Hindarso et al., 2001
GAC (commercial)	BTEX	1292.10	0.538	B: 217.32 T: 221.13 EB: 250.65 p-X: 301.4	pH: 7 T: 25°C	Su et al., 2010
PAC (commercial)	Benzene/ toluene	560	–	B: 40 T: 40	–	Koh and Dixon, 2001

material for activation, the extent of activation and the ability of regeneration are the factors responsible for wider pore size distribution. It is reported that the polymeric-based precursors (polyacrylonitrile, Novalak, polyvinylidene chloride, phenol formaldehyde, and Saran) have large surface area than that of coal-based sorbents, but the uptake of coal-based AC is higher than that of the rest (Liu et al., 2013; Wang et al., 2015). The formation of mesopores during the carbonization step creates more surface area and active sites for sorption, rendering it more graphitic than that of other precursors (Yang, 2003).

Hassan et al. (1999) investigated the effect of surface modification of activated carbon by KCl and calculated the adsorption capacity of benzene and toluene at two different solution concentrations, namely, 20 mg/l and 80 mg/l. They elucidated that at both concentrations toluene showed almost the same behavior with variation in adsorbent dose, whereas for benzene, at 80 mg/l, the sorption capacity is more influenced than that of 20 mg/l. This can be explained using the hydrophobicity index (toluene K_{OW} : 537; benzene K_{OW} : 131.8), which indicates that toluene has much higher affinity on carbon surface than that of benzene. Moreover, toluene saturates the carbon surface at a much lower solution

concentration by occupying the available sites. In contrast, benzene at a lower solution concentration, adsorbs only onto the available sites. However, the sorption capacity increases with occupying the rest of the sites. Similarly, Tham et al. (2011) modified the durian shell-based activated carbon with 30% H_3PO_4 at 500°C for 20 minutes for the removal of toluene. They prompted the research to analyze the effect of varying concentration of toluene on the removal efficiency of modified AC and showed that there was insignificant effect due to the reason that at low concentration, toluene occupies the maximum available adsorption sites (mesoporous/microporous).

Nevertheless, Wibowo et al. (2007) compared the chemical and thermal modification of activated carbon and concluded that both treatments caused insignificant impact on textural properties of activated carbon. Furthermore, pH_{PZC} values decrease with an increase in oxygen-containing acidic functional groups, while the opposite trend is observed for heat treatment. They inferred that the solution pH plays a vital role on the enhancement of benzene uptake (151.82, 183.29, and 219.42 mg/g) and toluene (166.27, 194.11 and 130.53 mg/g) as the adsorption capacity for benzene and toluene is observed to increase with the increase in pH value (3, 7, and 11) as compared to that of acidic treatment. Oxygen-bearing groups that confer the basic properties to the adsorbent give the best adsorption capacity, and thermal treatment plausibly favors the dispersion interaction between carbon basal planes and aromatic rings of benzene and toluene. On the contrary, Ferreira et al. (2015) inferred that acidic and neutral pH caused the sorption capacity to be enhanced because of electrostatic interactions between adsorbent and adsorbate.

Moreover, Aivalioti et al. (2012) deduced that in the process of heat treatment, most of the surface oxides decompose into CO and CO_2 , resulting in the production of free carbon atoms and free radical edge sites. Thus, the temperature rise improves the chances for the generation of active sites. They revealed that the thermal treatment at 750°C showed a remarkable increase in adsorption capacity. After cooling, the exposure of the surface to air, results in the formation of new surface oxides (carbonyls, pyrone, and chromene) having basic character, rendering the carbon surface less polar, which is a desirable trait for effective adsorption (Aivalioti et al., 2012).

HNO_3 is a strong oxidizing agent that oxidizes carbon atoms and causes the carbon surface to lose its electrons and become positively charged (Wibowo et al., 2007). But, the literature divulges that modification with H_3PO_4 gives higher sorption capacity than HNO_3 (Mangun et al., 2001). The only reason for this is the source of activated carbon. Rice husk has such a higher carbon-to-silica ratio and lower ash content than that of coal-based precursors that activation with a mild oxidizing agent makes it able to improve the sorption capacity up to 380 m^2/g . Daifullah and Girgis (2003) compared five different precursors of activated carbon and treated them with 50% H_3PO_4 along with air treatment. They concluded that the treatment with H_3PO_4 causes the incorporation of P_2O_5 and high content of acidic oxygen functional groups, which in turn increases the surface polarity and decreases the sorption of the hydrophobic BTEX. Hydration of (acidic) carboxylic groups either blocks the pore entrances, thus reducing the surface area available for adsorption (water cluster formation), or localizes free electrons over carbon basal planes, thus hampering the sorption capacity of activated carbon. However, Daifullah and Girgis postulated that the air treatment removes the phosphorus oxides, making the carbon surface basic in nature, which significantly improves the uptake of BTEX. They suggested that the oxygen atoms of carbonyl groups form electron donor–acceptor interactions with aromatic rings of BTEX. Table 13.6 summarizes the characteristics of modified activated carbon for removal of BTEX from aqueous solution.

TABLE 13.6

Summary of Characteristics of Modified Activated Carbon Used for the Removal of BTEX from Aqueous Solution

Adsorbent	Pollutant	Modifier	Surface Area (m ² /g)	Pore Volume (cm ³ /g)	pH	Adsorption Capacity, <i>q_e</i> (mg/g)	Reference
AC (coal based)	Benzene/toluene	Thermal treatment (800°C)	863.66	0.339	pH: 7 T: 30°C	B: 268.97 T: 279.16	Wibowo et al., 2007
Lignite (commercial)	BTEX	Thermal treatment (750°C)	95.19	0.090	pH: 10.79 15°C–25°C	B: 0.027 T: 0.003 EB: 0.003 m,p-X: 0.006 o-X: 0.003	Aivalioti et al., 2012
AC	Benzene/toluene	KOH	3216	1.59	pH: 7	B: 860 T: 1200 B/T: 1200	Asenjo et al., 2011
ACF (precursor polyacrylonitrile)	Toluene	Pd/Pt	1086	0.502	120°C–300°C	–	Liu et al., 2013
AC (fuel oil residue)	o-Xylene	ZnCl ₂	399.75	96.19	pH: 5.53	–	Mohammed et al., 2013
AC (date pits)	BTEX	H ₃ PO ₄	800	0.58	pH: 7.8 T: 25°C	B _{DP} : 8.8 T _{DP} : 5.0 EB _{DP} : 5.6 X _{DP} : 6.2	Daifullah and Girgis, 2003
AC (cotton stalks)	BTEX	H ₃ PO ₄	1183	1.055	pH: 7.8; T: 25°C	B _{CS} : 3 T _{CS} : 6.7 EB _{CS} : 8.7 X _{CS} : 9.3	Daifullah and Girgis, 2003
AC (peach stones)	BTEX	H ₃ PO ₄	1346	0.935	pH: 7.8 T: 25°C	B _{PS} : 3 T _{PS} : 6.5 EB _{PS} : 8.3 X _{PS} : 8.7	Daifullah and Girgis, 2003
AC (almond shells)	BTEX	H ₃ PO ₄	1279	1.011	pH: 7.8 T: 25°C	B _{AS} : 1.3 T _{AS} : 5 EB _{AS} : 6.5 X _{AS} : 7.4	Daifullah and Girgis, 2003
AC (olive stones)	BTEX	H ₃ PO ₄	848	0.632	pH: 7.8 T: 25°C	B _{OS} : 8.3 T _{OS} : 5.8 EB _{OS} : 6.6 X _{OS} : 7.2	Daifullah and Girgis, 2003
AC (rice husk)	BTEX	H ₃ PO ₄	956.5	0.726	pH: 6.5	B: 4.76, T: 5.5 E: 6.75 X: 7.33	Yakout, 2014
AC (rice husk)	Benzene	H ₃ PO ₄	–	–	pH: 6.5	365	Yakout, 2014
AC (coal based)	Benzene/toluene	HNO ₃	938.36	0.351	pH: 7 T: 30°C	B: 150.43 T: 157.07	Wibowo et al., 2007
ACF (phenolic resin-coated glass fiber)	BTEX	HNO ₃	483	0.176	pH: 7	B: 66 T: 85 EB: 237 X: 185	Mangun et al., 2001

Besides the advantages, activated carbon is faced with problems such as combustion risk, blocking of its pores because of the existence of polymerized aromatic compounds, little selectivity, high-temperature regeneration, and adsorption of moisture (Kadirvelu et al., 2003). However, activation at higher temperature can cope most of the drawbacks by improving surface properties and hence the adsorption capacity (Chang et al., 2000). Therefore, researchers are increasingly trying to find new adsorbents for the elimination of VOCs from environmental samples.

13.3 Conclusion and Way Forward

Activated carbons are widely accepted as one of the remarkably efficient adsorbents for BTEX removal from wastewater. The major sources of AC are the agricultural wastes that are abundantly available, a solution to environmental as well as waste disposal problems, and above all the potential replacement of expensive commercial adsorbents. Among different activation processes, chemical activation with three-stage activation has emerged as the most efficient process to generate carbon containing well-developed surface chemistry. During the activation stage, the H/C ratio governs the aromaticity and carbonaceous nature of the structure. Furthermore, the surface reactivity of activated carbon, produced by numerous sources, is principally influenced by the composition and the structure of the predecessor. Thus, the surface chemistry of activated carbon affects the interaction between BTEX and the active sites. Nevertheless, to further promote the practical application of ACs in abatement of BTEX, there are some important technical bottlenecks to be solved. For instance, the thermal regeneration of activated carbon, volatilization of BTEX in solution, and more efficient and cost effective ways for separation of these aromatic compounds still remain interesting but challenging. Fortunately, the surface modification of activated carbon has been observed to be an effective approach to respond to all the above technical issues. Researchers from diverse fields should come forward to move the theoretical knowledge into contemporary industrial application.

Additionally, the focal point of this particular study is the effect of sorption capacity of activated carbon from different agricultural sources, with or without modification. Researchers use the chosen set of publications (Tables 13.5 and 13.6) to compare the beneficial solution methodologies. A better compilation and understanding of the strengths and weaknesses of potential methodologies of the techniques used has been examined. Moreover, the researchers highlighted the point that in order to enhance sorption capacity, oxygen-bearing functional groups should be introduced over the surface of the adsorbent. Therefore, the detailed investigation in terms of regeneration of activated carbon is the future of wastewater treatment. In a nutshell, it can be concluded that the researchers should apply effective chemical modification techniques in order to resolve critical issues related to the attachment of targeted functional groups. A detailed review of the important available literature suggested that the basic treatment is the most impeccable of all functionalization techniques, as it introduces oxygen-enriched functional groups (pyrone, carbonyl, and ether-type oxygen-bearing groups) over the surface of activated carbon for the abatement of BTEX. The future directions of this study should be the green functionalization, which needs to be coupled with acid/base treatment to get the pronounced results in terms of BTEX uptake. Similarly, the introduction of a user-friendly regeneration technique could be a focal spot on forthcoming research in order to reduce the overall cost. Also the establishment of a quantitative method to ascertain the extent

of modification is another research domain requiring detailed analysis. However, various issues need to be addressed to obtain the desired adsorption capacity, the answer to the interplay between the modified activated carbon and BTEX, the long-term performance of adsorbents, and their commercial/industrial application in BTEX-contaminated water treatment.

References

- Adinata, D., Wan Daud, W. M. A., and Aroua, M. K. 2007. "Preparation and characterization of activated carbon from palm shell by chemical activation with K_2CO_3 ." *Bioresource Technology*, 98(1): 145–149.
- Ahmedna, M., Marshall, W. E., Hussein, A. A., Rao, R. M., and Goktepe, I. 2004. "The use of nutshell carbons in drinking water filters for removal of trace metals." *Water Research*, 38(4): 1062–1068.
- Ahmedna, M., Marshall, W. E., and Rao, R. M. 2000. "Production of granular activated carbons from select agricultural by-products and evaluation of their physical, chemical and adsorption properties1." *Bioresource Technology*, 71(2): 113–123.
- Ahnert, F., Arafat, H. A., and Pinto, N. G. 2003. "A study of the influence of hydrophobicity of activated carbon on the adsorption equilibrium of aromatics in non-aqueous media." *Adsorption*, 9(4): 311–319.
- Aivalioti, M., Pothoulaki, D., Papoulias, P., and Gidarakos, E. 2012. "Removal of BTEX, MTBE and TAME from aqueous solutions by adsorption onto raw and thermally treated lignite." *Journal of Hazardous Materials*, 207–208: 136–146.
- Akpa, J., and Nmegbu, C. 2014. "Adsorption of benzene on activated carbon from agricultural waste materials." *Research Journal of Chemical Sciences*, 4(9): 136–146.
- Alonso, L., Arce, A., Francisco, M., Rodríguez, O., and Soto, A. 2007. "Gasoline desulfurization using extraction with $[C_8mim][BF_4]$ ionic liquid." *AIChE Journal*, 53(12): 3108–3115.
- Ania, C., Cabal, B., Pevida, C., Arenillas, A., Parra, J., Rubiera, F., and Pis, J. 2007. "Effects of activated carbon properties on the adsorption of naphthalene from aqueous solutions." *Applied Surface Science*, 253(13): 5741–5746.
- Ariyadejwanich, P., Tanthapanichakoon, W., Nakagawa, K., Mukai, S., and Tamon, H. 2003. "Preparation and characterization of mesoporous activated carbon from waste tires." *Carbon*, 41(1): 157–164.
- Asenjo, N. G., Alvarez, P., Granda, M., Blanco, C., Santamaria, R., and Menendez, R. 2011. "High performance activated carbon for benzene/toluene adsorption from industrial wastewater." *Journal of Hazardous Materials*, 192: 1525–1532.
- Aygün, A., Yenisoğlu-Karakaş, S., and Duman, I. 2003. "Production of granular activated carbon from fruit stones and nutshells and evaluation of their physical, chemical and adsorption properties." *Microporous and Mesoporous Materials*, 66(2–3): 189–195.
- Baçaoui, A., Yaacoubi, A., Dahbi, A., Bennouna, C., Luu, R. P. T., Maldonado-Hodar, F., and Moreno-Castilla, C. 2001. "Optimization of conditions for the preparation of activated carbons from olive-waste cakes." *Carbon*, 39(3): 425–432.
- Bansode, R. R., Losso J. N., Marshall W. E., Rao R. M., and Portier R. J. 2003. "Adsorption of volatile organic compounds by pecan shell and almond shell-based granular activated carbons." *Bioresource Technology*, 90: 175–184.
- Beless, B., Rifai, H. S., and Rodrigues, D. F. 2014. "Efficacy of carbonaceous materials for sorbing polychlorinated biphenyls from aqueous solution." *Environmental Science and Technology*, 48(17): 10372–10379.
- Bhat, A., Ram Bheemarasetti, J. V., and Rajeswara Rao, T. 2001. "Kinetics of rice husk char gasification." *Energy Conversion and Management*, 42(18): 2061–2069.

- Branton, P., Lu, A. H., and Schüth, F. 2009. "The effect of carbon pore structure on the adsorption of cigarette smoke vapour phase compounds." *Carbon*, 47: 1005–1011.
- Chang, C.-F., Chang, C.-Y., and Tsai, W.-T. 2000. "Effects of burn-off and activation temperature on preparation of activated carbon from corn cob agrowaste by CO₂ and steam." *Journal of Colloid and Interface Science*, 232(1): 45–49.
- Daifullah, A. A. M., and Girgis, B. S. 2003. "Impact of surface characteristics of activated carbon on adsorption of BTEX." *Colloids and Surfaces A: Physicochemical and Engineering Aspects*, 214(1–3): 181–193.
- Daud, W. M. A. W., Ahmad, M. A., and Aroua, M. K. 2007. "Carbon molecular sieves from palm shell: Effect of the benzene deposition times on gas separation properties." *Separation and Purification Technology*, 57(2): 289–293.
- El-Hendawy, A.-N. A., Samra, S., and Girgis, B. 2001. "Adsorption characteristics of activated carbons obtained from corncobs." *Colloids and Surfaces A: Physicochemical and Engineering Aspects*, 180(3): 209–221.
- Ferreira, R. C., Couto Junior, O., Carvalho, K. Q., Arroyo, P., and Barros, M. 2015. "Effect of solution pH on the removal of paracetamol by activated carbon of dende coconut mesocarp." *Chemical Biochemical Engineering*, 29(1): 47–53.
- Franz, M., Arafat, H. A., and Pinto, N. G. 2000. "Effect of chemical surface heterogeneity on the adsorption mechanism of dissolved aromatics on activated carbon." *Carbon*, 38(13): 1807–1819.
- Girgis, B. S., Yunis, S. S., and Soliman, A. M. 2002. "Characteristics of activated carbon from peanut hulls in relation to conditions of preparation." *Materials Letters*, 57(1): 164–172.
- Gong, G., Liu, J., Yang W., Zhou Y., Sheng, H., and Fang, Y. 2016. "Preparation of coal-based columnar activated carbon for removal of benzene." *Material Science Forum*, 878: 101–107.
- Hackbarth, F. V., Vilar, V. J., De Souza, G. B., Souza, S., and Souza, A. 2014. "Benzene, toluene and o-xylene (BTX) removal from aqueous solutions through adsorptive processes." *Adsorption*, 20(4): 577–590.
- Hassan, A. A., Marcus, F., and Neville, G. P. 1999. "Effect of salt on the mechanism of adsorption of aromatics on activated carbon." *Langmuir*, 15(18): 5997–6003.
- Haykiri-Acma, H., Yaman, S., and Kucukbayrak, S. 2006. "Gasification of biomass chars in steam-nitrogen mixture." *Energy Conversion and Management*, 47(7–8): 1004–1013.
- Hindarso, H., Ismadji, S., Wicaksana, F., Mudjijati, A., and Indraswati, N. 2001. "Adsorption of benzene and toluene from aqueous solution onto granular activated carbon." *Journal of Chemical and Engineering Data*, 46(4): 788–791.
- Hu, Z., and Srinivasan, M. P. 2001. "Mesoporous high-surface-area activated carbon." *Microporous and Mesoporous Materials*, 43(3): 267–275.
- Hu, Z., Srinivasan, M. P., and Ni, Y. 2001. "Novel activation process for preparing highly microporous and mesoporous activated carbons." *Carbon*, 39(6): 877–886.
- Ioannidou, O., and Zabaniotou, A. 2007. "Agricultural residues as precursors for activated carbon production—A review." *Renewable and Sustainable Energy Reviews*, 11(9): 1966–2005.
- Jia, Q., and Lua, A. C. 2008. "Effects of pyrolysis conditions on the physical characteristics of oil-palm-shell activated carbons used in aqueous phase phenol adsorption." *Journal of Analytical and Applied Pyrolysis*, 83(2): 175–179.
- Kadirvelu, K., Kavipriya, M., Karthika, C., Radhika, M., Vennilamani, N., and Patabhi, S. 2003. "Utilization of various agricultural wastes for activated carbon preparation and application for the removal of dyes and metal ions from aqueous solutions." *Bioresource Technology*, 87(1): 129–132.
- Kalderis, D., Bethanis, S., Paraskeva, P., and Diamadopoulos, E. 2008. "Production of activated carbon from bagasse and rice husk by a single-stage chemical activation method at low retention times." *Bioresource Technology*, 99(15): 6809–6816.
- Kennedy, L. J., Vijaya, J. J., and Sekaran, G. 2004. "Effect of two-stage process on the preparation and characterization of porous carbon composite from rice husk by phosphoric acid activation." *Industrial and Engineering Chemistry Research*, 43(8): 1832–1838.

- Kerbach, R., Boughedaoui, M., Bounoua, L., and Keddam, M. 2006. "Ambient air pollution by aromatic hydrocarbons in Algiers." *Atmospheric Environment*, 40(21): 3995–4003.
- Kilduff, J. E., Karanfil, T., Chin, Y.-P., and Weber, W. J. 1996. "Adsorption of natural organic polyelectrolytes by activated carbon: A size-exclusion chromatography study." *Environmental Science and Technology*, 30(4): 1336–1343.
- Koh, S.-M., and Dixon, J. B. 2001. "Preparation and application of organo-minerals as sorbents of phenol, benzene and toluene." *Applied Clay Science*, 18(3–4): 111–122.
- Lehmann, C. M., Rostam-Abadi, M., Rood, M. J., and Sun, J. 1998. "Reprocessing and reuse of waste tire rubber to solve air-quality related problems." *Energy and Fuels*, 12(6): 1095–1099.
- Li, L., Quinlivan, P. A., and Knappe, D. R. U. 2002. "Effects of activated carbon surface chemistry and pore structure on the adsorption of trace organic contaminants from aqueous solution." *Carbon*, 40(12): 2085–2100.
- Lillo-Ródenas, M. A., Cazorla-Amorós, D., and Linares-Solano, A. (2003). Understanding chemical reactions between carbons and NaOH and KOH: An insight into the chemical activation mechanism. *Carbon*, 41(2): 267–275.
- Liu, Z.-S., Chen, J.-Y., and Peng, Y.-H. 2013. "Activated carbon fibers impregnated with Pd and Pt catalysts for toluene removal." *Journal of Hazardous Materials*, 256: 49–55.
- Lua, A. C., and Yang, T. 2004. "Effect of activation temperature on the textural and chemical properties of potassium hydroxide activated carbon prepared from pistachio-nut shell." *Journal of Colloid and Interface Science*, 274(2): 594–601.
- Lua, A. C., Yang, T., and Guo, J. 2004. "Effects of pyrolysis conditions on the properties of activated carbons prepared from pistachio-nut shells." *Journal of Analytical and Applied Pyrolysis*, 72(2): 279–287.
- Malik, P. K. 2003. "Use of activated carbons prepared from sawdust and rice-husk for adsorption of acid dyes: A case study of Acid Yellow 36." *Dyes and Pigments*, 56(3): 239–249.
- Mangun, C. L., Yue, Z., Economy, J., Maloney, S., Kemme, P., and Cropek, D. 2001. "Adsorption of organic contaminants from water using tailored ACFs." *Chemistry of Materials*, 13(7): 2356–2360.
- Marcilla, A., Garcia-Garcia, S., Asensio, M., and Conesa, J. 2000. "Influence of thermal treatment regime on the density and reactivity of activated carbons from almond shells." *Carbon*, 38(3): 429–440.
- Miguel, G. S., Fowler, G. D., Dall'Orso, M., and Sollars, C. J. 2002. "Porosity and surface characteristics of activated carbons produced from waste tyre rubber." *Journal of Chemical Technology and Biotechnology*, 77(1): 1–8.
- Minkova, V., Marinov, S., Zanzi, R., Björnbo, E., Budinova, T., Stefanova, M., and Lakov, L. 2000. "Thermochemical treatment of biomass in a flow of steam or in a mixture of steam and carbon dioxide." *Fuel Processing Technology*, 62(1): 45–52.
- Mohammed, A. M., and Haider, A. J. 2013. "Preparation of activated carbon from fuel oil wastes for removal of ortho-xylene from aqueous solution by new circulating system." *Advances in Environmental Biology*, 7(6): 1040–1049.
- Mohammed, J., Nasri, N. S., Zaini, M. A. A., Hamza, U. D., and Ani, F. N. 2015. "Adsorption of benzene and toluene onto KOH activated coconut shell based carbon treated with NH₃." *International Biodeterioration & Biodegradation*, 102: 245–255.
- Najm, I. N., Snoeyink, V. L., Lykins Jr, B. W., and Adams, J. Q. 1991. "Using powdered activated carbon: A critical review." *Journal (American Water Works Association)*, 83(1): 65–76.
- Nouri, S., and Haghseresht, F. 2005. "Estimation of adsorption capacity for dissociating and non dissociating aromatic compounds on activated carbon with different models." *Adsorption*, 11(1): 77–86.
- Oh, G. H., and Park, C. R. 2002. "Preparation and characteristics of rice-straw-based porous carbons with high adsorption capacity." *Fuel*, 81(3): 327–336.
- Ollero, P., Serrera, A., Arjona, R., and Alcantarilla, S. 2002. "Diffusional effects in TGA gasification experiments for kinetic determination." *Fuel*, 81(15): 1989–2000.
- Pan, B., and Xing, B. 2008. "Adsorption mechanisms of organic chemicals on carbon nanotubes." *Environmental Science & Technology*, 42(24): 9005–9013.

- Prahas, D., Kartika, Y., Indraswati, N., and Ismadji, S. 2008. "Activated carbon from jackfruit peel waste by H₃PO₄ chemical activation: Pore structure and surface chemistry characterization." *Chemical Engineering Journal*, 140(1–3): 32–42.
- Radovic, L. R., Silva, I. F., Ume, J. I., Menéndez, J. A., Leon, C. A. L. Y., and Scaroni, A. W. 1997. "An experimental and theoretical study of the adsorption of aromatics possessing electron-withdrawing and electron-donating functional groups by chemically modified activated carbons." *Carbon*, 35(9): 1339–1348.
- Ray, J. P., and Engelhardt, F. R. 2012. *Produced Water: Technological/Environmental Issues and Solutions*. Springer.
- Rossner Campos, A. A. 2008. "Removal of polar and emerging organic contaminants by alternative adsorbents." PhD dissertation, North Carolina State University.
- Şahin, Ö., Saka, C., Ceyhan, A. A., and Baytar, O. 2016. "The pyrolysis process of biomass by two-stage chemical activation with different methodology and iodine adsorption." *Energy Sources, Part A: Recovery, Utilization, and Environmental Effects*, 38(12): 1756–1762.
- Saka, C. 2012. "BET, TG-DTG, FT-IR, SEM, iodine number analysis and preparation of activated carbon from acorn shell by chemical activation with ZnCl₂." *Journal of Analytical and Applied Pyrolysis*, 95: 21–24.
- Savova, D., Apak, E., Ekinci, E., Yardim, F., Petrov, N., Budinova, T., and Minkova, V. 2001. "Biomass conversion to carbon adsorbents and gas." *Biomass and Bioenergy*, 21(2): 133–142.
- Schüth, C., Taubald, H., Bolaño, N., and Maciejczyk, K. 2003. "Carbon and hydrogen isotope effects during sorption of organic contaminants on carbonaceous materials." *Journal of Contaminant Hydrology*, 64(3): 269–281.
- Singla, V., Pachauri, T., Satsangi, A., Kumari, K. M., and Lakhani, A. 2012. "Comparison of BTX profiles and their mutagenicity assessment at two sites of Agra, India." *The Scientific World Journal*, article ID 272853.
- Skoulou, V., and Zabaniotou, A. 2007. "Investigation of agricultural and animal wastes in Greece and their allocation to potential application for energy production." *Renewable and Sustainable Energy Reviews*, 11(8): 1698–1719.
- Souza, S., Luz, A. D., Silva, A., and Souza, A. A. 2012. "Removal of mono-and multicomponent BTX compounds from effluents using activated carbon from coconut shell as the adsorbent." *Industrial and Engineering Chemistry Research*, 51(18): 6461–6469.
- Stavropoulos, G., and Zabaniotou, A. 2005. "Production and characterization of activated carbons from olive-seed waste residue." *Microporous and Mesoporous Materials*, 82(1): 79–85.
- Su, F., Lu, C., and Hu, S. 2010. "Adsorption of benzene, toluene, ethylbenzene and p-xylene by NaOCl-oxidized carbon nanotubes." *Colloids and Surfaces A: Physicochemical and Engineering Aspects*, 353(1): 83–91.
- Sudaryanto, Y., Hartono, S., Irawaty, W., Hindarso, H., and Ismadji, S. 2006. "High surface area activated carbon prepared from cassava peel by chemical activation." *Bioresource Technology*, 97(5): 734–739.
- Sun, J., Brady, T. A., Rood, M. J., Lehmann, C. M., Rostam-Abadi, M., and Lizzio, A. A. (1997). "Adsorbed natural gas storage with activated carbons made from Illinois coals and scrap tires." *Energy and Fuels*, 11(2): 316–322.
- Sun, L., Gu, Z. Z., Guo, D. Y., and Xu, M. 1997. "Demonstration systems of cooking gas produced by crop straw gasifier for villages." In A. V. Bridgwater and D. G. B. Boocock (Eds.), *Developments in Thermochemical Biomass Conversion*, vol. 1/2, pp. 973–984. Dordrecht: Springer Netherlands.
- Tham, Y. J., Puziah A. L., Abdulla A. M., Shamala, A., and Taufiq Y. H. 2011. "Performances of toluene removal by activated carbon derived from durian shell." *Bioresource Technology*, 102: 724–728.
- Thrower, P. A. 1993. *Chemistry and Physics of Carbon*, vol. 24. New York: Taylor & Francis.
- Tongpoothorn, W., Sriuttha, M., Homchan, P., Chanthai, S., and Ruangviriyachai, C. 2011. "Preparation of activated carbon derived from *Jatropha curcas* fruit shell by simple thermo-chemical activation and characterization of their physico-chemical properties." *Chemical Engineering Research and Design*, 89(3): 335–340.

- Tran, H. N., You, S.-J., and Chao, H.-P. 2017. "Fast and efficient adsorption of methylene green 5 on activated carbon prepared from new chemical activation method." *Journal of Environmental Management*, 188: 322–336.
- Tsai, W., Chang, C., Wang, S., Chang, C., Chien, S., and Sun, H. 2001. "Cleaner production of carbon adsorbents by utilizing agricultural waste corn cob." *Resources, Conservation and Recycling*, 32(1): 43–53.
- Veser, G., Ziauddin, M., and Schmidt, L. D. 1999. "Ignition in alkane oxidation on noble-metal catalysts." *Catalysis Today*, 47(1): 219–228.
- Wang, G., Dou, B., Zhang, Z., Wang, J., Liu, H., and Hao, Z. 2015. "Adsorption of benzene, cyclohexane and hexane on ordered mesoporous carbon." *Journal of Environmental Sciences*, 30: 65–73.
- Wibowo, N., Setyadhi, L., Wibowo, D., Setiawan, J., and Ismadji, S. 2007. "Adsorption of benzene and toluene from aqueous solutions onto activated carbon and its acid and heat treated forms: Influence of surface chemistry on adsorption." *Journal of Hazardous Materials*, 146(1–2): 237–242.
- Yakout, S. M. 2014. "Removal of the hazardous, volatile, and organic compound benzene from aqueous solution using phosphoric acid activated carbon from rice husk." *Chemistry Central Journal*, 8(1): 52.
- Yang, R. T. (2003). *Adsorbents: Fundamentals and Applications*. Hoboken, NJ: Wiley.
- Yin, C. Y., Aroua, M. K., and Daud, W. M. A. W. 2007. "Review of modifications of activated carbon for enhancing contaminant uptakes from aqueous solutions." *Separation and Purification Technology*, 52(3): 403–415.
- Zabaniotou, A. A., Kalogiannis, G., Kappas, E., and Karabelas, A. J. 2000a. "Olive residues (cuttings and kernels) rapid pyrolysis product yields and kinetics." *Biomass and Bioenergy*, 18(5): 411–420.
- Zabaniotou, A. A., Roussos, A. I., and Koroneos, C. J. 2000b. "A laboratory study of cotton gin waste pyrolysis." *Journal of Analytical and Applied Pyrolysis*, 56(1): 47–59.
- Zhang, R., and Somasundaran, P. 2006. "Advances in adsorption of surfactants and their mixtures at solid/solution interfaces." *Advances in Colloid and Interface Science*, 123–126: 213–229.
- Zhang, T., Walawender, P. W., Fan, T. L., Fan, M., Daugaard, D., Brown, C. R. 2004. "Preparation of activated carbon from forest and agricultural residues through CO₂ activation." *Chemical Engineering Journal*, 105(1): 53–59.
- Zhao, X. S., Ma, Q., and Lu, G. Q. 1998. "VOC removal: Comparison of MCM-41 with hydrophobic zeolites and activated carbon." *Energy and Fuels*, 12(6): 1051–1054.
- Zhu, D., Kwon, S., and Pignatello, J. J. 2005. "Adsorption of single-ring organic compounds to wood charcoals prepared under different thermochemical conditions." *Environmental Science & Technology*, 39(11): 3990–3998.
- Zolin, A., Jensen, A. D., Jensen, P. A., and Dam-Johansen, K. 2002. "Experimental study of char thermal deactivation." *Fuel*, 81(8): 1065–1075.

Index

A

AAS, *see* Atomic absorption spectroscopy (AAS)
Acid-activated sintering process red mud (ASRM), 147
Acid blue 113 (AB113) dye, 147
Acidosasa edulis, 209
Activated carbon, 41, 49

- activation process and, 82
- based on agricultural waste materials, 199–203
- BET surface areas of, 236
- CO₂ capture and, 41, 49
- definition of, 199
- fiber, 294
- grapeseed, 202
- high-microporosity, 225
- low-cost, 199
- surface modification of, *see* BTEX (Benzene, Toluene, Ethylbenzene, and Xylenes) removal from aqueous solutions, impact of surface modification of activated carbon on
- synthesis, hydrochar for, 235–246

Activated red mud (ARM), 143, 137
Advection, 302
Agricultural waste, 8–10

- adsorption capacities, 206–210
- copper ions and, 197–221
- gaseous pollutant removal and, 8–10
- removal of hazardous pollutants from water using, 79–108
- sustainable biochar derived from, 255–291
- synthesis of adsorbents, 8–9
- utilization, 10

Alumina extraction waste, 184–185
Amine-functionalized solid sorbents, 44
ARM, *see* Activated red mud (ARM)
Artificial neural network (ANN) modeling, 138
Artocarpus odoratissimus, 207
ASRM, *see* Acid-activated sintering process red mud (ASRM)
Atomic absorption spectroscopy (AAS), 167

B

Bacteria-modified red mud, 143
Bagasse carbon-red mud (BCRM), 148
Bauxsol-coated sand (BCS), 137

Bentonite, 202
BET (Brunauer–Emmett–Teller) surface area, 82, 1660
Bezafibrate (BZF), 151
Biochar, 82; *see also* Methylene green 5 (MG5), sustainable biochar for removal of (from aqueous solution)

- coconut shell, 257, 288
- golden shower pod, 257, 288
- orange peel, 257, 288
- wood-derived, 202

Biofiltration, volatile organic compounds (VOCs) removal by, 21–33

- “active thickness,” 24
- background and driving factors, 21
- biofiltration process, 21–22
- characterization of biofilter media, 23
- coconut coir, 30
- empty bed residence time, 27
- ground tire rubber, 27
- key parameters affecting biofilter performance, 22–27
- modeling solid phase adsorption, 31
- moisture content, issues relating to, 25
- recommendations, 31–32
- solid waste adsorbents and biofiltration process, 27–30
- sugarcane bagasse, 29
- wood charcoal, 29

Biomass, mesoporous adsorbents from, *see* Hydrothermal treatment (mesoporous adsorbents from biomass)
Black carbon, 256
Blast furnace slag, sludge, and flue dust, 183–184
BTEX (Benzene, Toluene, Ethylbenzene, and Xylenes) removal from aqueous solutions, impact of surface modification of activated carbon on, 293–312

- activated carbon and its sources, 294–307
- activation process, 295–298
- adsorption mechanism, 301–302
- advection, 302
- effect of textural properties of activated carbon without modification, 302–303
- effect of textural properties of modified activated carbon, 303–307

external diffusion, 302
 future directions, 307–308
 governing properties for activation process, 299
 internal diffusion, 302
 kinetic models for activation process, 300–301
 polycyclic aromatic compounds, 293
 raw materials used for preparation of activated carbon, 296
 BZF, *see* Bezafibrate (BZF)

C

Calcined limestone (CL), 13
 Calcium-based sorbents, 44
 Calcium looping process (CLP), carbon dioxide (CO₂) capture by calcium-based industrial solid wastes in, 57–76
 calcium-based industrial solid wastes as CO₂ sorbents, 58–61
 circulated fluidized bed boiler, 70
 coadsorption of CO₂ and other pollutants, 70–73
 CO₂ capture performance, 60–61
 CO₂/HCl adsorption, 70–73
 CO₂ and SO₂ adsorption, 70
 effects of reaction conditions on CO₂ capture performance, 61–65
 enhancing CO₂ capture performance, 65–69
 inert supports, 66–67
 microcrystalline cellulose, 69
 organic calcium precursors, 65–66
 particle size, 65
 pore structure, improvements of, 67–69
 reaction atmosphere, 62–65
 reaction temperature, 61
 refuse-derived fuel-fired boilers, 71
 steel slag, 60
 Carbon capture and storage (CCS), 36
 Carbon dioxide (CO₂) capture, *see* Calcium looping process (CLP), carbon dioxide (CO₂) capture by calcium-based industrial solid wastes in; Industrial flue gas, carbon dioxide (CO₂) capture from
 Carbon molecular sieves, 41
 Carbon nanotubes (CNTs), 41–42
Carica papaya, 210
 Cation exchange capacity (CEC), 256
 CATRM, *see* Concentrated sulfuric acid activated red mud (CATRM)
 CCB, *see* Coconut shell biochar (CCB)
 CCS, *see* Carbon capture and storage (CCS)

CDW, *see* Construction and demolition waste (CDW)
 CEC, *see* Cation exchange capacity (CEC)
Cicer arietinum, 200
Cinnamomum camphora, 205
 Circulated fluidized bed boiler (CFBB), 70
Citrus maxima, 209
 CL, *see* Calcined limestone (CL)
 CLP, *see* Calcium looping process (CLP), carbon dioxide (CO₂) capture by calcium-based industrial solid wastes in
 CNTs, *see* Carbon nanotubes (CNTs)
 Coconut coir, 30
 Coconut shell biochar (CCB), 257, 288
 Co-ion effect, 124
 Concentrated sulfuric acid activated red mud (CATRM), 146
 Construction and demolition waste (CDW), 13
 Copper ions, agricultural solid waste materials as potential adsorbents for (from water and wastewater), 197–221
 activated carbon based on agricultural waste materials, 199–203
 adsorption capacities (activated carbon), 200–201
 adsorption capacities (agricultural waste materials), 206–210
 agricultural waste materials, 203–212
 bentonite, 202
 pomegranate peel biosorbents, 211
 wood-derived biochars, 202
 Crystal violet (CV), 147
Cucumis sativus, 81

D

Direct reduction of iron (DRI), 164
 Dolochar (as low-cost adsorbent for the removal of Pb(II) from aqueous solutions), 163–177
 adsorbent for lead removal, 165
 adsorption isotherms, 172–173
 effect of adsorbent dosage, 169
 effect of adsorption particle size, 169–170
 effect of contact time, 169
 effect of solution pH on Pb adsorption, 168
 effect of temperature on Pb(II) adsorption, 173–174
 kinetic model, 171–172
 materials and methods, 165–166
 method of experiment, 167
 pore structure characterization, 166
 thermodynamic parameters, 174–175
 zero point charge (pH drift method), 167

DRI, *see* Direct reduction of iron (DRI)
 Dubinin–Raduskevich (DR) isotherm model,
 94, 114, 211

E

EBRT, *see* Empty bed residence time (EBRT)
 EDX fluorescence spectrophotometry, *see*
 Energy dispersive x-ray (EDX)
 fluorescence spectrophotometry
Eichhornia crassipes, 208
 Electrostatic screening, 266
 Elovich equation, 122
 Empty bed residence time (EBRT), 27
 Endocarp, 10
 Energy dispersive x-ray (EDX) fluorescence
 spectrophotometry, 84
Eriobotrya japonica, 210
Eupatorium adenophorum, 201
 External diffusion, 302

F

Fertilizer industry, 186
 Flue gas
 emission of, 191
 remediation, implementation of industrial
 solid wastes for, 192–193
 treatment, possible remedies in, 191–192
 Fourier transform infrared (FTIR) spectroscopy,
 84, 86–87, 211
 Freundlich isotherm, 96, 119, 137
Fumaria indica, 209

G

Gaseous pollutant removal, 3–19
 agricultural waste, 8–10
 construction waste, 12
 industrial waste, 4–8
 municipal solid waste, 11
 palm oil mill waste, 10
 plastic solid waste, 14
 pros and cons of separation technologies,
 14–15
 sources and types of solid waste, 11
 utilization of miscellaneous waste
 adsorbents for gas adsorption, 13–14
 Gasification, 37
 Golden shower pod biochar (GSB), 257, 288
 Granular red mud (GRM), 139, 142, 143, 147
 Graphene-based material, 42
 Ground tire rubber (GTR), 27

H

HAS, *see* Hyperbranched amino silica (HAS)
 Hazardous air pollutants (HAPs), 22
 Heavy metal
 pollution and its remediation, 180–181
 removal, comparative analysis of, 191
 Henry law isotherm, 92
 HMF, *see* Hydroxymethylfurfural (HMF)
 HPMC, *see* Hydroxypropyl methylcellulose
 (HPMC)
 Hydrated Portland cement (HPC), 13
 Hydrothermal treatment (mesoporous
 adsorbents from biomass), 225–253
 activated carbon synthesis, hydrochar for,
 235–246
 BET surface areas of activated carbons, 236
 BET surface areas of hydrochars, 234
 biomass and biomass-based adsorbents,
 227–230
 effect of higher ZnCl_2 amounts under
 different hydrothermal temperatures,
 239–240
 effect of hydrothermal pretreatment
 temperature, 235–237
 hydrochar formation, properties, and
 applications, 231–246
 hydrothermal carbonization, 230
 use of H_2O_2 as a catalyst, 240–243
 use of H_3PO_4 as a catalyst, 240
 use of ZnCl_2 as a catalyst, 237–239
 use of ZnCl_2 as a catalyst under different
 concentrations, 244–246
 Hydroxymethylfurfural (HMF), 231
 Hydroxypropyl methylcellulose (HPMC), 137
 Hyperbranched amino silica (HAS), 46

I

Industrial flue gas, carbon dioxide (CO_2)
 capture from, 35–55
 activated carbon, 41
 adsorption, definition of, 40
 advantages and disadvantages of
 adsorption, 48–49
 amine-functionalized activated
 carbonaceous materials, 46
 amine-functionalized solid sorbents, 44
 aqueous amines, 45
 calcium-based sorbents, 44
 carbon molecular sieves, 41
 carbon nanotubes, 41–42
 CO_2 capture technology, 36–38

- CO₂ separation technology, 38–47
 - effect of amine functional groups and structural properties of adsorbents, 47–48
 - gasification, 37
 - graphene-based material, 42
 - hyperbranched amino silica, 46
 - lithium-based sorbents, 43
 - mass transfer zone, 49
 - metal-organic frameworks, 42
 - molecular basket sorbent, 43
 - multiwalled carbon nanotubes, 41
 - natural gas combined cycle, 36
 - nonspecific interaction, 47
 - novel structured sorbents, 47
 - oxy-fuel combustion, 38
 - physisorption, 40
 - postcombustion capture, 36–37
 - potassium-based sorbents, 44
 - precombustion capture, 37
 - pyrene methyl picolinimide, 46
 - shift convertor, 37
 - single-walled carbon nanotubes, 41
 - temperature swing adsorption, 43
 - treatment and disposal of spent adsorbent (activated carbon), 49
 - zeolites, 42
 - zero emission coal processes, 44
 - Industrial solid wastes, potential reusability of (as adsorbents), 179–196
 - air pollution (emission of flue gas), 191
 - alumina extraction waste, 184–185
 - background and current scenario, 179
 - blast furnace slag, sludge, and flue dust, 183–184
 - comparative analysis of heavy metal removal, 191
 - competitive removal of metal ions, 187–188
 - cost incurred in using industrial solid wastes, 189–190
 - environmental concerns about industrial wastes, 180
 - fertilizer industry, 186
 - flue gas treatment, possible remedies in, 191–192
 - heavy metal pollution and its remediation, 180–181
 - implementation of industrial solid wastes for flue gas remediation, 192–193
 - industrial solid wastes (alternative solution), 181–187
 - leather industry waste, 185
 - miscellaneous industries, 186–187
 - paper industry waste, 185–186
 - postcombustion residue, 182–183
 - recommendations, 193–194
 - toxicity analysis of industrial waste-based adsorbents, 190
 - Industrial waste, 4–8
 - synthesis of adsorbents, 6
 - types, 5–6
 - utilization, 7–8
 - Internal diffusion, 302
 - Iron oxide-activated red mud (IOARM), 143
- J**
- Jatropha curcas*, 210, 211
- L**
- Langmuir isotherm, 118, 274
 - Lansium domesticum*, 81
 - Leather industry waste, 185
 - Lithium-based sorbents, 43
- M**
- Malachite green (MG), 147
 - MBS, *see* Molecular basket sorbent (MBS)
 - Metal-organic frameworks (MOFs), 42
 - Methylene blue (MB) dye, 84, 148
 - Methylene green 5 (MG5), sustainable biochar for removal of (from aqueous solution), 255–291
 - adsorption experiments, 259–261
 - adsorption isotherms, 272–274
 - adsorption kinetics, 267–272
 - adsorption reversibility, 278
 - adsorption thermodynamics, 274–278
 - batch adsorption experiment, 259–260
 - biochar characterization, 258
 - biochar preparation, 257–258
 - breakthrough half-breakthrough time, 281
 - characteristics of biochar, 261–265
 - column adsorption experiment, 260–261
 - continuous adsorption experiment, 279–282
 - electrostatic attraction and cation exchange, 282
 - electrostatic screening, 266
 - external diffusion, 270
 - hydrogen bonding formation, 283
 - ionic strength, effect of, 266–267
 - materials and methods, 257–261
 - n*– π interaction, 284
 - π – π interaction, 284–286

- point of zero charge and effect of solution pH, 265–266
- pore filling, 286–288
- possible adsorption mechanisms, 282–288
- separation factor, 274
- statistical analysis, 261
- transport processes, steps associated with, 270
- Yoon–Nelson sorption capacity, 281
- MG, *see* Malachite green (MG)
- MOFs, *see* Metal-organic frameworks (MOFs)
- Molecular basket sorbent (MBS), 43
- Moringa oleifera*, 200
- Morris–Weber equation, 122
- Multifunction red mud granule (RMGM), 140
- Multiwalled carbon nanotubes (MWCNTs), 41
- Municipal solid waste (MSW), 11

N

- Natural gas combined cycle (NGCC), 36
- Nitrobenzene (NB), 151

O

- Oil palm shell, 10
- Orange peel biochar (OPB), 257, 288
- Oxy-fuel combustion, 38

P

- PAHs, *see* Polynuclear aromatic hydrocarbons (PAHs)
- Palm oil mill waste, 10
- Paper industry waste, 185–186
- Pb(II) removal from aqueous solutions, *see* Dolochar (as low-cost adsorbent for the removal of Pb(II) from aqueous solutions)
- PC, *see* Pulverized coal (PC)
- PCBs, *see* Polychlorinated biphenyls (PCBs)
- PEI, *see* Polyethylenimine (PEI)
- Phosphate treated rice husk (PRH), 125; *see also* Rice husk, biosorption of divalent heavy metal ions by
- Physisorption, 40
- Plastic solid waste, 14
- PMP, *see* Pyrene methyl picolinimide (PMP)
- Polybrominated diphenyl ethers (PBDEs), 198
- Polychlorinated biphenyls (PCBs), 198
- Polyethylenimine (PEI), 43, 46
- Polynuclear aromatic hydrocarbons (PAHs), 198

- Polystyrene (PS)
 - microspheres, 147
 - modified red mud (MRM-PS), 147
 - waste, 14
- Polyvinyl chloride (PVC), 60
- Pore size distribution (PSD), 41
- Potassium-based sorbents, 44
- PRH, *see* Phosphate treated rice husk (PRH)
- PS, *see* Polystyrene (PS)
- PSD, *see* Pore size distribution (PSD)
- Pulverized coal (PC), 36
- PVC, *see* Polyvinyl chloride (PVC)
- Pyrene methyl picolinimide (PMP), 46
- Pyrolysis, 82

R

- Raw rice husk (RRH), 125; *see also* Rice husk, biosorption of divalent heavy metal ions by
- RBB dye, *see* Remazol Brilliant Blue (RBB) dye
- RDF (refuse-derived fuel)-fired boilers, 71
- Reactive black 5 (RB5) dye, 147
- Redlich–Peterson isotherm, 119
- Red mud for environmental applications, 135–161
 - bacteria-modified red mud, 143
 - iron oxide-activated red mud, 143
 - magnetic nanoparticles, synthesis of, 137
 - preparation of catalyst, 153–155
 - purification of toxic waste gases, 152–153
 - removal of anions from water and wastewater, 136–140
 - removal of dyes from aqueous solution, 145–149
 - removal of heavy metal ions from aqueous solution, 140–145
 - removal of organic pollutants from aqueous solution, 149–152
- Red mud granular adsorbent (RMGA), 139
- Red mud powders (RMPs), 155
- Reichenberg model, 122
- Remazol Brilliant Blue (RBB) dye, 146
- Rice husk, biosorption of divalent heavy metal ions by, 109–134
 - chemically and thermally modified rice husk, 111–115
 - co-ion effect, 124
 - column experiment, 124–126
 - effect of use of mixture of rice husk and other sorbents on sorption performance, 116–117

elution or recovery of sorbate (metal ions), 127–128
 impact of metal dose on sorption performance, 117
 impact of various parameters on sorption capacity of rice husk, 115–117
 kinetics of biosorption process by activated rice husk, 121–123
 mechanism of sorption, 126–127
 sorption isotherms, 117–121
 thermodynamics of sorption, 123–124
 RMGA, *see* Red mud granular adsorbent (RMGA)
 RMGM, *see* Multifunction red mud granule (RMGM)
 RMPs, *see* Red mud powders (RMPs)
Rosa centifolia, 205
 RRH, *see* Raw rice husk (RRH)

S

Sargassum sp., 200
 Scanning electron microscopy (SEM), 67, 84, 166, 231
 Seawater-neutralized red mud (SWRM), 147
 Shift convertor, 37
 Single-walled carbon nanotubes (SWCNTs), 41
 Sodium dodecyl sulfate-modified red mud (SDS/RM), 146
Sophora japonica, 209
 Steel slag, 60
 Sugarcane bagasse, 29
 SWCNTs, *see* Single-walled carbon nanotubes (SWCNTs)
 SWRM, *see* Seawater-neutralized red mud (SWRM)

T

Temkin isotherm, 95, 119
 Temperature swing adsorption (TSA), 43
 Thermal gravimetric analysis (TGA), 70, 84
Typha latifolia, 201

U

Ulva fasciata, 200
Uncaria gambir, 206

V

Volatile organic compounds (VOCs), 298
 Volatile organic compounds (VOCs) removal by biofiltration, 21–33
 “active thickness,” 24
 background and driving factors, 21
 biofiltration process, 21–22
 characterization of biofilter media, 23
 coconut coir, 30
 empty bed residence time, 27
 ground tire rubber, 27
 key parameters affecting biofilter performance, 22–27
 modeling solid phase adsorption, 31
 moisture content, issues relating to, 25
 recommendations, 31–32
 solid waste adsorbents and biofiltration process, 27–30
 sugarcane bagasse, 29
 wood charcoal, 29

W

Water, removal of hazardous pollutants from (using agricultural wastes), 79–108
 adsorption isotherm models, 92–99
 adsorption kinetic models, 99–101
 BET (Brunauer–Emmett–Teller) surface area, 82
 biochar, 82
 biocides and other organic contaminant removal, 90–91
 chemical modification of agricultural wastes, 82–84
 dye removal, 89
 environmental application, 87–91
 equilibrium, kinetics, and thermodynamic studies, 91–102
 Fourier transform infrared spectroscopy, 86–87
 future perspective, 102–103
 heavy metals removal, 87–89
 Langmuir–Freundlich equation, 96
 modification of agricultural wastes for adsorbents, 80–87
 nitrogen sorption, 85
 physical modification of agricultural wastes, 81

- pyrolysis, 82
- scanning electron microscopy, 87
- Sips equation, 96
- Temkin model, 96
- thermal modification of agricultural wastes,
 - 81–82
- thermodynamic of adsorption, 101–102
- versatile modification of agricultural wastes,
 - 80
- Wood charcoal, 29

X

- X-ray diffraction, 84
- X-ray fluorescence (XRF), 59, 165
- X-ray photo electron spectroscopy (XPS), 84

Y

- Yoon–Nelson sorption capacity, 281

Z

- Zeolites, 12–13, 42
- Zero emission coal (ZEC) processes, 44
- Zero point charge (ZPC), 167